INVESTIGATING THE INTRATHYMIC AND POST-THYMIC PROCESSES WHICH INSTRUCT THYMIC $CD25^{+}FOXP3^{+}$ REGULATORY T-CELL DEVELOPMENT

By
SARAH ELIZABETH INGLESFIELD

A thesis submitted to the University of Birmingham

For the Degree of DOCTOR OF PHILOSOPHY

Institute of Immunology and Immunotherapy

College of Medical and Dental Science

University of Birmingham

October 2021

ABSTRACT

The thymus is a key site of Treg development, however uncertainty remains regarding how intrathymic and post-thymic processes may contribute to the generation of a diverse peripheral Treg population. Therefore, we used the Rag-GFPxFoxp3-RFP mouse to characterise the development of newly produced Tregs in the thymus and periphery.

Our analysis identified that de novo thymic Tregs contained heterogeneous CD62L^{hi} and CD62L^{lo} subsets, generated through a post selection pathway, where some CD62L^{hi} Tregs differentiated into CD62L^{lo} Tregs, possibly mediated by interactions with mTEC^{hi}. Both Treg subsets appeared to undergo thymic egress, contributing to the peripheral pool from the earliest neonatal stages. We also identified post-selection proliferation of thymic Tregs, which was most prevalent within the neonate, where it correlated with the large expansion of the earliest thymic Treg population. Further analysis of neonatal thymic Tregs identified they proliferated more extensively than Tconvs, possibly in response to IL-2 and IL-15 signalling. Finally, we performed RNAseq analysis of recent thymic emigrants and their mature counterparts within Treg and Tconv lineages. This comparison identified that both lineages may undergo a modest post-thymic maturation upon egress, featuring some shared elements.

Collectively our findings highlight underappreciated processes involved in intrathymic and post-thymic Treg development.

ACKNOWLEDGMENTS

Firstly, I would like to express my sincere gratitude to Professor Graham Anderson for his attentiveness, commitment and counsel, in guiding the direction of my research. In addition, I would like to thank Dr William Jenkinson and Dr Sara Jabbari for the encouragement, support and advice they also provided.

My colleagues in the Anderson lab have all played a significant part in supporting me during my studies and I would like to thank them for all their help and kindness. I am also indebted to all members of the fourth floor of the IBR for their camaraderie and goodwill.

I would also like to take the opportunity to thank Dr Sascha Ott and his research group at the University of Warwick for their generous collaboration in this project and for their role in providing me bioinformatics analysis training.

I would like to acknowledge the essential support of the Wellcome Trust and the Mechanisms of Inflammatory Disease programme in funding my PhD studies. I would like to thank the coordinators of this programme, and in particular Professor Robin May for his advisory role throughout my studies.

Finally, thank you to my family and friends who have persevered with me throughout what has at times been a challenging but ultimately rewarding academic undertaking.

TABLE OF CONTENTS

CHAPTER ONE: GENERAL INTRODUCTION 1
1.1 $CD4^+CD8^-$ SP4 T-cells and Peripheral Tolerance 2
1.1.1 Overview of T-cells in the Immune System 2
1.1.2 T-cell Heterogeneity and $\alpha\beta$T-cell Subsets 2
1.1.3 SP4 T-cell Activation and Differentiation 4
1.1.4 Regulatory T-cells and Peripheral Tolerance 9
1.1.4.1 Identification of Tregs and the Role of Foxp3 10
1.1.4.2 Treg Mediated Suppression 13
1.1.4.3 Treg Heterogeneity 17
1.1.4.3.1 Peripheral vs Thymic Tregs 17
1.1.4.3.2 Phenotypically and Functionally Distinct Treg Subsets 19
1.2 Thymic Development and Post-Thymic Development of $CD4^+$ T-cells 24
1.2.1 The Thymus and T-cell Development: An Overview 24
1.2.2 Thymocyte Entry and Early Development 27
1.2.3 $CD4^+CD8^+$ Double Positive Thymocytes and Positive Selection 29
1.2.4 Single Positive Thymocytes: Central Tolerance and Maturation 33
1.2.5 Central Tolerance 34
1.2.5.1 Negative Selection by Clonal Deletion 36
1.2.5.2 Redirection to the Treg Lineage 37
1.2.6 Post-Selection Maturation and Thymic Egress 42
1.2.7 RTEs and Continued Post-Thymic Maturation 46
1.2.8 Influence of Development Stage on Thymic Output 49
1.3 Key Cellular Regulators of SP4 T-cell Development 51
1.3.1 Generation and Involution of the Thymic Microenvironment 51
1.3.2 TEC 52
1.3.2.1 cTEC 52
1.3.2.2 mTEC 54
1.3.2.2.1 $mTEC^{hi}$ 55
1.3.2.2.2 $mTEC^{lo}$ 58
1.3.3 Thymic Hematopoietic Regulators 59
1.3.3.1 Thymic DC 59
1.3.3.2 Autoreactive Thymocytes 63
1.3.3.3 Mature Thymic Tregs 64
1.3.4 Peripheral Support of SP4 RTE Development 66
1.4 General Aims 69

CHAPTER TWO: MATERIALS AND METHODS 71
2.1 Mice 72
2.2 Media For Cell Isolation, Cell Staining and Cell Culture Systems 74
2.3 Dissection of Mouse Tissues 75
2.4 Isolation of Cell Populations 76
2.4.1 Isolation of Lymphocytes from Tissues 76
2.4.1.1 Thymus, Spleen and Lymph Nodes (LNs) 76
2.4.1.2 Bone Marrow (BM) 76

2.4.1.3 Liver 77
2.4.1.4 Colon 77
2.4.1.5 Blood 78
2.4.2 Isolation of Lymphocytes from Organ Cultures 78
2.4.3 Isolation of Thymic Stromal Cells from Tissues 79
2.4.4 Isolation of Thymic Stromal Cells from Organ Cultures 79
2.5 Cell Counts 80
2.5.1 Counting with Sphero AccuCount cell count beads 80
2.5.2 Counting with a Haemocytometer 80
2.6 Flow Cytometry 81
2.6.1 Cell Surface Staining 81
2.6.2 Intracellular Fixation and Staining 83
2.6.3 Intracellular Fixation and Staining with Retention of GFP 83
2.6.4 Flow Cytometric Analysis 84
2.7 Bromodeoxyuridine (BRDU) Proliferation Analysis 85
2.7.1 *In Vivo* BRDU Labelling 86
2.7.2 *In Vitro* BRDU Labelling 86
2.7.3 Detection of BRDU with Foxp3 86
2.8 Isolation of Cell Populations by Cell Sorting 87
2.8.1 Preparation of Sample for Cell Sorting 87
2.8.1.1 Enrichment of Populations Prior to Cell Sorting 88
2.8.1.1.1 CD8 Depletion 88
2.8.1.1.2 Rag-GFP Enrichment 88
2.8.2 Purity Cell Sorting 88
2.9 Fetal Thymic Organ Cultures (FTOCs) 89
2.9.1 FTOC for Analysis of Lymphocyte Populations 90
2.9.2 FTOC for Analysis of Stromal Populations 90
2.9.3 Blockade of Common γ Chain Receptor Signalling in FTOC 90
2.10 Reaggregate Thymic Organ Cultures (RTOCs) 91
2.11 Pilot Colitis Model 92
2.11.1 Colitis Model Setup 92
2.11.2 Assessment of Colitis Model Endpoint 93
2.12 RNA Sequencing (RNAseq) 93
2.12.1 Single Cell RNAseq (scRNAseq) 93
2.12.1.1 Sample Generation 94
2.12.1.2 Sample Sequencing 94
2.12.1.3 Bioinformatics Processing 94
2.12.2 Bulk RNAseq 95
2.12.2.1 Sample Generation 95
2.12.2.2 Sample Sequencing 96
2.12.2.3 Bioinformatics Processing 96
2.13 Statistical Analysis 98

CHAPTER THREE: RE-EXAMINING *DE NOVO* THYMIC TREG DEVELOPMENT 99

3.1 Introduction 100
3.2 Results 102
3.2.1 Heterogeneous Thymic Treg Development 102

3.2.2 Treg Precursors and Heterogeneous Treg Development 131
3.2.3 Possible Regulators of the Treg Lineage 145
3.2.4 Assessing Functional Differences of Tregs: Pilot Colitis Model 170
3.3 Discussion 179
3.3.1 A Thymic Origin for Heterogeneous Tregs 179
3.3.2 Characterising Thymic Development of Heterogeneous Tregs 181
3.3.3 Concluding Remarks 189

CHAPTER FOUR: INTRATHYMIC PROLIFERATION OF NEONATAL TREGS 192
4.1 Introduction 193
4.2 Results 194
4.2.1 Identifying Proliferation of Neonatal Thymic Treg 194
4.2.2 Further Characterisation of Neonatal Treg Proliferation 212
4.2.3 Possible Regulators of Neonatal Intrathymic Proliferation 220
4.2.4 Changes to Intrathymic Proliferation with Age 243
4.3 Discussion 256
4.3.1 Neonatal Intrathymic Proliferation by Thymic Tregs 256
4.3.2 Possible Regulators of Intrathymic Proliferation of Thymic Tregs 259
4.3.3 Concluding Remarks 264

CHAPTER FIVE: DIFFERENTIATING RTES FROM THEIR MATURE COUNTERPARTS 267
5.1 Introduction 268
5.2 Results 270
5.2.1 Initial Generation and Processing of RNAseq Datasets 270
5.2.2 Characterising and Comparing SP4 RTEs and Non-RTEs Using RNAseq 286
5.3 Discussion 311
5.3.1 Gene Expression Changes Characterising RTE Maturation 311
5.3.1.1 Possible Common Features of Treg and Tconv RTEs 311
5.3.1.2 Possible Lineage Specific Features of Treg and Tconv RTEs 313
5.3.2 Similarity of SP4 RTE and Non-RTE Genetic Profiles 316
5.3.3 Concluding Remarks 318

CHAPTER SIX: GENERAL DISCUSSION 321
6.1 Considerations for Models Used to Investigate De Novo Treg Development 322
6.2 Complexities and Distinctions of Thymic Treg Development 328
6.3 Concluding Remarks 334

REFERENCES 335

APPENDIX: SUPPLEMENTARY DATA ACCOMPANYING CHAPTER FIVE 355

LIST OF FIGURES

CHAPTER ONE

Figure 1. 1 SP4 T-cell Activation and Differentiation Legend.....5
Figure 1. 2 Mechanisms of Treg Mediated Suppression.....15
Figure 1. 3 Treg Heterogeneity and Differentiation.....22
Figure 1. 4 SP4 T-cell Development.....25
Figure 1. 5 Treg Development: Two Pathways of a Two Step Process.....38

CHAPTER THREE

Figure 3. 1 The Foxp3-RFPxRag-GFP Reporter Confirms the Thymic Treg Population Consists of *De Novo* and Mature Tregs.....104
Figure 3. 2 The *De Novo* Thymic Treg Population Contains $CD62L^{hi}$ and $CD62L^{lo}$ Subsets.....106
Figure 3. 3 $CD62L^{hi}$ and $CD62L^{lo}$ *De Novo* Thymic Tregs Show Broadly Similar Expression of Markers Associated with Migration, Function, or Maturation.....109
Figure 3. 4 $CD62L^{hi}$ Tregs Appear Before $CD62L^{lo}$ Tregs in *De Novo* Thymic Treg Development.....113
Figure 3. 5 Treatment of Embryonic Thymic Stroma with dGuo Inhibits Development of $MTEC^{hi}$.....115
Figure 3. 6 $CD62L^{hi}$ *De Novo* Thymic Tregs Differentiate to $CD62L^{lo}$ Tregs in RTOC.....117
Figure 3. 7 *De Novo* Thymic Treg Subsets Both Show Evidence of Egress Competency..121
Figure 3. 8 $CD62L^{hi}$ and $CD62L^{lo}$ Tregs are Identifiable within the Splenic RTE Population.....123
Figure 3. 9 $CD62L^{hi}$ and $CD62L^{lo}$ Tregs are Present within the Early Neonatal Splenic RTE Population.....125
Figure 3. 10 Treg RTE can be Found in Lymphoid and Non-Lymphoid Peripheral Tissues.....127
Figure 3. 11 $CD62L^{hi}$ and $CD62L^{lo}$ Treg RTEs Display Different Homing Preferences.....129
Figure 3. 12 Thymic Treg Precursor Populations are a Mixture of *De Novo* and Mature Tregs.....132
Figure 3. 13 Early Developmental Appearance of Thymic $CD25^{+}Foxp3^{-}$ Precursors Relative to $CD25^{-}Foxp3^{+}$ Precursors and Tregs.....135
Figure 3. 14 SP4 T-cells with a $CD25^{-}Foxp3^{+}$ Thymic Treg Precursor Phenotype are Present in the Spleen.....138
Figure 3. 15 *De Novo* $CD25^{+}Foxp3^{-}$ Treg Precursors Comprise $CD62L^{hi}$ and $CD62L^{lo}$ Subsets.....140
Figure 3. 16 *De Novo* $CD25^{-}Foxp3^{+}$ Treg Precursors Comprise $CD62L^{hi}$ and $CD62L^{lo}$ Subsets.....143
Figure 3. 17 Formalin Fixation Retains Rag-GFP During Intracellular Staining.....147
Figure 3. 18 Thymic Treg Development Appears Normal in *Aire*$^{-/-}$ Adults.....150
Figure 3. 19 Treg Populations Appear Normal in the Spleen of *Aire*$^{-/-}$ Adults.....152
Figure 3. 20 Reduced *De Novo* Thymic Treg in D7 *Aire*$^{-/-}$ Neonates Does Not Appear to be a Consequence of Altered Heterogeneous Treg Development.....155

Figure 3. 21 Absence of Aire has a Limited Impact on D7 Neonatal Splenic Treg Populations.....157
Figure 3. 22 Identification of a Trend Suggestive of Altered Heterogeneous Thymic Treg Development in *Ltbr*$^{-/-}$ Adults.....160
Figure 3. 23 Specific Reduction of Splenic Treg RTEs in *Ltbr*$^{-/-}$ Adults.....162
Figure 3. 24 Evidence of Altered Heterogeneous Thymic Treg Development in D7 *Ltbr*$^{-/-}$ Neonates.....165
Figure 3. 25 Gross Reduction of Splenic SP4 T-cells in D7 *Ltbr*$^{-/-}$ Neonates.....168
Figure 3. 26 Colitis Model Setup.....171
Figure 3. 27 Preliminary Evidence Co-transferred Tregs Prevent Weight Loss in Colitis Model.....175
Figure 3. 28 Preliminary Evidence Co-transferred Tregs Protect Against Pathogenic Colonic T-cells in Colitis Model.....177
Figure 3. 29 Summary Diagram of Heterogeneous Thymic Treg Development.....190

CHAPTER FOUR

Figure 4. 1 Establishment of the Thymic Treg is Associated with Rapid Expansion in the Neonate.....196
Figure 4. 2 Early Appearance of Rag-GFP^{-} Thymic Tregs in Ontogeny.....198
Figure 4. 3 Early Appearance of Thymic Rag-GFP^{-} Tregs in Neonates is Unlikely Solely Due to Peripheral Recirculation.....202
Figure 4. 4 Expression of the Proliferation Marker Ki67 by Neonatal Thymic Tregs.....204
Figure 4. 5 Confirmation Neonatal Thymic Treg are Undergoing Active Proliferation.....207
Figure 4. 6 Rapid Expansion of Neonatal Treg Population Counters Initial Imbalance in the Peripheral Ratio of Tconv:Treg.....210
Figure 4. 7 Thymic Treg Precursors Show Evidence of Proliferation.....213
Figure 4. 8 Comparable Proliferation of Neonatal Thymic Treg Subsets.....216
Figure 4. 9 Neonatal Thymic Tcons Proliferate but to a Lesser Extent than Tregs.....218
Figure 4. 10 Differential Expression of γ_c Family Members by Neonatal SP4 Thymocyte Populations.....221
Figure 4. 11 FTOCs as a System to Investigate Intrathymic Proliferation: Evidence of Ongoing Thymic Treg Development.....225
Figure 4. 12 FTOCs as a System to Investigate Intrathymic Proliferation: Evidence of Active Thymocyte Proliferation.....227
Figure 4. 13 Specific Disruption of CD25+Foxp3- Treg Precursor Proliferation within Anti-CD25 Treated FTOCs.....230
Figure 4. 14 SP4 Thymocyte Proliferation Appears Normal within Anti-IL15/IL-15R Treated FTOCs.....232
Figure 4. 15 Loss of Aire has Only a Minor Impact on Intrathymic Proliferation of Thymocytes within the Treg Lineage.....235
Figure 4. 16 Slight Impairment of Thymic Treg Development in D7 *Tnfrsf4*$^{-/-}$ Neonates..239
Figure 4. 17 Proliferation of SP4 Thymocyte Populations is Reduced in D7 *Tnfrsf4*$^{-/-}$ Neonates.....241
Figure 4. 18 Thymocyte Proliferation Decreases with Age.....245
Figure 4. 19 Reduced Proliferation of De Novo Thymocytes in Adults.....247
Figure 4. 20 Differential Expression of CD25 by Adult and Neonatal Thymocytes.....249

Figure 4. 21 Differential Expression of CD127 by Adult and Neonatal Thymocytes.....252
Figure 4. 22 Differential Expression of CD122 by Adult and Neonatal Thymocytes.....254
Figure 4. 23 Summary Diagram of Intrathymic Proliferation in Neonates and Adults.....265

CHAPTER FIVE

Figure 5. 1 Overview of Generation of RTE and Non-RTE scRNAseq and Bulk RNAseq Datasets.....272
Figure 5. 2 Overview of Pre-Processing Stages of scRNAseq RTE and Non-RTE Datasets 275
Figure 5. 3 Treg and Naïve Tconvs Populations can be Identified within scRNAseq Datasets.....278
Figure 5. 4 Overview of Isolation and Reanalysis of Tconv and Treg RTE and Non-RTE Subsets within scRNAseq Dataset.....281
Figure 5. 5 Overview of Pre-Processing Stages of Bulk RNAseq RTE and Non-RTE Datasets 283
Figure 5. 6 Principal Component Analysis Identifies RTE vs Non-RTE Identity as the Largest Source of Variation within the SP4-Bulk RNAseq Dataset.....288
Figure 5. 7 Differentially Expressed Genes between Bulk SP4 RTE and Mature SP4 T-cells are Associated with Modest Fold Changes.....290
Figure 5. 8 Variation between Tconv RTE and Mature Tconv Associated with Modest Changes in Gene Expression.....294
Figure 5. 9 Variation between Treg RTE and Mature Treg Associated with Modest Changes in Gene Expression.....297
Figure 5. 10 Treg and Tconv RTEs Exhibit Some Common Changes in Gene Expression..300
Figure 5. 11 Changes in Gene Expression Observed in Naïve Tconv scRNAseq Analysis are Highly Comparable with Bulk RNAseq Analysis.....302
Figure 5. 12 Changes in Gene Expression Identified in Treg scRNAseq Analysis are Less Consistent with Bulk RNAseq Analysis.....304
Figure 5. 13 Summary Diagram of SP4 RTE Development Stage.....319

CHAPTER SIX

Figure 6. 1 Discriminating *De Novo* and Mature Thymic Tregs.....324

APPENDIX

Figure S. 1 Detail of QC Steps Taken in Processing scRNAseq Dataset from Figure 5.2...356
Figure S. 2 Enlarged Heatmap of Total RTE and Non-RTE Clusters DEGs Originally Presented in Figure 5.3.B.....358
Figure S. 3 Enlarged Heatmap of Naïve Tconv Clusters DEGs Originally Presented in Figure 5.4.B.....360
Figure S. 4 Enlarged Heatmap of Treg Clusters DEGs Originally Presented in Figure 5.4.C.....362
Figure S. 5 Specifics of Removal of B-cell Genes from Bulk RNAseq datasets from Figure 5.5.....364
Figure S. 6 Enlarged Heatmap of DEGs between Treg RTE and Non-RTE Originally Presented in Figure 5.9.E.....366

LIST OF TABLES

CHAPTER TWO

Table 2. 1 Details of Mouse Strains 73
Table 2. 2 RPMI-1640 Hepes (RF10) 74
Table 2. 3 2% Fetal Calf Serum Hanks Balanced Saline Solution (2% FCS HBSS) 74
Table 2. 4 Dulbecco's Modified Eagle Medium (DMEM) 74
Table 2. 5 MACs Buffer 75
Table 2. 6 FACs Buffer 75
Table 2. 7 Primary Extracellular Antibodies Used for Flow Cytometry Immunolabeling ... 84
Table 2. 8 Secondary Antibodies Used for Flow Cytometry Immunolabeling 85
Table 2. 9 Primary Intracellular Antibodies Used for Flow Cytometry Immunolabeling 85
Table 2. 10 Purified Functional Grade Antibodies Used for Signalling Blockade Experiments 91
Table 2. 11 R Packages Used in RNAseq Analysis 97
Table 2. 12 Parameters Used for Seurat Clustering of scRNAseq Data 97

CHAPTER FIVE

Table 5. 1 Selection of Markers Previously Suggested to be Differentially Expressed by RTE and Non-RTE 269
Table 5. 2 Details of Suspected Common DEGs between RTE and Non-RTEs Selected for Follow-Up Protein Validation Analysis 310

APPENDIX

Table S. 1 Contaminating B-cell Genes Identified and Removed from SP4-Bulk Dataset 368
Table S. 2 Specifics of DEGs (between RTEs and Non-RTEs) of Literature Genes Detected within the SP4-Bulk Dataset 369
Table S. 3 Specifics of DEGs identified between RTEs and Non-RTEs, which are Top 100 Contributors to PC1, within the SP4-Bulk Dataset 370
Table S. 4 Specifics of all DEGs Identified Between RTEs and Non-RTEs within the Tconv scRNAseq Dataset 373
Table S. 5 Specifics of all DEGs Identified Between RTEs and Non-RTEs within the Treg scRNAseq Dataset 374

ABBREVIATIONS

3PP	Third Pharyngeal Pouch
Aire	Autoimmune Regulator
APC	Antigen Presenting Cell
BM	Bone Marrow
BRDU	Bromodeoxyuridine
cDC	Conventional DC $CD8\alpha^+CD11c^+$, variants: cDC1 ($Sirp\alpha^-CD11b^-$) and cDC2 ($Sirp\alpha^+CD11b^+$)
CMJ	Corticomedullary Junction
CNS	Conserved Non-Coding Sequences
cTEC	Cortical Thymic Epithelial Cell
cTreg	Central Treg ($CD62L^{hi}CCR7^{hi}CD44^{lo}$)
D	Day
d3tx	Day 3 Thymectomy
DC	Dendritic Cell
DEG	Differentially Expressed Gene
dGuo	2-Deoxyguanosine
DMEM	Dulbecco's Modified Eagle Medium
DN	Double Negative ($CD4^-CD8^-$) Thymocyte
DP	Double Positive ($CD4^+CD8^+$) Thymocyte
DPBS	Dulbeccos Phosphate Buffered Saline
E	Embryonic Day
EDTA	Ethylenediaminetetraacetic Acid
ETP	Early Thymic Progenitor
eTreg	Effector Treg ($CD62L^{lo}CCR7^{lo}CD44^{hii}$)
FC	Fold Change
FCS	Fetal Calf Serum
Fezf2	Fez Family Zinc Finger 2
FMO	Fluorescence Minus One
Foxp3	Forkhead Box P3
FTOC	Fetal Thymic Organ Culture
γ_χ	Common Cytokine Receptor γ-Chain
GFP	Green Fluorescent Protein
HBSS	Hank's Balanced Salt Solution
iLN	Inguinal Lymph Nodes
iNKT-Cell	Invariant Natural Killer T-Cells
jTEC	Junctional Epithelial Cells
LN	Lymph Node
LSEC	Liver Sinusoidal Endothelial Cell
LTβR	Lymphotoxin β Receptor
MHC	Major Histocompatibility Complex, variants: MHCI and MHCII
Mir181	MicroRNA-181
mLN	Mesenteric Lymph Nodes
moDC	Monocyte-Derived DC (cDC2 subset $CD14^+Sirp\alpha^+$)
mTEC	Medullary Thymic Epithelial Cell

NK	Natural Killer cell
PC	Principal Component
PCA	Principal Component Analysis
pDC	Plasmacytoid DC ($PDCA1^{+}CD11c^{low}$)
pMHC	Peptide MHC
pTreg	Peripherally Derived Treg
PVS	Perivascular Space
QC	Quality Control
Rag	Recombination Activation Gene
RANK	Receptor Activator for NF-κB
RBC	Red Blood Cell
RF10	RPMI-1640 Hepes
RFP	Red Fluorescent Protein
RNAseq	RNA Sequencing
RT	Room Temperature
RTE	Recent Thymic Emigrant
RTOC	Reaggregate Thymic Organ Culture
S1P	Sphingosine-1-phosphate
S1PR1	Sphingosine-1-phosphate Receptor 1
Satb1	special AT-rich Sequence-binding Protein-1
scRNAseq	Single Cell RNA Sequencing
SLO	Secondary Lymphoid Organ
Sox4	SRY-Box Transcription Factor 4
SP	Single Positive T-cell, variants: SP4 ($CD4^{+}CD8^{-}$) and SP8 ($CD4^{-}CD8^{+}$)
Tconv	Conventional T-cell
TCR	T Cell Receptor, variants: $\alpha\beta$TCR and $\gamma\delta$TCR
TEPC	Thymic Epithelial Progenitor Cell
TF	Transcription Factor
Tfh	T-follicular Helper
Th	T-helper, variants: Th1, Th2, Th17
TLR	Toll-like Receptor
TNFRSF	Tumor Necrosis Factor Receptor Superfamily
TR	Transcriptional Regulator
TRA	Tissue Restricted Antigen
Treg	Regulatory T-cell
$Triple^{hi}$ Treg	$CD25^{hi}PD1^{hi}GITR^{hi}$ Treg
$Triple^{lo}$ Treg	$CD25^{lo}PD1^{lo}GITR^{lo}$ Treg
TSLP	Thymic Stromal Lymphopoietin
tSNE	t-distributed Stochastic Neighbour Embedding
TSP	Thymus Seeding Progenitor
tTreg	Thymic Derived Treg
V(D)J	Variable (Diverse) Joining Gene Segments
VAT	Visceral Adipose Tissue
WT	Wild-type

CHAPTER ONE:
GENERAL INTRODUCTION

1.1 $CD4^+CD8^-$ SP4 T-cells and Peripheral Tolerance

1.1.1 Overview of T-cells in the Immune System

The primary purpose of the immune system is to protect the host from harmful pathogens. To perform this function a variety of immune cells are required. These different cells are broadly categorised as belonging to the innate or adaptive arm of the immune system, although great interplay exists between the two[1]. One of the critical features of the adaptive immune system is that it mediates specific recognition of pathogens. Of particular relevance to this are T-cells, specifically those that express the $\alpha\beta$ form of the T-cell receptor ($\alpha\beta$TCR). The majority of these cells recognise peptides antigens presented by Major Histocompatibility Complex (MHC) molecules, and are termed conventional $\alpha\beta$T-cells. Owing to the random nature of $\alpha\beta$TCR generation, to be discussed in Section 1.2, each T-cell has a different TCR from a potential of $\sim 10^{15}$[2,3] meaning as a population, $\alpha\beta$T-cells have the potential to recognise virtually any antigen. Such potential is incredibly useful for the immune system in responding to a diverse range of ever-changing pathogens, however it is not without its challenges.

1.1.2 T-cell Heterogeneity and $\alpha\beta$T-cell Subsets

It should be noted that conventional $\alpha\beta$T-cells are not the only type of T-cell there are also $\gamma\delta$T-cells, which express the distinct $\gamma\delta$ form of the TCR[3,4], and invariant natural killer T (iNKT) cells, which express a semi-invariant $\alpha\beta$TCR[5]. Notably both also differ in their recognition of antigen, as iNKT-cells recognise glycolipid antigens presented by CD1d[5] while $\gamma\delta$T-cells recognise non-peptide antigen in a non-MHC restricted manner[4]. This differing antigen recognition combined with differing localisation and function enables these T-cell subsets to uniquely contribute to immune responses[4,5] however here the focus remains on the $\alpha\beta$T-cell

lineage. Within the αβT-cell lineage there is great subset diversity based on functional specialisation. Much of this is generated during development in the thymus, to be discussed in section 1.2.

αβT-cells circulate through lymphatics and secondary lymphoid organs (SLOs), engaging with cell types which may present an antigen their specific TCR recognises[4,6]. αβT-cells recognise peptide antigen in the context of two types of MHC molecules that present distinct antigen to different αβT-cell subsets. MHCI is universally expressed on all nucleated cells to present endogenous antigen. MHCII in contrast, is restricted to specialised antigen presenting cells (APCs) to present exogenous antigen[7]. The type of MHC (with peptide) an αβT-cell recognises determines which TCR co-receptor the cell expresses, either CD4 or CD8[8,9]. Consequently αβT-cells are sub-categorised as $CD4^+CD8^-$ (SP4) or $CD8^+CD4^-$ (SP8) due to their recognition of MHCII or MHCI accordingly. It should be noted that in the periphery these subsets are commonly referred to as $CD4^+$ T-cells and $CD8^+$ T-cells however here they are termed SP4 and SP8 respectively, for consistency with naming conventions of thymic populations.

This difference in MHC recognition translates to differing functional responses. SP8 T-cells are commonly termed "cytotoxic" T-cells as antigen recognition/activation results in direct killing of the presenting cell via apoptosis inducing mechanisms[10]. SP4 T-cells are referred to as "helper" T-cells (Th), as upon antigen recognition/ activation these cells produce appropriate cytokines which "help" direct/orchestrate an appropriate immune response[11]. The type of response induced is dependent upon what signals naïve SP4 T-cells receive. Owing to the specific relevance of SP4 T-cells to the thesis, they will be the primary focus.

1.1.3 SP4 T-cell Activation and Differentiation

Perhaps the most notable APC in initiating SP4 T-cell responses in SLOs is the dendritic cell (DC), although it should be noted that macrophages and B-cells can also perform as APCs. Appropriate activation and differentiation of naïve T-cells requires three signals from the same DC[6,12], as illustrated in Figure 1.1. Signal 1 is provided through $\alpha\beta$TCR mediated signalling, when a naïve T-cell recognises its cognate antigen presented by the DC. However in isolation signal 1 is insufficient to induce T-cell activation, signal 2 provided by DC co-stimulatory molecules, is also required[12]. Perhaps the most notable co-stimulatory pathway is mediated by CD86/CD80 and CD28, expressed by DCs and T-cells respectively, which results in T-cell proliferation, IL-2 production and survival[13]. CD28 signalling also induces T-cells to upregulate other costimulatory molecules including ICOS and OX40 which in conjunction with their respective ligands also support T-cell activation[13]. Activation of a naïve T-cell through signal 1 and 2 results in an effector T-cell. However different effector T-cell subsets exist and the exact type of effector T-cell produced is dependent upon signal 3, which is also influenced by the nature of the pathogen that initiated the immune response. This signal is provided predominantly by DC cytokine secretion[6,12]. Different cytokines induce different effector subsets, distinct in their signature transcription factors (TFs), and the type of immune response they orchestrate, primarily through their own cytokine secretion[11].

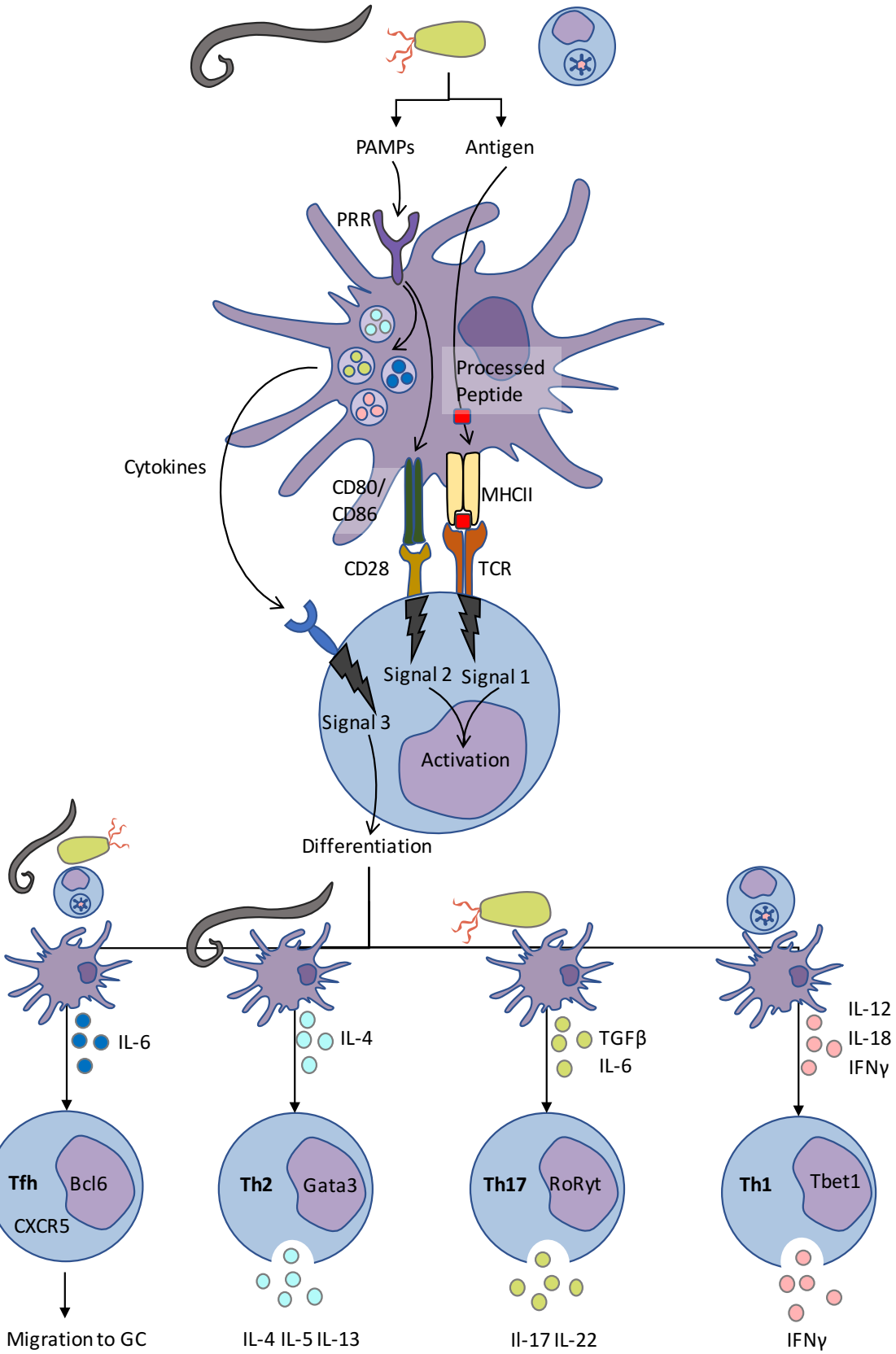
PAMPs
Antigen
PRR
Processed
Peptide
Cytokines
CD80/
CD86
MHCII
CD28
TCR
Signal 2
Signal 1
Signal 3
Activation
Differentiation
IL-6
IL-4
TGFβ
IL-6
IL-12
IL-18
IFNγ
Tfh
Bcl6
CXCR5
Th2
Gata3
Th17
RoRyt
Th1
Tbet1
Migration to GC
IL-4 IL-5 IL-13
Il-17 IL-22
IFNγ

Figure 1. 1 SP4 T-cell Activation and Differentiation Legend

Broadly DCs receive two pieces of material from pathogenic invaders, which are key for their ability to induce SP4 T-cell activation. Firstly, pathogenic antigens which the DC process to peptide antigen for presentation by MHC II. Secondly there are molecular motifs specifically associated with, and conserved across classes of pathogens, termed pathogen-associated molecular patterns (PAMPS) which are recognised by pattern recognition receptor (PRR) on immune cells such as DCs. Recognition of PAMPS by PRRs causes maturation of the DC including the upregulation of CD80/86 alongside secretion of specific cytokines depending on the type of invader. The DC then provides three signals to the $CD4^{+}$ T-cell. Signal 1 is peptide MHCII to TCR and signal 2 is CD80/86 to CD28 (expressed by the DC and T-cell respectively). In combination signal 1 and 2 result in activation of the T-cell. Signal 3 is provided by DC derived cytokines. Depending on the type of pathogen different DCs secrete different cytokines to induce an appropriate Th effector subset. The principle DC cytokines which induce a Th effector subset, through induction of that subsets signature transcription factor, and the principle cytokines that Th effector then secretes to elicit an immune response are shown. Intracellular pathogens induce DCs to secrete IFNγ which in turn induces T-bet^{+} Th1 effectors that secrete IFNγ. Extracellular pathogens induce DCs to secrete IL-6 and TGFβ which in turn induces $RoRyt^{+}$ Th17 effectors that secrete IL-17 and IL-22. Large parasites and helminths induce DCs to secrete IL-4 which in turn induces $Gata3^{+}$ Th2 effectors that secrete IL-4,IL-5,IL-13. Finally $Bcl6^{+}$ Tfh are not induced in response to a specific infection but by IL-6 from activated DCs which causes upregulation of CXCR5 allowing migration to germinal centres (GCs) to support B-cell responses.

Two highly proinflammatory responses are mediated by Th1 and Th17 effectors, which are necessary to deal with intracellular pathogens or extracellular bacteria and fungi (respectively)[11]. Th1 effectors are induced by IFN-γ activated TFs STAT1 and ultimately the signature TF T-bet, alongside IL-12 activated TF STAT4[11,14,15]. T-bet acts in consort with STAT4 to induce IFN-γ secretion, a signature cytokine, which polarises the T-cell response towards Th1 as it promotes further STAT1/T-bet induction[11,14,15]. Alongside an autocrine role IFN-γ is vital in orchestrating the wider highly pro-inflammatory immune response[11]. Induction of Th17 effectors can be driven by a combination of IL6, IL21, IL23, IL-1β and TGF-β cytokine signalling[11,16,17]. Downstream STAT-3 and the master TF RORγt then promote differentiation of Th17 effectors and secretion of vital mediators of Th17 functions, notably IL-17 and IL-22[11,16,17].

Unlike Th1 or Th17, Th2 effectors mediate a more restrained response, against extracellular parasites and the tissue damage such parasites cause[18]. Th2 differentiation occurs in response to IL-4 which induces STAT6 and ultimately the signature Th2 TF Gata3, these TFs then induce expression of the signature Th2 cytokines, IL-4, IL-5 and IL-13. These cytokines help eliminate extracellular parasites, through mechanism such as expulsion or granuloma formation[18]. Furthermore they also, along with other factors such as IL-10, ameliorate associated tissue damage, by promoting an anti-inflammatory environment that is conducive to wound repair, and inducing other cell types to mediate repair[18]. Given the vital anti-inflammatory nature of the Th2 response it is perhaps unsurprising that there is strong antagonism to other Th subsets, as exemplified by the antagonism between Gata3 and Th1 induction[19].

Finally, the T follicular helper (Tfh) subset, rather than orchestrating a response against a defined type of pathogen, instead specifically supports another adaptive immune cell response, the B-cell[20]. Tfh are induced by IL-6 to express the signature TF Bcl6 which upregulates CXCR5 to direct Tfh to germinal centres where they can support various aspects of the B-cell response including survival and affinity maturation[20].

As different SP4 T-cell subsets are necessary to react to different pathogen-specific circumstances, signal 3 is vital in insuring an appropriately directed immune response. DCs are informed by recognition of characteristic pathogen-associated molecular patterns and other environmental signals as to the type of threat and hence the appropriate effector Th lineage[11,12]. Furthermore, these cues also enable maturation of DCs from an immature to mature state. This maturation involves the expression and upregulation of co-stimulatory molecules including CD80/86 (which are not constitutively expressed) and also of peptide MHCII, thus mature DCs that migrate to SLOs are more adept at inducing T-cell activation[12,21]. While the conditions described above help ensure naïve T-cells are activated appropriately, this is not always the case. Th subsets have been described as mediators of various conditions. For instance, Th2 responses are involved in allergies while Th1 and Th17 have both been implicated in different autoimmune diseases[11,18], demonstrating the potential for SP4 T-cell dysregulation. This problem stems at least in part from the random generation of the TCR, which is a double-edged sword as virtually anything can be recognised. While this means recognition of potentially any pathogen, it comes at the cost of generating TCRs which recognise innocuous antigens from self-cells, environmental or food particles, and commensals. Immune responses directed against such antigens can cause tissue damage, autoimmunity and allergy, which ultimately can be fatal.

1.1.4 Regulatory T-cells and Peripheral Tolerance

The challenge presented by T-cells recognising host cells has necessitated mechanisms which prevent inappropriate activation and maintain a diverse but crucially self-tolerant T-cell repertoire. Maintaining an unresponsive state towards self-antigen is commonly referenced as maintaining tolerance. Mechanisms which enforce tolerance are constantly prevalent throughout the life of a T-cell, beginning with mechanisms which screen and eliminate developing T-cells with potentially harmful TCR clones (e.g. those recognising self-antigen) in the thymus (termed central tolerance) and continuing into the peripheral tissues with mechanisms which target mature T-cells (termed peripheral tolerance).

Mechanisms of central tolerance, are encompassed through thymic negative selection processes, covered in greater detail in section 1.2. In brief the outcome for an autoreactive T-cell detected during thymic negative selection is either clonal deletion or clonal diversion into the regulatory T-cell (Treg) lineage. While certainly a vital process, as demonstrated by autoimmune disease seen in patients and mice with defects in central tolerance processes[22,23] it would appear that negative selection is not 100% effective. This is evident from the reports of auto-reactive clones in the T-cell repertoire isolated from both healthy humans[24] and (transgenic) mice[25]. A lack of complete coverage is perhaps not unsurprising, as while the thymus is an impressively robust organ, its' screening of autoreactive T-cells (discussed in section 1.2) is limited by both time and available repertoire[26,27].

Furthermore a wider trade-off exists between deleting clones with some self-reactive potential but may contribute to a protective immune response e.g. against pathogenic invaders[2]. Indeed in models where the diversity of the TCR repertoire is reduced, the result

is a reduced ability to respond to as wide a range of antigens[2]. As such there may be some benefits to a "leaky" negative selection process, however it does necessitate peripheral tolerance mechanisms to ensure those autoreactive T-cells that escape negative selection are kept in check. Therefore, peripheral tolerance mechanisms are also vital in restraining the immune system. A range of mechanisms are employed including some which overlap with central tolerance approaches: namely clonal deletion and clonal diversion into the Treg lineage[28,29].

Of the mechanisms specific to peripheral tolerance, in the first instance there is ignorance. Here peripheral auto-reactive T-cells remain inactivate despite the presence of their cognate antigen, due to either inherent low TCR affinity, low antigen density or restriction of antigen to sites with limited accessibility[30,31]. Regarding this latter point certain tissues, such as the brain, are associated with anatomical barriers which cause sequestering of antigen and limit T-cell access. This isolation contributes to these sites "immune privilege", characterised by a limited immune response on antigen challenge[30,31]. Alternatively, when autoreactive T-cells do encounter their antigen, they can be subject to a process called anergy. Here T-cells recognising antigen in the absence of an appropriate second signal are rendered unresponsive to future encounters with cognate antigen[28]. Finally the most relevant mechanism to this thesis, which shall be considered in greater detail, is that of immune suppression carried out by Tregs[29].

1.1.4.1 Identification of Tregs and the Role of Foxp3

The existence of a suppressive T-cell subset, later termed regulatory T-cells (Tregs), was first suggested by work in the 1970s which highlighted that distinct T-cells could dampen immune

responses[32–34]. Much research then focused on determining phenotypic markers to distinguish this suppressive subset. In mice CD25, the IL2Rα chain expressed as part of the high-affinity IL2R complex, was identified as the distinguishing marker of peripheral SP4 T-cells capable of enacting immune suppression on $CD25^-$SP4 T-cells[35,36]. However, CD25 alone was not sufficient to fully distinguish Tregs as upon activation non-Tregs upregulate CD25. Therefore a more distinctive lineage marker was necessary, which in mice, proved to be the forkhead/winged-helix family TF forkhead box P3 (Foxp3)[37–39]. In mice, Foxp3 was found to be co-expressed by $CD4^+CD25^+$ T-cells but, unlike CD25, not upregulated by activated $CD25^-$ SP4 T-cells[37,39].

Compelling evidence of the link between cellular expression of Foxp3 and immune regulation came from scurfy mice, a naturally occurring X-linked mutant in which a frameshift in the Foxp3 gene results in a non-functional Foxp3 protein[40]. Typically, within the first 4 weeks of life mice hemizygous for the scurfy mutation suffer fatal multi-organ autoimmune disease, predominantly mediated by SP4 T-cells[41]. Similar observations were made with the $Foxp3^{DTR}$ mouse, which featured a diphtheria toxin receptor construct under the control of the Foxp3 locus, meaning $Foxp3^+$ Tregs could be selectively ablated upon injection of diphtheria toxin[42–44]. Using this system to specifically deplete Tregs in neonates and adults resulted in severe autoimmune disease, reminiscent of the phenotype observed in scurfy mice[42–44]. Critically both scurfy neonates and Treg depleted $Foxp3^{DTR}$ mice could be rescued from autoimmune disease development by transfer of exogenous $CD4^+CD25^+Foxp3^+$ Tregs[38,44]. Collectively demonstrating that specific loss of $Foxp3^+$ Treg was sufficient to induce autoimmunity and hence indicating the importance of the Treg population and their expression of Foxp3 in maintaining peripheral tolerance.

Further evidence that Foxp3 was the critical TF inducing the regulatory phenotype required to enforce this tolerance came from transduction experiments which aimed to determine if Foxp3 express alone could force a regulatory phenotype[37,38]. Here viral vectors were used to induce Foxp3 gene expression in Foxp3$^-$ SP4 T-cells. Ectopic expression of Foxp3 in these cells resulted in the upregulation of several regulatory molecules associated with the CD25$^+$Foxp3$^+$ Treg population[37]. However perhaps most critically these Foxp3-transduced T-cells demonstrated regulatory function. Firstly *in vitro* assays showed Foxp3-transduced T-cells were capable of limiting proliferation of activated Foxp3$^-$ SP4 T-cells[37]. While *in vivo* autoimmune colitis models, where disease is induced by transfer of Foxp3$^-$ T-cells into lymphocyte deficient hosts and can be ameliorated by co-transfer of Tregs, identified that co-transfer of Foxp3-transduced T-cells prevented colitis disease onset as effectively as naturally occurring Tregs[37,38]. Overall these findings demonstrate the critical role of Foxp3 in driving the regulatory function and phenotype of Tregs, and hence Foxp3 is often referred to as the master TF of the Treg lineage.

The vital role of Foxp3 in immune regulation is not limited to mice, in humans Immunodysregulation Polyendocrinopathy Enteropathy X-linked syndrome is akin to scurfy with patients suffering, often fatal, early onset systemic autoimmune disease due to an impaired Treg population stemming from mutations in the Foxp3 gene[45]. However, while Foxp3 is certainly an important marker of human Tregs it appears to be less specific as it can become upregulated in non-Tregs upon activation or proliferation without conferring a regulatory role[46]. Other markers of human Tregs have been proposed, most notably low expression of CD127 [47], although again this phenotype can be shared by activated non-Tregs[46]. As such confident identification of Tregs in humans is more challenging than in mice

but widely accepted definitions of Tregs within the two species are SP4 T-cells which are, in mice, $CD25^{+}Foxp3^{+}$ and in humans $CD25^{+}Foxp3^{+}CD127^{lo}$[48].

1.1.4.2 Treg Mediated Suppression

The models used to identify Tregs suggest their vital role in enforcing tolerance. Using inducible Treg depletion models it was shown that Tregs actively prevented autoimmune disease throughout life[42,43]. So how do Tregs, which represent only 5-10%, of peripheral SP4 T-cells[49], control the larger highly diverse $CD25^{-}Foxp3^{-}$ conventional T-cell (Tconv) population? Firstly while Treg suppression necessitates antigen specific recognition[50,51], they respond to much lower antigen concentrations than those required to activate Tconv, at least *in vitro*[51]. This could enable Tregs, unlike Tconvs, to be activated by immature DC and thus circumvent responses through tonic suppression[29]. Secondly, following antigen specific activation subsequent Treg suppression may occur in an antigen non-specific manner[51], through a wide variety of mechanisms. To give an overview of those targeting SP4 T-cells they are divided as follows: limiting Tconv access to survival/growth factors, release/expression of products which suppress or kill target Tconvs, and modulation of DC function (Figure 1.2).

Regarding limiting Tconv access to survival/growth factors Tregs are capable of outcompeting Tconvs for contact with DCs[52] along with competing for, and even removing, DC derived signals. This has been illustrated as a function for CTLA-4 which has high affinity for CD80/86 and can induce transendocytosis of CD80/86[53], more recently transendocytosis of peptide-MHCII complexes has also been observed[54]. Tregs do not only restrict access to surface DC products, the survival cytokine IL-2 is also more readily consumed by Tregs due to their constitutive expression of the high affinity IL2R (CD25), and as Tregs do not produce IL-

2 their consumption results in cytokine deprivation induced apoptosis in Tconvs[55]. More direct suppression of Tconvs by Tregs have been described by secretory and cell contact mechanisms. Tregs are described to secrete known inhibitory cytokines such as IL-10[56], TGFβ[57] and IL-35[58] to mediate suppression. Tconvs are also suppressed by Treg mediated increase in cAMP levels, either through direct delivery by GAP junctions or Treg expressed CD73/CD39 generation of adenosine[59]. Induction of apoptosis in Tconvs through granzyme B mediated pathways have also been reported[60]. Tregs also modulate the DC they interact with, inhibiting their maturation through pathways involving Treg expressed CTLA-4/LAF-1[52] or LAG-3[61]. Furthermore Tregs can induce a more toleragenic phenotype in DC. CTLA-4 induces Indoleamine 2,3-dioxygenase and consequently tryptophan catabolism, which results in toxic metabolic products capable of causing apoptosis in neighbouring T-cells[62]. While Treg expressed TIGIT can induce DC to produce IL-10[63]. In addition to the suppressive effects of these cytokines, toleragenic DC produce TGFβ along with retinoic acid, which mediate conversion of Tconvs to Tregs[64].

This wide range of mechanisms may reflect redundancy, as suggested by singular knock-out models which lack extensive autoimmune phenotypes[58,60,65]. However it may also indicate that certain responses necessitate specific suppression, as is suggested for instance by reports that Treg derived IL-10 is required in mucosal but not systemic regulation[65]. An idea that raises the question of heterogeneity within the Treg population.

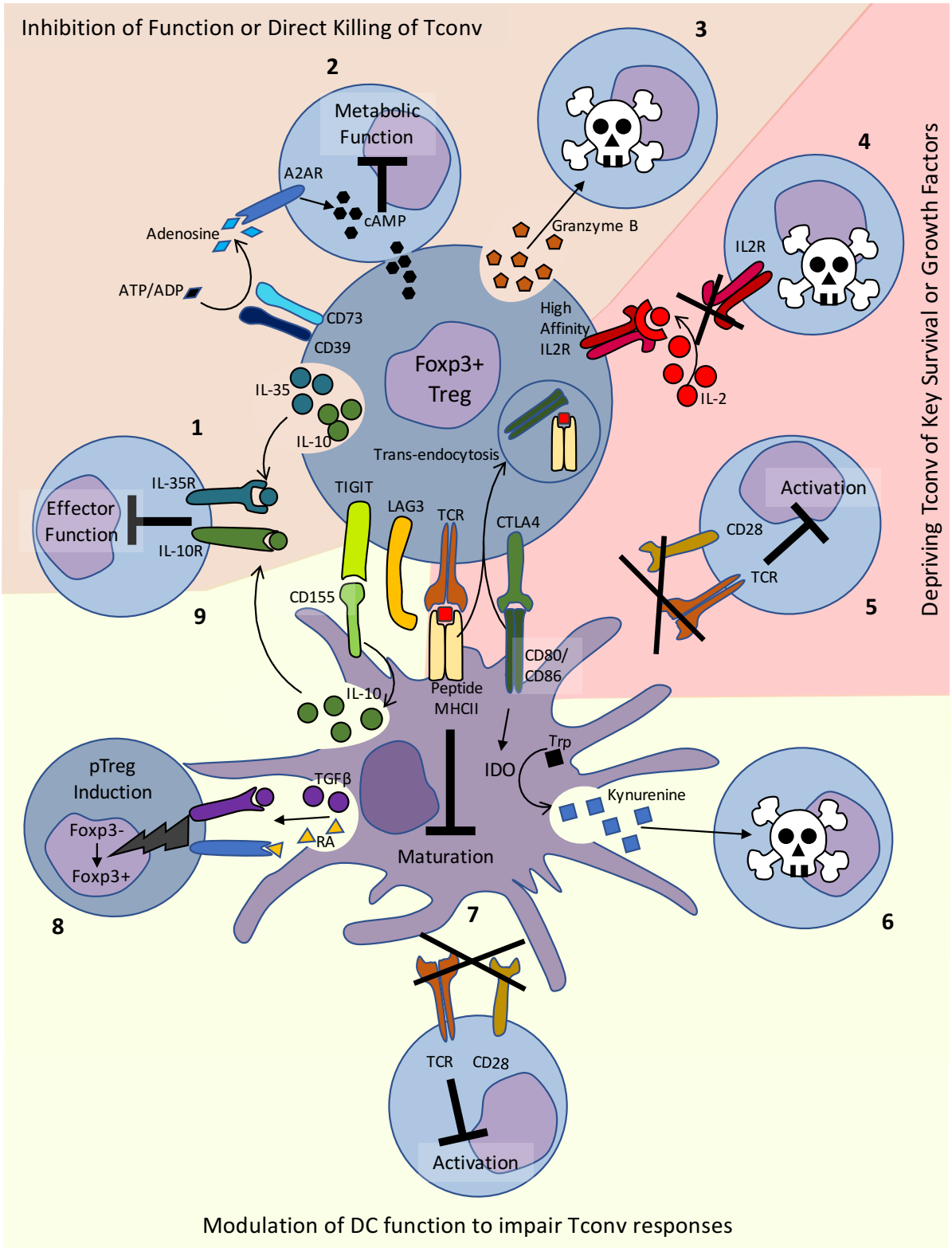

Modulation of DC function to impair Tconv responses

Figure 1. 2 Mechanisms of Treg Mediated Suppression

The mechanisms used by Foxp3^{+} Treg (dark blue) to target Foxp3^{-} Tconv (light blue) are grouped into 3 categorise as indicated by background colour. First shown are those that suppress Tconv function or induce cell death (orange). **(1)** Treg secrete immunosuppressive cytokines IL-10 and IL-35 which impair Tconv function. **(2)** Treg upregulate cAMP in Tconv either by, adenosine (generated from CD39 and CD73 mediated conversion of ATP/ADP) acting on Tconv adenosine A2A receptor (A2AR) or by direct delivery from Treg via gap junctions. cAMP mediates suppression of Tconv through disruption of their metabolic function. **(3)** Treg also cause apoptosis of Tconv by secretion of factors such as granzyme B which induce apoptosis. The next grouping of mechanisms (red) describe those that limit Tconv access to key survival or growth factors. **(4)** Through expression of the high affinity IL2R (CD25) Treg outcompete Tconv (which do not express CD25 so have a lower affinity IL2R) for the growth factor IL-2, resulting in cytokine deprivation induced apoptosis of Tconv. **(5)** Treg can directly deprive Tconv of activation signals through their TCR and CD28 by directly competing for peptide MHCII and CD80/86 with their TCR and CTLA4 (respectively) these molecules can also then be stripped from the DC surface by Treg trans-endocytosis. Overall this deprives the Tconv of activation signals. The final grouping of Treg mechanisms (yellow) are those that modulate the function of DCs for downstream effects on Tconv. **(6)** CTLA4 engagement with CD80/86 can induce Indoleamine 2,3-dioxygenase (IDO) mediated tryptophan catabolism resulting in the toxic product Kynurenine which can induce apoptosis in neighbouring Tconv. **(7)** Broadly DC maturation is impaired by engagement with Treg CTLA4 or LAG-3. This means that DCs do not upregulate peptide MHCII or CD80/86 so are thereby less capable of inducing activation of Tconv. **(8)** Modulated DC may also secrete TGβ along with retinoic acid (RA) which induce Foxp3 expression causing conversion of Tconv to peripherally induced pTregs. **(9)** Interaction of Treg TIGIT with DC CD155 induces DC to secrete the immunosuppressive cytokine IL-10 which suppresses Tconv functions.

1.1.4.3 Treg Heterogeneity

1.1.4.3.1 Peripheral vs Thymic Tregs

One clear source of heterogeneity within the Treg population origin is clonal diversion that occurs in both the thymus and periphery resulting in $CD25^{+}Foxp3^{+}$ thymic Tregs (tTregs) and peripheral Tregs (pTregs) respectively (other described pTreg subsets e.g. Tr1[66] and Th3[67] will not be discussed). Interestingly, fundamental regulation of the Foxp3 locus may differ between tTregs and pTregs. Investigation into the 5' regulatory region of the Foxp3 gene has identified four conserved non-coding DNA sequences, CNS0 within the promoter, CNS1 and CNS2 within the first intron and CNS3 in the intron after exon 1[68,69]. These regulatory regions play an essential role in many aspects of Treg development/maintenance to differing degrees in tTregs and pTregs. Firstly regarding induction, CNS1 proved a vital mediator of pTreg induction but dispensable for tTreg generation[69]. While in contrast special AT-rich sequence-binding protein-1 (Satb1) binding CNS0 proved essential for tTreg development but not pTreg induction[68]. Finally CNS3 seems to regulate generation of both tTregs and pTregs, by inducing a poised state of the Foxp3 promoter which increases the efficiency of Foxp3 induction[69].

CNS2 is not implicated in induction but rather maintenance/stability of Tregs, with demethylation of this region vital to continued Foxp3 and Treg identity[69,70]. Generally, stability of Tregs is a contentious topic, with several studies reporting Treg reprogramming under various conditions[71,72], while others demonstrate Treg stability[73,74]. Reprogramming of both tTregs and pTregs has been suggested *in vivo*[71] while , *in vitro* exposure to inflammatory cytokines causes reprogramming of tTregs and pTregs to a Th17 phenotype demonstrating instability may be induced in either[72]. Further investigations into the

methylation status of the CNS2 region in pTregs and tTregs have suggested that pTregs are more prone to instability as they have a less demethylated CNS2 region than tTregs[75]. However it should be noted that this could be an artefact of the *in vitro* system as notably once returned to an *in vivo* environment some pTregs maintained their regulatory phenotype over a 3 month period and increased methylation of their CNS2 region[76]. Therefore, differences between pTregs and tTregs in Treg lineage stability remains unclear.

While dependence on certain CNS elements may distinguish tTregs and pTregs, this is largely impractical in most experimental settings and hence more overt phenotypic markers of the two populations are highly sought after. Transcriptomic analysis of pTregs (generated *in vitro* and *in vivo*) alongside tTregs have highlighted that *in vivo* pTregs and tTregs are broadly similar but do display some differences, while *in vitro* pTregs differ from both *in vivo* pTregs and tTregs[77,78]. Interestingly returning *in vitro* pTregs to an *in vivo* environment results in acquisition of a transcriptional phenotype more akin to tTregs[76]. Overall suggesting that pTregs and tTregs are broadly phenotypically and functionally similar. However individual distinguishing markers have emerged, with Helios[79] and Neuropilin-1[80] widely used as specific markers of tTregs. Although reports of Helios^{hi}/Neuropilin-1^{hi} pTregs and Helios^{lo}/Neuropilin-1^{lo} tTregs, suggest neither Helios nor Nrp1 faithfully distinguish the populations fully[81].

While pTregs and tTregs appear highly similar phenotypically, their function must somehow differ, because both are necessary for comprehensive regulation. *In vivo* when pTregs or tTregs populations are present individually, as opposed to a combined population, immunopathology is observed[78,82,83]. Interestingly the specific absence of pTregs does not

result in multi-organ autoimmunity but rather Th2 mediated pathology at mucosal sites, akin to an allergic/asthmatic response[82]. Therefore, it has been suggested that in part the synergy of pTreg and tTreg regulation stems from distinct predominate control of responses to non-self-antigen and self-antigen (respectively). This is supported by observed differences in TCR repertoires of tTregs and pTregs[78]. Overall this identifies a fundamental difference in the repertoires of pTregs and tTregs which likely mediates their divergent but harmonic immunoregulation to self and non-self-antigens.

1.1.4.3.2 Phenotypically and Functionally Distinct Treg Subsets

While pTregs and tTregs appear broadly similar, aside from origin, the total Treg population has emerged as being highly heterogeneous (Figure 1.3). Notably, the circulating Treg population can broadly be divided on the basis of the adhesion molecule CD62L, the chemokine receptor CCR7 and the activation marker CD44, into $CD62L^{hi}CCR7^{hi}CD44^{lo}$ central Tregs (cTregs) and $CD62L^{lo}CCR7^{lo}CD44^{hi}$ effector Tregs (eTregs). Analogous $Foxp3^{lo}CD45RA^{hi}CD25^{lo}$ resting and $Foxp3^{hi}CD45RA^{hi}CD25^{hi}$ effector subsets have been identified in humans[84]. These two subsets fundamentally differ. cTregs predominantly recirculate through SLOs, and owing to this localisation have been proposed as ideally positioned to enact their regulation by limiting antigenic priming of Tconvs by DC[85]. cTregs appear quiescent and long-lived, undergoing little proliferation while highly expressing anti-apoptotic markers. This homeostasis is IL-2 dependent, with CCR7 mediating localisation to IL-2 produced in T-cell zones[85]. This cTreg population is thought to originate in the thymus then upon antigenic stimulation in the periphery cTregs may differentiate into eTregs[85–87]. eTregs are a more complex population to consider as they display further phenotypic diversity dependent upon their localisation/surrounding microenvironment. Broadly speaking eTregs

are predominant in non-lymphoid tissue, display a more activated phenotype with higher expression of activation/effector markers, and are potent producers of IL-10[85,88]. They are also largely IL-2 independent, instead relying on ICOS signalling for their maintenance[85].

The specific polarised fates of eTregs appears highly dependent on context. For instance eTregs can be influenced by inflammatory Th responses, upregulating canonical Th TFs T-bet[89], IRF4 [90], STAT3[91] and Bcl6[92] in the context of Th1, Th2, Th17 and Tfh responses (respectively). Expression these TFs by Tregs appears key to their regulation as specific ablation of different canonical Th TFs impaired Treg regulation of the respective Th response. One role for canonical Th TFs in mediating Treg regulation could be linked to the chemokine receptors they induce (e.g. CXCR3 by T-bet[89], CXCR5 by Bcl6[92] and CCR6 by STAT3[91]) which enable Treg recruitment to the inflammatory site. Furthermore eTregs also reside in non-lymphoid tissues under steady state conditions, as more specialised tissue resident Tregs, where they perform unique functions. For instance visceral adipose tissue (VAT) Tregs, distinct in phenotype and TCR repertoire, produce large amounts of IL-10 and suppress local inflammation to regulate insulin resistance[93,94]. While the intestinal RORγt$^+$ and GATA3$^+$ tissue Tregs, control inflammation in response to commensal microbiota and tissue damage respectively[95,96]. Similarly skin Tregs, with distinctive phenotypes and TCR repertoires[97], are implicated in regulating the local microbiota[98] and wound healing[99]. Collectively demonstrating how different and specialised Tregs are at distinct tissue sites.

The process by which eTreg differentiate from cTregs into their distinct phenotypes is complicated. Recent analysis of VAT Tregs in TCR transgenic mice and single cell RNA sequencing (scRNAseq) trajectory analysis of colonic and skin Tregs, suggest a progressive

differentiation process initiated in SLOs and becoming more tissue specialised upon entry into the tissue site[100,101]. Notably the scRNAseq analysis also identified conserved signatures of colon and skin tissue Tregs[101]. Similarly, there are certain TFs/axis that seem to be a common requirement for eTregs compared to those that are more response/tissue specific[88,94,102]. Overall suggesting both a core conserved programme of eTreg identity alongside more specific tissue/inflammatory programmes.

One critical factor for these differentiation programmes appears to be TCR signalling. Broadly TCR signalling appears vital in the maintenance and differentiation of eTregs, as ablation of the TCR in Tregs resulted in a specific impairment of this population[103]. The critical role for TCR signalling likely relates to its induction of the IRF4-Blimp-1 axis which is essential for differentiation of functional eTregs[88]. Alongside TCR signalling, recent work also identified an essential role for tumor necrosis factor receptor superfamily (TNFRSF) signalling induced RelA, in regulating eTreg survival and effector differentiation independently of the TCR-IRF4-axis[102]. Importantly, deficiency of either IRF4 or RelA results in specific impairment of eTreg differentiation/maintenance indicating essential non-redundant roles for both pathways[88,102]. TCR signalling also appears to direct eTreg fate more specifically, as Tregs with similar TCR sequences were found to adopt the same transcriptional programme[104]. This study also highlighted signal strength as important in dictating Treg fate[104], in keeping with the observation that weaker TCR signalling generated SLO residing IL-35 producing eTregs rather than IL-10 producing eTregs[105]. Again, though TCR signalling appears to act in concert with other pathways to direct cell fate. For instance PPAR-γ, a TF indispensable in VAT Tregs, is induced and maintained in response to both TCR and IL-33-ST2 mediated signalling[100,106].

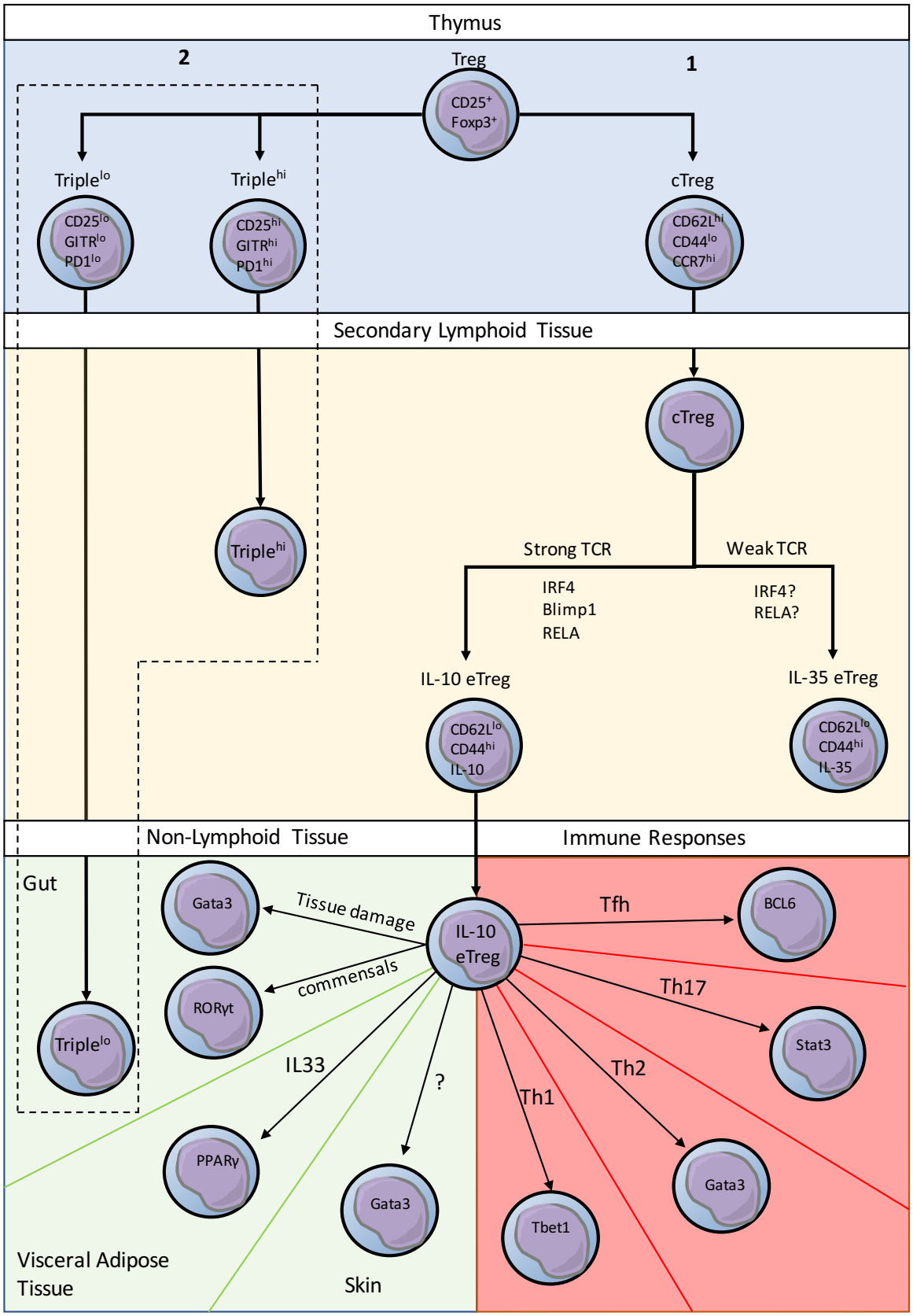
Thymus
2
Treg
1
CD25+ Foxp3+
Triplelo
Triplehi
cTreg
CD25lo GITRlo PD1lo
CD25hi GITRhi PD1hi
CD62Lhi CD44lo CCR7hi
Secondary Lymphoid Tissue
cTreg
Triplehi
Strong TCR
Weak TCR
IRF4
Blimp1
RELA
IRF4?
RELA?
IL-10 eTreg
IL-35 eTreg
CD62Llo CD44hi IL-10
CD62Llo CD44hi IL-35
Non-Lymphoid Tissue
Immune Responses
Gut
Gata3
Tissue damage
IL-10 eTreg
Tfh
BCL6
commensals
RORγt
Th17
Stat3
Triplelo
IL33
?
Th1
Th2
PPARγ
Gata3
Gata3
Tbet1
Visceral Adipose Tissue
Skin

Figure 1. 3 Treg Heterogeneity and Differentiation

An overview of the development of the different Treg ($CD25^{+}Foxp3^{+}$) subsets split into two paths. Path **(1)** begins with central Tregs (cTregs) defined as $CD62L^{hi}CD44^{lo}CCR7^{hi}$ which is generated in the thymus then exported to secondary lymphoid organs (SLOs). In SLOs cTregs may remain or convert to effector Tregs (eTregs) characterised as $CD62L^{lo}CD44^{hi}$. Under strong TCR signalling IL-10 secreting eTregs are induced through expression of key TFs IRF4,RelA and Blimp1. Under weak TCR signalling IL-35 eTregs are induced, currently it is unclear if TFs IRF4 or RelA drive this although Blimp1 is known not be involved. IL-35 eTregs remain in SLOs while IL-10 eTregs are recruited to non-lymphoid tissue or sites of immune responses/inflammation for further differentiation. Different inflammatory conditions result in different eTregs as distinguished primarily by their TF. Tregs express the same signature TFs as the Th subset driving the inflammation i.e. Tbet, Gata3, STAT3 and Bcl6 by Tregs in the context of Th1, Th2, Th17 and Tfh responses (respectively). Under steady state conditions Tregs are still recruited to non-lymphoid sites and adopt different phenotypes accordingly, while there are several changes we focus on TF for simplicity. In the skin Tregs express TF Gata3, while in adipose tissue IL-33 drives expression of TF PPARγ, finally in the gut RORγt and Gata3 Tregs are driven by signals from commensals and tissue damage respectively. Path **(2)** is based on the relatively recent discovery that different Treg subsets can be identified in the thymus. $Triple^{hi}$ and $Triple^{lo}$ Tregs are believed distinct from cTregs and characterised by high or low (respectively) expression of CD25, PD1 and ICOS. $Triple^{lo}$ Tregs are directed to the gut, while $Triple^{hi}$ Tregs are present in SLOs.

Overall this suggests that heterogeneity in the Treg population arises from peripheral cTregs differentiating to eTregs which then, depending on the context, adopt specialised phenotypes (Figure 1.3). However, this sole peripheral origin of Treg heterogeneity does not account for recent observations of two Treg subsets, distinct from cTregs and eTregs, within the developing thymic Treg pool[107] (Figure 1.3). Differentiation of these thymic Treg subsets, defined as $CD25^{hi}PD1^{hi}GITR^{hi}$ ($Triple^{hi}$ Tregs) or $CD25^{lo}PD1^{lo}GITR^{lo}$ ($Triple^{lo}$ Tregs), was driven by differing TCR signalling strength, reminiscent of eTreg differentiation. Furthermore, $Triple^{hi}$ and $Triple^{lo}$ Tregs proved distinct in their function, suppressing lymphoproliferation in lymph nodes (LNs) or limited colitis via induction of pTregs, respectively [107]. Thereby identifying a clear thymic source of heterogeneous Tregs in lymphoid and non-lymphoid tissue. Similarly in neonates skin seeding Tregs have been proposed to migrate directly from the thymus[98]. Collectively suggesting a poorly appreciated role for the thymus in directing the heterogeneity of the peripheral Treg population.

1.2 Thymic Development and Post-Thymic Development of $CD4^+$ T-cells

1.2.1 The Thymus and T-cell Development: An Overview

The thymus is a primary lymphoid organ, which provides a unique microenvironment conducive to T-cell development. The thymus consists of 2 lobes each of which primarily comprise of a central medulla, composed of medullary thymic epithelial cells (mTEC) and an outer cortex, composed of cortical thymic epithelial cells (cTEC). The critical role of the thymus in T-cell development was demonstrated in 1961 by investigations into neonatal thymectomy, which found a subsequent lack of peripheral T-cells and an accompanying increased susceptibility to infection[108]. Subsequent research has made great progress in uncovering the stages of T-cell development, both within and beyond the thymus, and how they are supported/instructed by the thymic microenvironment (outlined in Figure 1.4).

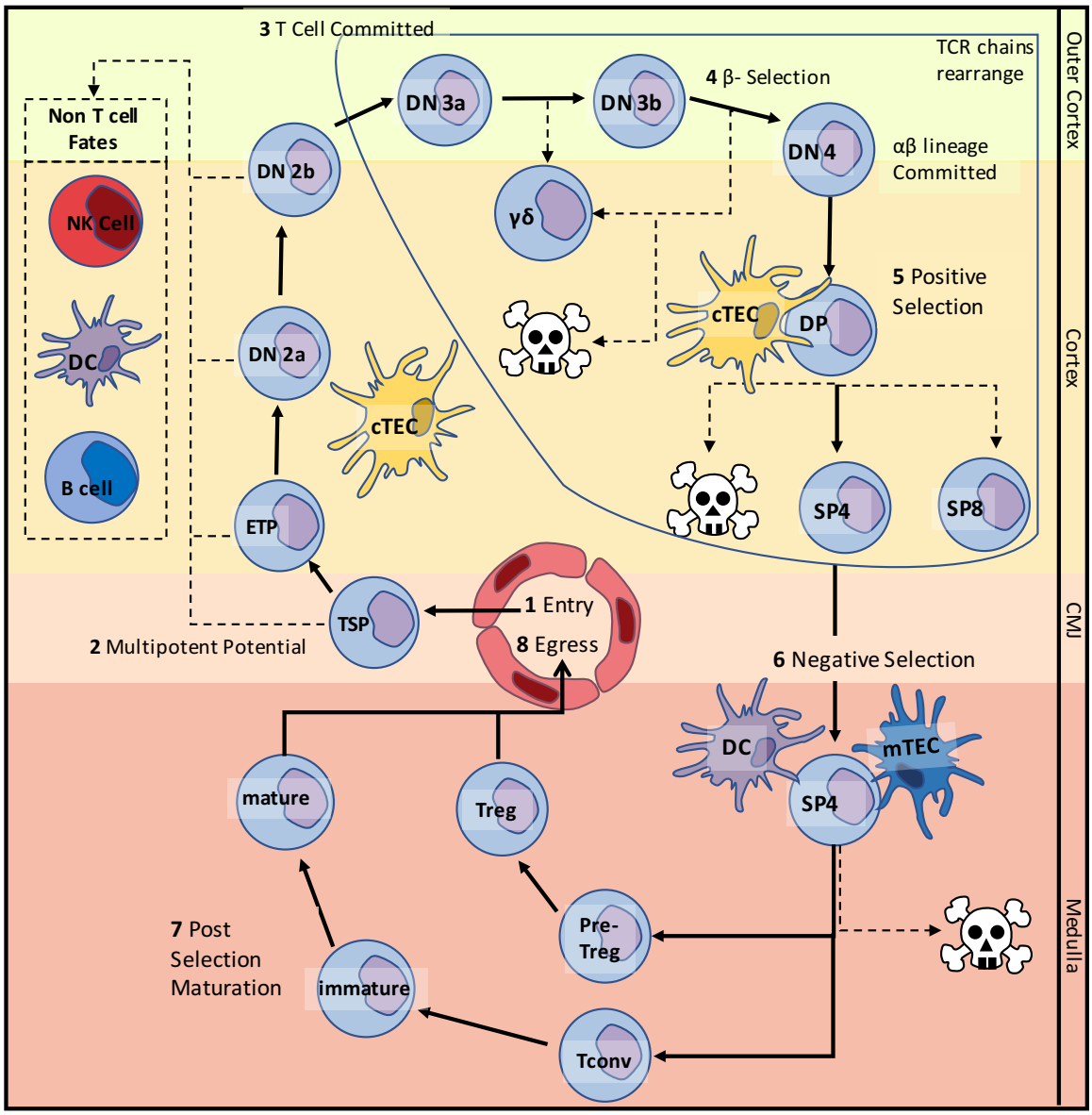

A. Intrathymic Development

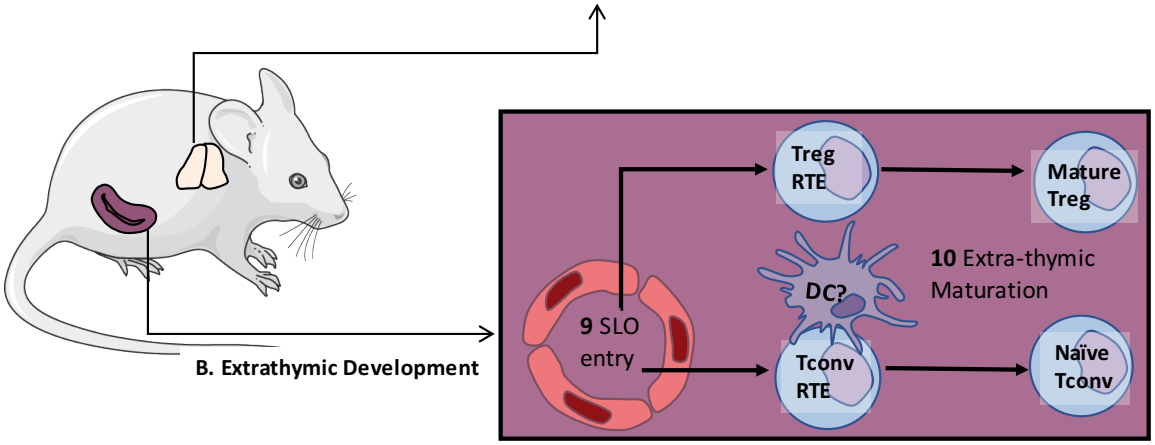

B. Extrathymic Development

Figure 1. 4 SP4 T-cell Development

Overview of the pathway of **(A)** intrathymic and **(B)** post-thymic $CD4^+CD8^-$ (SP4) T-cell development. **(1)** Entry of thymus seeding progenitor (TSP) through the blood vessels at the corticomedullary junction (CMJ). **(2)** Early stages of thymocyte differentiation, at this stage the thymocytes have multi-lineage potential and may differentiate to non-T-cell fates (dashed lines). Interacting with cortical epithelial cells (cTECs) is important in determining this lineage choice. Assuming they remain on a T-cell development pathway thymocytes progress through the intermediate stages of early thymic progenitor (ETP), DN2a and DN2b simultaneously moving outward from the cortex to the outer-cortex. **(3)** T-cell lineage commitment occurs upon transition to the DN3a development stage. With this is a massive increase in VDJ recombination to produce the TCR chain. TCRβ, TCRγ, TCRδ, chains rearrange simultaneously, thus there is a potential branch point where if TCRγ and TCRδ chains are successfully expressed the thymocyte diverges into the γδ T-cell lineage. If a TCRβ chain is expressed the cell transitions to DN3b to undergo β-selection. **(4)** In β-selection the TCRβ chain is tested for functionality, alternative fates at this stage are death by apoptosis or redirection to the γδ T-cell lineage. Upon successful completion of β-selection the thymocyte transitions to DN4 and αβ T-cell lineage commitment is complete. The DN4 thymocyte migrates back towards the cortex, begins TCRα chain rearrangement upregulates CD4 and CD8 and transitions to a $CD4^+CD8^+$ double positive (DP) phenotype. **(5)** DP thymocytes then undergo positive selection, mediated by cTECs, to test the functionality of the fully rearranged αβ TCR. Recognition of pMHCII results in differentiation to an SP4 thymocyte. Alternatively recognising pMHCI results in differentiation to an SP8 fate while failure to recognise pMHC results in death by apoptosis. **(6)** SP4 thymocytes then transition to the medulla to undergo negative selection. Here the thymocytes are tested by medullary TEC (mTEC) and dendritic cells (DCs) for recognition of pMHC. Recognition of pMHC results in either death by apoptosis or entry into the regulatory T-cell (Treg) lineage via an intermediary Treg precursor (pre-Treg). If pMHC is not recognised the thymcoyte escapes negative selection to enter the conventional T-cell (Tconv) lineage. **(7)** Following negative selection thymocytes undergo a post-selection maturation process. **(8)** Mature thymocytes are egress competent and exit the thymus via the blood vessels at the CMJ. **(9)** Upon exiting the thymus newly exported T-cells termed recent thymic emigrants (RTE) enter secondary lymphoid organs (SLOs). **(10)** SP4 RTE then undergo an extra-thymic maturation process believed to be mediated in some way by SLO DCs. Upon completion of this maturation RTE enter the mature naïve T-cell pool.

1.2.2 Thymocyte Entry and Early Development

The thymus, while essential for T-cell development is not the source of the earliest T-cell precursors as it does not produce haematopoietic stem cells for precursors to differentiate from. Rather it is the bone marrow (BM) that possess this capacity, and thus the thymus is colonised by a blood-borne progenitor cell[109] termed the thymus seeding progenitor (TSP), whose exact phenotype remains somewhat uncertain[110], which enter via blood vessels at the corticomedullary junction (CMJ)[111]. This colonisation occurs in waves, with the thymus being receptive to precursor entry for approximately 1 week then refractive for the following 3 weeks, regulated by the relative occupancy/availability of intrathymic niches[112].

The onset of T-cell lineage commitment requires pre-thymic Notch signalling in TSPs[113]. Within the thymus T-cell lineage commitment begins with the differentiation of the TSP to the early thymic progenitor (ETP), which have multi-lineage potential[110,114]. ETPs sit within the $CD4^-CD8^-CD25^-CD44^+$ double negative (DN) 1 thymocyte population, which can be further divided into 5 subsets (DN1a-e) by differential CD117 and CD24 expression[110,115]. Specifically ETPs with T-cell potential are located in the $CD117^+$ DN1a-b population[115]. ETPs differentiate to $CD4^-CD8^-CD25^+CD44^+$ DN2 thymocytes, which are divided into $pLCK^+$ DN2a and $pLCK^-$ DN2b[110,116]. DN2a thymocytes have lost B-cell potential, while DN2b have additionally lost DC/NK potential[110,116]. Finally DN2 thymocytes transition to $CD4^-CD8^-CD25^+CD44^+$ DN3, at which point they are fully committed to the T-cell lineage[110,114]. At each of these development stages, thymocytes undergo proliferation, although it is relatively reduced in the later stages[110].

The signalling pathways and subsequent transcriptional changes underpinning this T-cell development pathway are complex[110]. Broadly, they are TCR independent and mediated by the thymic microenvironment, with distinct development stages occurring in distinct cortex regions[111]. Migration begins with ETPs transitioning from the perimedullary cortex to the inner cortex, differentiating to DN2 thymocytes which subsequently migrate to the outer cortex[111]. cTEC derived CXCL12 plays a critical role in directing this migration through its receptor CXCR4 which is expressed on DN1-3 populations[117]. During this migration thymocytes interact with local stroma to instruct their differentiation. For instance, notably cTECs provide Notch ligands (particularly delta-like ligand 4) which interact with Notch receptors on the thymocytes to instruct differentiation at both the ETP:DN2 and DN2:DN3 transition via the Notch signalling pathway[110,118].

Upon differentiation to DN3, thymocyte development becomes TCR signalling dependent and TCR rearrangement is massively increased[110,119]. Here in-frame genes encoding the TCR chains are generated by random rearrangement of variable (V), joining (J) and, in the case of the TCRβ or TCRδ chain, diversity (D) gene segments. This process is termed V(D)J recombination, and is orchestrated by recombination-activating gene 1 and 2 (Rag-1 and Rag-2). Once V(D)J recombination is complete the V(D)J exon and downstream constant region exons are transcribed and spliced together to generate the TCR chain mRNA[120]. The number of possible V(D)J segments to choose from, in addition to diversity introduced by the recombination mechanism, underpins the discussed potential TCR repertoire diversity of $\sim 10^{15}$[2,3,120].

Rearrangement of the TCRβ, TCRδ and TCRγ chains occurs almost simultaneously, with the lineage fate of αβ vs γδ T-cell largely dependent on which yields a successful rearrangement first[119,121]. Here we focus on the αβ fate which is finalised by successful expression of a functional TCRβ chain. Functionality of a produced TCRβ chain is determined by a process termed β-selection[110]. DN3 thymocytes which have successfully rearranged a TCRβ chain and are about to undergo β-selection are distinguishable as $CD27^+$ DN3b as opposed to $CD27^{lo}$ DN3a[122]. In β-selection the rearranged TCRβ chain pairs with an invariant pre-Tα chain (a surrogate for the TCRα chain that is yet to be rearranged) and CD3 chains to give a pre-TCR complex which must be signalled through to pass β-selection[110,123]. Thymocytes which fail β-selection undergo apoptosis[123] although they can first attempt to rearrange upstream V(D)J segments to generate a new TCRβ chain. Alongside pre-TCR signalling, Notch1 and CXCR4 signalling are also necessary for the survival, proliferation and further differentiation of the DN3b thymocyte[124,125]. Having completed β-selection, TCRβ rearrangement permanently ceases, a process termed allelic exclusion, and commitment to the αβ T-cell lineage is complete[114]. DN3b thymocytes differentiate to $CD44^-CD25^-$ DN4 an intermediary population to the $CD4^+CD8^+$ double positive (DP) thymocyte[126]. DN4 thymocytes migrate back to the cortex, upregulate CD4 and CD8 and initiate TCRα chain rearrangement to progress to the DP development stage[114].

1.2.3 $CD4^+CD8^+$ Double Positive Thymocytes and Positive Selection

Cortical DP thymocytes are then screened for their ability to undergo positive selection, to determine if the generated TCR is capable of recognition of peptide MHC (pMHC), and thereby represents a functionally useful clone. While undergoing positive selection DP thymocytes are kept in an immature state. This has been connected to the basic helix-loop-helix TFs, encoded

by E2a and HEB[127]. Notably E2a is highly expressed in DP thymocytes and promotes genes associated with the DP phenotype, including CXCR4 and RORyt, while also repressing genes that characterise mature thymocytes such as CCR7[127,128]. Importantly both E2a and HEB seem essential in enforcing positive selection, as in their absence, an increased proportion of DPs mature to single positives (SPs), including thymocytes with non-functional TCRs[127].

The process of positive selection is mediated by cTEC, which present pMHCI and pMHCII complexes to highly motile DP thymocytes[129]. There are three possible outcomes for the DP thymocyte at this stage. Firstly, failure to recognise pMHC complexes, results in apoptosis due to a lack of survival signals, termed death by neglect[128]. However in the absence of a positive selection signal the surface TCRα can be replaced to give a new $\alpha\beta$TCR[130] as E2a keeps the Rag locus active allowing DP thymocytes continue to undergo TCRα chain rearrangement. Thereby, allowing DP thymocytes to maximise the chance of generating a functional receptor and passing positive selection, akin to β selection. While theoretically TCR rearrangement could be an exhaustive process with cell death occurring only once all possible V and J segments have been combined, it is actually limited by the lifespan of the cell. The survival of DP thymocytes is regulated by TFs RORγ and TCF-1 which in turn control the anti-apoptotic factor Bcl-X_L[131,132]. This pathway is essential for positive selection, as demonstrated by the premature death by neglect of DP thymocytes upon its disruption[131,132].

The remaining two outcomes result from recognition of pMHC but with different affinity. High affinity recognition of cTEC presented pMHC results in negative selection, through programmed cell death by apoptosis mediated by cortical DCs[133,134]. As will be discussed, negative selection is more synonymous with the medulla, and while the removal of clones in

the cortex is significant, indeed exceeding that of SP thymocytes deleted in the medulla[135], it only offers screening against ubiquitous peptide[133]. Conversely, low affinity recognition of pMHC results in survival and progression to a SP thymocyte. DP thymocytes are intrinsically more sensitive to low affinity pMHC[136], which can be attributed, at least partially, to modulation of TCR signalling by factors such as CD5[137] and mir181a[138]. Downstream TCR signalling pathways are vital to initiate positive selection, with one notable example being the RAS-ERK-MAP kinase pathway whose constituents act to inhibit E2A activity[139]. Termination of E2a (which as discussed maintains an immature DP state and expression of Rag genes) is vital for DP thymocytes progression and for their associated TCR arrangement to become permanent. The essential antagonism between the RAS-ERK-MAP kinase pathway and E2a, is demonstrated by the impaired positive selection observed in *Id3*$^{-/-}$ mice (where the RAS-ERK-MAP kinase pathway is disrupted) but not *Id3*$^{-/-}$*E2a*$^{-/-}$ mice[140]. Overall, only approximately 5% of DPs thymocytes meet the requirements of positive selection[141].

Positive selection also results in SP lineage commitment to either a SP4 or a SP8 thymocyte. TCR recognition of MHC is vital in determining thymocyte fate, as mice deficient for MHCI or MHCII lack SP8 or SP4 thymocytes respectively[142,143]. There are several theories as to how this recognition directs commitment to either the SP4 or SP8 lineage. Two early theories were the stochastic selection model and the strength of signal instructional model[144]. The stochastic selection model, proposed that positively selected thymocytes terminated one of their co-receptors at random, with long-term survival dependent on a secondary rescue signal from an appropriate co-receptor[144]. However findings such as, the >50% selection of TCR transgenic thymocytes oppose a random process[145] . In contrast the strength of signal instructional model proposed that distinct TCR signals were generated in the context of MHCI

or MHCII[144]. These differences were believed to stem from a stronger signal from TCR engagement with CD4 due to its higher association of Lck (relative to CD8)[144]. However, subsequent analysis of chimeric CD8 co-receptors expressing CD4 cytosolic domains identified no impact on the CD4:CD8 ratio and hence no impact of increased signalling strength on lineage choice[146].

An alternative model proposed to rectify these experimental discrepancies was the kinetic signalling model, where TCR signal duration along with common cytokine receptor γ-chain (γ_c) signalling, notably IL-7, direct lineage choice[144,147]. Here upon TCR stimulation DP thymocytes initially downregulate CD8 gene expression adopting a $CD4^+CD8^{lo}$ intermediate phenotype. If TCR signalling persists, indicative of engagement of CD4 with MHCII, SP4 lineage commitment occurs. Whereas if TCR signalling were interrupted, the cell becomes responsive to IL-7 mediated co-receptor reversal, terminating CD4 transcription and reinstating CD8, and thereby restoring TCR signalling and an SP8 fate[147]. However again the kinetic model is not without contradiction. For instance, using inducible Zap70 transgenic mouse models to specifically terminate TCR signalling of selecting DPs it was shown that loss of TCR signalling did not prevent lineage diversion of SP4 thymocytes, but did impair SP8 lineage development and long-term survival/maturation of both lineages[148]. Conflicting with the proposed role of TCR termination in the kinetic model, while implicating TCR signalling in survival of both SP4 and SP8 thymocytes[148].

While the model of lineage divergence remains unclear, important downstream TFs which direct the two lineages have been identified. SP8 development requires Runx3 binding and activating of CD4 silencers to repress CD4 transcription[149]. In contrast ThPOK, which binds

and antagonizes CD4 silencers preventing downregulation[150], appears to be the key SP4-lineage specifying factor as forced expression of ThPOK was sufficient to force development of the SP4 lineage[151].

1.2.4 Single Positive Thymocytes: Central Tolerance and Maturation

Thus, with positive selection and lineage divergence specificity for the SP4 lineage is complete. The next step for SP4 thymocytes is to migrate to the medulla, mediated by newly upregulated CCR7 responding to mTEC derived CCR7 ligands[152]. SP4 thymocyte migration into the medulla marks their final development stage prior to thymic egress. During this time SP4 thymocytes undergo central tolerance by negative selection, and a maturation process tied to thymic egress.

Regarding the exact timings of these processes, initially the medullary dwell time was estimated at 12-16 days[153], however this has been challenged by findings using Rag-GFP reporter mice[26,154]. In these mice green fluorescent protein (GFP) is expressed under either the *Rag1* or *Rag2* promoter, meaning that thymocytes undergoing TCR rearrangement produce and accumulate GFP in their cytosol[155,156]. Upon successful positive selection Rag expression, and hence GFP production, is terminated. The accumulated GFP then undergoes an exponential decay over a period of several weeks. This not only enables identification of newly produced thymocytes and recent thymic emigrants (RTEs) as GFP^+ but also the intensity of GFP serves as a molecular clock with younger cells having a higher expression of GFP[26,157]. As such the Rag-GFP mouse has been an invaluable tool in studying T-cell development. Using this system the estimated medullary dwell time is 4-5 days[26] a significant reduction on previous work. Intriguingly the dwell time also seems to differ between SP4 subsets as Tregs

reportedly remain longer than their Tconv counterparts[154]. This perhaps hints at the differential requirements of medullary access between the two populations and indeed Tregs fail to develop in the absence of the medulla while Tconvs are less impacted and still able to emigrate[158]. The essential role of the medulla in mediating central tolerance is further highlighted by the autoimmunity observed in mice where thymocyte cannot access the medulla, either because it is absent (e.g. *Relb*$^{-/-}$) or because they cannot enter (e.g. *Ccr7*$^{-/-}$)[158,159]. Overall this suggests a non-redundant role for the medulla in supporting central tolerance mechanisms but not necessarily Tconv maturation to egress competency.

1.2.5 Central Tolerance

As previously discussed central tolerance is necessary to eliminate, either by clonal deletion or redirection into the Treg lineage, thymocytes which have self-reactive TCRs. The vital role of the medulla largely relates to the ability of its stroma (discussed in greater detail in Section 1.3.) to present a wide variety of self-antigen including tissue restricted antigens (TRAs) normally exclusively expressed by tissue cell types. Thus, SP4 thymocytes are tested for recognition of self-peptide, if minimal they escape negative selection and enter the CD25^{-} Foxp3^{-} Tconv lineage, otherwise the outcome is death or diversion. TCR signalling is therefore critical but exactly how cell fate is determined is debatable.

Much research has indicated that the signal strength thymocytes receive is critical, these are encapsulated by the affinity/avidity models of negative selection[160]. The affinity model posits that it is the TCR affinity, defined as the strength of a singular interaction between the TCR and pMHC, for self-peptide that determines cell fate. Such that low affinity TCRs escape negative selection and become Tconvs, intermediate affinity TCRs are directed into the Treg

lineage and high affinity TCRs undergo clonal deletion[160]. This principle has been supported by an ovalbumin transgenic system in which stronger affinity dictated clonal deletion or Treg differentiation[161]. This system has also shown that the difference in affinity that drives survival or deletion is minimal, with only a two-fold difference in affinity between the weakest negative and positive selector[162]. Interestingly the outcome of thymocytes exposed to peptide whose affinity falls within this two-fold range is dependent on the peptide concentration[162]. Furthermore, other studies have indicated that the density of pMHC also influences selection[163,164] thereby challenging a model of T-cell selection based solely upon affinity. Hence the avidity model builds on the affinity model to propose a role for avidity, which is proportional to the combined affinity interactions and thereby dependent on TCR affinity and the density of pMHC. Thus, increasing or decreasing the cognate pMHC density can modulate the outcome of a thymocyte with a fixed TCR affinity[160]. For instance, a low affinity TCR combined with a low pMHC density would still result in escape to the Tconv lineage, however increasing pMHC density could drive it to a Treg or deletion fate.

Furthermore distinct antigen expression patterns and when/how thymocytes encounter this antigen, may also contribute to driving different central tolerance fates[160]. Ubiquitous antigen and TRA exhibit different expression patterns, with specific TRA being sparser, and these characteristic expression patterns were noted to drive alternative fates of clonal deletion or Treg differentiation, respectively[165,166]. These different fates can be explained by the avidity model but have also been connected to the timing and repetition of antigen interactions[160]. This is suggested by work in thymic slice systems, in which medullary thymocytes are highly motile in a random walk pattern, engaging briefly with APCs[167]. When abundant cognate antigen (mimicking a ubiquitous antigen) is provided, receptive thymocytes

rapidly cease migration and are subsequently deleted[168]. In contrast, cognate antigen mimicking a sparser TRA pattern results in reduced but not absent motility[167]. This suggests that unlike ubiquitous antigens, TRA may promote transient TCR triggering, which may facilitate Treg induction, as discontinuous TCR signalling has been linked favourably to Foxp3 induction[160,169]. Indeed, mathematical modelling has suggested a signal integration model whereby singular strong interactions result in clonal deletion while repeated transient signals result in Treg differentiation[170]. If TRA but not the ubiquitous antigen expression patterns are conducive to Treg fate this may explain why Treg induction is largely restricted to medullary SP4 thymocytes[171].

Additionally, cell-intrinsic regulation may be important in determining cell fate. It has been observed that increasing SP4 thymocyte maturity inversely correlates with Treg induction[172] and sensitivity to clonal deletion[173]. Thereby suggesting a progressive decline in responsivity to tolerance mechanisms and hence a limited "window of opportunity"[172]. Furthermore, within this "window" it is suggested that thymocytes start as most receptive to deletion which is progressively lost in favour of Treg induction[160,172]. Overall suggesting there may be intrinsic signalling within thymocytes to direct cell fate, integrated with antigen expression and signalling strength[160]. Thus cell fate is determined but how then is it enacted?

1.2.5.1 Negative Selection by Clonal Deletion

First to consider, albeit briefly, is clonal deletion. TCR signalling is heavily implicated in the activation of apoptosis through the downstream MAP kinase pathway member ERK[162,174]. As previously discussed ERK is also a key mediator of positive selection, and its ability to facilitate such opposing fates seems dependent on the kinetics and intensity of activation induced by

antigen affinity. High affinity TCR binding results in rapid and intense ERK induction, associated with apoptosis, where low affinity recognition does not[162,174]. Further downstream apoptosis is vitally directed by the pro-apoptotic BH3-only proteins, notably Bim and Puma, which activate Bax and Bak to induce the mitochondrial apoptosis pathway[175]. There is some redundancy in the BH3-only proteins as loss of Bim alone does not cause autoimmunity however combined loss of Bim and Puma does[175].

1.2.5.2 Redirection to the Treg Lineage

Broadly, commitment to the Treg lineage is proposed to occur through a two-step model (Figure 1.5). Initial TCR signalling supports differentiation to a Treg precursor before TCR independent signalling permits differentiation to the final Treg state[160,176]. Interestingly antagonism of the clonal deletion apoptotic pathway may be an important factor in the TCR dependent step. Notably Treg differentiation seems to require CD28, as *Cd28*$^{-/-}$ and *Cd80*$^{-/-}$ *Cd86*$^{-/-}$ mice exhibit a drastically reduced intrathymic Treg pool[177]. Interestingly CD28 deficiency in a transgenic model of Treg induction resulted in loss of the population rather than escape into the Tconv lineage. Suggesting CD28 supports Treg development not by amplifying TCR signalling but by providing a pro-survival signal, and thereby acts as a delineating factor between deletion and Treg differentiation[178]. Supporting this CD28 can regulate Bim, a mediator of clonal deletion [179].

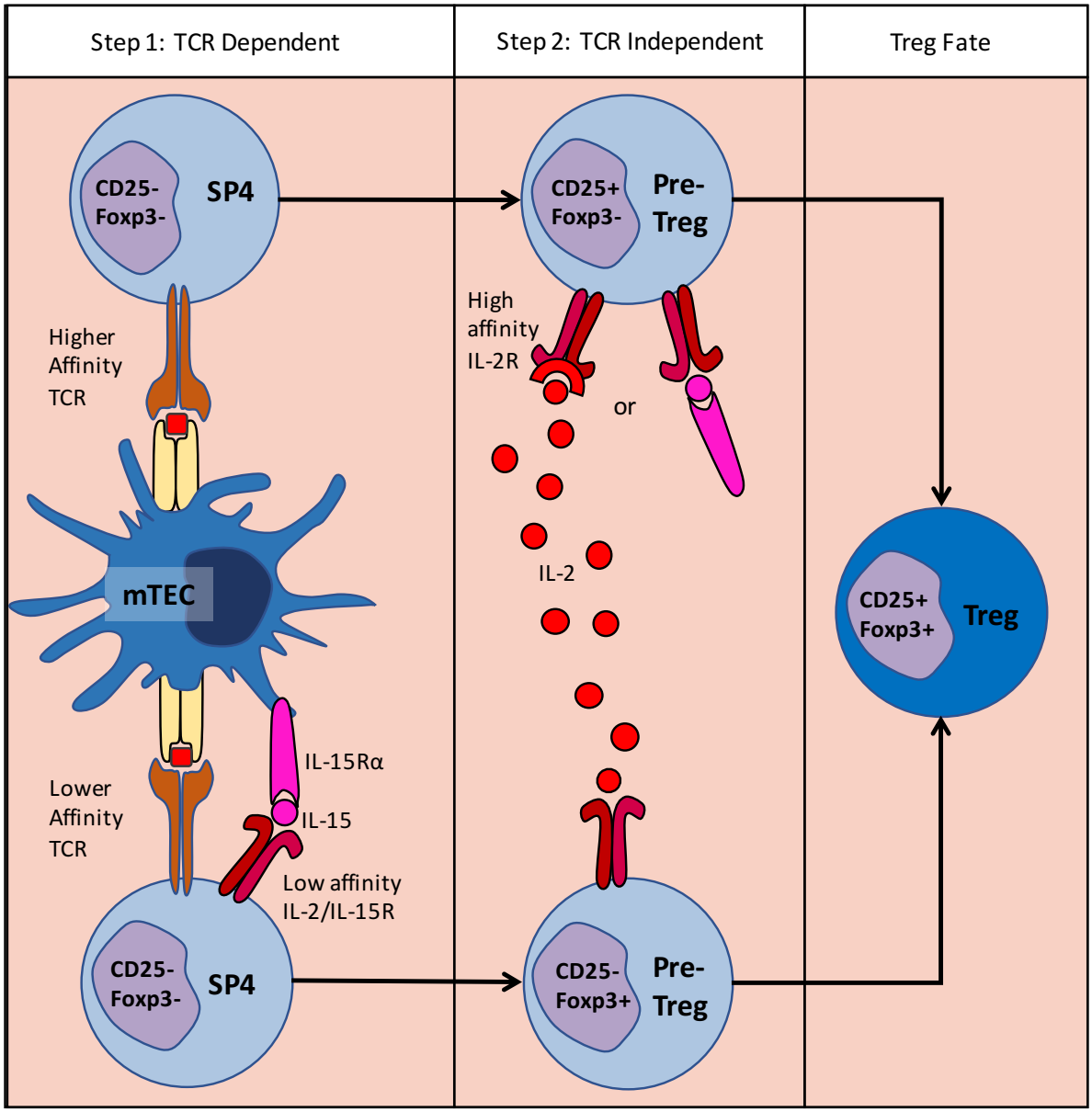
Step 1: TCR Dependent
Step 2: TCR Independent
Treg Fate
CD25-
Foxp3-
SP4
CD25+
Foxp3-
Pre-
Treg
High
affinity
IL-2R
or
Higher
Affinity
TCR
mTEC
IL-2
CD25+
Foxp3+
Treg
IL-15Rα
IL-15
Lower
Affinity
TCR
Low affinity
IL-2/IL-15R
CD25-
Foxp3-
SP4
CD25-
Foxp3+
Pre-
Treg

Figure 1. 5 Treg Development: Two Pathways of a Two Step Process

There are two pathways through which SP4 thymocytes can enter the Treg lineage and in both cases commitment occurs in two steps. In step 1, an SP4 thymocyte undergoing negative selection recognises pMHC with a (top pathway) higher affinity or (bottom pathway) lower affinity TCR. Higher affinity recognition results in differentiation to a $CD25^{+}Foxp3^{-}$ Treg precursor (pre-Treg). Lower affinity recognition must be coupled with IL-15 signalling via the low affinity IL-2R on the SP4 thymocyte (IL-15 is trans-presented by the IL-15Rα expressed on another cell type, possibly mTEC). This combination results in differentiation of the $CD25^{-}Foxp3^{+}$ Treg precursor (pre-Treg). In step 2, the two Treg precursors respond to cytokines to promote final differentiation to $CD25^{+}Foxp3^{+}$ Treg (dark blue). Regarding the $CD25^{+}Foxp3^{-}$ Treg precursor (upper) either IL-2 signalling via the high affinity IL-2R or IL-15 signalling via the low affinity IL-2R is sufficient. Regarding the $CD25^{-}Foxp3^{+}$ Treg precursor (lower) IL-2 signalling is necessary, which is believed to occur via the low affinity IL-2R initially.

Regarding the secondary TCR independent signal, cytokines belonging to the γ_c family, which includes IL-2, IL-4, IL-7 and IL-15, are heavily implicated. Signalling by these cytokines induces STAT5, which in turn binds directly to the CNS2 region of the Foxp3 promoter to mediate its expression[180]. Importantly reduced thymic Tregs are observed in $\gamma c^{-/-}$[181–183], implicating all γ_c members. IL-4 has since been ruled out due to normal Treg development in *Il4r*$\alpha^{-/-}$ mice[184]. The role of IL-7 was more complex to dissect as broadly IL-7 is required to support thymocyte development and by extension Tregs. However, while targeted deletion of IL-7 in DP thymocytes did not impair later Treg development *in vivo*[185], IL-7 could induce Treg differentiation *in vitro*[184], making a specific role for IL-7 in Treg differentiation unclear. In contrast IL-2 and IL-15 have both been strongly implicated in Treg development as *Il2r*$\beta^{-/-}$ mice, which lack a subunit common to both the IL-2 and IL-15 receptor signalling complexes, have drastically reduced Tregs[183,186]. However individual loss of either IL-15 or IL-2 signalling appears to have mixed results, with reports of either normal or modestly impaired thymic Tregs, respectively[183,186]. These results suggest some functional redundancy between these two cytokines in supporting thymic Treg development and indeed *Il2*$^{-/-}$*Il15*$^{-/-}$ mice display a similar Treg development defect to *Il2r*$\beta^{-/-}$[183].

The overlapping roles of IL-2 and IL-15 may relate to how they instruct Treg precursors[187]. Two Treg precursors have been identified within the SP4 thymocyte compartment, with both CD25$^-$Foxp3$^+$ and CD25$^+$Foxp3$^-$ capable of differentiation to CD25$^+$Foxp3$^+$ Tregs *in vitro*[182,188]. These findings were corroborated by *in vivo* Treg differentiation following intrathymic injection of CD25$^+$Foxp3$^-$ or adoptive cell transfer of CD25$^-$Foxp3$^+$[182,188]. For differentiation into Tregs both these precursors require IL-2, although it may be a more stringent requirement for CD25$^-$Foxp3$^+$ precursors[182,184,187,188], in which IL-2 signalling prevents Fopx3 mediated

apoptosis[182]. In contrast $CD25^+Foxp3^-$ precursors seem able to differentiate in response to IL-2 or IL-15[182,184,188]. Furthermore, development of $CD25^+Foxp3^-$ precursors requires neither IL-15 nor IL-2 whereas $CD25^-Foxp3^+$ development seems IL-15 dependent[187]. This suggests differing roles for IL-2/IL-15 in the induction of these Treg precursors, and additional differences have also been highlighted. For instance, while both precursors subsets were reduced in *Cd28*$^{-/-}$ the loss of $CD25^-Foxp3^+$ precursors were more substantive[189]. This was linked to a critical role for downstream NF-κB in $CD25^-Foxp3^+$ but not $CD25^+Foxp3^-$ precursors[189]. The role of epigenetic regulators also differed with CNS3 and CaRE4 required for development of $CD25^-Foxp3^+$ or $CD25^+Foxp3^-$ precursors respectively[189]. Taken together this suggests two separate pathways of Treg development (Figure 1.5). In the first TCR signalling alone induces $CD25^+Foxp3^-$ precursors which then rely on IL-15/IL-2 for final differentiation to Tregs. In the second TCR signalling alongside IL-15 signalling induces $CD25^-Foxp3^+$ precursors which then rely on IL-2 to become Tregs[176].

The relative contribution of these two pathways in Treg development remains uncertain. A predominant role for $CD25^+Foxp3^-$ precursors has been suggested by several studies. Developmentally in neonates $CD25^+Foxp3^-$ appear before either $CD25^+Foxp3^+$ or $CD25^-Foxp3^+$[171]. More recently the Treg precursor product dynamics have been readdressed using the Nr4a3–Tocky mice[190]. In this system TCR signalling dynamics are tracked by an unstable fluorescent timer protein, such that when cells first receive a TCR trigger they are transiently $blue^+red^-$ (new), with persistent signalling they become $blue^+red^+$ (persistent) and without further signalling $blue^-red^+$ (arrested). In this system, $CD25^+Foxp3^-$, $CD25^+Foxp3^+$ and $CD25^-Foxp3^+$ were predominantly in the new, persistent and arrested populations respectively. Collectively suggesting $CD25^+Foxp3^-$ as a transient precursor that provides a major pathway

for Treg differentiation through persistent TCR signalling[190]. Contradictory to this are findings that relatively few $CD25^{+}Foxp3^{-}$ actually upregulate Foxp3 *in vitro* or *in vivo*[182,187,188]. Furthermore, recently an inducible Zap70 system investigating the kinetics of $GITR^{hi}$ precursor and Treg subpopulations suggested that the kinetics of $CD25^{-}Foxp3^{+}$ were more consistent with a major precursor role whereas $CD25^{+}Foxp3^{-}$ appearance was too rapid and suggestive of high death rate[187]. Indeed, $CD25^{+}Foxp3^{-}$ precursors are expanded when mechanisms mediating negative selection by deletion are impaired[189]. Consequently, the dynamics of Treg precursors remains unresolved. Importantly though, recent work suggests that both Treg precursors are required to generate a Treg population with a diverse TCR repertoire[189].

1.2.6 Post-Selection Maturation and Thymic Egress

Alongside negative selection SP4 thymocytes undergo a phenotypic and functional maturation prior to thymic egress. The phenotypic changes associated with maturation include upregulation of CD62L, Qa2, MHCI and IL-7Rα alongside downregulation of CD69 and CD24[26,173,191,192]. These maturation markers have been utilised in various combinations to define relative states of maturity. A detailed breakdown using MHCI and CD69 determined 3 stages of progressive maturation defined as $CD69^{+}MHCI^{-}$ SM, $CD69^{+}MHCI^{+}$ M1, and $CD69^{-}MHCI^{+}$ M2[191]. Recently further work has shown that M2, which are $CD69^{-}$ $CD62L^{+}$, can be further subdivided into $CD62L^{lo}$ M2a, $CD62L^{int}$ M2b and $CD62L^{hi}$ M2c[192]. In determining these different maturation stages Rag-GFP mice have been an essential tool, as it can be demonstrated that the described phenotypic maturation correlates with a gradual loss of Rag-GFP and hence an increase in thymocyte age[26,191].

Phenotypic maturation accompanies an increase in thymocyte competency which is not unsurprising given some of the defining markers. For instance, increased CD62L is indicative of increased emigration competency, as CD62L mediates peripheral T-cell entry into SLO, a necessary step for further T-cell development (discussed in Section 1.2.7 and 1.3.4) and future functionality. More generally maturation is also reported to accompany increased thymocyte proliferative ability and cytokine responsiveness[191].

An important regulator of thymocyte maturation is the NF-κB signalling pathway. Initial work suggested signalling through the NF-κB pathway was required for maturation, proliferation and also cell survival[191,193]. Specifically, there have been strong links between IL-7Rα and NF-κB, as mediators of increased proliferative competence and general homeostasis[193–195]. IL-7Rα is upregulated with maturation of SP4 thymocytes, in a TCR signalling dependent manner[195]. IL-7 signalling through IL-7Rα can mediate both intra-thymic and extra-thymic T-cell proliferation (predominantly under lymphop5enic conditions)[196–198]. Significantly, impairment of this thymic IL-7Rα maturation process subsequently constrains peripheral T-cell proliferation and survival[195,199]. With regard to NF-κB it was originally thought to mediate maturation by thymocyte survival but it has recently emerged that survival is in fact dependent upon the upstream IKK complex's inhibition of RIPK1[194]. Similarly, TAK1, another component of the NF-κB pathway, also mediates NF-κB independent mechanisms that regulate cytokine responsivity, in response to type I interferon signalling[191]. Separate from the NF-κB signalling pathway, Runx1 is another broad intrinsic regulator required early on in SP4 thymocyte maturation[200]. As will be discussed, T-cell maturation continues beyond thymic egress and interestingly both Runx1 and NF-κB remain essential regulators[199,200].

Indicating perhaps that this thymic maturation programme marks the start of a progressive process required for peripheral preparedness.

Notably, regulators of thymocyte maturation such as Runx1 are not required for negative selection[200] indicating some separation between the two processes. Indeed thymocyte maturation seems to occur post-selection as while immature $CD24^{hi}$ thymocytes were susceptible to tolerance induction their mature $CD24^{lo}$ counterparts were resistant[173]. Furthermore, it is within the immature thymocyte population, as defined by $CD24^{hi}Qa2^{lo}$ or $CD69^{+}MHCI^{+}$, that Treg precursors first emerge[189]. Overall suggesting that negative selection processes may be restricted to the early stages of maturation. This is perhaps not unsurprising as one important purpose of thymocyte maturation seems to be preparation for thymic egress.

The association with egress is clear as mature thymocytes upregulate Sphingosine-1-phosphate receptor 1 (S1PR1), a G protein coupled receptor, which is an essential mediator of thymic egress (at least in adults)[201]. Upregulation of S1PR1 is regulated by Foxo1 and Klf2 both of which are also upregulated during post-selection maturation and also control the upregulation of the maturation marker CD62L[202,203]. While conversely CD69 expression, associated with immature thymocytes, has an antagonistic relationship with the S1PR1 axis, with S1PR1 signalling accelerating CD69 downregulation[204] while interaction of CD69 with S1PR1 causes its internalisation and degradation[205]. S1PR1 mediates thymocyte migration along a gradient of its ligand Sphingosine-1-phosphate (S1P)[201]. Disruption to this axis dramatically impairs thymic egress, as demonstrated by the intrathymic accumulation within FTY720 (a potent S1PR1 agonist) treated mice[206,207].

For S1PR1 mediated egress the S1P gradient must be high specifically near exit vessels and within the blood, as such S1P levels necessitate tight regulation. Near sites of thymic egress S1P generation has been linked to thymic pericytes which ensheath blood vessels. These pericytes express the enzymes sphingosine kinase 1 and sphingosine kinase 2 which catalyse phosphorylation of sphingosine to generate S1P[208]. Conversely it is necessary that S1P remains low at the source of emigrating thymocytes which is achieved through negative regulators of S1P expressed by to TEC, endothelial cells and also possibly DCs[209–211]. These negative regulators include lipid phosphate phosphatase 3 and S1P lyase which inactivate or degrade S1P, and ceramide synthase 2 which competes with sphingosine kinases for sphingosine[209–211]. Overall this ensures an appropriate S1P gradient that enables egress competent thymocytes to migrate towards CMJ blood vessels[208]. Thymocytes then enter into the perivascular space (PVS) which is an intermediate space between blood vessel and pericytes. Notably this step is dependent on lymphotoxin β receptor (LTβR) expression by endothelial cells, independent of S1P[192]. Finally, thymocytes migrate across the thymic blood endothelium, exiting the PVS and entering the peripheral blood, again following a heightened S1P gradient[208].

Exactly which thymocytes are capable of emigrating from the thymus is again subject to some debate and two major conflicting models have emerged[153]. The conveyor belt model suggests an ordered linear thymic egress where only the most mature thymocytes leave, in contrast the lucky dip model proposes a more stochastic exit of egress competent thymocytes[153]. Evidence is conflicting, some work identifying that younger thymocytes can exit prior to older fractions, supporting a lucky dip[212]. In contrast others have reported the phenotype of RTEs

to be that of the most mature thymocytes[26,192], which correlates with the observed accumulation of these most mature thymocytes in the PVS[192].

1.2.7 RTEs and Continued Post-Thymic Maturation

SP4 T-cells which have most recently left the thymus are termed RTEs. Various methods to study RTEs in mice have been utilised including intrathymic injection of fluorescent labels and surgical grafting of congenic thymic lobes[213]. While these methods allow snapshot identification of RTEs there are drawbacks, particularly the impact of surgical stress on the steady state. An un-manipulated system to study RTEs was therefore preferable and presented by the previously discussed Rag-GFP mouse[155–157].

Using Rag-GFP mice it has been identified that bulk SP4 RTEs undergo a progressive maturation over a period of 2-3 weeks[26,157], characterised by modulation of maturation markers such as CD24, Qa2, CD45RB, IL7Rα[157] and CD55[214]. The cellular interactions that mediate RTE maturation, as will be discussed in section 1.3.5, remain unclear. However, independent intrinsic regulators of RTE survival and maturation have been identified including IKK2[199],NKAP[214,215] and Runx1[200]. Regulation of NF-κB signalling by IKK2 mediates upregulation of IL7Rα in RTEs which is necessary for their homeostatic survival and proliferation as mature cells[199]. However, interestingly several RTE maturation markers proved to be independent of IKK, with its deficiency specifically impairing IL7Rα upregulation, a process identified to normally take only 6-9 days[199]. Indeed both Runx1[200] and NKAP[214,215] are required for upregulation of CD55 and α2,8-sialyltransferase by maturing RTEs, both of which are important in protecting RTEs from elimination by complement and hence seem to promote RTE maturation through survival[200,214,215]. It is perhaps not unsurprising therefore

that both *Cd4*^{cre}*Runx1*$^{fl/fl}$ and *Cd4*^{cre}*Nkap*$^{fl/fl}$ mice exhibit a broad block in RTE maturation[200,215]. Another proposed regulator of RTE maturation is downregulation of mitochondrial metabolism which is proposed to occur very rapidly post egress[216]. Overall this suggests that the 2-3 week RTE maturation period may be made up of several mechanisms independently regulating specific aspects of the overall process[199].

RTE maturation is not just phenotypic but also functional, as SP4 (and SP8) RTEs display reduced functionality relative to their mature counterparts. Notably stimulated non-polarised RTEs are poor producers of IL-2, IFN-γ and IL-4[217]. However poor cytokine production is not universal but rather dependent on context. RTEs under Th1 or Th17 polarising conditions are poor cytokine producers, whereas under Th2 polarising conditions RTEs exceed mature T-cells in IL-4, IL-5 and IL-13 production[217]. More recent work identifies inflammation as a broader contextual requirement for RTEs function. Exposure of RTEs and mature T-cells to antigen in the presence of either alum, or a mixture of IL-1β, IL-33 and IL-18 (cytokines which alum indirectly induces) resulted in comparable proliferation and IL-2 production [218]. However not all inflammatory settings seem to mediate function of RTEs. In mice with chronic *Leishmania donovani* infection RTEs were able to home to sites of infection but failed to mediate effector responses[219]. However, transfer of RTEs to *Rag2*$^{-/-}$ host subsequently infected with *Leishmania donovani* did result in effective protection. This indicates that RTEs can mount effective immune responses against infections but were blocked under chronic conditions. One possibility is that the disrupted splenic architecture caused by the parasite impaired RTE maturation[219].

While in the context of inflammation RTEs can become responsive effector cells, in general they are incredibly sensitive to peripheral tolerance**.** RTEs not only mount poor responses to self-antigen but are also more sensitive to tolerance mechanisms such as Treg suppression and anergy than their older counterparts[218]. Furthermore, RTEs seem to be preferentially directed into the pTregs population which is in part mediated by an increased sensitivity to TGFβ through heightened retinoic acid expression[220,221]. The benefit to increased tolerance susceptibility in RTEs may relate to the discussed gaps in central tolerance, which mean that RTEs may be responsive to novel innocuous antigens encountered only in the periphery. Supporting this, transfer of *Pdcd1*$^{-/-}$ (but not *Pdcd1*$^{+/+}$) RTEs into lymphopenic hosts induced severe autoimmunity[222,223]. Thus identifying both the presence of self-reactive clones in the RTE population and the vital role tolerance mechanisms such as PD-1 play in restraining them. Moreover in an oral tolerance model RTEs were preferentially tolerised[221]. Therefore, one purpose of post-thymic maturation may be to enforce tolerance to peripheral antigens.

Importantly this tolerance process seems to be tightly controlled by environmental cues such as inflammation, presumably helping to prevent tolerance of RTEs to infectious agents. Metabolomics and epigenetic regulation of RTEs may be key to this dynamic balance of tolerance vs responsiveness. Poor production of IL-2 by RTEs has been linked to hypermethylation of the IL-2 locus, as methylation in RTEs is more extensive than in mature T-cells or thymocytes and removing methylation enhanced cytokine production by RTEs[224]. Importantly RTEs were found to highly express both the DNA methyltransferase DNMT3a and demethylase TET, enabling dynamic rapid modulation of gene expression[224]. Similarly, impaired IFN-γ production in SP8 RTEs has been linked to a reduced glycolysis rate which can

be modulated by exogeneous IL-2[225,226]. Interestingly this metabolic control is independent of mitochondria metabolism[226] which is reduced in both SP4[216] and SP8[226] RTEs.

1.2.8 Influence of Development Stage on Thymic Output

The thymocyte development process described here is largely representative of an adult mouse and while broadly consistent there is some variation across the lifespan. Not least is thymic involution with age (discussed further in section 1.3.1) which negatively impacts on thymic output[227,228]. In addition to this broad impact on the overall thymocyte development process, specific changes to individual development steps have also been observed. For instance the source of TSP switches from the fetal liver in the embryo to the BM postnatally[229]. Similarly regulation of thymic egress switches between neonates and adults, regulated by CCR7 and CCL19 in the former[152,230] and S1PR1:S1P in the latter. Thus, from entry to egress there can be variation in thymocyte development.

The thymic Treg population is also heavily influenced by age. Initially neonatal thymic Treg development appears delayed due to a less permissive medullary environment[171,231]. However when thymic Tregs are generated, they appear to represent a unique neonatal Treg population which persists into adulthood[232,233]. These neonatal Tregs seem superior, compared to their adult counterparts, in protecting against autoimmunity in specific organs[232,233]. Thus while clearly Tregs are required throughout life[43], evidence is mounting that Tregs generated in the neonatal period are distinct and necessary to enforce tolerance. Beyond neonatal development, important changes to the thymic Treg compartment have been observed with increasing age. Using Rag-GFP mice it has been found that mature GFP^- Tregs can recirculate to the thymus and in adults constitute the majority of the total Treg pool

relative to de novo Tregs[234,235]. This accumulation of mature thymic Tregs is initially observed at lower levels in young adults and increases throughout life, such that in aged mice approximately 90% of thymic Tregs are mature[235]. While mature thymic Tconvs, have also been observed in the thymus, relative to de novo Tconvs, they are the minority, even in aged mice[235]. With increasing age there is also a reduction in thymic output as measured by RTEs, and notably Treg RTEs are more dramatically reduced than Tconv RTEs[235]. Taken together these finding have led to the suggestion that mature thymic Tregs modulate de novo Treg development (discussed further in Section 1.3.3.3).

Increasing host age also impacts on the total RTE population, more than just a reduction in output, those that are exported seem impaired. Notably RTEs in aged mice exhibit sluggish peripheral maturation[228], and were less responsive to antigen stimulation than younger counterparts[236]. This change has been linked to the combined impact of increasing age on both the BM progenitors and the thymic environment[236]. Interestingly this study also identified that under lymphopenic conditions the responsiveness of aged RTEs improved[236]. Broadly RTEs favour lymphopenic conditions, able to out-compete mature T-cells only under these circumstances[237]. RTEs propensity for lymphopenia may be of particular importance in the neonate, which are initially lymphopenic[238]. Interestingly neonatal RTEs were found to be more responsive in both cytokine production and proliferation than adults[239]. Overall this suggests as a population RTEs are highly dynamic across life.

1.3 Key Cellular Regulators of SP4 T-cell Development

1.3.1 Generation and Involution of the Thymic Microenvironment

The thymus represents a unique and complex microenvironment comprised of both stromal and hematopoietic cell types which, as will be discussed, are essential regulators of thymocyte development. The earliest stages of thymic organogenesis can be observed around day 10 of embryogenesis (E10)[240]. Here the thymus, concurrent with other pharyngeal organs, arises from the third pharyngeal pouch (3PP) [240]. The endoderm of the 3PP gives rise to the thymic epithelium[241], and is believed to contain a bipotent thymic epithelial progenitor cell (TEPC) that generates both cTEC and mTEC[242]. The 3PP is surrounded by neural crest derived mesenchyme, which ultimately forms the thymic capsule[240]. By E12.5 following expansion of both epithelium and mesenchyme compartments the thymus separates from both the pharynx and parathyroid glands, becoming more discrete[240]. Colonisation of the thymus by hematopoietic progenitors begins around E11.25-11.5[243], and while initially TEC development proceeds independently of these progenitors, around E13.5-E15.5 cross-talk from developing thymocytes helps to direct further TEC differentiation and organisation[244].

Regarding this later organogenesis, one particularly important TF in thymic development is Foxn1[240]. The importance of Foxn1 was highlighted by the phenotype of nude mice, which lack a thymus owing to a mutation in the Foxn1 gene[240,245]. However initial thymic organogenesis seems to be Foxn1 independent, with development arresting at TEC lineage commitment[240,246]. Rather Foxn1 is essential for various aspects of later thymic development, from regulating TEC differentiation and proliferation, influencing the thymic architecture and mediating recruitment of hematopoietic progenitors[240,246–248]. Foxn1 has also been linked with age dependent thymic involution[240], which as discussed has a negative impact on

thymocyte output. Thymic involution is associated with increased adipose tissue and reduced TEC numbers alongside alterations to the ratios of TEC subsets, causing disruption to the stromal architecture[227].

1.3.2 TEC

TEC can be subdivided into two major populations, $Epcam^{+}Ly51^{+}UEA1^{-}$ cTEC and $Epcam^{+}UEA1^{+}Ly51^{-}$ mTEC[249]. During embryonic development, the two subsets are believed to arise from a bipotent TEPC, however whether this remains the case after birth is a contentious issue[249]. Regardless, once differentiated the two TEC subsets perform distinct functions.

1.3.2.1 cTEC

cTEC are able to support both the early stages of T-cell commitment and later positive selection. cTEC are implicated in various aspects of early thymocyte development, including correct DN thymocyte localisation through their expression of CXCL12[117] and lineage commitment by provision of Notch ligands[118]. However perhaps most notable is the unique role they perform in mediating positive selection of thymocytes.

This specific requirement for cTEC has primarily been linked to their unique expression of specialised peptide processing machinery. This is perhaps most clearly demonstrated in the generation of MHCI restricted peptide by a specialised proteasome. cTEC uniquely express the thymoproteasome, which contains the catalytic subunit β5t, and hence differs from both the housekeeping proteasome and immunoproteasome, formed with β5 and β5i subunits respectively[250]. Importantly this differing composition translates into distinctive substrate

preference and processing, favouring hydrophilic substrates[251] and exhibiting distinct cleavage preferences[252]. This results in a unique peptide repertoire, notably enriched for low affinity TCR ligands[252,253]. Similarly, distinct processing of MHCII restricted peptide by cTEC has been suggested owing to their specific expression of lysosomal proteases, cathepsin L[254,255] and thymus-specific serine protease (TSSP)[256]. While the subsequent uniqueness of the MHCII bound peptide repertoire is less clear, it has been noted that deficiency in either protease impairs SP4 positive selection[254,256]. In *Ctsl*$^{-/-}$ (cathepsin L) mice this presents as a reduction in SP4 thymocyte number[254] whereas *Prss16*$^{-/-}$ (TSSP) mice show specific impairment of certain TCR clones[256]. In addition to proteases, macroautophagy, a process which enables unconventional loading of endogenous antigen onto MHCII, has also been linked to optimal positive selection of SP4 thymocytes by cTEC[257]. The significance of this distinct peptide processing may be at least partially linked to negative selection[27]. Notably reconstitution of *Prss16*$^{-/-}$ mice with MHCII deficient BM, largely restored the SP4 thymocyte population, suggesting the reduction of SP4 thymocytes in *Prss16*$^{-/-}$ was owing to increased negative selection by thymic DCs[255]. This indicates that one purpose of unique cTEC peptide processing may be to generate peptides distinct from those presented during negative selection[27].

However, at least for SP8 development, the situation may be more complex as in *Psmb11*$^{-/-}$ (β5t) mice, while positive selection is impaired[252,253], negative selection was not increased[253]. Furthermore, substitution of β5t with β5i did not restore SP8 development[253]. Overall this suggests that β5t dependent processing is also required to generate peptides which specifically support positive selection. This may relate to the low affinity nature of the

peptides β5t generates because, as previously discussed, low affinity interaction between pMHC and thymocytes is crucial to their successful traversing of positive selection[27,252,253].

cTEC do not only support positive selection through provision of an appropriate pMHC repertoire. Thymic nurse cells were identified as a cTEC subset able to engulf multiple DP thymocytes[258,259], for the purpose of supporting TCRα rearrangement [259]. While this function was not essential for positive selection, it seems to optimise the process. This highlights how functional heterogeneity within the cTEC compartment may mediate differential support of positive selection, a topic that is generally poorly understood and possibly underappreciated[249].

1.3.2.2 mTEC

The other TEC compartment within the thymus is the mTEC, comprising the medullary region, which as discussed plays a vital role in supporting negative selection and Treg development. Within the mTEC compartment there is further heterogeneity, the extent of which is only recently being fully uncovered. Classically, mTEC have been divided as $MHCII^{low}CD80^{low}$ $mTEC^{lo}$ and $MHCII^{high}CD80^{high}$ $mTEC^{hi}$[260,261]. However recent scRNAseq analysis redefined mTEC into four subsets (mTECI-IV) on the basis of differential gene expression analysis[262]. This reclassification in particular highlights cells which would classically all be termed $mTEC^{lo}$ as distinct mTEC subsets. As will be discussed there is clear heterogeneity within the $mTEC^{lo}$ population and this reclassification helps highlight and distinguish distinct mTEC subpopulations. However, whether this mTECI-IV nomenclature will be adopted in future is unclear, thus here we will discuss mTEC using the classical $mTEC^{hi}$ and $mTEC^{lo}$ definition while highlighting additional heterogeneous subsets within these phenotypes.

1.3.2.2.1 mTEC^{hi}

The mTEC^{hi} compartment is perhaps most synonymous with negative selection, largely owing to the expression of the transcriptional regulator (TR) autoimmune regulator (Aire) specifically within this population[261]. An essential role for Aire in central tolerance was suggested after AIRE deficiency was identified as the underlying cause behind the multi-organ autoimmunity observed in individuals with autoimmune-polyendocrinopathy-candidiasis-ectodermal dystrophy[23]. A similar highly specific multi-organ autoimmunity was observed in *Aire*$^{-/-}$ mice, and importantly this disease phenotype could be traced to a requirement for Aire mediated promiscuous gene expression of TRAs by mTEC[263]. Indeed, there are thousands of Aire-dependent TRAs[264–266] however there are also Aire-independent genes suggesting a role for other TFs/TRs in TRA expression. Fez family zinc finger 2 (Fezf2) has emerged as one such TF, shown to regulate expression of approximately 400 TRA genes, the majority of which are Aire-independent[267]. Interestingly, unlike Aire, Fezf2 expression is not restricted to mTEC^{hi} but was also present in a subset of mTEC^{lo}[267]. Nor does co-expression of Aire and Fezf2 seem necessary, the two have been proposed to regulate their respective TRAs independently as Aire-dependent and Fezf2-dependent TRAs, were expressed normally in *Fezf2*$^{-/-}$ and *Aire*$^{-/-}$ mice, respectively[267]. Importantly *Fezf2*$^{-/-}$ mice, despite intact expression of Aire dependent TRAs, exhibit a multi-organ autoimmunity distinct from an *Aire*$^{-/-}$[267]. Consequently, Fezf2 and Aire have been proposed to operate independently to drive distinct TRA expression.

Subsequent investigations have identified that as a population mTEC express approximately 85-90% of all the genes[264–266,268], and can generate even greater diversity through mechanisms such as alternative splicing[265,268]. scRNAseq analysis has identified that this broad coverage is achieved through heterogeneous TRA expression by individual mTECs[264–

[266]. Consequently, any given Aire-dependent TRA gene is expressed in only ~1% of all mTECs[264], but those mTECs express that gene very highly[264–266]. This results in the sparse expression pattern of TRAs discussed previously. Interestingly these scRNAseq analyses also offer insight into how complete coverage may be coordinated across the mTEC compartment [265,266]. An ordered stochasticity mechanism for complete coverage is suggested by observations that distinct clusters of co-expressed Aire-dependent genes are observed between groups of mTEC [269]. These co-expressed gene clusters varied between individuals suggesting a stochastic origin which maintains individual diversity[265]. Further to this, mTEC are suggested to progressively transition through different TRA clusters across their lifespan, again maximising TRA coverage[266].

As well as generating this diverse antigen repertoire, mTEC must present it to developing thymocytes to enable negative selection. Traditionally endogenous antigen is restricted to MHCI presentation however mTEC must also present TRAs to SP4 thymocytes. mTEC achieve this in two ways, firstly by utilising macroautophagy to enable unconventional MHCII loading of endogenous peptide[270] and secondly by transferring TRAs to other thymic APCs (discussed in later sections). Direct presentation via macroautophagy seems of particular importance as disruption to this pathway drastically impairs clonal deletion[270]. While this study did not conclusively identify the impact of macroautophagy on Treg differentiation, other work indicates a critical role for mTEC derived TRA in Treg development. For instance, Aire derived TRAs are implicated in the generation of the previously discussed unique neonatal Treg population[233].

In addition to provision of antigen, mTEC may also support Treg development through other signalling pathways. A vital role for stromal derived IL-15 in Treg development was identified by generating hematopoietic chimeras with *Rag1*$^{-/-}$*Il15r*$\alpha^{-/-}$ hosts, in which the thymic stroma is unable to transpresent IL-15[187]. Consequently, these mice exhibited reduced development of both CD25^{-}Foxp3^{+} Treg precursors and CD25^{+}Foxp3^{+} Tregs[187]. Specifically mTEC^{hi} have been identified as a major source of IL-15 in the thymus, with little to no IL-15 observed in mTEC^{lo} and DCs respectively[271], although interestingly mTEC^{lo} may be important in transpresentation of IL-15 as suggested by their higher expression of IL-15Rα[272]. However, mTEC do not seem to be the source of the other vital γ_c cytokine IL-2, as Treg development appeared normal in hematopoietic chimeras generated using *Il2*$^{-/-}$*Rag1*$^{-/-}$ hosts[187], indicating a hematopoietic, rather than stromal, origin of IL-2[187] (discussed in later sections). However, mTEC may still contribute to IL-2 signalling, in a TNFRSF dependent manner. It has been reported that signalling through GITR, OX40 and TNFR2 increases Treg precursor IL-2 responsiveness, and that mTEC express the respective ligands for all these molecules[273].

Considering this myriad of functions it is perhaps unsurprising that mTEC have emerged as essential mediators of negative selection. This issue was neatly addressed by grafting *Relb*$^{-/-}$ lobes into suitable hosts to investigate thymocyte development where mTEC specifically were impaired[158]. Notably Treg development was abolished in this system and *Relb*$^{-/-}$ lobes grafted into nude hosts caused autoimmunity, indicating a fundamental loss of both tolerance mechanisms associated with negative selection[158]. Subsequent studies have drawn similar conclusions, noting in particular the vital requirement for mTEC in Treg development[274,275].

1.3.2.2.2 mTEC^{lo}

Originally, the function of the mTEC^{lo} population appeared to be as an mTEC^{hi} precursor, where mTEC^{lo} differentiated to Aire^{-} mTEC^{hi} before progressing to Aire^{+} mTEC^{hi}[261]. This progression is dependent upon appropriate signalling, with a critical role for TNFRSF members, receptor activator of nuclear factor-κ B (RANK) and CD40[276], with RANK in particular necessary for Aire expression[277]. However, more recent work suggests that a precursor population may constitute only a small fraction of the mTEC^{lo} population. Podoplanin expressing junctional thymic epithelial cells (jTEC) so termed because they reside at the CMJ, are one such postnatal mTEC^{lo} subpopulation considered to possess mTEC precursor potential[278]. Notably, subsequent scRNAseq analysis of mTEC identified a jTEC subset which trajectory analysis determined to be an initial mTEC precursor[279].

Alongside this precursor subset the mTEC^{lo} compartment seems to contain a heterogeneous mixture of mature cell-types, the full extent of which is only recently being appreciated. Earlier work identified a CCL21^{+} mTEC^{lo} population, dependent on LTβR signalling[280]. In ontogeny this population appeared after the mTEC^{hi} so originally it was proposed to develop from Aire^{+} mTEC[280]. However, while a recent scRNAseq analysis of mTEC did identify a CCL21^{+} mTEC^{lo} population, subsequent analysis using a Csn2^{Cre}Rosa26^{tdtomato} reporter determined that this population did not originate from an mTEC^{hi} precursor[262]. Although it was noted that this population was reduced in *Aire*$^{-/-}$ mice suggesting some cross-talk between the two populations[262]. Functionally this population seems to support negative selection by CCL21 mediated recruitment of thymocytes[281]. Additionally, CCL21^{+} mTEC may also influence iNKT-cell development, as recent work identified that transpresentation of IL-15 by CCL21^{+} mTEC specifically supported development of iNKT-cell subsets iNKT1 and iNKT17[282].

Whilst CCL21 may not represent a post-Aire phenotype, fate tracking mice including Aire reporters and $Csn2^{Cre}Rosa26^{tdtomato}$ reporters have identified $Aire^{-}mTEC^{lo}$ which previously were $Aire^{+}mTEC^{hi}$[262,283]. These post-Aire $mTEC^{lo}$ have been divided into two distinct subsets, a previously identified corneocyte-like mTEC subset[262,284,285] and a novel thymic tuft cell subset[262,283]. Similar to the development of CCL21 mTEC both these post-AIRE subsets are dependent upon LTβR signalling[282,285]. The exact functional significance of corneocyte-like mTEC is a little unclear. In humans it has been connected to thymic stromal lymphopoietin (TSLP) conditioning of thymic DCs to mediate Treg development[286], but the same has not been observed in mice[249,262]. In contrast, the tuft cell, similar to the $CCL21^{+}$ mTEC, has been connected to iNKT-cell development, supporting the iNKT2 subset through IL-25 secretion[282]. Taken together, these findings highlight that the $mTEC^{lo}$ compartment is more than a source of $mTEC^{hi}$ precursors, and rather represents a highly heterogeneous mixture of mature cell types, capable of supporting conventional and unconventional thymocyte development.

1.3.3 Thymic Hematopoietic Regulators

1.3.3.1 Thymic DC

The thymic DC pool is heterogeneous, comprised of three major subsets, $CD8\alpha^{+}CD11c^{+}$ conventional DC (cDCs) which are further subdivided into $CD8\alpha^{+}Sirp\alpha^{-}CD11b^{-}$ cDC1 and $CD8\alpha^{-}Sirp\alpha^{+}CD11b^{+}$ cDC2 and $PDCA1^{+}CD11c^{low}$ plasmacytoid DC (pDC)[287,288]. Recent scRNAseq data has identified a further subset present in the $Sirp\alpha^{+}$ cDC2 population defined as $CD14^{+}Sirp\alpha^{+}$ monocyte-derived DC (moDC)[289]. These DC subsets differ in their origin, distribution and seemingly their functional contribution to negative selection.

The origin of these DC subsets can be defined broadly as peripheral or intrathymic. Both pDC and cDC2 subsets are well documented to develop in the periphery before migrating to the thymus. Both subsets rely on the cell adhesion molecule α4 integrin[288,290] to mediate thymic entry, but are recruited by different chemokine axes with TEC derived CCL8 or CCL25 mediating recruitment of $CCR2^+$ cDC2[291] or $CCR9^+$ pDCs[288], respectively. In contrast cDC1s develop intrathymically from a migrant precursor, which is itself recruited from the BM to the thymus via a CCR7-CCL21 chemokine axis[292]. Thymic CCL21 is predominantly derived from mTEC[281], which are also heavily implicated in the intrathymic positioning of cDC1[293]. This intrathymic positioning appears dependent upon cDC1 expression of XCR1, with $mTEC^{hi}$ providing XCR1 ligand XCL1[293]. As discussed $mTEC^{hi}$ contain $Aire^+$ cells and intriguingly Aire seems to regulate this XCR1-XCL1 axis, as both *Aire*$^{-/-}$ and *Xcl1*$^{-/-}$ mice exhibited mis-positioning of cDC1 with fewer located in the medulla[293]. Positioning of pDC and cDC2 may differ slightly from cDC1 as both have also been identified at the CMJ[288,291], with cDC2 specifically identified within perivascular spaces and around small vessels[291].

This differential origin and positioning may contribute to how DCs support negative selection, at least in terms of antigen presentation. It has been proposed that migratory DCs localised close to blood vessels are ideally positioned to capture and present blood-borne antigen. Indeed, intravenously injected antigen were detected in the thymic PVS cDC2 within 30 minutes[291]. Further comparison of the ability of intrathymic DCs to uptake injected antigen from the blood, suggested that pDCs were also highly proficient, more so than cDC2, while cDC1 displayed the lowest uptake[294]. In addition to efficient capture of soluble blood-borne peripheral antigens both cDC2 and pDCs seem capable of bringing peripheral antigen into the thymus on their migration[288,290]. Using beads unable to cross thymic blood vessels, it was

shown that after either intravenous or subcutaneous injection, the beads were still present within both thymic pDC and cDC2 but not cDC1[288]. Similarly, thymic DCs were also shown to acquire FITC exclusively painted on the skin and antigens restricted to cardiac myocytes, in an α4 integrin dependent manner[290], suggesting a major role for cDC2 and pDC in presentation of a variety of peripheral antigens. Thymic DCs have also been reported to present both ubiquitous antigen and Aire-dependent TRA sourced from mTECs[275,295,296]. Interestingly cDC1 seem more proficient at this mode of presentation than cDC2, a difference speculated to relate to XCR1 dependent interaction of cDC1 with mTEC[275]. However more recent work suggests other DC subsets present mTEC derived antigen with equal efficiency[289]. Furthermore there may be similar recruitment by mTEC of other DCs as it was observed that Toll-like receptor (TLR) signalling in $mTEC^{hi}$ induced a programme of chemokines believed to recruit moDC to the medulla[289].

As well as presenting different types of antigen for negative selection it has also been proposed that DCs provide additional signals in Treg development. Induction of a Treg phenotype seems to be a role that all three DC subsets can perform, at least *in vitro*, with variable efficiency[297,298]. One mechanism that may contribute to this is IL-2 dependent, as purified thymic DCs were identified as a significant, albeit not sole, source of IL-2[299]. Furthermore, $Il2^{-/-}$ BM-derived DC were poorer at supporting Treg differentiation in a thymic slice system, compared to WT counterparts[299]. DCs may also mediate the same TNFSRF dependent pathway as mTEC to alter thymocyte IL-2 responsiveness, as all three DC subsets express ligands for GITR and TNFR2[273]. CD70 represents another TNFSRF pathway through which DCs can promote Treg development, with CD70 from DC (and mTEC) interacting with Treg CD27 to prevent Treg apoptosis[298]. Interestingly cDC1 may rely more heavily on this

pathway, as reduced Treg differentiation was observed following *in vitro* culture of $SP4^{+}$ thymocytes with *Cd70*$^{-/-}$ cDC1 but not *Cd70*$^{-/-}$ cDC2[298].

Overall, this identifies that DCs can support negative selection and more specifically Treg development, but evidently there is also some redundancy with mTEC. This raises the question as to whether, like mTECs, thymic DCs are essential for the negative selection process. One study has addressed this by offering new insight into the role of LTβR in the thymus[300]. Previous investigation into *Ltβr*$^{-/-}$ mice identified autoimmunity believed to be connected to a disrupted medulla and reduced mTECs[301]. However, when LTβR deficiency was restricted to TEC by virtue of the *Foxn1*^{cre}*Ltβr*$^{fl/fl}$ mouse, tolerance mechanisms proved independent of this disrupted phenotype and did not result in overt autoimmunity[300]. Rather, the loss of tolerance in the *Ltβr*$^{-/-}$ mouse stemmed from reduced negative selection owing to an altered thymic DC compartment[300]. Similarly, another study investigating the impact of depletion of cDC1 vs mTEC determined a cooperative role for cDC1 and mTEC in negative selection[274]. This was suggested because the combined absence of cDC1 and mTEC resulted in a multi-organ autoimmune phenotype more severe than the autoimmunity observed when mTEC alone were depleted[274]. Furthermore, recent two-photon microscopy analysis identifies a roughly equal contribution of both mTECs and cDCs to antigen presentation during negative selection[302], implicating both DCs and mTECs as important regulators of negative selection.

Conversely, the role of DCs in Treg development is less clear from these studies as a defect in Treg development is not identified in either *Ltβr*$^{-/-}$ or cDC1 depleted mice[274,300]. Indeed Treg development is noted to be impaired only upon mTEC depletion, and is not further reduced with additional DC depletion[274]. While this suggests a redundant role for DC in Treg

development, an alternative explanation is suggested by findings into the impact of DCs on TCR clones[275]. This work suggests that mTEC and DC perform complimentary roles in Treg development by selecting for Tregs with distinct TCRs[275]. This study also identified that cDCs, not pDCs, were required for Treg development and predominantly it was cDC1s which acquire and present Aire-dependent antigens to mediate Treg development[275]. However more recent work suggests more redundancy in Aire-dependent antigen presentation by DC, as two Aire-dependent Treg clones reliant on antigen presentation by DC still developed in mice lacking cDC1[303]. Furthermore moDCs also seem to play a distinct role in Treg development as reduction of this subset as a consequence of TEC specific *Myd88*$^{-/-}$ impaired de novo Treg development and was associated with subsequent colitis[289]. Thus, overall it appears that the thymic DC compartment does make an important cooperative contribution to negative selection and Treg development.

1.3.3.2 Autoreactive Thymocytes

Intriguingly thymocytes themselves may participate in thymic Treg development. As discussed, studies implicated a hematopoietic, rather than stromal, source of IL-2[187] and initially thymic DCs were identified as one source[299]. Interestingly subsequent work identified thymic T-cells as another important source of thymic IL-2[187,304,305]. To address the requirement for different potential IL-2 producing hematopoietic populations, IL-2 deficiency was specifically induced in either B-cells, DCs, or T-cells, by using *Cd79a*^{Cre}*Il2*$^{fl/fl}$, *Cd11c*^{Cre}*Il2*$^{fl/fl}$, *Cd4*^{Cre}*Il2*$^{fl/fl}$ mice, respectively[304]. When these mice were crossed to an *Il15*$^{-/-}$, thereby eliminating IL-2 independent Treg development, impaired IL-2 specific Treg development was observed only in the *Cd4*^{Cre}*Il2*$^{fl/fl}$[304]. Furthermore, additional crossing of *Cd4*^{Cre}*Il2*$^{fl/fl}$ mice with *Cd11c*^{Cre}*Il2*$^{fl/fl}$ or *Cd79a*^{Cre}*Il2*$^{fl/fl}$ either singularly or together did not exacerbate the reduction

of thymic Tregs[304]. Together, these findings indicate that IL-2 expression by thymic T-cells is both essential and sufficient for thymic Treg development.

This in turn prompts the question of exactly which thymic T-cells are required. iNK T-cells and peripheral T-cells, including memory SP4 T-cells, have been ruled out[187,305], as has autocrine production by Tregs[187], rather developing thymocytes seem to be the essential source of IL-2[187,305]. Interestingly the type of developing thymocyte population matters, with optimal Treg development observed under polyclonal, but not monoclonal, thymocyte development[187], prompting speculation that a specific subset of developing thymocytes absent from the monoclonal setting produced IL-2[187]. Recent findings support this, and identify a small pool of autoreactive thymocytes which on receiving a TCR trigger secrete IL-2 necessary to support Treg development[305]. These autoreactive IL-2 secreting cells predominantly reside within the $CD25^{+}Foxp3^{-}$ Treg precursor population and experience different fates, either further differentiating into Tregs, undergoing apoptosis or escaping negative selection[305]. Overall, this indicates that developing autoreactive thymocytes play a vital role in supporting the development of their fellow thymic Tregs.

1.3.3.3 Mature Thymic Tregs

As previously discussed, studies using Rag-GFP mice have identified that mature $Rag\text{-}GFP^{-}$ Tregs contaminate the intrathymic Treg pool. The origin of these Tregs has been ascertained primarily through thymus transplantation models[234], in which embryonic thymic lobes are surgically grafted to congenically different hosts, and adoptive intravenous cell transfer of cogenically marked cells[235,306]. Tracking these graft-derived or transferred cells identified their presence in the thymus, demonstrating thymic recirculation of peripheral Tregs in

mice[234,235,306]. Thymic transplantation models also suggest a role for long-term retention of thymic Treg, as it was shown that the proportion of graft derived Tregs is greater in the grafted thymic lobes than the host thymus[306]. Thus, both thymic recirculation and retention may contribute to the mature thymic Treg population, although recirculation seems to play a larger role[306].

Interestingly the medulla has emerged as a key regulator of thymic Treg recirculation[307]. Investigations into *Aire*$^{-/-}$ Rag-GFP mice identified a reduction in mature thymic Tregs, which through thymic transplant models, was linked to impaired Treg recirculation[307]. Similarly, recirculation of mature Tregs to the thymus was also impaired in *Ccr6*$^{-/-}$ Rag-GFP mice[307]. These two findings were connected by the CCR6 ligand CCL20 which was produced primarily by the Aire^{+}mTEC^{hi} compartment, and notably reduced in *Aire*$^{-/-}$[307]. Taken together this suggests an Aire^{+}mTEC mediated CCL20-CCR6 axis which controls the recirculation of mature Tregs to the thymus and subsequent localisation within the medulla[307]. Interestingly this axis may itself be subject to regulation by TLR signalling, as TLR9 stimulation increased both mTEC^{hi} CCL20 expression and the size of the mature thymic Treg population[289].

Mature Tregs recirculating to/remaining within the thymus seems somewhat counterintuitive, given their discussed role in enforcing peripheral tolerance. As previously eluded to, their return has been connected with regulation of de novo Treg development. This has been supported by studying *de novo* Treg development using *in vitro* systems such as fetal thymic organ cultures (FTOCs) and thymic slices, which mimic the thymic microenvironment and structure and support thymocyte development[235,299]. Notably addition of mature Tregs to either FTOCs[235] or thymic slices[299] specifically impaired de novo Treg development. This

block in Treg development appears to occur at the transition of Treg precursor to Treg, as Treg precursor development itself was not impacted by addition of de novo Tregs[235]. In keeping with this, it was shown that mature Tregs did not interfere with TCR signalling of de novo Tregs[299], which as previously discussed is required for Treg precursor differentiation. Instead evidence pointed to an IL-2 dependent mechanism, as addition of IL-2 increased Treg development[299], while conversely treatment with an anti-CD25 monoclonal antibody decreased Treg development[235]. Furthermore, combined treatment of anti-CD25 and mature Tregs did not result in a greater reduction[235]. Together this suggests that mature thymic Tregs compete with developing thymocytes for IL-2 and thereby limit the differentiation of Treg precursors to Tregs[235,299]. Thus, the larger mature thymic Treg population in older mice is thought to be responsible for the reduction in thymic Treg output[235], as previously discussed. However, findings from systems with altered thymic Treg recirculation challenge this idea. *Aire*$^{-/-}$ mice have reduced thymic Treg recirculation but no increase in de novo Treg development[307], while *Tnfrsf11b*$^{-/-}$ mice have increased thymic Treg recirculation but no decrease in de novo Treg development[308]. Thus, the relationship between mature thymic Tregs and de novo Tregs remains uncertain.

1.3.4 Peripheral Support of SP4 RTE Development

As previously discussed SP4 T-cell development continues in the periphery with the maturation of RTEs. While intrinsic regulators of the RTE maturation programme have been identified, it appears that initiation of this programme is not cell-intrinsic but requires peripheral signalling, and hence thymic egress. Thymocytes prevented from undergoing thymic egress exhibited a less mature phenotype than their age matched peripheral RTE

counterparts[309]. However interestingly, the 'stuck' thymocytes exhibited an intermediate maturation phenotype, and indeed expressed certain markers, notably Qa2, at mature levels, suggesting that either the early phases of RTE development are cell-intrinsic or that the thymus can compensate for some peripheral signals at this stage[309].

Whilst the thymus may regulate some early aspects of maturation, for its completion RTEs must exit the thymus and ultimately access SLOs. In splenectomised mice where LN access was also blocked, so called "homeless RTEs' were unable to enter SLOs for their development and proved to be phenotypically and functionally immature relative to RTEs which could access SLOs[309]. Interestingly maturation was not impaired when RTEs were prevented from accessing either the spleen or the LNs alone, nor when following access to a given LN subsequent recirculation to other LNs was blocked[309]. Thus suggesting that a common mechanism present in all SLOs can promote RTE maturation independently[309]. However, exactly what this common mechanism is, remains elusive. Several molecules have proved superfluous to RTE maturation, including MHC[310], CD80/CD86, IL-7, and the CCR7 ligands, CCL19 and CCL21[311]. Rather the only essential requirement identified thus far is an intact DC compartment, which supports RTE maturation in some unknown way[311]. This finding may also explain the limited maturation of trapped thymic RTEs[309], as it has been found that egress competent $CD69^{-}Qa2^{+}$ thymocytes, termed "pre-RTE", upregulate Qa2 in response to migratory DCs in the thymic PVS[312].

RTEs are not restricted to SLOs, and can be found in non-lymphoid tissue, notably the gut[313] and the liver[314,315]. Whether this migration is maturation related, has not been fully addressed although evidently it cannot compensate for loss of SLO access[309]. Furthermore,

RTE maturation progressed normally under S1P blockade which as well as blocking LN egress, should prevent RTE entry to the gut[309], suggesting that non-lymphoid tissue access is not necessary for supporting RTE maturation. Instead, non-lymphoid tissues may be important for tolerance induction in RTE. This idea largely arises from analysis of a small population of SP4 RTEs which are retained within the liver[314,315]. Transplant experiments have demonstrated that RTEs home to the liver early on and, by using splenectomised *Ltβr*$^{-/-}$ recipients (lacking SLOs), independently of SLO derived signals[314]. RTEs which are subsequently retained by the liver appear activated, CD44^{hi}, but express regulatory markers like Lag3 and secrete both IL-10 and TGFβ on stimulation[314,315]. Furthermore they respond poorly to IL-7 survival signals and express high levels of apoptotic factors Fas-L and Bim[314,315]. Consequently under homeostatic conditions the ultimate fate for these RTEs is likely apoptosis[315]. Importantly retained liver RTEs have high autoreactive potential, as upon transfer to *Rag1*$^{-/-}$ hosts, liver RTEs caused more severe inflammation in the lung, liver and intestine relative to LN RTEs[314]. This suggests that the liver may retain autoreactive RTEs that escape negative selection to enforce peripheral tolerance.

Regarding how this tolerance may be mediated, the liver is an established site of peripheral tolerance capable of presenting many peripheral specific innocuous antigens, via specialised liver cells, notably liver sinusoidal endothelial cells (LSEC), and liver-resident macrophages Kupffer cells[316]. Co-culturing liver RTEs with LSECs, induced a tolerogenic phenotypic characterised by, Lag3, Fas-L and IL-10 expression alongside reduced IL-7 responsiveness[315]. In contrast co-culturing with Kupffer cells only induced LAG3 expression. Indicating that LSECs may primarily mediate tolerance of liver RTEs[315]. The pathways utilised by LSECs are unclear but cell-contact seems essential as does Notch signalling[315]. Surprisingly Aire may also be

involved, as previous work identified post-thymic expression of both MHCII and Aire were necessary to induce the toleragenic RTE phenotype[314]. Interestingly, this same liver retention was not observed in SP8 RTEs[314] possibly due to their direct homing to the intestine[313]. SP8 RTE expression of CCR9 and $\alpha_4\beta_7$ was proposed to facilitate their migration to the gut and again this seemed SLO independent[313]. While this study does not identify a toleragenic phenotype of SP8 RTE they do note that despite an activated phenotype there is no overt inflammation[313]. Certainly, the intestine is another site where novel innocuous peripheral antigens may be encountered, so it is tempting to speculate that this migration to non-lymphoid tissue may also facilitate tolerance.

1.4 General Aims

The thymus plays a key role in tolerance and immunity by carefully balancing the intrathymic production of Tconvs and Tregs. As such, thymus function is central to the formation of a safe and effective immune system. However, uncertainty remains regarding how the thymus controls the development of multiple SP4 T-cell lineages. In particular, while commitment of self-reactive SP4 thymocytes to the Treg lineage in the thymic medulla is increasingly well characterised, subsequent events during Treg development, within the thymus and periphery are less clear. Specifically, it is unclear how thymic developmental processes might contribute quantitatively and qualitatively to the Treg population, and whether thymic Tregs undergo further post-thymic maturation.

Broadly, we hypothesised that Treg-lineage specific post-selection processes within the thymus and post-thymic processes were important in the formulation of the observed peripheral Treg population. Specifically, we hypothesised that post-selection maturation of

thymic Tregs contributes to the heterogeneous Treg subsets in the periphery, therefore we expected the thymus to support the generation and export of distinct Treg subsets. We also hypothesised that thymic post-selection processes contribute to the variation in the peripheral Treg population observed with age, therefore these processes should differ in the neonate and adult. Finally, we hypothesised Treg RTE undergo lineage-specific post-thymic maturation, meaning Treg RTE should be immature relative to their mature counterparts and undergo a distinct maturation process to Tconv RTEs.

Therefore, we sought to re-examine and characterise the process of de novo thymic Treg development to address the following specific aims:

1. Provide a detailed understanding of the developmental stages that give rise to intrathymically produced Tregs.
2. Examine the role of intrathymic proliferation in the production of the neonatal thymic/ peripheral Treg pool.
3. Define RTE populations of both Tconv and Treg lineages.

CHAPTER TWO:
MATERIALS AND METHODS

2.1 Mice

All mice used for experimental work were maintained within the Biomedical Service Unit at the University of Birmingham. All matters regarding animal use, including breeding, procedures and culling were conducted in accordance with Home Office regulations. Table 2.1 details the mouse strains used within this study, which are all on a C57Bl/6 background.

Wild-type (WT) and genetically modified animals were used, under steady state conditions unless otherwise stated. Genetically modified animals fell within two categories: WT fluorescent reporters or genetic knockout (often crossed with fluorescent reporters). Where fluorescent reporters were used a WT non-fluorescent reporter served as a negative staining control (see Section 2.6). Where genetic knockouts were used, an age matched WT (either fluorescent or non-fluorescent dependent upon the knockout) acted as a control. Animals aged 8-12 weeks were classified adults, all other ages investigated are specifically stated. Animals aged >Day (D)5 were culled by the schedule 1 procedure cervical dislocation, while those aged <D5 were culled by decapitation.

Timed matings were setup to supply embryonic or neonatal (pre-weaning) tissue. Detection of a vaginal plug was classified as day 0 of gestation (embryonic day 0, E0). To harvest embryonic tissue pregnant females were culled between E14-E17. For neonatal tissue, pregnant females were left to complete gestation, pups were classified as D0 on birth and subsequently harvested for tissue at indicated ages.

Table 2. 1 Details of Mouse Strains

Mouse Strain	Phenotype	Source
C57BL/6	Wild Type	BMSU and Charles River
BoyJ	Congenic CD45.1 C57BL/6 Wild Type	BMSU
Rag2-GFP (Rag-GFP)	Transgenic mice which encode a green fluorescent protein (GFP) reporter within the *Rag2* gene[155]. This means that GFP expression can be used as a molecular timer of T cell development	The Jackson Laboratory
Foxp3-RFP	Transgenic mice which encode a red fluorescent protein (RFP) reporter within the Foxp3 gene. This means that RFP can be used to discriminate Treg and non-Treg populations	The Jackson Laboratory
Rag2-GFPxFoxp3-RFP	Generated from crossing Rag-GFP reporter mice with Foxp3-RFP mice. Meaning the Rag-GFPxFoxp3-RFP reporter can discriminate Treg and non-Treg alongside reporting as a molecular timer of T cell development	Generated in house at the BMSU
Aire$^{-/-}$ x Rag-2-GFP	Generated from crossing Aire deficient mice with Rag-GFP reporter mice. Resulting in mice which display an Aire deficient phenotype	Generated in house at the BMSU (*Aire*$^{-/-}$ used in breeding originally from Professor Katja Simon University of Oxford)
Ltbr$^{-/-}$ x Rag-2-GFP	Generated from crossing LTβR deficient mice with Rag-GFP reporter mice. Resulting in mice which display an LTβR deficient phenotype (which causes disruption to the thymic medulla and also absence of peripheral LNs and disrupted splenic architecture) alongside Rag-GFP as a molecular timer of T cell development	Generated in house at the BMSU (*Ltbr*$^{-/-}$ used in breeding originally from Professor Klaus Pfeffer University of Düsseldorf)
Tnfrsf4$^{-/-}$	Mice are deficient for Ox40 and therefore lack Ox40:Ox40L costimulatory interactions between T cells and APCs	Professor Dave Withers University of Birmingham
Rag2$^{-/-}$	Mice are deficient for Rag2 and therefore lack mature T-cell and B-cell populations because they are unable to progress beyond the generation of the TCR/BCR (respectively) during their development.	BMSU, via the Jackson Laboratory

2.2 Media For Cell Isolation, Cell Staining and Cell Culture Systems

Tables 2.2-2.6 indicate the composition of various media used throughout the study. RF10 (Table 2.2) or 2% FCS HBSS (Table 2.3) were used in the initial dissection, storage and processing of cell populations (Section 2.3). DMEM (Table 2.4) was used to culture cells in FTOCs/ reaggregate thymic organ cultures (RTOC) (Section 2.9-2.10). To perform flow cytometry and fluorescence activated cell sorting (Section 2.6 and 2.8), MACs buffer (Table 2.5) or FACs buffer (Table 2.6) was used as staining buffer for stromal or lymphocyte populations, respectively. In addition, where indicated, Dulbeccos phosphate buffered saline (DPBS) with or without magnesium and calcium, $Mg^{2+}Ca^{2+}$DPBS or $Mg^{-}Ca^{-}$DPBS, respectively (both Sigma-Aldrich) were used without any additional additives, for staining or washing processes.

Table 2. 2 RPMI-1640 Hepes (RF10)

Component	Volume	Final Concentration	Source
RPMI-1640+ 20mM Hepes with L-glutamine, without bicarbonate	500ml	-	Sigma-Aldrich
Heat-inactivated fetal calf serum	50ml	10%	Sigma-Aldrich
200mM L-Glutamine	5ml	2mM	Sigma-Aldrich
5000 IU/ml Penicillin and Streptomycin	10ml	100 IU/ml	Sigma-Aldrich

Table 2. 3 2% Fetal Calf Serum Hanks Balanced Saline Solution (2% FCS HBSS)

Component	Volume	Final Concentration	Source
Hank's Balanced Salt Solution	500ml	-	Sigma-Aldrich
Heat-inactivated fetal calf serum	10ml	2%	Sigma-Aldrich

Table 2. 4 Dulbecco's Modified Eagle Medium (DMEM)

Component	Volume	Final Concentration	Source
Dulbecco's Medium with 3.7g/l bicarbonate, without glutamine	20ml	-	Sigma-Aldrich
Heat inactivated fetal calf serum	2ml	10%	Sigma-Aldrich
5000 IU/ml	400µl	100 IU/ml	Sigma-Aldrich
200mM L-Glutamine	400µl	4mM	Sigma-Aldrich

1M Hepes	200µl	10mM	Sigma-Aldrich
5x103 M2 Mercaptoethanol	200µl	-	Sigma-Aldrich
100x non-essential amino acids	200µl	-	Sigma-Aldrich

Table 2. 5 MACs Buffer

Component	Volume	Final Concentration	Source
Dulbeccos phosphate buffered saline without calcium or magnesium	500ml	-	Sigma-Aldrich
Heat inactivated fetal calf serum	2.5ml	0.5%	Sigma-Aldrich
EDTA 0.05M	2ml	0.02M	Sigma-Aldrich

Table 2. 6 FACs Buffer

Component	Volume	Final Concentration	Source
Dulbeccos phosphate buffered saline with calcium and magnesium	500ml	-	Sigma-Aldrich
Heat inactivated fetal calf serum	15ml	3%	Sigma-Aldrich

2.3 Dissection of Mouse Tissues

Tissue including, thymus, spleen, LNs, liver and bone marrow, were dissected from culled mice at BMSU and placed into RF10. Where necessary excess fat or blood was removed from tissues. Tissues were then stored in RF10 on ice until processing (Section 2.4). The colon was dissected from below the cecum to the rectum and placed in 2% FCS HBSS. Any fat was removed, then the colon was cut open longitudinally and the tissue washed with 2% FCS HBSS to remove the contents. The colon was then cut into approximately 5mm pieces and kept in 2% FCS HBSS on ice until processing (Section 2.4).

To isolate fetal tissue, the womb was first removed from culled pregnant mice, then within a laminar flow hood embryos were separated from the womb and amniotic sac. Embryonic thymic lobes were then dissected using a dissection microscope and placed in RF10 temporarily before further use.

2.4 Isolation of Cell Populations

2.4.1 Isolation of Lymphocytes from Tissues

2.4.1.1 Thymus, Spleen and Lymph Nodes (LNs)

Lymphocytes were isolated from thymus, spleen and LNs via mechanical disaggregation, by using two glass slides to tease apart the tissues, with the resultant released cells collected in a petri-dish containing RF10. Once a single cell suspension was obtained the slides were then washed with RF10 and discarded. The resulting cell suspension was then filtered through a membrane-mesh filter into 15ml Falcon tubes (Corning), then centrifuged (1400rpm, 4 minutes). The supernatant was removed and the pellet resuspended in either 2mls of RF10 for thymic and LN samples, or 2mls of Red Blood Cell (RBC) lysis buffer Hybri-max (Sigma-Aldrich) for splenic samples. Thymic and LN samples were placed on ice while splenic samples were left at room temperature (RT) for 10 minutes to deplete erythrocytes. An equal volume of RF10 was then added and centrifuged as before. If erythrocyte lysis was incomplete this process was repeated, otherwise splenocytes were resuspended in 2ml of RF10 and placed on ice to be counted (Section 2.5.1).

2.4.1.2 Bone Marrow (BM)

BM was obtained from tibia and femur bones, which were first cleaned and then cut at either end. A 25g needle attached to a syringe containing RF10 was used to flush out the BM into a 35mm petri dish containing RF10. Extracted BM was passed through the needle several times until a single cell suspension was obtained, this was then passed through a filter into a Falcon tube and centrifuged (1400rpm, 10 minutes). The sample was then resuspended in 2ml RBC lysis buffer Hybri-max for 10 minutes at RT. An equal volume of RF10 was then added and

centrifuged as before and the sample resuspended in RF10 and placed on ice to be counted (Section 2.5.1).

2.4.1.3 Liver

To isolate lymphocytes from liver the tissue was first mechanically disaggregated in RF10 by pushing through a 70µm cell strainer. The suspension was then centrifuged (1400rpm, 4 minutes) and the pellet resuspended in 5ml RF10. To separate out the lymphocytes an OptiPrep density gradient was employed. In a 15ml Falcon tube 1.3ml OptiPrep (Sigma-Aldrich) was mixed with 3.7ml $Mg^{2+}Ca^{2+}$DPBS. The liver suspension was then gently pipetted on top of the OptiPrep. This mixture was then centrifuged (1000RCF, 25 minutes, brake speed 1). The cloudy layer containing the lymphocyte was then carefully transferred to a fresh Falcon tube and topped up with 10ml FACs buffer then centrifuged (1400rpm,4 minutes). The resulting pellet was then resuspended in 2ml RF10 and placed on ice to be counted (Section 2.5.1).

2.4.1.4 Colon

The colon segments were removed from solution by filtering through a nitex mesh. Using forceps the segments were then transferred into a Falcon tube containing 10ml HBSS 2mM Ethylenediaminetetraacetic acid (EDTA, Sigma-Aldrich). This tube was then shaken vigorously for 20 seconds, then incubated for 15 minutes at 37°C under agitation. The colon was then washed by first filtering it through a nitex mesh (as before) before it was resuspended in 10ml warm HBSS, shaken again and re-filtered. The tissue fragments were then transferred to a tube containing 10ml HBSS 2mM EDTA and shaken and incubated as before. Following this incubation the colon was washed twice as before. An enzyme mix comprising 10ml RF10,

0.85mg/ml collagenase V (Sigma-Aldrich), 1.25mg/ml Collagenase D (Roche), 1mg/ml Dispase (Gibco) and 30μg/ml DNAse (Roche) was prepared and the colon segments added. This mixture was then incubated at 37°C under agitation, with manual shaking every 5-7 minutes, for 30-45 minutes until no tissue remained. The single cell suspension was filtered through a 100μm filter followed by a 70μm filter, and centrifuged (1400rpm,4 minutes). The pellet was resuspended in RF10 and centrifuged again, twice. Finally the pellet was resuspended in 2ml RF10 and placed on ice ready to be counted (Section 2.5.1).

2.4.1.5 Blood

Blood samples collected from live mice by saphenous bleed (up to approximately 100μl), were transferred to 1.5ml Eppendorfs and 500μl of RBC lysis buffer Hybri-max was added at RT for 10 minutes. An equal volume of RF10 was then added and centrifuged (1400rpm, 4 minutes). This process was then repeated twice, then the sample resuspended in 1ml of RF10 and placed on ice.

2.4.2 Isolation of Lymphocytes from Organ Cultures

Cultured thymic lobes were removed from filters by submerging the filter in a petri-dish containing RF10 and gently pushing off any lobes that did not immediately detach. Lymphocytes were isolated by mechanical disaggregation, with thymic lobes teased apart using the closed ends of two pairs of forceps, in a 1ml standing drop of RF10. Multiple lobes (as indicated in specific methods) were pooled and teased together, to ensure sufficient lymphocytes for staining. The media was transferred to a 1.5ml Eppendorf tube, and briefly left for any large stromal clumps to sink to the bottom. The supernatant (containing the single cell suspension of lymphocytes) was transferred to a second 1.5ml Eppendorf tube, leaving

behind any stromal clumps. The single cell suspension was then centrifuged (1400rpm, 4 minutes) and the supernatant discarded and the pellet resuspended in 1ml of RF10 and placed on ice to be counted (Section 2.5.2).

2.4.3 Isolation of Thymic Stromal Cells from Tissues

To isolate thymic stromal cells, thymi were added to 1.5ml Eppendorfs containing an enzyme mix of 1ml RF10, 0.4mg/ml DNase1 (Sigma-Aldrich) and 2.5mg/ml Collagenase Dispase (Sigma-Aldrich). Using scissors the thymi were chopped into fine pieces, then the media and tissue transferred into a polypropylene round bottom digest tube (Falcon) and incubated at 37°C under agitation, with resuspension by pipetting every 10 minutes, for up to 30 minutes, until the tissue had completely digested. Samples were filtered into a 15ml Falcon tube topped up with MACs buffer, then centrifuged (1400rpm, 4 minutes). Next a CD45-depletion was performed by first incubating the sample with (vortexed) anti-CD45 beads (Miltenyi Biotec) in MACs buffer for 20 minutes at 4°C. Samples were then passed through a primed LS MACs separation column (Miltenyi Biotec) placed on QuadroMACs separator magnets. The column run-off (containing the $CD45^-$ cells) was collected in 15ml Falcon tubes, centrifuged (1400rpm, 4 minutes) and resuspended in MACs buffer for analysis.

2.4.4 Isolation of Thymic Stromal Cells from Organ Cultures

Cultured thymic lobes were removed from filters as described in Section 2.4.2. Lobes were then transferred using a P1000 Gilson pipette to a 1.5ml Eppendorf tube. The lobes were left to settle to the bottom before the supernatant was removed. Lobes were then washed by addition of 1ml Mg^-Ca^-DPBS, which was removed once the lobes had resettled to the bottom, this process was repeated 3 times. Then the lobes were resuspended in 600µl of 0.25% trypsin

solution (pre-prepared as 1:10 dilution of 2.5% trypsin stock (Sigma-Aldrich): 0.02% EDTA in $Mg^{-}Ca^{-}$DPBS (Sigma-Aldrich). The tube was then incubated at 37°C for 15 minutes. Lobes were then resuspended using a P1000 Gilson pipette and returned to the incubator for 5-10 minutes. A P1000 Gilson pipette was then used to complete disaggregation of the lobes to generate a single cell suspension. 400µl of RF10 was added to neutralise the trypsin before the suspension was centrifuged (1400rpm, 4 minutes). The pellet was then resuspended in 1ml RF10 and placed on ice to be counted (Section 2.5.2).

2.5 Cell Counts

2.5.1 Counting with Sphero AccuCount cell count beads

Isolated populations which yielded large numbers of cells (e.g. from tissues) were counted using AccuCount Blank Beads (Spherotech Inc). The count sample consisted of a known number of AccuCount beads (5000), and an aliquot of the sample to be counted (diluted in FACs buffer to give a 1:40 dilution). The count sample was then run on a BD LSR Fortessa flow cytometer to record the number of cells and beads acquired. This information was used to calculate the total cell number in the 2ml sample as follows:

$$Total\ Cell\ Number = \left(\left(\frac{Number\ of\ cells}{Number\ of\ beads} \right) \times 5000 \right) \times 40$$

2.5.2 Counting with a Haemocytometer

Counting with a haemocytometer was reserved for populations which yielded low cell numbers, including lymphocyte/stromal populations recovered from FTOC and RTOC, and sorted populations with low recovery. Samples were re-suspended in 1ml to count and a 10µl

aliquot was taken for the count (if the number of cells was too large to count this aliquot was further diluted). 10μl of sample was loaded onto the hemocytometer, and counts were made of cells within each of the four corner squares, then these counts averaged. This average was multiplied by 10^4 (and if necessary by the dilution factor) to give the final cell count/ml of the sample.

2.6 Flow Cytometry

For flow cytometric analysis $5x10^6$ cells per sample were loaded into a 96 well-plate (Corning) for staining. If less than $5x10^6$ cells were recovered (e.g. some early neonatal timepoints) the total sample was stained. In situations of particularly low cell numbers (e.g. lymphocyte populations recovered from RTOC) cells were stained in 1.5ml Eppendorfs. Alongside samples additional staining controls (e.g. single colours and negative staining controls) were also stained simultaneously in the same manner. Samples were first stained for extracellular markers (Section 2.6.1) then if necessary stained for intracellular markers (Section 2.6.2-3). Exposure of samples to light was minimised and all staining incubations were completed in darkness. Throughout staining, cells were washed by addition of 100-150μl of the indicated buffer to the required wells, the plate was then centrifuged (1400rpm,2 minutes) and the contents flicked out. Where cells were stained in Eppendorfs, cells were centrifuged (1400rpm, 4 minutes) and the supernatant removed by pipette. The antibodies used for cell staining alongside their working dilutions are detailed in Table 2.7-9.

2.6.1 Cell Surface Staining

Prior to cell surface staining, the transferred $5x10^6$ cells to be stained were either washed with FACs buffer (for experiments involving only lymphoid tissues) or stained with a cell viability

dye (for experiments involving non-lymphoid tissue). In this latter process, cells were first washed with $Mg^{-}Ca^{-}$DPBS, then stained with 50μl Zombie Aqua (Biolegend) diluted 1:500 in $Mg^{-}Ca^{-}$DPBS at RT for 20 minutes. Cells were then washed initially with $Mg^{-}Ca$ PBS followed by a second wash with FACs buffer.

Cells were then stained with primary antibodies (details Table 2.7) in 50μl FACs buffer on ice for 20 minutes, except for any chemokine receptors which were stained at 37°C for 30 minutes. Following this staining incubation, cells were washed twice with FACs buffer. If necessary cells were then resuspended for staining with secondary antibodies (details Table 2.8) adhering to the same conditions as primary antibody staining.

S1PR1 staining was an exception to this general cell surface staining protocol. Here cells were first stained with 75μl of unconjugated S1PR1 in FACs buffer on ice for 30 minutes. Cells were then washed twice with FACs buffer and stained with 100μl anti-Rat IgG2a biotin in FACs buffer for 30 minutes on ice. Cells were then washed twice with FACs buffer and incubated with rat serum (R&D Systems) diluted 1:10 in FACs buffer for 15 minutes on ice. Cells were then washed twice with FACs buffer and stained with a conjugated streptavidin (alongside other primary surface markers) as previously described.

Following cell surface staining, cells were either subject to further intracellular staining (Section 2.6.3-4) or resuspended in FACs buffer and transferred to FACs tubes (Scientific Laboratory Supplies) for flow cytometric analysis (Section 2.6.5).

2.6.2 Intracellular Fixation and Staining

For analysis of intracellular proteins such as Foxp3, Ki67 and Aire, intracellular fixation and staining was performed following cell surface staining (Section 2.6.2). For this cells were permeabilised using reagents from the eBioscience Foxp3/Transcription Factor Staining Buffer Set (ThermoFisher) in accordance with manufacturer's instructions.

Here cells were first resuspended in 150µl of Fixation/Permeabilisation solution (comprising 3 parts diluent: 1 part concentrate), on ice for 40 minutes. Cells were then washed twice with Permeabilisation buffer (consisting of 1 part 10X Permeabilization Buffer: 9 parts dH20) before being stained for intracellular antibodies (Table 2.9) diluted in 50µl Permeabilisation buffer, for 30 minutes at RT. Cells were then washed twice with Permeabilisation buffer, then resuspended in FACs buffer and transferred to FACs tubes for flow cytometry analysis (Section 2.6.5).

2.6.3 Intracellular Fixation and Staining with Retention of GFP

The fixation described in Section 2.6.3 resulted in loss of intracellular reporters such as GFP, therefore for analysis of Rag2-GFP alongside intracellular proteins (e.g. Foxp3 and Ki67), an alternative fixation process, adapted from Heinen *et al*[317], was utilised. Here following initial cell surface staining (Section 2.6.2), cells were resuspended in 200µl of 2% formaldehyde in $Mg^{-}Ca^{-}$DPBS (prepared from 10% neutral-buffered formalin (Sigma-Aldrich) diluted 1:1 in $Mg^{-}Ca^{-}$DPBS) for 60 minutes at RT. Cells were then washed twice, with Permeabilisation buffer (eBioscience) as detailed in Section 2.6.3. Cells were then stained for intracellular antibodies (Table 2.9) diluted in 100µl Permeabilisation buffer, overnight at 4°C. Cells were then washed

twice with Permeabilisation buffer, then resuspended in FACs buffer and transferred to FACs tubes for flow cytometric analysis (Section 2.6.5).

2.6.4 Flow Cytometric Analysis

Samples were run on the BD LSR Fortessa flow cytometer, using the BD FACSDiva software for initial data collection. Voltages for each detection channel and compensation between fluorochromes were set on the basis of single colour staining controls. Negative staining controls, such as isotype controls or fluorescence minus one (FMO) controls, were used to determine positive staining. Cells were initially pre-gated on forward scatter and side scatter gates, followed by forward scatter-height and forward scatter-area to discriminate viable cells and single cells, respectively. Analysis of exported Flow Cytometry Standard files was performed using FlowJo (version 10.6.1). Where MFI was measured, this was taken as the median fluorescent intensity.

Table 2. 7 Primary Extracellular Antibodies Used for Flow Cytometry Immunolabeling

Specificity	Clone	Conjugate	Working Dilution	Supplier
CD4	RM4-5	BV711	1:200	BioLegend
CD8	53-6.7	BV785	1:200	BioLegend
TCRβ	H57-597	APC-eFluor 780	1:200	eBioscience
CD25	PC61	BV650	1:2000	Biolegend
	PC61.5	PE Cy7	1:2000	eBioscience
	3C7	BV421	1:200	Biolegend
CD62L	MEL-14	APC	1:2000	eBioscience
	MEL-14	PE Cy7	1:2000	eBioscience
CD44	IM7	PercpCy5.5	1:200	Biolegend
CD69	H1.2F3	PercpCy5.5	1:200	eBioscience
CCR7	4B12	PE	1:100	eBioscience
CCR6	29-2L17	BV421	1:200	Biolegend
CD127	A7R34	APC	1:200	eBioscience
CD122	TM-b1	PE Cy7	1:100	eBioscience
ICOS	15F9	Biotin	1:100	eBioscience
PD1	29F.1A12	BV421	1:200	Biolegend

GITR	DTA-1	APC	1:200	eBioscience
CD73	TY/11.8	BV605	1:800	Biolegend
CD24	M1/69	PercpCy5.5	1:1000	eBioscience
Qa2	695H1-9.9	Biotin	1:200	Biolegend
CD55	RIKO-3	PE	1:400	Biolegend
S1PR1 Monoclonal	713412	-	1:10	R&D Systems
Rat IgG_{2a}	MRG 2a-83	Biotin	1:100	Biolegend
CD45	30-F11	APC Cy7	1:800	eBioscience
	30-F11	PE Cy7	1:400	eBioscience
CD45.1	A20	PE Cy7	1:400	eBioscience
CD45.2	104	AF700	1:100	eBisocience
Epcam	G8.8	PerCpCy5.5	1:2000	eBioscience
UEA	-	Biotin	1:12000	Vector Laboratories
Ly51	6C3	APC	1:1000	Biolegend
MHC II	M5/114.15.2	AF700	1:2000	eBioscience
CD80	16-10A1	BV605	1:800	Biolegend

Table 2. 8 Secondary Antibodies Used for Flow Cytometry Immunolabeling

Specificity	Conjugate	Working Dilution	Supplier
Streptavidin	PE Cy7	1:1500	eBioscience

Table 2. 9 Primary Intracellular Antibodies Used for Flow Cytometry Immunolabeling

Specificity	Clone	Conjugate	Working Dilution		Supplier
			ebioscience Fixation	2% Formaldehyde Fixation	
Foxp3	FJK-16s	PE-eFluor610	1:200	1:100	eBioscience
Ki67	SolA15	PE Cy7	1:2000	1:500	eBioscience
BRDU	MoBU-1	APC	1:50	-	Invitrogen
AIRE	5H12	FITC	1:1000	-	eBioscience

2.7 Bromodeoxyuridine (BRDU) Proliferation Analysis

To detect actively proliferating cells, we used BRDU labelling and subsequent detection by flow cytometry. For this approach, 10mg/ml BRDU stock was prepared (under sterile

conditions) by reconstituting 100mg BRDU powder (Sigma-Aldrich) in 9.9ml pre-warmed sterile $Mg^{-}Ca^{-}$DPBS for 1 hour at 37°C. Aliquots of 10mg/ml BRDU stock were stored at -80°C for subsequent administration.

2.7.1 *In Vivo* BRDU Labelling

For *in vivo* labelling of proliferating cells, 1.5mg/mouse of BRDU was administered by intraperitoneal injection and mice were culled and thymocytes isolated (per Section 2.4.1) 1 hour later.

2.7.2 *In Vitro* BRDU Labelling

To label proliferating cells from neonatal tissues or FTOCs an *in vitro* BRDU labelling approach, post lymphocyte isolation and counting (Sections 2.4-2.5), was adopted. Regarding neonatal tissues, $5x10^6$ cells were resuspended in 5ml RF10 with 10μg/ml BRDU in a 6 well-plate (Corning) for 1 hour at 37°C. Similarly, lymphocytes isolated from FTOCs were labelled with BRDU by resuspending them in 1.5ml of RF10 with 10μg/ml BRDU in a 1.5ml Eppendorf tube for 1 hour at 37°C. After 1 hour, the suspension was then centrifuged (1400rpm, 4 minutes) then washed by resuspension in RF10 and centrifuged as before.

2.7.3 Detection of BRDU with Foxp3

To detect BRDU with Foxp3, a method adapted from Zabransky *et al*[318] was utilised. Thymocytes were first stained for surface markers as described in Section 2.6.1. Samples were then resuspended in 150μl of Fixation/Permeabilisation solution (Section 2.6.3) for 16 hours at 4°C. The samples were then washed with Permeabilisation buffer (Section 2.6.3), twice. Samples were then resuspended in 100μl of diluted DNAse (30μl of 1mg/ml DNAse stock

(BrdU Flow Kit, BD Pharmingen), 70µl $Mg^{2+}Ca^{2+}$DPBS) and incubated at 37°C for 1 hour. Samples were then washed with Permeabilisation buffer, twice, and stained for Foxp3 and BRDU (concentrations detailed in Table 2.9) in 100µl perm buffer, for 1 hour at RT. Samples were then washed twice and resuspended in FACs buffer and transferred to FACs tubes for flow cytometric analysis (Section 2.6.5).

2.8 Isolation of Cell Populations by Cell Sorting

Fluorescence activated cell sorting was used to isolate pure populations of cell subsets for staining, RNA sequencing (RNAseq, Section 2.12), culture (Section 2.10) and transfer (Section 2.11) purposes. For cell culture and cell transfer experiments, but not RNAseq analysis or staining of individual mice, cells from multiple mice were pooled together for cell sorting, to ensure that a sufficiently sized sorted population was recovered. In addition, for cell culture and cell transfer experiments, sample preparation, cell sorting and subsequent sample handling were all performed under sterile conditions.

2.8.1 Preparation of Sample for Cell Sorting

Samples were subject to cell surface labelling as described in Section 2.6, except all cells recovered from processing were stained. Accordingly, all staining volumes were increased so that cells were stained in 50µl buffer per $5x10^6$ cells. In addition, to reduce the number cells which had to be sorted, samples were enriched for the population of interest prior to cell sorting through one of two enrichment approaches.

2.8.1.1 Enrichment of Populations Prior to Cell Sorting

2.8.1.1.1 CD8 Depletion

With the exception of cells sorted for RNAseq analysis, thymic and splenic SP4 subpopulations where initially enriched for, by depletion of $CD8^+$ cells using mouse CD8a (Ly-2) MicroBeads (Miltenyi Biotech). As per manufacturer's instructions isolated and counted thymocytes were resuspended in 90μl MACs buffer per 10^7 total cells with 10μl vortexed CD8α microbeads per 10^7 cells and incubated for 10 minutes at 4°C. Samples were then passed through primed LS MACs separation columns (Miltenyi Biotec), and the run-off from the column (containing the $CD8^-$ cells) collected in 15ml Falcon tubes, centrifuged (1400rpm, 4 minutes) and resuspended in FACs buffer. Where multiple mice were used samples were pooled before being counted (Section 2.5.1) and stained (Section 2.8.1).

2.8.1.1.2 Rag-GFP Enrichment

Splenocytes sorted for RNAseq analysis were initially enriched for RTEs by performing a GFP^+ enrichment sort. Here isolated stained splenocytes (Section 2.8.1) were resuspended in RF10 and subject to an enrichment sort on the BD FACSAria Fusion to collect Rag-GFP^+ cells. Cells were collected in 15ml Falcon tubes containing RF10, and subsequently collected tubes were centrifuged (1400rpm, 4 minutes) and pooled.

2.8.2 Purity Cell Sorting

Following enrichment and cell surface staining, samples were resuspended in RF10, and filtered through a 30μm pre-separation filter (Miltenyi Biotec) into a polypropylene FACS tube. Purity cell sorting was performed using the BD FACSAria Fusion. Depending on the anticipated cell number recovery, sorted cells were collected into 1.5ml Eppendorfs, FACs tubes or 15ml Falcon tubes each of which contained a small volume of RF10 to prevent shear damage to the

sorted cells. A small aliquot of the sorted population was taken to ascertain the purity, via comparison to a pre-sorted sample run on the BD LSR Fortessa.

2.9 Fetal Thymic Organ Cultures (FTOCs)

FTOCs were utilised for analysis of both lymphocyte and stromal populations. The initial FTOC setup for both these purposes was broadly similar, except that for FTOC setup to analyse stromal (but not lymphocyte) populations, 9mM 2-deoxyguanosine (dGuo) stock (Sigma-Aldrich) was added to the cultures at final concentration of 1.35mM as indicated.

All work was performed under sterile conditions within a laminar flow cabinet. Prior to FTOC setup, 0.8μm nucleopore filters (Millipore) and anti-wrap sponges (Medipost Ltd) cut into approximately $1cm^2$ squares, were sterilised by boiling (separately) for 30 minutes or 2 hours, respectively. After boiling these were left to air dry in a laminar flow cabinet for later use.

On the day of FTOC setup, embryonic thymic lobes were dissected (Section 2.3). Then cultures were setup by adding DMEM to a Petri dish and placing a pre-prepared anti-wrap sponge square into the media, before finally positioning a nucleopore filter atop the sponge. Thymic lobes were then transferred onto these filters using a mouth-controlled sterile glass pipette. The embryonic age/size of the lobes dictated how many were added to a single filter, up to 6 lobes were added for ages E14-E15 whereas up to 4 lobes were added for ages E16-E17. Depending on the number of lobes recovered different sizes of petri-dish were used, either 35mm or 90mm petri-dish (Sterilin). 35mm petri-dishes held 1.8ml DMEM (+/- dGuo) to which one sponge/filter were added whereas 90mm petri-dishes held 4ml DMEM (+/- dGuo) to which two sponge/filter were added. Following setup of all embryonic lobes petri dishes were

placed inside a sterile humidified chamber at 37°C, 10% CO_2 for 30 minutes (to normalise the medium pH to between 7.2-7.4) before the chamber was sealed and incubated at 37°C for between 4-7 days of culture, as indicated.

2.9.1 FTOC for Analysis of Lymphocyte Populations

To investigate intrathymic proliferation of lymphocyte populations with BRDU, FTOC were cultured for between 4-7 days (as indicated). 4 thymic lobes were pooled together for BRDU lymphocyte analysis (Section 2.7).

2.9.2 FTOC for Analysis of Stromal Populations

Following 5-7 days culture with dGuo, filters were transferred to a petri-dish containing RF10 and any lobes that did not detach were gently pushed off. For those lobes not treated with anti-RANK (R&D Systems), stromal populations were then isolated (Section 2.4.4). When treating with anti-RANK, lobes were set-up in new cultures consisting of a centre well culture dish (Falcon) with the outer section filled with 2ml $Mg^{2+}Ca^{2+}$DPBS and the inner section containing 200µl DMEM +/- anti-RANK at a final concentration of 10µg/ml. A nucleopore filter was then placed onto the DMEM and thymic lobes transferred to the filter as previously described. Following setup of all embryonic lobes, culture dishes were placed inside a sterile humidified chamber and cultured for 4-5 days. After which stromal populations were isolated (Section 2.4.4).

2.9.3 Blockade of Common γ Chain Receptor Signalling in FTOC

FTOCs were also used to investigate the impact of blockade of γ_c family members on intrathymic proliferation. Here E17 FTOC were cultured as per Section 2.9.1, for 4 days. On D4

of culture the lobes were setup in new cultures in centre well culture dishes (as described in Section 2.9.2 except the inner well) where each FTOC condition consisted of 4 embryonic lobes. For treated FTOC, the inner section contained 200µl of DMEM + either purified anti-CD25 or anti-IL-15/IL-15R Complex antibodies (Table 2.10) at a final concentration of 20µg/ml. Control FTOC received the appropriate isotype control (Table 2.10) at the same concentration. FTOCs were then cultured for 24 hours after which they were harvested for BRDU lymphocyte analysis (as per Section 2.9.1).

Table 2. 10 Purified Functional Grade Antibodies Used for Signalling Blockade Experiments

Antibody	Clone	Supplier
Biolegend Ultra-LEAF™ Purified anti-mouse CD25	PC61	BioLegend
Ultra-LEAF™ Purified Rat IgG1, λ Isotype Control (control for Anti-CD25)	G0114F7	BioLegend
Anti-IL-15/IL-15R Complex, Functional Grade	GRW15PLZ	eBioscience
Rat IgG1 kappa Isotype Control, Functional Grade (control for Anti-IL-15/IL-15R Complex)	eBRG1	eBioscience

2.10 Reaggregate Thymic Organ Cultures (RTOCs)

RTOCs represent an *in vitro* 3D thymic microenvironment, which can be used to assess thymic development of a specific thymocyte population, under malleable thymic stromal conditions. Within this study RTOCs were used to assess precursor potential of $CD62L^{hi}$ *de novo* thymic Tregs. RTOC generation required sorted $CD62L^{hi}$ *de novo* thymic Treg (sorted as per Section 2.8) and thymic stroma, sourced from FTOCs treated with dGuo and with/without anti-RANK (Section 2.9). Under sterile conditions, the sorted lymphocytes (numbers varied between 20-100x10^3 cells owing to the variable sort recovery) were combined with the stroma (approximately 500x10^3) in a 1.5ml Eppendorf tube. This mixture was then centrifuged (1400rpm, 4 minutes), the pellet resuspended in DMEM then centrifuged as before. The supernatant was removed to leave a minimal volume of liquid. The pellet was vortexed to

generate a slurry which was drawn up using a mouth-controlled sterile glass pipette. Under a dissection microscope the slurry was dropped onto the centre of a 0.8μm Whatman filter atop an anti-wrap sponge (both sterilised) in DMEM. This culture setup was as described in Section 2.9, except here each filter held maximum one RTOC. RTOC were then cultured akin to FTOC (Section 2.9) for 3-4 days, before lymphocytes were isolated (Section 2.4.2).

2.11 Pilot Colitis Model

To assess the functional ability of Tregs to control inflammatory responses previous studies have utilised an adoptive transfer colitis model[189,319,320]. Here non-Treg effector cells are transferred to T-cell deficient hosts, in the presence or absence of Treg or different Treg populations. Hosts receiving only non-Tregs develop colitis, and the prevalence/severity of this disease can be compared to those hosts which also received Treg populations, to gain insight into the co-transferred Tregs regulatory function. We therefore performed a pilot study, adapted from previous methodology[189,319,320], to assess this model as an *in vivo* system of Treg function.

2.11.1 Colitis Model Setup

The populations to be transferred were prepared by sorting simultaneously $CD4^+CD8^-$Foxp3-RFP^+ and $CD4^+CD8^-$Foxp3-RFP^- splenocytes from Foxp3-RFP mice (Section 2.8). Samples were counted post-sort to calculate the cell numbers to be resuspended in Mg^-Ca^-DPBS PBS for transfer into *Rag2*$^{-/-}$ hosts. Hosts either received $5x10^5$ $CD4^+CD8^-$Foxp3-RFP^- splenocytes alone or with $1x10^5$ $CD4^+CD8^-$Foxp3-RFP^+, administered by intravenous injection in a carrier volume of 200μl. Host were weighed immediately prior to transfer to record their starting weight. Following transfer *Rag2*$^{-/-}$ hosts were monitored closely by BMSU staff and weighed at regular

intervals. After 4 weeks *Rag2*$^{-/-}$ were blood samples were collected (by saphenous bleed) and analysed by flow cytometry to ensure that transferred populations had been maintained. Hosts continued to be monitored and ultimately *Rag2*$^{-/-}$ hosts which received CD4^{+}CD8^{-}Foxp3-RFP^{-} splenocytes alone had to be culled for welfare reasons. When this endpoint occurred a *Rag2*$^{-/-}$ host which had received CD4^{+}CD8^{-}Foxp3-RFP^{-} and CD4^{+}CD8^{-}Foxp3-RFP^{+} splenocytes was also culled for direct comparative analysis.

2.11.2 Assessment of Colitis Model Endpoint

To assess the disease outcome of the model several observations were made. Firstly prior to cull, *Rag2*$^{-/-}$ mice were weighed a final time and this, along with all weights recorded throughout the timecourse, were used to calculate the percentage weight change. The colon was dissected and with cecum attached, then measured and imaged. The cecum was then removed for further dissection of the colon. The colon and the spleen were then processed for flow cytometry analysis (Sections 2.3, 2.4 and 2.6).

2.12 RNA Sequencing (RNAseq)

The following sections contains technical detail to accompany the descriptive overview of the generation and processing of RNAseq datasets described in Section 5.2.1.

2.12.1 Single Cell RNAseq (scRNAseq)

It should be noted that while one scRNAseq dataset was generated by sequencing (termed total SP4 dataset) this dataset was subsequently subsetted, generating two additional datasets termed Treg and Tconv scRNAseq datasets, further detailed in Section 5.2.1.

2.12.1.1 Sample Generation

Splenocytes were isolated from a single Rag-GFP mouse and two populations, Live $CD4^+CD8^-$ Rag-GFP^- mature SP4 T-cells and Live $CD4^+CD8^-$Rag-GFP^+ SP4 RTEs, were sorted simultaneously (Section 2.8). Samples were sorted into LoBind eppendorfs (Fisher), and stored on ice while counts and purity checks were performed. Cells were then resuspended at 1000 cells/μl in RF10 and taken for immediate sequencing.

2.12.1.2 Sample Sequencing

Sequencing was performed by Genomics Birmingham. Approximately 8000 live cells of the sorted Rag-GFP^+ and Rag-GFP^- were loaded separately on to the Chromium Controller (10x Genomics) for library generation using Chromium Single Cell 3' Library and Gel Bead Kit v2. Subsequently the libraries were pooled and sequenced on an Illumina NextSeq 500.

2.12.1.3 Bioinformatics Processing

Sequencing data was aligned and quantified using **cellranger mkfastq** and **cellrangercount** from the CellRanger software package (version 3.1.0) using a standard reference murine genome (GRCm38). This was completed in accordance with default parameters with the exception of quantification by **cellrangercount** where the option **force-cells 4000** was included to force the software to return 4000 cells for each sample.

Subsequent processing and analysis was performed in R studio (version 1.2.5019, with R version 3.6.1). Analysis was primarily conducted using the Seurat package[321] with additional packages used for subsequent specific analysis (Table 2.11). Unless otherwise stated processing steps and function parameters are set according to standard Seurat processing recommendation as described in the package associated vignettes. Initial quality control (QC)

steps removed cells with >5% mitochondrial counts and <700 unique genes. The data was the normalised, 2000 highly variable features identified, then all features were scaled. Principal component analysis (PCA) was then performed using the selected highly variable features. The elbow plot method was then used to determine the number of PCs (dims) used as input for clustering (by shared nearest neighbour) and non-linear dimensionality reduction by t-distributed stochastic neighbour embedding (tSNE), the variable dims and res values supplied to these Seurat functions for the three datasets are detailed in Table 2.12.

Differentially expressed genes were identified using the Seurat function **FindMarkers** with default settings. Where multiple clusters are compared only the positive markers were reported. Where RTE and non-RTE are compared the two populations were defined according to their original sorted identity. Here statistical significance was determined using the default Wilcoxon Rank Sum test, and p-values were adjusted by bonferroni correction (adjusted p-values <0.05 were considered significant).

2.12.2 Bulk RNAseq

2.12.2.1 Sample Generation

Splenocytes were isolated from a single Rag-GFP mouse and two populations, Live $CD4^+CD8^-CD62L^+$Rag-GFP^- naïve mature SP4 T-cells and Live $CD4^+CD8^-CD62L^+$Rag-GFP^+ naïve SP4 RTEs, were sorted simultaneously (Section 2.8). Samples were sorted into LoBind eppendorfs, and stored on ice while counts and purity checks were performed. Samples were then centrifuged (1400rpm, 4 minutes), the supernatant removed and the pellet snap frozen on dry ice. Samples were stored at -80°C prior to sequencing.

2.12.2.2 Sample Sequencing

Sequencing was performed by Source Bioscience. The cDNA library was prepared using the NEBNext Ultra II Directional kit (New England Biolabs). Sequencing was then performed on Illumina HiSeq 4000, 75bp paired end.

2.12.2.3 Bioinformatics Processing

Reads were mapped with HISAT2 (version 2.1.0) to a standard reference murine genome (GRCm38). The subsequent SAM files were then converted to BAM files using Samtools (version 0.1.8) then the reads mapping to exons were counted for each annotated gene using LiBiNorm (version 2.0).

Subsequent processing and analysis was performed in R studio primarily using the DESeq2 package[322], with additional packages used for subsequent specific analysis (Table 2.11). Unless otherwise stated processing steps and function parameters are set according to standard DESeq2 processing recommendation as described in the package associated vignettes. QC steps resulted in the removal of 1 paired RTE and non-RTE outlier samples and 47 B-cell genes. The Deseq2 function **DESeq** was used to perform differential expression analysis with default settings. Here statistical significance was determined using the default Wald test, and p-values were adjusted by Benjamini-Hochberg algorithm (adjusted p-values <0.05 were considered significant). PCA was performed on rlog transformed data generated by DESeq analysis using the function **prcomp** with default settings.

Table 2. 11 R Packages Used in RNAseq Analysis

Package	Version	Analysis	Description of Package Use
Seurat	3.2.2	scRNAseq	Pre-processing, clustering, dimensional reduction and differential gene expression analysis of scRNAseq data. Visualisation of analysed scRNAseq data via dimensional reduction plots, heatmaps and dotplots
DESeq2	1.26.0	Bulk RNAseq	Pre-processing and differential gene expression analysis of bulk RNAseq data
stats	3.6.3	scRNAseq and Bulk RNAseq	The function prcomp was used to perform PCA on data generated by DESeq analysis
			The function cor.test was used to test for correlation of fold change data generated by DESeq and Seurat analysis
Enhanced-Volcano	1.4.0	Bulk RNAseq	Produce Volcano Plots from data generated by DESeq analysis
pheatmap	1.0.12	Bulk RNAseq	Produce Heatmaps from data generated by DESeq analysis
ggplot2	3.3.3	scRNAseq and Bulk RNAseq	Generic plotting, used to generate bar plots, histogram plots and scatter plots from data generated by DESeq and Seurat analysis
VennDiagram	1.6.20	scRNAseq	Produce Volcano Plots from data generated by Seurat analysis

Table 2. 12 Parameters Used for Seurat Clustering of scRNAseq Data

scRNAseq Seurat Object	findNeighbours dims	findClusters res
Total SP4 scRNAseq dataset	1:13	0.5
Tconv dataset (Subsetted from total SP4 scRNAseq dataset)	1:12	0.5
Treg dataset (Subsetted from total SP4 scRNAseq dataset)	1:13	0.6

2.13 Statistical Analysis

For graphical and statistical analysis of quantifiable data, GraphPad Prism (version 8.2.1) software was used. The statistical test used depended on the context of the data. Analysis which compared two groups from the same mouse were analysed with a paired statistical test, whereas analysis which compared independent groups of mice were analysed with an unpaired statistical test. Normality tests were used to ascertain whether data was normally distributed. Where data was normally distributed a parametric test was used, otherwise a non-parametric test was used. For data analysis of two groups a Student's T test (or non-parametric equivalent) was used. For data analysis of three or more groups for the same parameter a One-Way ANOVA, with multiple corrections (or non-parametric equivalent) was used. The exact type of test used is noted in the corresponding figure legend. The outcome of these statistical tests was considered statistically significantly if the p-value <0.05. This significance is noted within the figure as: ns >0.05 *<0.05, **<0.01, ***<0.001,****<0.0001.

CHAPTER THREE:
RE-EXAMINING *DE NOVO* THYMIC TREG DEVELOPMENT

3.1 Introduction

Heterogeneity within the peripheral Treg population seems critical to its ability to respond appropriately to different types of inflammatory responses across disparate tissue sites. While peripheral Tregs can differ greatly in their phenotype, localisation and function it has been proposed that fundamentally the population may be broadly divided as $CD62L^{hi}CCR7^{hi}CD44^{lo}$ cTregs and $CD62L^{lo}CCR7^{lo}CD44^{hi}$ eTregs[85,323]. Here cTregs are believed to give rise to eTregs, which then undergo further differentiation to a more specialised phenotype[85,323]. Interestingly diversification of Tregs has been proposed to stem solely from the periphery, as initial studies identified thymic Tregs as homogenous, containing only cTreg[85]. However more recently two additional distinct Treg subsets, $CD25^{hi}PD1^{hi}GITR^{hi}$ $Triple^{hi}$ and $CD25^{lo}PD1^{lo}GITR^{lo}$ $Triple^{lo}$ Tregs, have been identified within the developing thymic Treg pool[107]. Importantly these Treg subsets were also identified within the periphery, suggesting that historically the contribution made by thymic Tregs towards peripheral heterogeneity may have been underappreciated. These findings also raise questions about how and when heterogeneous Tregs are generated during thymic development.

Broadly, thymic Tregs arise through lineage divergence of autoreactive SP4 thymocytes in a process that is heavily dependent upon the thymic medulla. However, the exact pathway of thymic Treg development is less clear. Initial commitment to the Treg lineage is fairly well characterised and is believed to proceed via one of two precursor populations, defined as $CD25^{+}Foxp3^{-}$[188] and $CD25^{-}Foxp3^{+}$[182]. However, some controversy exists regarding the relative roles of the two precursors in the Treg developmental pathway, with disagreement over which represents the major Treg precursor population[187,190]. Interestingly recent work suggests that both precursor populations are required to generate a Treg population with a

diverse TCR repertoire. This was first suggested by work in Nur77-GFP mice identifying differing TCR affinity between thymic Treg precursors[187,189]. Furthermore, the TCR repertoires of $CD25^{+}Foxp3^{-}$ and $CD25^{-}Foxp3^{+}$ precursors, while themselves distinct, individually overlapped with the Treg TCR repertoire, suggesting the precursors separately contribute to overall Treg diversity[189]. Interestingly differing Treg TCR affinity is heavily implicated in Treg heterogeneity, being a key driver of the divergence of both $Triple^{hi}$ and $Triple^{lo}$ Tregs and the differentiation of eTregs. Furthermore, Tregs derived from the different precursors differed functionally, with only $CD25^{+}Foxp3^{-}$ derived Treg protective against experimental autoimmune encephalitis[189]. Perhaps hinting that Treg heterogeneity may in part be initiated at the precursor stage.

Following commitment to the Treg lineage it remains unclear whether Tregs undergo further thymic development. In contrast, Tconv thymocytes are known to undergo a post-selection maturation from an immature $CD69^{+}CD62L^{-}$ phenotype to a mature $CD69^{-}CD62L^{+}$ phenotype, associated with increased competency and egress ability[191,324]. Therefore, raising the question of whether Tregs undergo their own phenotypic differentiation, and whether this period could coincide with the appearance of heterogeneous subsets.

Overall this highlights a lack of detail regarding the exact process of thymic Treg development, particularly with regard to the generation of heterogeneous Treg subsets. Furthermore, previous investigations into Treg development may have been confounded due to the unknowing inclusion of mature Tregs in the analysis, as recent observations made using Rag-GFP mice identifies that the thymic Treg pool comprises both *de novo* developing thymic Tregs and mature Tregs[234,235].

We therefore decided to re-examine *de novo* thymic Treg development to gain further insight into how the thymus may contribute to peripheral Treg diversity. We identified heterogeneity within the thymic Treg compartment, which we subsequently characterised and studied within the wider context of the developing Treg lineage. Through our investigations we aimed to understand the programme of heterogeneous Treg development within the thymus, and the role of the thymic microenvironment in directing this process.

3.2 Results

3.2.1 Heterogeneous Thymic Treg Development

To ensure that our investigation of *de novo* thymic Treg development was not contaminated by mature thymic Tregs we used Foxp3-RFPxRag-GFP mice. As outlined in Figure 3.1.A, the Foxp3-RFPxRag-GFP mouse combines two separate reporter systems, Rag-GFP and Foxp3-RFP which inform on cell age and identity respectively. In brief, the Foxp3-RFP reporter identifies Foxp3$^+$ cells as RFP$^+$ and hence in combination with CD25 can be used to distinguish Tregs and Tconvs. While Rag-GFP functions as a molecular timer of T-cell development (discussed in Section 1.2.4), being maximal in DP thymocytes before decreasing with increasing age, meaning that developing SP4 thymocytes and RTE, but not mature SP4 T-cells, are Rag-GFP$^+$. Thus, in combination *de novo* Tregs are Rag-GFP$^+$Foxp-RFP$^+$. To ensure stringency in identification of *de novo* cells by flow cytometry analysis we used the level of Rag-GFP present in DP thymocytes to define Rag-GFP$^+$, as the entire population should be Rag-GFP$^+$, and a non-fluorescent WT control to define the Rag-GFP$^-$ level (Figure 3.1.B). When we applied this system to SP4 thymocytes in an adult mouse we determined that we could identify Tregs and Tconvs as CD25$^+$Foxp3-RFP$^+$ and CD25$^-$Foxp3-RFP$^-$ SP4 thymocytes (pre-gated as CD4$^+$CD8$^-$ TCRβ^+) respectively. Analysis of Rag-GFP expression within these populations confirmed

previous observations[234,235] that the majority of thymic Treg are Rag-GFP$^-$ and hence mature, in contrast only a small minority of Tconv thymocytes were Rag-GFP$^-$ (Figure 3.1.B-C). Thereby demonstrating the importance of identifying and considering only Rag-GFP$^+$ thymic Treg in our developmental analysis.

We therefore set out to characterise adult *de novo* thymic Treg population using flow cytometry analysis, defining *de novo* Tregs as CD4$^+$CD8$^-$TCRβ^+Rag-GFP$^+$CD25$^+$Foxp3-RFP$^+$ (Figure 3.2.A). We observed that *de novo* thymic Tregs were heterogeneous regarding CD62L expression and could be divided into CD62L^{hi} and CD62L^{lo} subsets (Figure 3.2.B). Interestingly differing levels of CD62L are a key distinguisher of the previously identified cTreg and eTreg subsets, which are CD62L^{hi} and CD62L^{lo} respectively. However there were some discrepancies between the phenotype of the CD62L^{hi} and CD62L^{lo} thymic Treg we observed and cTregs and eTregs. Firstly, cTregs and eTregs have been identified as CCR7^{hi} and CCR7^{lo} respectively whereas we detected high expression of CCR7 by both CD62L^{hi} and CD62L^{lo} thymic Tregs (Figure 3.2B). Furthermore, cTregs and eTregs are primarily identified as CD62L^{hi}CD44^{lo} and CD62L^{lo}CD44^{hi} which we can roughly identify within the bulk splenic Treg population (Figure 3.2.C). However, within the thymus both CD62L^{hi} and CD62L^{lo} Tregs express high levels of CD44, such that applying the same gating of splenic cTreg to thymus, results in the loss of a large proportion of CD44^{hi}CD62L^{hi} Tregs (Figure 3.2.D). Overall this suggests that the CD62L^{hi} and CD62L^{lo} thymic Treg we observed are similar but distinct from previously defined cTregs and eTregs.

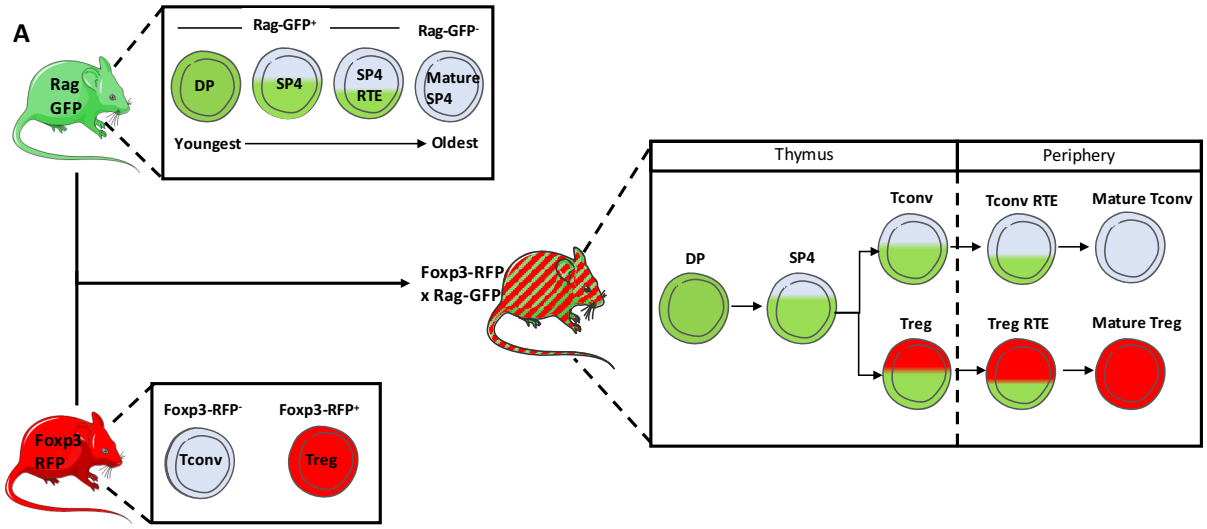
A
Rag GFP
Rag-GFP+
Rag-GFP-
DP
SP4
SP4 RTE
Mature SP4
Youngest
Oldest
Foxp3-RFP x Rag-GFP
Thymus
Periphery
Tconv
Tconv RTE
Mature Tconv
DP
SP4
Treg
Treg RTE
Mature Treg
Foxp3 RFP
Foxp3-RFP-
Foxp3-RFP+
Tconv
Treg

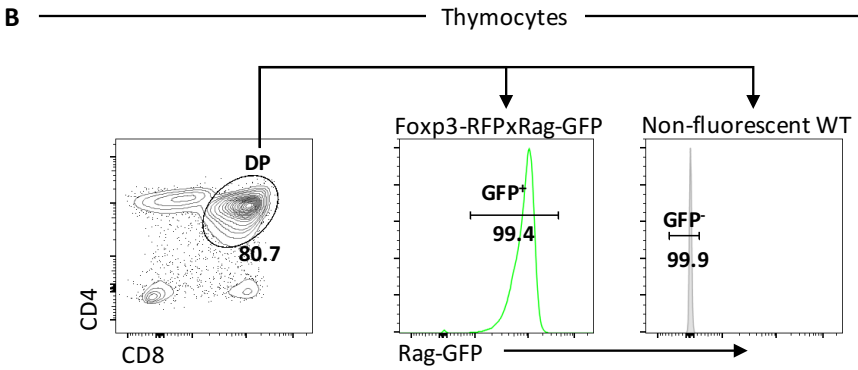
B
Thymocytes
Foxp3-RFPxRag-GFP
Non-fluorescent WT
DP
80.7
CD4
CD8
GFP+
99.4
GFP-
99.9
Rag-GFP

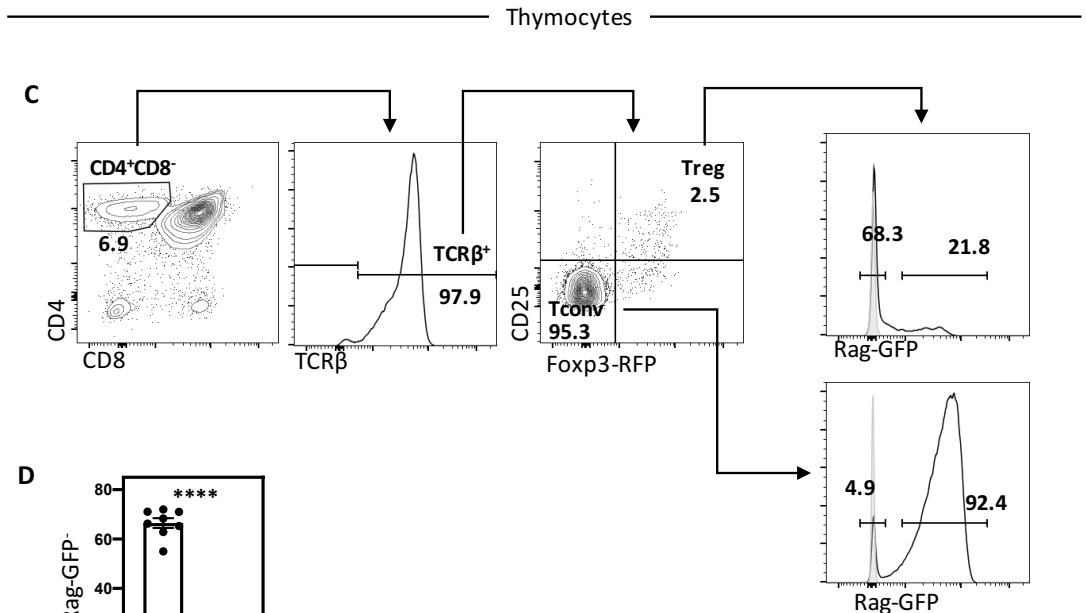
Thymocytes
C
CD4+CD8-
6.9
CD4
CD8
TCRβ+
97.9
TCRβ
Treg
2.5
Tconv
95.3
CD25
Foxp3-RFP
68.3
21.8
Rag-GFP
4.9
92.4
Rag-GFP

D
****
% Rag-GFP-
80
60
40
20
0
Treg
Tconv

Figure 3.1 The Foxp3-RFPxRag-GFP Reporter Confirms the Thymic Treg Population Consists of *De Novo* and Mature Tregs

Identification and characterisation of *de novo* and mature thymocyte populations in Foxp3-RFPx Rag-GFP adult (8-12 weeks) mice. All data representative of n=8 across 6 independent experiments.

(A) Diagram depicting the generation of Rag-GFPxFoxp3-RFP mice and the fluorescent labelling this system offers. The of Rag-GFPxFoxp3-RFP mouse is generated by crossing Rag-GFP and Foxp3-RFP single reporters. Top left, depicts the how the Rag-GFP mouse acts as a reporter of T-cell age. GFP is produced when Rag is expressed by double positive (DP) thymocytes. Rag gene expression and hence new GFP production is then terminated. The accumulated GFP within the thymocyte then undergoes exponential decay with time, during which the thymocyte develops and ultimately exits the thymus to become a RTE until Rag-GFP is lost completely and the cell is termed mature. Thus *de novo* and mature SP4 T-cells are discriminated as Rag-GFP^{+} and Rag-GFP^{-} respectively. In addition because GFP level is inversely proportional to cell age, the level can be used to compare the relative ages of *de novo* cells. Bottom left, shows the Foxp3-RFP mouse as a reporter of T-cell identity. Here RFP is expressed when the Foxp3 gene is expressed by a cell and thus can be used (in conjuncture with other markers) to discriminate Treg identity. The combination of these two reporters, Foxp3-RFPxRag-GFP enables simultaneous discrimination of both T-cell age and identity.

(B) Gating strategy used to define Rag-GFP^{+} (*de novo*) and Rag-GFP^{-} (mature) T-cell populations. CD4^{+}CD8^{+} DP thymocytes were gated on in both Foxp3-RFPxRag-GFP and WT (non-fluorescent) mice. In the Foxp3-RFPxRag-GFP sample the level of Rag-GFP expression by the DP thymocytes was then used to define the Rag-GFP^{+} population. Whereas in the WT sample the level of Rag-GFP expression by the DP thymocytes was then used to define the Rag-GFP^{-} population. Gating strategy presented as representative FACs plots from an adult (8-12 weeks) including gate title and percentage of cells within the gate given underneath.

(C) Identification of *de novo* (Rag-GFP^{+}) and mature (Rag-GFP^{-}) SP4 (CD4^{+}CD8^{-}TCRβ^{+}) thymocyte populations. Initial gating strategy used to define SP4 thymocytes as CD4^{+}CD8^{-}TCRβ^{+} which is then further subdivided on the basis of CD25 and Foxp3 to give the SP4 populations: Treg (CD25^{+}Foxp3-RFP^{+}) and Tconv (CD25^{-}Foxp3-RFP^{-}). Using the Rag-GFP gating depicted in **(A)** the Treg and Tconv can then be divided into Rag-GFP^{+} (*de novo*) and Rag-GFP^{-} (mature) populations. Data presented as representative FACs plots including gate title and percentage of cells within the gate given underneath.

(D) Quantification of the percentage of Rag-GFP^{-} (mature) cells within Treg (CD4^{+}CD8^{-}TCRβ^{+}CD25^{+}Foxp3-RFP^{+}) and Tconv (CD4^{+}CD8^{-}TCRβ^{+}CD25^{-}Foxp3-RFP^{-}) thymocytes. Statistical analysis performed using a paired t-test where, where **** $p<0.0001$.

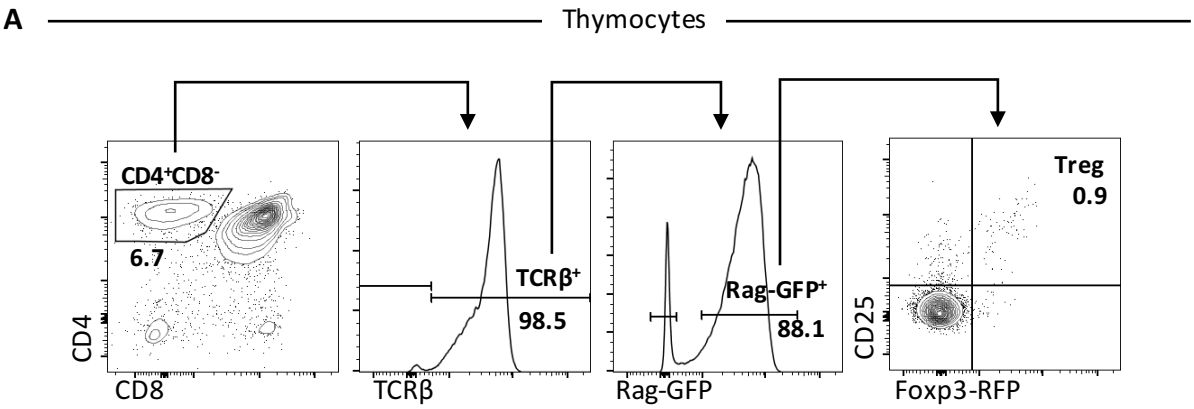
A
Thymocytes
CD4+CD8-
6.7
CD4
CD8
TCRβ+
98.5
TCRβ
Rag-GFP+
88.1
Rag-GFP
Treg
0.9
CD25
Foxp3-RFP

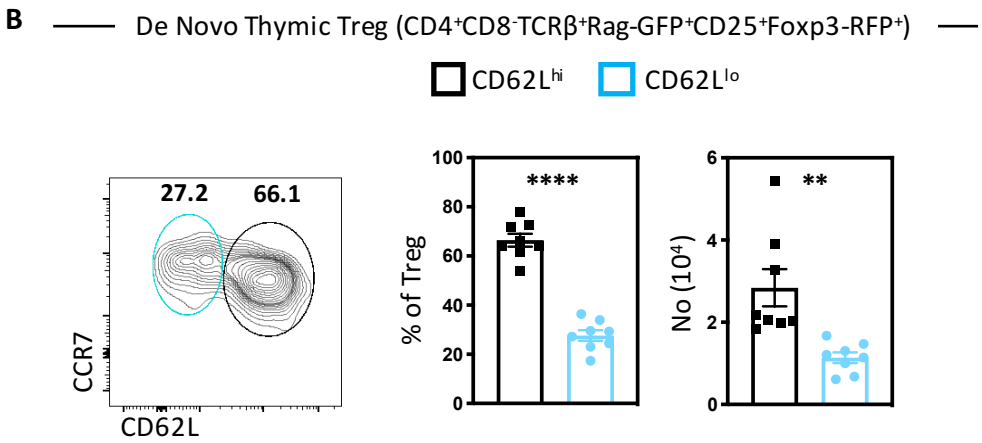
B
De Novo Thymic Treg (CD4+CD8-TCRβ+Rag-GFP+CD25+Foxp3-RFP+)
CD62Lhi
CD62Llo
27.2
66.1
CCR7
CD62L
100
80
60
40
20
0
% of Treg
****
6
4
2
0
No (10⁴)
**

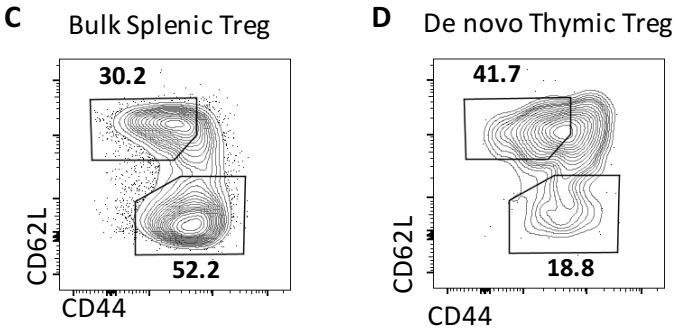
C
Bulk Splenic Treg
30.2
52.2
CD62L
CD44
D
De novo Thymic Treg
41.7
18.8
CD62L
CD44

Figure 3.2 The *De Novo* Thymic Treg Population Contains CD62L^{hi} and CD62L^{lo} Subsets

Identification and characterisation of de novo thymic Treg in Foxp3-RFPx Rag-GFP adult (8-12 weeks) mice. All data representative of n=8 across 6 independent experiments. All statistics presented were generated using paired t- tests, where ** p<0.01, **** p<0.0001.

(A) Gating strategy used for the identification of de novo thymic Treg (CD4^{+}CD8^{-}TCRβ^{+}Rag-GFP^{+}CD25^{+}Foxp3-RFP^{+}). The total SP4 thymocyte population is initially gated as CD4^{+}CD8^{-}TCRβ^{+}. De novo SP4 thymocytes are then gated as Rag-GFP^{+} and subsequently de novo Treg are gated as CD25^{+}Foxp3-RFP^{+}. Gating strategy presented as representative FACs plots including gate title and percentage of cells within the gate given underneath.

(B) Phenotypic analysis of CD62L and CCR7 expression on de novo thymic Tregs. Representative FACs plot of CD62L/CCR7 profile with two populations gated as CD62L^{hi} (black) and CD62L^{lo} (blue). Graphs quantify the percentage (left) and number (right) of the two CD62L^{hi} (black) and CD62L^{lo} (blue) Treg populations.

(C-D) Investigation of cTreg and eTreg phenotype within Tregs. Treg populations gated based on the previously defined CD62L^{hi}CD44^{lo} (cTreg) and CD62L^{lo}CD44^{hi} (eTreg). Phenotypic analysis of CD62L and CD44 expression on **(C)** total splenic Treg(CD4^{+}CD8^{-}TCRβ^{+} CD25^{+}Foxp3-RFP^{+}) and **(D)** de novo thymic Tregs (CD4^{+}CD8^{-}TCRβ^{+}Rag-GFP^{+}CD25^{+}Foxp3-RFP^{+}) presented as representative FACs plot of CD62L/CD44 profile.

Having identified heterogeneity within thymic Tregs for CD62L, we wondered whether there were further differences between the two CD62L Treg populations. To broadly address this, we investigated expression of phenotypic markers linked to migration (Figure 3.3.A), effector function (Figure 3.3.B) and maturity (Figure 3.3.C). Markers such as CCR9, CXCR4, TIGIT and KLRG1 were not readily detectable on either Treg subset. While markers including ICOS, GITR, Qa2 and CD55, were detectable but showed little difference between the two subsets. Finally, we identified a few statistically significant differently expressed markers, although the difference in expression between $CD62L^{hi}$ and $CD62L^{lo}$ subsets in all cases was slight. For instance, $CD62L^{lo}$ Tregs exhibited slightly higher expression of chemokine receptors CCR6 and CCR7 (Figure 3.3.A), associated with entry to non-lymphoid or lymphoid tissue, respectively. Similarly, $CD62L^{lo}$ Tregs also more highly expressed the functional molecules PD1 and CD73, although not CD44 (Figure 3.3.B), a marker associated with a general Treg effector phenotype, which was more highly expressed by $CD62L^{hi}$ Tregs. Conversely $CD62L^{lo}$ Tregs had lower expression of CD24 (Figure 3.3.C), a molecule whose downregulation has been tied to increasing T-cell maturity. Collectively these small differences may hint that $CD62L^{lo}$ Tregs are more primed towards a mature effector-like phenotype, however generally our analysis highlights many similarities between $CD62L^{hi}$ and $CD62L^{lo}$ Tregs.

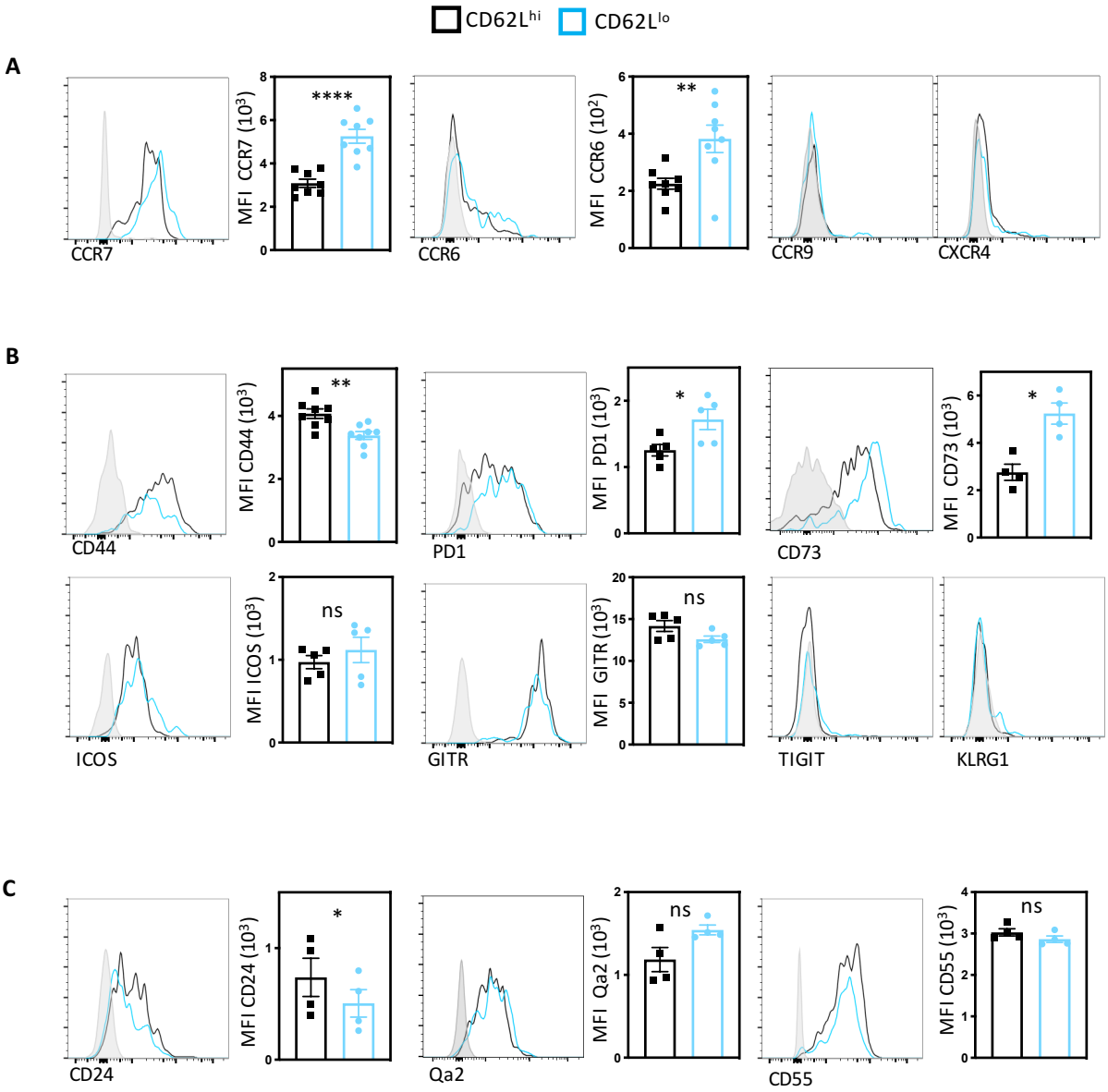
CD62L^{hi}
CD62L^{lo}
A
CCR7
MFI CCR7 (10^3)
****
CCR6
MFI CCR6 (10^2)
**
CCR9
CXCR4
B
CD44
MFI CD44 (10^3)
**
PD1
MFI PD1 (10^3)
*
CD73
MFI CD73 (10^3)
*
ICOS
MFI ICOS (10^3)
ns
GITR
MFI GITR (10^3)
ns
TIGIT
KLRG1
C
CD24
MFI CD24 (10^3)
*
Qa2
MFI Qa2 (10^3)
ns
CD55
MFI CD55 (10^3)
ns

Figure 3. 3 CD62L^{hi} and CD62L^{lo} *De Novo* Thymic Tregs Show Broadly Similar Expression of Markers Associated with Migration, Function, or Maturation

Further phenotypic analysis of thymic CD62L^{hi} (black) and CD62L^{lo} (blue) Rag-GFP^{+} Treg from adult (8-12 weeks) Foxp3-RFPxRag-GFP mice. Phenotypic markers investigated can be broadly categorised as relating to **(A)** migration, **(B)** function, or **(C)** maturation. Data presented is representative of **(A)** n ≥ 4 across ≥ 2 independent experiments, **(B)** n ≥ 4 across ≥ 2 independent experiments, and **(C)** n = 4 across ≥ 2 independent experiments. All statistics presented were generated using a paired t-test where, where ns $p>0.05$, * $p<0.05$, ** $p<0.01$, **** $p<0.0001$.

Data presented as representative FACs plots which show the expression level of the indicated marker on CD62L^{hi} (black) and CD62L^{lo} (blue) thymic Treg (CD4^{+}CD8^{-}TCRβ^{+}Rag-GFP^{+}CD25^{+}Foxp3-RFP^{+}) relative to a negative control (filled grey histogram). If marker expression is greater than negative control then the accompanying bar chart quantifying the MFI of the marker on the two Treg subsets is given.

We were next interested in understanding how the two CD62L^{hi} and CD62L^{lo} Tregs might fit within the thymic Treg development pathway, and whether there was any connection between them. Using Rag-GFP we compared the relative ages of the two CD62L subsets and determined that CD62L^{lo} Treg have a lower level of Rag-GFP (Figure 3.4.A) and hence were older as a population. Furthermore, when we analysed the appearance of the two Treg populations across an ontogeny series we found that at the very early stages of Treg development, the CD62L^{hi} Treg subset predominates with a more gradual appearance of the CD62L^{lo} population (Figure 3.4.B). Together this suggests that a developmental pathway may exist whereby CD62L^{hi} Treg arise first and then may differentiate into CD62L^{lo} Tregs. To further investigate this possible precursor product relationship, we decided to utilise RTOCs (3D organ cultures in which developmental trajectories of isolated thymocyte subsets can be monitored) to determine the fate of CD62L^{hi} Tregs.

To generate RTOC we required an appropriate source of thymic stroma. The thymic stromal compartment present within the adult is diverse, dividing firstly into cTEC or mTEC, with mTEC further split into mTEC^{lo} and mTEC^{hi}, the latter of which includes a sizeable Aire^{+} fraction (Figure 3.5.A). Given the significance of mTEC^{hi}, particularly Aire^{+}mTEC^{hi}, in bulk thymic Treg development (discussed in Section 1.3.2.2.1) we wondered if this subset may also influence heterogeneous Treg development. We therefore sought to generate stroma which either contained or lacked mTEC^{hi}. Previous work[277] has identified embryonic lobes setup as dGuo treated FTOC then subsequently treated either with or without anti-RANK, generates mixed thymic stroma which either does or does not contain mTEC^{hi}, respectively (Figure 3.5.B). In agreement with these findings, we observed that FTOC treated with or without anti-RANK both contained cTEC and mTEC populations, although the proportion of mTEC was far smaller

in the latter (Figure 3.5.C). Furthermore, while mTEC^{lo} were present in both FTOCs, mTEC^{hi} and Aire^{+}mTEC^{hi} were restricted to anti-RANK treated FTOC (Figure 3.5.C). This malleable source of thymic stroma was then combined with our isolated thymocyte population of interest, CD62L^{hi} Tregs, to form RTOCs (Figure 3.6.A).

The starting CD62L^{hi} Treg population, was isolated by fluorescence activated cell sorting as CD4^{+}CD8^{-}TCRβ^{+}CD25^{+}Foxp3^{+}Rag^{-}GFP^{+}CD62L^{hi} (Figure 3.6.B). The RTOCs were then cultured to determine the fate of CD62L^{hi} Tregs, to identify if CD62L^{hi} Tregs were capable of differentiating into CD62L^{lo} Tregs and if so whether this process was dependent upon the mTEC^{hi} population (Figure 3.6.A). The general Treg phenotype seemed fairly stable with or without mTEC^{hi}, as following 3-4 days in culture we observed that the majority of Tregs remained CD25^{+}Foxp3^{+}, although some appeared to transition to a CD25^{-}Foxp3^{+} phenotype (Figure 3.6.C). However, closer analysis of Tregs cultured in the presence of mTEC^{hi}, identified a large proportion were CD62L^{lo} (Figure 3.6.C) suggesting that some input CD62L^{hi} Tregs had transitioned to CD62L^{lo} Tregs. To determine if mTEC^{hi} were required to support this transition we examined the CD62L phenotype following culture in their absence (Figure 3.6.C-D). Our findings were inconclusive, as an initial experiment identified a large reduction in CD62L^{lo} Treg without mTEC^{hi}, however when repeated the opposite was observed. Therefore, no conclusive difference in the ratio of CD62L^{lo}:CD62L^{hi} Tregs was observed between the different stromal conditions (Figure 3.6.D).

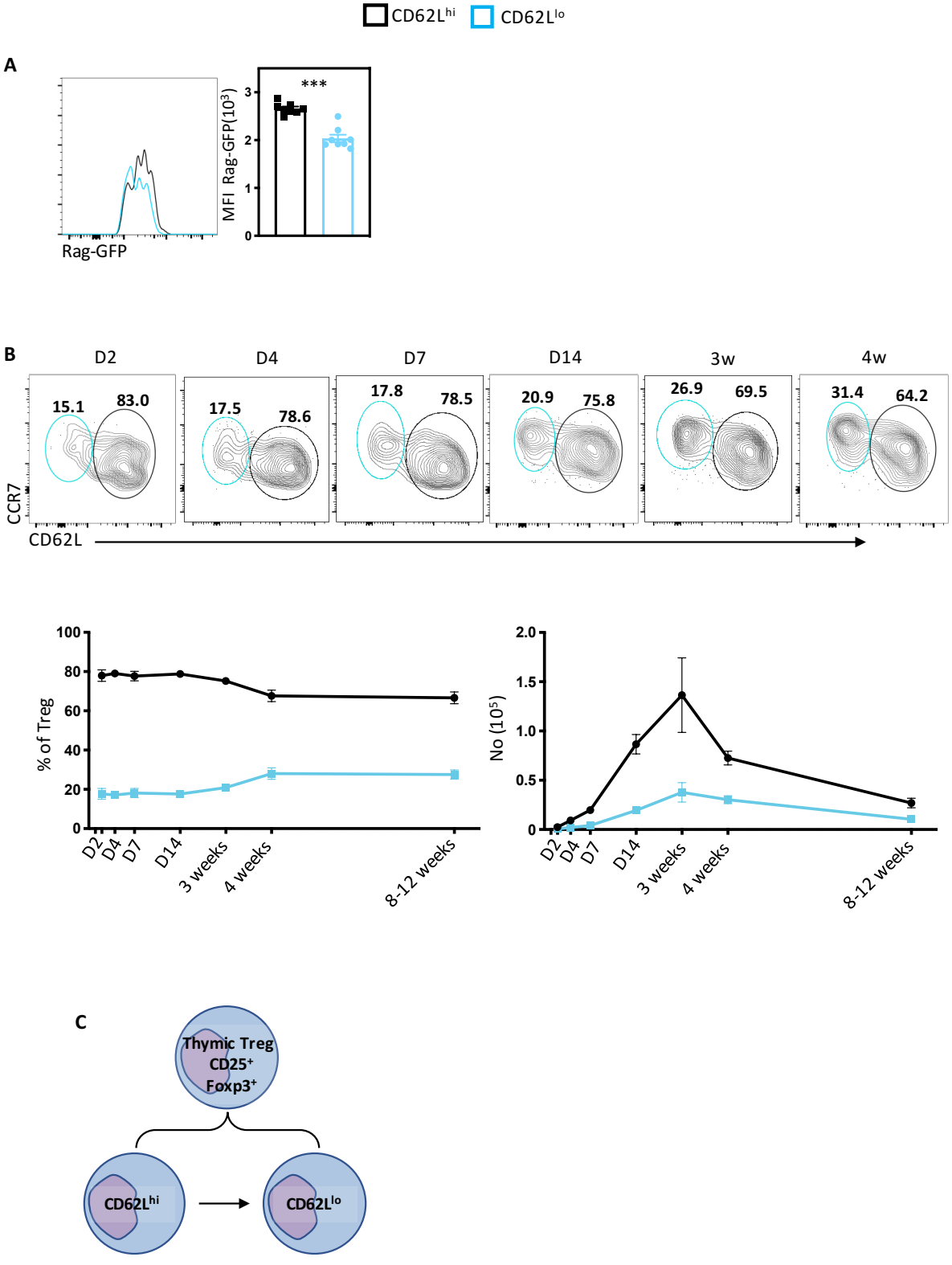
CD62L^hi
CD62L^lo
A
Rag-GFP
MFI Rag-GFP(10³)
***
B
D2
D4
D7
D14
3w
4w
15.1
83.0
17.5
78.6
17.8
78.5
20.9
75.8
26.9
69.5
31.4
64.2
CCR7
CD62L
% of Treg
No (10⁵)
D2
D4
D7
D14
3 weeks
4 weeks
8-12 weeks
C
Thymic Treg
CD25⁺
Foxp3⁺
CD62L^hi
CD62L^lo

Figure 3. 4 CD62L^{hi} Tregs Appear Before CD62L^{lo} Tregs in *De Novo* Thymic Treg Development

(A) Comparison of Rag-GFP expression on CD62L^{hi} (black) and CD62L^{lo} (blue) Rag-GFP^{+} (*de novo*) thymic Treg in adult (8-12 week) Foxp3-RFPxRag-GFP mice. Data is representative of n=8 across 6 independent experiments. Representative FACs plot shows Rag-GFP levels of CD62L^{hi} and CD62L^{lo} Treg relative to a non-fluorescent staining control (filled grey). Bar chart quantifies the the MFI of Rag-GFP for the two Treg populations. Statistical analysis performed using a paired t-test where, where *** $p<0.001$.

(B) Appearance of *de novo* CD62L^{hi} and CD62L^{lo} Treg (CD4^{+}CD8^{-}TCRβ^{+}Rag-GFP^{+}CD25^{+}Foxp3-RFP^{+}) across ontogeny of Foxp3-RFPxRag-GFP mice. All timepoints representative of $n \geq 5$ across ≥ 2 independent experiments. Representative FACs plots show the CD62L/CCR7 profile of Rag-GFP^{+} Treg and gating of the two Treg subsets CD62L^{hi} (black) and CD62L^{lo} (blue) at the indicated age. Below graphs quantify, (left) the percentage of the two subsets within the Treg population and (right) the number of the two Treg subsets, across the timecourse.

(C) Schematic of proposed order of appearance of the two *de novo* Treg subsets, where CD62L^{hi} Treg appear first and may give rise to the CD62L^{lo} Treg.

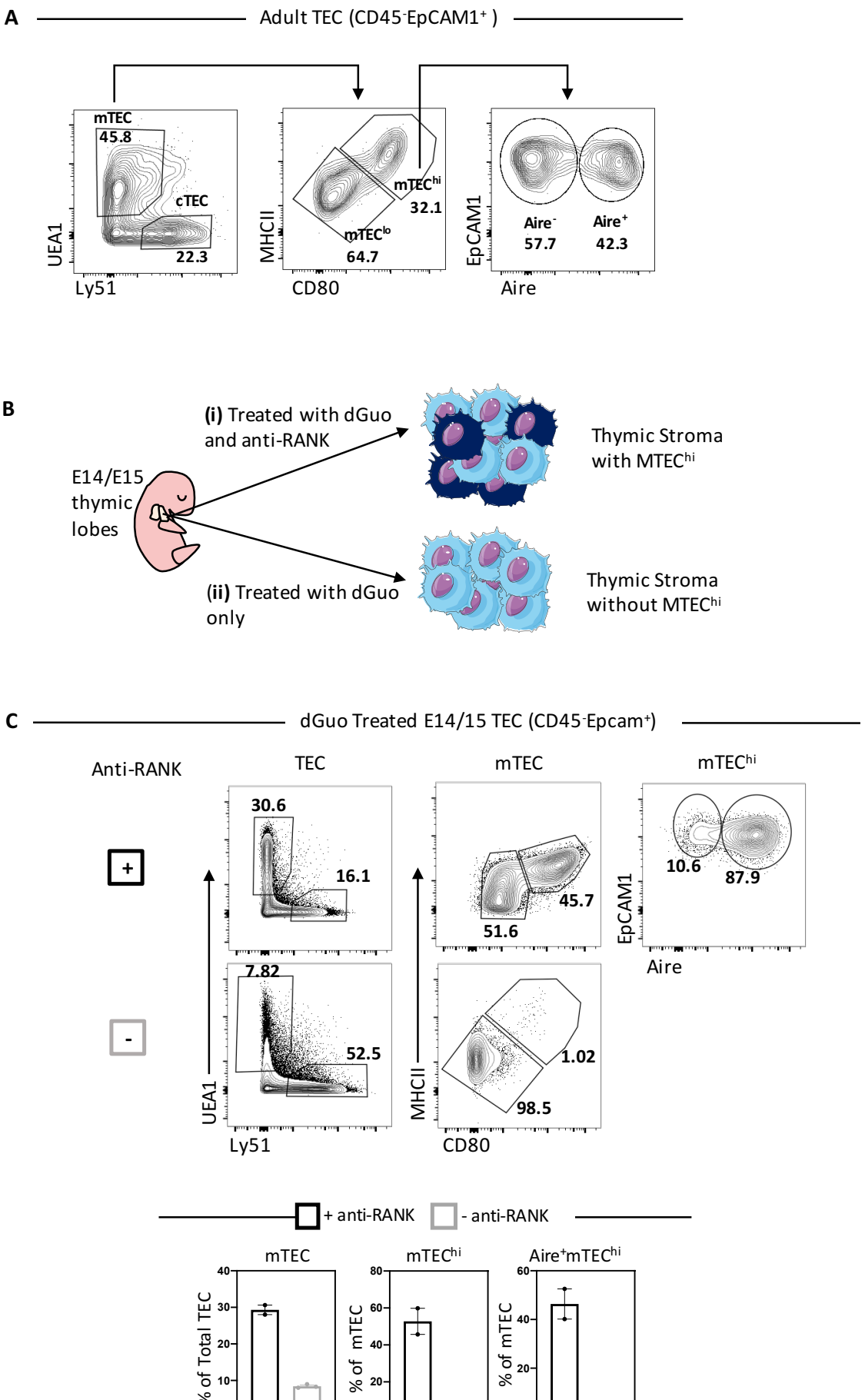
A
Adult TEC (CD45-EpCAM1+)
mTEC
45.8
cTEC
22.3
UEA1
Ly51
mTEChi
32.1
mTEClo
64.7
MHCII
CD80
Aire-
57.7
Aire+
42.3
EpCAM1
Aire
B
(i) Treated with dGuo and anti-RANK
E14/E15 thymic lobes
(ii) Treated with dGuo only
Thymic Stroma with MTEChi
Thymic Stroma without MTEChi
C
dGuo Treated E14/15 TEC (CD45-Epcam+)
Anti-RANK
TEC
mTEC
mTEChi
+
-
30.6
16.1
7.82
52.5
45.7
51.6
10.6
87.9
1.02
98.5
UEA1
Ly51
MHCII
CD80
EpCAM1
Aire
+ anti-RANK
- anti-RANK
mTEC
mTEChi
Aire+mTEChi
% of Total TEC
% of mTEC
% of mTEC

Figure 3. 5 Treatment of Embryonic Thymic Stroma with dGuo Inhibits Development of MTEC^{hi}

(A) TEC populations present in the WT adult (8-12 weeks) thymus. TEC (pre-gated as CD45$^-$ Epcam$^+$) can be initially subdivided into mTEC (Ly51$^-$UEA$^+$) and cTEC (Ly51$^+$UEA$^-$). mTEC can then be further divided into mTEC^{hi} (MHCII^{hi}CD80^{hi}) and mTEC^{lo} (MHCII^{lo}CD80^{lo}) subsets. Finally the mTEC^{hi} population can be divided into AIRE$^+$ and AIRE$^-$ cells.
(B) Schematic depicting different culturing conditions used to promote different stromal subsets *in vitro.* Embryonic thymic lobes are isolated at embryonic day (E) 15/14 and treated with dGuo, then either receive stimulation with anti-RANK. Treatment with anti-RANK induces mTEC^{hi}, hence in the absence of anti-RANK this population fails to develop.
(C) Analysis of mTEC in dGuo pre-treated E14/E15 thymic lobes either stimulated with anti-RANK or unstimulated, as indicated. FACS plots show (left) breakdown of mTEC (Ly51$^-$UEA$^+$) within total TEC (CD45$^-$Epcam$^+$), (middle) breakdown of mTEC subsets mTEC^{hi} (MHCII^{hi}CD80^{hi}) and mTEC^{lo} (MHCII^{lo}CD80^{lo}), and (right) the proportion of AIRE$^+$ mTEC^{hi} and mTEC^{lo}. Graphs quantify the frequency of mTEC as a proportion of total TEC (left), and the frequency of mTEC^{hi} (middle) and AIRE$^+$mTEC^{hi} (right) as a proportion of mTEC, comparative between thymic lobes stimulated with anti-RANK (black) or unstimulated (grey). Data representative of n ≥ 2 across ≥ 2 independent experiments.

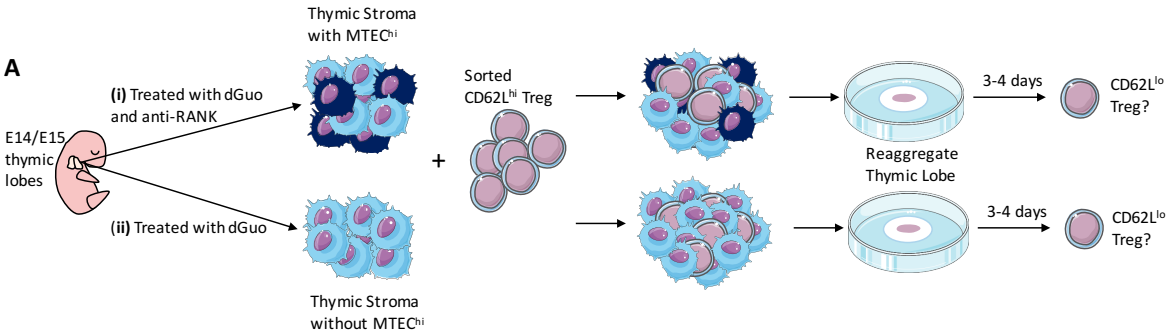
A
Thymic Stroma with MTEC^hi
(i) Treated with dGuo and anti-RANK
E14/E15 thymic lobes
(ii) Treated with dGuo
Thymic Stroma without MTEC^hi
Sorted CD62L^hi Treg
+
Reaggregate Thymic Lobe
3-4 days
CD62L^lo Treg?
3-4 days
CD62L^lo Treg?

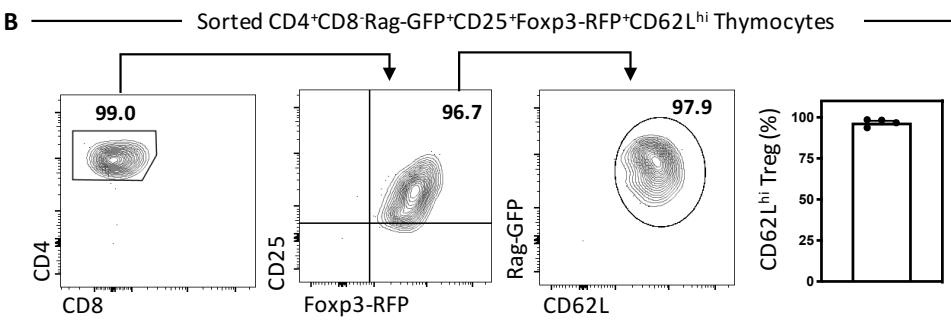
B
Sorted CD4+CD8-Rag-GFP+CD25+Foxp3-RFP+CD62L^hi Thymocytes
99.0
CD4
CD8
96.7
CD25
Foxp3-RFP
97.9
Rag-GFP
CD62L
CD62L^hi Treg (%)
100
75
50
25
0

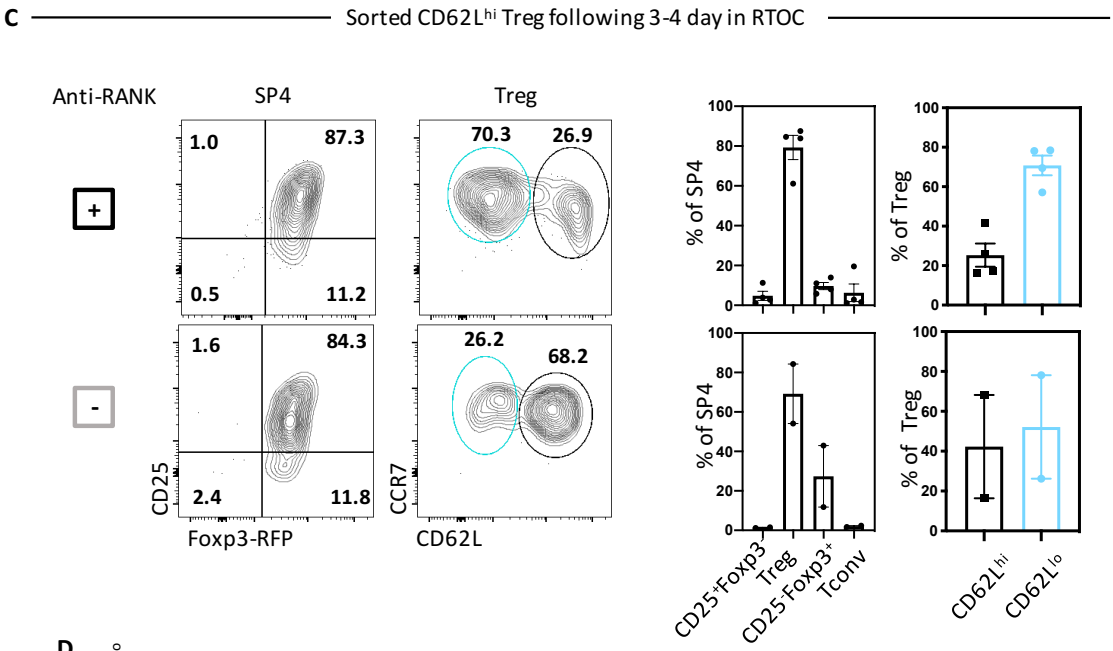
C
Sorted CD62L^hi Treg following 3-4 day in RTOC
Anti-RANK
SP4
Treg
+
-
1.0
87.3
0.5
11.2
70.3
26.9
1.6
84.3
2.4
11.8
26.2
68.2
CD25
Foxp3-RFP
CCR7
CD62L
% of SP4
% of Treg
CD25+Foxp3 Treg
CD25-Foxp3+ Tconv
CD62L^hi
CD62L^lo

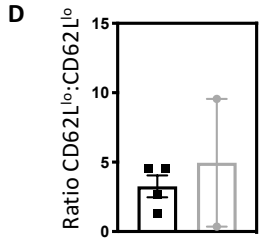
D
Ratio CD62L^lo:CD62L^lo
15
10
5
0

Figure 3. 6 CD62L^{hi} *De Novo* Thymic Tregs Differentiate to CD62L^{lo} Tregs in RTOC

Analysis of phenotypic changes to *de novo* thymic CD62L^{hi} Treg following 3-4 days in RTOC. RTOCs were generated by combing between 20-100x10^{3} sorted CD62L^{hi} Tregs with 500x10^{3} stroma treated with/without anti-RANK. Data presented on RTOC generated from stroma treated with anti-RANK, is representative of n=4 across 4 independent experiments. Data presented on RTOC generated from stroma treated without anti-RANK, is representative of n=2 across 2 independent experiments

(A) RTOC schematic: isolated embryonic thymic lobes are treated with dGuo then either receive stimulation (i) with anti-RANK (which induced production of mTEC^{hi}) or (ii) are left unstimulated. The pre-generated thymic stroma is then combined with sorted Treg of interest to generate a reaggregated thymic lobe which is cultured to determine developmental changes in the sorted thymocyte population.

(B) Phenotypic analysis of sorted CD62L^{hi} *de novo* thymic Treg (sorted as CD4^{+}CD8^{-}CD25^{+}Foxp3-RFP^{+}Rag-GFP^{+}CD62L^{hi}) at D0 of RTOC. Data presented as representative FACs plots which show the sorted CD62L^{hi} Treg phenotype, which was initially gated as CD4^{+}CD8^{-} then gated as CD25^{+}Foxp3-RFP^{+} Treg and finally as Rag-GFP^{+}CD62L^{hi} Treg. The purity of the CD62L^{hi} Treg is quantified as the percentage of CD4^{+}CD8^{-}CD25^{+}Foxp3-RFP^{+}Rag-GFP^{+} Tregs.

(C) Phenotypic analysis of sorted CD62L^{hi} *de novo* thymic Treg (sorted as CD4^{+}CD8^{-}CD25^{+}Foxp3-RFP^{+}Rag-GFP^{+}CD62L^{hi}) following 3-4 days of culture in RTOC generated from stroma treated with (black) or without (grey) anti-RANK. Representative FACs plots show (left) the CD25/Foxp3 profile of SP4 (CD4^{+}CD8^{+}TCRβ^{+}) thymocytes and (right) the CD62L/CCR7 profile of Treg (CD4^{+}CD8^{+}TCRβ^{+}CD25^{+}Foxp3-RFP^{+}) with two populations gated as CD62L^{hi} (black) and CD62L^{lo} (blue). The accompanying graphs quantify (left) the percentage of the four SP4 thymocyte populations as indicated and (right) the percentage of CD62L^{hi} and CD62L^{lo} Treg.

(D) Graph shows the ratio of CD62L^{lo}:CD62L^{hi} Treg in RTOC generated from stroma treated with (black) or without (grey) anti-RANK.

It is notable that even in the presence of mTEC^{hi} not all CD62L^{hi} Tregs transitioned to CD62L^{lo} phenotype in this experimental timeframe, suggesting a bifurcated fate for CD62L^{hi} Tregs. We therefore questioned whether thymic Treg development generated two heterogeneous Treg subsets which were both subsequently exported to the periphery. To determine if both Treg subsets were capable of thymic egress we examined S1PR1 expression. As discussed in Section 1.2.6, S1PR1 is a key mediator of Tconv thymocyte egress, expressed by mature egress competent CD62L^{hi}CD69^{lo} Tconvs but not immature CD62L^{lo}CD69^{hi} Tconvs (Figure 3.7.A). Interestingly both CD62L^{hi} and CD62L^{lo} Tregs expressed S1PR1 at a comparable level to mature Tconvs and significantly higher than immature Tconvs (Figure 3.7.B). Similarly, both CD62L^{hi} and CD62L^{lo} Tregs also lacked CD69, a key antagonist of S1PR1 expression, expressing levels similar to mature Tconvs and significantly lower than immature Tconvs (Figure 3.7.C). Taken together this suggests both CD62L^{hi} and CD62L^{lo} Treg subsets are capable of thymic egress.

If both CD62L^{hi} and CD62L^{lo} thymic Tregs were exported, we would expect to find them within the Treg RTE population within peripheral lymphoid tissues. We therefore examined this population in the adult spleen (Figure 3.8.A) and as anticipated found Treg RTE to be heterogeneous, containing CD62L^{hi} and CD62L^{lo} subsets. However, the presence of both subsets within splenic RTE could be the result of CD62L^{hi} Treg differentiating into CD62L^{lo} Treg within the spleen following thymic export. To address this possibility, we investigated the phenotype of the earliest splenic Tregs reasoning that these Tregs would have just been exported from the thymus and therefore had limited opportunity to further differentiate. In keeping with previous observations[36], the earliest time point we observed a notable splenic Treg population was D4 (Figure 3.9.A), and at this time we observed both CD62L^{hi} and CD62L^{lo}

Treg subsets present at a similar ratio to that of adult Tregs (Figure 3.9.B). This would suggest that the heterogeneity of Treg RTEs reflects the export of the two different thymic subsets.

Thus far our analysis had focussed on the splenic RTE population, however previous studies have suggested that different types of Treg exhibit distinct homing preferences[85,107]. A tendency that may be suggested by our own phenotypic data, not least by the difference in CD62L expression due to its role as a key mediator of entry into SLOs. We also observed slight differences in the expression of certain chemokine receptors such as CCR6 (Figure 3.3.A), which could also drive differential homing preferences. Therefore we decided to look for evidence of Treg RTE in a variety of tissues including, the inguinal LNs (iLNs), mesenteric LNs (mLN), BM, and liver (Figure 3.10). This analysis identified that SP4 RTEs were most prevalent in SLOs such as iLNs and mLNs, but were also detectable, at lower frequencies, in non-lymphoid tissues like the liver (Figure 3.10.B). Within this bulk population similar proportions of Treg RTEs were observed in all tissues except BM, which contained a higher proportion of Tregs (Figure 3.10.B).

Having identified Treg RTEs in a variety of tissues, we next examined their CD62L phenotype (Figure 3.11). We found that the ratio of $CD62L^{hi}$:$CD62L^{lo}$ Tregs within the spleen, iLNs and mLNs was similar, with the majority being $CD62L^{hi}$. In contrast, very few $CD62L^{hi}$ Tregs were present within the BM Treg population, which largely consisted of $CD62L^{lo}$ Tregs. While within the liver we observed virtually no $CD62L^{hi}$ Tregs, only $CD62L^{lo}$ Tregs.

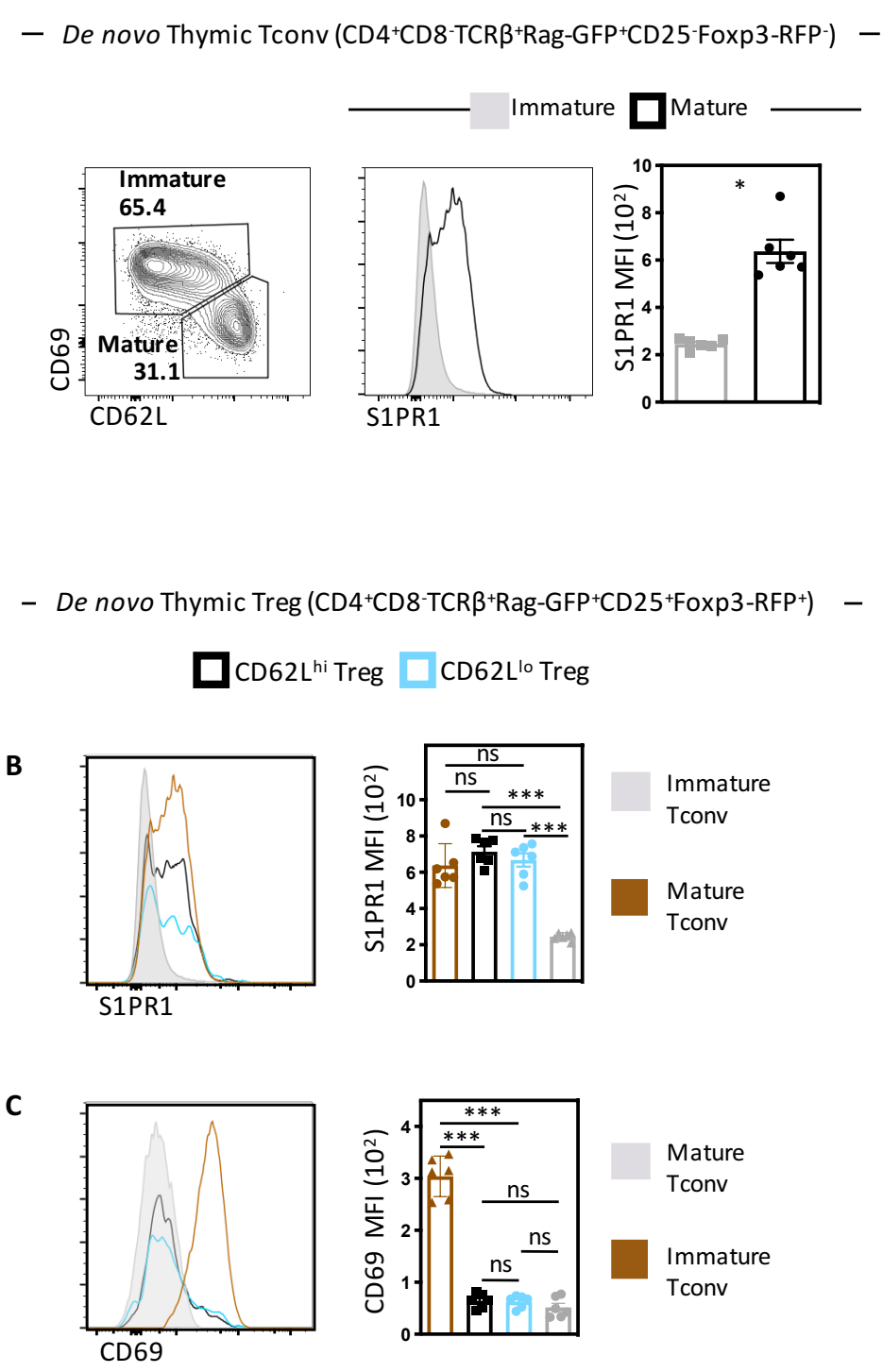
A
De novo Thymic Tconv (CD4+CD8-TCRβ+Rag-GFP+CD25-Foxp3-RFP-)
Immature
Mature
Immature
65.4
Mature
31.1
CD69
CD62L
S1PR1
S1PR1 MFI (10²)
*
De novo Thymic Treg (CD4+CD8-TCRβ+Rag-GFP+CD25+Foxp3-RFP+)
CD62Lhi Treg
CD62Llo Treg
B
S1PR1
S1PR1 MFI (10²)
ns
ns
***
ns
***
Immature Tconv
Mature Tconv
C
CD69
CD69 MFI (10²)
***
***
ns
ns
ns
Mature Tconv
Immature Tconv

Figure 3. 7 *De Novo* Thymic Treg Subsets Both Show Evidence of Egress Competency

Analysis of S1PR1 and CD69 expression by *de novo* thymocytes in adult (8-12 weeks) Foxp3-RFPxRag-GFP mice. Data representative of n=6 across 3 independent experiments. All statistics presented were generated using a repeated measures one way anova, ns $p>0.05$, *** $p<0.001$.

(A) Analysis of immature ($CD69^{+}CD62L^{-}$) and mature ($CD62L^{+}CD69^{-}$) *de novo* Tconv ($CD4^{+}CD8^{-}TCR\beta^{+}Rag\text{-}GFP^{+}CD25^{-}Foxp3\text{-}RFP^{-}$) thymocyte subsets. Representative FACs plots show (left) the gating of the immature and mature populations, and (right) the expression of S1PR1 by immature (filled grey) and mature (black) Tconv subsets. The bar chart quantifies the MFI of S1PR1 on mature (black) and immature (grey).

(B) Comparison of S1PR1 expression on $CD62L^{hi}$ (black) and $CD62L^{lo}$ (blue) *de novo* Treg ($CD4^{+}CD8^{-}TCR\beta^{+}Rag\text{-}GFP^{+}CD25^{+}Foxp3\text{-}RFP^{+}$), with immature Tconv (filled grey) and mature Tconv (brown) as internal positive and negative staining controls, respectively. Data presented as FACs plots showing S1PR1 expression levels of the four populations, with accompanying bar chart quantifying the MFI of S1PR1 for each population.

(C) Comparison of CD69 expression on $CD62L^{hi}$ (black) and $CD62L^{lo}$ (blue) *de novo* Treg, with mature Tconv (filled grey) and immature Tconv (brown) as internal positive and negative staining controls, respectively. Data presented as FACs plots showing CD69 expression levels of the four populations, with accompanying bar chart quantifying the MFI of CD69 for each population.

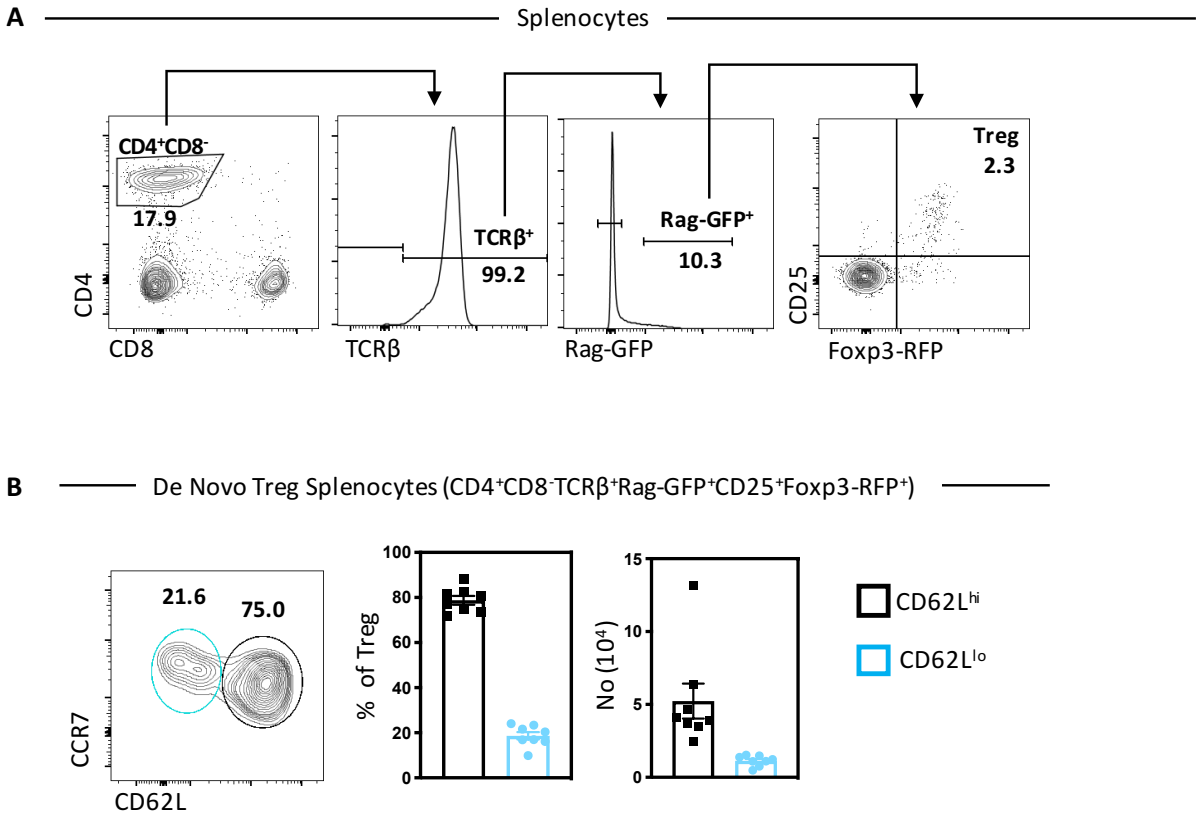
A
Splenocytes
CD4+CD8-
17.9
CD4
CD8
TCRβ+
99.2
TCRβ
Rag-GFP+
10.3
Rag-GFP
Treg
2.3
CD25
Foxp3-RFP
B
De Novo Treg Splenocytes (CD4+CD8-TCRβ+Rag-GFP+CD25+Foxp3-RFP+)
21.6
75.0
CCR7
CD62L
% of Treg
100
80
60
40
20
0
No (10^4)
15
10
5
0
CD62Lhi
CD62Llo

Figure 3. 8 CD62L^{hi} and CD62L^{lo} Tregs are Identifiable within the Splenic RTE Population

Identification and characterisation of splenic Treg RTEs in Foxp3-RFPx Rag-GFP adult (8-12 weeks) mice. All data representative of n=8 across 6 independent experiments.

(A) Gating strategy used for the identification of splenic Treg RTEs (CD4^{+}CD8^{+}TCRβ^{+}CD25^{+}Foxp3-RFP^{+}). The total SP4 splenocyte population is initially gated as CD4^{+}CD8^{-}TCRβ^{+}. SP4 RTEs are then gated as Rag-GFP^{+} and subsequently *de novo* Treg are gated as CD25^{+}Foxp3-RFP^{+}. Gating strategy presented as representative FACs plots including gate title and percentage of cells within the gate given underneath.

(B) Phenotypic analysis of CD62L and CCR7 expression on splenic Treg RTEs. Representative FACs plot of CD62L/CCR7 profile with two populations gated as CD62L^{hi} (black) and CD62L^{lo} (blue). Graphs quantify the percentage (left), number (middle) of the two CD62L^{hi} (black) and CD62L^{lo} (blue) Treg populations.

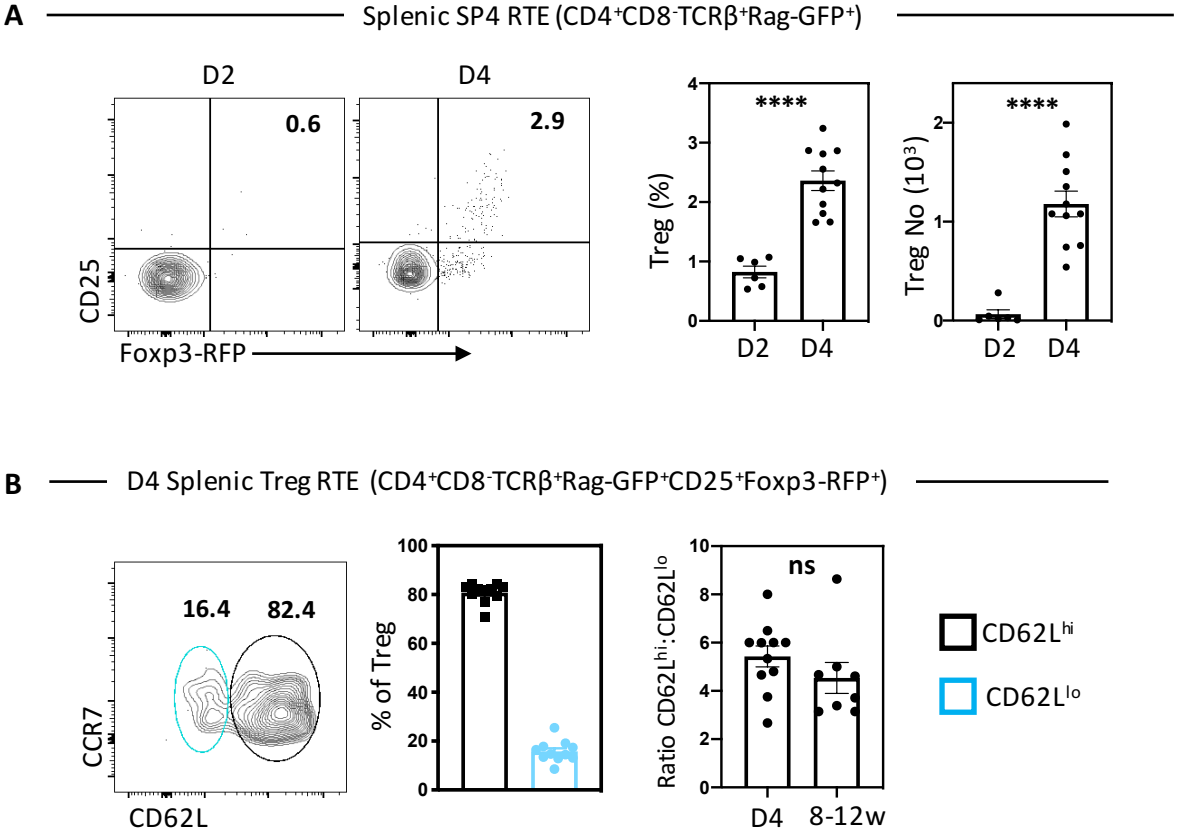
A
Splenic SP4 RTE (CD4+CD8-TCRβ+Rag-GFP+)
D2
D4
0.6
2.9
CD25
Foxp3-RFP
****
Treg (%)
D2
D4
****
Treg No (10³)
D2
D4
B
D4 Splenic Treg RTE (CD4+CD8-TCRβ+Rag-GFP+CD25+Foxp3-RFP+)
16.4
82.4
CCR7
CD62L
% of Treg
ns
Ratio CD62Lhi:CD62Llo
D4
8-12w
CD62Lhi
CD62Llo

Figure 3. 9 CD62L^{hi} and CD62L^{lo} Tregs are Present within the Early Neonatal Splenic RTE Population

Identification and characterisation of splenic Treg RTEs in Foxp3-RFPx Rag-GFP neonatal and adult mice. For all timepoints n ≥ 6 across ≥ 2 independent experiments. All statistics presented were generated using a unpaired student's t-tests, where ns p>0.05, **** p<0.0001.

(A) Analysis of the appearance of the CD25^{+}Foxp3-RFP^{+} Treg RTE within the Rag-GFP^{+} SP4 (CD4^{+}CD8^{-}TCRβ^{+}Rag-GFP^{+}) population in the neonatal spleen. Data presented as representative FACs plots of CD25/Foxp3 profile of Rag-GFP^{+} SP4 RTEs at D2 and D4 and accompanying graphs quantify Rag-GFP^{+} Treg percentages and numbers comparative between D2 and D4.

(B) Phenotypic analysis of CD62L and CCR7 expression on D4 splenic Treg RTEs. Representative FACs plot of CD62L/CCR7 profile with two populations gated as CD62L^{hi} (black) and CD62L^{lo} (blue). Left graph quantifies the percentage of the two CD62L^{hi} (black) and CD62L^{lo} (blue) Treg populations. Right graph compares the ratio of CD62L^{hi}:CD62L^{lo} Treg RTE in D4 and adult (8-12 weeks) mice.

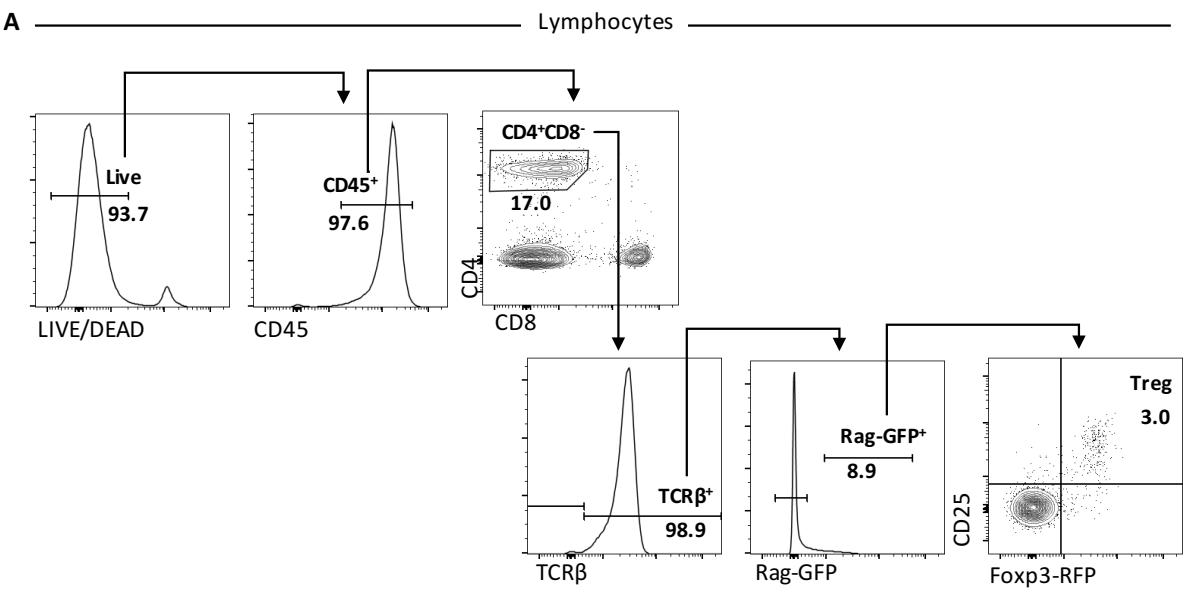
A
Lymphocytes
Live
93.7
LIVE/DEAD
CD45+
97.6
CD45
CD4+CD8-
17.0
CD4
CD8
TCRβ+
98.9
TCRβ
Rag-GFP+
8.9
Rag-GFP
Treg
3.0
CD25
Foxp3-RFP

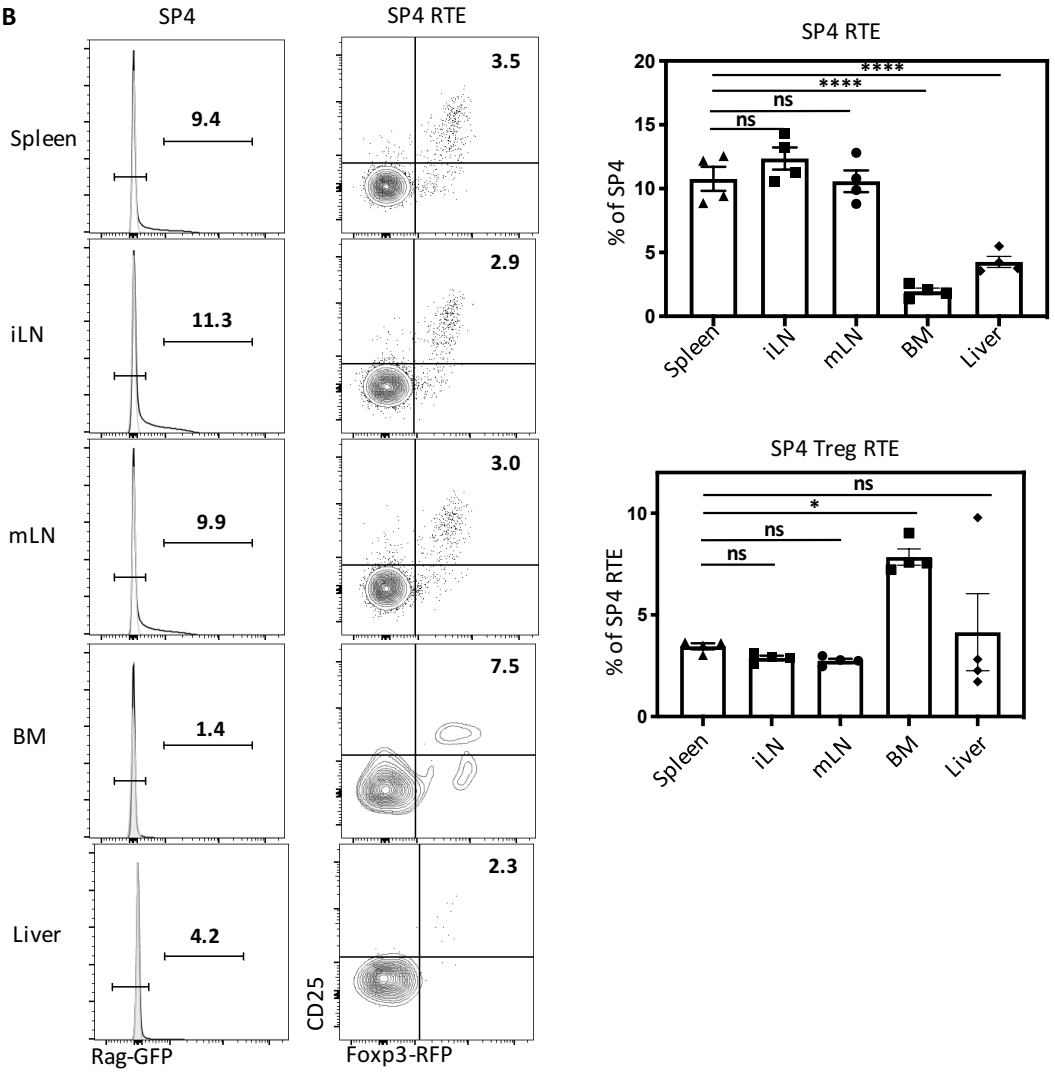
B
SP4
SP4 RTE
Spleen
9.4
3.5
iLN
11.3
2.9
mLN
9.9
3.0
BM
1.4
7.5
Liver
4.2
2.3
Rag-GFP
CD25
Foxp3-RFP
SP4 RTE
% of SP4
20
15
10
5
0
****
****
ns
ns
Spleen
iLN
mLN
BM
Liver
SP4 Treg RTE
% of SP4 RTE
10
5
0
ns
*
ns
ns
Spleen
iLN
mLN
BM
Liver

Figure 3. 10 Treg RTE can be Found in Lymphoid and Non-Lymphoid Peripheral Tissues

Identification and characterisation of SP4 RTE (LIVE/DEAD^{-}CD45^{+}CD4^{+}CD8^{-}TCRβ^{+}Rag-GFP^{+}) in spleen, iLN, mLN, BM, and liver from adult (8-12 weeks) Foxp3-RFPxRag-GFP mice. For all tissues data representative of n =4 across 2 independent experiments. All statistics presented were generated using a ordinary one way anova where, ns>0.05, * p<0.05, **** p<0.0001.

(A) Gating strategy used for the identification of Treg RTE (LIVE/DEAD^{-}CD45^{+}CD4^{+}CD8^{-}TCRβ^{+}Rag-GFP^{+}CD25^{+}Foxp3-RFP^{+}) in tissues. Live cells are initially gated upon as LIVE/DEAD^{-}. Then hematopoietic cells are gated as CD45$^{+.}$ Next the total SP4 thymocyte population is gated as CD4^{+}CD8^{-}TCRβ^{+}. Splenic SP4 RTE are then gated as Rag-GFP^{+} and subsequently Treg RTE are gated as CD25^{+}Foxp3-RFP^{+}. Gating strategy presented as representative FACs plots from splenic tissue including gate title and percentage of cells within the gate given underneath.

(B) Comparison of the proportions of Treg RTE present in different tissues. Representative FACs plots show (left) the Rag-GFP expression of SP4 T-cells and (right) the of CD25/Foxp3 profile of the Rag-GFP^{+} SP4 RTEs, from the indicated tissues. Graphs quantify (top) the percentage of Rag-GFP^{+} cells within the SP4 population and (bottom) cells the percentage of CD25^{+}Foxp3-RFP^{+} cells within the Rag-GFP^{+} SP4 population for each tissue.

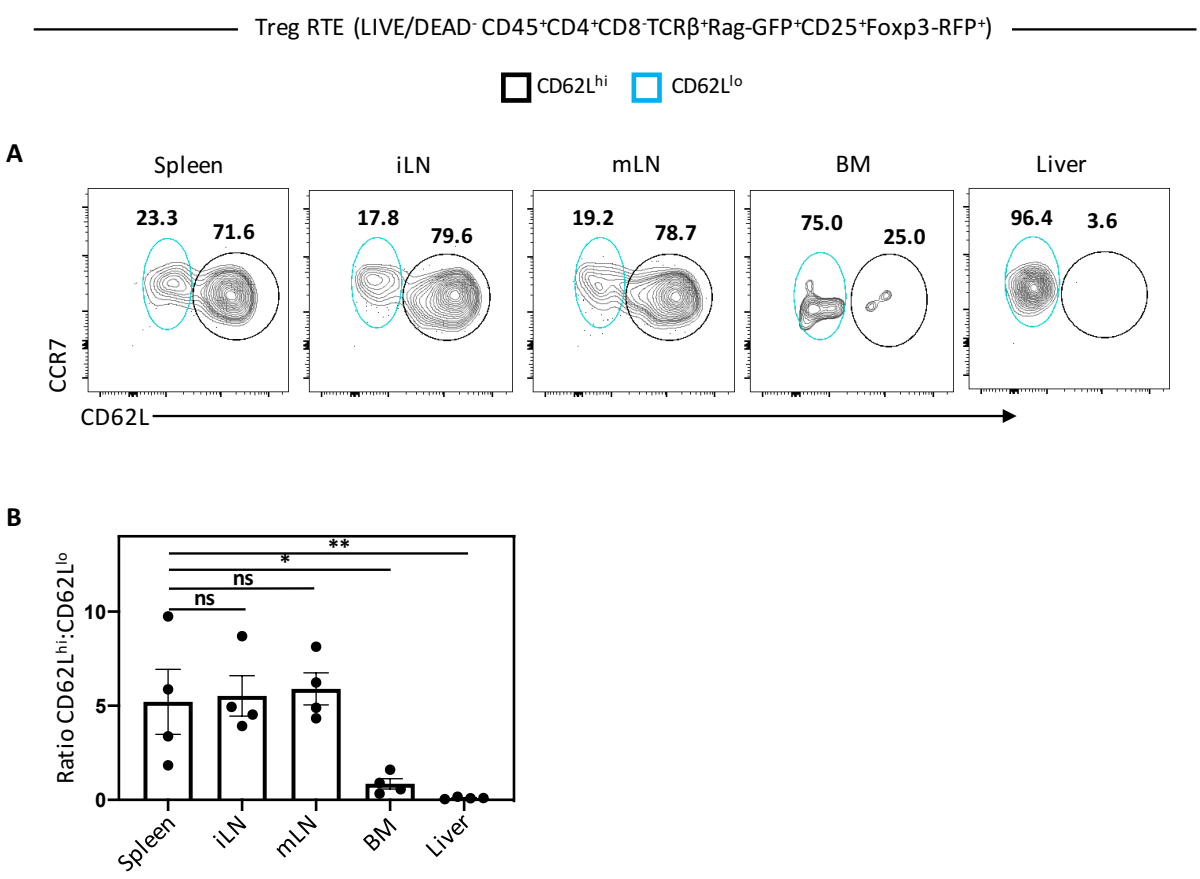
Treg RTE (LIVE/DEAD- CD45+CD4+CD8-TCRβ+Rag-GFP+CD25+Foxp3-RFP+)
CD62Lhi
CD62Llo
A
Spleen
iLN
mLN
BM
Liver
23.3
71.6
17.8
79.6
19.2
78.7
75.0
25.0
96.4
3.6
CCR7
CD62L
B
Ratio CD62Lhi:CD62Llo
**
*
ns
ns
10
5
0
Spleen
iLN
mLN
BM
Liver

Figure 3. 11 CD62L^{hi} and CD62L^{lo} Treg RTEs Display Different Homing Preferences

Identification and characterisation of Treg RTE (LIVE/DEAD^{-}CD45^{+}CD4^{+}CD8^{-}TCRβ^{+}Rag-GFP^{+}CD25^{+}Foxp3-RFP^{+}) in spleen, iLN, mLN, BM, and liver from adult (8-12 weeks) Foxp3-RFPxRag-GFP mice. For all tissues data representative of n =4 across 2 independent experiments. All statistics presented were generated using an ordinary one way anova, where ns $p>0.05$,* $p<0.05$, **$p<0.01$.

(A) Comparison of CD62L and CCR7 expression on Treg RTEs from different tissues. Presented as representative FACs plot of CD62L/CCR7 profile from the indicated tissue with two Treg populations gated as CD62L^{hi} (black) and CD62L^{lo} (blue).

(B) Graph compares the ratio of CD62L^{hi}:CD62L^{lo} Treg RTE from the different tissues as indicated.

3.2.2 Treg Precursors and Heterogeneous Treg Development

Having identified heterogeneous thymic Tregs we were interested in more fully characterising their thymic development. Importantly bulk thymic Treg development has been linked to two thymic Treg precursor populations, $CD25^{+}Foxp3^{-}$ and $CD25^{-}Foxp3^{+}$ SP4 thymocytes, however there remains some controversy as to how these two precursor populations contribute to Treg development. We were therefore interested in characterising how the two proposed Treg precursor populations may contribute to both bulk and heterogeneous Treg development.

We began by identifying $CD25^{+}Foxp3^{-}$ and $CD25^{-}Foxp3^{+}$ populations within the total SP4 thymocyte population using Foxp3-RFPxRag-GFP mice (Figure 3.12). In agreement with previous findings[234] we found that both populations were contaminated with mature $Rag\text{-}GFP^{-}$ thymocytes to different extents (Figure 3.12.A-B). Similar to Tregs, the majority of $CD25^{-}Foxp3^{+}$ precursors were $Rag\text{-}GFP^{-}$ while in contrast a much smaller proportion of $CD25^{+}Foxp3^{-}$ precursors were $Rag\text{-}GFP^{-}$. Thus confirming that to accurately investigate the developmental role of these Treg precursor populations, $Rag\text{-}GFP^{-}$ thymocytes must be excluded. We therefore gated as before (Figure 3.2.A) in order to examine only the *de novo* SP4 population (Figure 3.12.C). Within this population we observed that $CD25^{+}Foxp3^{-}$ precursors were the most prevalent while $CD25^{-}Foxp3^{+}$ precursors and Tregs were present at lower but similar levels.

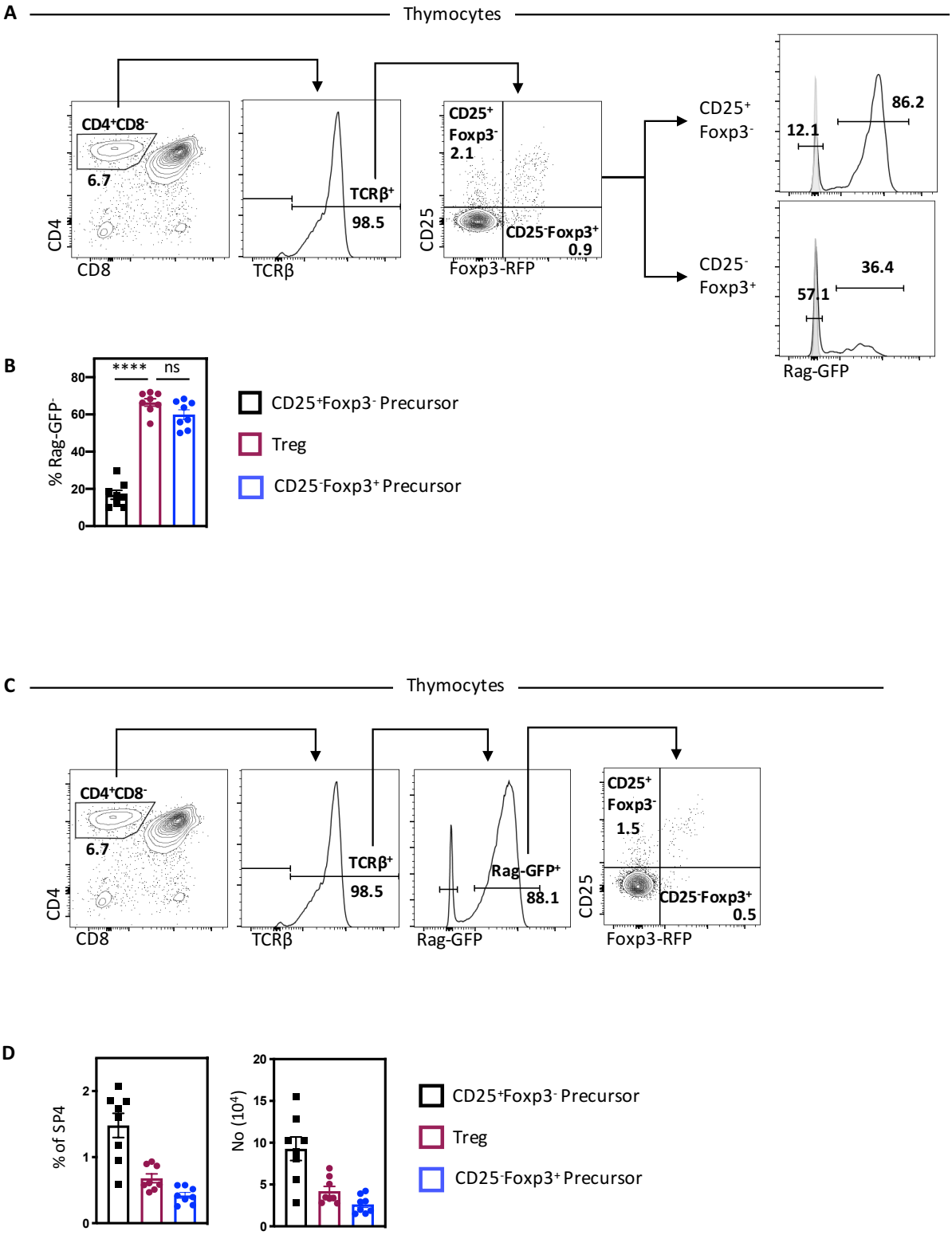
A
Thymocytes
CD4+CD8-
6.7
CD4
CD8
TCRβ+
98.5
TCRβ
CD25+
Foxp3-
2.1
CD25
Foxp3-RFP
CD25-Foxp3+
0.9
CD25+
Foxp3-
12.1
86.2
CD25-
Foxp3+
57.1
36.4
Rag-GFP
B
% Rag-GFP-
****
ns
CD25+Foxp3- Precursor
Treg
CD25-Foxp3+ Precursor
C
Thymocytes
CD4+CD8-
6.7
CD4
CD8
TCRβ+
98.5
TCRβ
Rag-GFP+
88.1
Rag-GFP
CD25+
Foxp3-
1.5
CD25
CD25-Foxp3+
0.5
Foxp3-RFP
D
% of SP4
No (10⁴)
CD25+Foxp3- Precursor
Treg
CD25-Foxp3+ Precursor

Figure 3. 12 Thymic Treg Precursor Populations are a Mixture of *De Novo* and Mature Tregs

Identification of the two thymic Treg precursor populations in Foxp3-RFPx Rag-GFP adult (8-12 weeks) mice. All data representative of n=8 across 6 independent experiments.

(A) Identification of *de novo* (Rag-GFP^{+}) and mature (Rag-GFP^{-}) cells within thymic Treg precursor populations. SP4 thymocytes are initially gated as CD4^{+}CD8^{-}TCRβ^{+}, this populations is then subdivided on the basis of CD25 and Foxp3 to identify thymic Treg precursors as CD25^{+}Foxp3-RFP^{-} and CD25^{-}Foxp3-RFP^{+}. The two precursor populations are then divided into Rag-GFP^{+} (*de novo*) and Rag-GFP^{-} (mature) subsets.

(B) Quantification of the percentage of Rag-GFP^{-} (mature) cells within CD25^{+}Foxp3-RFP^{-} Treg precursors (black), CD25^{-}Foxp3-RFP^{+} Treg precursors (blue) and CD25^{+}Foxp3-RFP^{+} Treg (purple) thymocyte populations. Statistical analysis performed using a repeated measures one way anova, where ns $p>0.05$, **** $p<0.0001$.

(C) Gating strategy used for the identification of *de novo* thymic Treg precursors. The total SP4 thymocyte population is initially gated as CD4^{+}CD8^{-}TCRβ^{+}. *De novo* SP4 thymocytes are then gated as Rag-GFP^{+} and subsequently *de novo* Treg precursors are gated as CD25^{+}Foxp3-RFP^{-} and CD25^{-}Foxp3-RFP^{+}. Gating strategy presented as representative FACs plots including gate title and percentage of cells within the gate given underneath.

(D) Quantification of the (left) percentage and (right) number of CD25^{+}Foxp3-RFP^{-} Treg precursors (black), CD25^{-}Foxp3-RFP^{+} Treg precursors (blue) and CD25^{+}Foxp3-RFP^{+} Treg (purple) within the *de novo* SP4 (CD4^{+}CD8^{-}TCRβ^{+}Rag-GFP^{+}) thymocyte population.

Having identified the proposed *de novo* precursor populations, we then sought to assess their precursor role in thymic Treg development (Figure 3.13). We began by comparing the Rag-GFP expression of Tregs with $CD25^{-}Foxp3^{+}$ and $CD25^{+}Foxp3^{-}$ precursors to establish their ages relative to one another (Figure 3.13.A). We observed that both precursor populations expressed higher average levels of Rag-GFP compared to Tregs, suggesting they are younger than Treg. $CD25^{+}Foxp3^{-}$ precursors appeared to be the youngest population expressing the highest level of Rag-GFP, which was fairly uniform across the population and largely distinct from the Treg population. Whereas Rag-GFP expression within the $CD25^{-}Foxp3^{+}$ precursor population was far more spread and included lower levels of Rag-GFP which overlapped with the Treg population, suggesting these two populations were much closer in age.

To better understand the developmental appearance of the two precursors we next investigated their appearance in an ontogeny sequence (Figure 3.13.B). At D2 a very small Treg population could be observed, in agreement with previous findings that suggest D2 as the first appearance of Tregs[171]. At this time, we also observed a large population of $CD25^{+}Foxp3^{-}$ precursor but very few $CD25^{-}Foxp3^{+}$ precursors. Across ontogeny $CD25^{+}Foxp3^{-}$ precursors remained the largest population although Treg and $CD25^{-}Foxp3^{+}$ precursors increased in size following D2, particularly in the first week of life, at a seemingly similar rate. This suggests that $CD25^{+}Foxp3^{-}$ precursors are established as a population prior to Treg and $CD25^{-}Foxp3^{+}$ precursors, whose developmental appearance is similar. Overall, both the Rag-GFP expression and ontogeny appearance of $CD25^{+}Foxp3^{-}$ precursors suggest that as a population they precede Tregs, in keeping with a precursor role. In contrast both Rag-GFP expression and ontogeny appearance of $CD25^{-}Foxp3^{+}$ precursors suggest much greater overlap with Tregs, making the developmental relationship between the two less clear cut.

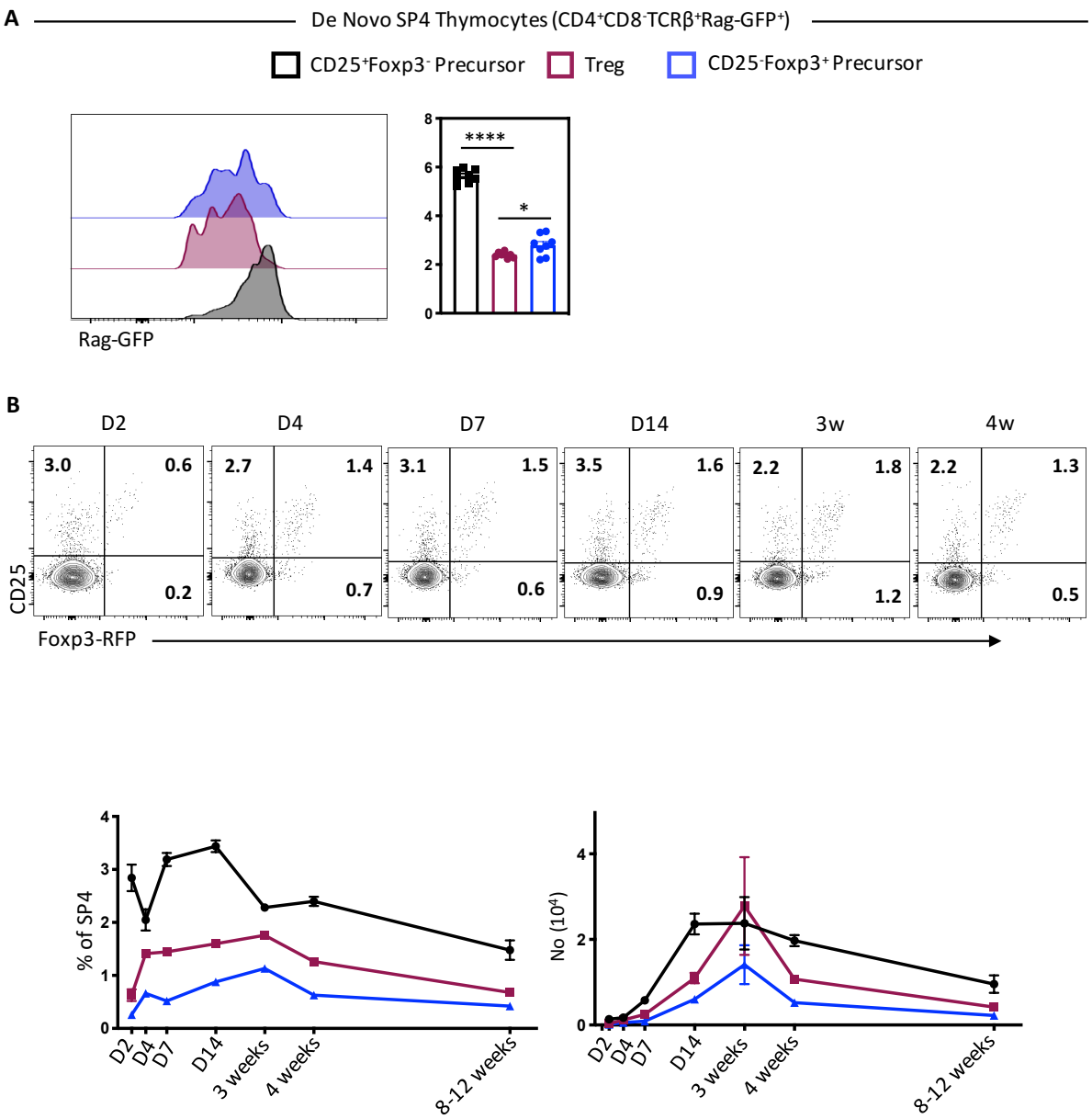
A
De Novo SP4 Thymocytes (CD4+CD8-TCRβ+Rag-GFP+)
CD25+Foxp3- Precursor
Treg
CD25-Foxp3+ Precursor
Rag-GFP
****
*
B
D2
D4
D7
D14
3w
4w
3.0
0.6
0.2
2.7
1.4
0.7
3.1
1.5
0.6
3.5
1.6
0.9
2.2
1.8
1.2
2.2
1.3
0.5
CD25
Foxp3-RFP
% of SP4
No (10⁴)
D2
D4
D7
D14
3 weeks
4 weeks
8-12 weeks

Figure 3. 13 Early Developmental Appearance of Thymic CD25^{+}Foxp3^{-} Precursors Relative to CD25^{-}Foxp3^{+} Precursors and Tregs

(A) Comparison of Rag-GFP expression of *de novo* SP4 (CD4^{+} CD8^{-} TCRβ^{+} Rag-GFP^{+}) thymocyte populations, CD25^{+} Foxp3-RFP^{+} Treg (purple), CD25^{+} Foxp3-RFP^{-} Treg precursors and CD25^{-} Foxp3-RFP^{+} Treg precursors, from adult (8-12 week) Foxp3-RFPxRag-GFP mice. Data is representative of n=8 across 6 independent experiments. Representative FACs plot shows Rag-GFP levels of Treg, CD25^{+} Foxp3-RFP^{-} and CD25^{-} Foxp3-RFP^{+} Treg precursors. Bar chart quantifies the the MFI of Rag-GFP for the three populations. Statistical analysis performed using a repeated measures one way anova, where * $p<0.05$, **** $p<0.0001$.

(B) Appearance of *de novo* SP4 thymocyte populations, CD25^{+} Foxp3-RFP^{+} Treg (purple), CD25^{+} Foxp3-RFP^{-} Treg precursors and CD25^{-} Foxp3-RFP^{+} Treg precursors, across ontogeny of Foxp3-RFPxRag-GFP mice. All timepoints representative of $n \geq 5$ across ≥ 2 independent experiments. Representative FACs plots show the CD25/Foxp3 profile of the *de novo* SP4 thymocytes at indicated ages, with the percentage of Treg, CD25^{+} Foxp3-RFP^{-} and CD25^{-} Foxp3-RFP^{+} Treg precursors given in the respective quadrant. Below graphs quantify, (left) the percentage and (right) the numbers, of the three populations within the SP4 population across the timecourse.

Furthermore, surprisingly we were also able to identify $CD25^{-}Foxp3^{+}$ precursors alongside Tregs within both the Rag-GFP^{+} RTE and Rag-GFP^{-} mature SP4 splenocyte population (Figure 3.14). Moreover, mature $CD25^{-}Foxp3^{+}$ precursors were present at a similar proportion to Tregs (Figure 3.14.B). In contrast, very few $CD25^{+}Foxp3^{-}$ splenocytes were detected within either the RTE or mature SP4 splenocyte fraction. The presence of $CD25^{-}Foxp3^{+}$ precursors extra-thymically is conflicting with a purely thymic Treg precursor role and may instead indicate a more complex dynamic relationship between Tregs and $CD25^{-}Foxp3^{+}$ precursors.

Having investigated the two thymic Treg precursors in the context of bulk thymic Treg development, we wondered whether some of the observed differences, and indeed the requirement for both precursor populations may relate to differential roles in heterogeneous Treg development. Previously we had identified $CD62L^{hi}$ and $CD62L^{lo}$ *de novo* thymic Treg subsets, we therefore looked at CD62L expression within Treg precursors to gain some insight into the relationship between them (Figure 3.15-16). Examining $CD25^{+}Foxp3^{-}$ thymic precursors revealed heterogeneous expression of CD62L within this population, with the majority being $CD62L^{lo}$ while a smaller proportion were $CD62L^{hi}$ (Figure 3.15.A). To try and unpick a possible ordered development pathway we compared Rag-GFP expression of the precursor subsets and CD62L Treg subsets (Figure 3.15.B). We observed that levels of Rag-GFP were fairly distinct and gradually decreased from highest average expression to lowest in the order $CD62L^{lo}CD25^{-}Foxp3^{+}$ precursor, $CD62L^{hi}CD25^{-}Foxp3^{+}$ precursor, $CD62L^{hi}$ Treg then $CD62L^{lo}$ Treg. This may suggest a sequential order of development beginning with $CD62L^{lo}CD25^{-}Foxp3^{+}$ precursor transitioning to $CD62L^{hi}$ which give rise to $CD62L^{hi}$ Tregs.

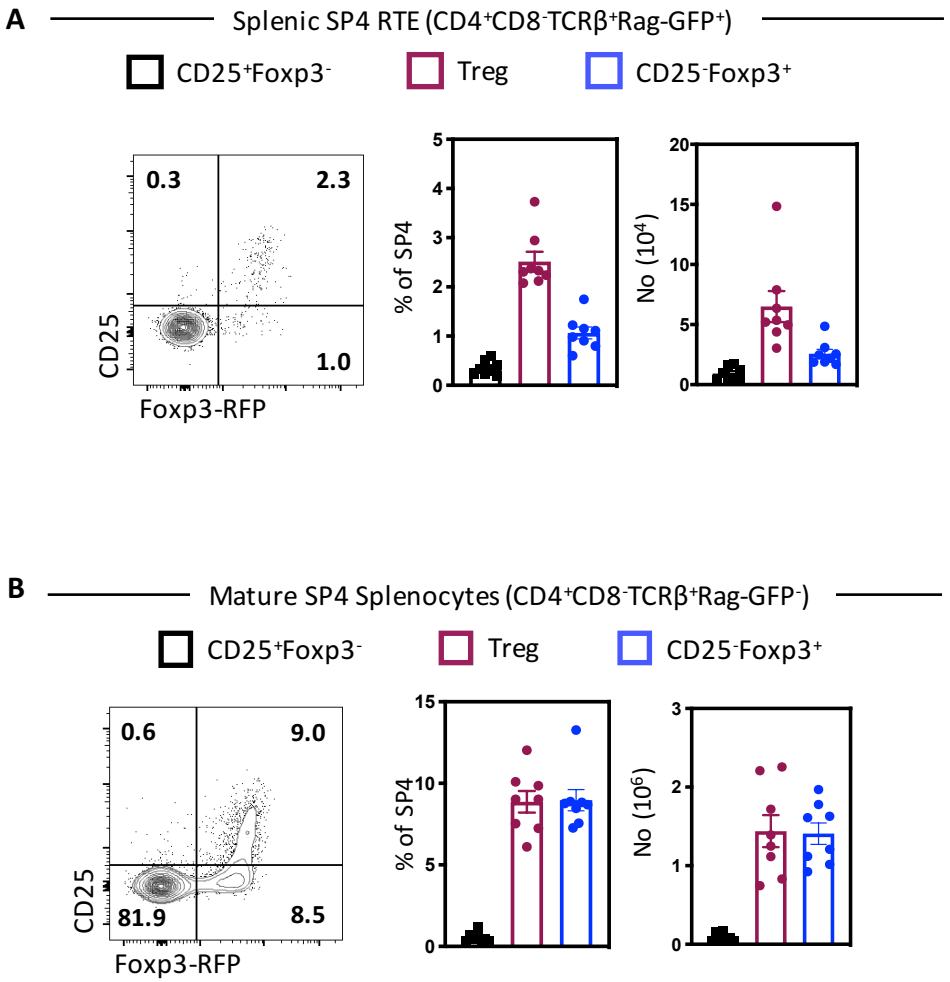
A
Splenic SP4 RTE (CD4+CD8-TCRβ+Rag-GFP+)
CD25+Foxp3-
Treg
CD25-Foxp3+
0.3
2.3
1.0
CD25
Foxp3-RFP
% of SP4
No (10^4)
B
Mature SP4 Splenocytes (CD4+CD8-TCRβ+Rag-GFP-)
CD25+Foxp3-
Treg
CD25-Foxp3+
0.6
9.0
81.9
8.5
CD25
Foxp3-RFP
% of SP4
No (10^6)

Figure 3. 14 SP4 T-cells with a CD25$^-$Foxp3$^+$ Thymic Treg Precursor Phenotype are Present in the Spleen

Analysis of SP4 splenocyte populations which resemble CD25$^+$Foxp3-RFP$^-$ or CD25$^-$Foxp3-RFP$^+$ thymic Treg precursors within adult Foxp3-RFPx Rag-GFP adult (8-12 weeks) mice. All data representative of n=8 across 6 independent experiments.

(A) Analysis of splenic SP4 RTE (CD4$^+$CD8$^-$TCRβ$^+$Rag-GFP$^+$) populations: CD25$^+$Foxp3-RFP$^+$ Treg (purple), CD25$^+$Foxp3-RFP$^-$ (black) and CD25$^-$Foxp3-RFP$^+$ (blue). Data presented as representative FACs plot of the CD25/Foxp3 profile of SP4 RTE and bar char which quantify the percentages and numbers of the SP4 populations as indicated.

(B) Analysis of mature SP4 (CD4$^+$CD8$^-$TCRβ$^+$Rag-GFP$^-$) splenocyte populations: CD25$^+$Foxp3-RFP$^+$ Treg (purple), CD25$^+$Foxp3-RFP$^-$ (black) and CD25$^-$Foxp3-RFP$^+$ (blue). Data presented as representative FACs plot of the CD25/Foxp3 profile of SP4 splenocytes and bar char which quantify the percentages and numbers of the SP4 populations as indicated.

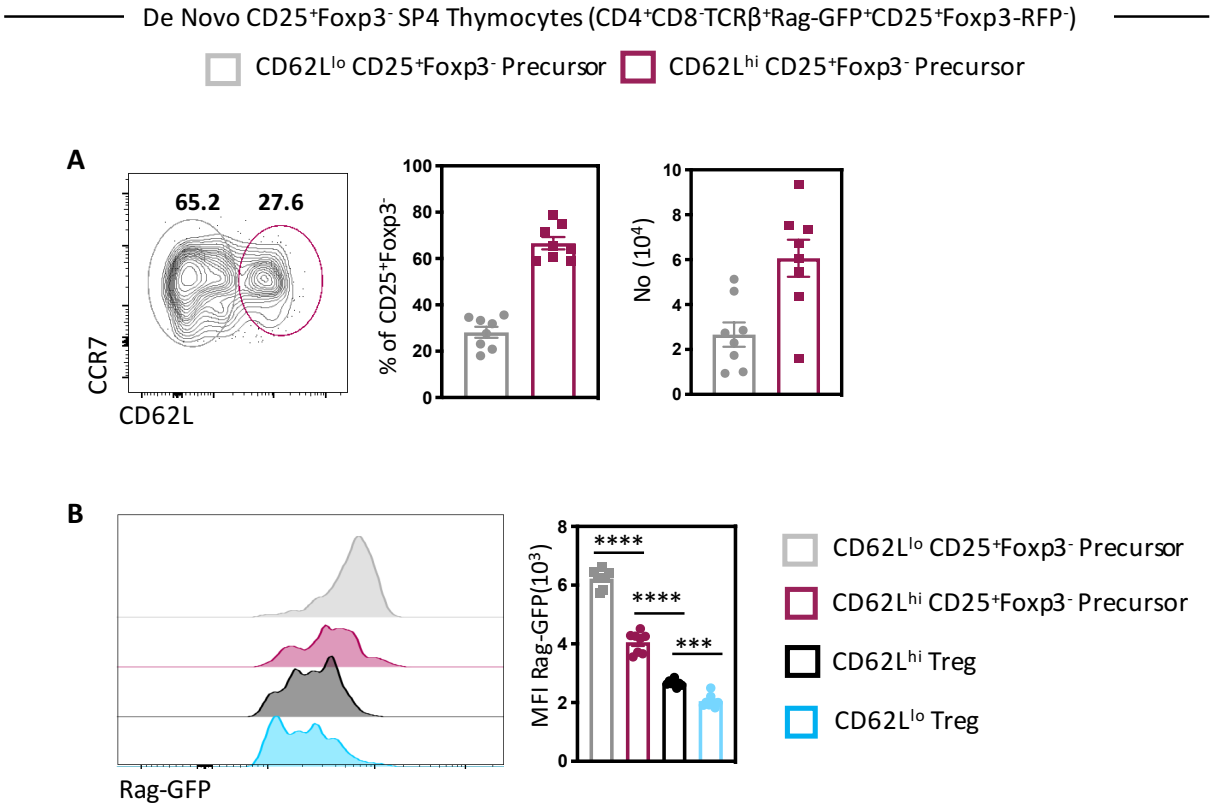
De Novo CD25+Foxp3- SP4 Thymocytes (CD4+CD8-TCRβ+Rag-GFP+CD25+Foxp3-RFP-)
CD62Llo CD25+Foxp3- Precursor
CD62Lhi CD25+Foxp3- Precursor
A
65.2
27.6
CCR7
CD62L
% of CD25+Foxp3-
No (10^4)
B
Rag-GFP
MFI Rag-GFP(10^3)
****
****
***
CD62Llo CD25+Foxp3- Precursor
CD62Lhi CD25+Foxp3- Precursor
CD62Lhi Treg
CD62Llo Treg

Figure 3. 15 *De Novo* CD25^{+}Foxp3^{-} Treg Precursors Comprise CD62L^{hi} and CD62L^{lo} Subsets

Identification and characterisation of de novo thymic CD25^{+}Foxp3-RFP^{-} Treg precursors in Foxp3-RFPx Rag-GFP adult (8-12 weeks) mice. All data representative of n=8 across 6 independent experiments.

(A) Phenotypic analysis of CD62L and CCR7 expression on de novo thymic CD25^{+}Foxp3-RFP^{-} Treg precursors (pre-gated as CD4^{+}CD8^{-}TCRβ^{+}Rag-GFP^{+}). Representative FACs plot of CD62L/CCR7 profile with two populations gated as CD62L^{hi} (purple) and CD62L^{lo} (grey). Graphs quantify the percentage (left) and number (right) of the two CD62L^{hi} (purple) and CD62L^{lo} (grey) CD25^{+}Foxp3-RFP^{-} Treg precursor populations.

(B) Comparison of Rag-GFP expression of de novo CD25^{+}Foxp3-RFP^{-} Treg precursor and Treg (CD25^{+}Foxp3-RFP^{+}) subsets. Representative FACs plot shows Rag-GFP levels of CD25^{+}Foxp3-RFP^{-}CD62L^{lo} (grey), CD25^{+}Foxp3-RFP^{-}CD62L^{hi} (purple), CD25^{+}Foxp3-RFP^{+}CD62L^{hi} (black) and CD25^{+}Foxp3-RFP^{+}CD62L^{lo} (blue) thymocytes. The accompanying bar chart quantifies the MFI of Rag-GFP for the four thymocyte populations. All statistics presented were generated using a repeated measures one way anova, *** $p < 0.001$, **** $p < 0.0001$.

Similarly, we found that $CD25^{-}Foxp3^{+}$ thymic precursors were also heterogonous for CD62L, although here the population was more evenly split between $CD62L^{hi}$ and $CD62L^{lo}$ thymocytes, with the former being slightly more abundant (Figure 3.16.A). Again, we examined Rag-GFP expression to try and discern a developmental order however while we observed some slight differences in the average expression, the populations all showed a lot of overlap in Rag-GFP levels (Figure 3.16.B). Suggesting little difference in age between the populations, thereby making it challenging to infer a developmental progression.

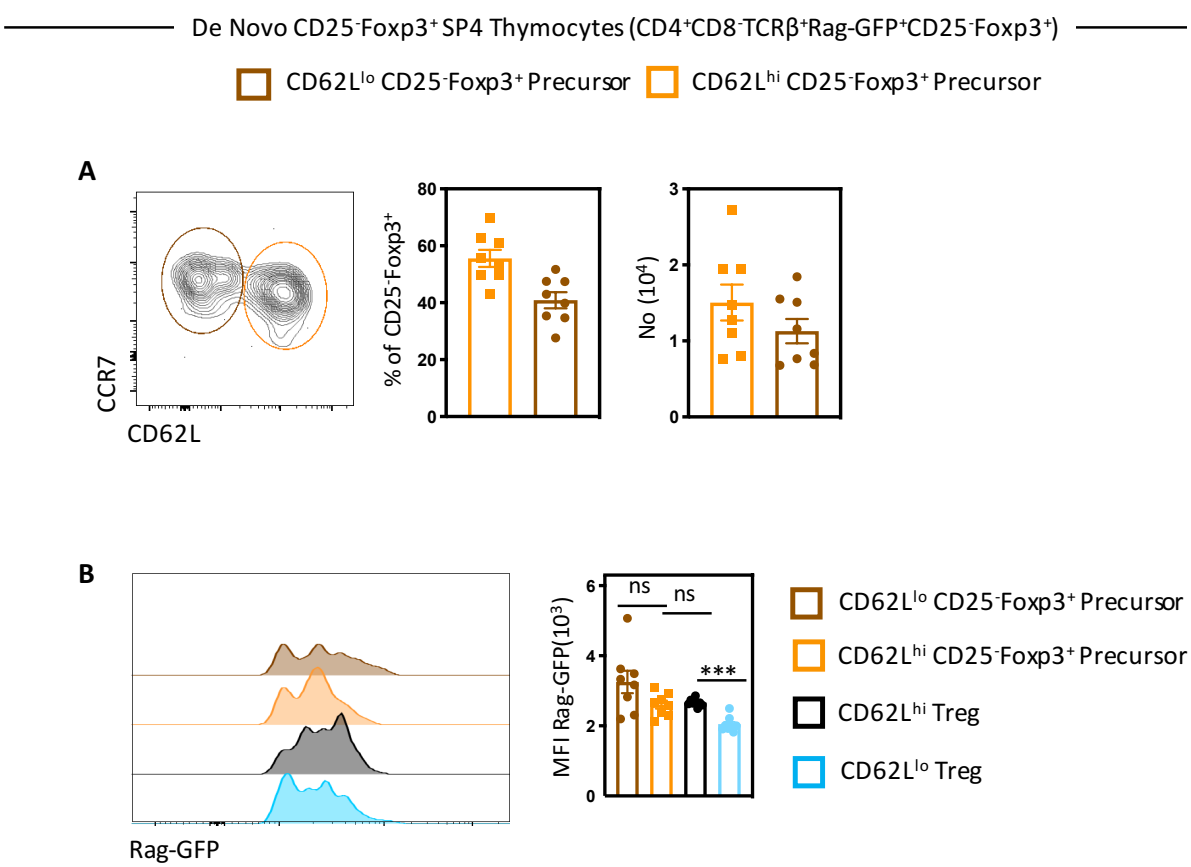
De Novo CD25-Foxp3+ SP4 Thymocytes (CD4+CD8-TCRβ+Rag-GFP+CD25-Foxp3+)
CD62Llo CD25-Foxp3+ Precursor
CD62Lhi CD25-Foxp3+ Precursor
A
CCR7
CD62L
% of CD25-Foxp3+
No (10^4)
B
Rag-GFP
MFI Rag-GFP(10^3)
ns
ns
***
CD62Llo CD25-Foxp3+ Precursor
CD62Lhi CD25-Foxp3+ Precursor
CD62Lhi Treg
CD62Llo Treg

Figure 3. 16 *De Novo* CD25$^-$Foxp3$^+$ Treg Precursors Comprise CD62L^{hi} and CD62L^{lo} Subsets

Identification and characterisation of de novo thymic CD25$^-$Foxp3-RFP$^+$ Treg precursors in Foxp3-RFPx Rag-GFP adult (8-12 weeks) mice. All data representative of n=8 across 6 independent experiments.

(A) Phenotypic analysis of CD62L and CCR7 expression on de novo thymic CD25$^-$Foxp3-RFP$^+$ Treg precursors (pre-gated as CD4$^+$CD8$^-$TCRβ$^+$Rag-GFP$^+$). Representative FACs plot of CD62L/CCR7 profile with two populations gated as CD62L^{hi} (orange) and CD62L^{lo} (brown). Graphs quantify the percentage (left) and number (right) of the two CD62L^{hi} (orange) and CD62L^{lo} (brown) CD25$^+$Foxp3-RFP$^-$ Treg precursor populations.

(B) Comparison of Rag-GFP expression of de novo CD25$^-$Foxp3-RFP$^+$ Treg precursor and Treg (CD25$^+$Foxp3-RFP$^+$) subsets. Representative FACs plot shows Rag-GFP levels of CD25$^-$ Foxp3-RFP$^+$CD62L^{lo} (brown), CD25$^-$Foxp3-RFP$^+$CD62L^{hi} (orange), CD25$^+$Foxp3-RFP$^+$CD62L^{hi} (black) and CD25$^+$Foxp3-RFP$^+$CD62L^{lo} (blue) thymocytes. The accompanying bar chart quantifies the the MFI of Rag-GFP for the four thymocyte populations. All statistics presented were generated using a repeated measures one way anova, ns $p>0.05$, *** $p<0.001$.

3.2.3 Possible Regulators of the Treg Lineage

Having investigated and broadly characterised heterogeneous *de novo* thymic Treg development we next questioned how the process may be orchestrated by the thymic microenvironment. Given the essential role of the thymic medulla in regulating bulk Treg development[158], we wondered whether it may also direct development of our two identified CD62L Treg subsets. Furthermore, in some animal models with altered medullary environments bulk thymic Treg development has been described as normal[300,307], which prompted us to wonder whether in these models a subtler phenotype relating to Treg heterogeneity may have been missed. We therefore decided to investigate heterogeneous *de novo* Treg development in two such models, namely *Aire*$^{-/-}$ (which lack Aire mediated TRA expression by mTEC) and *Ltbr*$^{-/-}$ (which lack LTβR, a critical regulator of medullar organisation and mTEC development).

One complication with investigating *de novo* Treg development in *Aire*$^{-/-}$ and *Ltbr*$^{-/-}$, was that these KOs were crossed to Rag-GFP but not Foxp3-RFP reporter, meaning that Foxp3 had to be detected through intracellular staining that retained Rag-GFP. We therefore adapted a previously described formalin-based protocol[317] to retain the GFP while staining for intracellular markers (Section 2.6.4). We then compared the expression of both Rag-GFP and Foxp3 detected when thymocytes from Rag-GFP mice were subject to different fixation and intracellular staining approaches (Figure 3.17). Thymocytes were either left unfixed, or underwent fixation and intracellular staining following either our standard approach using ebioscience fixation or our Rag-GFP retention protocol using formalin-based fixation (Section 2.6.3-4).

Initially we compared Rag-GFP expression of DP thymocytes, which should virtually all be Rag-GFP$^+$ (Figure 3.17.A). We found that relative to the non-fluorescent control virtually all DP thymocytes appeared Rag-GFP$^+$ following formalin, but not ebioscience, fixation. However, whist the Rag-GFP levels of DP thymocytes fixed using formalin were distinct from the non-fluorescent control, the intensity of the Rag-GFP signal was reduced compared to the unfixed Rag-GFP sample (Figure 3.17.A). Therefore, it was important to assess how well the formalin fixation method reported Rag-GFP$^+$ cells in populations with lower Rag-GFP intensity. Within the SP4 thymocyte population a clear Rag-GFP$^+$ population was identified following formalin fix, with the percentage of Rag-GFP$^+$ thymocytes detected similar to the unfixed Rag-GFP sample, although again the Rag-GFP intensity was reduced (Figure 3.17.B). Furthermore, within the SP4 population we could also detect Foxp3, with the percentage of Foxp3$^+$ cells detected similar to ebioscience fixation (Figure 3.17.B). We also examined Foxp3 and Rag-GFP expression of splenocytes following formalin fixation (Figure 3.17.C). Similar to the thymus Foxp3 detection was clear however while Rag-GFP$^+$ splenocytes were detected, the frequency was much lower than the unfixed control. Possibly this reduction is a consequence of failing to retain cells with low intensity Rag-GFP$^+$, which are more prominent in the spleen. However overall formalin fixation offered a viable compromise between retaining Rag-GFP and detecting Foxp3, particularly within the thymus.

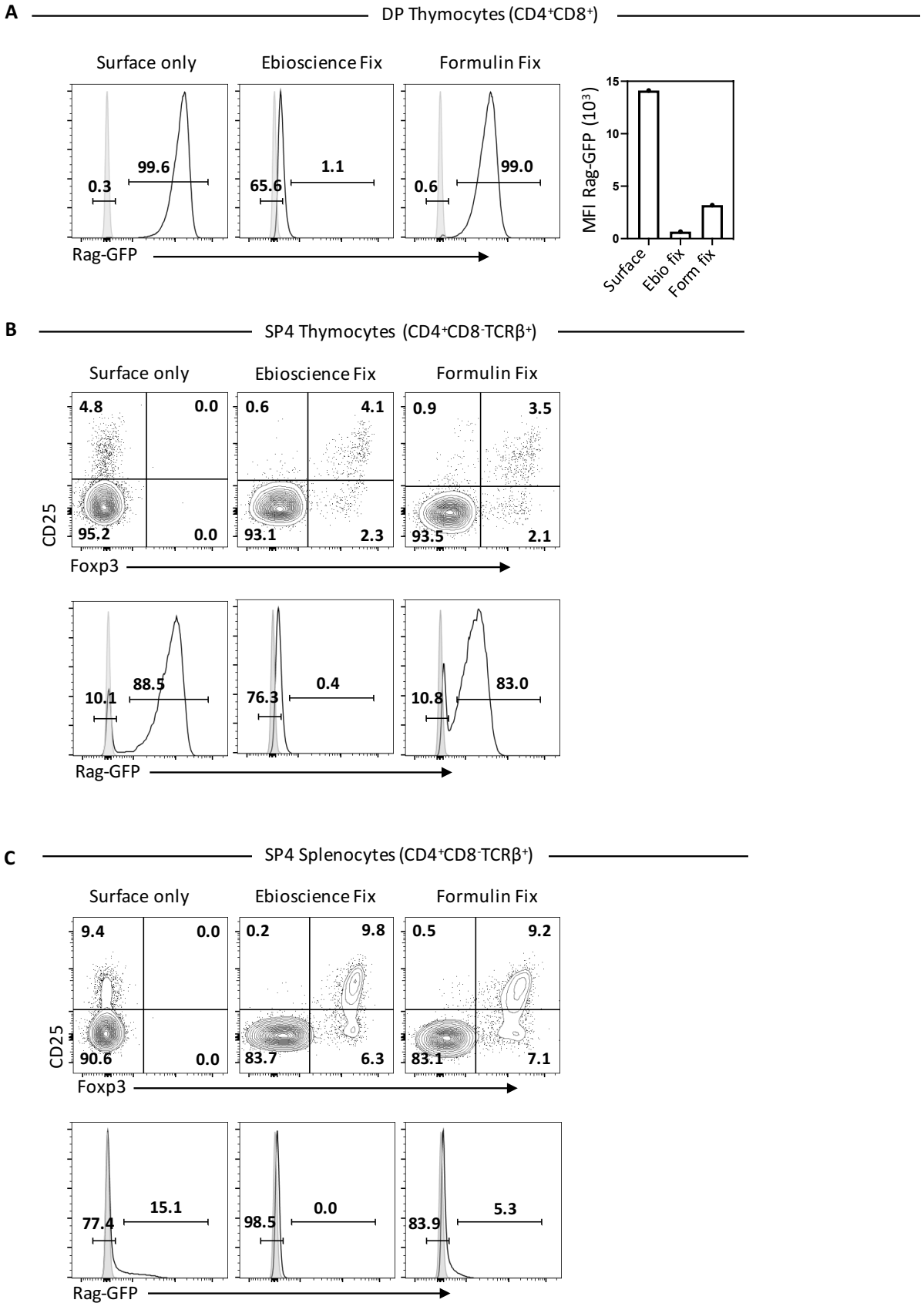
A
DP Thymocytes (CD4+CD8+)
Surface only
Ebioscience Fix
Formulin Fix
99.6
0.3
1.1
65.6
99.0
0.6
Rag-GFP
MFI Rag-GFP (10³)
15
10
5
0
Surface
Ebio fix
Form fix
B
SP4 Thymocytes (CD4+CD8-TCRβ+)
Surface only
Ebioscience Fix
Formulin Fix
4.8
0.0
95.2
0.0
0.6
4.1
93.1
2.3
0.9
3.5
93.5
2.1
CD25
Foxp3
88.5
10.1
0.4
76.3
83.0
10.8
Rag-GFP
C
SP4 Splenocytes (CD4+CD8-TCRβ+)
Surface only
Ebioscience Fix
Formulin Fix
9.4
0.0
90.6
0.0
0.2
9.8
83.7
6.3
0.5
9.2
83.1
7.1
CD25
Foxp3
15.1
77.4
0.0
98.5
5.3
83.9
Rag-GFP

Figure 3. 17 Formalin Fixation Retains Rag-GFP During Intracellular Staining

Comparison of Rag-GFP retention and intracellular Foxp3 detection using different fixation/ intracellular staining approaches. All cells underwent simultaneous surface staining then were subject to different fixation/intracellular staining approaches as follows: surface only cells did not undergo fixation or intracellular staining, Ebioscience Fix cells were fixed with the eBioscience™ Foxp3 then stained for Foxp3 (Section 2.6.3), and Formulin Fix cells were fixed with 1:1 formalin (4% formaldehyde): PBS then stained for Foxp3 (Section 2.6.4). Analysis performed in Rag-GFP adult (8-12 weeks) mice, all data representative of n=1 across n=1 experiments

(A) Analysis of Rag-GFP expression of DP ($CD4^+CD8^+$) thymocytes stained by the three described methods. Data presented as representative FACs plots which show Rag-GFP levels relative to a non-fluorescent staining control (filled grey). Rag-GFP^+ and Rag-GFP^- gating defined as detailed in Figure 3.1.B. Accompanying graph quantifies Rag-GFP MFI of Rag-GFP^+ DP thymocytes detected by each method.

(B) Comparison of Rag-GFP expression and Foxp3 detection within SP4 ($CD4^+CD8^-TCR\beta^+$) thymocytes stained by the three described methods. Data presented as representative FACs plots which show (top) the CD25/Foxp3 profile and (bottom) the Rag-GFP levels of SP4 thymocytes stained by the indicated method.

(C) Comparison of Rag-GFP expression and Foxp3 detection within SP4 ($CD4^+CD8^-TCR\beta^+$) splenocytes. Data presented as representative FACs plots which show (top) the CD25/Foxp3 profile and (bottom) Rag-GFP of SP4 thymocytes stained by the indicated method.

We therefore utilised this method to assess thymic Treg development in adult Rag-GFPx*Aire*$^{-/-}$ relative to Rag-GFPx*Aire*$^{+/+}$ WT controls (Figure 3.18). Comparison of the general thymic phenotype revealed little difference in either total thymic cellularity (Figure 3.18.A) or the size of the bulk SP4 population (3.18.B). Similarly, Rag-GFP^{+} *de novo* SP4 thymocyte populations, including Tregs, were comparable in Aire$^{-/-}$ and WT controls, in keeping with previous analysis[307] (Figure 3.18.C). To more closely assess the *de novo* Treg population, we examined the split of CD62L^{hi} to CD62L^{lo} Tregs. Again, we identified little difference between Aire$^{-/-}$ and WT (Figure 3.18.D), suggesting that Aire is a non-essential regulator of heterogeneous Treg development in the adult thymus.

Whilst the thymic phenotype of *Aire*$^{-/-}$ appeared normal we wondered if there was any difference in the export of Tregs. We therefore examined the spleen, initial characterisation confirmed that the splenic cellularity and bulk SP4 population were broadly comparable between *Aire*$^{-/-}$ and WT controls (Figure 3.19.A-B). We then examined the SP4 RTEs, finding that within this population there appeared to be little difference in the export of bulk Tconv or Treg RTEs between WT and *Aire*$^{-/-}$(Figure 3.19.C). Similarly, the two CD62L Treg subsets were also present within the Treg RTEs at similar proportions (Figure 3.19.D). Overall indicating that Aire deficiency had little impact on the export of bulk or heterogeneous Tregs.

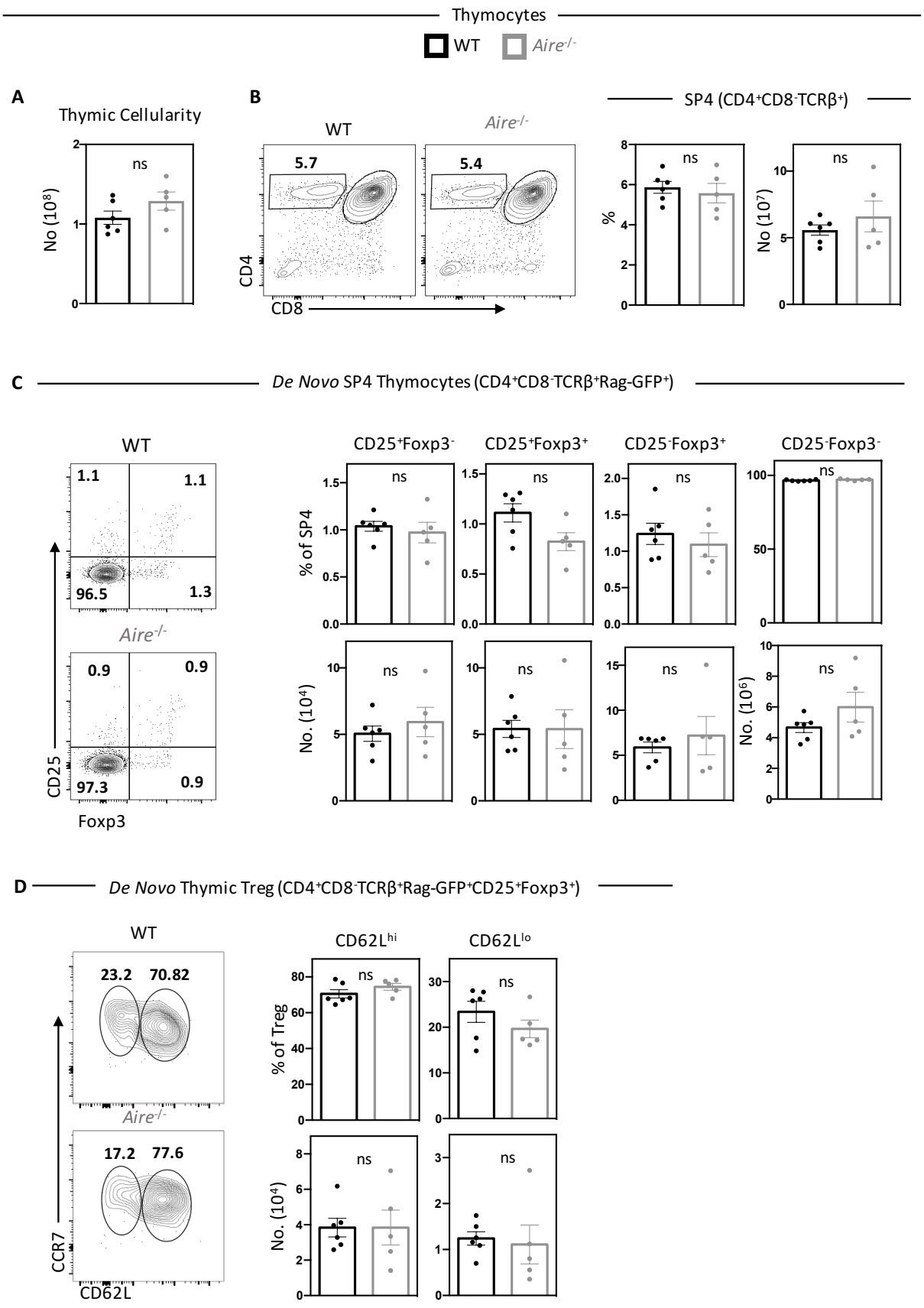
Thymocytes
WT
Aire-/-
A
Thymic Cellularity
No (10⁸)
ns
B
WT
Aire-/-
5.7
5.4
CD4
CD8
SP4 (CD4+CD8-TCRβ+)
%
No (10⁷)
ns
C
De Novo SP4 Thymocytes (CD4+CD8-TCRβ+Rag-GFP+)
WT
1.1
1.1
96.5
1.3
Aire-/-
0.9
0.9
97.3
0.9
CD25
Foxp3
CD25+Foxp3-
CD25+Foxp3+
CD25-Foxp3+
CD25-Foxp3-
% of SP4
No. (10⁴)
No. (10⁶)
ns
D
De Novo Thymic Treg (CD4+CD8-TCRβ+Rag-GFP+CD25+Foxp3+)
WT
23.2
70.82
Aire-/-
17.2
77.6
CCR7
CD62L
CD62Lhi
CD62Llo
% of Treg
No. (10⁴)
ns

Figure 3. 18 Thymic Treg Development Appears Normal in *Aire*$^{-/-}$ Adults

Comparison of thymic phenotype in *Aire*$^{-/-}$ x Rag-GFP (grey) and WT x Rag-GFP (black) adult (8-12 weeks) mice. Data representative of n=5 for *Aire*$^{-/-}$ and n=6 for WT across 5 independent experiments. All statistics were generated using a unpaired student's t-tests, where ns $p>0.05$.

(A) Comparison of total thymic cellularity between *Aire*$^{-/-}$ and WT depicted as graphical quantification of numbers.

(B) Comparison of SP4 (CD4^{+}CD8^{-}TCRβ^{+}) thymocyte population. Representative FACs plots of CD4/CD8 profile of thymocytes for *Aire*$^{-/-}$ and WT mice as indicated. The graphs on the right quantifies the percentages and numbers of SP4 thymocytes across the two conditions as indicated.

(C) Comparison of *de novo* SP4 thymocyte (CD4^{+}CD8^{-}TCRβ^{+}Rag-GFP^{+}) populations: CD25^{+}Foxp3^{-} and CD25^{-}Foxp3^{+} Treg precursors, CD25^{+}Foxp3^{+} Treg and CD25^{-}Foxp3^{-} Tconv. Representative FACs plots of CD25/Foxp3 profile of SP4 thymocytes for *Aire*$^{-/-}$ and WT mice as indicated. Accompanying graphs quantify the percentages (top) and numbers (bottom) of the four SP4 thymocyte populations across the two conditions as indicated.

(D) Comparison of CD62L phenotype of *de novo* thymic Treg (CD4^{+}CD8^{-}TCRβ^{+}Rag-GFP^{+}CD25^{+}Foxp3^{+}). Representative FACs plots of the CD62L/CCR7 profile of the Treg for each condition for *Aire*$^{-/-}$ and WT mice as indicated. Accompanying graphs quantify the percentages (top) and numbers (bottom) of the CD62L^{hi} and CD62L^{lo} Tregs across the two conditions as indicated.

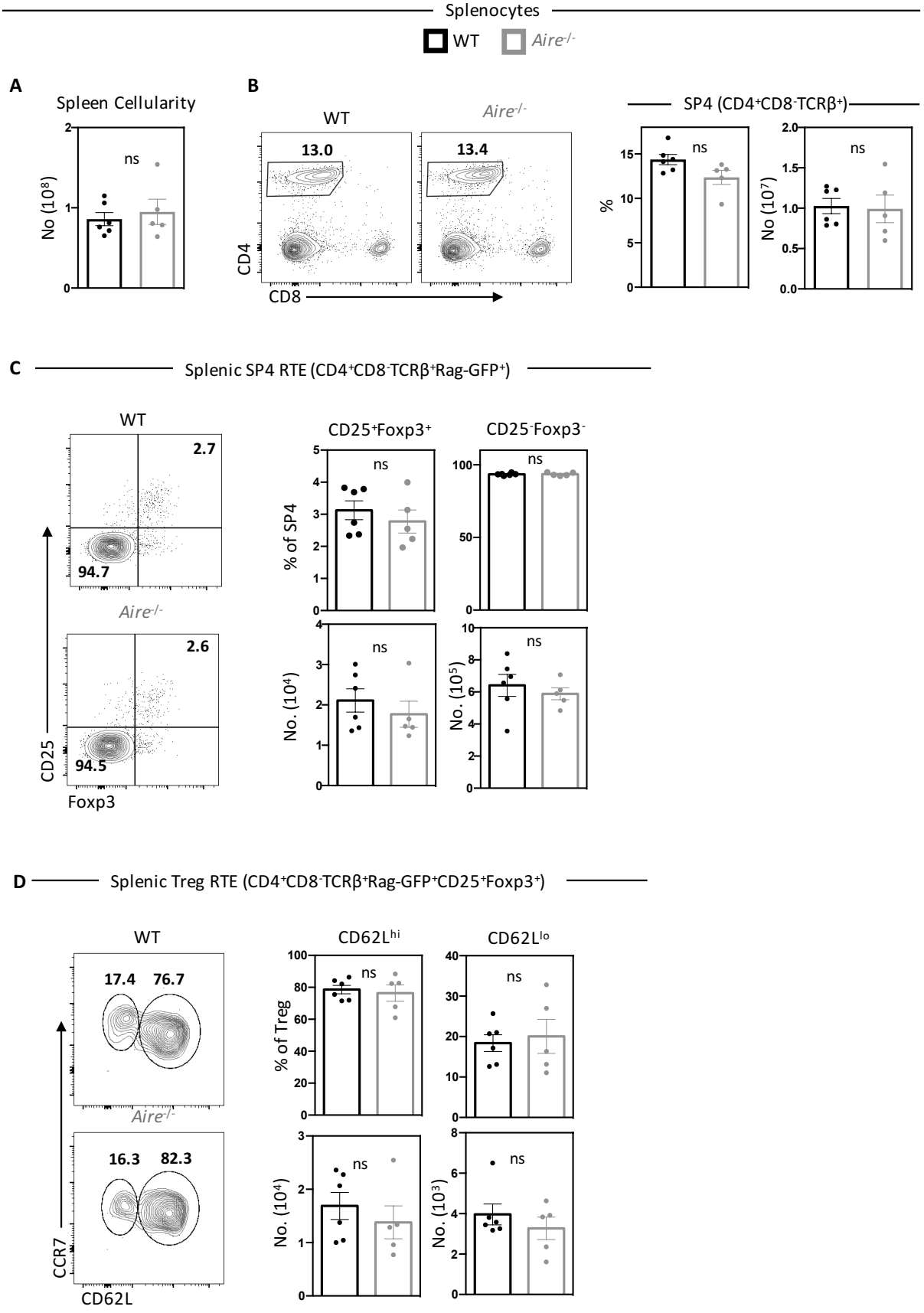
Splenocytes
WT
Aire-/-
A
Spleen Cellularity
No (10^8)
ns
B
WT
Aire-/-
13.0
13.4
CD4
CD8
SP4 (CD4+CD8-TCRβ+)
%
No (10^7)
ns
C
Splenic SP4 RTE (CD4+CD8-TCRβ+Rag-GFP+)
WT
2.7
94.7
Aire-/-
2.6
94.5
CD25
Foxp3
CD25+Foxp3+
CD25-Foxp3-
% of SP4
No. (10^4)
No. (10^5)
ns
D
Splenic Treg RTE (CD4+CD8-TCRβ+Rag-GFP+CD25+Foxp3+)
WT
17.4
76.7
Aire-/-
16.3
82.3
CCR7
CD62L
CD62Lhi
CD62Llo
% of Treg
No. (10^4)
No. (10^3)
ns

Figure 3. 19 Treg Populations Appear Normal in the Spleen of *Aire*$^{-/-}$ Adults

Comparison of splenic phenotype in *Aire*$^{-/-}$ x Rag-GFP (grey) and WT x Rag-GFP (black) adult (8-12 weeks) mice. Data representative of n=5 for *Aire*$^{-/-}$ and n=6 for WT across 5 independent experiments. All statistics were generated using a unpaired student's t-tests, where ns $p>0.05$.

(A) Comparison of total splenic cellularity between *Aire*$^{-/-}$ and WT depicted as graphical quantification of numbers.

(B) Comparison of SP4 (CD4^{+}CD8^{-}TCRβ^{+}) splenocyte population. Representative FACs plots of CD4/CD8 profile of splenocytes for *Aire*$^{-/-}$ and WT mice as indicated. The graphs on the right quantifies the percentages and numbers of SP4 splenocytes across the two conditions as indicated.

(C) Comparison of SP4 recent thymic emigrant (RTE) (CD4^{+}CD8^{-}TCRβ^{+}Rag-GFP^{+}) populations: CD25^{+}Foxp3^{+} Treg and CD25^{-}Foxp3^{-} Tconv. Representative FACs plots of CD25/Foxp3 profile of SP4 RTE for *Aire*$^{-/-}$ and WT mice as indicated. Accompanying graphs quantify the percentages (top) and numbers (bottom) of the Tconv and Treg RTEs across the two conditions as indicated.

(D) Comparison of CD62L phenotype of Treg RTE (CD4^{+}CD8^{-}TCRβ^{+}Rag-GFP^{+}CD25^{+}Foxp3^{+}). Representative FACs plots of the CD62L/CCR7 profile of the Treg for for *Aire*$^{-/-}$ and WT mice as indicated. Accompanying graphs quantify the percentages (top) and numbers (bottom) of the CD62L^{hi} and CD62L^{lo} Tregs across the two conditions as indicated.

Previous studies have proposed that the role of Aire in Treg development may be more critical in early neonatal stages compared to the adult[232,233]. Thus, whilst we found little difference in Treg development in the adult Treg, it is possible a more prominent impact on Treg development may be observed at a neonatal time point. We therefore investigated Treg development in D7 *Aire*$^{-/-}$ neonates relative to D7 WT littermate controls, here we did not use Rag-GFP as given the early timepoint recirculation was assumed to be minimal. The gross thymic phenotype, assessed by comparing thymic cellularity and bulk SP4 thymocyte population, seemed similar between WT and *Aire*$^{-/-}$ neonates (Figure 3.20.A-B). However, within the SP4 population we identified a reduction in Tregs (as previously observed[233]) and CD25^{-}Foxp3^{+} precursors, but not thymic Tconvs or CD25^{+}Foxp3^{-} precursors (Figure 3.20.C). Analysis of CD62L phenotype of the Treg population did not reveal any large differences between WT and *Aire*$^{-/-}$ neonates although the proportion of CD62L^{lo} Tregs was slightly higher in *Aire*$^{-/-}$ (Figure 3.20.D). Despite this proportional increase in CD62L^{lo} Tregs we did not see a numerical increase, possibly due to the general reduction in Tregs observed in *Aire*$^{-/-}$ neonates (Figure 3.20.D).

Following our thymic analysis we also examined the exported T-cell population by analysing the spleen (Figure 3.21). Our initial characterisation suggested that splenic cellularity was comparable and while the frequency of total SP4 splenocytes was slightly reduced this didn't result in a numerical difference (Figure 3.21.A-B). Within the SP4 population, Tconv splenocytes were largely unchanged and whilst the proportion of Tregs was slightly increased in *Aire*$^{-/-}$ neonates, this did not translate to a numerical difference (Figure 3.21.C). However on closer examination of the Treg population we did identify a proportional and numerical increase in CD62L^{lo} Tregs, while the CD62L^{hi} subset was largely comparable (Figure 3.21.D).

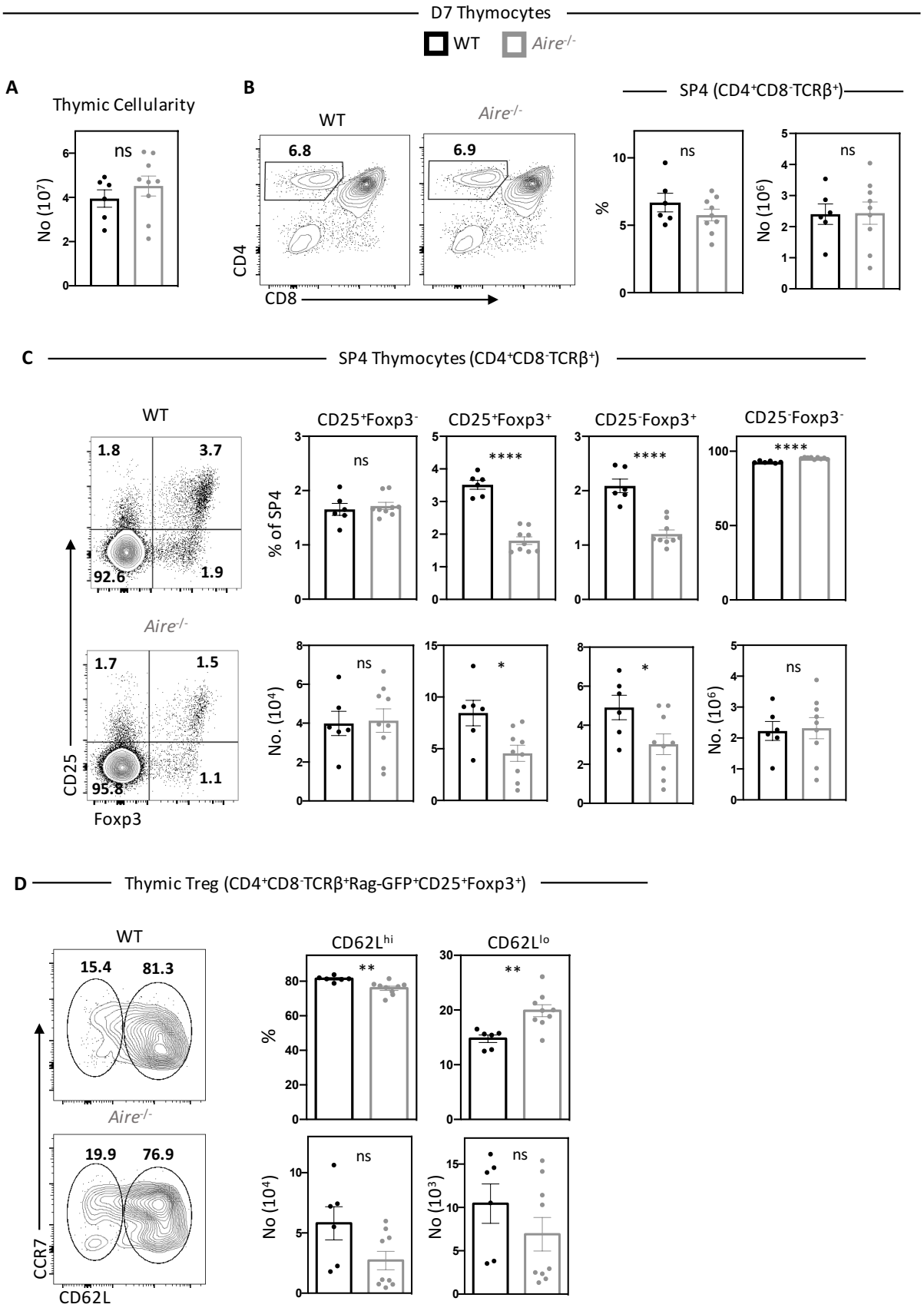
D7 Thymocytes
WT
Aire-/-
A
Thymic Cellularity
No (10^7)
ns
B
WT
Aire-/-
6.8
6.9
CD4
CD8
SP4 (CD4+CD8-TCRβ+)
%
No (10^6)
ns
C
SP4 Thymocytes (CD4+CD8-TCRβ+)
WT
1.8
3.7
92.6
1.9
Aire-/-
1.7
1.5
95.8
1.1
CD25
Foxp3
CD25+Foxp3-
CD25+Foxp3+
CD25-Foxp3+
CD25-Foxp3-
% of SP4
No. (10^4)
No. (10^6)
ns
****
*
D
Thymic Treg (CD4+CD8-TCRβ+Rag-GFP+CD25+Foxp3+)
WT
15.4
81.3
Aire-/-
19.9
76.9
CCR7
CD62L
CD62Lhi
CD62Llo
%
No (10^4)
No (10^3)
**
ns

Figure 3. 20 Reduced De Novo Thymic Treg in D7 *Aire*$^{-/-}$ Neonates Does Not Appear to be a Consequence of Altered Heterogeneous Treg Development

Comparison of thymic phenotype in D7 *Aire*$^{-/-}$ (grey) and WT littermate control (black) neonates. Data representative of n=9 for *Aire*$^{-/-}$ and n=6 for WT across 4 independent experiments. All statistics were generated using a unpaired student's t-tests, where ns $p>0.05$, * $p<0.05$, ** $p<0.01$, **** $p<0.0001$.

(A) Comparison of total thymic cellularity between *Aire*$^{-/-}$ and WT depicted as graphical quantification of numbers.

(B) Comparison of SP4 (CD4^{+}CD8^{-}TCRβ^{+}) thymocyte population. Representative FACs plots of CD4/CD8 profile of thymocytes for *Aire*$^{-/-}$ and WT neonates as indicated. The graphs on the right quantifies the percentages and numbers of SP4 thymocytes across the two conditions as indicated.

(C) Comparison of SP4 thymocyte (CD4^{+}CD8^{-}TCRβ^{+}) populations: CD25^{+}Foxp3^{-} and CD25^{-}Foxp3^{+} Treg precursors, CD25^{+}Foxp3^{+} Treg and CD25^{-}Foxp3^{-} Tconv. Representative FACs plots of CD25/Foxp3 profile of SP4 thymocytes for *Aire*$^{-/-}$ and WT neonates as indicated. Accompanying graphs quantify the percentages (top) and numbers (bottom) of the four SP4 thymocyte populations across the two conditions as indicated.

(D) Comparison of CD62L phenotype of thymic Treg (CD4^{+}CD8^{-}TCRβ^{+}CD25^{+}Foxp3^{+}). Representative FACs plots of the CD62L/CCR7 profile of the Treg for each condition for *Aire*$^{-/-}$ and WT neonates as indicated. Accompanying graphs quantify the percentages (top) and numbers (bottom) of the CD62L^{hi} and CD62L^{lo} Tregs across the two conditions as indicated.

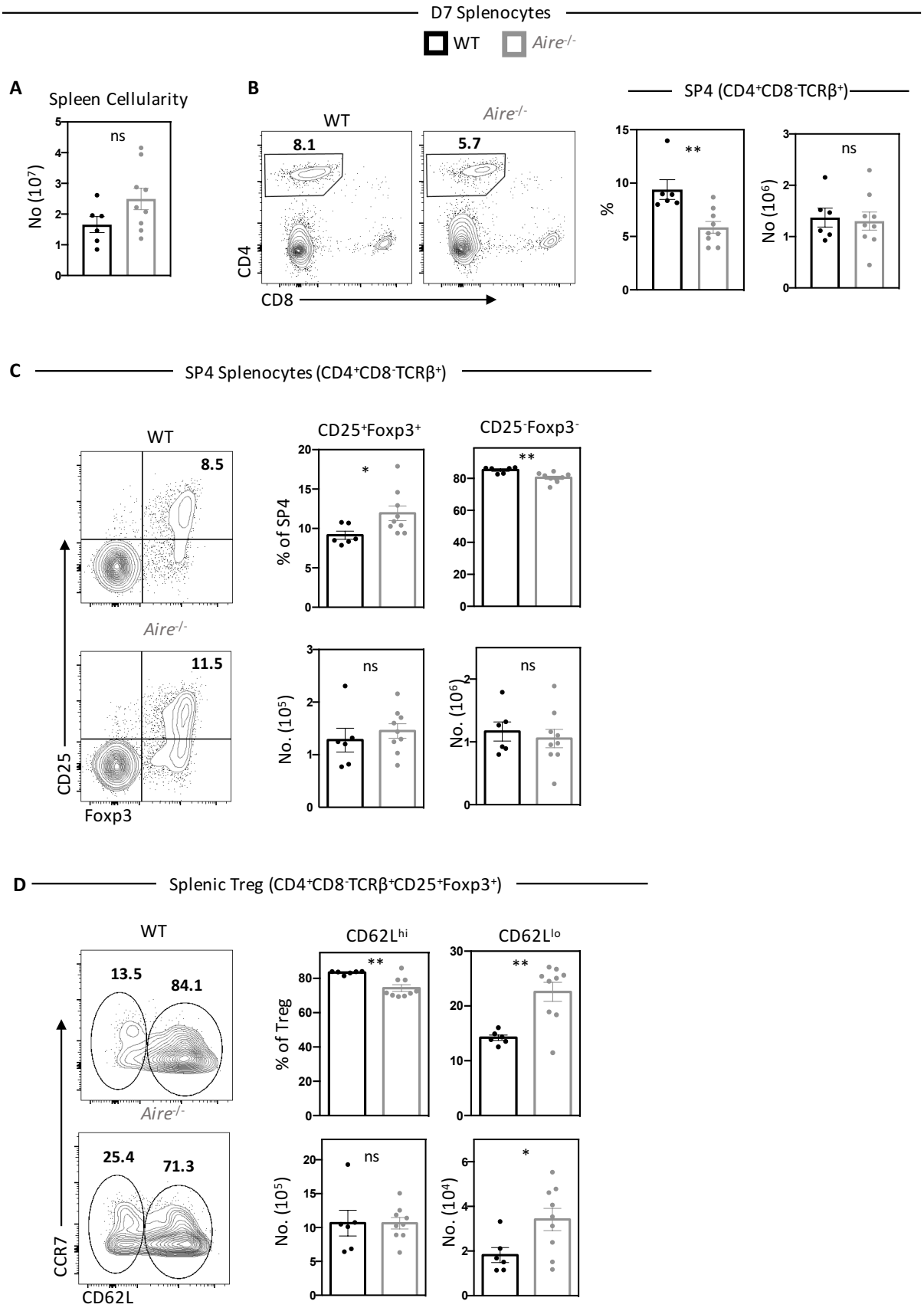
D7 Splenocytes
WT
Aire-/-
A
Spleen Cellularity
No (10^7)
ns
B
WT
Aire-/-
8.1
5.7
CD4
CD8
SP4 (CD4+CD8-TCRβ+)
%
**
No (10^6)
ns
C
SP4 Splenocytes (CD4+CD8-TCRβ+)
WT
8.5
Aire-/-
11.5
CD25
Foxp3
CD25+Foxp3+
CD25-Foxp3-
% of SP4
*
**
No. (10^5)
No. (10^6)
ns
ns
D
Splenic Treg (CD4+CD8-TCRβ+CD25+Foxp3+)
WT
13.5
84.1
Aire-/-
25.4
71.3
CCR7
CD62L
CD62Lhi
CD62Llo
% of Treg
**
**
No. (10^5)
No. (10^4)
ns
*

Figure 3. 21 Absence of Aire has a Limited Impact on D7 Neonatal Splenic Treg Populations

Comparison of splenic phenotype in D7 *Aire*$^{-/-}$ (grey) and WT littermate control (black) neonates. Data representative of n=9 for *Aire*$^{-/-}$ and n=6 for WT across 4 independent experiments. All statistics were generated using a unpaired student's t-tests, where ns $p>0.05$, * $p<0.05$, ** $p<0.01$.

(A) Comparison of total splenic cellularity between *Aire*$^{-/-}$ and WT depicted as graphical quantification of numbers.

(B) Comparison of SP4 ($CD4^{+}CD8^{-}TCR\beta^{+}$) splenocyte population. Representative FACs plots of CD4/CD8 profile of splenocytes for *Aire*$^{-/-}$ and WT neonates as indicated. The graphs on the right quantifies the percentages and numbers of SP4 splenocytes across the two conditions as indicated.

(C) Comparison of SP4 splenocyte populations: $CD25^{+}Foxp3^{+}$ Treg and $CD25^{-}Foxp3^{-}$ Tconv. Representative FACs plots of CD25/Foxp3 profile of SP4 splenocytes for *Aire*$^{-/-}$ and WT neonates as indicated. Accompanying graphs quantify the percentages (top) and numbers (bottom) of the Tconvs and Tregs across the two conditions as indicated.

(D) Comparison of CD62L phenotype of splenic Treg ($CD4^{+}CD8^{-}TCR\beta^{+}CD25^{+}Foxp3^{+}$). Representative FACs plots of the CD62L/CCR7 profile of the Treg for for *Aire*$^{-/-}$ and WT neonates as indicated. Accompanying graphs quantify the percentages (top) and numbers (bottom) of the $CD62L^{hi}$ and $CD62L^{lo}$ Tregs across the two conditions as indicated.

Alongside our analysis of Treg development in *Aire*$^{-/-}$ we also examined *Ltbr*$^{-/-}$, similarly beginning by assessing thymic Treg development in adult Rag-GFPx*Ltbr*$^{-/-}$ relative to Rag-GFP WT controls (Figure 3.22). Comparison of the general thymic phenotype revealed that while thymic cellularity was similar (Figure 3.22.A), the SP4 thymocyte population was increased in both proportion and number (Figure 3.22.B). Possibly this increase is the consequence of a problem with thymic emigration, which has previously been observed in the *Ltbr*$^{-/-[192,301]}$. Comparison of Rag-GFP^{+} *de novo* SP4 thymocytes populations, suggested that WT and *Ltbr*$^{-/-}$ were broadly similar, however we noted a few differences (Figure 3.22.C). Firstly, there was a slight decrease in the proportion, but not numbers, of CD25^{+}Foxp3^{-} precursors. Conversely we observed a numerical increase of Tconv thymocytes despite no proportional difference, which may again relate to an emigration issue. Importantly we saw no change in the bulk *de novo* Treg population, however our data on CD62L^{hi} and CD62L^{lo} Tregs was suggestive of a trend. As in the *Ltbr*$^{-/-}$ we observed that the percentage, though not numbers, of Tregs with a CD62L^{lo} and CD62L^{hi} phenotype was increased or decreased respectively (Figure 3.22.D).

We then investigated the splenic phenotype of *Ltbr*$^{-/-}$ to determine if the slight changes observed in the thymus also altered the exported Tregs. Initial characterisation of the splenic cellularity and bulk SP4 population suggested that the general splenic phenotype was similar between *Ltbr*$^{-/-}$ and WTs controls (Figure 3.23.A-B). However, analysis of SP4 RTE populations revealed a proportional and numerical reduction of Tregs, but not Tconvs, in *Ltbr*$^{-/-}$ (Figure 2.23.C). Closer examination of Treg RTE CD62L subsets, identified a slight statistical decrease in the proportion of CD62L^{hi} Tregs, but not CD62L^{lo} Tregs. Correspondingly we also observed a large numerical decrease in CD62L^{hi} Tregs, in keeping with the general reduction of Treg RTEs, but again no statistical difference in CD62L^{lo} Tregs (Figure 3.23.D).

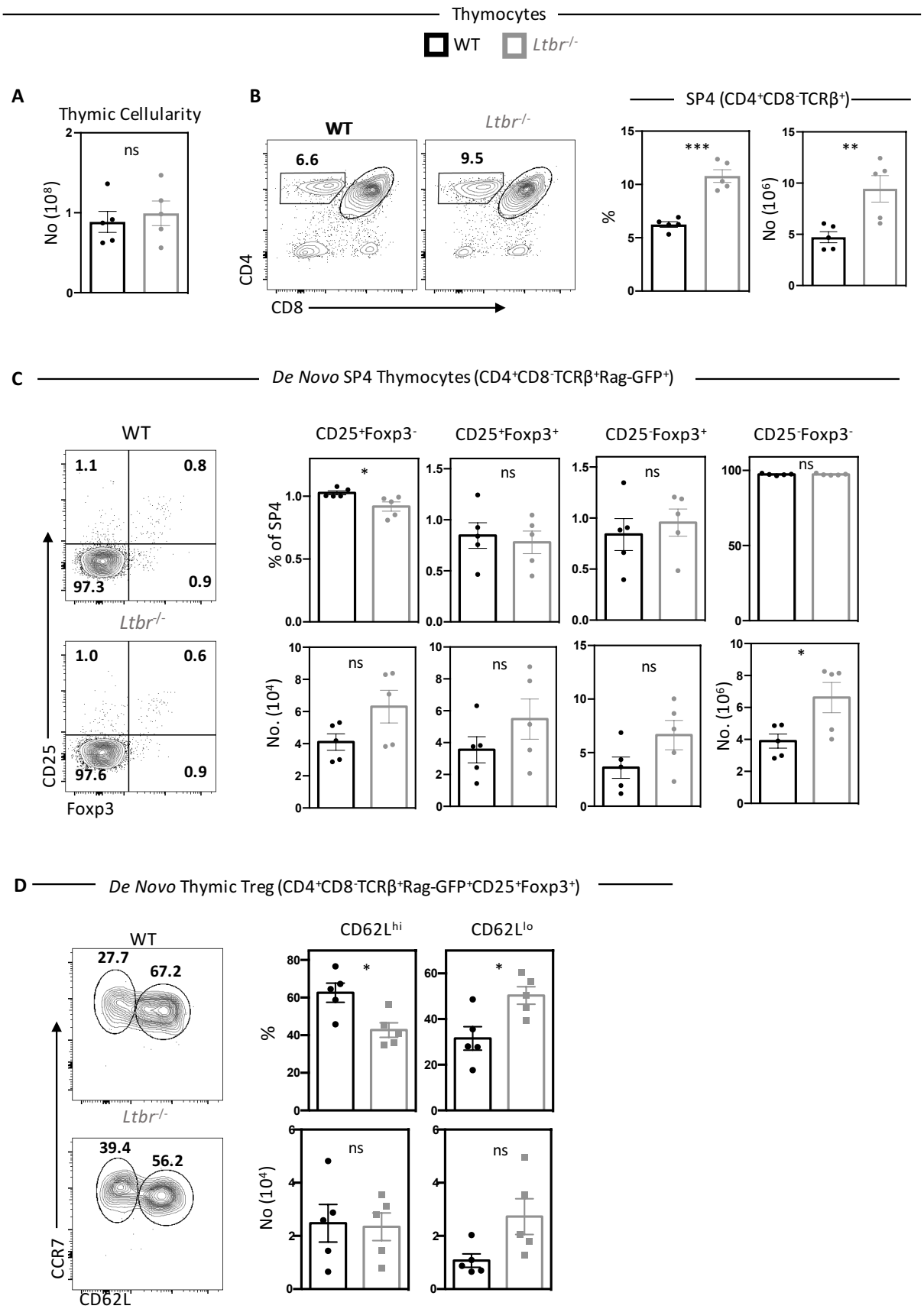
Thymocytes
WT
Ltbr-/-
A
Thymic Cellularity
ns
No (10⁸)
B
WT
Ltbr-/-
6.6
9.5
CD4
CD8
SP4 (CD4+CD8-TCRβ+)
***
**
%
No (10⁶)
C
De Novo SP4 Thymocytes (CD4+CD8-TCRβ+Rag-GFP+)
WT
1.1
0.8
97.3
0.9
Ltbr-/-
1.0
0.6
97.6
0.9
CD25
Foxp3
CD25+Foxp3-
CD25+Foxp3+
CD25-Foxp3+
CD25-Foxp3-
% of SP4
No. (10⁴)
No. (10⁶)
D
De Novo Thymic Treg (CD4+CD8-TCRβ+Rag-GFP+CD25+Foxp3+)
WT
27.7
67.2
Ltbr-/-
39.4
56.2
CCR7
CD62L
CD62Lhi
CD62Llo
%
No (10⁴)

Figure 3. 22 Identification of a Trend Suggestive of Altered Heterogeneous Thymic Treg Development in *Ltbr*$^{-/-}$ Adults

Comparison of thymic phenotype in *Ltbr*$^{-/-}$ x Rag-GFP (grey) and WT x Rag-GFP (black) adult (8-12 weeks) mice. Data representative of n=5 for *Ltbr*$^{-/-}$ and n=5 for WT across 3 independent experiments. All statistics were generated using a unpaired student's t-tests, where ns $p>0.05$, * $p<0.05$, ** $p<0.01$, *** $p<0.001$.

(A) Comparison of total thymic cellularity between *Ltbr*$^{-/-}$ and WT depicted as graphical quantification of numbers.

(B) Comparison of SP4 (CD4^{+}CD8^{-}TCRβ^{+}) thymocyte population. Representative FACs plots of CD4/CD8 profile of thymocytes for *Ltbr*$^{-/-}$ and WT mice as indicated. The graphs on the right quantifies the percentages and numbers of SP4 thymocytes across the two conditions as indicated.

(C) Comparison of *de novo* SP4 thymocyte (CD4^{+}CD8^{-}TCRβ^{+}Rag-GFP^{+}) populations: CD25^{+}Foxp3^{-} and CD25^{-}Foxp3^{+} Treg precursors, CD25^{+}Foxp3^{+} Treg and CD25^{-}Foxp3^{-} Tconv. Representative FACs plots of CD25/Foxp3 profile of SP4 thymocytes for *Ltbr*$^{-/-}$ and WT mice as indicated. Accompanying graphs quantify the percentages (top) and numbers (bottom) of the four SP4 thymocyte populations across the two conditions as indicated.

(D) Comparison of CD62L phenotype of *de novo* thymic Treg (CD4^{+}CD8^{-}TCRβ^{+}Rag-GFP^{+}CD25^{+}Foxp3^{+}). Representative FACs plots of the CD62L/CCR7 profile of the Treg for each condition for *Ltbr*$^{-/-}$ and WT mice as indicated. Accompanying graphs quantify the percentages (top) and numbers (bottom) of the CD62L^{hi} and CD62L^{lo} Tregs across the two conditions as indicated.

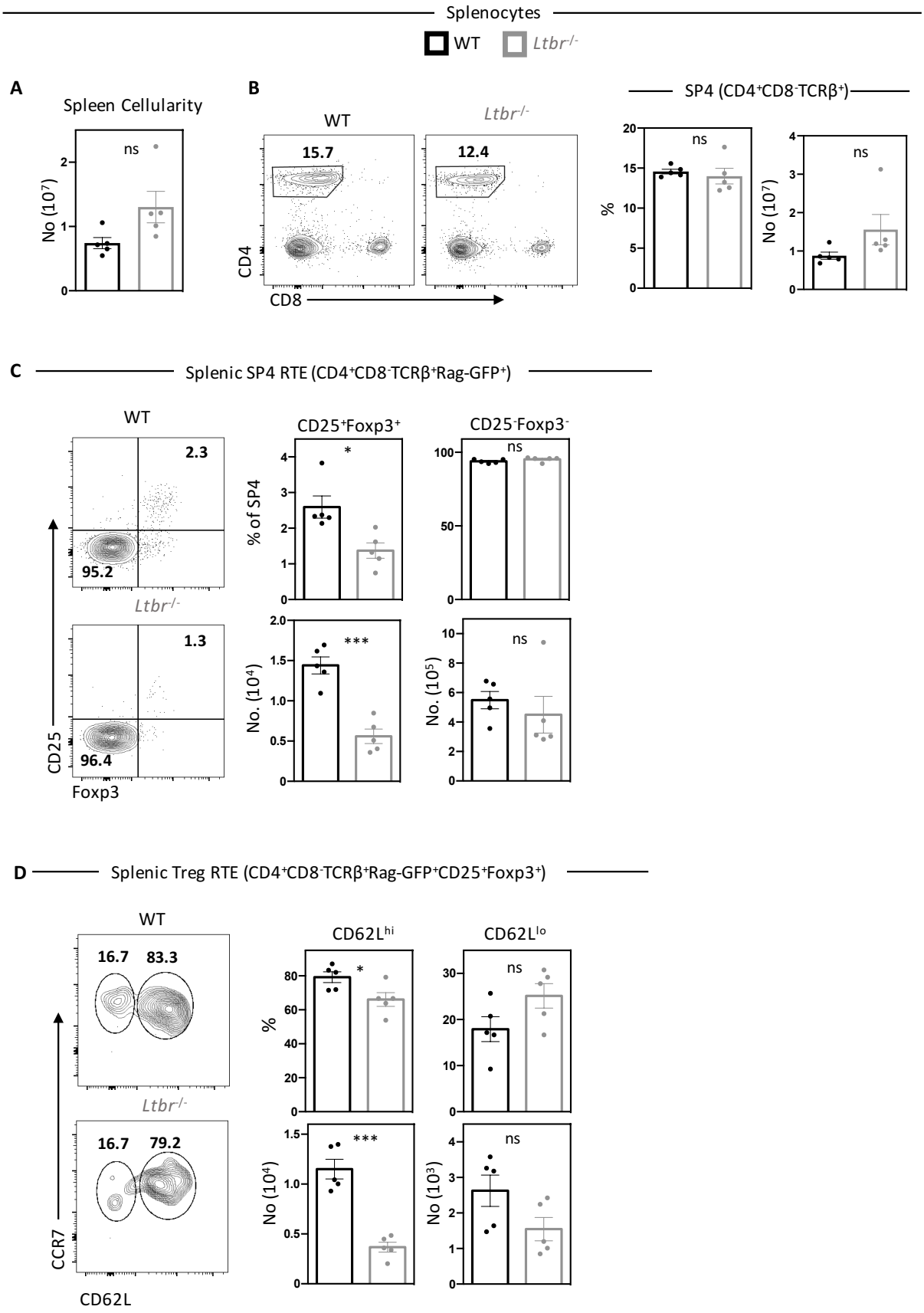
Splenocytes
WT
Ltbr-/-
A
Spleen Cellularity
No (10^7)
ns
B
WT
Ltbr-/-
15.7
12.4
CD4
CD8
SP4 (CD4+CD8-TCRβ+)
%
No (10^7)
ns
C
Splenic SP4 RTE (CD4+CD8-TCRβ+Rag-GFP+)
WT
2.3
95.2
Ltbr-/-
1.3
96.4
CD25
Foxp3
CD25+Foxp3+
CD25-Foxp3-
% of SP4
No. (10^4)
No. (10^5)
*
***
ns
D
Splenic Treg RTE (CD4+CD8-TCRβ+Rag-GFP+CD25+Foxp3+)
WT
16.7
83.3
Ltbr-/-
16.7
79.2
CCR7
CD62L
CD62Lhi
CD62Llo
%
No (10^4)
No (10^3)
*
***
ns

Figure 3. 23 Specific Reduction of Splenic Treg RTEs in *Ltbr*$^{-/-}$ Adults

Comparison of splenic phenotype in *Ltbr*$^{-/-}$ x Rag-GFP (grey) and WT x Rag-GFP (black) adult (8-12 weeks) mice. Data representative of n=5 for *Ltbr*$^{-/-}$ and n=5 for WT across 3 independent experiments. All statistics were generated using a unpaired student's t-tests, where ns $p>0.05$, * $p<0.05$, *** $p<0.001$.

(A) Comparison of total splenic cellularity between *Ltbr*$^{-/-}$ and WT depicted as graphical quantification of numbers.

(B) Comparison of SP4 (CD4^{+}CD8^{-}TCRβ^{+}) splenocyte population. Representative FACs plots of CD4/CD8 profile of splenocytes for *Ltbr*$^{-/-}$ and WT mice as indicated. The graphs on the right quantifies the percentages and numbers of SP4 splenocytes across the two conditions as indicated.

(C) Comparison of SP4 recent thymic emigrant (RTE) (CD4^{+}CD8^{-}TCRβ^{+}Rag-GFP^{+}) populations: CD25^{+}Foxp3^{+} Treg and CD25^{-}Foxp3^{-} Tconv. Representative FACs plots of CD25/Foxp3 profile of SP4 RTE for *Ltbr*$^{-/-}$ and WT mice as indicated. Accompanying graphs quantify the percentages (top) and numbers (bottom) of the Tconv and Treg RTEs across the two conditions as indicated.

(D) Comparison of CD62L phenotype of Treg RTE (CD4^{+}CD8^{-}TCRβ^{+}Rag-GFP^{+}CD25^{+}Foxp3^{+}). Representative FACs plots of the CD62L/CCR7 profile of the Treg for for *Ltbr*$^{-/-}$ and WT mice as indicated. Accompanying graphs quantify the percentages (top) and numbers (bottom) of the CD62L^{hi} and CD62L^{lo} Tregs across the two conditions as indicated.

Collectively our analysis of thymic and splenic *de novo* Treg, did identify some proportional differences of heterogeneous Tregs in the *Ltbr*$^{-/-}$ however these changes were only slight suggesting a fairly limited role for LTβR in adult Treg development. However, we wondered if, akin to Aire, LTβR may be more important in Treg development in the neonate. We therefore examined Treg development in D7 *Ltbr*$^{-/-}$ neonates relative to D7 *Ltbr*$^{+/-}$ littermate controls (substituting for a WT control as *Ltbr*$^{+/-}$ did not display overt features of *Ltbr*$^{-/-}$ phenotype such as lack of LNs), as before we did not use Rag-GFP to define *de novo* cells.

Our initial characterisation of the thymic phenotype identified that the D7 *Ltbr*$^{-/-}$ and *Ltbr*$^{+/-}$ neonates had comparable thymic cellularity (Figure 3.24.A), but there was a slight reduction numerically in SP4 thymocytes in the *Ltbr*$^{-/-}$ (Figure 3.24.B). In keeping with this observed reduction of SP4 thymocyte numbers we saw a general reduction in numbers of all four SP4 thymocyte populations, however only the proportions of Treg and CD25^{-}Foxp3^{+} precursors were reduced (Figure 3.24.C). Within the Treg population we observed a proportional increase of CD62L^{lo} Tregs, and a corresponding decrease of CD62L^{hi} Tregs which were also reduced numerically (Figure.3.24.D). However, we did not see a corresponding numerical increase of CD62L^{lo} Tregs in *Ltbr*$^{-/-}$ possibly due to the general reduction in Tregs associated with the *Ltbr*$^{-/-}$ phenotype (Figure 3.24.D).

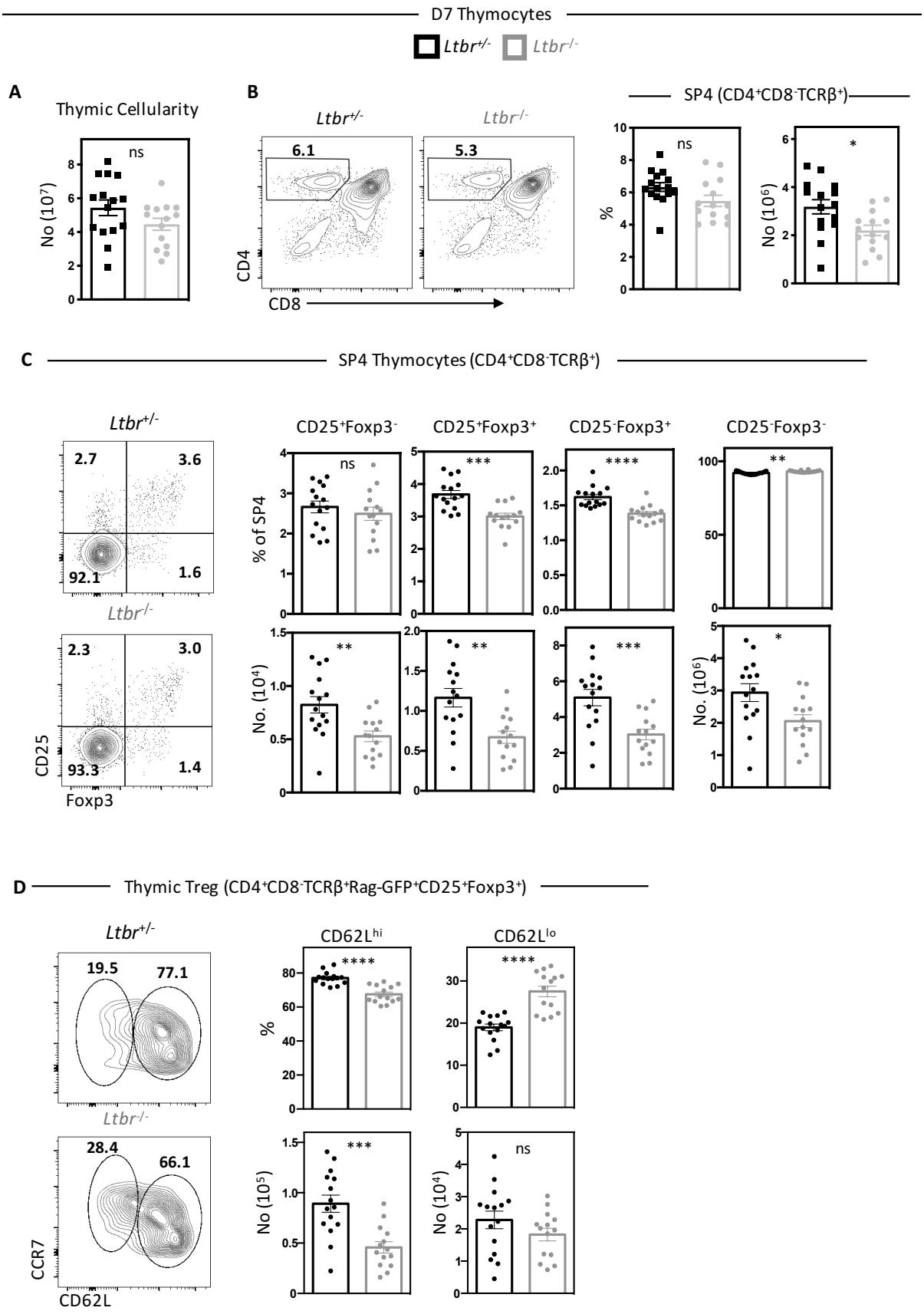
D7 Thymocytes
Ltbr+/-
Ltbr-/-
A
Thymic Cellularity
ns
No (10^7)
B
Ltbr+/-
Ltbr-/-
6.1
5.3
CD4
CD8
SP4 (CD4+CD8-TCRβ+)
ns
%
*
No (10^6)
C
SP4 Thymocytes (CD4+CD8-TCRβ+)
Ltbr+/-
2.7
3.6
92.1
1.6
Ltbr-/-
2.3
3.0
93.3
1.4
CD25
Foxp3
CD25+Foxp3-
CD25+Foxp3+
CD25-Foxp3+
CD25-Foxp3-
% of SP4
No. (10^4)
No. (10^6)
ns
***
****
**
*
D
Thymic Treg (CD4+CD8-TCRβ+Rag-GFP+CD25+Foxp3+)
Ltbr+/-
19.5
77.1
Ltbr-/-
28.4
66.1
CCR7
CD62L
CD62Lhi
CD62Llo
%
No (10^5)
No (10^4)

Figure 3. 24 Evidence of Altered Heterogeneous Thymic Treg Development in D7 *Ltbr*$^{-/-}$ Neonates

Comparison of thymic phenotype in D7 *Ltbr*$^{-/-}$ (grey) and *Ltbr*$^{+/-}$ littermate control (black) neonates. Data representative of n=14 for *Ltbr*$^{-/-}$ and n=15 for *Ltbr*$^{+/-}$ across 5 independent experiments. All statistics were generated using a unpaired student's t-tests, where ns p>0.05, * p<0.05, ** p<0.01, *** p<0.001, **** p<0.0001.

(A) Comparison of total thymic cellularity between *Ltbr*$^{-/-}$ and *Ltbr*$^{+/-}$ depicted as graphical quantification of numbers.

(B) Comparison of SP4 (CD4^{+}CD8^{-}TCRβ^{+}) thymocyte population. Representative FACs plots of CD4/CD8 profile of thymocytes for *Ltbr*$^{-/-}$ and *Ltbr*$^{+/-}$ neonates as indicated. The graphs on the right quantifies the percentages and numbers of SP4 thymocytes across the two conditions as indicated.

(C) Comparison of SP4 thymocyte (CD4^{+}CD8^{-}TCRβ^{+}) populations: CD25^{+}Foxp3^{-} and CD25^{-}Foxp3^{+} Treg precursors, CD25^{+}Foxp3^{+} Treg and CD25^{-}Foxp3^{-} Tconv. Representative FACs plots of CD25/Foxp3 profile of SP4 thymocytes for *Ltbr*$^{-/-}$ and *Ltbr*$^{+/-}$ neonates as indicated. Accompanying graphs quantify the percentages (top) and numbers (bottom) of the four SP4 thymocyte populations across the two conditions as indicated.

(D) Comparison of CD62L phenotype of thymic Treg (CD4^{+}CD8^{-}TCRβ^{+}CD25^{+}Foxp3^{+}). Representative FACs plots of the CD62L/CCR7 profile of the Treg for each condition for *Ltbr*$^{-/-}$ and *Ltbr*$^{+/-}$ neonates as indicated. Accompanying graphs quantify the percentages (top) and numbers (bottom) of the CD62L^{hi} and CD62L^{lo} Tregs across the two conditions as indicated.

Having identified some phenotypic changes to Treg development in the *Ltbr*$^{-/-}$ neonate we then analysed the spleen to investigate the impact on the exported T-cell population (Figure 3.25). Interestingly whilst the total cellularity of the spleen was comparable between *Ltbr*$^{-/-}$ and *Ltbr*$^{+/-}$ neonates (Figure 3.25.A), the SP4 population was dramatically reduced in *Ltbr*$^{-/-}$ (Figure 3.25.B). In keeping with this reduction of SP4 splenocytes numbers we saw a general numerical reduction in both Tregs and Tconvs, however proportionally only Tregs were reduced (Figure 3.25.C). This reduction of splenic Tregs did not seem to result from specific reduction of CD62L^{hi} or CD62L^{lo} Tregs as, while both numerically reduced, the proportional split of the two was comparable between *Ltbr*$^{-/-}$ and *Ltbr*$^{+/-}$ neonates (Figure 3.25.D).

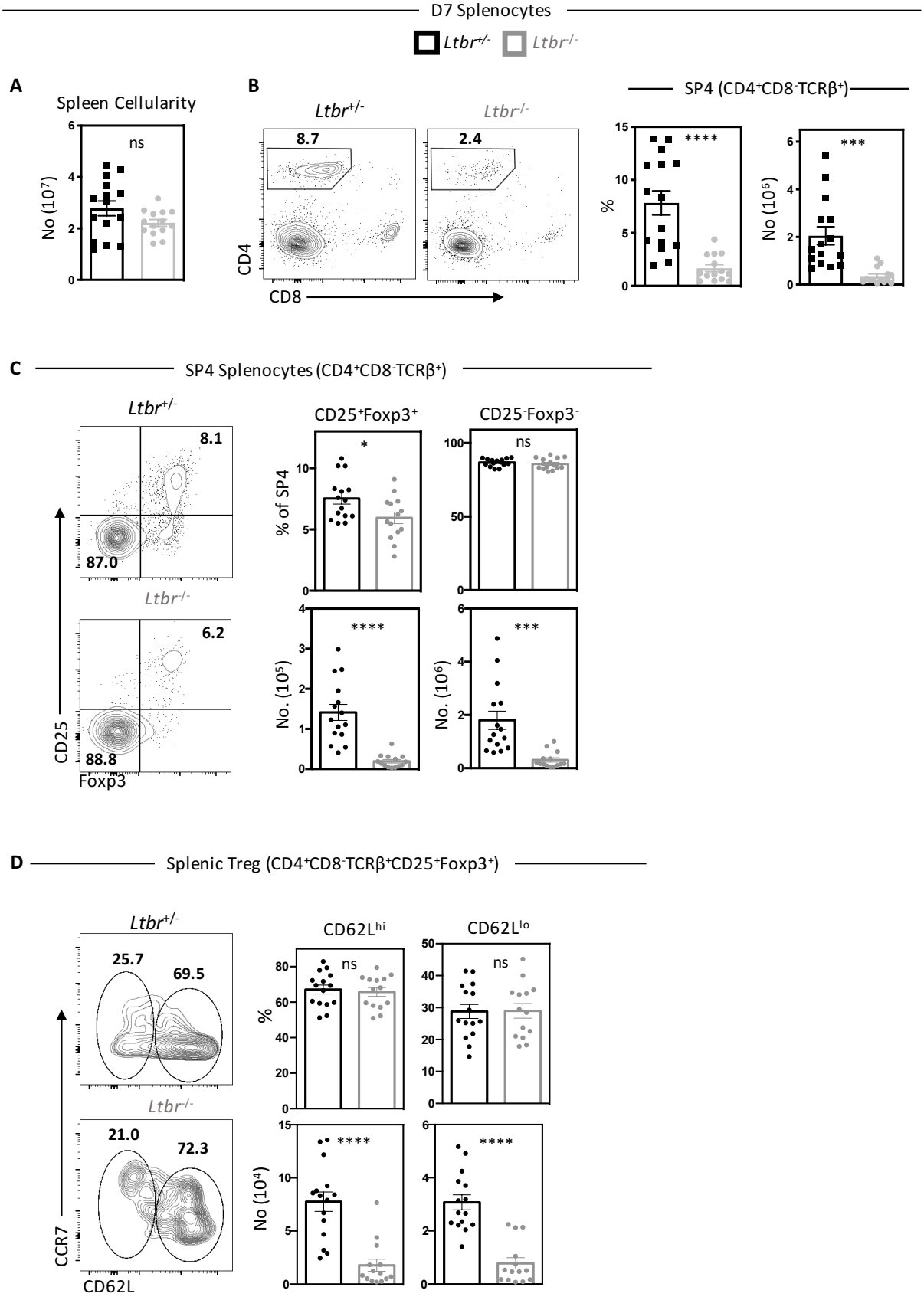
D7 Splenocytes
Ltbr+/-
Ltbr-/-
A
Spleen Cellularity
No (10^7)
ns
B
Ltbr+/-
Ltbr-/-
8.7
2.4
CD4
CD8
SP4 (CD4+CD8-TCRβ+)
%
****
No (10^6)
***
C
SP4 Splenocytes (CD4+CD8-TCRβ+)
Ltbr+/-
8.1
87.0
Ltbr-/-
6.2
88.8
CD25
Foxp3
CD25+Foxp3+
CD25-Foxp3-
% of SP4
*
ns
No. (10^5)
****
No. (10^6)
***
D
Splenic Treg (CD4+CD8-TCRβ+CD25+Foxp3+)
Ltbr+/-
25.7
69.5
Ltbr-/-
21.0
72.3
CCR7
CD62L
CD62Lhi
CD62Llo
%
ns
No (10^4)
****

Figure 3. 25 Gross Reduction of Splenic SP4 T-cells in D7 *Ltbr*$^{-/-}$ Neonates

Comparison of splenic phenotype in D7 *Ltbr*$^{-/-}$ (grey) and *Ltbr*$^{+/-}$ littermate control (black) neonates. Data representative of n=14 for *Ltbr*$^{-/-}$ and n=15 for *Ltbr*$^{+/-}$ across 5 independent experiments. All statistics were generated using unpaired student's t-tests, where ns $p>0.05$, * $p<0.05$, *** $p<0.001$, **** $p<0.0001$.

(A) Comparison of total splenic cellularity between *Ltbr*$^{-/-}$ and *Ltbr*$^{+/-}$ depicted as graphical quantification of numbers.

(B) Comparison of SP4 (CD4^{+}CD8^{-}TCRβ^{+}) splenocyte population. Representative FACs plots of CD4/CD8 profile of splenocytes for *Ltbr*$^{-/-}$ and *Ltbr*$^{+/-}$ neonates as indicated. The graphs on the right quantifies the percentages and numbers of SP4 splenocytes across the two conditions as indicated.

(C) Comparison of SP4 splenocyte populations: CD25^{+}Foxp3^{+} Treg and CD25^{-}Foxp3^{-} Tconv. Representative FACs plots of CD25/Foxp3 profile of SP4 splenocytes for *Ltbr*$^{-/-}$ and *Ltbr*$^{+/-}$ neonates as indicated. Accompanying graphs quantify the percentages (top) and numbers (bottom) of the Tconvs and Tregs across the two conditions as indicated.

(D) Comparison of CD62L phenotype of splenic Treg (CD4^{+}CD8^{-}TCRβ^{+}CD25^{+}Foxp3^{+}). Representative FACs plots of the CD62L/CCR7 profile of the Treg for for *Ltbr*$^{-/-}$ and *Ltbr*$^{+/-}$ neonates as indicated. Accompanying graphs quantify the percentages (top) and numbers (bottom) of the CD62L^{hi} and CD62L^{lo} Tregs across the two conditions as indicated.

3.2.4 Assessing Functional Differences of Tregs: Pilot Colitis Model

So far our investigations had focussed on understanding how heterogeneous thymic Tregs develop, without addressing why such heterogeneity is necessary. Interestingly previous work has linked phenotypic and functional heterogeneity in Tregs[107], and we therefore wondered if the same was true for CD62L^{hi} and CD62L^{lo} Tregs. To compare the function of different types of Tregs previous studies have utilised a colitis model[107,189], where colitis is induced by transfer of non-Tregs and controlled by co-transferring Tregs[319,320]. We therefore planned to compare CD62L^{hi} and CD62L^{lo} Tregs using this system, but first needed to establish the model in our lab with a pilot experiment. Our aim was to determine firstly if we could induce colitis through adoptive transfer of Tconv splenocytes, and secondly if we could protect against disease by co-transfer of bulk Foxp3^{+} Tregs.

The setup schematic for this pilot is outlined in Figure 3.26.A. In brief CD4^{+}Foxp3-RFP^{-} Tconvs and CD4^{+}Foxp3-RFP^{+} Tregs were sorted from CD45.1^{+}CD45.2^{-} Foxp3-RFP mice for injection in CD45.1^{-}CD45.2^{+} *Rag2*$^{-/-}$ hosts (which lack endogenous T-cells). The *Rag2*$^{-/-}$ hosts were divided into two groups which received either, Tconvs only (Foxp3^{-}*Rag2*$^{-/-}$ hosts) or both Tconvs and Tregs (Foxp3^{+}*Rag2*$^{-/-}$ hosts), and were expected to either develop or be protected from colitis onset, respectively. Following transfer the *Rag2*$^{-/-}$ hosts were bled after 4 weeks, to confirm the longevity of transferred cells (Figure 3.26.B). In all hosts, we could detect transferred cells and confirmed they had maintained their starting phenotype as Foxp3^{+} Tregs were restricted to Foxp3^{+}*Rag2*$^{-/-}$ hosts (Figure 3.26.B-C).

A

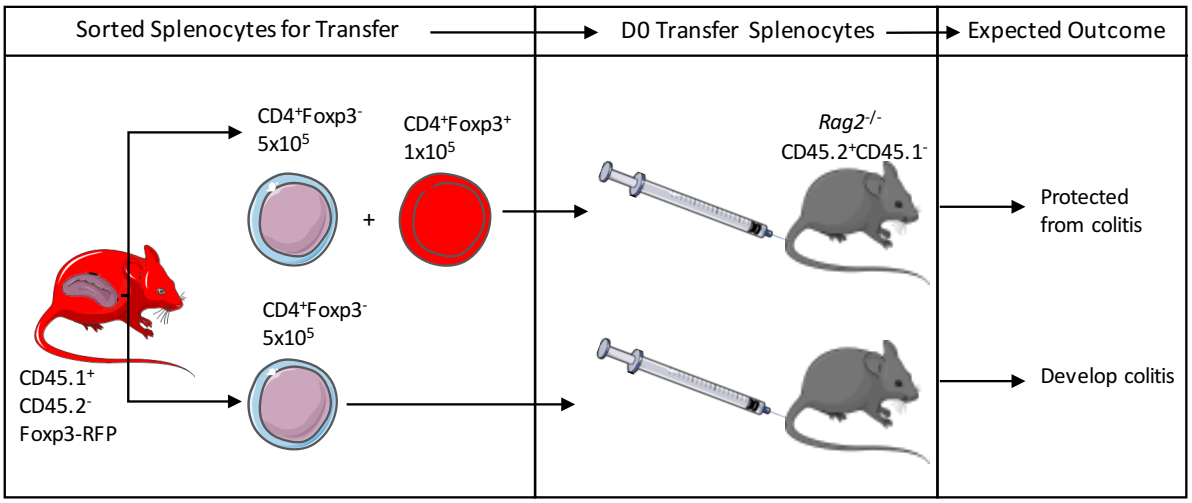
Sorted Splenocytes for Transfer
D0 Transfer Splenocytes
Expected Outcome
CD4+Foxp3-
5x10^5
CD4+Foxp3+
1x10^5
+
CD4+Foxp3-
5x10^5
CD45.1+
CD45.2-
Foxp3-RFP
Rag2-/-
CD45.2+CD45.1-
Protected
from colitis
Develop colitis

B

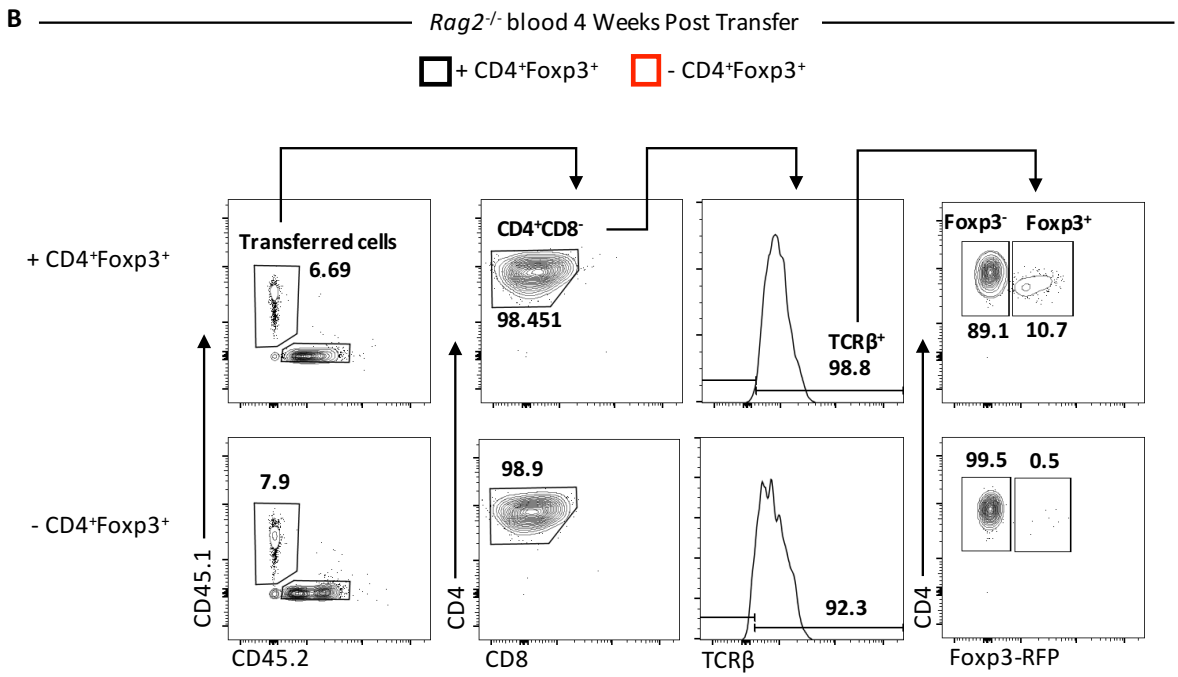
Rag2-/- blood 4 Weeks Post Transfer
+ CD4+Foxp3+
- CD4+Foxp3+
+ CD4+Foxp3+
- CD4+Foxp3+
Transferred cells
6.69
CD4+CD8-
98.451
TCRβ+
98.8
Foxp3-
Foxp3+
89.1
10.7
7.9
98.9
92.3
99.5
0.5
CD45.1
CD45.2
CD4
CD8
TCRβ
CD4
Foxp3-RFP

C

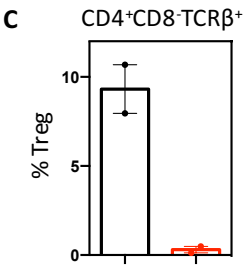
CD4+CD8-TCRβ+
% Treg
10
5
0

Figure 3. 26 Colitis Model Setup

Setup of pilot experiment to establish an adoptive transfer model of colitis induction. All data representative of n=2 *Rag2*$^{-/-}$ recipients of 5x10^5 CD4$^+$Foxp3-RFP$^-$ splenocytes alone (-CD4$^+$Foxp3-RFP$^+$, red) and n= 2 *Rag2*$^{-/-}$ recipients of 5x10^5 CD4$^+$Foxp3-RFP$^-$ and 1x10^5 CD4$^+$Foxp3-RFP$^+$ splenocytes (+CD4$^+$Foxp3-RFP$^+$, black), setup across 1 experiment.
(A) Adoptive transfer schematic: *Rag2*$^{-/-}$ CD45.2$^+$ hosts are injected at D0 with splenocytes from WT CD45.1$^+$CD45.2$^-$ Foxp3-RFP$^+$ mice. *Rag2*$^{-/-}$ recipients receive 5x10^5 CD4$^+$Foxp3-RFP$^-$ splenocytes alone or with 1x10^5 CD4$^+$Foxp3-RFP$^+$.
(B) Identification of transferred SP4 (CD45.1$^+$CD45.2$^-$CD4$^+$CD8$^-$TCRβ$^+$) in blood from *Rag2*$^{-/-}$ recipients 4 weeks post initial transfer. Gating strategy to identify the phenotype of the transferred SP4 T cells. Transferred cells are initially identified as CD45.1$^+$CD45.2$^-$, then as CD4$^+$CD8$^-$TCRβ$^+$ SP4 T cells. Then subsequently Foxp3 expression is examined to identify the presence of CD4$^+$Foxp3-RFP$^-$ (Tconv) vs CD4$^+$Foxp3-RFP$^+$ (Treg). Data presented as representative FACs plots (including gate title and percentage of cells within the gate given underneath) from a *Rag2*$^{-/-}$ host receiving CD4$^+$Foxp3-RFP$^-$ and CD4$^+$Foxp3-RFP$^+$ splenocytes (top) and a *Rag2*$^{-/-}$ host receiving CD4$^+$Foxp3-RFP$^-$ splenocytes only (bottom).
(C) Quantification of the percentage of CD4$^+$Foxp3-RFP$^+$ Treg detected within transferred SP4 T cells in the blood of *Rag2*$^{-/-}$ host receiving CD4$^+$Foxp3-RFP$^-$ and CD4$^+$Foxp3-RFP$^+$ splenocytes (black) and a *Rag2*$^{-/-}$ host receiving CD4$^+$Foxp3-RFP$^-$ splenocytes only (red).

Following adoptive transfer *Rag2*$^{-/-}$ hosts were closely monitored for evidence of colitis onset. The general well-being of animals was judged by their appearance and behaviour, and animals were also weighed at regular intervals as weight loss has frequently been used as an indicator of colitis. Tracking weight change of *Rag2*$^{-/-}$ hosts relative to their starting weight (Figure 3.27.A), showed that whilst initially all hosts gained weight, Foxp3^{-}*Rag2*$^{-/-}$ hosts then began to lose weight whereas Foxp3^{+}*Rag2*$^{-/-}$ hosts either maintained or further increased their weight. Ultimately the two Foxp3^{-}*Rag2*$^{-/-}$ hosts had to be culled, at D76 and D133 post transfer, due to general welfare concerns. The Foxp3^{+}*Rag2*$^{-/-}$ hosts remained healthy throughout the time course, but were also culled at D76 and D133 post transfer respectively to act as a comparative control in colitis endpoint analysis. Comparing the final weights of all hosts, identified Foxp3^{+}*Rag2*$^{-/-}$ hosts were heavier (relative to their starting weight) than Foxp3^{-}*Rag2*$^{-/-}$ hosts (Figure 3.27.B). This reduction in weight of *Rag2*$^{-/-}$ hosts which received only Tconvs is consistent with a colitis phenotype.

To further assess possible inflammation within *Rag2*$^{-/-}$ hosts, we looked for macroscopic and cellular changes consistent with a colitis phenotype upon experimental endpoint (Figure 3.28). One macroscopic change associated with colitis is shortening of the colon, therefore we compared colon lengths and indeed colons from Foxp3^{-}*Rag2*$^{-/-}$ hosts were slightly shorter than Foxp3^{+}*Rag2*$^{-/-}$ hosts (Figure 3.28.A). We also performed flow cytometry analysis of the colon and spleen to identify if there were any specific differences in the colonic T-cell populations which could underpin a colitis phenotype. We began by examining bulk Tconv and Treg populations in Foxp3^{-}*Rag2*$^{-/-}$ and Foxp3^{+}*Rag2*$^{-/-}$ hosts, as we anticipated that Treg should only be present to control inflammation in the latter (Figure 3.28.B). Surprisingly we identified Tregs within the spleen and colon of all hosts, although they were present at a lower frequency

and number in Foxp3^{-}*Rag2*$^{-/-}$ hosts. This suggests that peripheral Tregs have been induced from transferred Tconvs in Foxp3^{-}*Rag2*$^{-/-}$ hosts, however this population is seemingly insufficient to prevent sickness in these mice. Possibly this lack of protection relates to the increased numbers of Tconvs, specifically within the colon, in Foxp3^{-}*Rag2*$^{-/-}$ hosts relative to Foxp3^{+}*Rag2*$^{-/-}$ hosts. Indeed when we examined the ratio of Tconvs:Tregs we observed this was far higher in Foxp3^{-}*Rag2*$^{-/-}$ hosts. We therefore wondered whether this numerical increase of colonic Tconvs might be a consequence of a specific increase in effector Tconvs relative to naïve Tconvs within Foxp3^{-}*Rag2*$^{-/-}$ hosts. However, we observed little difference in in the proportion of effector Tconvs between Foxp3^{+}*Rag2*$^{-/-}$ and Foxp3^{-}*Rag2*$^{-/-}$ hosts with the majority of Tconv CD44^{hi}CD62L^{lo} effector phenotype (Figure 3.28.C).

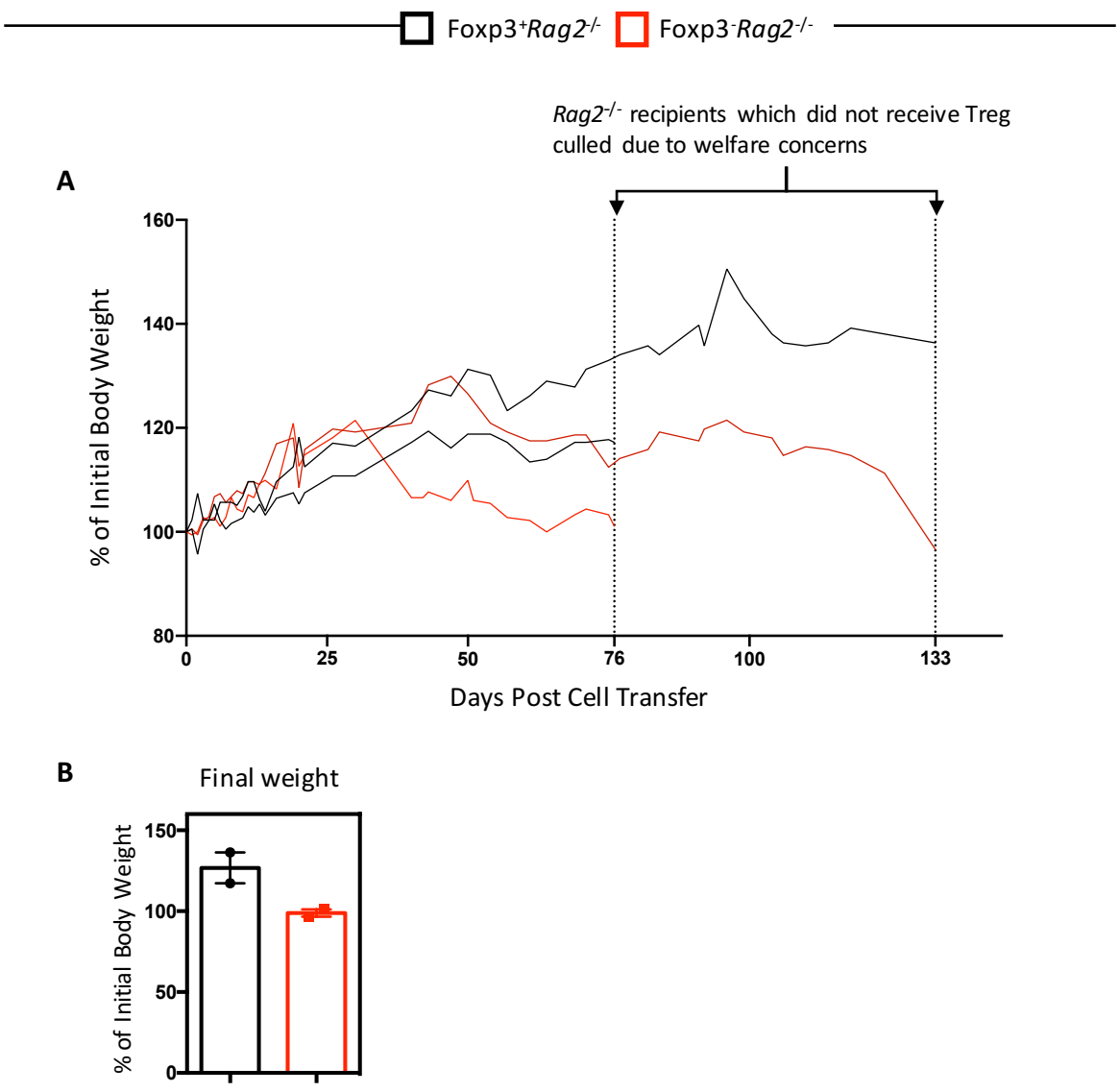
Foxp3+Rag2-/-
Foxp3-Rag2-/-
Rag2-/- recipients which did not receive Treg culled due to welfare concerns
A
% of Initial Body Weight
160
140
120
100
80
0
25
50
76
100
133
Days Post Cell Transfer
B
Final weight
% of Initial Body Weight
150
100
50
0

Figure 3. 27 Preliminary Evidence Co-transferred Tregs Prevent Weight Loss in Colitis Model

Monitoring of *Rag2*$^{-/-}$ host body weight following setup of adoptive transfer model of colitis induction. All data representative of n=2 *Rag2*$^{-/-}$ recipients of 5x10^{5} CD4^{+}Foxp3-RFP^{-} splenocytes alone (Foxp3^{-}*Rag2*$^{-/-}$, red) and n= 2 *Rag2*$^{-/-}$ recipients of 5x10^{5} CD4^{+}Foxp3-RFP^{-} and 1x10^{5} CD4^{+}Foxp3-RFP^{+} splenocytes (Foxp3^{+}*Rag2*$^{-/-}$, black), setup across 1 experiment. **(A)** Timecourse of *Rag2*$^{-/-}$ host body weight across the length of experiment starting at D0 when cells were adoptively transferred. Data depicts weight of *Rag2*$^{-/-}$ hosts as percentage of the host starting weight (measured at D0 of transfer), against days post adoptive transfer. Each line represents an individual *Rag2*$^{-/-}$ host which either received CD4^{+}Foxp3-RFP^{-} and CD4^{+}Foxp3-RFP^{+} splenocytes (black) or CD4^{+}Foxp3-RFP^{-} splenocytes only (red). Dashed line indicates where a *Rag2*$^{-/-}$ host which received CD4^{+}Foxp3-RFP^{-} splenocytes alone had to be culled due to welfare concerns over the animals condition, at the same time a *Rag2*$^{-/-}$ host which received CD4^{+}Foxp3-RFP^{-} and CD4^{+}Foxp3-RFP^{+} splenocytes was also culled to act as a control.
(B) Comparison of the final body weight (measured immediately prior to culling of hosts) of *Rag2*$^{-/-}$ hosts which either received CD4^{+}Foxp3-RFP^{-} and CD4^{+}Foxp3-RFP^{+} splenocytes (black) or CD4^{+}Foxp3-RFP^{-} splenocytes only (red). Presented as percentage of the host starting weight.

A

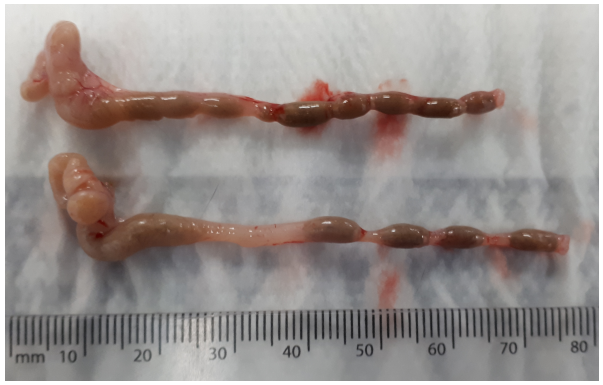

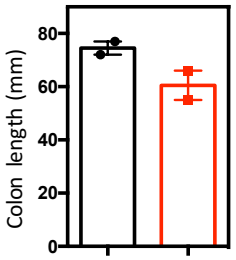

B SP4 T-cells (LIVE/DEAD-CD45.1+CD45.2-CD4+CD8-TCRβ+)

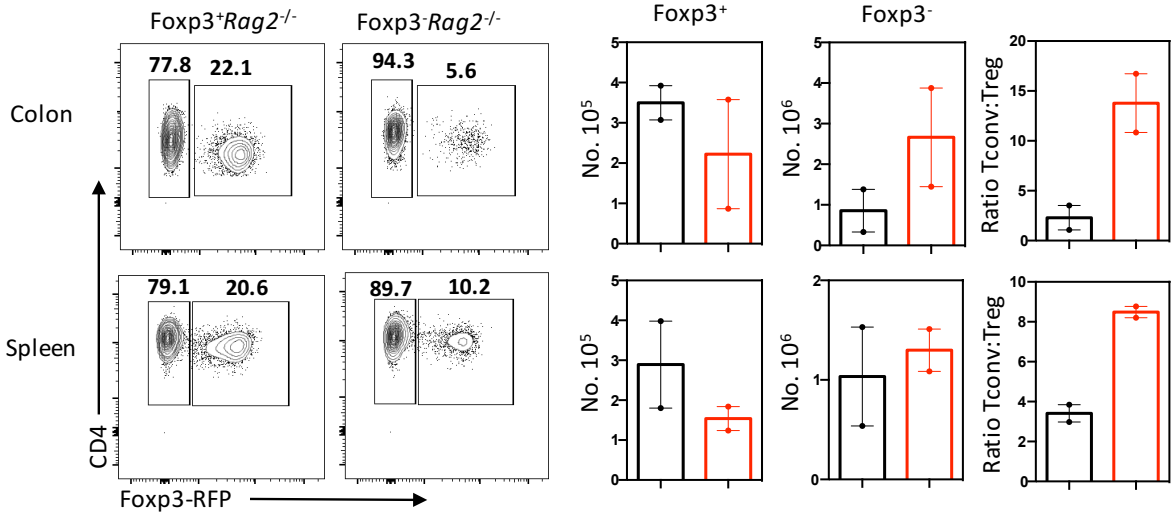

C Tconv (LIVE/DEAD-CD45.1+CD45.2-CD4+CD8-TCRβ+Foxp3-)

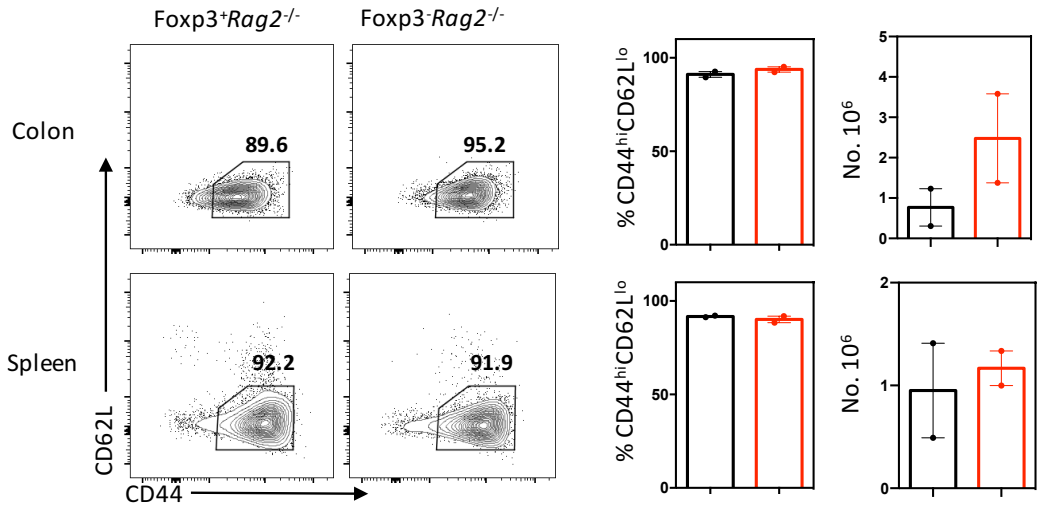

Figure 3. 28 Preliminary Evidence Co-transferred Tregs Protect Against Pathogenic Colonic T-cells in Colitis Model

Analysis of *Rag2*$^{-/-}$ hosts for evidence of colitis following end of adoptive transfer model of colitis induction. All data representative of n=2 *Rag2*$^{-/-}$ recipients of 5x10^{5} CD4^{+}Foxp3-RFP^{-} splenocytes alone (Foxp3^{-} *Rag2*$^{-/-}$, red) and n= 2 *Rag2*$^{-/-}$ recipients of 5x10^{5} CD4^{+}Foxp3-RFP^{-} and 1x10^{5} CD4^{+}Foxp3-RFP^{+} splenocytes (Foxp3^{+} *Rag2*$^{-/-}$, black), setup across 1 experiment and harvested at 2 timepoints (n=1 for each condition across these two timepoints).

(A) Left shows a representative image of colons from *Rag2*$^{-/-}$ hosts receiving CD4^{+}Foxp3-RFP^{-} and CD4^{+}Foxp3-RFP^{+} splenocytes (bottom) or CD4^{+}Foxp3-RFP^{-} splenocytes only (top). Right quantifies the colon length from *Rag2*$^{-/-}$ hosts which either received CD4^{+}Foxp3-RFP^{-} and CD4^{+}Foxp3-RFP^{+} splenocytes (black) or CD4^{+}Foxp3-RFP^{-} splenocytes only (red).

(B) FACs analysis of transferred SP4 T-cells (LIVE/DEAD^{-}CD45.1^{+}CD45.2^{-}CD4^{+}CD8^{-}TCRβ^{+}) from the colon (top) and spleen (bottom) of *Rag2*$^{-/-}$ hosts which received either CD4^{+}Foxp3-RFP^{-} and CD4^{+}Foxp3-RFP^{+} splenocytes (black) or CD4^{+}Foxp3-RFP^{-} splenocytes only (red), as indicated. Representative FACs plots show the CD4/Foxp3 profile of SP4 T-cells (from the indicated tissue and indicated host) with Tconv and Treg gated as CD4^{+}Foxp3-RFP^{-} and CD4^{+}Foxp3-RFP^{+} respectively. Accompanying bar chats quantify (left) the number of Treg (middle) the number of Tconv, and (right) the ratio of Treg:Tconv across the two conditions.

(C) FACs analysis of transferred Tconv (LIVE/DEAD^{-}CD45.1^{+}CD45.2^{-}CD4^{+}CD8^{-}TCRβ^{+}Foxp3-RFP^{-}) from the colon (top) and spleen (bottom) of *Rag2*$^{-/-}$ hosts which received either CD4^{+}Foxp3-RFP^{-} and CD4^{+}Foxp3-RFP^{+} splenocytes or CD4^{+}Foxp3-RFP^{-} splenocytes only, as indicated. Representative FACs plots show the CD62L/CD44 profile of Tconv (from the indicated tissue and indicated host) with effector cells gated as CD44^{hi} CD62L^{lo}. Accompanying bar charts quantify (left) the frequency and (right) the number of effector Tconv across the two conditions.

3.3 Discussion

3.3.1 A Thymic Origin for Heterogeneous Tregs

Our analysis revealed *de novo* Tregs as heterogeneous comprising both CD62L^{hi} and CD62L^{lo} subsets, present at fairly consistent proportions across the studied lifetime, suggesting that heterogeneous Treg development occurs throughout life (Figure 3.4). Importantly we found these two subsets within both *de novo* Treg thymocytes (Figure 3.2) and exported Treg RTEs (Figure 3.8), identifying that the heterogeneity we observed in the thymus is not transient and may contribute to peripheral Treg heterogeneity.

Therefore, our findings are in agreement with reports that the thymus does generate heterogeneous Treg subsets[107], and opposes previous findings which report only CD62L^{hi} Tregs among *de novo* thymocytes[85]. Possibly this discrepancy is linked to how *de novo* Tregs were identified between studies. Here, like Wyss *et al*[107], we utilised the Rag-GFPxFoxp3-RFP model meaning *de novo* thymic Tregs could be characterised with minimal experimental manipulation. In contrast Smigiel *et al*[85] used a Rag-GFP model and therefore had to perform intracellular staining to detect Foxp3, and consequently initially sorted *de novo* thymocytes by Rag-GFP levels. Here, ensuring that pure Rag-GFP^{+} populations were isolated may have resulted in the loss of Tregs with lower Rag-GFP intensities, which our analysis would suggest to be predominantly CD62L^{lo} (Figure 3.4), resulting in the assumption that all Rag-GFP^{+} Tregs were CD62L^{hi}.

Interestingly the CD62L^{hi} and CD62L^{lo} Treg subsets we identified have some characteristics reminiscent of previously described peripheral Treg subsets. Most notably differential CD62L expression is strongly associated with the CD62L^{hi} cTreg and CD62L^{lo} eTreg phenotype [85],

although Triple^{hi} and Triple^{lo} Tregs also differentially express CD62L, being CD62L^{hi} or CD62L^{lo}, respectively[107]. Moreover, while RTEs were generally more prominent in SLOs, we saw some evidence of differential homing by CD62L^{hi} and CD62L^{lo} Tregs (Figure 3.11). As the former preferentially homed to SLOs, while the latter also homed to non-lymphoid tissues, mirroring the homing of cTregs and eTregs respectively[85].

However, in contrast with the previously defined eTregs/cTregs and the Triple^{hi}/Triple^{lo} Tregs both our thymic CD62L subsets showed high expression of CCR7 and CD44 (Figure 3.3). Furthermore, both CD62L^{hi} and CD62L^{lo} Tregs appeared fairly quiescent in phenotype, which for the former is in keeping with the expected cTreg/Triple^{hi} Treg phenotype but regarding the latter opposes the previously described activated/effector-like phenotype of the eTregs/Triple^{lo} Tregs[85,107]. Although our analysis did suggest that, relative to CD62L^{hi} Tregs, CD62L^{lo} Tregs might be slightly more mature and effector-like in their phenotype (Figure 3.3), possibly indicative of differential functionality which would be interesting to assess further using the model outlined in Section 3.2.4.

Therefore overall, exactly how the Treg subsets we identified relate to those previously described remains unclear. This may in part relate to discrepancies in defining the bulk Treg population between studies. Here we defined Tregs as CD25^{+}Foxp3^{+} as our interest was in thymic development and we aimed to exclude the proposed CD25^{+}Foxp3^{-} and CD25^{-}Foxp3^{+} thymic Treg precursor populations[182,188]. However previous studies of both cTregs/eTregs and Triple^{hi}/Triple^{lo} Tregs are based on definitions of Tregs as CD4^{+}Foxp3^{+}[85,107].

Another challenge in directly relating our findings to those of previous studies might be the existence of further undetected heterogeneity within our identified subsets. From our analysis, we were only confidently able to separate Tregs into two subsets by their clear differential expression of CD62L (Figure 3.2). However recent work has suggested that cTregs and eTregs comprise further subsets[104,325]. Moreover, the phenotypic characteristics of Triple^{lo} Tregs and Triple^{hi} Tregs also place them within the cTreg and eTreg populations, respectively[107]. Therefore, it is possible that our thymic CD62L Treg subsets also encompass further subsets, which we have not discriminated and hence this unappreciated heterogeneity confounds phenotyping the subset as a whole. To address this, a global approach such as scRNAseq, could be used to identify Treg subsets, in an unbiased manner, through clustering analysis.

Overall whilst the exact relationship between our findings of thymic Treg heterogeneity and previously described Treg subsets remains somewhat unclear, importantly our analysis confirms a thymic origin for some heterogeneous Tregs.

3.3.2 Characterising Thymic Development of Heterogeneous Tregs

To understand how the thymus orchestrates heterogeneous Treg development we first assessed at what stage of development the subsets emerged. Our analysis suggested that heterogeneity may arise once thymocytes have diverted into the Treg lineage as Rag-GFP and ontogeny analysis suggested that CD62L^{hi} Tregs precede CD62L^{lo} Tregs (Figure 3.4). Subsequent RTOC experiments confirmed that some CD62L^{hi} Tregs undergo intrathymic differentiation into CD62L^{lo} Tregs (Figure 3.6). Therefore, suggesting that heterogeneous Treg differentiation occurred post-selection, following Treg lineage divergence. However, unlike

the differentiation programme associated with Tconv thymocytes post-selection maturation[192], this differentiation did not result in a uniform naïve Treg population, as we identified thymic export of both CD62L^{hi} and CD62L^{lo} Tregs (Figure 3.8). This differential Treg fate is perhaps dependent upon the signals developing Tregs receive from thymic regulators of this differentiation (discussed below), but there may also be other factors. For instance, our RTOC analysis may suggest a temporal factor, as we observed a greater proportion of CD62L^{lo} Tregs in RTOCs, relative to *in vivo*, which could be a consequence of the lack of emigration in RTOCs. Therefore, suggesting Treg thymic dwell time as a regulator of differentiation. However, even within RTOCs some CD62L^{hi} Tregs remained undifferentiated (Figure 3.6), which may suggest that as a population CD62L^{hi} Tregs vary in their intrinsic potential for differentiation. Relatedly cTregs show varied ability to differentiate into eTregs, an observation subsequently explained by the presence of Ly6C^{+} and Ly6C^{-} subsets within the cTreg population, with the former proving a poorer progenitor for eTregs[325]. Therefore, perhaps similar variation is prevalent within our thymic CD62L^{hi} Treg population.

While we identified that one route by which heterogeneous Tregs emerge occurred after Treg lineage divergence, we were also interested in what influence thymic Treg precursors might have in heterogeneous Treg development. As previously, CD25^{+}Foxp3^{-} and CD25^{-}Foxp3^{+} Treg precursors have been reported to generate Tregs distinct in TCR repertoire and function[189]. Therefore, we decided to examine more closely these thymic Treg precursors to better understand their contribution to thymic Treg development.

Previous reports suggest the CD25^{+}Foxp3^{-} precursors appear earliest in thymic development and rapidly undergo differentiation into Tregs[171,189,190]. Accordingly, here we observed

$CD25^{+}Foxp3^{-}$ precursors were well established in the D2 neonatal thymus when Tregs and $CD25^{-}Foxp3^{+}$ precursors were only just emerging (Figure 3.13.B), supporting $CD25^{+}Foxp3^{-}$ precursors as youngest in the Treg lineage. Furthermore, the Rag-GFP levels of $CD25^{+}Foxp3^{-}$ population were distinctly higher than thymic Tregs and showed limited spread (Figure 3.13.A), suggesting a younger population fairly uniform in age. Therefore, $CD25^{+}Foxp3^{-}$ precursors appear to be an early short-lived population, in keeping with rapid differentiation to Tregs.

$CD25^{+}Foxp3^{-}$ precursors also displayed variation in CD62L expression (Figure 3.15), with the majority expressing low levels ($CD62L^{lo}CD25^{+}Foxp3^{-}$) alongside a small population with higher levels ($CD62L^{hi}CD25^{+}Foxp3^{-}$). The $CD62L^{lo}CD25^{+}Foxp3^{-}$ precursors appeared to be younger, with fairly uniform high levels of Rag-GFP. In contrast the Rag-GFP levels of $CD62L^{hi}CD25^{+}Foxp3^{-}$ precursors were intermediary, between $CD62L^{lo}CD25^{+}Foxp3^{-}$ precursors and $CD62L^{hi}$ Tregs. In combination, this might suggest a highly speculative linear developmental pathway where $CD62L^{lo}CD25^{+}Foxp3^{-}$ precursors fairly rapidly differentiate into $CD62L^{hi}CD25^{+}Foxp3^{-}$ precursors before upregulating Foxp3. Meaning that $CD25^{+}Foxp3^{-}$ precursors generate only one product, at least by CD62L expression. One method to test the developmental pathway of $CD25^{+}Foxp3^{-}$ precursors would be to use an RTOC time course to determine the fate of purified $CD62L^{lo}CD25^{+}Foxp3^{-}$ precursors. This could confirm firstly if they produce only $CD62L^{hi}$ Tregs and secondly if these Tregs are generated via a $CD62L^{hi}CD25^{+}Foxp3^{-}$ intermediary.

Regarding $CD25^{-}Foxp3^{+}$ precursors, previous studies proposed they are at a more mature stage of development and undergo a prolonged period of differentiation into Tregs[187,189]. Fittingly $CD25^{-}Foxp3^{+}$ precursors and Tregs appeared in unison during ontogeny (Figure 3.13.B), supporting a later emergence, similar to Tregs, of $CD25^{-}Foxp3^{+}$ precursors in thymic development. In addition, $CD25^{-}Foxp3^{+}$ precursors displayed a broad spread of Rag-GFP levels, which overlapped considerably with the levels observed within the Treg population (Figure 3.13.A). Possibly these older $CD25^{-}Foxp3^{+}$ cells are a consequence of a protracted differentiation to thymic Tregs[187,189]. However, our analysis of peripheral populations might offer an alternative explanation, as we identified cells with a $CD25^{-}Foxp3^{+}$ phenotype within both the RTE and mature splenic SP4 populations (Figure 3.14). Whilst these cells could be the result of mature Tregs downregulating CD25 following thymic egress, this evidence is suggestive that some $CD25^{-}Foxp3^{+}$ precursors leave the thymus and therefore represent a mature stage of development. Potentially these could be Tregs which have lost CD25 as a result of thymic differentiation, as downregulation of CD25 characterises both eTregs and $Triple^{lo}$ Tregs[85,107]. This possibility could be assessed *in vitro* using RTOCs generated with *de novo* thymic Tregs and $CD25^{-}Foxp3^{+}$ precursors to identify if they produce mature $CD25^{-}Foxp3^{+}$ cells.

The possibility that the $CD25^{-}Foxp3^{+}$ precursor population may also contain terminally differentiated cells, in addition to the suggested extensive differentiation time of the precursor population makes interpreting possible differentiation pathways by Rag-GFP levels challenging. Indeed, while we identified $CD62L^{hi}$ and $CD62L^{lo}$ $Foxp3^{+}$ precursors subsets, their ages were comparable to both one another and $CD62L^{hi}$ and $CD62L^{lo}$ Tregs (Figure 3.16). Therefore, by Rag-GFP the developmental pathway remains unclear but again an RTOC time

course might determine the fate of purified CD62L$^{hi/lo}$CD25^{-}Foxp3^{+} precursors. Furthermore, whilst our analysis does not determine if CD25^{-}Foxp3^{+} and CD25^{+}Foxp3^{-} generate distinct Tregs, we did observe a more even distribution of CD62L^{hi} and CD62L^{lo} cells within CD25^{-} Foxp3^{+} precursors, compared to CD25^{+}Foxp3^{-} precursors, which may hint at differential Treg production.

Alongside our efforts to characterise the thymic Treg development pathway we also sought to identify thymic regulators of this process. Notably bulk *de novo* Treg development is highly dependent on the medulla and specifically mTEC^{hi} [158], therefore we wondered if these cells might similarly be fundamental regulators of heterogeneous Treg development.

Significantly CD62L^{hi} Tregs differentiated into CD62L^{lo} Tregs in RTOCs containing mTEC (including mTEC^{hi}) but lacking additional lymphoid populations due to dGuo treatment [326,327] (Figure 3.6). Implying that a stromal environment alone is conducive to heterogeneous Treg development, with other thymocytes and DCs non-essential. However, this does not demonstrate an absolute requirement for mTEC^{hi} as Treg differentiation could be orchestrated in a cell intrinsic manner. To specifically investigate the role of mTEC^{hi} we generated RTOCs lacking mTEC^{hi}, and examined the impact on CD62L^{hi} to CD62L^{lo} Treg differentiation. However, our results were contradictory with an initial experiment identifying a large reduction in CD62L^{hi} differentiation in the absence of mTEC^{hi}, that was not replicated by a subsequent repeat (Figure 3.6.C-D). These conflicting findings may suggest an issue with the experimental setup, possibly related to the generation of stroma without mTEC^{hi}. One confounding issue could be incomplete elimination of thymocytes by dGuo, as some thymocytes express RANK-ligand[277] and thereby could promote mTEC^{hi} development even in

the absence of anti-RANK stimulation. If so, then the reduced differentiation we initially observed hints of a role for mTEC^{hi} in orchestrating thymic Treg differentiation. However this experiment needs to be repeated in a system with more reliable ablation of mTEC^{hi}, possibly in RTOC generated from *Relb*$^{-/-}$ thymic stroma as here mTEC development is intrinsically impaired[260].

If mTEC^{hi} do support heterogeneous thymic Treg development, the next question is how. Notably TCR signalling has been implicated as an important driver of Treg heterogeneity within both the thymus[107,189] and the periphery[103,328], and importantly mTEC^{hi} are key mediators of TCR signalling expressing a diverse range of TRAs[263–266]. Therefore, we wondered whether mTEC^{hi} might drive heterogeneous thymic Treg development by providing appropriate TCR stimulation through their expression of a unique TRA repertoire.

We therefore investigated the role of Aire, a fundamental regulator of the diverse mTEC^{hi} TRA repertoire[261], in heterogeneous Treg development. Similar to previous reports[307], bulk *de novo* thymic Treg development appeared normal in the adult *Aire*$^{-/-}$ (Figure 3.18). Importantly though, unlike earlier studies, we also examined heterogeneous thymic Treg subsets to determine if the composition of the thymic Treg population was altered. However, we observed little impact of *Aire*$^{-/-}$ on the balance of the two thymic CD62L Treg subsets (Figure 3.18.D), suggesting that Aire dependent TRA expression is non-essential in heterogeneous Treg development. Though TCR signalling may still be involved, as possibly there is redundancy between Aire and other TRs, for instance Fezf2[267] or simply TRAs are non-essential.

Furthermore, our results may also reflect previous reports that Aire is an essential regulator of neonatal but not of adult thymic Treg development[232,233]. Indeed, in *Aire*$^{-/-}$ neonates we observed reduced thymic Tregs , as previously described[232], and importantly alongside this general reduction we observed a slight phenotypic shift of both thymic and peripheral Tregs towards the CD62L^{lo} phenotype (Figure 3.20 and Figure 3.21). Suggestive that Aire may regulate the balance of CD62L^{hi} and CD62L^{lo} Tregs more prominently in the neonate. This may be connected to the role of Aire in driving development of neonatal Tregs with a distinct phenotype[233], though a more detailed analysis is necessary to assess this.

Alongside the more targeted impairment of Aire expression in mTEC, we also examined *Ltbr*$^{-/-}$ which are associated with a much broader disruption to the medullary environment including reduced mTEC[301]. Similar to *Aire*$^{-/-}$, we observed normal bulk *de novo* thymic Treg development in *Ltbr*$^{-/-}$ adults, as previously reported[300] (Figure 3.22). However, our assessment of heterogeneous Treg subsets did identify a percentage increase and corresponding decrease of CD62L^{lo} and CD62L^{hi} Tregs, respectively(Figure 3.22.D). Though not statistically significant numerically, possibly due to insufficient replicates, this is suggestive of a trend. Interestingly this skewed CD62L^{lo} phenotype could relate to the described defect in thymic emigration associated with *Ltbr*$^{-/-}$ [192,301], as we observed reduced Treg RTEs within the spleen (Figure 3.23). Possibly indicating that thymic Tregs undergo a protracted dwell time in the *Ltbr*$^{-/-}$ which, if so, our previously discussed RTOC analysis would suggest results in greater differentiation of CD62L^{hi} Tregs. Therefore, potentially the increase of CD62L^{lo} thymic Tregs in the *Ltbr*$^{-/-}$ is a consequence of increased differentiation of “stuck” CD62L^{hi} Tregs.

Identifying if Treg differentiation was similarly altered in *Ltbr*$^{-/-}$ neonates, was complicated as we observed a broad impairment to thymic development, with all SP4 populations reduced in both the thymus and spleen, including Tregs (Figure 3.24 and Figure 3.25). Notably, the composition of the thymic *Ltbr*$^{-/-}$ Tregs was again skewed towards a CD62L^{lo} phenotype (Figure 3.24.D), which might still be the consequence of a thymic egress issue as neonatal egress is heavily reliant on CCR7 and its ligands[230] which are regulated by LTβR[280]. However, it is challenging to assess a specific role of LTβR in Treg development given the more general disruption observed in the *Ltbr*$^{-/-}$ neonate, which suggests a more fundamental issue with thymic SP4 development in the neonate.

Indeed, the untargeted *Ltbr*$^{-/-}$, while useful for broadly assessing the impact of impaired LTβR signalling, represents a challenge in terms of intuiting specific roles for LTβR in Treg development, because the loss of LTβR across many cell types presents as multiple thymic defects[192,300,301,329]. More recent studies have utilised targeted models where LTβR ablation is restricted to specific cell types in order to identify associated thymic defects. For instance, specific deletion of LTβR from TEC in *Foxn1*^{Cre}*Ltbr*$^{fl/fl}$, was associated with a disrupted medulla but not impaired central tolerance, nor defective thymic emigration[192,300]. The former was instead linked with DCs[300] while the latter was associated, by use of the *Flk1*^{Cre}*Ltbr*$^{fl/fl}$, with the thymic endothelium[192]. Therefore, it would be interesting to use these models to assess if the increase in CD62L^{lo} Tregs is related to impaired egress, as if so, we would expect CD62L^{lo} thymic Tregs to increase in *Flk1*^{Cre}*Ltbr*$^{fl/fl}$ but not *Foxn1*^{Cre}*Ltbr*$^{fl/fl}$. Alternatively, the impact of increased thymic dwell time on Treg differentiation could similarly be assessed using FTY720 to inhibit thymic egress[206,207].

3.3.3 Concluding Remarks

As summarised in Figure 3.29, overall we identify that the thymus supports development and export of CD62L^{hi} and CD62L^{lo} Tregs. Meaning the thymus directly contributes to peripheral Treg diversity, though the exact relationship between these thymic subsets and described peripheral subsets remains uncertain. The origin of these two Treg subsets appears connected to a post-selection differentiation pathway, although there may also be a role for the two previously described thymic Treg precursor populations. Finally, the thymic regulators of this post- selection differentiation remain unclear although some provisional evidence suggests a role for mTEC, specifically mTEC^{hi}.

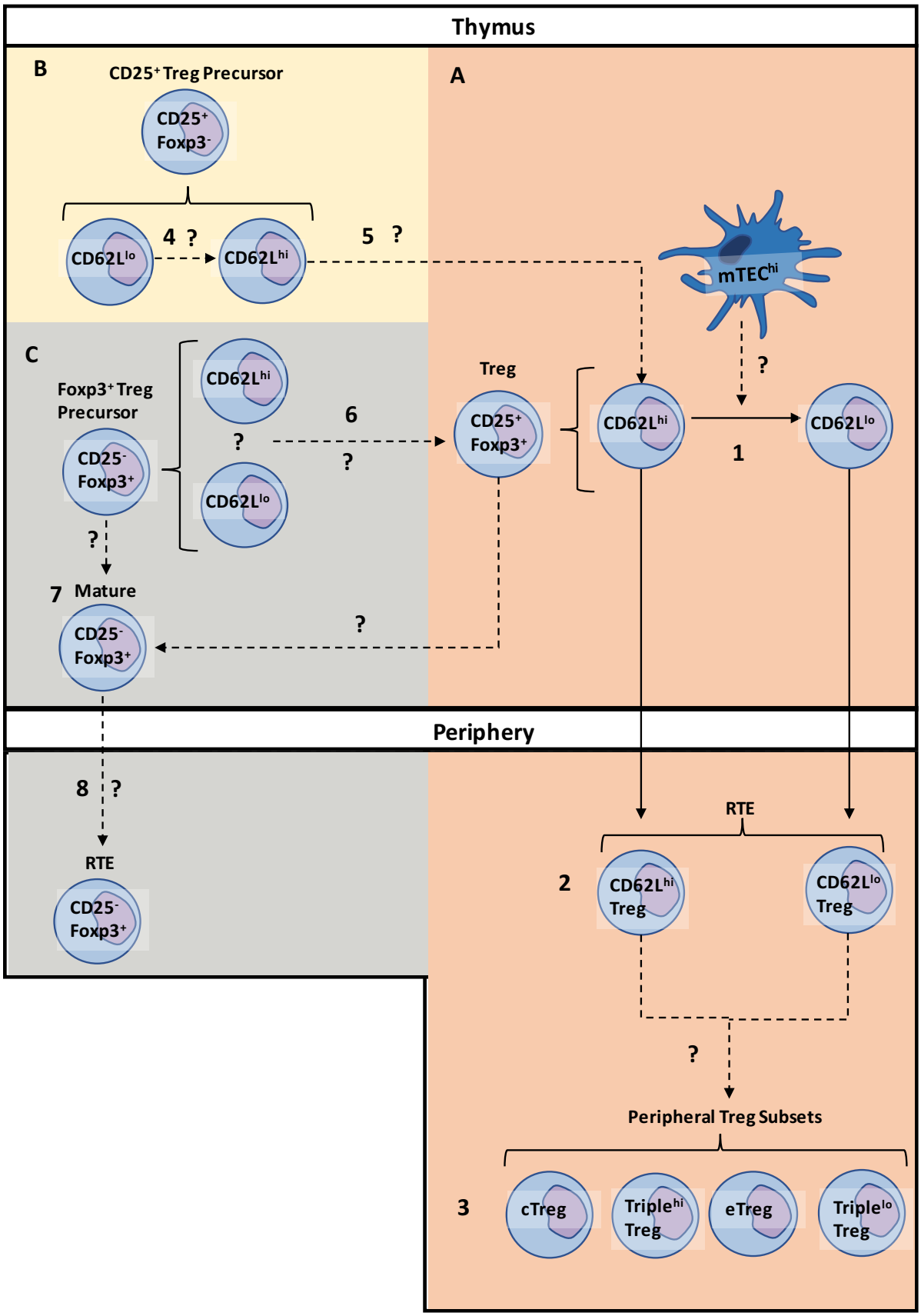
Thymus
B
CD25+ Treg Precursor
CD25+ Foxp3-
CD62Llo
4 ?
CD62Lhi
5 ?
A
mTEChi
?
C
Foxp3+ Treg Precursor
CD25- Foxp3+
CD62Lhi
?
CD62Llo
6
?
Treg
CD25+ Foxp3+
CD62Lhi
1
CD62Llo
?
7 Mature
CD25- Foxp3+
?
Periphery
8 ?
RTE
CD25- Foxp3+
RTE
2
CD62Lhi Treg
CD62Llo Treg
?
Peripheral Treg Subsets
3
cTreg
Triplehi Treg
eTreg
Triplelo Treg

Figure 3. 29 Summary Diagram of Heterogeneous Thymic Treg Development

Proposed overview of how the processes of intrathymic Treg development may contribute to the intrathymic generation and export of heterogeneous Treg. The development pathway is broadly divided into **(A)** $CD25^{+}Foxp3^{+}$ Treg (orange background), **(B)** $CD25^{+}Foxp3^{-}$ Treg precursor (yellow background) and **(C)** $CD25^{-}Foxp3^{+}$ Treg precursor stages (grey background). Dashed lines and question marks indicate the proposed relationship/pathway is somewhat speculative.

(A) Regarding Treg stages: **(1)** $CD25^{+}Foxp3^{+}$ Tregs begin as $CD62L^{hi}$, some of these $CD62L^{hi}$ Tregs undergo intrathymic differentiation giving rise to $CD62L^{lo}$ Tregs, in a process which may be mediated by $mTEC^{hi}$. **(2)** Both $CD62L^{hi}$ and $CD62L^{lo}$ Tregs undergo thymic egress and can be found within the peripheral RTE population. **(3)** How these $CD62L^{hi}$ and $CD62L^{lo}$ Tregs fit with previously described peripheral Treg subsets remains unclear.

(B) Regarding $CD25^{+}Foxp3^{-}$ Treg precursor stages: **(4)** $CD25^{+}Foxp3^{-}$ Treg precursors are suspected to begin as $CD62L^{lo}$ before differentiating to $CD62L^{hi}$. **(5)** these $CD62L^{hi}CD25^{+}Foxp3^{-}$ are then believed to upregulate Foxp3 producing $CD62L^{hi}CD25^{+}Foxp3^{+}$ Tregs.

(C) Regarding $CD25^{-}Foxp3^{+}$ Treg precursor stages: **(6)** $CD25^{+}Foxp3^{-}$ Treg precursors contain $CD62L^{hi}$ and $CD62L^{lo}$ subsets however the developmental order of these subsets and their relationship to $CD62L^{hi}$ and $CD62L^{lo}$ Tregs is currently unclear. **(7)** There may be also a pathway by which mature $CD25^{+}Foxp3^{-}$ thymocytes are generated, possibly via $CD25^{+}Foxp3^{+}$ Tregs which downregulate CD25. **(8)** There is some evidence these mature $CD25^{+}Foxp3^{-}$ thymocytes may then be exported and are found within the peripheral RTE population.

CHAPTER FOUR:
INTRATHYMIC PROLIFERATION OF NEONATAL TREGS

4.1 Introduction

Tregs play an essential role in establishing peripheral tolerance, and there is increasing evidence that thymic Tregs generated at the neonatal stage are of particular importance [98,232,233]. For example, a temporally controlled *Aire*$^{-/-}$ was used to demonstrate that Aire expression prior to weaning was both necessary and sufficient to prevent multi-organ autoimmune disease[232,233]. Similarly colonisation with commensal bacteria in the skin induced tolerance in the neonate but not the adult[98]. In both cases the induction of tolerance in the neonate was linked to thymic derived Tregs, which were phenotypically distinct from their adult counterparts[98,233]. Furthermore, adult and neonatal Tregs were also suggested to differ in their TCR repertoire as a consequence of distinct antigen processing by adult and neonatal mTECs[233]. Thus, distinct thymic Tregs essential for tolerance induction are generated in the neonate, and age dependent mechanisms may subtly influence thymic Treg development.

Given this vital role for neonatal thymic Tregs, it is perhaps surprising that initially neonates lack thymic Tregs, which first appear in the thymus after approximately 2-3 days, a notable lag behind their Tconv counterparts[171,231]. It has been postulated that this delay in Treg development is due to the absence of key signalling requirements as in D1 neonates the medulla, an essential support system for Treg development, was reported to be reduced and disorganised[171]. Indeed provision of TSLP a medullary derived cytokine enhanced Foxp3 induction in neonatal Tregs[231]. Furthermore, constitutive expression of STAT5 was sufficient to induce Foxp3 Tregs in D1 thymocytes indicating the potential for Treg differentiation at this time[181], suggesting that the medullary environment in early neonates may be less permissive to Treg development. Interestingly this delayed appearance of thymic Tregs appears to

translate to a peripheral delay which is implicated in the autoimmunity observed following neonatal day 3 thymectomy (d3tx)[36], however this is not without controversy. Reports of thymic delay do not provide a comparative periphery[171,231] and indeed Foxp3 expression has been observed in day 3 newborn spleens and LNs[330]. Moreover in d3tx mice peripheral Tregs are capable of regulation but are insufficient to prevent autoimmune disease[331]. Intriguingly the disease phenotype of d3tx reportedly mirrors *Aire*$^{-/-}$[263,331,332] suggesting that d3tx disease stems from the loss of the discussed unique neonatal Treg population[233].

While these findings suggest that neonatal thymic Treg development is a critical and potentially distinct process, it is not fully understood. We therefore investigated the appearance of the bulk Treg population in the thymus and periphery to understand the developmental processes underpinning neonatal tolerance. Surprisingly we found a phase of extensive intrathymic proliferation of neonatal Treg which may be an important driver in the rapid expansion of the Treg population. We also investigated possible drivers of intrathymic proliferation, and whether these differed between SP4 thymocyte populations. Overall, the findings in this chapter suggests that an age-dependent phase of intrathymic proliferation specifically contributes to neonatal thymic Treg development.

4.2 Results

4.2.1 Identifying Proliferation of Neonatal Thymic Treg

To better understand the initial establishment of the thymic Treg population we used flow cytometric analysis to monitor the total thymic Treg population across an ontogeny series in Rag-GFPxFoxp3-RFP mice (Figure 4.1A). This ontogeny series identified a large increase in the percentage of thymic Treg within the first week of life (D2-D7), however subsequently the

proportion of Treg did not increase further but rather remained fairly stable into adulthood (Figure 4.1.B). This percentage increase in neonatal Treg also reflected a large numerical increase in Tregs (Figure 4.1.C). However, this numerical increase could simply relate to the increasing size of the aging neonate as we also observed an increase in both total thymic cellularity and Tconv thymocyte population size (Figure 4.1.C). Therefore, to directly compare the amount of change occurring within each population we calculated the average log2 fold change between time points (Figure 4.1.D). Generally, the fold change of the thymocyte populations mirrored changes in thymic cellularity, suggesting that at these times fluctuations within the respective thymocyte population were linked to changing thymus size. However, between D2 and D4 the increase in Tregs was disproportionately larger than both Tconvs and thymic cellularity, suggesting that the neonatal Treg population increases at a rate above that expected by increasing thymus size with age.

From this, we wondered why there was such a large increase in Treg numbers in neonates, particularly between D2 and D4. This time period also proved notable when we examined Rag-GFP levels of neonatal thymic Treg. Given that Rag-GFP is documented to undergo exponential decay with a half-life of approximately 56 hours[26], and thereby remain detectable for around 3 weeks, we anticipated that in early neonatal time points, Rag-GFP$^-$ Treg would be absent. As expected at D2 there were virtually no Rag-GFP$^-$ thymic Treg, however by D4 a clear proportion of Treg were Rag-GFP$^-$. This Rag-GFP$^-$ population increased throughout the first week of life, before a large drop in proportion was observed at D14 (Figure 4.2.A). Throughout the remainder of the time course the proportion of Rag-GFP$^-$ Tregs steadily increased, in keeping with the expected recirculation/retention of mature Tregs[234,235].

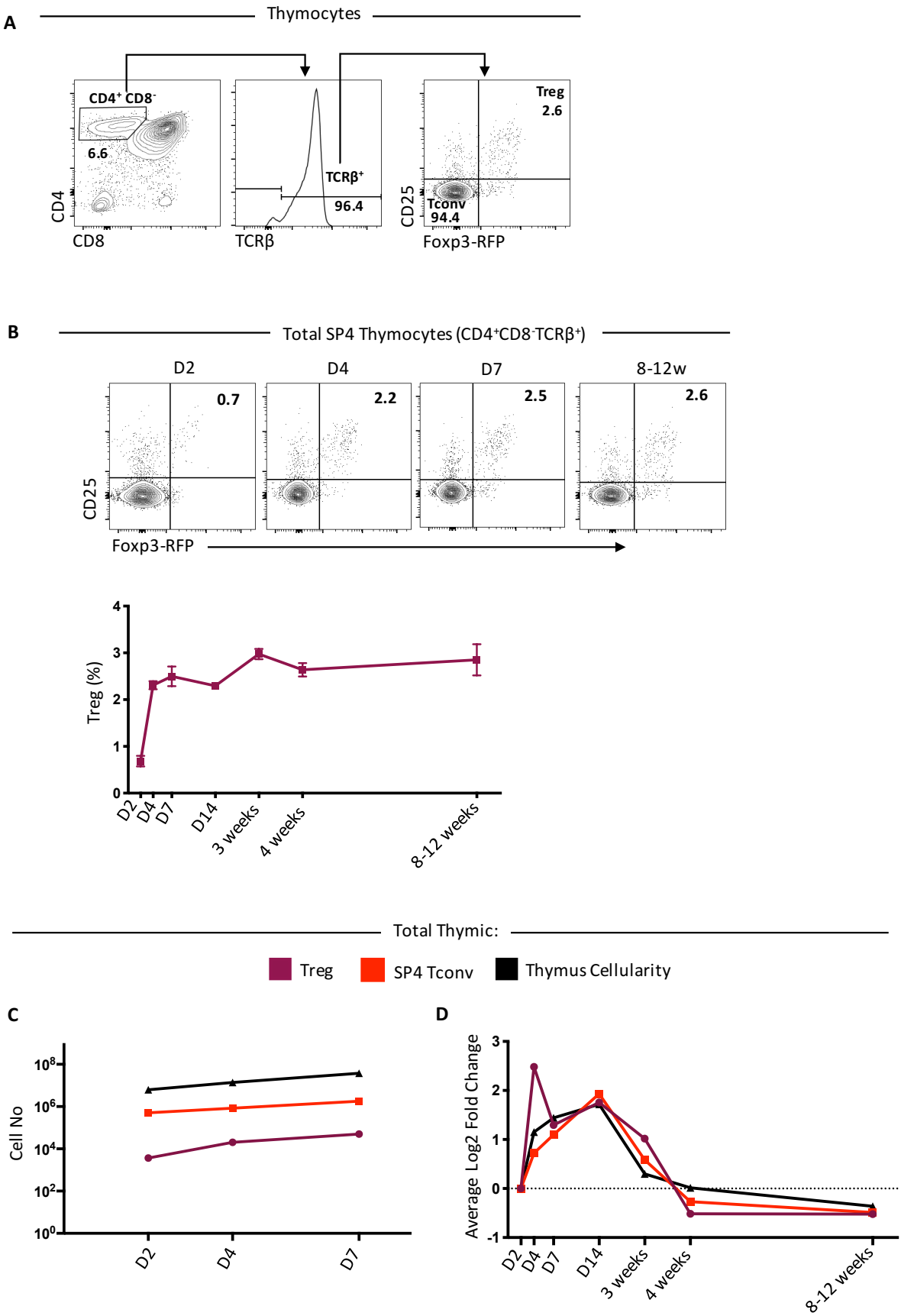
A
Thymocytes
CD4+ CD8-
6.6
CD4
CD8
TCRβ+
96.4
TCRβ
Treg
2.6
Tconv
94.4
CD25
Foxp3-RFP
B
Total SP4 Thymocytes (CD4+CD8-TCRβ+)
D2
D4
D7
8-12w
0.7
2.2
2.5
2.6
CD25
Foxp3-RFP
Treg (%)
D2
D4
D7
D14
3 weeks
4 weeks
8-12 weeks
Total Thymic:
Treg
SP4 Tconv
Thymus Cellularity
C
Cell No
D2
D4
D7
D
Average Log2 Fold Change
D2
D4
D7
D14
3 weeks
4 weeks
8-12 weeks

Figure 4. 1 Establishment of the Thymic Treg is Associated with Rapid Expansion in the Neonate

Changes in the total thymic Treg population in Foxp3-RFPx Rag-GFP mice during ontogeny. All timepoints representative of n ≥ 5 across ≥ 2 independent experiments.

(A) The gating strategy used for the identification of SP4 thymocyte populations. The total SP4 thymocyte population is initially gated as $CD4^{+}CD8^{-}TCR\beta^{+}$. Subsequently this SP4 population can be further divided on the basis of CD25 and Foxp3 to give the SP4 populations: Treg ($CD25^{+}Foxp3^{+}$) and Tconv ($CD25^{-}Foxp3^{-}$). Gating strategy presented as representative FACs plots from an adult (8-12 weeks) including gate title and percentage of cells within the gate given underneath.

(B) Analysis of the frequency (%) of $CD25^{+}Foxp3^{+}$ Treg within the total SP4 thymocyte ($CD4^{+}CD8^{-}TCR\beta^{+}$) population throughout ontogeny. Left shows representative plots of CD25/Foxp3 profile of total SP4 thymocytes at indicated ages, with the percentage of Treg given in the respective quadrant. Right shows quantification of Treg percentages across the timecourse.

(C) Changes to numbers of $CD4^{+}CD8^{-}TCR\beta^{+}CD25^{+}Foxp3^{+}$ Treg (purple), $CD4^{+}CD8^{-}TCR\beta^{+}CD25^{-}Foxp3^{-}$ Tconv (red) and thymus cellularity (black) in the first week of life.

(D) Average log 2 fold change of Treg (purple), Tconv (red) and thymus cellularity (black) across ontogeny. Fold changes were calculated from the average total number for each timepoint for each population.

A Total Thymic Treg ($CD4^+CD8^-TCR\beta^+CD25^+Foxp3^+$)

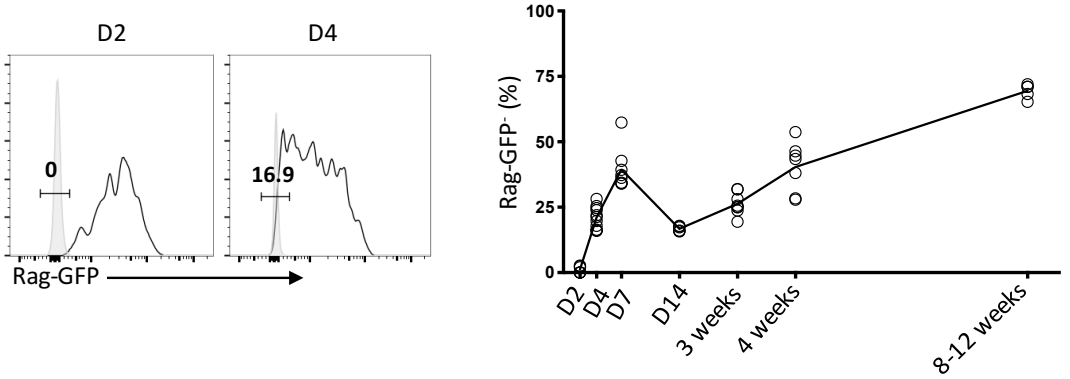

B $N_t = N_0 \times e^{-\lambda \times t}$ and $\lambda = \frac{\ln 2}{t_{1/2}}$ ∴ $t = \ln\left(\frac{N_t}{N_0}\right) \div -\left(\frac{\ln 2}{t_{1/_2}}\right)$

N_t = final amount of GFP = average MFI of D4 Tregs = 1162

N_0 = initial amount of GFP = average MFI of D2 Tregs = 3882

$t_{1/2}$ = half-life = cell cycle ≈ 56 hours

t = elapsed time

$t = \mathrm{In}\left(\frac{1162}{3882}\right) \div -\left(\frac{\mathrm{In}\ 2}{56}\right)$ = 97.5 ≈ 5 days ≈

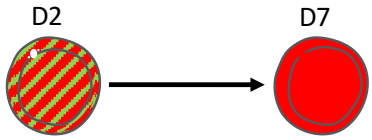

C $N_t = N_0 \times e^{-\lambda \times t}$ and $\lambda = \frac{\ln 2}{t_{1/2}}$ ∴ $t = \ln\left(\frac{N_t}{N_0}\right) \div -\left(\frac{\ln 2}{t_{1/_2}}\right)$

N_t = final amount of GFP = average MFI of D4 Rag-GFP⁻ Tregs = 1162

N_0 = initial amount of GFP = average MFI of D2 Tregs = 3882

$t_{1/2}$ = half-life = cell cycle ≈ 8 hours

t = elapsed time

$t = \mathrm{In}\left(\frac{1162}{3882}\right) \div -\left(\frac{\mathrm{In}\ 2}{8}\right)$ = 13.9 ≈ 1.8 divisions ≈

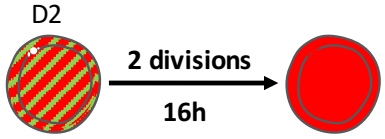

Figure 4. 2 Early Appearance of Rag-GFP$^-$ Thymic Tregs in Ontogeny

Changes in the Rag-GFP$^-$ thymic Treg in Foxp3-RFPx Rag-GFP mice during ontogeny. For all timepoints n ≥ 5 across ≥ 2 independent experiments.

(A) Analysis of the frequency (%) of Rag-GFP$^-$Treg (pre-gated as CD4$^+$CD8$^-$ TCRβ$^+$CD25$^+$Foxp3$^+$) within the total thymic Treg population throughout ontogeny. Left shows representative histogram plots of Rag-GFP expression of total thymic Treg at indicated ages (black), relative to non-fluorescent staining control (filled grey). The percentage of Rag-GFP$^-$ Treg is given above the gate. Right shows quantification of Rag-GFP$^-$ Treg percentages across the timecourse.

(B-C) Calculation of elapsed timed based on exponential decay with a half-life based on **(B)** approximate half-life of Rag-GFP or **(C)** approximate cell cycle time. Values substituted into the equation as shown. Calculated elapsed time between starting and final levels of Rag-GFP given in hours and number of cell divisions, and illustrated in schematic diagram.

The appearance of Rag-GFP$^-$ Tregs by D4 was surprising, especially as this seemed insufficient time for Rag-GFP loss by exponential decay. Indeed, we calculated that approximately 5 days would be necessary for the level of Rag-GFP observed in D2 thymic Tregs to decay to that of D4 thymic Tregs following Rag-GFPs estimated 56-hour half-life (Figure 4.2.B). Thus, loss of Rag-GFP in D4 neonatal Tregs is unlikely to simply be a consequence of loss of Rag-GFP by exponential decay over its natural half-life. We therefore considered what else could drive an artificial loss of Rag-GFP, and noted that the Rag-GFP expression of Tregs appeared as successively decreasing discrete peaks (Figure 4.2.A), which was highly evocative of the loss of proliferative tracking dyes during cell division. Consequently, we wondered if proliferation could be involved, with each cell division causing the level of Rag-GFP to half, and thereby mimicking exponential decay. To determine if Rag-GFP could theoretically be depleted by extensive proliferation within the observed timeframe of 48 hours we performed the same exponential decay calculation as detailed in Figure 4.2.B but replaced the half-life of Rag-GFP with the cell cycle time, approximately 8 hours (Figure 4.2.C). Our calculations showed that, assuming constant division, 13.9 hours or 1.8 divisions were necessary for Rag-GFP to decay to negligible levels, as we assumed a complete division would be necessary for Rag-GFP decay, this rounded to 2 divisions, taking 16 hours. Therefore, our findings suggest that it was feasible for extensive proliferation to cause loss of Rag-GFP within a 48-hour time period.

Having identified Treg proliferation as a cause of the appearance of Rag-GFP$^-$ Tregs, we sought to determine the site of this proliferation. One possibility was that Rag-GFP$^+$ Treg were exported from the thymus, underwent extensive proliferation within the periphery then recirculated to the thymus as Rag-GFP$^-$ Tregs, akin to the recirculation of mature Rag-GFP$^-$ Treg in post-neonatal mice. We therefore examined the total splenic Treg population (Figure 4.3.A)

in D2 and D4 neonates. In agreement with previous observations[36] we found that at D2 the splenic Treg population was negligible but by D4 a clear population was present (Figure 4.3.B), suggesting that substantive thymic egress of Tregs does not occur prior to D3. Of the D4 splenic Treg population we found that relative to their thymic counterparts, a larger proportion were Rag-GFP$^-$ (Figure 4.3.C). However, Rag-GFP$^-$ thymic Tregs still vastly outnumbered their splenic counterparts numerically (Figure 4.3.C). Overall this suggests that recirculation of peripheral Treg is unlikely to be the sole source of the thymic Rag-GFP$^-$ population, because firstly there is little time between export and supposed recirculation and secondly the number of Rag-GFP$^-$ Treg which recirculate would be very large comparative to the numbers of peripheral Treg present.

Given peripheral tissues seemed an unlikely source of thymic Rag-GFP$^-$ Tregs, we looked for evidence of intrathymic proliferation. Ki67 is commonly used as a marker of proliferating cells, therefore we looked at Ki67 by flow cytometry analysis across a series of neonatal ages in WT mice (Figure 4.4.A). At all stages, we could identify Ki67$^+$ Treg however proportionally this population was largest between D2 and D4, then slightly reduced by D7 and smallest at D14. To further support a connection between the appearance of Rag-GFP$^-$ thymic Treg and proliferation, we examined Ki67 expression alongside Rag-GFP expression in D7 Rag-GFP WT neonates (Figure 4.4.B). Within these mice a larger percentage of Ki67$^+$ Treg were Rag-GFP$^-$ compared to Ki67$^-$ Treg suggesting that loss of Rag-GFP correlates with Ki67 and hence is linked to proliferation.

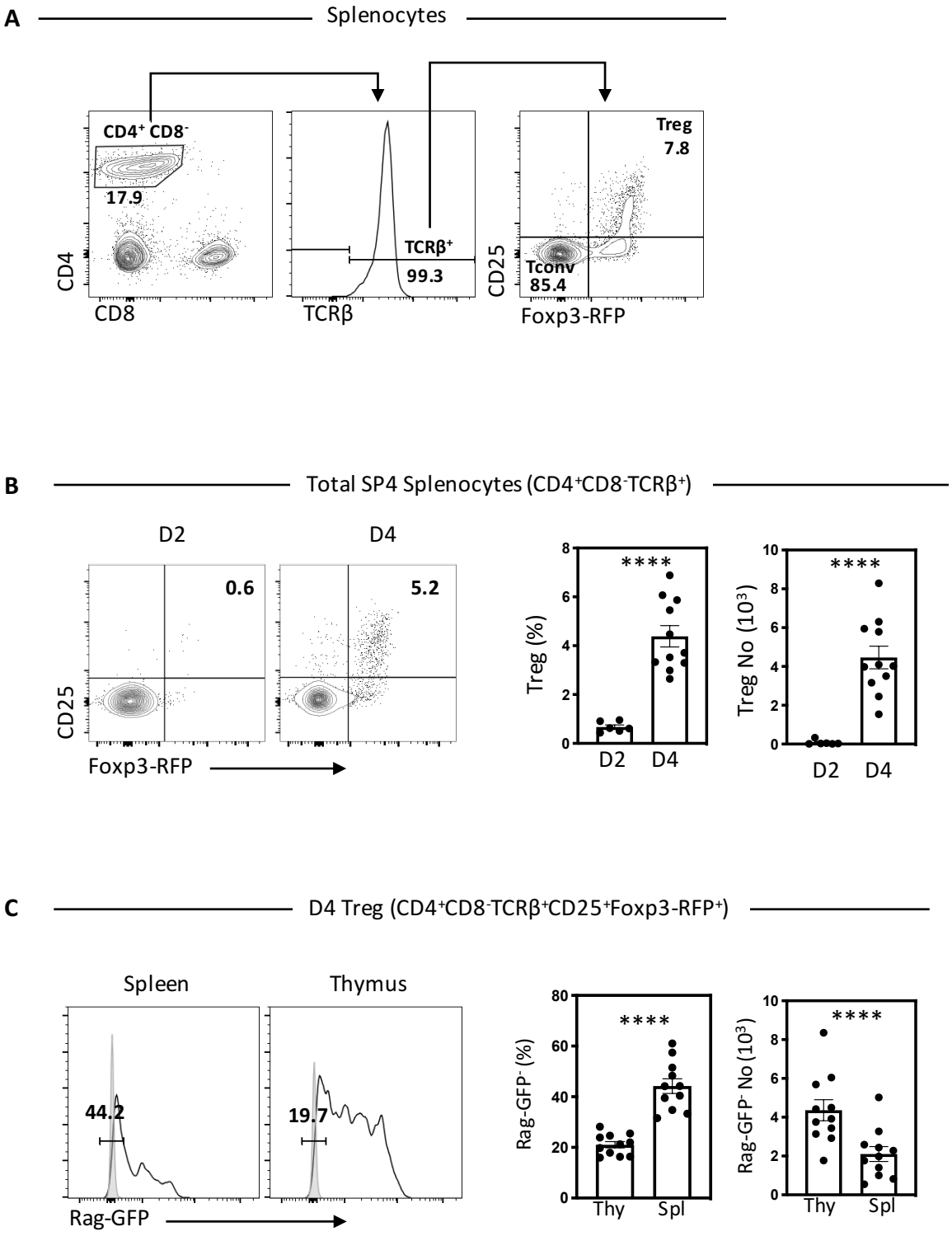
A
Splenocytes
CD4+ CD8-
17.9
CD4
CD8
TCRβ+
99.3
TCRβ
Treg
7.8
Tconv
85.4
CD25
Foxp3-RFP
B
Total SP4 Splenocytes (CD4+CD8-TCRβ+)
D2
D4
0.6
5.2
CD25
Foxp3-RFP
****
Treg (%)
D2
D4
****
Treg No (10³)
D2
D4
C
D4 Treg (CD4+CD8-TCRβ+CD25+Foxp3-RFP+)
Spleen
Thymus
44.2
19.7
Rag-GFP
****
Rag-GFP- (%)
Thy
Spl
****
Rag-GFP- No (10³)
Thy
Spl

Figure 4. 3 Early Appearance of Thymic Rag-GFP$^-$ Tregs in Neonates is Unlikely Solely Due to Peripheral Recirculation

Analysis of the early splenic Treg population in Foxp3-RFPx Rag-GFP mice. All timepoints n ≥ 6 across ≥ 2 independent experiments. All statistics presented were generated using a unpaired student's t- tests, where **** p<0.0001.

(A) The gating strategy used for the identification of SP4 splenocyte populations. The total SP4 splenocyte population is initially gated as CD4$^+$CD8$^-$TCRβ$^+$. Subsequently this SP4 population can be further divided on the basis of CD25 and Foxp3 to give the SP4 populations: Treg (CD25$^+$Foxp3-RFP$^+$) and Tconv (CD25$^-$Foxp3-RFP$^-$). Gating strategy presented as representative FACs plots from an adult (8-12 weeks) including gate title and percentage of cells within the gate given underneath.

(B) Analysis of the appearance of CD25$^+$Foxp3-RFP$^+$ Treg within the total SP4 splenic (CD4$^+$CD8$^-$TCRβ$^+$) population. Left shows representative plots of CD25/Foxp3-RFP profile of total SP4 splenocytes at D2 and D4. Right shows quantification of Treg percentages and numbers comparative between D2 and D4.

(C) Comparison of Rag-GFP$^-$ Tregs (pre-gated as CD4$^+$CD8$^-$TCRβ$^+$CD25$^+$Foxp3-RFP$^+$) present in the thymus and spleen of D4 neonates. Left shows representative histogram plots of Rag-GFP expression of total thymic or splenic (as indicated) Treg, relative to non-fluorescent staining control (filled grey). The percentage of Rag-GFP$^-$ Treg is given above the gate. Right shows quantification of Rag-GFP$^-$ Treg percentages and numbers comparative between thymus and spleen.

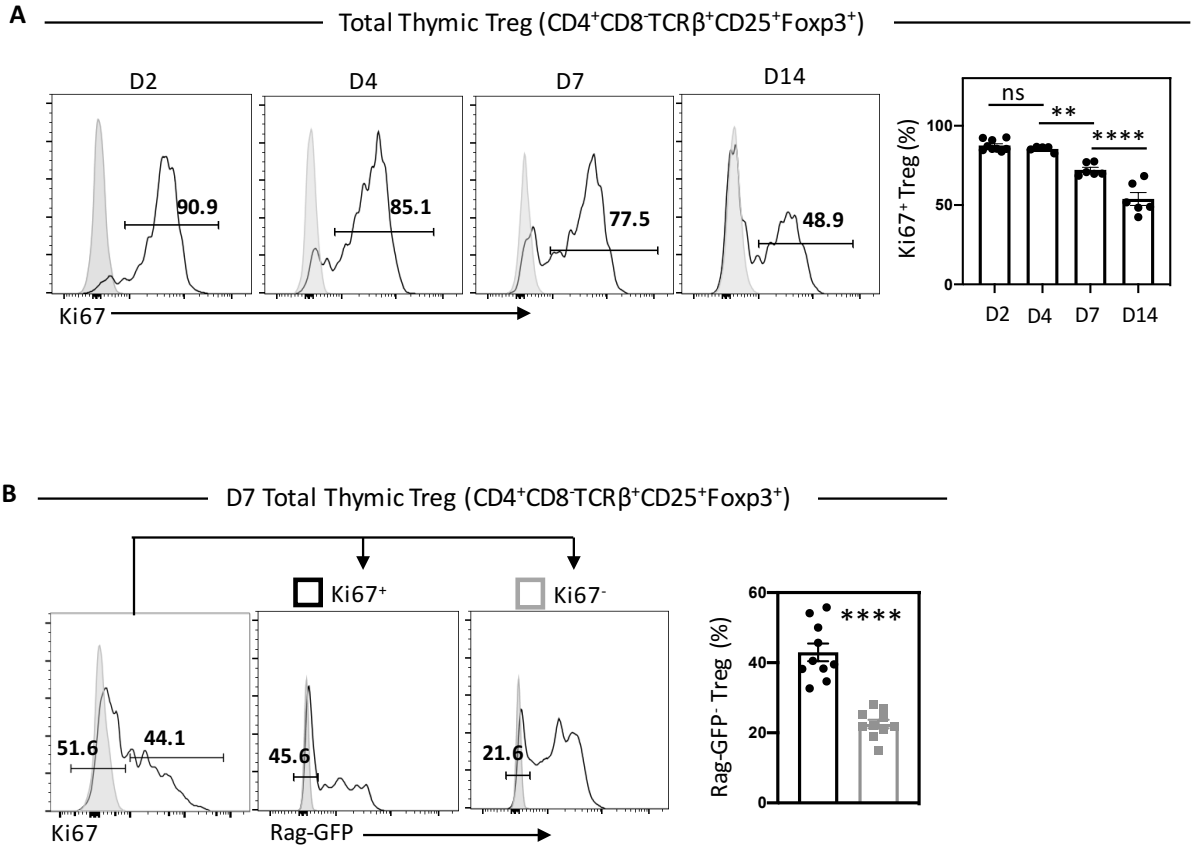
A
Total Thymic Treg (CD4+CD8-TCRβ+CD25+Foxp3+)
D2
D4
D7
D14
90.9
85.1
77.5
48.9
Ki67
ns
**
****
Ki67+ Treg (%)
100
50
0
D2
D4
D7
D14
B
D7 Total Thymic Treg (CD4+CD8-TCRβ+CD25+Foxp3+)
Ki67+
Ki67-
51.6
44.1
45.6
21.6
Ki67
Rag-GFP
****
Rag-GFP- Treg (%)
60
40
20
0

Figure 4. 4 Expression of the Proliferation Marker Ki67 by Neonatal Thymic Tregs

(A) Analysis of Ki67 expression on thymic Treg in WT neonates at indicated neonatal ages. Plots shows representative FACs plots of Ki67 levels on thymic Treg (pre-gated as $CD4^{+}CD8^{-}TCR\beta^{+}CD25^{+}Foxp3^{+}$) at the indicated ages, relative to isotype control (filled grey). Right shows quantification of $Ki67^{+}$ Treg percentages across the indicated ages. All timepoints n ≥ 5 across ≥ 2 independent experiments. Statistical analysis performed using an ordinary one way anova, where ns p>0.05,** p<0.01, **** p<0.0001

(B) Analysis of Ki67 expression on thymic Treg in D7 Rag-GFP neonates. Representative FACs plots show, on the left, Ki67 staining on Treg, relative to isotype control (filled grey) with the gated $Ki67^{+}$ and $Ki67^{-}$ Treg populations subsequently depicted in the two right plots. These two right plots show Rag-GFP expression of the $Ki67^{+}$ and $Ki67^{-}$ Treg (as indicated), relative to non-fluorescent staining control (filled grey). Right graph shows quantification of $Rag\text{-}GFP^{-}$ Treg percentages comparative between $Ki67^{+}$ Treg (black) and $Ki67^{+}$ Treg (grey). Data represents n=10 across 3 independent experiments. Statistical analysis performed using a paired t-test, where **** indicates a p value <0.0001.

Whilst Ki67 is widely used as a marker of proliferation it may not provide the most accurate measure of active proliferation because it marks all stages of the cell cycle (except G_0) and may also be expressed/retained in non-proliferating cells[333,334]. Therefore, we sought to confirm our findings regarding Ki67 and intrathymic proliferation of Treg using BRDU, a more accurate marker of active proliferation as it is incorporated only by cells in S phase of cell cycle. Normally, in adult mice, BRDU would be administered *in vivo***,** however there were several welfare concerns around injecting neonatal pups with BRDU. Therefore, we administered BRDU to thymocytes *in vitro* following their isolation from neonatal tissue (detailed in Section 2.7.2). To directly compare the *in vivo* and *in vitro* approaches we performed them side by side in adult mice and examined BRDU incorporation, across the two conditions, by two thymocyte populations ($CD4^-CD8^+TCR\beta^-$ and $CD4^+CD8^+$) known to contain a proliferating fraction (Figure 4.5.A). Importantly BRDU incorporation was observed in the expected populations under both routes of administration and these different conditions were broadly comparable, although a greater proportion of BRDU incorporation was observed under *in vitro* administration. Overall this suggested that *in vitro* administration of BRDU was a viable method to detect proliferation of thymocytes. When we used this approach to examine BRDU incorporation by D4 neonatal thymic Treg (Figure 4.5.B), we observed a large proportion of $BRDU^+$ Treg. This is in agreement with our previous findings using Ki67, that neonatal thymic Treg are actively proliferating.

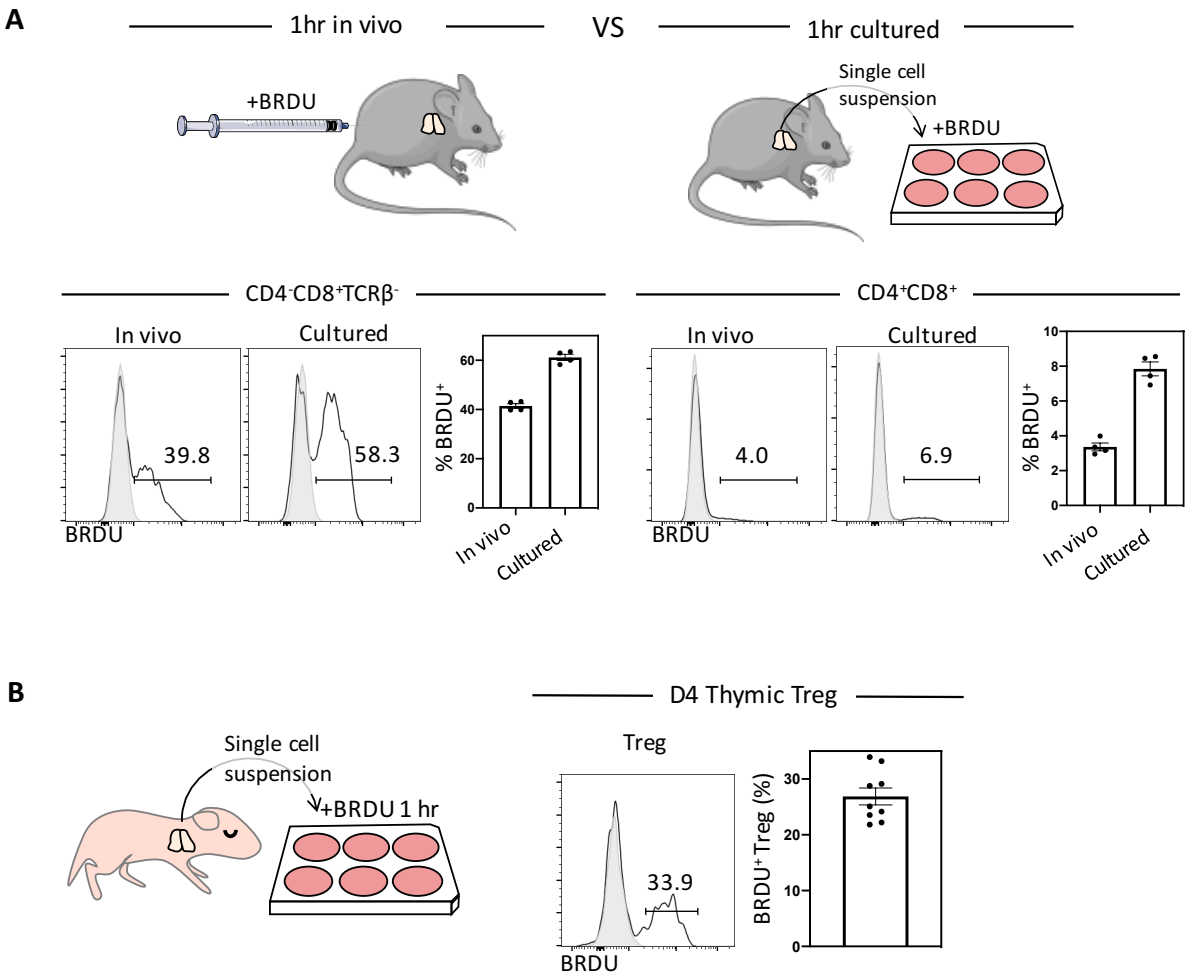
A
1hr in vivo
VS
1hr cultured
+BRDU
Single cell suspension
+BRDU
CD4-CD8+TCRβ-
CD4+CD8+
In vivo
Cultured
39.8
58.3
BRDU
% BRDU+
In vivo
Cultured
4.0
6.9
BRDU
% BRDU+
B
D4 Thymic Treg
Single cell suspension
+BRDU 1 hr
Treg
33.9
BRDU
BRDU+Treg (%)

Figure 4. 5 Confirmation Neonatal Thymic Treg are Undergoing Active Proliferation

(A) Comparison of *in vivo* vs *in vitro* (cultured) BRDU labelling of thymocytes in WT adults (8-12 weeks), associated data is presented on the left and right, respectively. Top shows a schematic of each method. Bottom shows the BRDU analysis of two thymocyte populations ($CD4^{-}CD8^{+}TCR\beta^{-}$ and $CD4^{+}CD8^{+}$) known to harbour a proliferating fraction. FACs plots show BRDU trace as histogram relative to the without BRDU control (filled grey). Bar charts quantify the percentages of $BRDU^{+}$ cells in each condition. Data representative of n=4 injected, 4 cultured across 2 independent experiments.

(B) Analysis of BRDU incorporation by thymic Treg from D4 neonates. Left shows a schematic of BRDU labelling method. Right shows BRDU analysis from thymic Treg ($CD4^{+}CD8^{-}TCR\beta^{+}CD25^{+}Foxp3^{+}$). FACs plots show BRDU trace as histogram relative to the without BRDU control in grey. Bar chart quantifies the percentages of $BRDU^{+}$ Treg within the Treg population. Data representative of n= 9 across 3 independent experiments.

To examine whether intrathymic Treg proliferation may be important in establishing the balance of peripheral Treg:Tconv necessary to maintain tolerance, we examined the dynamics of these two peripheral population sizes across ontogeny (Figure 4.6), starting with their initial appearance within the spleen. Studies of d3tx mice suggest that Tregs are slightly delayed in their peripheral appearance relative to Tconvs[36]. To confirm this, we looked for evidence of the two populations in D2 spleens, and observed a small population of SP4 T-cells (Figure 4.6.A) predominantly comprised of Tconvs while Tregs were virtually undetectable (Figure 4.6.B). This suggests, in agreement with d3tx studies, that Tconv exit to the periphery prior to Treg, a finding also in keeping with our own, and others[171,231], observations that at D2 the thymic Treg population is only just emerging. Following the appearance of both populations we saw that both Treg and Tconv splenocytes continually increase numerically throughout life, however proportionally within the SP4 compartment Treg and Tconv reach a plateau by D7, and for Treg this involves a steep increase in proportion from D2 (Figure 4.6.C).

To more directly address how these numerical and proportional changes impacted on the balance of Treg:Tconv we calculated the ratio of Tconv:Treg splenocytes across the ontogeny series (Figure 4.6.D). We saw that at D2 the ratio of Tconv:Treg is heavily skewed towards Tconv with a ratio of over 150 Tconv per 1 Treg. However, by D7 the ratio of Tconv to Treg is dramatically reduced to nearer 10 Tconvs: 1 Treg, a ratio that remains stable into adulthood. Collectively our analysis suggests that extensive intrathymic proliferation of Treg between D2 and D7 may be necessary to rapidly expand the peripheral Treg population to achieve a Tconv:Treg ratio conducive to protective peripheral tolerance in the neonate.

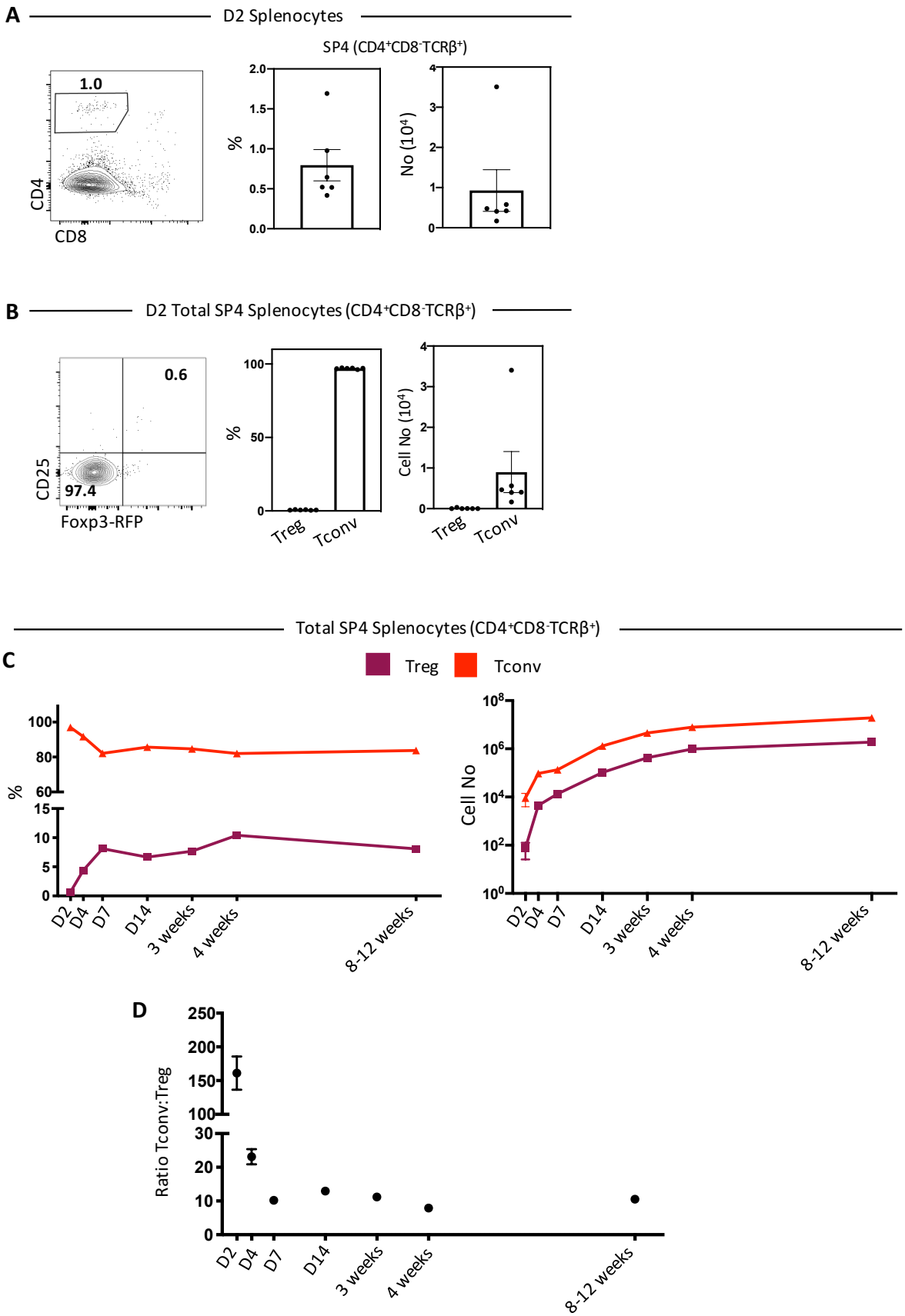
A
D2 Splenocytes
SP4 (CD4+CD8-TCRβ+)
1.0
CD4
CD8
%
No (10⁴)
B
D2 Total SP4 Splenocytes (CD4+CD8-TCRβ+)
0.6
97.4
CD25
Foxp3-RFP
%
Cell No (10⁴)
Treg
Tconv
Total SP4 Splenocytes (CD4+CD8-TCRβ+)
C
Treg
Tconv
%
Cell No
D2
D4
D7
D14
3 weeks
4 weeks
8-12 weeks
D
Ratio Tconv:Treg

Figure 4. 6 Rapid Expansion of Neonatal Treg Population Counters Initial Imbalance in the Peripheral Ratio of Tconv:Treg

Analysis of the early splenic SP4 ($CD4^+CD8^-TCR\beta^+$) T cell population in Foxp3-RFPx Rag-GFP mice. All timepoints n ≥ 6 across ≥ 2 independent experiments.

(A) Analysis of the splenic SP4 ($CD4^+CD8^-TCR\beta^+$) T cell population in D2 neonates. Left shows representative FACs plots of CD4/CD8 profile. Right shows quantification of the SP4 T cell percentages and numbers.

(B) Proportion of Treg ($CD4^+CD8^-TCR\beta^+$ $CD25^+Foxp3^+$) and Tconv ($CD4^+CD8^-TCR\beta^+$ $CD25^-$ $Foxp3^-$) within the D2 SP4 splenocyte population. Left shows representative FACs plots of CD25/Foxp3 profile of total SP4 splenocytes. Right shows quantification of the Treg and Tconv percentages and numbers.

(C) Analysis of Treg (purple) and Tconv (red) within the total splenic SP4 T cell population throughout ontogeny. Left shows the changes to percentages of the populations with the changes to the numbers on the right.

(D) Analysis of the ratio of the number of Tconv:Treg within the spleen throughout ontogeny. Ratios were calculated from total number of Treg and Tconv within the spleen for each individual mouse, for each timepoint.

4.2.2 Further Characterisation of Neonatal Treg Proliferation

Having identified proliferation of neonatal thymic Treg we then sought to better understand how proliferation related to distinct stages of thymic Treg development. We therefore looked for evidence of proliferation, by analysing Ki67 expression and BRDU incorporation, within the two thymic Treg precursor populations, $CD25^{+}Foxp3^{-}$ and $CD25^{-}Foxp3^{+}$ SP4 thymocytes, in D4 neonates (Figure 4.7A). While both Ki67 and BRDU analysis identified a proliferating fraction within $CD25^{+}Foxp3^{-}$ and $CD25^{-}Foxp3^{+}$ precursors, they differed between the precursor populations. Ki67 analysis suggested that a larger proportion of $CD25^{-}Foxp3^{+}$ than $CD25^{-}Foxp3^{+}$ were $Ki67^{+}$, and that the proportion of $Ki67^{+}$ Tregs were larger still. In contrast, by BRDU incorporation $CD25^{+}Foxp3^{-}$ precursors seemed to proliferate more, as they contained the larger proportion of $BRDU^{+}$ cells, which was roughly equivalent to the proportion of $BRDU^{+}$ Tregs. This discrepancy between the two measures of proliferation may reflect the previously noted limitations of Ki67 analysis, hence the BRDU analysis likely provides a more accurate measure on the relative amount of proliferation occurring. Importantly though, both analyses support that proliferation occurs to some degree within both Treg precursor populations and, based on the BRDU analysis, these precursors proliferate to different extents, with the $CD25^{+}Foxp3^{-}$ precursors exhibiting more extensive proliferation reminiscent of Tregs.

A

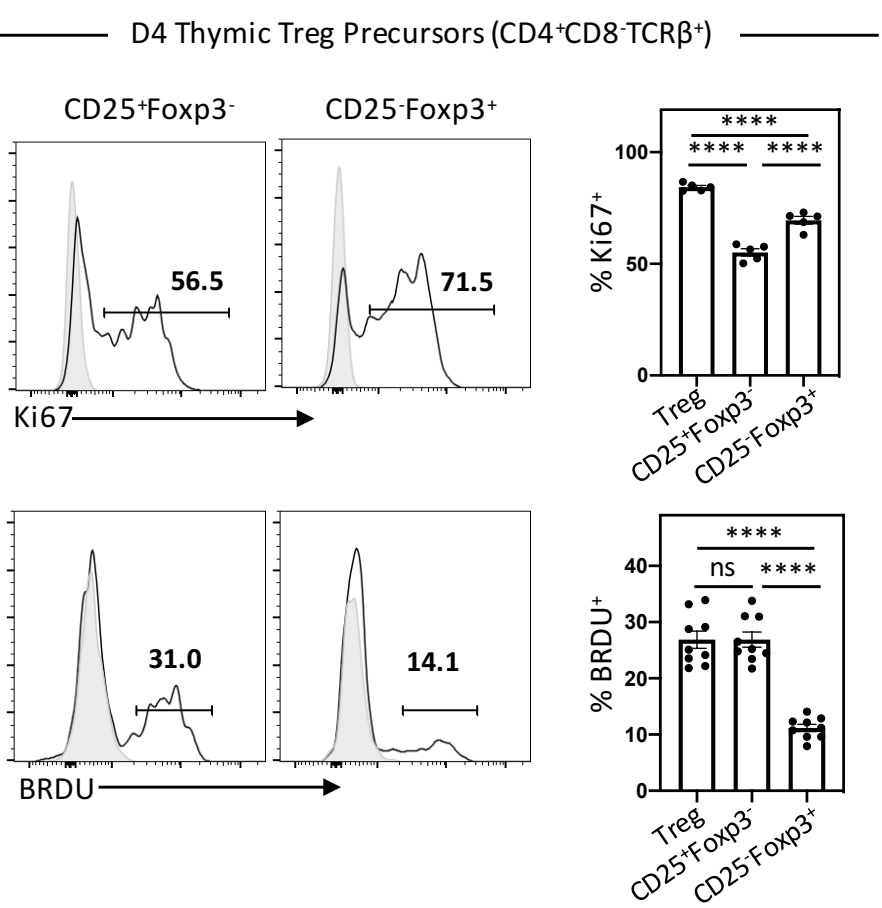
D4 Thymic Treg Precursors (CD4+CD8-TCRβ+)
CD25+Foxp3-
CD25-Foxp3+
56.5
71.5
Ki67
% Ki67+
****
****
****
100
50
0
Treg
CD25+Foxp3-
CD25-Foxp3+
31.0
14.1
BRDU
% BRDU+
****
ns
****
40
30
20
10
0
Treg
CD25+Foxp3-
CD25-Foxp3+

Figure 4. 7 Thymic Treg Precursors Show Evidence of Proliferation

(A) Analysis of proliferation in the two thymic Treg Precursor populations ($CD4^{+}CD8^{-}TCR\beta^{+}CD25^{+}Foxp3^{-}$ and $CD4^{+}CD8^{-}TCR\beta^{+}CD25^{-}Foxp3^{+}$) from D4 WT neonates by (top) Ki67 and (bottom) BRDU. Data representative of (top/Ki67) n= 5 across 2 independent experiments(bottom/BRDU) n= 9 across 3 independent experiments. Representative FACs plots show Ki67 and BRDU trace relative to isotype or without BRDU control, respectively (filled grey). Bar charts quantify percentages of $Ki67^{+}$ or $BRDU^{+}$ $CD25^{+}Foxp3^{-}$, $CD25^{-}Foxp3^{+}$ and $CD25^{+}Foxp3^{+}$ Treg. Statistical analysis performed using repeated measures one way anova, ns $p>0.05$, **** $p<0.0001$.

As well as considering the proliferation of thymocytes upon entry into the Treg lineage we examined whether there were differences in later stages of Treg development. Previously (Chapter 3) we identified two subsets of thymic Treg, $CD62L^{hi}$ and $CD62L^{lo}$ both of which are present in the neonatal thymus. Therefore we looked for evidence of proliferation within these two Treg populations using BRDU and Ki67 in D4 neonates (Figure 4.8.A). Unlike our analysis of Treg precursors, here BRDU and Ki67 analysis yielded similar results. Within both Treg populations we identified a clear $Ki67^{+}$ or $BRDU^{+}$ proliferating fraction, and the proportion of $Ki67^{+}/BRDU^{+}$ cells was slightly higher in $CD62L^{hi}$ Treg. Overall this suggests that both Treg subsets are proliferating in the neonatal thymus, and that this process is slightly more extensive in the $CD62L^{hi}$ Treg population.

Having identified proliferation throughout the Treg lineage we next wondered whether intrathymic proliferation was specific to this lineage or if non-Treg thymocytes also proliferated to a similar extent. To address this, we examined proliferation of SP4 Tconv thymocytes using BRDU and Ki67 in D4 neonates (Figure 4.9.A). While Tconv thymocytes contained a $Ki67^{+}/BRDU^{+}$ population, by both methods of analysis this population was significantly smaller than the population observed within thymic Tregs. Thus, thymic Tconvs proliferate, but to a lesser extent than thymic Tregs. This is further supported by analysis of the Rag-GFP trace in thymic Tconvs (Figure 4.9.B), which consisted of far fewer peaks of low level Rag-GFP compared to thymic Tregs.

A D4 Thymic Treg ($CD4^+CD8^-TCR\beta^+CD25^+Foxp3^+$)

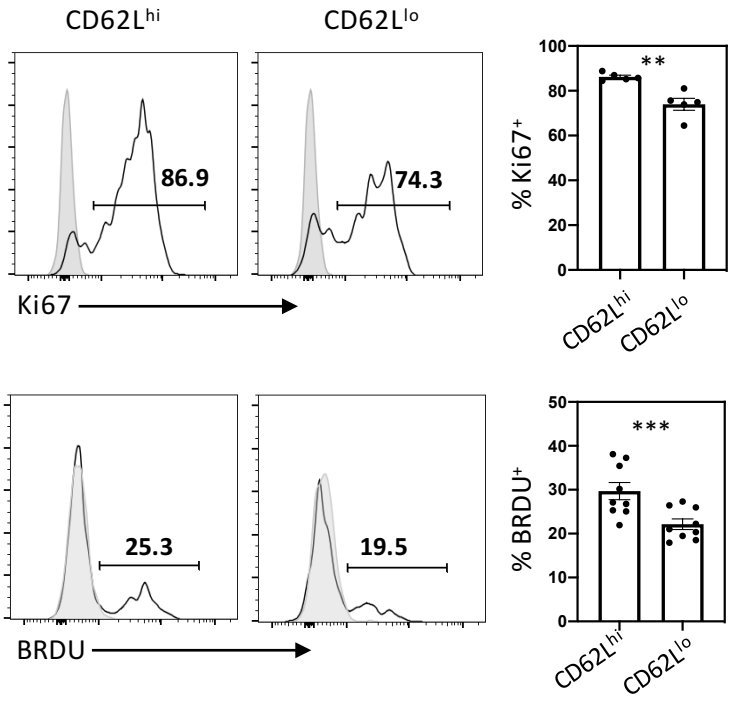

Figure 4. 8 Comparable Proliferation of Neonatal Thymic Treg Subsets

(A) Analysis of proliferation in the two thymic Treg populations ($CD4^+CD8^-TCR\beta^+CD25^+Foxp3^+CD62L^{hi}$ and $CD4^+CD8^-TCR\beta^+CD25^+Foxp3^+CD62L^{lo}$) from D4 WT neonates by (top) Ki67 and (bottom) BRDU. Data representative of (top/Ki67) n= 5 across 2 independent experiments(bottom/BRDU) n= 9 across 3 independent experiments. Representative FACs plots show Ki67 and BRDU trace relative to isotype or without BRDU control, respectively (filled grey). Bar charts quantify percentages of $Ki67^+$ or $BRDU^+$ $CD62L^{hi}$ and $CD62L^{lo}$ Treg. Statistical analysis performed using paired t-test, ** $p<0.01$, *** $p<0.001$.

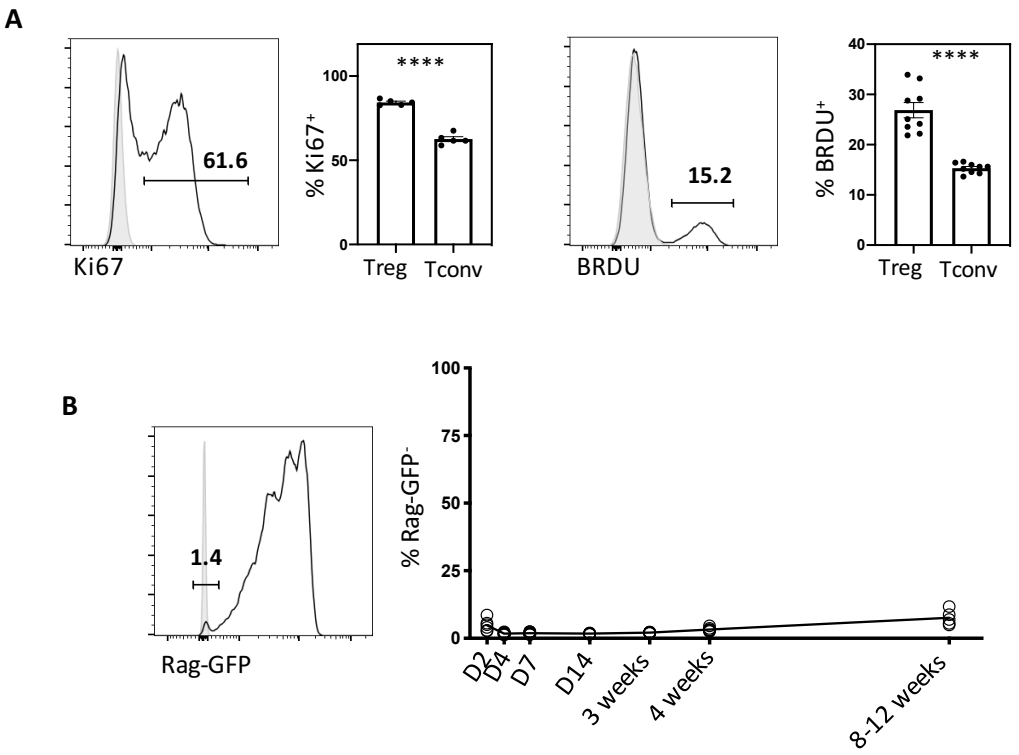
A
61.6
Ki67
****
% Ki67+
100
50
0
Treg
Tconv
15.2
BRDU
****
% BRDU+
40
30
20
10
0
Treg
Tconv
B
1.4
Rag-GFP
% Rag-GFP-
100
75
50
25
0
D2
D4
D7
D14
3 weeks
4 weeks
8-12 weeks

Figure 4. 9 Neonatal Thymic Tcons Proliferate but to a Lesser Extent than Tregs

(A) Analysis of proliferation markers, Ki67 (left) and BRDU (right) on thymic Tconv ($CD4^{+}CD8^{-}TCR\beta^{+}CD25^{-}Foxp3^{-}$) in D4 WT neonatal mice. Data representative of (left/ Ki67) n= 5 across 2 independent experiments (right/BRDU) n= 9 across 3 independent experiments. Representative FACs plots show Ki67 and BRDU trace relative to isotype or without BRDU control, respectively (filled grey). Bar charts quantify percentages of $Ki67^{+}$ or $BRDU^{+}$ Tconv comparative to thymic Treg. All statistical analysis performed using paired t-test, **** $p \leq 0.0001$.

(B) Analysis of Rag-GFP levels on thymic Tconv across ontogeny in Foxp3-RFPx Rag-GFP mice. All timepoints representative of $n \geq 5$ across ≥ 2 independent experiments. Left shows representative FACs plot of Rag-GFP expression on D4 Tconv ($CD4^{+}CD8^{-}TCR\beta^{+}CD25^{-}Foxp3\text{-}RFP^{-}$) thymocytes, relative to non-fluorescent staining control (filled grey). Right shows quantification of $Rag\text{-}GFP^{-}$ Tconv percentages across the timecourse.

4.2.3 Possible Regulators of Neonatal Intrathymic Proliferation

Our analysis identified that within the neonatal thymus all four SP4 populations (Tconv, Treg, $CD25^{+}Foxp3^{-}$ and $CD25^{-}Foxp3^{+}$ precursors) proliferated with variable intensity, with Treg and $CD25^{+}Foxp3^{-}$ proliferating to the greatest extent. We therefore wondered what factors might drive intrathymic proliferation and if the observed variation in proliferation intensity may reflect different underpinning mechanisms.

Notably, γ_c family members have previously been connected to both thymic development and homeostasis. In particular, IL-7, IL-2 and IL-15 seemed prime candidates for potential regulators of intrathymic proliferation due to their historic association with thymocyte proliferation and/or thymic Treg development[182,184,187,188,196,335]. To determine if the four SP4 thymocyte populations might be receptive to such cytokine signalling, we looked for expression of the respective cytokine receptor within each population. The receptors for γ_c cytokines are formed from distinct combinations of subunits with CD25(IL2Rα), CD122 (IL2Rβ), and CD127 (IL7Rα), forming key components of the receptors for IL-2, IL-15 and IL-7 cytokines respectively (although it should also be noted that CD122 also forms part of the IL-2R complex). Inherently the four SP4 thymocyte subsets differentially express CD25, owing to its role as a distinguishing positive marker of both Tregs and $CD25^{+}Foxp3^{-}$ Treg precursors, and as such these two populations are likely more receptive to IL-2 signalling. Therefore, we focused on whether CD127 or CD122 were also differentially expressed across the four SP4 thymocyte populations (Figure 4.10).

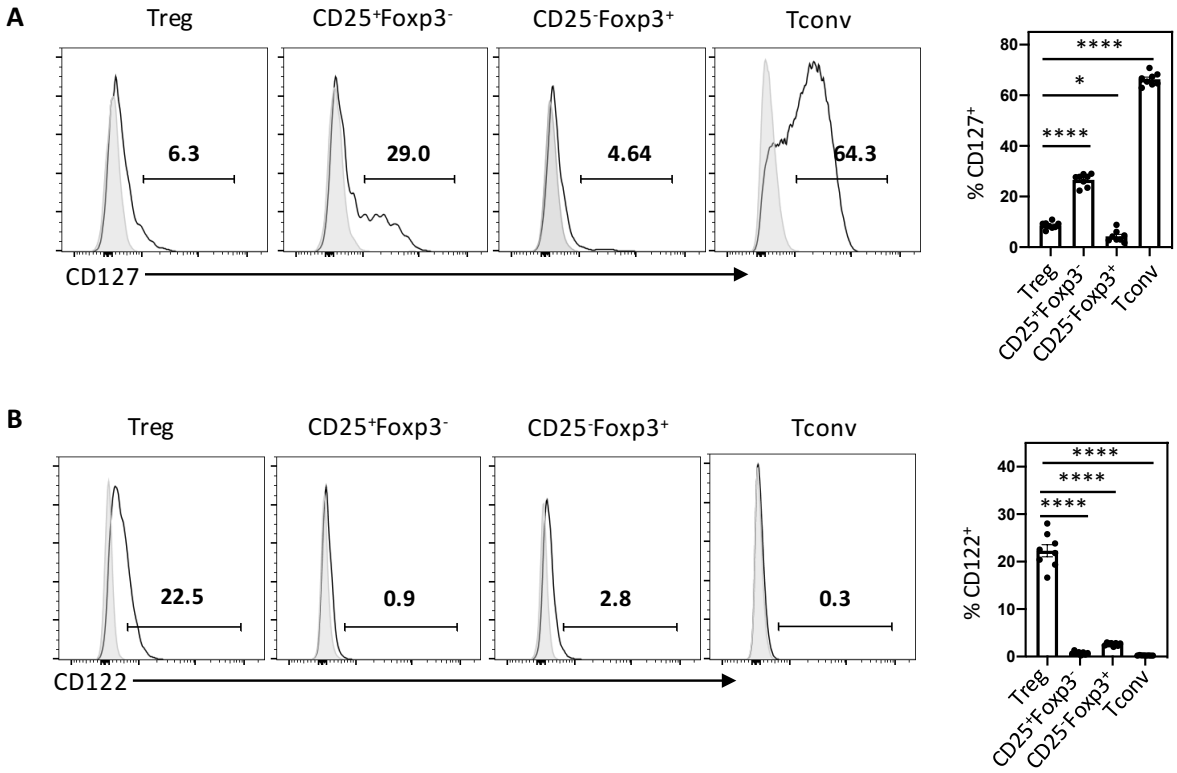
A
Treg
CD25+Foxp3-
CD25-Foxp3+
Tconv
6.3
29.0
4.64
64.3
CD127
% CD127+
****
*
****
Treg
CD25+Foxp3-
CD25-Foxp3+
Tconv
B
Treg
CD25+Foxp3-
CD25-Foxp3+
Tconv
22.5
0.9
2.8
0.3
CD122
% CD122+
****
****
****
Treg
CD25+Foxp3-
CD25-Foxp3+
Tconv

Figure 4. 10 Differential Expression of γ_c Family Members by Neonatal SP4 Thymocyte Populations

Analysis of γ_c family members **(A)** CD127 and **(B)** CD122 expression by SP4 thymocyte ($CD4^+CD8^-TCR\beta^+$) populations in D4 WT neonatal mice. Data representative of n=8 across 2 independent experiments. Expression of **(A)** CD127 and **(B)** CD122, by $CD25^+Foxp3^-$ and $CD25^-Foxp3^+$ Treg precursors, $CD25^+Foxp3^+$ Treg and $CD25^-Foxp3^-$ Tconv, as indicated, presented as representative FACs plots with trace relative to FMO control (filled grey). Bar charts quantify percentages of **(A)** $CD127^+$ and **(B)** $CD122^+$ SP4 thymocyte populations as indicated. All statistics are relative to Treg percentage and were generated using repeated measures one way anovas, where * $p<0.05$, **** $p<0.0001$.

Expression of CD127 differed across the four SP4 thymocyte populations (Figure 4.10.A). Notably, the majority of Tconv thymocytes expressed CD127, while very little CD127 expression was detected within the Treg population. Similarly, CD127 was not strongly expressed by $CD25^{-}Foxp3^{+}$ Treg precursors and while, comparatively, $CD25^{+}Foxp3^{-}$ precursors were found to contain a larger proportion of $CD127^{+}$ thymocytes this was significantly lower relative to the Tconv population. Overall this indicates that CD127 expression is primarily restricted to the Tconv thymocyte lineage, suggesting that Tconvs would be more receptive to IL-7 signalling. In contrast, we detected very little CD122 expression on any of the SP4 thymocyte populations apart from Treg, and even within this population there was only a small proportion of $CD122^{+}$ thymocytes (Figure 4.10.B). Whether this expression would drive IL-15 or IL-2 signalling is unclear owing to the overlapping role of CD122 in both cytokine receptors.

Collectively this γ_c receptor analysis suggests receptivity to different γ_c cytokines varies across the four SP4 thymocyte populations, with most notably Treg and Tconv diametrically opposing in their sensitivity to IL-2 and IL-7. To determine if these γ_c cytokines do differentially control intrathymic proliferation of different SP4 thymocyte populations we aimed to examine the impact of specific γ_c cytokines on proliferation. Due to welfare concerns surrounding the use of neonates, *in vivo* manipulation of γ_c cytokines signalling was not possible, so we aimed to establish an *in vitro* system which closely mimicked thymic proliferation in the neonate. FTOCs represent an established *in vitro* system used to investigate thymocyte development within a 3D thymic stromal structure. Here thymic lobes are isolated from embryos (approximately E17) and placed whole in culture. The thymocyte precursors present within the embryonic thymic lobes then undergo development, akin to *in vivo*, and ultimately give rise to mature T-

cell populations including SP4 thymocytes. Therefore, we utilised FTOC to investigate the proliferation of the developing SP4 thymocytes. However firstly, we needed to characterise the culture period required for the development of all SP4 thymocyte populations (Figure 4.11) and whether there was any evidence of intrathymic proliferation under FTOC conditions (Figure 4.12).

Initially we characterised the proportions of different thymocyte populations present within FTOC harvested at day 4 (D4) and day 7 (D7) and compared these observations to the phenotype of a D4 neonate (Figure 4.11). By D4 of culture, bulk thymocyte development within FTOC appeared similar to the D4 neonate, in particular the proportion of SP4 thymocytes. However, by D7 thymocyte development within FTOC appeared more skewed towards mature differentiated thymocytes, as evidenced by a decreased proportion of DP thymocytes and corresponding increase in SP4 and SP8 thymocytes (Figure 4.11.A). Within the SP4 compartment, Tconv, $CD25^{+}Foxp3^{-}$ and $CD25^{-}Foxp3^{+}$ Treg precursors and Treg could all be identified within FTOC at both D4 and D7 of culture (Figure 4.11.B). Culture D4 appeared to coincide with the emergence of the Treg population as the proportion of Treg observed was lower than in D4 neonates. In contrast by D7 the proportion of Treg was far larger than observed in the neonate, possibly reflective of an accumulation of mature differentiated Treg that could not undergo emigration from isolated thymus lobes. Overall this suggests that at D4 of culture, FTOC thymocyte development appears to be more actively ongoing and reflective of the *in vivo* D4 neonate, whereas by D7 of culture the thymocyte population contains an accumulating fraction of mature thymocytes.

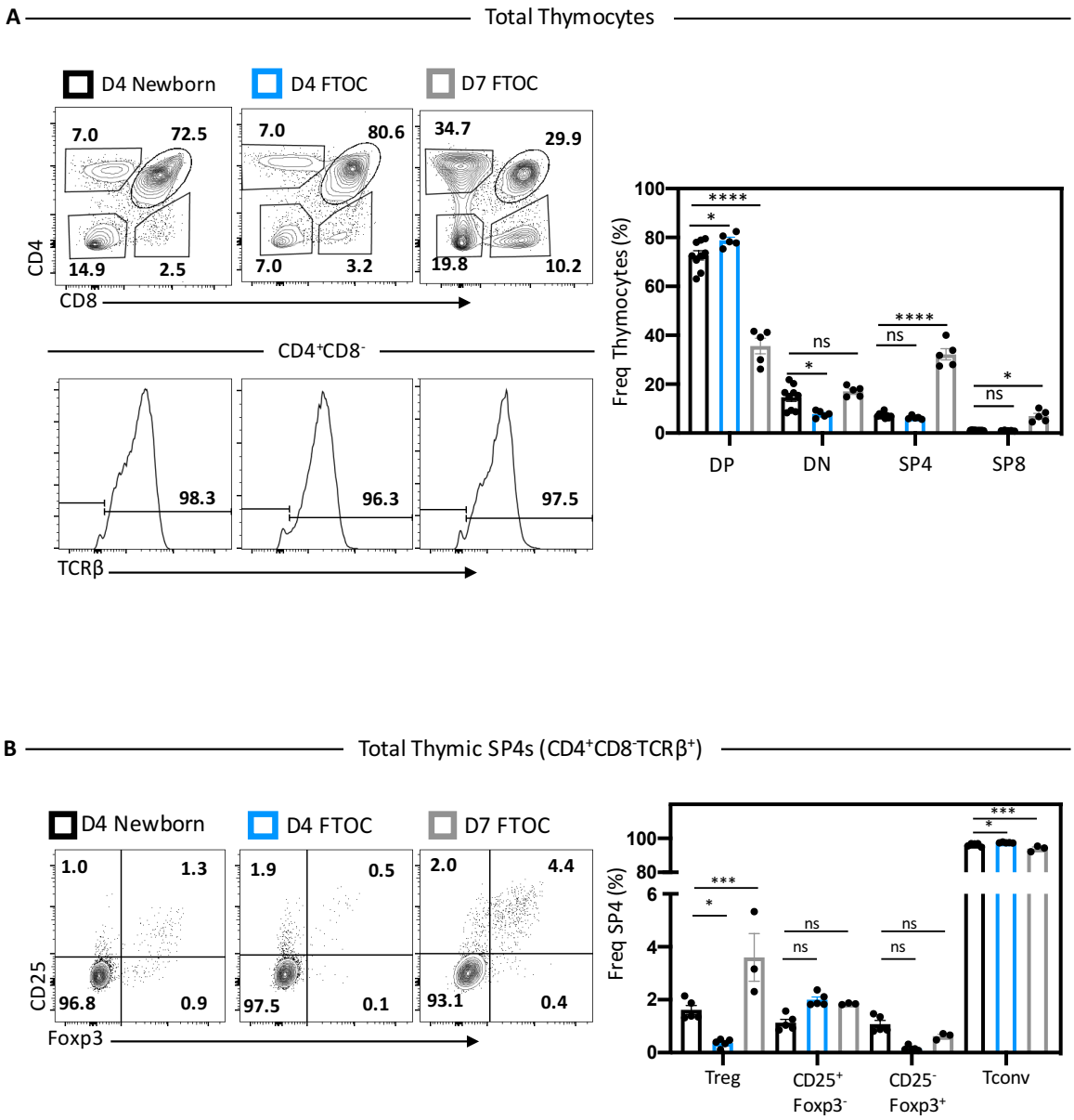
A
Total Thymocytes
D4 Newborn
D4 FTOC
D7 FTOC
7.0
72.5
14.9
2.5
7.0
80.6
7.0
3.2
34.7
29.9
19.8
10.2
CD4
CD8
CD4+CD8-
98.3
96.3
97.5
TCRβ
Freq Thymocytes (%)
DP
DN
SP4
SP8
B
Total Thymic SP4s (CD4+CD8-TCRβ+)
D4 Newborn
D4 FTOC
D7 FTOC
1.0
1.3
96.8
0.9
1.9
0.5
97.5
0.1
2.0
4.4
93.1
0.4
CD25
Foxp3
Freq SP4 (%)
Treg
CD25+ Foxp3-
CD25- Foxp3+
Tconv

Figure 4. 11 FTOCs as a System to Investigate Intrathymic Proliferation: Evidence of Ongoing Thymic Treg Development

Comparison of thymocyte development in D4 neonates (black), D4 FTOC (blue) and D7 FTOC (grey). Data representative of n ≥ 5 across ≥ 2 independent experiments. All statistics are relative to the D4 neonate group and were generated using ordinary one way anovas, where ns $p>0.05$, * $p<0.05$,** $p\leq0.01$, *** $p\leq0.001$, **** $p\leq0.0001$

(A) Comparison of the frequency of thymocyte populations: DN ($CD4^-CD8^-$), DP ($CD4^+CD8^+$), SP4 ($CD4^+CD8^-TCR\beta^+$) and SP8 ($CD4^-CD8^+TCR\beta^+$). Top left shows representative FACs plots of CD4/CD8 profile of total thymocytes for each condition. Bottom left shows representative FACs plots of TCRβ expression within the $CD4^+CD8^-$ thymocyte population. The graph on the right quantifies the percentages of the four thymocyte populations.

(B) Comparison of the frequency of SP4 thymocyte ($CD4^+CD8^-TCR\beta^+$) populations: $CD25^+Foxp3^+$ Treg, $CD25^+Foxp3^-$ and $CD25^-Foxp3^+$ Treg precursors, and $CD25^-Foxp3^-$ Tconv. Left shows representative FACs plots of CD25/Foxp3 profile for each condition. The graph on the right quantifies the percentages of the four SP4 thymocyte populations.

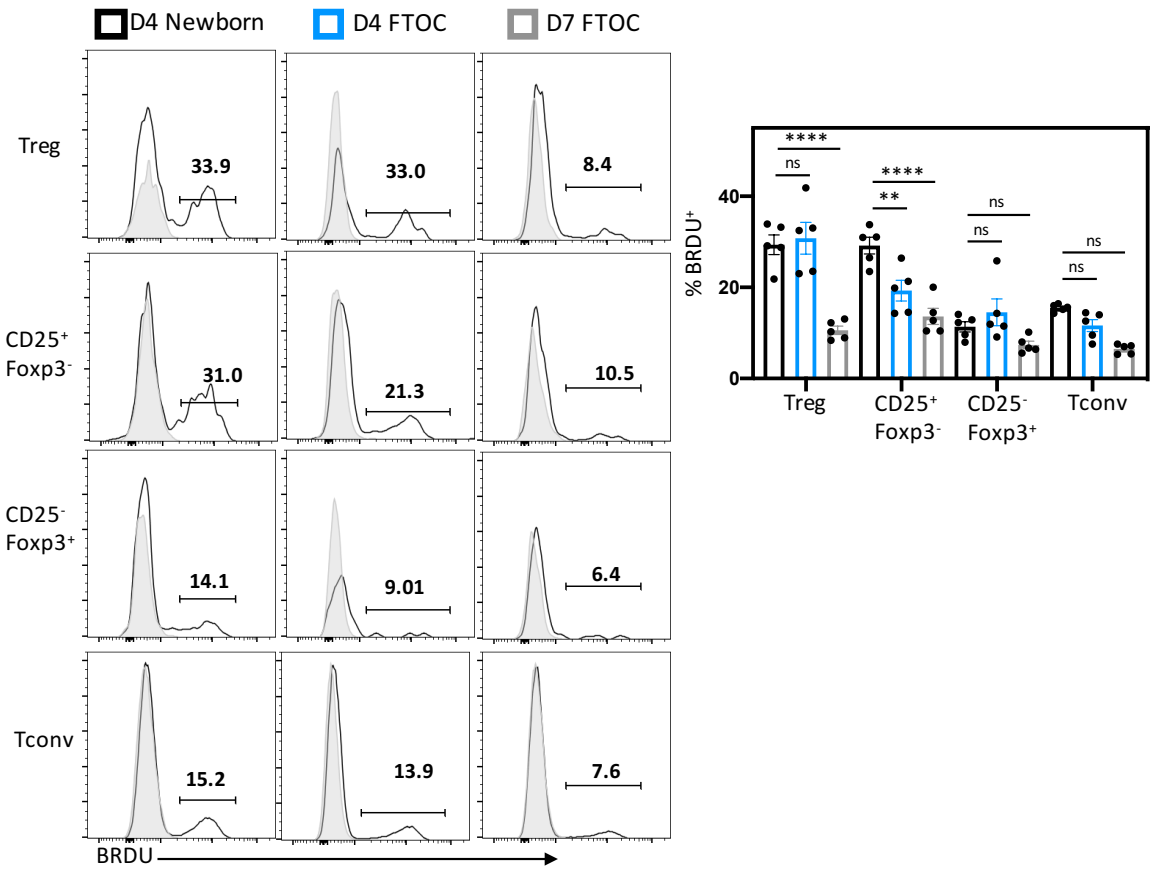
A
Total Thymic SP4s (CD4+CD8-TCRβ+)
D4 Newborn
D4 FTOC
D7 FTOC
Treg
CD25+ Foxp3-
CD25- Foxp3+
Tconv
33.9
33.0
8.4
31.0
21.3
10.5
14.1
9.01
6.4
15.2
13.9
7.6
BRDU
% BRDU+
****
ns
**
Treg
CD25+ Foxp3-
CD25- Foxp3+
Tconv

Figure 4. 12 FTOCs as a System to Investigate Intrathymic Proliferation: Evidence of Active Thymocyte Proliferation

(A) Comparison of frequency of BRDU incorporation by SP4 thymocyte ($CD4^+CD8^-TCR\beta^+$) populations: $CD25^+Foxp3^+$ Treg, $CD25^+Foxp3^-$ and $CD25^-Foxp3^+$ Treg precursors, and $CD25^-Foxp3^-$ Tconv in D4 neonates (black), D4 FTOC (blue) and D7 FTOC (grey). Data representative of n ≥ 5 across ≥ 2 independent experiments. Data presented as representative FACS plots and percentages are quantified as bar charts. FACS plots show BRDU incorporation relative to a without BRDU control (filled grey). All statistics were generated using ordinary one way anovas, ns $p>0.05$, * $p<0.05$,** $p<0.01$, **** $p<0.0001$

Following characterisation of broad SP4 thymocyte development in the FTOC system we examined intrathymic proliferation of the SP4 thymocyte subsets akin to our observations from the D4 neonate. BRDU incorporation was used to assess proliferation of SP4 thymocytes in D4 and D7 FTOCs, and again this was compared to BRDU incorporation observed in D4 neonates (Figure 4.12). BRDU incorporation by all four thymocyte populations in D4 FTOCs was relatively comparable to the level observed in D4 neonates, with high incorporation by Tregs and $CD25^{+}Foxp3^{-}$ Treg precursors and lower BRDU incorporation by $CD25^{-}Foxp3^{+}$ Treg precursors and Tconvs. In contrast BRDU incorporation by all four thymocyte populations was reduced in D7 FTOCs, with far lower levels of incorporation by Tregs and $CD25^{+}Foxp3^{-}$ Treg precursors in particular. This reduced BRDU incorporation by D7 of organ culture possibly reflects the accumulation of mature thymocytes (identified in Figure 4.11) which are no longer proliferating and likely would have egressed *in vivo*.

Combined, our initial characterisation of SP4 development and proliferation identified that D4 FTOC represent a viable *in vitro* system to investigate the impact of disruption to γ_c cytokine signalling on SP4 thymocyte proliferation. Therefore, we aimed to identify regulators of thymic Treg proliferation by disrupting the signalling of IL-2 (Figure 4.13) and IL-15 (Figure 4.14) through use of blocking antibodies with FTOCs (detailed in Section 2.9.3).

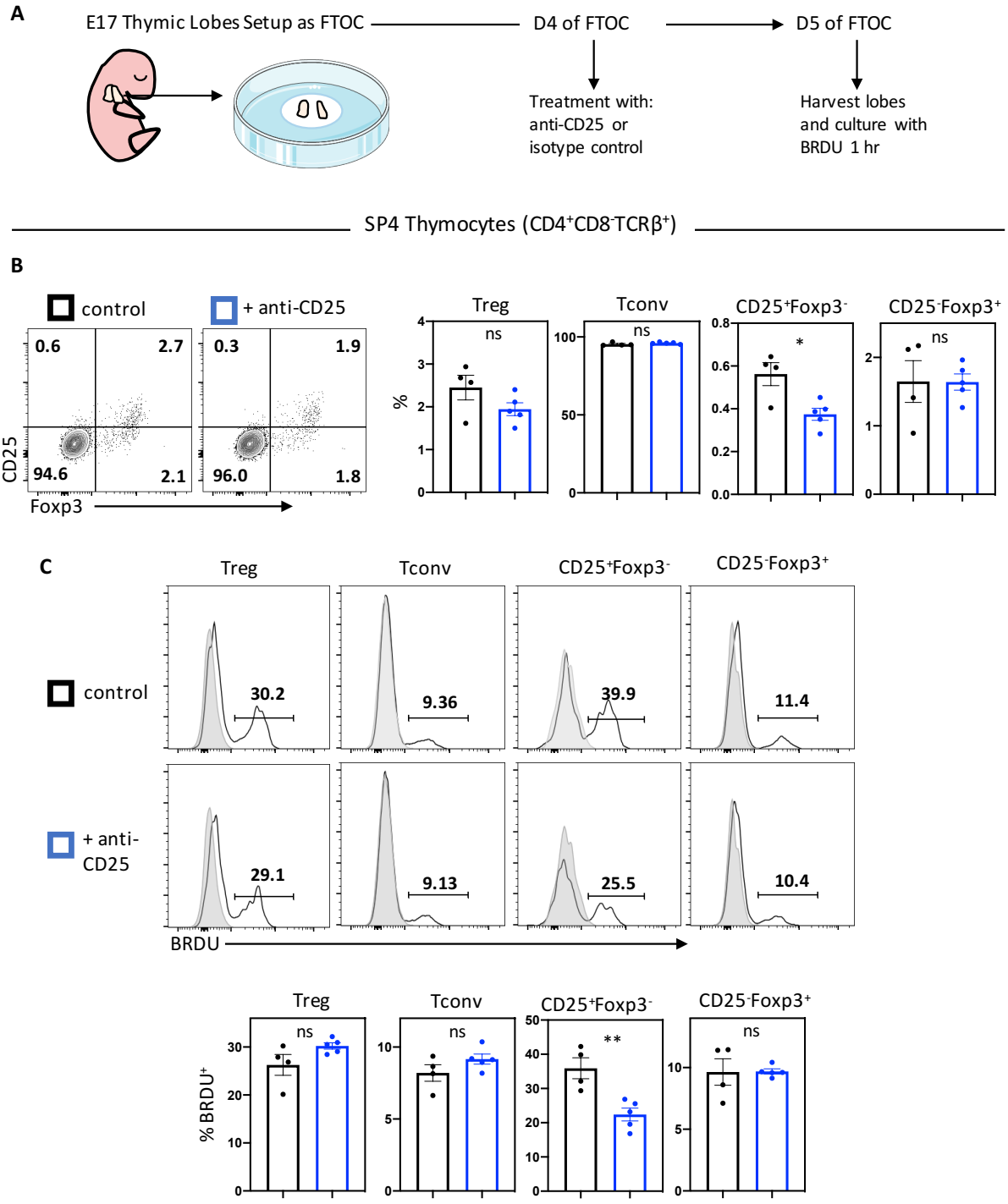
A
E17 Thymic Lobes Setup as FTOC
D4 of FTOC
D5 of FTOC
Treatment with: anti-CD25 or isotype control
Harvest lobes and culture with BRDU 1 hr
SP4 Thymocytes (CD4+CD8-TCRβ+)
B
control
+ anti-CD25
0.6
2.7
94.6
2.1
0.3
1.9
96.0
1.8
CD25
Foxp3
Treg
Tconv
CD25+Foxp3-
CD25-Foxp3+
%
ns
*
C
control
+ anti-CD25
30.2
9.36
39.9
11.4
29.1
9.13
25.5
10.4
BRDU
% BRDU+
**

Figure 4. 13 Specific Disruption of $CD25^{+}Foxp3^{-}$ Treg Precursor Proliferation within Anti-CD25 Treated FTOCs

(A) Schematic of FTOC combined with BRDU labelling as an *in vitro* approach to investigate intrathymic proliferation of SP4 thymocytes. E17 embryonic lobes are dissected and cultured as FTOCs. On day 4 (D4) FTOCs are then treated with either anti-CD25 or an isotype control for 24 hours. On day 5 (D5) lobes are harvested and reduced to a single cell suspension and incubated with BRDU for 1 hour.
(B-C) Comparison of thymocyte development and proliferation in D5 FTOC treated with either anti-CD25 (blue) or an isotype control (black). Analysis of **(B)** total frequency and **(C)** frequency of BRDU incorporation by SP4 ($CD4^{+}CD8^{-}TCR\beta^{+}$) thymocyte populations: $CD25^{+}Foxp3^{+}$ Treg, $CD25^{+}Foxp3^{-}$ and $CD25^{-}Foxp3^{+}$ Treg precursors, and $CD25^{-}Foxp3^{-}$ Tconv. **(B)** Data presented as representative FACs plots of CD25/Foxp3 profile for each condition with accompanying graph quantifying the percentages of the four SP4 thymocyte populations. **(C)** Data presented as representative FACs plots of BRDU incorporation by each SP4 population across the two conditions relative to a without BRDU control (filled grey). The accompanying bar chart quantifies the percentage of $BRDU^{+}$ thymocytes. All statistical analysis performed using a student's t-test, where ns $p>0.05$, * $p<0.05$,** $p\leq0.01$. Data presented for all conditions is representative of n=4 (isotype control) and n=5 (anti-CD25) across 2 independent experiments.

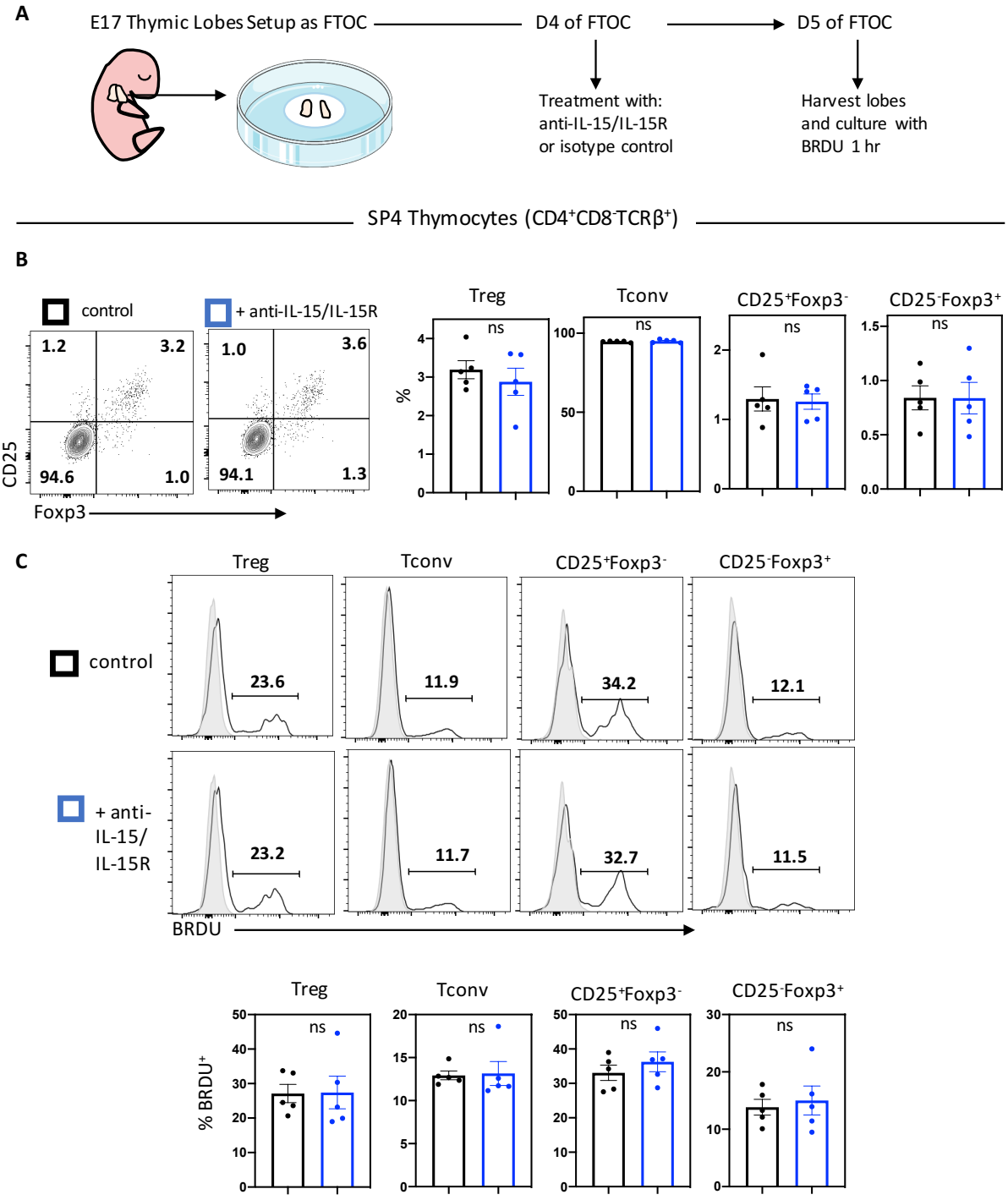
A
E17 Thymic Lobes Setup as FTOC
D4 of FTOC
D5 of FTOC
Treatment with:
anti-IL-15/IL-15R
or isotype control
Harvest lobes
and culture with
BRDU 1 hr
SP4 Thymocytes (CD4+CD8-TCRβ+)
B
control
+ anti-IL-15/IL-15R
1.2
3.2
94.6
1.0
1.0
3.6
94.1
1.3
CD25
Foxp3
Treg
Tconv
CD25+Foxp3-
CD25-Foxp3+
%
ns
C
control
+ anti-IL-15/IL-15R
23.6
11.9
34.2
12.1
23.2
11.7
32.7
11.5
BRDU
% BRDU+

Figure 4. 14 SP4 Thymocyte Proliferation Appears Normal within Anti-IL15/IL-15R Treated FTOCs

(A) Schematic of FTOC combined with BRDU labelling as an *in vitro* approach to investigate intrathymic proliferation of SP4 thymocytes. E17 embryonic lobes are dissected and cultured as FTOCs. On day 4 (D4) FTOCs are then treated with either anti-IL15/IL15R or an isotype control for 24 hours. On day 5 (D5) lobes are harvested and reduced to a single cell suspension and incubated with BRDU for 1 hour.
(B-C) Comparison of thymocyte development and proliferation in D5 FTOC treated with either anti-IL15/IL15R (blue) or an isotype control (black). Analysis of **(B)** total frequency and **(C)** frequency of BRDU incorporation by SP4 ($CD4^+CD8^-TCR\beta^+$) thymocyte populations: $CD25^+Foxp3^+$ Treg, $CD25^+Foxp3^-$ and $CD25^-Foxp3^+$ Treg precursors, and $CD25^-Foxp3^-$ Tconv. **(B)** Data presented as representative FACs plots of CD25/Foxp3 profile for each condition with accompanying graph quantifying the percentages of the four SP4 thymocyte populations. **(C)** Data presented as representative FACs plots of BRDU incorporation by each SP4 population across the two conditions relative to a without BRDU control (filled grey). The accompanying bar chart quantifies the percentage of $BRDU^+$ thymocytes. All statistical analysis performed using a students t-test, where ns $p>0.05$.
Data presented for all conditions is representative of n=5 (isotype control) and n=5 (anti-CD25) across 2 independent experiments.

Regarding the impact of anti-CD25 treatment on the SP4 thymocyte populations, we observed a reduction in the proportion of $CD25^{+}Foxp3^{-}$ Treg precursors (relative to isotype treated controls), but not Tconv, $CD25^{-}Foxp3^{+}$ Treg precursors or Tregs following treatment (Figure 4.13.B). Similarly, with regard to BRDU incorporation, anti-CD25 treatment resulted in a reduction of $BRDU^{+}$ cells within the $CD25^{-}Foxp3^{+}$ Treg precursor population only (Figure 4.13.C). Overall identifying that IL-2 blockade specifically reduces the $CD25^{-}Foxp3^{+}$ Treg precursor population possibly due, at least partially, to reduced proliferation within this population.

In contrast following anti-IL-15/IL-15R treatment we observed very little difference between the treated and control samples with regard to the overall proportions of the SP4 thymocyte populations, or the proportion of $BRDU^{+}$ cells within them (Figure 4.14.B-C). Suggesting IL-15 blockade alone has little impact on the intrathymic proliferation of any of the SP4 thymocyte subsets. Overall the impact of blockading IL-2 or IL-15 signalling individually appeared limited, and notably showed no significant effect on Treg proliferation.

In addition to cytokine signalling another important signal in both thymocyte development and T-cell proliferation is TCR signalling. We therefore wondered if factors tied to TCR signalling may also modulate neonatal intrathymic proliferation. Furthermore Aire has been identified as a key regulator of neonatal Treg development specifically [232,233], which is also suggested by our observations, of reduced numbers of Tregs (and $CD25^{-}Foxp3^{+}$ precursors), but not Tconvs in D7 *Aire*$^{-/-}$ neonates (Figure 3.20). Therefore, we wondered if Aire might act to regulate neonatal Treg development, at least partially, through promotion of intrathymic proliferation via TCR signalling.

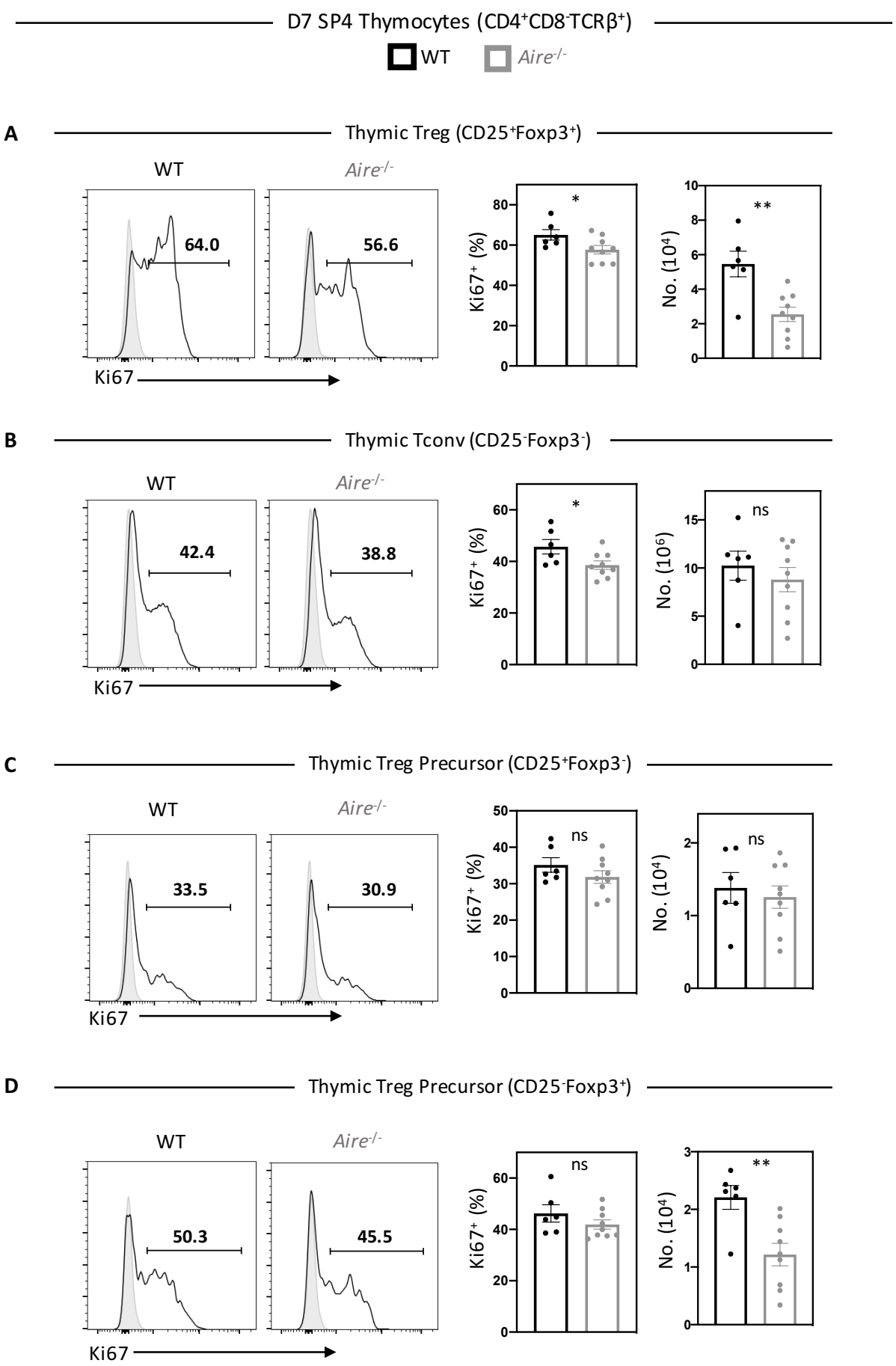
D7 SP4 Thymocytes (CD4+CD8-TCRβ+)
WT
Aire-/-
A
Thymic Treg (CD25+Foxp3+)
WT
Aire-/-
64.0
56.6
Ki67
Ki67+ (%)
No. (10⁴)
*
**
B
Thymic Tconv (CD25-Foxp3-)
42.4
38.8
No. (10⁶)
ns
C
Thymic Treg Precursor (CD25+Foxp3-)
33.5
30.9
D
Thymic Treg Precursor (CD25-Foxp3+)
50.3
45.5

Figure 4. 15 Loss of Aire has Only a Minor Impact on Intrathymic Proliferation of Thymocytes within the Treg Lineage

Comparison of Ki67 expression by SP4 ($CD4^+CD8^-TCR\beta^+$) thymocyte populations: **(A)** $CD25^+Foxp3^+$ Treg **(B)** $CD25^-Foxp3^-$ Tconv **(C)** $CD25^+Foxp3^-$ and **(D)** $CD25^-Foxp3^+$ Treg precursors in D7 *Aire*$^{-/-}$ (grey) and WT (black) littermate control neonates. Data representative of n=9 for *Aire*$^{-/-}$ and n=6 for WT across 4 independent experiments. Data presented as representative FACs plots of Ki67 expression by the indicated SP4 thymocyte population, relative to isotype control (filled grey), from WT or *Aire*$^{-/-}$ neonates. Graphs on the right quantify the percentages and numbers of $Ki67^+$ cells within the indicated SP4 population across the two conditions. All statistics were generated using unpaired student's t- tests, where * $p<0.05$, ** $p<0.01$.

To investigate whether the reduced thymic Treg population in *Aire*$^{-/-}$ neonates was a consequence of altered intrathymic proliferation, we analysed Ki67 expression by SP4 thymocyte populations in D7 *Aire*$^{-/-}$ compared to WT littermate controls (Figure 4.15). This comparison identified that both the proportion and number of Ki67^{+} Tregs were slightly reduced in the *Aire*$^{-/-}$. Similarly, while there was a slight reduction in the proportion of Ki67^{+} Tconvs, this did not translate to a numerical difference. In contrast, the proportion of Ki67^{+} CD25^{+}Foxp3^{-} and CD25^{-}Foxp3^{+} Treg precursors appeared normal although the number of Ki67^{+} CD25^{-}Foxp3^{+} was reduced. Overall there appears to be little difference in Ki67 expression between WT and *Aire*$^{-/-}$ neonates. The most notable difference was the numerical reduction of Ki67^{+} Tregs and CD25^{-}Foxp3^{+} precursors, however the lack of a large proportional reduction in Ki67^{+} thymocytes within these populations suggests this numerical reduction is likely a consequence, rather than causative, of the observed reduction in their total population sizes (Figure 3.20). Taken together, these observations suggest that Aire has little influence in the intrathymic proliferation of any of the SP4 thymocyte subsets.

Similar to TCR signalling, co-stimulation is another signalling pathway that may be a likely candidate in the modulator of proliferation. Ox40 in particular has been identified as a modulator of both thymic Treg development and proliferation [336]. Therefore we wondered whether Ox40 may specifically drive thymic Treg proliferation in the neonate. To investigate this, we examined SP4 thymocytes in D7 *Tnfrsf4*$^{-/-}$ neonates, compared to age matched WT controls (Figure 4.16-17). Our initial characterisation of general thymocyte development determined that total thymic cellularity and the bulk SP4 thymocyte population were comparable between WT and *Tnfrsf4*$^{-/-}$ neonates (Figure 4.16.A-B). However, within the SP4

thymocyte population we identified a reduction in the proportion and numbers of Tregs and $CD25^{-}Foxp^{+}$ precursors but not Tconvs or $CD25^{+}Foxp3^{-}$ precursors (Figure 4.16.C).

To examine if the reduced Treg/$CD25^{+}Foxp3^{-}$ precursor populations were linked to impaired intrathymic proliferation, we analysed Ki67 expression within SP4 thymocyte populations in D7 *Tnfrsf4*$^{-/-}$ neonates compared to controls. This analysis identified a reduction in the frequency and number of $Ki67^{+}$ Tregs and both $CD25^{+}Foxp3^{-}$ and $CD25^{-}Foxp3^{+}$ precursors (Figure 4.17.A,C,D), suggesting that the reduced Treg and $CD25^{-}Foxp3^{+}$ precursor population sizes may partly result from reduced intrathymic proliferation. However, given the relatively small reduction in $Ki67^{+}$ Treg/ $CD25^{-}Foxp3^{+}$ thymocytes, impaired intrathymic proliferation seems unlikely to be the underlying reason for the reduced population sizes. Furthermore, this reduction in $Ki67^{+}$ thymocytes was not restricted to the Treg lineage as the frequency and number of $Ki67^{+}$ Tconv was also reduced (Figure 4.17.B). Therefore, it seems that Ox40 signalling contributes in a non-specific manner to the intrathymic proliferation of all SP4 thymocyte populations. However, the observed decrease in Ki67 within all of the SP4 thymocyte populations was relatively small suggesting either Ox40 is not an essential mediator of intrathymic proliferation, or redundancy exists between Ox40 and other co-stimulatory pathways.

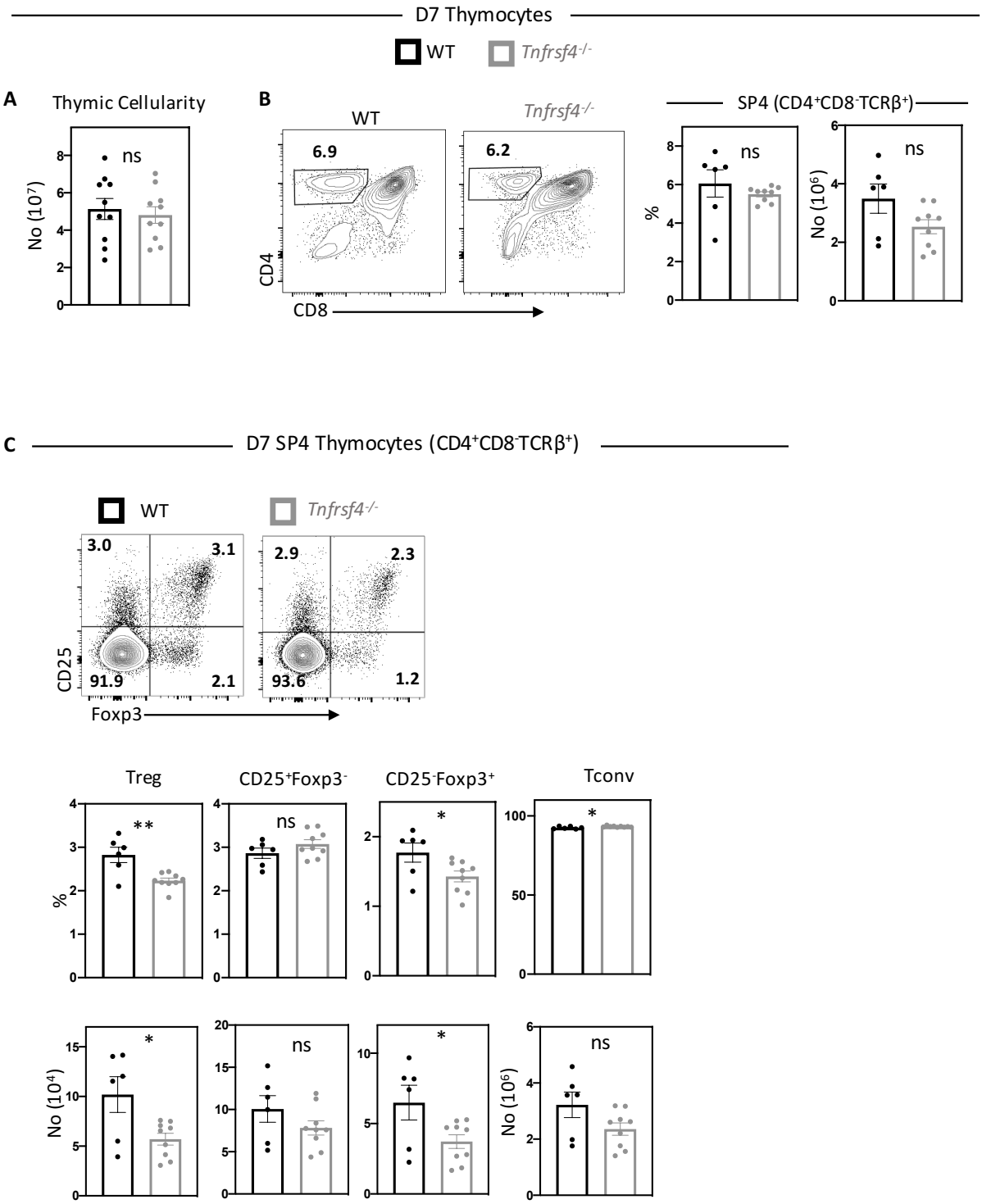
D7 Thymocytes
WT
Tnfrsf4-/-
A
Thymic Cellularity
No (10^7)
ns
B
WT
Tnfrsf4-/-
6.9
6.2
CD4
CD8
SP4 (CD4+CD8-TCRβ+)
%
No (10^6)
ns
C
D7 SP4 Thymocytes (CD4+CD8-TCRβ+)
WT
Tnfrsf4-/-
3.0
3.1
2.9
2.3
91.9
2.1
93.6
1.2
CD25
Foxp3
Treg
CD25+Foxp3-
CD25-Foxp3+
Tconv
%
**
ns
*
*
No (10^4)
No (10^6)

Figure 4. 16 Slight Impairment of Thymic Treg Development in D7 *Tnfrsf4*$^{-/-}$ Neonates

Comparison of thymic phenotype in D7 *Tnfrsf4*$^{-/-}$ (grey) and WT (black) neonates. Data representative of n=9 across 2 independent experiments for *Tnfrsf4*$^{-/-}$ and n=6 across 2 independent experiments for WT. All statistics were generated using unpaired student's t-tests, where ns $p>0.05$, * $p<0.05$,** $p\leq0.01$.

(A) Comparison of total thymic cellularity between *Tnfrsf4*$^{-/-}$ and WT depicted as graphical quantification of numbers.

(B) Comparison of SP4 (CD4^{+}CD8^{-}TCRβ^{+}) thymocyte population. Left shows representative FACs plots of CD4/CD8 profile of thymocytes for *Tnfrsf4*$^{-/-}$ and WT neonates as indicated. The graphs on the right quantifies the percentages and numbers of SP4 thymocytes across the two conditions as indicated.

(C) Comparison of the frequency of SP4 thymocyte (CD4^{+}CD8^{-}TCRβ^{+}) populations: CD25^{+}Foxp3^{+} Treg, CD25^{+}Foxp3^{-} and CD25^{-}Foxp3^{+} Treg precursors, and CD25^{-}Foxp3^{-} Tconv in for *Tnfrsf4*$^{-/-}$ and WT neonates as indicated. Top shows representative FACs plots of CD25/Foxp3 profile for each condition. Bottom graphs quantify the percentages and numbers of the four SP4 thymocyte populations as indicated.

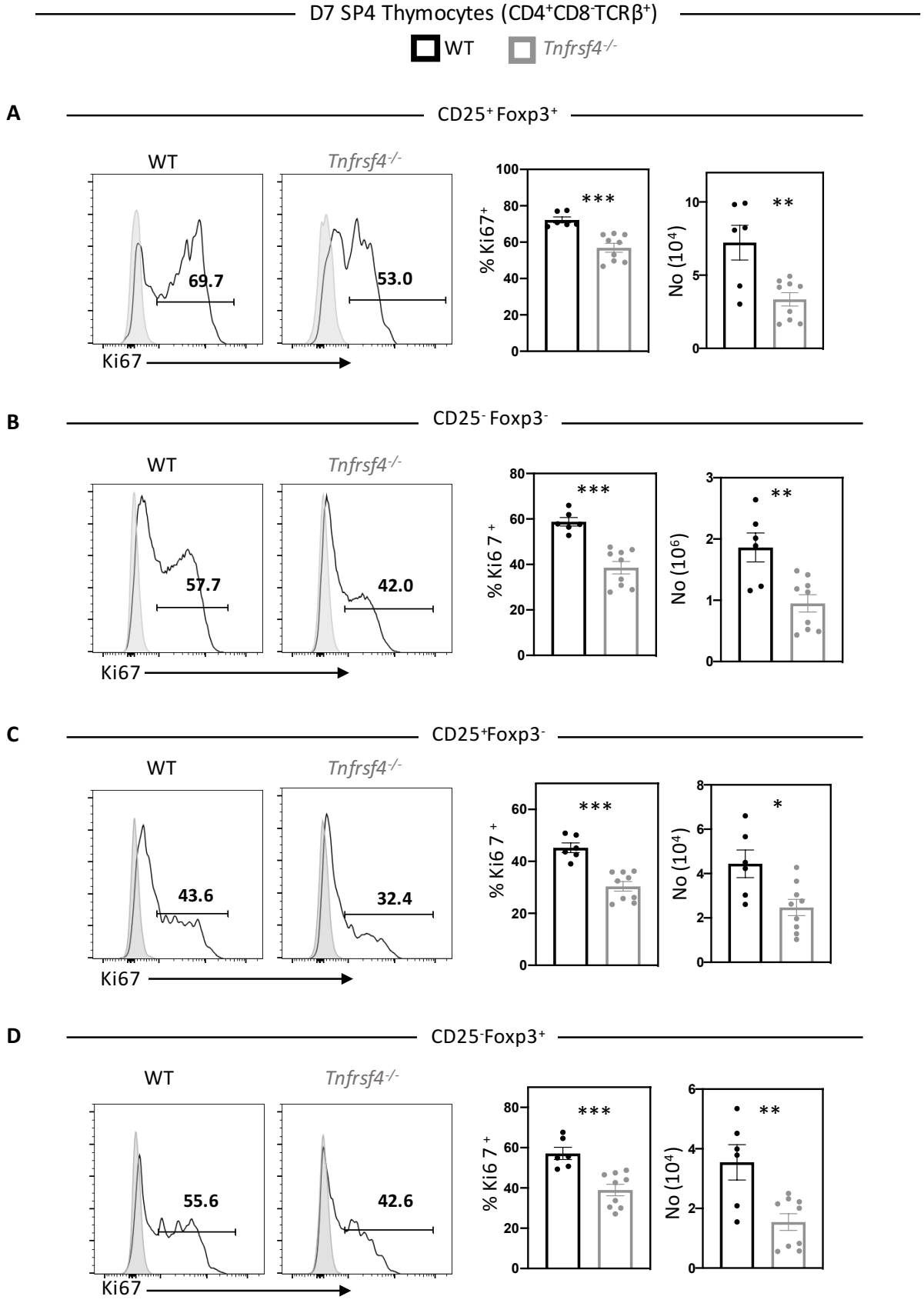
D7 SP4 Thymocytes (CD4+CD8-TCRβ+)
WT
Tnfrsf4-/-
A
CD25+ Foxp3+
WT
Tnfrsf4-/-
69.7
53.0
Ki67
% Ki67+
No (10⁴)
***
**
B
CD25- Foxp3-
57.7
42.0
% Ki6 7 +
No (10⁶)
C
CD25+Foxp3-
43.6
32.4
*
D
CD25-Foxp3+
55.6
42.6

Figure 4. 17 Proliferation of SP4 Thymocyte Populations is Reduced in D7 *Tnfrsf4*$^{-/-}$ Neonates

Comparison of Ki67 expression by SP4 ($CD4^{+}CD8^{-}TCR\beta^{+}$) thymocyte populations: **(A)** $CD25^{+}Foxp3^{+}$ Treg **(B)** $CD25^{-}Foxp3^{-}$ Tconv **(C)** $CD25^{+}Foxp3^{-}$ and **(D)** $CD25^{-}Foxp3^{+}$ Treg precursors, in D7 *Tnfrsf4*$^{-/-}$ (grey) and WT (black) neonates. Data representative of n=9 across 2 independent experiments for *Tnfrsf4*$^{-/-}$ and n=6 across 2 independent experiments for WT. Data presented as representative FACs plots of Ki67 expression by the indicated SP4 thymocyte population, relative to isotype control (filled grey), from WT or *Tnfrsf4*$^{-/-}$ neonates. Graphs on the right quantify the percentages and numbers of $Ki67^{+}$ cells within the indicated SP4 population across the two conditions. All statistics were generated using unpaired student's t- tests, where * $p<0.05$, ** $p\leq0.01$, *** $p\leq0.001$.

4.2.4 Changes to Intrathymic Proliferation with Age

Thus far, we had identified and focused on the extensive proliferation of thymic SP4 populations, particularly thymic Treg, within the neonatal thymus. As this analysis hinted that proliferation decreased in older neonates (Figure 4.4), we examined Treg proliferation in the thymus across the life course. Here, we analysed the Ki67 expression of Treg, Tconv and $CD25^{+}Foxp3^{-}$ and $CD25^{-}Foxp3^{+}$ precursors across an ontogeny series in WT mice (Figure 4.18). This analysis identified a general decline in the proportion of $Ki67^{+}$ thymocytes with age within all four SP4 populations, with the peak proportion of $Ki67^{+}$ observed within the first week of life and the lowest proportion observed in mature adults (8-12 weeks). However, the extent of the reduction varied. The decrease of $Ki67^{+}$ thymocytes was particularly steep within the Treg and the $CD25^{-}Foxp3^{+}$ precursor populations (although it should be noted that comparative BRDU and Ki67 analysis from Figure 4.7, suggests Ki67 may over represent the number of actively proliferating $CD25^{-}Foxp3^{+}$ thymocytes in the neonate), whereas by comparison decreases within Tconv and $CD25^{+}Foxp3^{-}$ thymocytes appeared relatively modest.

The decline of $Ki67^{+}$ thymocytes within all the SP4 populations suggests that with age there is a general reduction in intrathymic proliferation which is particularly notably within the thymic Treg population. However, there are limitations to this interpretation because this analysis was performed in WT mice meaning that *de novo* and mature Treg are not distinguishable. Given that the mature thymic Treg population is known to increase with age, one possibility was that the decrease in the proportion of $Ki67^{+}$ thymic Treg was a consequence of recirculating mature Treg increasingly masking the proliferation of the *de novo* Treg population with age. Therefore, we sought to assess the Ki67 expression of *de novo* thymic Tregs in adults specifically. However, unlike in our neonatal analysis (Figure 4.4), we could not

achieve clear Ki67 staining while retaining Rag-GFP in the adult. Therefore, we isolated Rag-GFP$^+$ thymocytes then performed Ki67 staining without Rag-GFP retention (Figure 4.19). Analysis of Ki67 expression by Treg, Tconv and CD25$^+$Foxp3$^-$ and CD25$^-$Foxp3$^+$ precursors within the sorted SP4 thymocytes were largely in keeping with the findings of the WT Ki67 timecourse (Figure 4.18). Relative to the neonate, the proportion of Ki67$^+$ cells observed was lower across all four populations, with Tregs containing the lowest proportion. Suggesting intrathymic proliferation of *de novo* thymocytes, particularly Tregs, decreases with age.

One possible reason for this age-related change could be an intrinsic difference in Treg receptivity to proliferative signals between the adult and neonate. Therefore, we examined expression of γ_c receptor expression in adult thymic Tregs. Firstly, we compared CD25 expression on Treg from WT D4 neonates and adults. While we identified Treg were present at a similar proportion we noted within this population the level of CD25 appeared lower on adult Treg (Figure 4.20.A). To better quantify this reduction, we compared the MFI of CD25 on D4 and adult Treg and again found adults to have a lower level (Figure 4.20.B). Interestingly this reduction in CD25 MFI was not observed between D4 and adult CD25$^+$Foxp3$^-$ precursors. Overall this suggested that neonatal Treg specifically express more CD25. However, this analysis was performed in WT mice, meaning that mature thymic Treg are a confounding factor in the adult and may account for the lower level of CD25 observed. To address this possibility, we compared CD25 expression of Rag-GFP$^+$ and Rag-GFP$^-$ Treg in Foxp3-RFPxRag-GFP adults. Identifying that, the MFI of Rag-GFP$^-$ mature Treg was significantly lower than Rag-GFP$^+$ *de novo* Treg (Figure 4.20.C). However, when we then compared the CD25 MFI of Rag-GFP$^+$ adult Treg to total Treg from D4 Foxp3-RFPxRag-GFP neonates we still observed a significant reduction in the adult (Figure 4.20.D).

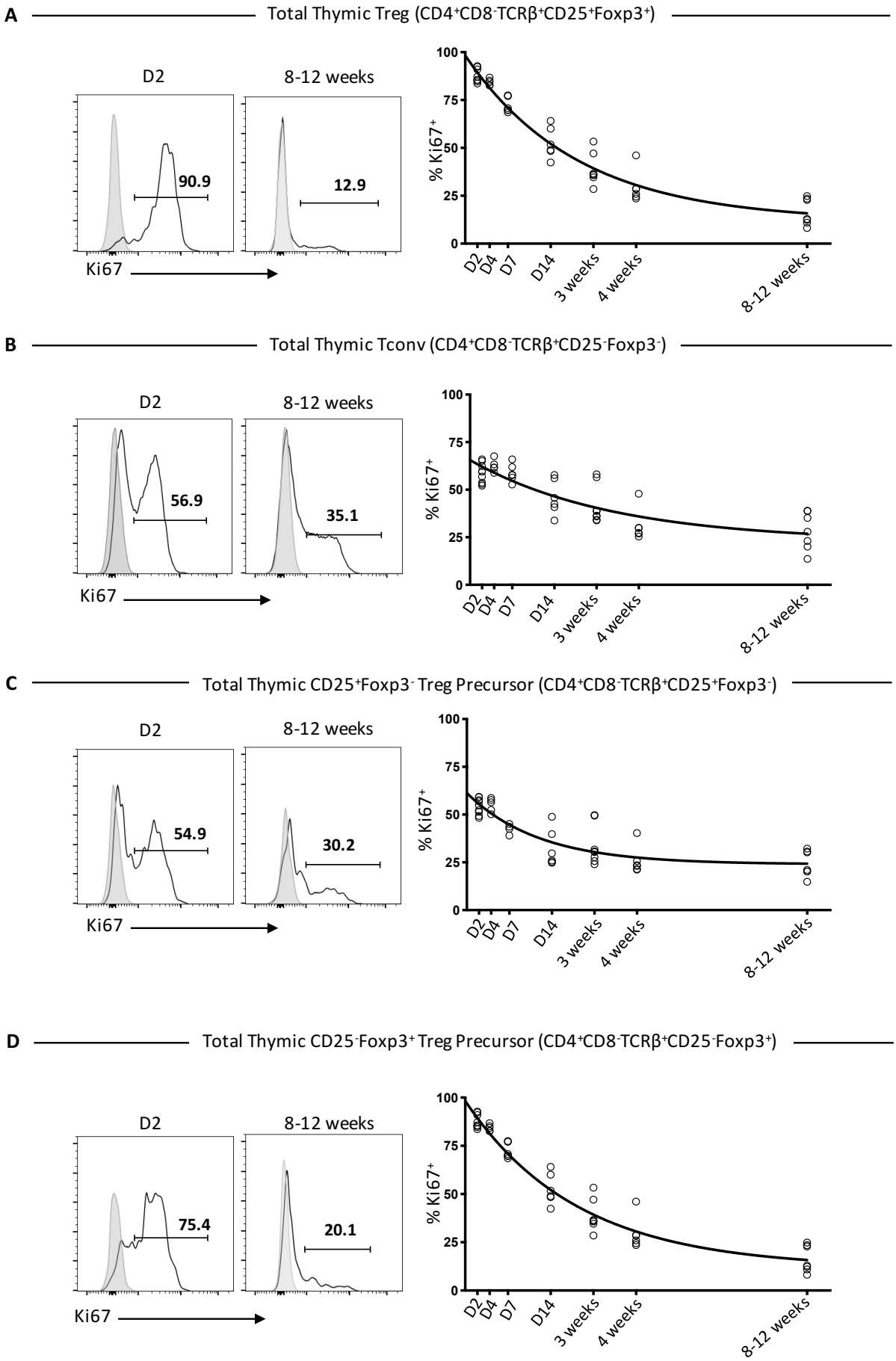
A
Total Thymic Treg (CD4+CD8-TCRβ+CD25+Foxp3+)
D2
8-12 weeks
90.9
12.9
Ki67
% Ki67+
100
75
50
25
0
D2
D4
D7
D14
3 weeks
4 weeks
8-12 weeks
B
Total Thymic Tconv (CD4+CD8-TCRβ+CD25-Foxp3-)
D2
8-12 weeks
56.9
35.1
Ki67
% Ki67+
C
Total Thymic CD25+Foxp3- Treg Precursor (CD4+CD8-TCRβ+CD25+Foxp3-)
D2
8-12 weeks
54.9
30.2
Ki67
% Ki67+
D
Total Thymic CD25-Foxp3+ Treg Precursor (CD4+CD8-TCRβ+CD25-Foxp3+)
D2
8-12 weeks
75.4
20.1
Ki67
% Ki67+

Figure 4. 18 Thymocyte Proliferation Decreases with Age

Age related changes in Ki67 expression by thymic SP4 ($CD4^+CD8^-TCR\beta^+$) populations: **(A)** $CD25^+Foxp3^+$ Treg **(B)** $CD25^-Foxp3^-$ Tconv **(C)** $CD25^+Foxp3^-$ and **(D)** $CD25^-Foxp3^+$ Treg precursors. All data is from WT mice and for all timepoints n ≥ 5 across ≥ 2 independent experiments.

Plots shows representative FACs plots of Ki67 levels, relative to isotype control (filled grey), on the indicated SP4 population at D2 or adult (8-12 weeks), as indicated. Right graphs shows quantification of the percentages of $Ki67^+$ thymocytes within the respective SP4 population across the timecourse.

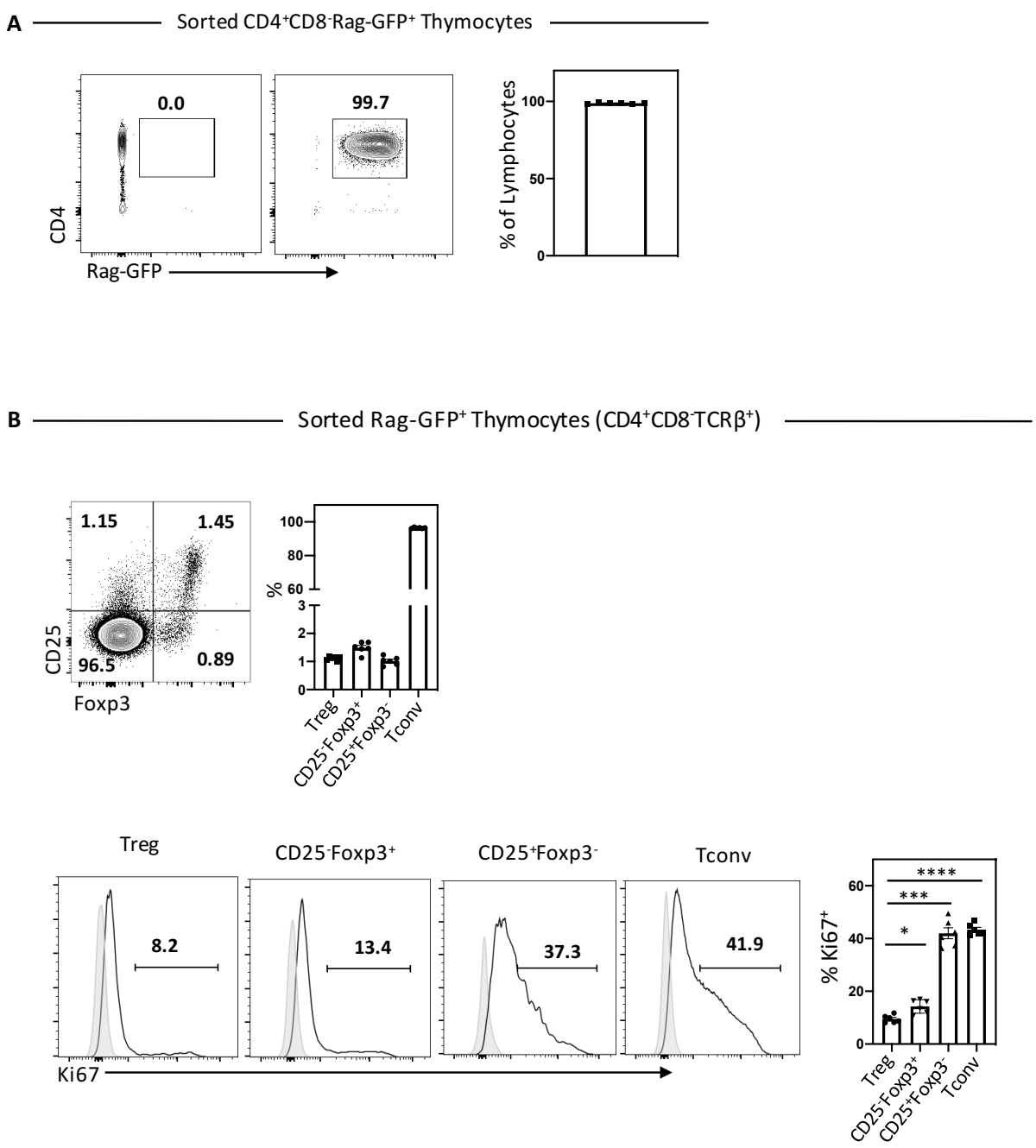
A
Sorted CD4+CD8-Rag-GFP+ Thymocytes
0.0
99.7
CD4
Rag-GFP
% of Lymphocytes
100
50
0
B
Sorted Rag-GFP+ Thymocytes (CD4+CD8-TCRβ+)
1.15
1.45
96.5
0.89
CD25
Foxp3
%
Treg
CD25-Foxp3+
CD25+Foxp3-
Tconv
Treg
CD25-Foxp3+
CD25+Foxp3-
Tconv
8.2
13.4
37.3
41.9
Ki67
% Ki67+
****
***
*

Figure 4. 19 Reduced Proliferation of *De Novo* Thymocytes in Adults

Analysis of sorted *de novo* thymocytes ($CD4^+CD8^-$Rag-GFP^+) from 8-10 week adult Rag-GFP mice. Data representative of n=6, from two independent experiments.

(A) Purity of the sorted $CD4^+CD8^-$Rag-GFP^+ thymocytes. Left shows representative FACs plot of the CD4/Rag-GFP profile of WT non-fluorescent control (left) and sorted $CD4^+CD8^-$Rag-GFP^+ (right) thymocytes. The graph on the right quantifies the purity of the sorted population as the frequency of the target population found within the total sorted thymocyte population.

(B) Analysis of Ki67 expression by SP4 populations within sorted $CD4^+CD8^-$Rag-GFP^+ thymocytes. Top shows the frequency of SP4 thymocyte ($CD4^+CD8^-TCR\beta^+$) populations: $CD25^+Foxp3^-$ and $CD25^-Foxp3^+$ Treg precursors, $CD25^+Foxp3^+$ Treg and $CD25^-Foxp3^-$ Tconv within the sorted samples. Presented as representative FACs plot of CD25/Foxp3 profile with right graph quantifying the percentages of the four SP4 thymocyte populations. Bottom compares the Ki67 expression within the four SP4 populations. Left shows representative FACs plots of Ki67 levels of each SP4 population, as indicated, relative to isotype control (filled grey). The graph on the right quantifies the percentages of $Ki67^+$ thymocytes within each population as indicated. Statistical analysis performed using a repeated measures one way anova, * $p<0.05$, *** $p<0.001$, **** $p<0.0001$.

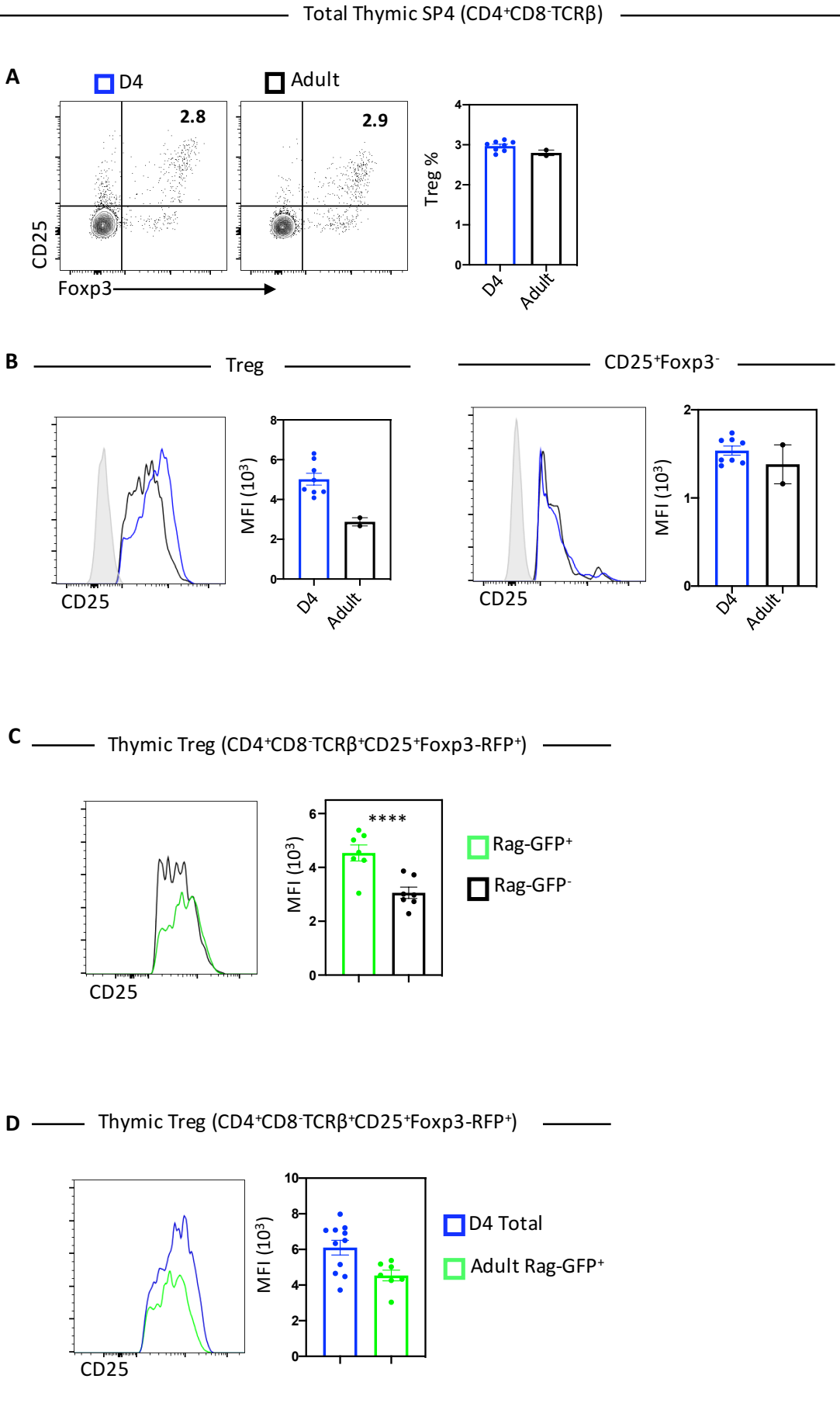
Total Thymic SP4 (CD4+CD8-TCRβ)
A
D4
Adult
2.8
2.9
CD25
Foxp3
Treg %
B
Treg
CD25+Foxp3-
CD25
MFI (10³)
C
Thymic Treg (CD4+CD8-TCRβ+CD25+Foxp3-RFP+)
****
Rag-GFP+
Rag-GFP-
D
Thymic Treg (CD4+CD8-TCRβ+CD25+Foxp3-RFP+)
D4 Total
Adult Rag-GFP+

Figure 4. 20 Differential Expression of CD25 by Adult and Neonatal Thymocytes

Comparative analysis of γ_c family member CD25 expression by thymic Treg ($CD4^+CD8^-TCR\beta^+CD25^+Foxp3^+$) in D4 (blue) and adult (black) mice. Data presented in **(A)** and **(B)** is from WT mice and represents n=8 for D4 neonates, and n=2 for adults (aged 8-12 weeks) across 2 independent experiments. Data in **(C)** is from Foxp3-RFPxRag-GFP mice and represents n=7 adults (aged 8-12 weeks) across 6 independent experiments. Data in **(D)** is from Foxp3-RFPxRag-GFP mice and represents n= 11 for D4 neonates and n=7 for adults (aged 8-12 weeks) across 2 and 6 independent experiments, respectively.

(A) Comparison of frequency of thymic Treg within SP4 ($CD4^+CD8^-TCR\beta^+$) thymocytes from D4 neonatal or adult mice. Data presented as representative FACS plots, showing the CD25/Foxp3 profile of SP4 thymocytes with the percentages of Treg quantified in the graph on the right.

(B) Comparison of the level of CD25 expression by thymic Treg (left) or $CD25^+Foxp3^-$ Treg precursors (right) from D4 neonatal or adult mice. Data presented as representative FACs plots showing an overlay of D4 (blue) and adult (black) CD25 expression relative to an FMO control (grey). Data is quantified in the accompanying graph which shows the the MFI of CD25 for the two ages within the indicated population.

(C) Comparison of the level of CD25 expression by *de novo* Rag-GFP^+ (green) and mature Rag-GFP^- (black) thymic Treg in adult mice. Representative FACs plots show an overlay of Rag-GFP^+ (green) and Rag-GFP^- (black) thymic Treg CD25 expression. Accompanying graph quantifies the MFI of CD25 for the two Treg populations. Statistical analysis performed using a paired t-test, **** $p<0.0001$.

(D) Comparison of the level of CD25 expression by adult *de novo* Rag-GFP^+ (green) and D4 total thymic Treg (blue). Representative FACs plots show an overlay of Rag-GFP^+ (green) and D4 (black) thymic Treg CD25 expression. Accompanying graph quantifies the MFI of CD25 for the two Treg populations.

We next compared CD127 expression on thymocytes from WT D4 neonates and adults (Figure 4.21). Within the Tconv population, we observed little difference in expression between the neonate and adult, and both contained a high proportion of $CD127^+$ thymocytes. Similarly, the proportion of $CD127^+$ thymocytes in neonates and adults was also comparable within the $CD25^+Foxp3^-$ precursor population. However, there was some discrepancy between the two ages within the $CD25^-Foxp3^+$ precursor and Treg populations, as both exhibited an increased proportion of $CD127^+$ thymocytes within the adult, with the largest change occurring within the Treg population. Again, the use of WT mice, and hence the potential confounding impact of mature Treg, makes interpreting this data challenging. However, these findings, along with those presented in Figure 4.20, together suggest that Treg in particular may change receptivity to γ_c signalling with age, with neonatal Treg being more sensitive to IL-2 signalling and less receptive to IL-7 signalling and vice versa in the adult.

Finally, we compared CD122 expression on thymocytes from WT D4 neonates and adults (Figure 4.22). In the neonate, we only detected a notable proportion of $CD122^+$ thymocytes within the Treg population, which was relatively modest in size. In contrast in the adult we detected very little CD122 expression within any of the SP4 thymocyte populations, including Treg. Suggesting that fewer adult Treg express CD122, which could impact on either IL-2 or IL-15 signalling. However again, interpreting these findings is complicated due to the possibility of unaccounted mature thymocytes within the WT.

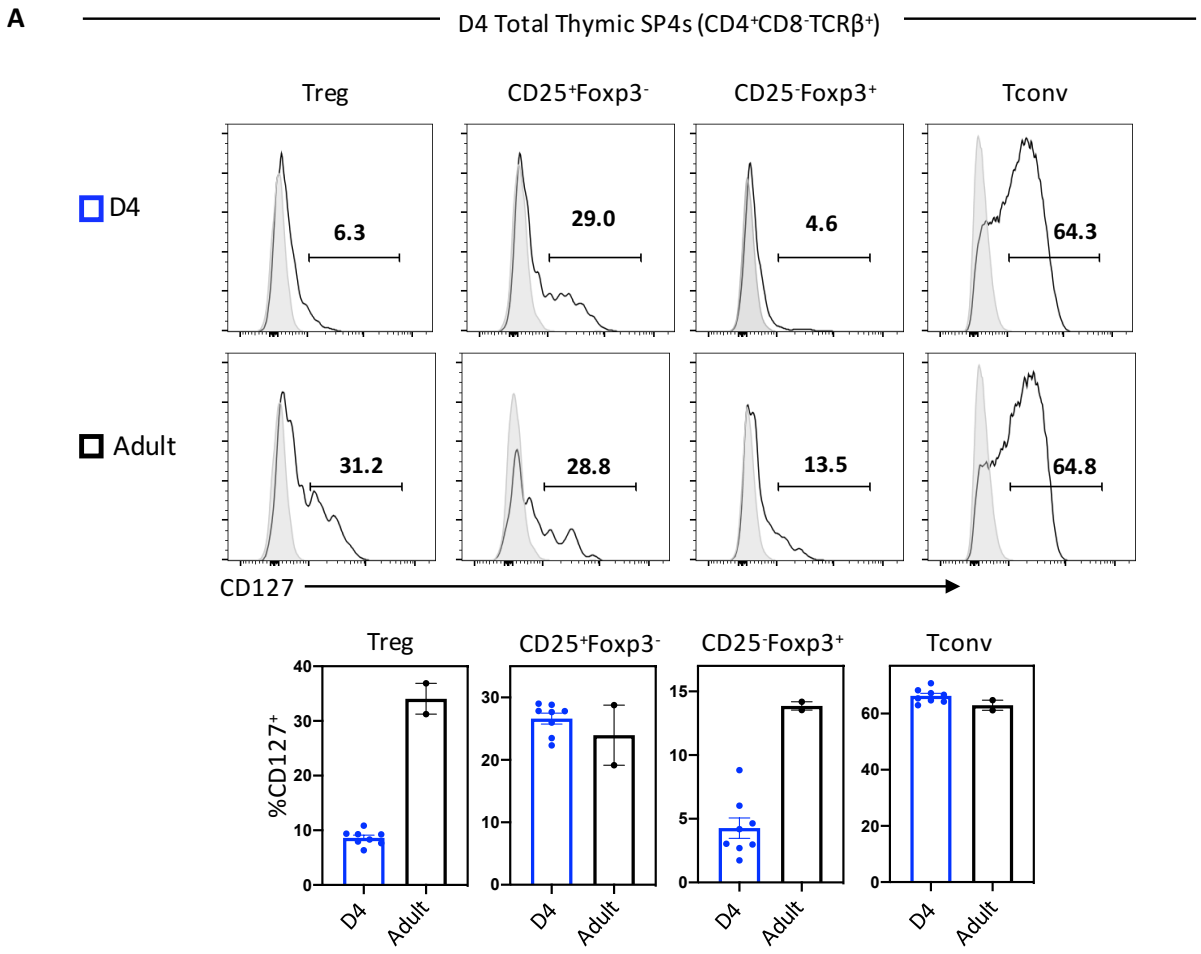
A
D4 Total Thymic SP4s (CD4+CD8-TCRβ+)
Treg
CD25+Foxp3-
CD25-Foxp3+
Tconv
D4
Adult
6.3
29.0
4.6
64.3
31.2
28.8
13.5
64.8
CD127
%CD127+
D4
Adult

Figure 4. 21 Differential Expression of CD127 by Adult and Neonatal Thymocytes

Comparative analysis of γ_c family member CD127 expression by SP4 thymocyte ($CD4^+CD8^-TCR\beta^+$) populations in D4 (blue) and adult (black) WT mice. Data representative of n=8 for D4 neonates, and n=2 for adults across 2 independent experiments.

(A) Expression of CD127 by SP4 thymocyte populations: $CD25^+Foxp3^-$ and $CD25^-Foxp3^+$ Treg precursors, $CD25^+Foxp3^+$ Treg and $CD25^-Foxp3^-$ Tconv, as indicated. Data presented as representative FACs plots with trace relative to FMO control (filled grey), top plots are from D4 neonates while bottom plots are from adults. Bar charts quantify percentages of $CD127^+$ SP4 thymocyte populations as indicated, comparing D4 (blue) and adults (black).

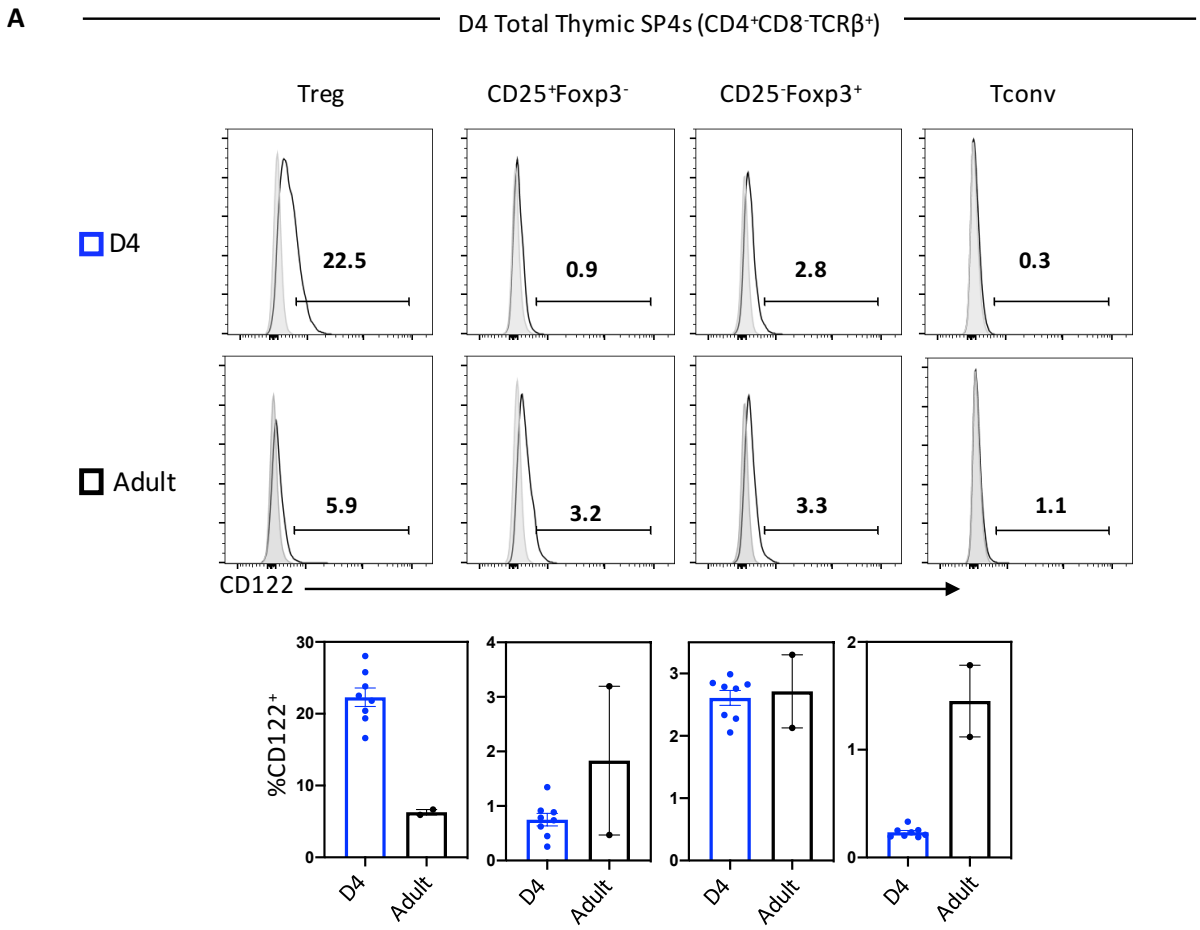
A
D4 Total Thymic SP4s (CD4+CD8-TCRβ+)
Treg
CD25+Foxp3-
CD25-Foxp3+
Tconv
D4
Adult
22.5
0.9
2.8
0.3
5.9
3.2
3.3
1.1
CD122
%CD122+
D4
Adult

Figure 4. 22 Differential Expression of CD122 by Adult and Neonatal Thymocytes

Comparative analysis of γ_c family member CD122 expression by SP4 thymocyte ($CD4^+CD8^-TCR\beta^+$) populations in D4 (blue) and adult (black) WT mice. Data representative of n=8 for D4 neonates, and n=2 for adults across 2 independent experiments.

(A) Expression of CD122 by SP4 thymocyte populations: $CD25^+Foxp3^-$ and $CD25^-Foxp3^+$ Treg precursors, $CD25^+Foxp3^+$ Treg and $CD25^-Foxp3^-$ Tconv, as indicated. Data presented as representative FACs plots with trace relative to FMO control (filled grey), top plots are from D4 neonates while bottom plots are from adults. Bar charts quantify percentages of $CD127^+$ SP4 thymocyte populations as indicated, comparing D4 (blue) and adults (black).

4.3 Discussion

4.3.1 Neonatal Intrathymic Proliferation by Thymic Tregs

Our initial characterisation of neonatal thymic Treg development, in agreement with previous observations of a delayed appearance of thymic Tregs relative to Tconvs[171,231], identified the early beginnings of a thymic Treg population in the D2 neonate (Figure 4.1). Interestingly following this initial appearance there was then a dramatic rapid increase in population size, between D2 and D4, beyond what might be expected from increasing cellularity (Figure 4.1.D). Importantly during this period, we uncovered evidence of proliferation by thymic Tregs, including dilution of Rag-GFP and expression of proliferative markers Ki67 and BRDU (Figure 4.2, Figure 4.4 and Figure 4.5). This proliferation appeared to be a feature of developing thymic Tregs, rather than a recirculating peripheral population, as thymic Tregs proliferated at times when there was little evidence of a peripheral Treg population and within FTOCs which lack a periphery (Figure 4.3 and Figure 4.12). Thus, while it is challenging to fully eliminate the possibility that *in vivo* recirculation of very recently exported Tregs could contribute to thymic proliferation (for example from non-lymphoid tissues not characterised here) they seem unlikely to be the major source. In combination, this evidence led us to suspect that intrathymic proliferation is a feature of thymic Treg development, which may in turn contribute to the rapidly expanding thymic Treg population in the early neonate.

Interestingly intrathymic proliferation within the SP4 lineage has previously been noted in a neonatal setting. Notably using a DNA binding dye (7-Aminoactinomycin D) it has been previously suggested around 25% of D4 neonatal CD4 SP thymocytes were proliferating[335]. Similarly RTOC analysis of CFSE labelled isolated D0-3 neonatal $CD4^+CD8^+CD69^+$ thymocytes suggested SP4 thymocytes underwent up to 6 divisions[337]. However, as these studies

analysed gross SP4 thymocytes they do not offer a direct comparison of Treg and Tconv intrathymic proliferation. Our comparison of the two populations identified that while neonatal Tconv thymocytes proliferate, it is to a much lesser extent than Tregs (Figure 4.9).

The timing of intrathymic proliferation within the Treg lineage was also reminiscent of previous studies which describe SP4 proliferation during post-selection maturation[196]. Here we identified intrathymic proliferation of Tregs and Treg precursors (Figure 4.7), the latter of which in particular suggests proliferation begins imminently following selection signals which drive divergence into the Treg lineage. Interestingly though, the proportion of proliferation within these two Treg precursor populations is not equal, as our BRDU analysis (which as discussed represents a more reliable measure of proliferation) suggests that $CD25^{+}Foxp3^{-}$ precursors proliferated to a greater extent than $CD25^{-}Foxp3^{+}$ precursors (Figure 4.7). This is reminiscent of previous reports of distinctions between the two populations, including different TCR repertoires[187,189] and differing responsivity to cytokines[182,184,187,188]. Moreover, these two precursors have also been proposed to differ in their contribution to Treg development, reportedly generating different types of functional Tregs[189]. Therefore, these reports in combination with our findings, may hint to differing contributions of precursors to early Treg generation. Perhaps with the proliferative $CD25^{+}Foxp3^{-}$ precursors (also notably the largest Treg lineage population at D2) being major contributors to early establishment of thymic Treg development. While the greater proliferative ability of $CD25^{+}Foxp3^{-}$ precursors, may be linked to their expression of CD25 and consequential increased responsivity to proliferative IL-2 signalling (discussed in Section 4.3.2).

One feature of the intrathymic proliferation which appears conserved between our observations and previous reports of neonatal SP4 thymocyte proliferation is a reduction of proliferative ability with age[337,338]. In our analysis, a decline in proliferation of all four SP4 populations (Tconv, Treg, $CD25^{+}Foxp3^{-}$ and $CD25^{-}Foxp3^{+}$ precursors) was observed with increasing age (Figure 4.18 and Figure 4.19). Though notably in the adult this decreased proliferation appeared most pronounced in the *de novo* Treg population, particularly compared to the more modest reduction of proliferation by the *de novo* Tconv and $CD25^{+}Foxp3^{-}$ precursor populations. These findings regarding proliferation of adult thymic SP4 populations are also in line with reports from *TcrdH2BeGFP* reporters[339]. Here the amount of proliferation a cell has undergone is inferred from the cellular intensity of the long-lived *TcrdH2BeGFP* reporter, and this identified that in adults there was limited proliferation within the Tconv and Treg lineage, and regarding the latter that proliferation appeared to occur at a $CD25^{+}Foxp3^{-}$ precursor stage[339].

Overall this suggests that extensive thymic Tregs proliferation is specific to the early neonate, raising the question of why such intense proliferation is necessary. It has been suggested that the greater proliferative ability of neonatal total SP4 thymocytes, relative to their adult counterparts, might aid the expansion of a positively-selected cohort at a time when the peripheral T-cell pool is in the process of being established[337]. Therefore, might the proliferation of thymic Tregs be similarly related to establishing the peripheral pool. Notably we observed that relative to Tconvs, Treg development in the thymus is delayed and importantly this appears to translate to a delayed peripheral appearance of Tregs (Figure 4.6). This delay has previously been observed in the neonate[171,231] and would also be in keeping with the suggestion that Tregs undergo a longer dwell time than Tconvs[154].

Furthermore the autoimmunity associated with dt3x studies also suggest a clear requirement for thymic Tregs in establishing a peripheral Treg pool capable of enforcing tolerance[36,331]. Indeed regarding the regulation of Tconvs by Tregs it is notable that while initially Tconvs dominated the periphery we found that the ratio of splenic Tconvs:Tregs reaches a fairly consistent equilibrium by D7 (Figure 4.6.D). This equilibrium was achieved by large increases in Treg proportions between D2 and D4 and to a lesser extent between D4 and D7, which coincides with the intensive proliferation period and expansion of the thymic Treg population. Therefore, it is tempting to speculate that the intense proliferation within the thymic Treg lineage might be necessary to rapidly export a regulatory population and thereby enforce tolerance of egressed Tconvs. Furthermore, as well as the rapid export of a sufficiently sized Treg population, intrathymic proliferation might also contribute to the expansion of a necessary type of Treg. As the intrathymic proliferation we observed coincides with the timeframe for the generation of distinct neonatal Tregs necessary for long-term tolerance[232,233].

4.3.2 Possible Regulators of Intrathymic Proliferation of Thymic Tregs

Following our identification of differential proliferation of thymic SP4 populations, we were interested in how the thymus might orchestrate this process, and particularly what signals might drive intrathymic Treg proliferation. Our investigations were concentrated on two broad factors associated with proliferation, TCR signalling and γ_c signalling.

Regarding TCR signalling, one interesting candidate was Aire which has previously been linked to the generation of distinct neonatal Tregs via differential processing of Aire-dependent TRAs in the neonatal thymus[232,233]. However while thymic Tregs were numerically reduced in *Aire*$^-$

$^{/-}$ neonates (as previously reported[232,233]), they proliferated to the same extent as *Aire*$^{+/+}$ controls (Figure 4.15), suggesting that TCR stimulation via Aire dependent-TRAs is not an essential driver of thymic Treg proliferation. However, there still may be a broad role for TCR signalling in intrathymic proliferation. As analysis of *Tnfrsf4*$^{-/-}$ neonates did identify a slight global reduction in proliferation of thymocytes (Figure 4.17), suggesting a general role for TCR associated co-stimulation pathways in driving proliferation. Overall though, our limited analysis of regulators of TCR signalling did not identify a clear essential role for TCR signalling specifically in intrathymic Treg proliferation. This is not dissimilar to reports that proliferation of bulk SP4 thymocytes was not impacted by mismatched MHCII stroma, implying that TCR signalling may not be required for post-selection proliferation[337]. This mismatched MHCII stroma system could similarly be utilised to specifically address whether TCR signalling is also non-essential in thymic Treg proliferation.

Our second potential regulator of proliferation was the γ_c cytokine receptor family, whose members have been associated with both thymocyte proliferation and development. Indeed, IL-7 and IL-2 have been implicated in bulk SP4 thymocyte proliferation in neonates[196,335], while IL-15, IL-2, and to a lesser extent IL-7, are key regulators of thymic Treg development[182,184,187,188]. Our analysis of the specific receptor components for these three cytokines identified a distinct pattern of expression by thymic Tregs (Figure 4.10). Notably, while Tconv thymocytes expressed high levels of CD127 (as expected[196]), Tregs had much lower levels of CD127 but higher expression of CD122 and CD25. Therefore, we suspected that IL-15 and IL-2 signalling rather than IL-7 signalling may be critical in driving intensive Treg proliferation.

However, individual blockade of IL-2 and IL-15 signalling had limited impact on intrathymic proliferation (Figure 4.13 and Figure 4.14). Although, IL-2 blockade did impair proliferation of $CD25^{+}Foxp3^{-}$ precursors (Figure 4.13), suggesting a reliance on IL-2 to mediate proliferation of this population, in contrast to its ability to differentiate into Tregs in response to IL-2 or IL-15[187]. Importantly though neither IL-2 nor IL-15 signalling blockade resulted in impaired Treg proliferation. Possibly this is due to redundancy between IL-2 and IL-15 in Treg proliferation, as our analysis of receptor expression suggests Tregs could be responsive to both, and redundancy between the two cytokines in orchestrating Treg development (discussed in Section 1.2.5.2) has previously been described[184,187]. If such redundancy exists, we would anticipate that combined blockade of IL-2 and IL-15 signalling would cause impaired Treg proliferation. Alternatively, it could be that IL-7 signalling, rather than IL-2 or IL-15, is the essential regulator of intrathymic Treg proliferation. As while the low expression of CD127 by neonatal Tregs (Figure 4.10.A) is suggestive of lower responsivity to IL-7, it might in fact be the consequence of endocytosis of CD127 following IL-7 signalling[340]. Therefore, while overall our initial investigations are somewhat inconclusive, there may still be a role for γ_c family members in driving intrathymic proliferation which warrants further investigation.

Furthermore, whilst our initial analysis focused on the identification of the signals driving proliferation it would also be interesting to determine their cellular origin. Largely our current analysis does not address this, however importantly we detected intrathymic proliferation of Tregs in FTOCs was comparable to Tregs in early neonates (Figure 4.12), indicating that the necessary cellular mediators of proliferation are present by E17, at least in some form (i.e. precursor). This could include mTECs, DCs (both cDCs and pDCs[341]) and other thymocytes, all of which, as discussed in Section 1.3, have some association with both Treg development and

γ_c cytokines[158,187,299,304]. One possible way to investigate the cellular origins would be to utilise RTOCs, where neonatal Treg proliferation could be assessed following culture with variable stromal and lymphoid compartments.

While the exact mechanisms driving intrathymic proliferation in the neonate remains unclear, we do identify that the process is subject to age-dependent changes, as relative to neonates, proliferation of adult thymic Tregs is reduced (Figure 4.18 and Figure 4.19). The lack of a definitive mechanism in the neonate means it is somewhat challenging to assess what might change between the neonate and adult, however previous assessment of neonatal and adult SP4 proliferation may offer some insight. As in RTOCs, adult SP4 thymocytes proved to be less proliferative than their neonatal counterparts[337]. This is significant because thymic stroma of RTOCs is from an embryonic source, suggesting that even within a mock-neonatal thymic environment adult thymocyte proliferation was impaired, thus implying proliferative ability is influenced by an intrinsic thymocyte factor.

One such intrinsic difference we identified between neonatal and adult thymic Tregs was their differential expression levels of γ_c family receptors, with adult Tregs showing increased CD127 (Figure 4.21) but decreased CD25 (Figure 4.20) and CD122 (Figure 4.22). Possibly hinting at differential responsivity to these cytokines at different ages, and specifically reduced receptivity to IL-2/IL-15 signalling in the adult. This may be particularly pertinent to the reduced proliferative ability, given the suspected (albeit unproven) role for IL-2/IL-15 in driving neonatal Treg proliferation suggested here. However, an important caveat of this comparison between neonatal and adult thymic Tregs is that it was performed in WT mice and thus,

recirculating mature Tregs were not excluded and therefore could be a confounding factor in the adult.

Whilst this evidence is suggestive of an intrinsic regulator it is also notable that there are several changes in the thymic microenvironment between neonates and adults which may harbour additional extrinsic age-related regulators. Broadly the thymus is known to involute with age, altering the cellular composition of the thymus[227] which may impact the availability of cellular mediators of proliferation. Furthermore, there is also evidence of age-dependent functions of thymic cells, for instance altered TRA processing by mTECs in neonates and adults[233]. Finally another notable change to the thymic Treg pool with increasing age is the increasing dominance of the mature recirculating Treg population[234,235], which purportedly compete with *de novo* Tregs for IL-2 to regulate thymic Treg differentiation. If IL-2 is a regulator of intrathymic proliferation this competition would also provide a mechanism by which mature Tregs could regulate the intrathymic proliferation of their *de novo* counterparts.

Therefore, it is possible that both intrinsic and extrinsic age-related regulators of Treg proliferation exist. One way to address intrinsic vs extrinsic factors could be to utilise an RTOC system to combine *de novo* adult thymic Tregs with embryonic stroma. If within this neonatal-like setting the adult Tregs proliferated to the same extent as neonatal Tregs this would suggest their intrinsic potential for proliferation and thereby identify an extrinsic age-related regulator. Whereas if adult Treg proliferation was still impaired, this would imply an intrinsic age-related regulator. Furthermore, recirculating mature thymic Tregs could also be included alongside *de novo* Tregs to determine their impact as a possible extrinsic regulator of intrathymic proliferation.

4.3.3 Concluding Remarks

As summarised in Figure 4.23, overall this chapter identifies extensive intrathymic proliferation as an underappreciated aspect of neonatal thymic Treg development. This intrathymic proliferation appears fairly restricted to the neonatal phase, and we hypothesise this extensive proliferation may be necessary in rapidly establishing the peripheral Treg population. The mediators of this proliferation currently remain unclear, warranting further investigation into both the regulation of the extensive proliferation in the neonate and the reduced proliferation in the adult. Collectively the findings of this chapter suggest that thymic Treg development is subject to distinct mechanisms in the neonatal thymus, which may ultimately help to establish the neonatal Treg population.

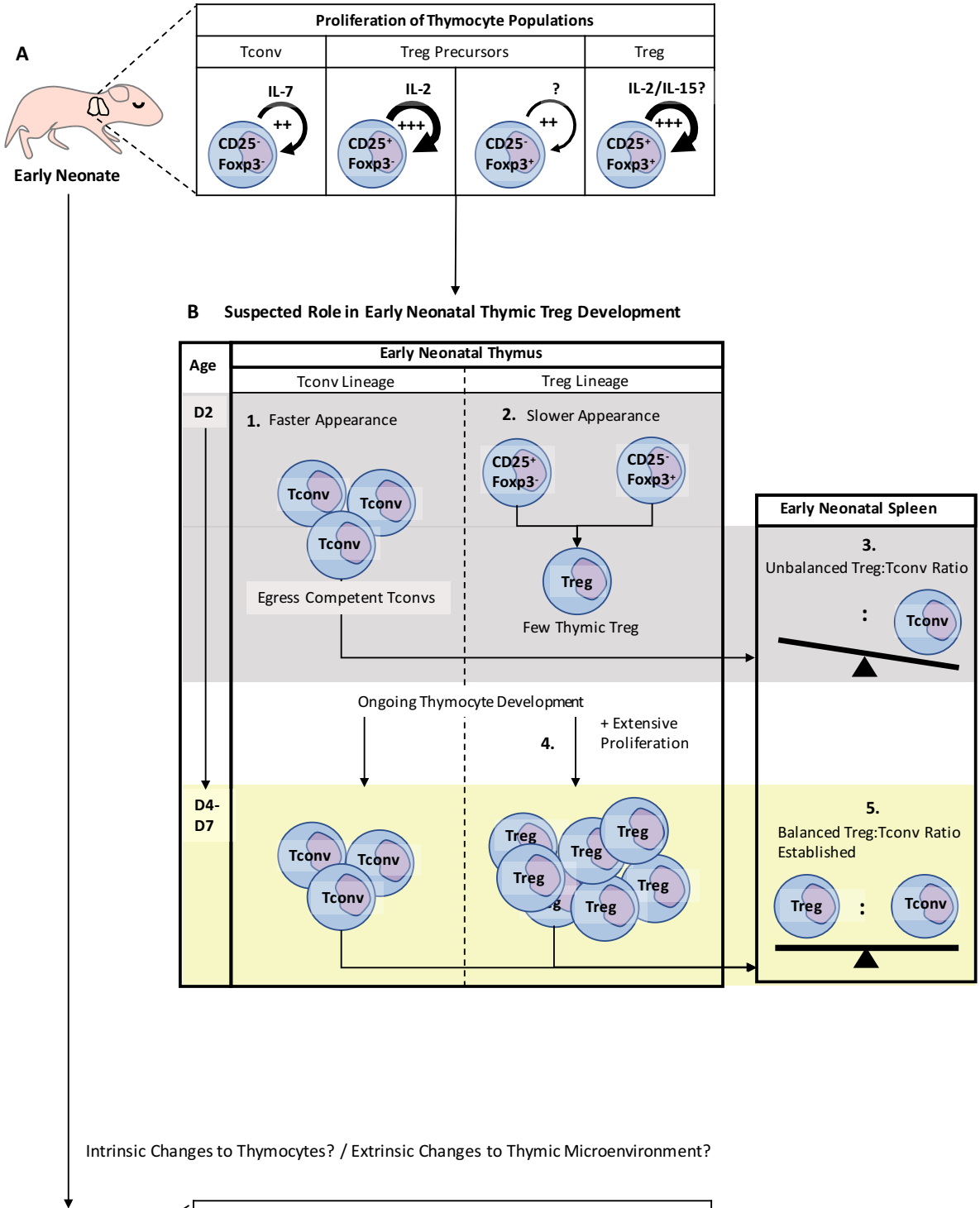
A
Early Neonate
Proliferation of Thymocyte Populations
Tconv
Treg Precursors
Treg
IL-7
++
IL-2
+++
?
++
IL-2/IL-15?
+++
CD25- Foxp3-
CD25+ Foxp3-
CD25- Foxp3+
CD25+ Foxp3+
B Suspected Role in Early Neonatal Thymic Treg Development
Age
Early Neonatal Thymus
Tconv Lineage
Treg Lineage
D2
1. Faster Appearance
2. Slower Appearance
Tconv
Egress Competent Tconvs
Few Thymic Treg
Early Neonatal Spleen
3.
Unbalanced Treg:Tconv Ratio
:
Ongoing Thymocyte Development
4.
+ Extensive Proliferation
D4-D7
5.
Balanced Treg:Tconv Ratio Established
Intrinsic Changes to Thymocytes? / Extrinsic Changes to Thymic Microenvironment?
C Adult
+
-/+

Figure 4. 23 Summary Diagram of Intrathymic Proliferation in Neonates and Adults

Proposed overview of **(A)** intrathymic proliferation of SP4 thymocyte populations in neonates and **(B)** how this might contribute to establishing the Treg population at this stage. While **(C)** gives an overview of intrathymic proliferation of SP4 thymocyte populations in adults. In **(A)** and **(C)** proliferation of SP4 thymocyte populations ($CD25^{-}Foxp3^{-}$ Tconvs, $CD25^{+}Foxp3^{+}$ Tregs, $CD25^{+}Foxp3^{-}$ and $CD25^{-}Foxp3^{+}$ Treg precursors) are indicated by circular arrows and proliferative intensity by plus by scale, with: +++ indicating most proliferative through to -/+ indicating little evidence of proliferation.

(A) In the early neonatal thymus there is evidence of differential proliferation between SP4 thymocyte populations with Tregs and $CD25^{+}Foxp3^{-}$ Treg precursors proliferating most intensely, and Tconvs and $CD25^{-}Foxp3^{+}$ Treg precursors proliferating to a lesser extent. The suspected cytokine regulators of each populations proliferation is indicated above, with ? indicating speculation.

(B) Overview of how particularly extensive intrathymic proliferation within the Treg lineage may contribute to rapid establishment of the Treg population. Beginning with the D2 (grey background) thymus **(1)** an egress competent Tconv thymocyte population can be observed as a consequence of rapid thymic development (and some intrathymic proliferation). **(2)** In contrast thymic development of the Treg lineage is slower, resulting in very few thymic Tregs in the D2 thymus. **(3)** Consequently thymocytes exported to the spleen are predominantly Tconvs with virtually no Tregs**,** resulting in an imbalanced peripheral Tconv:Treg ratio. **(4)** Thymocyte development continues in both Tconv and Treg lineages, contributing to the generation of Tconv/Treg populations. However the Treg population also expands dramatically as a consequence of extensive proliferation within the Treg lineage. **(5)** Meaning between D4 and D7 (yellow background) there is a expanded thymic Treg pool which undergoes export to the periphery alongside Tconvs to establish a balanced peripheral Tconv:Treg ratio.

(C) Arrow indicates aging which is accompanied by possible changes to the thymic microenvironment and/or intrinsic changes to thymocytes. Consequently in the adult the proliferation of all SP4 thymocyte populations is reduced with Treg proliferation particularly decreased, as indicated.

CHAPTER FIVE:
DIFFERENTIATING RTES FROM THEIR MATURE COUNTERPARTS

5.1 Introduction

RTEs are distinguished as peripheral SP4/SP8 T-cells which have newly exited the thymus[342]. Importantly RTEs have been shown to differ in more than just age to their more mature naïve peripheral T-cell counterparts. Primarily using Rag-GFP mice, which as previously discussed (Section 1.2) offer an un-manipulated system to discriminate RTEs, studies have identified that following thymic egress SP4/SP8 RTEs undergo a 2-3 week maturation period[157,342], dependent upon RTE entry into SLOs[309]. SP4/SP8 RTE maturation has been associated with phenotypic changes of markers connected to various aspects of T-cell biology ([157] and Table 5.1). Furthermore, this maturation has also been linked with differences in function[157], tolerance receptivity[218], metabolism[225,226], epigenetic regulation[224] and survival of complement[214]. With RTEs broadly displaying reduced functionality, increased tolerance sensitivity and impaired survival relative to their mature counterparts (previously discussed in Section 1.2.7). Consequently, RTEs are proposed to represent a distinct stage of T-cell development between mature thymocytes and mature naïve T-cells.

The prospect of a unique SP4 RTE population is not only intriguing from a developmental sense but also as a means to study thymic output. However, while significant progress has been made characterising RTE biology, they remain a challenging population to confidently isolate outside of the Rag-GFP model. While phenotypic differences between RTEs and mature naïve T-cells have been observed, these have often been modest changes in expression which occur incrementally with increasing RTE age. This lack of discrete markers may hint of the underlying similarity between RTEs and mature naïve T-cells. However, it is also notable that as yet no large-scale comparative study of RTE and mature T-cell

phenotypes have been conducted and thus only a limited selection of markers have been investigated.

Another limitation of previous investigations into RTE maturation is they have only considered RTE as gross SP4 or SP8 T-cell populations, and therefore not addressed heterogeneity within these RTE populations. Notably bulk SP4 T-cells contain both Tconv and Treg subsets, which differ dramatically in phenotype and function. Accordingly, whilst these populations undergo highly comparable thymic development, some aspects are lineage specific. Thus, raising the question of whether post-thymic maturation may also be a mixture of common and lineage specific processes.

We therefore sought to comprehensively investigate the differences between SP4 RTEs and their naïve mature counterparts, by performing bulk RNAseq and scRNAseq. We aimed to determine firstly, if SP4 RTEs display a unique gene expression profile, relative to mature naïve counterparts, and secondly if this gene expression profile may also be subject to lineage specific variation between Treg and Tconv RTE specifically.

Table 5. 1 Selection of Markers Previously Suggested to be Differentially Expressed by RTE and Non-RTE

Marker Type	Marker	Reported Status (in RTE)	Reference
T-cell markers broadly linked to: maturation/ homeostasis/ signalling	CD24	Upregulated	[157,342]
	Qa2	Downregulated	[157,342]
	Ly6C	Downregulated	[342,343]
	IL-7Ra	Downregulated	[157,342]
	CD28	Downregulated	[157,342]
	CD3/TCR	Upregulated	[157,342]

Metabolism	Glut1	Downregulated	[225,344]
	Hexokinase II	Downregulated	[225,344]
	CD98	Downregulated	[225,344]
	CD71	Downregulated	[225,344]
	MTORC1	Downregulated	[225,344]
	MTORC2	Upregulated	[225,344]
Anergy Factors	DGK-α	Upregulated	[218,344]
	DGK-ζ	Upregulated	[218,344]
	Cbl-b	Upregulated	[218,344]
	PD-1	Upregulated	[222,342,344]
	CTLA-4	Upregulated	[342,345]
Trafficking Molecules	$\alpha_4\beta_2$ integrin	Upregulated	[313,344]
	CCR9	Upregulated	[313,344]
	VLA-4	Upregulated	[344,346]
Susceptibility to Complement Activity	CD55	Downregulated	[214,344]
Methylation	DNMT1	Upregulated	[224]
	DNMT3a	Upregulated	[224]
	TET1	Upregulated	[224]

5.2 Results

5.2.1 Initial Generation and Processing of RNAseq Datasets

We therefore decided to compare SP4 RTEs with their suspected immediate subsequent T-cell stage (hereafter referred to as non-RTE), meaning mature naïve T-cells for bulk SP4/Tconv RTEs and mature Tregs for Treg RTEs. For a comprehensive analysis, we decided to utilise both bulk RNAseq and scRNAseq analysis. These two approaches complimented one another as bulk RNAseq presented a technically reliable platform which could be used to address SP4 RTE as a total population while scRNAseq could be used to assess heterogeneous SP4 RTE Treg and Tconv subsets albeit with some technical limitation associated with the platform (e.g. dropout).

An overview of the two approaches taken to generate the bulk RNAseq and scRNAseq datasets is shown in Figure 5.1.A (and Section 2.12). In the generation of both datasets, RTE and non-RTE populations were isolated simultaneously from the same source, namely from the splenocytes of adult Rag-GFP mice. This source offered both an enriched site of RTEs (which traffic to SLOs to complete their maturation) and a means to discriminate live RTE and non-RTE as Rag-GFP^{+} and Rag-GFP^{-} (respectively) by fluorescent activated cell sorting. However, the sequencing approach did not determine the specifics of the sorted populations collected. For scRNAseq, where different cell subsets could be distinguished in later bioinformatics analysis, we broadly sorted RTE and non-RTE as SP4 T-cells defined as CD4^{+}CD8^{-} (Figure 5.1.A and C). In contrast, as the bulk RNAseq would only inform on the average gene expression of the total sorted population we sorted RTE and non-RTE as naïve SP4 T-cells defined as CD4^{+}CD8^{-}CD62L^{hi} (Figure 5.1.A and B). This definition was particularly important to remove activated CD62L^{lo} effector T-cells from the non-RTE population and thereby ensure RTEs were compared to the next closest stage of T-cell development (i.e. mature naïve T-cells).

In total the described strategy resulted in the generation of one paired RTE and non-RTE scRNAseq samples and 4 paired RTE and non-RTE bulk RNAseq samples. These samples then underwent bioinformatic processing steps to generate appropriate RNAseq datasets for downstream comparative analysis of RTEs and non-RTEs.

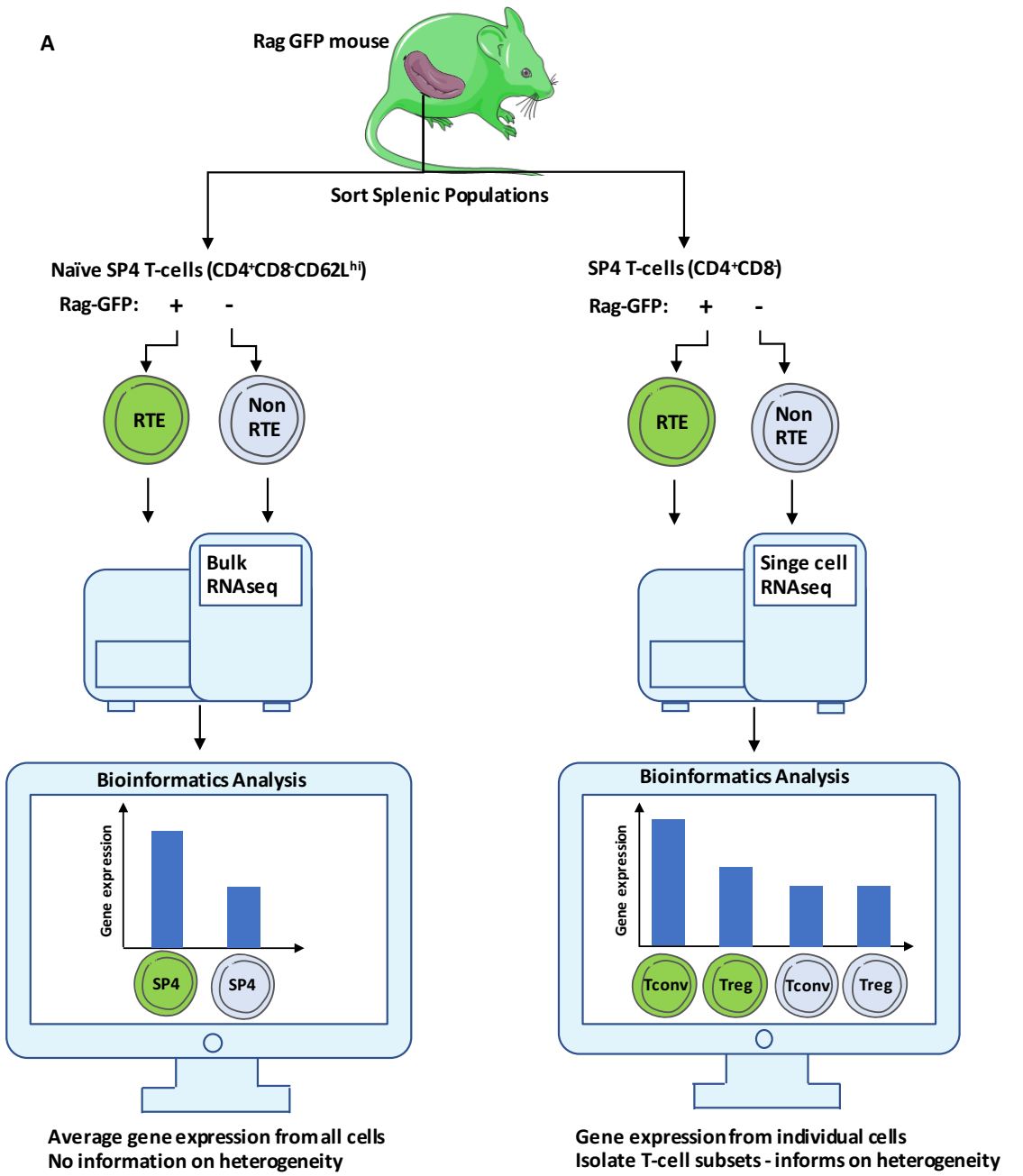
A
Rag GFP mouse
Sort Splenic Populations
Naïve SP4 T-cells (CD4+CD8-CD62Lhi)
Rag-GFP: + -
RTE
Non RTE
Bulk RNAseq
Bioinformatics Analysis
Gene expression
SP4
SP4
Average gene expression from all cells
No information on heterogeneity
SP4 T-cells (CD4+CD8-)
Rag-GFP: + -
RTE
Non RTE
Singe cell RNAseq
Bioinformatics Analysis
Gene expression
Tconv
Treg
Tconv
Treg
Gene expression from individual cells
Isolate T-cell subsets - informs on heterogeneity
B
Sorted Naive SP4s (CD4+CD8-CD62Lhi Rag-GFP+/-)
RTE
Non-RTE
CD62L
0.51 98.9
97.6 0.00
Rag-GFP
% Lymphocytes
100
50
0
C
Sorted Total SP4s (CD4+CD8- Rag-GFP+/-)
RTE
Non-RTE
0.67 99.1
99.4 0.06
CD4
Rag-GFP
% Lymphocytes
100
50
0

Figure 5. 1 Overview of Generation of RTE and Non-RTE scRNAseq and Bulk RNAseq Datasets

(A) Schematic of workflow for collection and analysis of splenic RTE and non-RTE RNAseq data. Two different strategies were employed to investigate SP4 RTEs and non-RTEs both as either (left) gross or (right) heterogeneous populations. (Left) total Naïve SP4 RTE ($CD4^{+}CD8^{-}CD62L^{hi}$Rag-GFP^{+}) and non-RTE ($CD4^{+}CD8^{-}CD62L^{hi}$Rag-GFP^{-}) were sorted from the spleens of Rag-GFP mice. The sorted RTE and non-RTE samples then underwent bulk RNAseq (separately). Finally the resultant two datasets were then pooled for bioinformatics analysis. This approach informs on differences in average gene expression across the total populations without providing any information regarding heterogeneity. (Right) total SP4 RTE ($CD4^{+}CD8^{-}$Rag-GFP^{+}) and non-RTE ($CD4^{+}CD8^{-}$Rag-GFP^{-}) were sorted from the spleens of Rag-GFP mice. The sorted RTE and non-RTE samples then underwent scRNAseq (separately). Finally the resultant two datasets were then pooled for bioinformatics analysis, which included the identification of T-cell subsets e.g. Treg within the total SP4 populations. This approach enables analysis of gene expression within individual cells of the total population and thereby provide additional insight into population heterogeneity. **(B-C)** Phenotype and purity of sorted SP4 splenocytes for **(B)** bulk RNAseq (n= 4 paired RTE and non-RTE samples) and **(D)** scRNAseq analysis (n= 1 paired RTE and non-RTE sample), sorted from WTxRag-GFP mice (5-6 weeks). Data presented as representative FACs plots which show **(C)** the Rag-GFP CD62L profile and **(C)** the CD4 Rag-GFP profile of sorted splenic SP4 **(C)** naive ($CD62L^{hi}$) or **(D)** total RTE and non-RTE as indicated, both of which are pre-gated as LIVE/$DEAD^{-}CD4^{+}CD8^{-}$. Accompanying bar charts present the purity of the respective sorted RTE and non-RTE populations as a percentage of the total lymphocytes.

Figure 5.2 (and Section 2.12.1) gives an overview of the processing of the scRNAseq dataset. In brief following the sequencing of RTE and non-RTE using the 10x Chromium platform, the generated scRNAseq samples were then separately processed using CellRanger pipeline tools to generate the digital expression matrix, which conveys the number of detected transcripts per gene per individual cell. Initial processing using default conditions resulted in the recovery of >4000 cells, however inspection of barcode rank plots suggested this may have resulted in inclusion of droplets with low RNA quantity (Figure S.1.A). Therefore, to ensure stringency in subsequent analysis, processing was re-performed with the algorithm instructed to recover 4000 cells in total (this value representing the expected recovery yield from the sequencing process). The associated barcode rank plots suggested this approach resulted in a more stringent cut-off between cells and empty droplets (Figure S.1.B).

The digital expression matrices were then read into R studio, where the RTE and non-RTE samples were merged into one dataset (referred to as the total SP4 scRNAseq dataset) and processed using the Seurat package (Figure 5.2 and Section 2.12.1.3). Of note, alongside the standard QC step to remove cells with >5% mitochondrial counts (Figure S.1.C) we also noted a prevalence of cells with low numbers of unique genes within the RTE sample, therefore cells were also removed with <700 unique genes (Figure S.1.D). After further processing (detailed in Section 2.12.1.3) the data was then ready for further downstream analysis, beginning with the identification of T-cell subsets of interest, namely naïve Tconvs and Tregs.

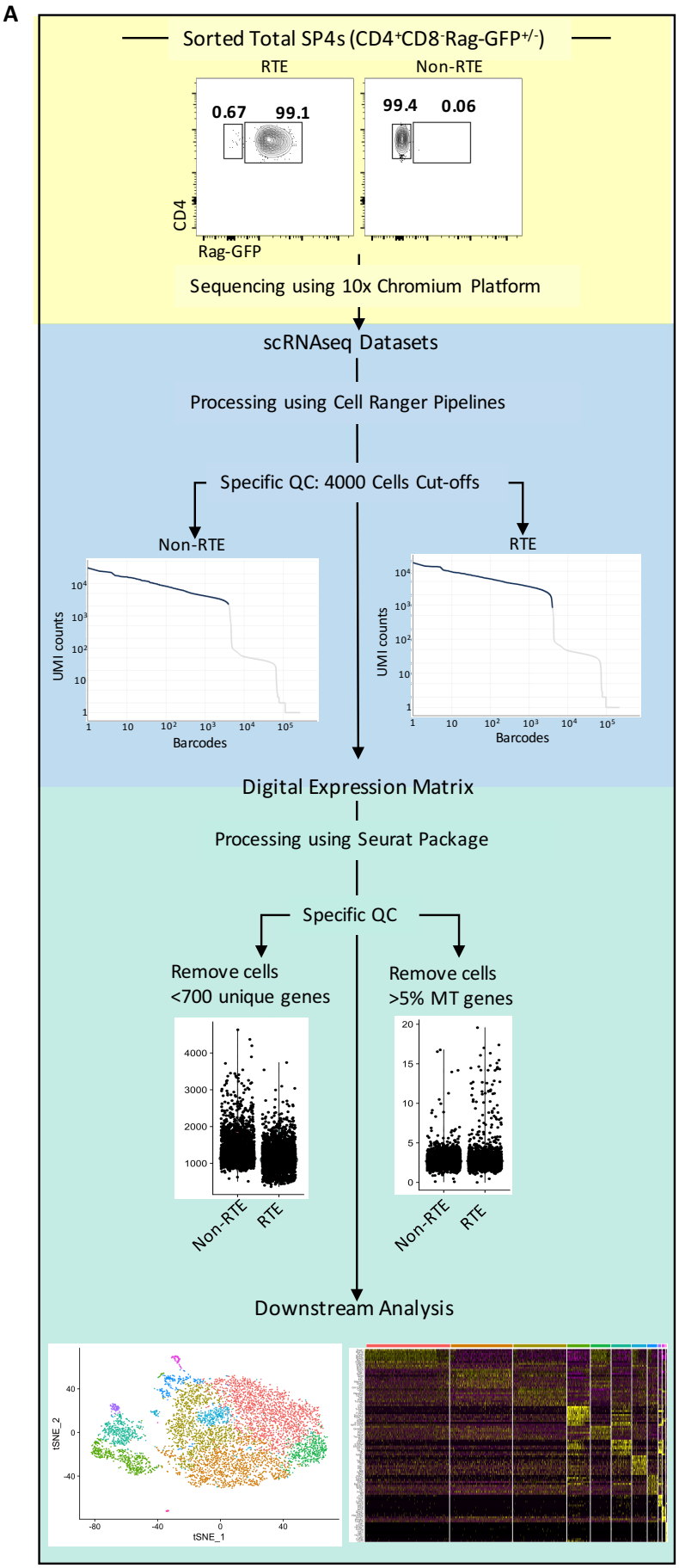
A
Sorted Total SP4s (CD4+CD8-Rag-GFP+/-)
RTE
Non-RTE
0.67
99.1
99.4
0.06
CD4
Rag-GFP
Sequencing using 10x Chromium Platform
scRNAseq Datasets
Processing using Cell Ranger Pipelines
Specific QC: 4000 Cells Cut-offs
Non-RTE
RTE
UMI counts
Barcodes
Digital Expression Matrix
Processing using Seurat Package
Specific QC
Remove cells
<700 unique genes
Remove cells
>5% MT genes
Non-RTE
RTE
Downstream Analysis
tSNE_1
tSNE_2

Figure 5. 2 Overview of Pre-Processing Stages of scRNAseq RTE and Non-RTE Datasets

(A) Schematic overview of the pre-processing stages involved in generating and preparing the scRNAseq RTE and non-RTE datasets for subsequent downstream analysis which addresses the biological questions of interest. Background colour indicates the type of analysis: wet lab (yellow), high performance computing using Cell Ranger (blue) and *in silico* analysis using R studio and Seurat (green). In brief, sorted $CD4^{+}CD8^{-}$Rag-GFP^{+} RTE and $CD4^{+}CD8^{-}$Rag-GFP^{-} non-RTE splenocytes were subject to sequencing using the 10x Chromium Platform to generate RTE and non-RTE scRNAseq datasets (n=1 paired experiment). The raw RNAseq datasets were then separately processed through the Cell Ranger analysis pipeline, using the reference genome GRCm38 (mm10) for alignment. Here a specific QC step was taken to force a 4000 cell cut-off of the both the RTE and non-RTE sample (see Figure S.1.A-B for enlarged version). The resulting digital expression matrices for both samples were read into R studio, merged and processed using Seurat. Initial QC steps removed low quality cells defined by < 700 unique genes and/or >5% mitochondrial (MT) genes(see Figure S.1.C-D for enlarged version). The data was then normalized, highly variable features identified, scaled and subject to linear dimensional reduction. The data was then ready for future downstream analysis including clustering and differential gene expression analysis.

To distinguish T-cell subsets, cell clustering was performed (detailed in Section 2.12.1.3 and Table 2.11) on the total SP4 scRNAseq dataset which identified 11 clusters (Figure 5.3.A). Clusters were then subject to differential expression analysis using the Seurat function **FindMarkers** (Figure 5.3.B). The differentially expressed genes (DEGs) combined with analysis of known biological markers for lymphocyte populations were used to assign cell subset identities to the clusters (Figure 5.3.C). Importantly we were able to identify clusters belonging to Treg and naïve Tconv subsets. A total of 6128 cells contained within five clusters displayed a naïve Tconv phenotype (cluster 1-5), expressing generic SP4 T-cell markers CD3 and CD4 as well as high expression of CCR7 and CD62L and low expression of CD44. An additional two clusters also appeared similar to the described naïve T-cell phenotype, however these clusters also expressed markers broadly linked to tolerance (cluster 10, 266 cells) or proliferation (cluster 11, 80 cells). These clusters were therefore designated as other, and excluded from naïve T-cell analysis. One cluster (cluster 6) containing 597 cells were identified as Tregs, again these cells expressed CD3 and CD4 but also specifically Treg markers CD25 and Foxp3. Of the remaining three clusters, two clusters were identified as the SP4 T-cell subsets effector T-cells (cluster 7, 521 cells) and iNKT-cells (cluster 8, 83 cells), respectively. While the remaining cluster was identified as small contaminating B-cell population (cluster 9, 23 cells).

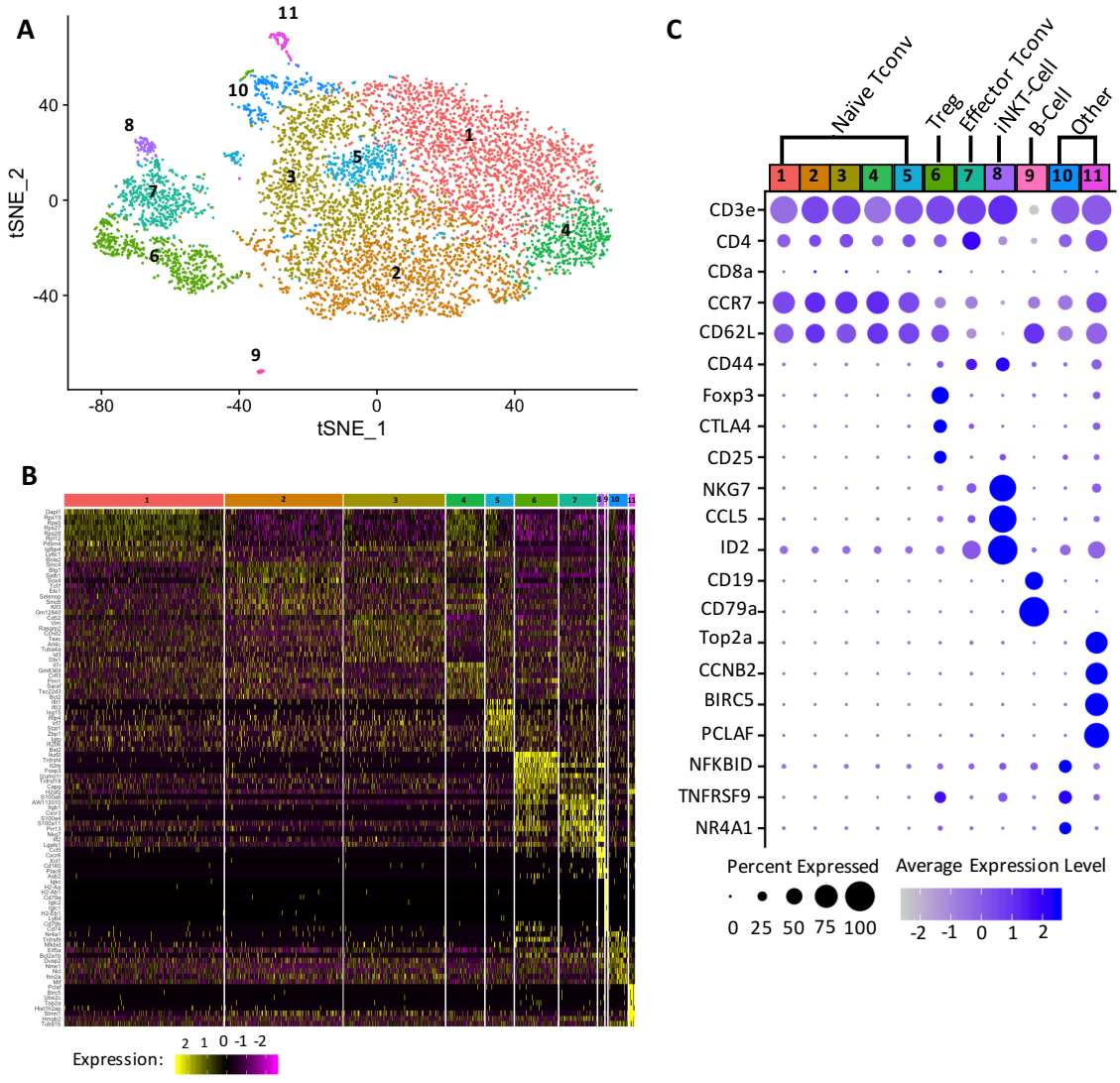
A
tSNE_2
tSNE_1
B
Expression:
C
Naïve Tconv
Treg
Effector Tconv
iNKT-Cell
B-Cell
Other
CD3e
CD4
CD8a
CCR7
CD62L
CD44
Foxp3
CTLA4
CD25
NKG7
CCL5
ID2
CD19
CD79a
Top2a
CCNB2
BIRC5
PCLAF
NFKBID
TNFRSF9
NR4A1
Percent Expressed
Average Expression Level

Figure 5. 3 Treg and Naïve Tconvs Populations can be Identified within scRNAseq Datasets

(A) t-SNE visualisation of merged RTE and non-RTE datasets coloured by clustering. **(B)** Heatmap of the top 10 most positively differentially expressed genes for each cluster, with the colour scale indicating gene expression level (see Figure S.2 for enlarged heatmap). **(C)** Visualisation of definitive markers for different lymphocyte populations within the different clusters (as indicated by the colours running along the top). The size of each circle reflects the percentage of cells in a cluster where the gene is detected, and the colour reflects the average expression level within each cluster. The suspected identity of the cluster is indicated above its colour.

Following identification of SP4 T-cell populations within the scRNAseq dataset, cells belonging to naïve Tconv or Treg clusters were isolated for further analysis as separate scRNAseq datasets (Figure 5.4), hereafter referred to as the Tconv and Treg datasets, respectively. Importantly, and as expected, these cells were a mixture of RTE and non-RTE (Figure 5.4.A). Following the formation of Tconv and Treg datasets, they were then subject to the same pre-processing steps and clustering (detailed in Section 2.12.1.3 and Table 2.11). A total of 6 clusters were found within the naïve Tconv dataset (Figure 5.4.B) while 4 clusters were present within the Treg dataset (Figure 5.4.C).

The bulk RNAseq dataset also had to undergo processing steps, as illustrated by the overview presented in Figure 5.5 (and Section 2.12.2). Following sequencing using the Illumina HiSeq 4000 platform the generated RTE and non-RTE bulk RNAseq samples were first processed separately using HISAT2, Samtools and LibiNorm to generate the digital expression matrix, which conveys the number of detected transcripts per gene per sample. The resultant matrices were then read into R studio and processed together as one dataset using the DESeq2 package (Section 2.12.2.3). Prior to downstream analysis, an additional two QC steps were taken. Firstly, initial PCA of the four paired RTE and non-RTE samples identified that while PC1 seemed to split RTE and non-RTE consistently for all samples, PC2 resulted in the separation of one paired RTE and non-RTE samples (replicate 4) from the remaining samples (Figure 5.5). Suggesting that the samples belonging to replicate 4 were outliers relative to the remaining three replicates. Therefore, to reduce the influence of batch effect from any subsequent differential analysis, the RTE and non-RTE samples belonging to this outlier experiment were removed.

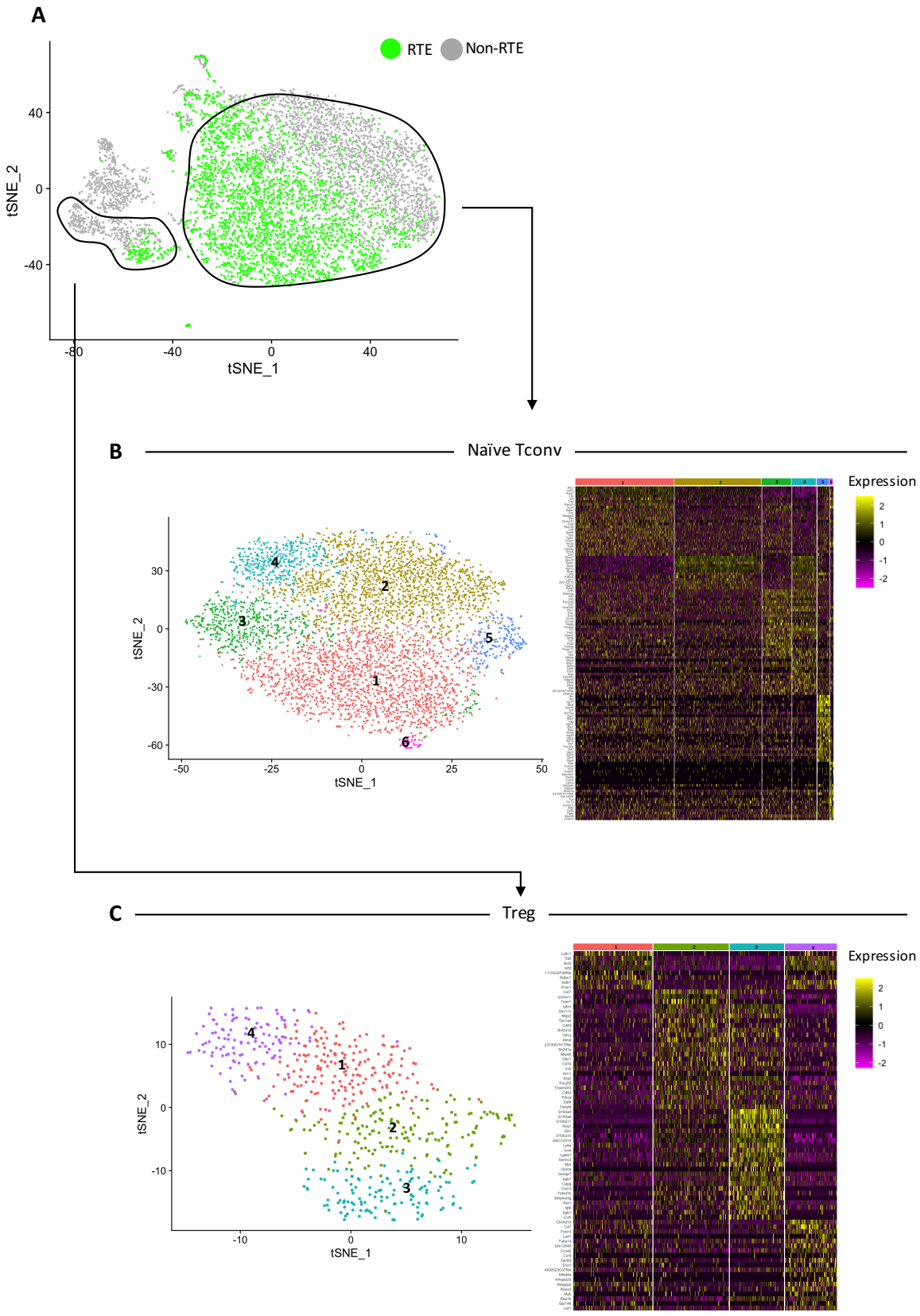
A
RTE
Non-RTE
tSNE_2
tSNE_1
B
Naïve Tconv
Expression
C
Treg
Expression

Figure 5. 4 Overview of Isolation and Reanalysis of Tconv and Treg RTE and Non-RTE Subsets within scRNAseq Dataset

(A) t-SNE plot with cells coloured by original sorted RTE (green) or non-RTE (grey) identity. Black outline encloses cells identified in Figure 5.4 as belonging to Treg or naïve Tconv clusters. These outlined cells were subsequently isolated and reanalysed to investigate individual **(B)** naïve Tconv and **(C)** Treg subsets. Subsequent clustering analysis of separate Treg and naïve Tconv populations (as indicated) is presented as t-SNE plots with associated heatmaps of the top 10 positive differentially expressed genes for each cluster separately as individual datasets (see Figure S.3-4 for enlarged heatmaps). For heatmap colour scale indicates gene expression level.

A

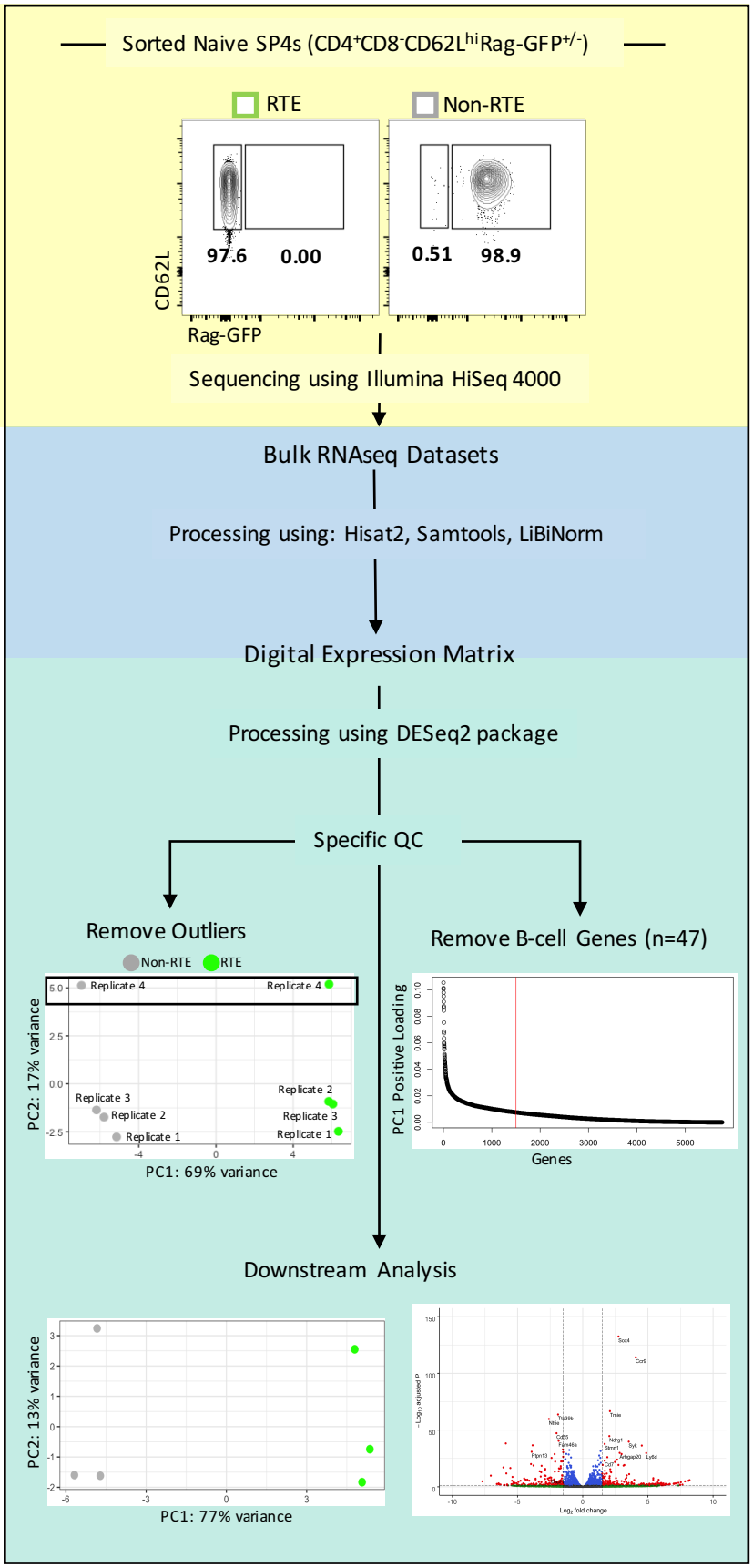
Sorted Naive SP4s (CD4+CD8-CD62LhiRag-GFP+/-)
RTE
Non-RTE
97.6
0.00
0.51
98.9
CD62L
Rag-GFP
Sequencing using Illumina HiSeq 4000
Bulk RNAseq Datasets
Processing using: Hisat2, Samtools, LiBiNorm
Digital Expression Matrix
Processing using DESeq2 package
Specific QC
Remove Outliers
Remove B-cell Genes (n=47)
Non-RTE
RTE
Replicate 4
Replicate 4
Replicate 3
Replicate 2
Replicate 2
Replicate 3
Replicate 1
Replicate 1
PC2: 17% variance
PC1: 69% variance
PC1 Positive Loading
Genes
Downstream Analysis
PC2: 13% variance
PC1: 77% variance

Figure 5. 5 Overview of Pre-Processing Stages of Bulk RNAseq RTE and Non-RTE Datasets

(A) Schematic overview of the pre-processing stages involved in generating and preparing the bulk RNAseq RTE and non-RTE datasets for subsequent downstream analysis which addresses the biological questions of interest. Background colour indicates the type of analysis: wet lab (yellow), high performance computing using Hisat2, Samtools and LiBiNorm(blue) and *in silico* analysis using R studio and DESeq2. In brief, sorted $CD4^{+}CD8^{-}CD62L^{hi}Rag\text{-}GFP^{+}$ RTE and $CD4^{+}CD8^{-}CD62L^{hi}Rag\text{-}GFP^{-}$ non-RTE SP4 splenocytes were subject to sequencing using the Illumina HiSeq 4000 Platform to generate RTE and non-RTE scRNAseq datasets (n=4 paired experiments). The raw RNAseq data was then processed using Hisat2, Samtools and LibiNorm, using the reference genome GRCm38 (mm10) for alignment. The resulting digital expression matrices were then processed in R using DEseq2. Datasets were normalised and two specific QC steps were taken. Firstly one experiment was identified as an outlier so its associated RTE and non-RTE samples were excluded from further analysis. In addition B-cell genes were also identified in the RTE sample, resulting in the exclusion of 47 B-cell genes from the top 1500 genes making the largest positive contribution to PC1 (see Figure S.5 for detailed overview). The data was then ready for future downstream analysis including differential gene expression analysis.

Secondly several B-cell genes were identified as more highly expressed by the RTE samples (Figure S.5.A). The presence of these genes indicated a small number of contaminating B-cells more prevalent within the RTE fraction. This is feasible as immature B-cells that are present in the spleen are Rag-GFP^{+} and possibly the contamination of the RTE fraction is greater because, relative to Rag-GFP^{-}, the pool of Rag-GFP^{+} T-cells is smaller meaning contaminants are more prominent. To prevent these contaminating genes confounding the underlying differences that may be present between RTE and non-RTE populations, they were removed in a process outlined in Figure S.5. In brief, as preliminary analysis had implicated PC1 to contain the majority of variation between RTE and non-RTE samples, we screened the top 1500 genes positively contributing to PC1 (hence upregulated in RTE). We then examined the expression of these genes within the B-cell cluster identified within our own scRNAseq dataset, in addition to cross referencing the gene names with known B-cell markers described in the literature. This approach resulted in the flagging and removal of 47 genes, detailed in Table S.1.

The processed bulk RNAseq dataset (now comprising of 3 paired naïve SP4 RTE and non-RTE samples) hereafter referred to as the SP4-bulk dataset, alongside the aforementioned Tconv and Treg datasets were then all ready for downstream differential expression analysis to compare RTEs and non-RTEs.

5.2.2 Characterising and Comparing SP4 RTEs and Non-RTEs Using RNAseq

We began by examining RTE as a mass population, in keeping with previous studies, through differential analysis of our SP4-bulk dataset. Notably the first two PCs explained the vast majority of variation within our dataset, in combination accounting for approximately 90% of the total variance (Figure 5.6.A). Indeed, PC1 alone accounted for approximately 77% of the total variance, and importantly plotting samples by PC1 identifies that PC1 separates the samples on the basis of their RTE / non-RTE identity (Figure 5.6.B). Suggesting that the difference in sorted identity was the main source of variation within our dataset. The next largest source of variation, explained by PC2, seems to be linked to the variation between the mice which the paired RTE and non-RTE samples were sorted from (Figure 5.6.C). However, given the far lower variance accounted for by PC2, this batch effect seems to be minimal relative to the variance between RTEs and non-RTEs.

Following our PCA determining RTE vs non-RTE identity as the main source of variation within the SP4-bulk dataset we were then interested in further exploring which genes were underpinning the differences between the populations. We therefore performed differential expression analysis (Figure 5.7) and identified a total of 1953 significant (adjusted p-value <0.05) differentially expressed genes (DEGs) between RTEs and non-RTEs (Figure 5.7.A-B). Of the DEGs identified 991 were downregulated and 962 were upregulated with respect to their expression by RTEs (Figure 5.7.B). It was notable however, that while statistically significant the fold change (FC) associated with these DEGs generally appeared relatively modest (Figure 5.7.A). Indeed, closer examination of the log2

fold change of DEGs identified that only 316 upregulated DEGs and 242 downregulated DEGs exhibited a log2 fold change of greater than 1 or -1, respectively (Figure 5.7.C). Meaning that the majority of DEGs identified are associated with very small changes in expression between RTEs and non-RTEs. It is also clear that some of the DEGs with the greatest statistical significance display relatively modest changes in gene expression (Figure 5.7.D). For example, the most statistically significant DEG identified in our dataset was SRY-Box Transcription Factor 4 (*Sox4)*, which is upregulated in RTE with log2 fold change of 2.7. Interestingly Sox4 has previously been associated with SP4 thymocyte development[347,348]. Two other notable highly statistically significant DEGs were *Cd55* and *Ccr9* as, while again their downregulation or upregulation in RTE (respectively) was fairly modest, previous studies have associated these changes with RTE maturation (Table 5.1).

The identification of *Ccr9* and *Cd55* as notable statistically significant DEGs in our analysis also prompted us to further question the relationship between our analysis and previous investigations into RTE maturation. We therefore examined the genes in Table 5.1, which represent a selection of genes identified by previous studies of bulk SP4 or SP8 T-cell populations in mouse models as potential distinguishers of RTEs from their mature counterparts. We detected 19 of these literature genes within the bulk-SP4 dataset, 11 of which represented significant DEGs between RTEs and non-RTEs (Figure 5.7E and Table S.2). In addition to aforementioned *Cd55* and *Ccr9,* the expression of several of these significant genes was in keeping with previous observations regarding their expression by RTEs. With RTEs showing upregulation of the CD3 component *CD3g*, and the DNA methyltransferase *Dnmt3a* and downregulation of *Ly6c1* (Ly6C) and the metabolism mediators *Rptor* and *Slc7a5*.

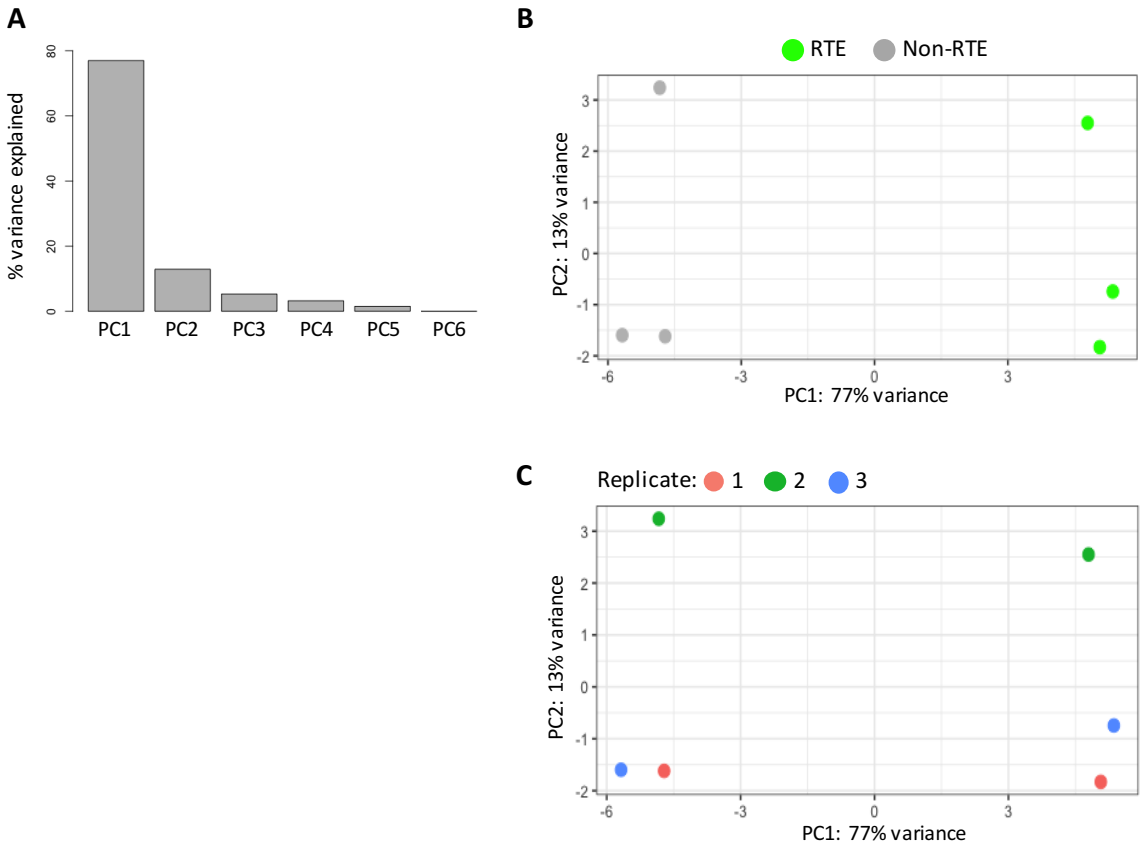
A
% variance explained
0
20
40
60
80
PC1
PC2
PC3
PC4
PC5
PC6
B
RTE
Non-RTE
PC2: 13% variance
PC1: 77% variance
C
Replicate: 1 2 3
PC2: 13% variance
PC1: 77% variance

Figure 5. 6 Principal Component Analysis Identifies RTE vs Non-RTE Identity as the Largest Source of Variation within the SP4-Bulk RNAseq Dataset

Analysis of naïve SP4 RTE and non-RTE bulk RNAseq datasets. **(A)** Scree plot of the percentage of variance explained by the top 6 principal components. **(B-C)** Individual sequenced samples plotted by the first two principal components, PC1 and PC2 (with the amount of variation each PC explains given as % of the variance). Samples are coloured by **(B)** their sorted RTE (green) or non-RTE (grey) identity or **(C)** their paired experimental replicate identity (red, green or blue).

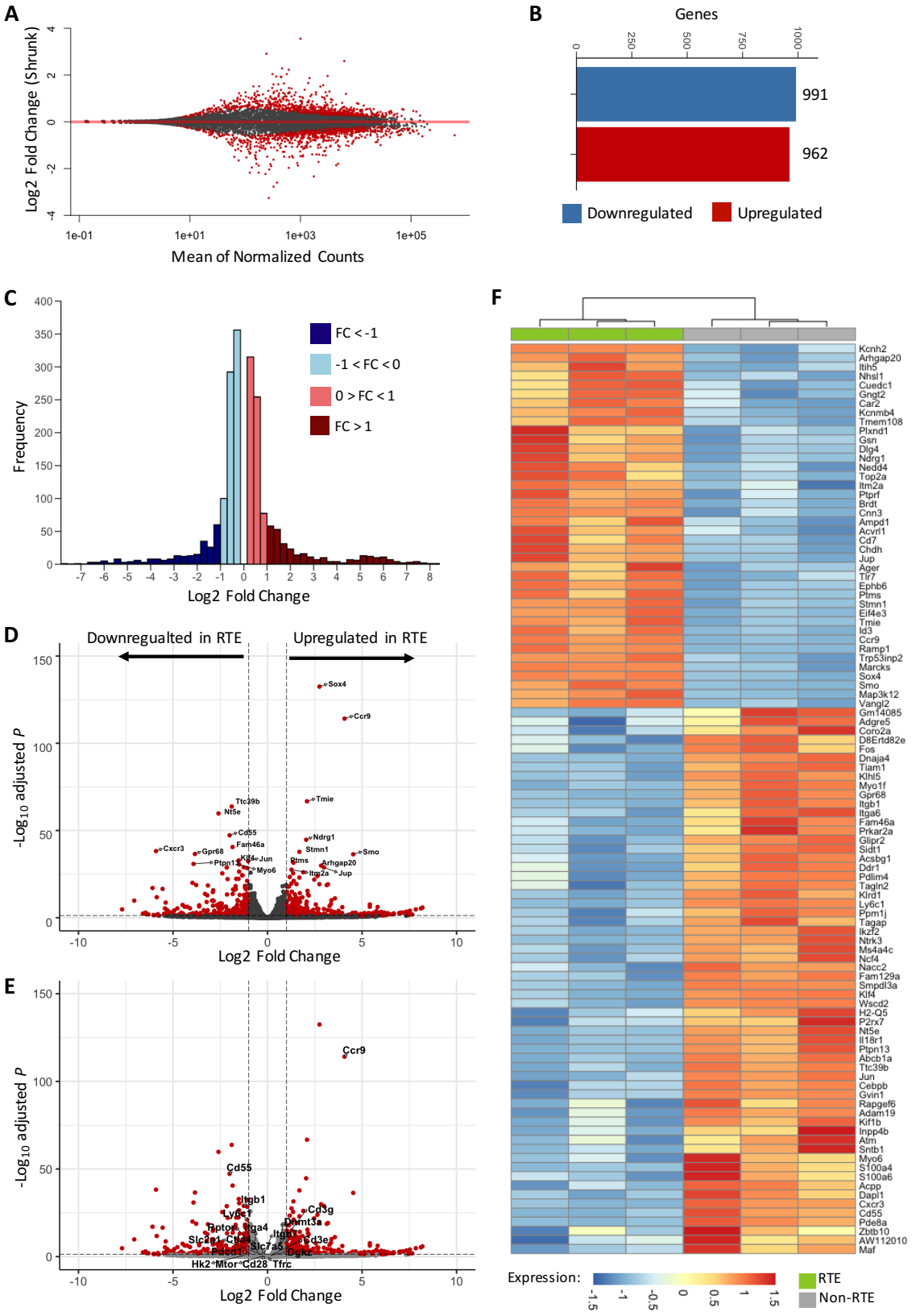
A
Log2 Fold Change (Shrunk)
Mean of Normalized Counts
B
Genes
991
962
Downregulated
Upregulated
C
Frequency
FC < -1
-1 < FC < 0
0 > FC < 1
FC > 1
Log2 Fold Change
D
Downregualted in RTE
Upregulated in RTE
-Log10 adjusted P
Log2 Fold Change
E
-Log10 adjusted P
Log2 Fold Change
F
Expression:
RTE
Non-RTE

Figure 5. 7 Differentially Expressed Genes between Bulk SP4 RTE and Mature SP4 T-cells are Associated with Modest Fold Changes

(A) MA plot comparing gene expression between RTE and non-RTE samples by plotting mean normalised counts against associated shrunken log2 fold change. Each dot represents a gene with red colouration indicating the differential expression of the gene is significant (adjusted p-value <0.05). **(B)** Bar plot of total number of significant (adjusted p-value <0.05) differentially expressed genes (DEGs) identified between RTE and non-RTE samples. Bars are grouped by whether the genes are upregulated (red) or downregulated (blue) in RTE. Numbers above bars indicate the total number of genes in each condition. **(C)** Histogram plot of the log2 fold changes of significant (adjusted p-value <0.05) DEGs. Colour scale of bars indicates differences in fold change (FC), such that genes with FC < 0 are blue with light blue indicating FC <-1 and dark blue indicating FC > -1 whereas genes with FC >0 are red, with light red indicating FC <1 and dark red indicating FC >1. Analysis of naïve SP4 RTE and non-RTE bulk RNAseq datasets. **(D-E)** Volcano plot visualising DEGs between RTE and non-RTE. Positive FCs and negative FCs of genes indicate they are up-regulated or downregulated in RTE, respectively. Red colouring indicates genes are above the statistical significant threshold (adjusted p-value < 0.05) and log2 fold change threshold (-1 >FC < 1). **(D)** Labelled genes represent the top 10 upregulated and downregulated genes by significance (adjusted p-value). **(E)** labelled genes are markers which previous studies have associated identification of RTE (detailed in Table 5.1) which were also identified within our dataset. **(F)** Heatmap showing the expression of the top 100 genes contributing to PC1 (rows) by bulk RNAseq samples (columns). Columns are grouped by unsupervised clustering and are coloured by their sorted RTE (green) or non-RTE (grey) identity. Colour scale indicates gene expression level.

However, in contrast to the previous findings, *Pdcd1* (PD1), *Ctla4*, *Itga4* and *Itgb1* were all significantly downregulated by RTEs. This differing expression pattern in our dataset may be explained to some extent by discrepancies in the type/ source of RTE examined. For instance upregulation of PD1 was reported when RTEs were defined by CD24 expression[222] but when RTEs were defined using Rag-GFP mouse models the opposite was shown[342], akin to our analysis. Regarding upregulation of CTLA4 by RTEs this has been proposed from FTOC analysis[345] while upregulation of $\alpha_4\beta_2$ integrin (comprising Itgα4 and Itgβ1) has been described in SP8 RTEs[344,346,349]. Therefore, the RTE populations in these studies may differ somewhat from our analysed RTE population (SP4 RTEs derived from an *in vivo* system) accounting for some of the discrepancy between our findings. Overall while we identified some overlap with markers previously proposed to characterise RTEs, notably many of these DEGs did not appear to be strong discriminators of RTEs and non-RTEs.

In order to better address the relevance of the identified DEGs in differentiating RTE identity, we examined which DEGs made the greatest contribution to PC1 as PCA implicated these as critical in underpinning the variation between RTE and non-RTE. Among the top 100 genes contributing to PC1 were several genes of interest (Figure 5.7.F and Table S.3). As might be expected some of the most significant DEGs were present, including *Sox4*, *Cd55* and *Ccr9*. Other DEGs of note included *Cd7* (upregulated by RTE), a marker associated with both thymocyte lymphoid lineage restriction[350] and function[351] and *Ly6c1* (which as discussed has previously been linked to RTE maturation).

Overall this differential expression analysis identifies many DEGs between RTEs and non-RTEs, some of which are particularly notable due to their previously identified relationship

with RTE identity or thymocyte development. However, it is also clear that the magnitude of the majority of gene expression changes between RTE and non-RTE populations are relatively small, suggesting a large degree of similarity between the two. However, this analysis still only considers differences between mass populations, therefore we next compared RTEs and non-RTEs from heterogeneous SP4 T-cell populations.

We began by comparing RTEs and non-RTEs within the Tconv dataset (Figure 5.8). Initial dimensional reduction approaches tSNE (Figure 5.8.A) and PCA (Figure 5.8.B) showed broad separation of cells on the basis of their RTE vs non-RTE identity, akin to findings from PCA of the total SP4-bulk dataset. Again, suggestive that RTE/non-RTE identity is critical to the variation prevalent within the dataset. Subsequent differential expression analysis between RTEs and non-RTEs identified a total of 34 significant DEGs, 11 downregulated and 23 upregulated, with respect to their expression by RTEs (Figure 5.8.C and Table S.4). Similar to findings from the SP4-bulk dataset, the magnitude of the fold changes associated with these DEGs were relatively modest (Figure 5.8.D), but the identified DEGs showed a consistent discriminatory pattern of expression between RTEs and non-RTEs (Figure 5.8.E-F). Furthermore, closer examination of some of the DEGs with the largest fold changes identified some genes of particular interest (Figure 5.8.F). These include proposed RTE markers *Ly6c1* and *Cd55*, both previously flagged in our SP4-bulk analysis, as well as *Il7r* as a downregulated DEG (with respect to RTE). Interestingly *Sox4* and *Cd7* are also among the top 10 upregulated DEGs, identifying further overlap with DEGs from our SP4-bulk analysis. Another upregulated DEG of note is *Satb1*, which has previously been identified as a post-selection lineage director for SP thymocytes[352], and from our analysis appears to be widely expressed in the RTEs but not non-RTEs.

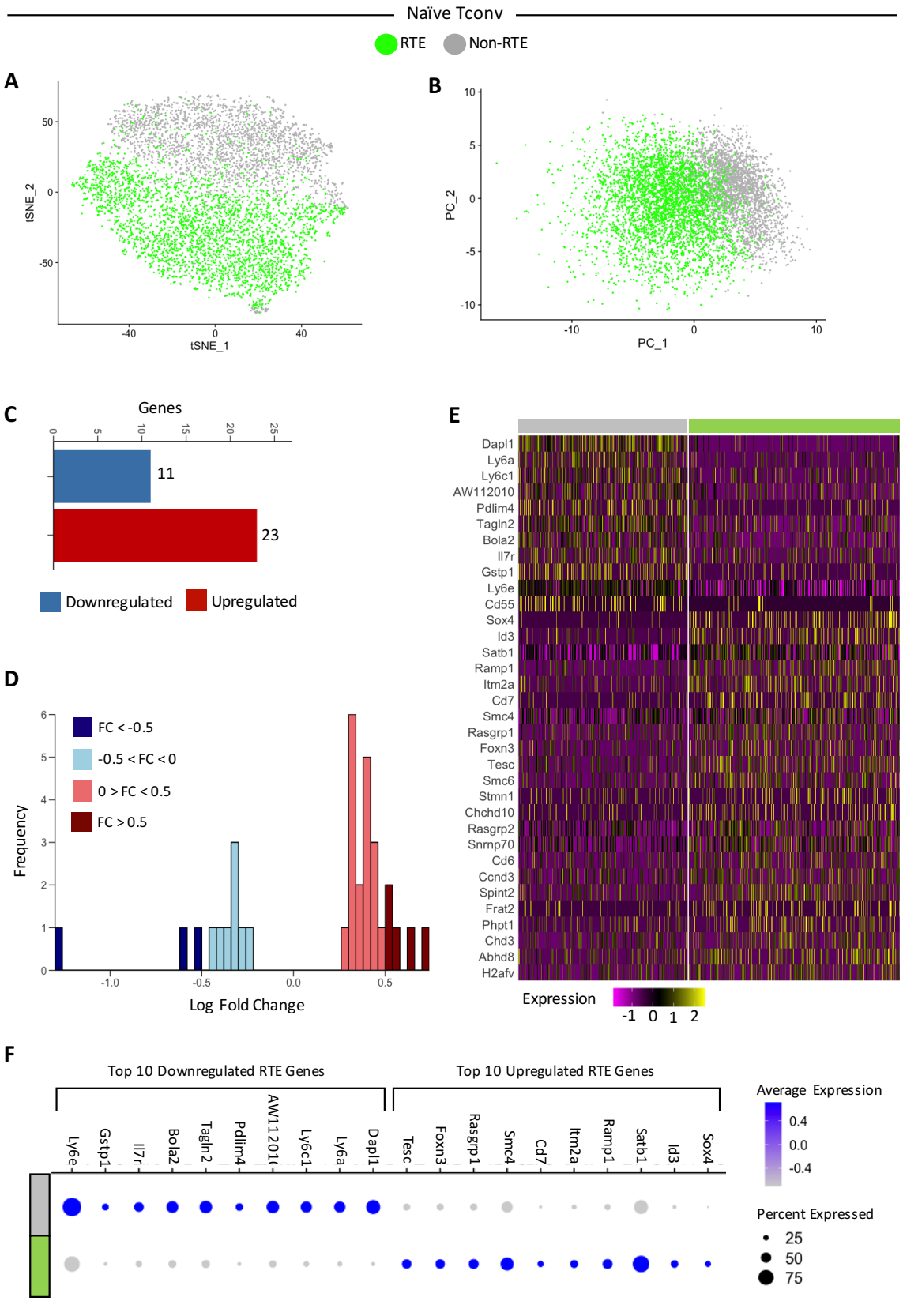
Naïve Tconv
RTE
Non-RTE
A
tSNE_2
tSNE_1
B
PC_2
PC_1
C
Genes
11
23
Downregulated
Upregulated
D
FC < -0.5
-0.5 < FC < 0
0 > FC < 0.5
FC > 0.5
Frequency
Log Fold Change
E
Dapl1
Ly6a
Ly6c1
AW112010
Pdlim4
Tagln2
Bola2
Il7r
Gstp1
Ly6e
Cd55
Sox4
Id3
Satb1
Ramp1
Itm2a
Cd7
Smc4
Rasgrp1
Foxn3
Tesc
Smc6
Stmn1
Chchd10
Rasgrp2
Snrnp70
Cd6
Ccnd3
Spint2
Frat2
Phpt1
Chd3
Abhd8
H2afv
Expression
F
Top 10 Downregulated RTE Genes
Top 10 Upregulated RTE Genes
Average Expression
Percent Expressed
25
50
75

Figure 5. 8 Variation between Tconv RTE and Mature Tconv Associated with Modest Changes in Gene Expression

Analysis of subsetted naïve SP4 Tconv RTE and non-RTE scRNAseq dataset. **(A-B)** Dimensional reduction analysis presented as **(A)** t-SNE plot of naïve Tconv cells and **(B)** PCA plot of naïve Tconv cells plotted by the first two principal components PC1 and PC2, with cells coloured by their original sort identity RTE (green) or non-RTE (grey). **(C)** Bar plot of total number of significant (adjusted p-value <0.05) differentially expressed genes (DEGs) identified between RTE and non-RTE samples. Bars are grouped by whether the genes are upregulated (red) or downregulated (blue) in RTE. Numbers above bars indicate the total number of genes in each condition. **(D)** Histogram plot of the log fold changes of significant (adjusted p-value <0.05) DEGs. Colour scale of bars indicates differences in fold change (FC), such that genes with FC < 0 are blue with light blue indicating FC <-0.5 and dark blue indicating FC > -0.5 whereas genes with FC >0 are red, with light red indicating FC <0.5 and dark red indicating FC >0.5. **(E)** Heatmap of all significant (adjusted p<0.05) DEGs (rows), with cells grouped as RTE or non-RTE (columns) as indicated. Colour scale indicates gene expression level. **(F)** Dotplot showing the expression of the top 10 upregulated and downregulated (by FC magnitude) significant RTE genes (rows) within cells grouped by their sorted RTE (green) or non-RTE (grey) identity. The size of each circle reflects the percentage of cells where the gene is detected, and the colour reflects the average expression level within the grouped cells.

We then compared RTEs and non-RTEs within the Treg dataset (Figure 5.9). Again, dimensional reduction approaches tSNE (Figure 5.9.A) and PCA (Figure 5.9.B) resulted in some separation of cells by their RTE vs non-RTE identity, although by PC1 there did appear to be greater overlap between RTEs and some non-RTEs (Figure 5.9.B). Differential expression analysis identified 140 significant DEGs, 100 downregulated and 40 upregulated, with respect to their expression by RTEs (Figure 5.9.C and Table S.5). As before though, these DEGs were generally associated with fairly modest fold changes (Figure 5.9.D). However, the identified DEGs did display a consistent discriminatory pattern of expression between RTEs and non-RTEs (Figure 5.9.E-F). Furthermore, the top 10 DEGs associated with the largest positive fold changes showed some overlap with previously identified genes, namely *Cd7* and *Satb1*. Interestingly these top DEGs also included several linked to Treg function. Notably RTEs appeared to downregulate eTreg associated genes *Klrg1*[85], *S100a11*, *S100a4* and *S100a6*[101,104,353], while upregulating cTreg associated genes *Bcl2*[85], *Klf2* and *Sell* (CD62L), the latter two of which are also important for SLO trafficking[354].

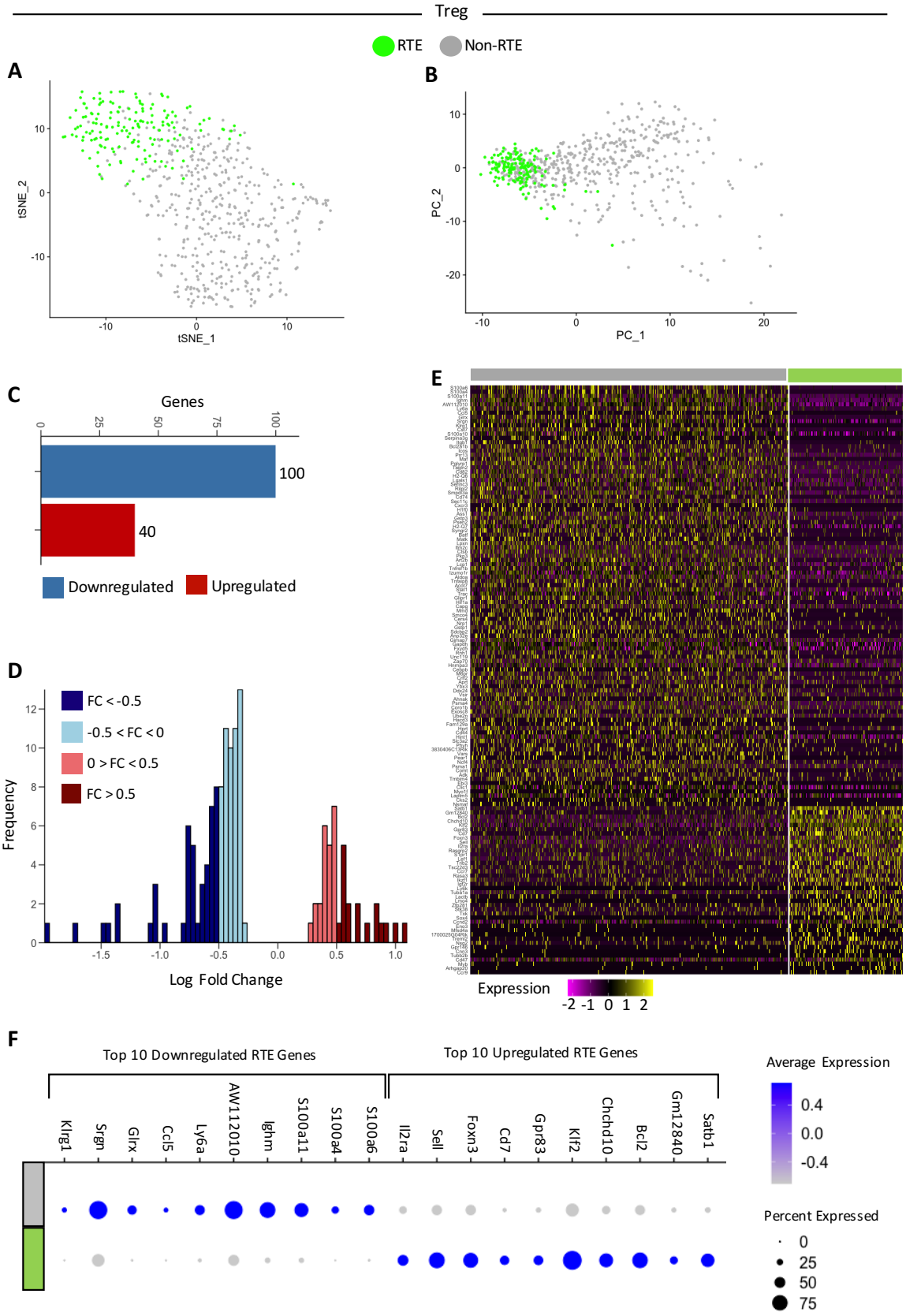
Treg
RTE
Non-RTE
A
tSNE_2
tSNE_1
B
PC_2
PC_1
C
Genes
100
40
Downregulated
Upregulated
D
FC < -0.5
-0.5 < FC < 0
0 > FC < 0.5
FC > 0.5
Frequency
Log Fold Change
E
Expression
F
Top 10 Downregulated RTE Genes
Top 10 Upregulated RTE Genes
Klrg1
Srgn
Glrx
Ccl5
Ly6a
AW112010
Ighm
S100a11
S100a4
S100a6
Il2ra
Sell
Foxn3
Cd7
Gpr83
Klf2
Chchd10
Bcl2
Gm12840
Satb1
Average Expression
Percent Expressed

Figure 5. 9 Variation between Treg RTE and Mature Treg Associated with Modest Changes in Gene Expression

Analysis of subsetted Treg RTE and non-RTE scRNAseq dataset. **(A-B)** Dimensional reduction analysis presented as **(A)** t-SNE plot of Treg cells and **(B)** PCA plot of Treg cells plotted by the first two principal components PC1 and PC2, with cells coloured by their original sort identity RTE (green) or non-RTE (grey). **(C)** Bar plot of total number of significant (adjusted p-value <0.05) differentially expressed genes (DEGs) identified between RTE and non-RTE samples. Bars are grouped by whether the genes are upregulated (red) or downregulated (blue) in RTE. Numbers above bars indicate the total number of genes in each condition. **(D)** Histogram plot of the log fold changes of significant (adjusted p-value <0.05) DEGs. Colour scale of bars indicates differences in fold change (FC), such that genes with FC < 0 are blue with light blue indicating FC <-0.5 and dark blue indicating FC > -0.5 whereas genes with FC >0 are red, with light red indicating FC <0.5 and dark red indicating FC >0.5. **(E)** Heatmap of all significant (adjusted p<0.05) DEGs (rows), with cells grouped as RTE or non-RTE (columns) as indicated. Colour scale indicates gene expression level (see Figure S.6 for enlarged heatmap). **(F)** Dotplot showing the expression of the top 10 upregulated and downregulated (by FC magnitude) significant RTE genes (rows) within cells grouped by their sorted RTE (green) or non-RTE (grey) identity. The size of each circle reflects the percentage of cells where the gene is detected, and the colour reflects the average expression level within the grouped cells.

The identification of some common DEGs between RTEs and non-RTEs from separate Treg and Tconv populations prompted us to more comprehensively compare all significant DEGs from the populations (Figure 5.10). This comparison showed a large amount of variation between the DEGs from the two populations, however we did identify 10 shared DEGs including the aforementioned *Satb1*, *Sox4* and *Cd7* (Figure 5.10.A). Furthermore, while there was some variation in both the proportion and level of expression of these DEGs between Treg and Tconv RTEs/non-RTEs (Figure 5.10.A), we observed strong correlation between the fold changes of the 10 common DEGs from Treg and Tconv datasets (Figure 5.10.B). Suggesting that the expression changes associated with these common DEGs during RTE maturation is highly similar between Treg and Tconv subsets. Overall hinting at both common and distinct maturation processes in Treg and Tconv RTE development.

In addition to comparing the DEGs generated from Treg and Tconv datasets to one another, we also decided to compare these more defined T-cell subsets with the gross SP4-bulk dataset (Figure 5.11-12). The intention being, that the identification of common DEGs across two independent analyses highlight the significance of these DEGs as consistent markers of RTE identity. Furthermore, comparable trends between the two datasets would also support the reproducibility of our findings between different sequencing approaches, in turn helping to counter the limited sample number of our scRNAseq approach.

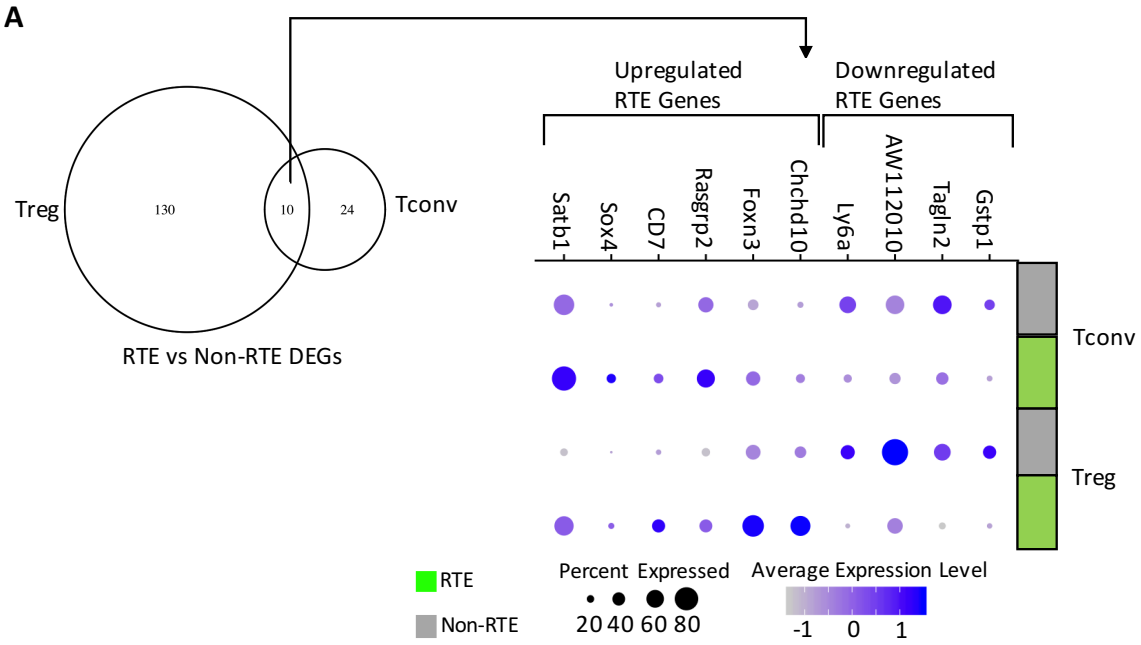
A
Treg
130
10
24
Tconv
RTE vs Non-RTE DEGs
Upregulated RTE Genes
Downregulated RTE Genes
Satb1
Sox4
CD7
Rasgrp2
Foxn3
Chchd10
Ly6a
AW112010
Tagln2
Gstp1
Tconv
Treg
RTE
Non-RTE
Percent Expressed
20 40 60 80
Average Expression Level
-1 0 1

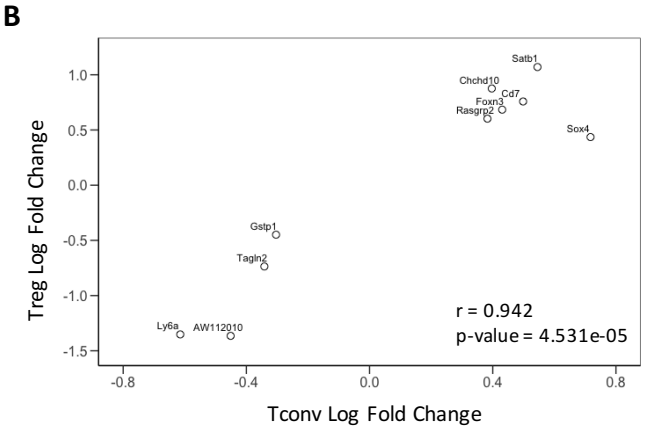
B
Treg Log Fold Change
Tconv Log Fold Change
Satb1
Chchd10
Cd7
Foxn3
Rasgrp2
Sox4
Gstp1
Tagln2
Ly6a
AW112010
r = 0.942
p-value = 4.531e-05

Figure 5. 10 Treg and Tconv RTEs Exhibit Some Common Changes in Gene Expression

Comparison of RTE and non-RTE differentially expressed genes (DEGs) between Treg and naïve Tconv. **(A)** Data presented as (left) a Venn diagram of all DEGs within Treg and naïve Tconv populations with genes common to both in the centre overlap. The numbers indicate how many genes are present within each condition. (Right) The identified 10 common genes are named and their expression visualised within RTE (green) and non-RTE (grey) from Treg and Tconv using a dotplot. The size of each circle reflects the percentage of cells where the gene is detected, and the colour reflects the average expression level within the grouped cells. **(B)** Plot comparing the fold changes (FCs) of the the 10 common RTE and non-RTE DEGs identified in (**A**) within the Treg and naïve Tconv scRNaseq datasets. Plot shows the FC of DEGs (as labelled) within the naïve Tconv dataset against the same DEGs FC within the Treg dataset. Strength of the correlation given by Pearson's correlation coefficient (r) with associated p-value.

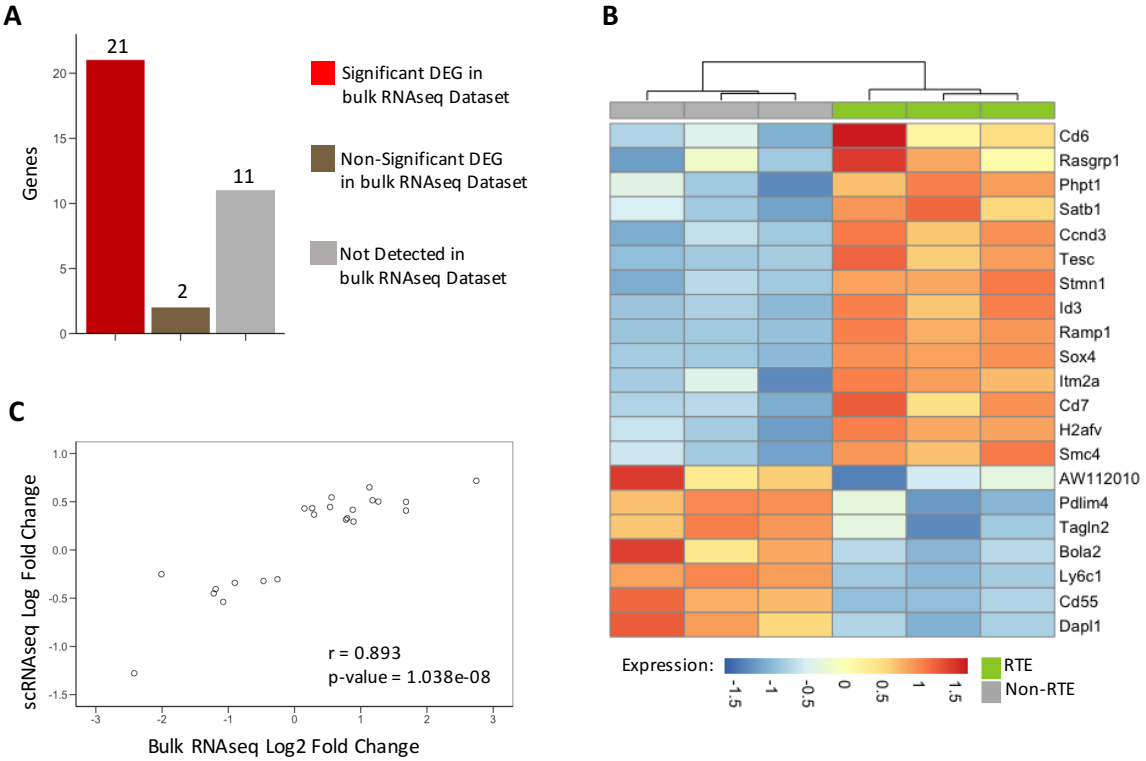
A
21
2
11
Genes
Significant DEG in bulk RNAseq Dataset
Non-Significant DEG in bulk RNAseq Dataset
Not Detected in bulk RNAseq Dataset
B
Cd6
Rasgrp1
Phpt1
Satb1
Ccnd3
Tesc
Stmn1
Id3
Ramp1
Sox4
Itm2a
Cd7
H2afv
Smc4
AW112010
Pdlim4
Tagln2
Bola2
Ly6c1
Cd55
Dapl1
Expression:
RTE
Non-RTE
C
scRNAseq Log Fold Change
Bulk RNAseq Log2 Fold Change
r = 0.893
p-value = 1.038e-08

Figure 5. 11 Changes in Gene Expression Observed in Naïve Tconv scRNAseq Analysis are Highly Comparable with Bulk RNAseq Analysis

Comparison of RTE and non-RTE DEGs detected from subsetted naïve SP4 Tconv scRNAseq analysis with DEGs detected by naïve SP4 Tconv Bulk RNAseq Analysis. **(A)** Barplot of the DEGs detected in the naïve Tconv scRNAseq dataset categorised by their relationship with the bulk RNAseq dataset. Genes are quantified in three categories: the gene is also a significant DEG in the bulk RNAseq dataset (red), the gene is a non-significant DEG in the bulk RNAseq dataset (brown), the gene was not detected in the bulk RNAseq dataset (grey). Numbers above bars indicate the total number of genes in each condition. **(B)** Heatmap showing the expression of the DEGs which are significant in both the naïve Tconv scRNAseq dataset and bulk RNAseq dataset (rows) by bulk RNAseq samples (columns). Columns are grouped by unsupervised clustering and are coloured by their sorted RTE (green) or non-RTE (grey) identity. Colour scale indicates gene expression level. **(C)** Plot comparing the fold changes (FCs) of all DEGs that were detected in both the bulk RNAseq dataset and the naïve Tconv scRNAseq dataset. Plot shows the FC of DEGs within the bulk RNAseq dataset against the same DEGs FC within the naïve Tconv scRNAseq dataset. Strength of the correlation given by Pearson's correlation coefficient (r) with associated p-value.

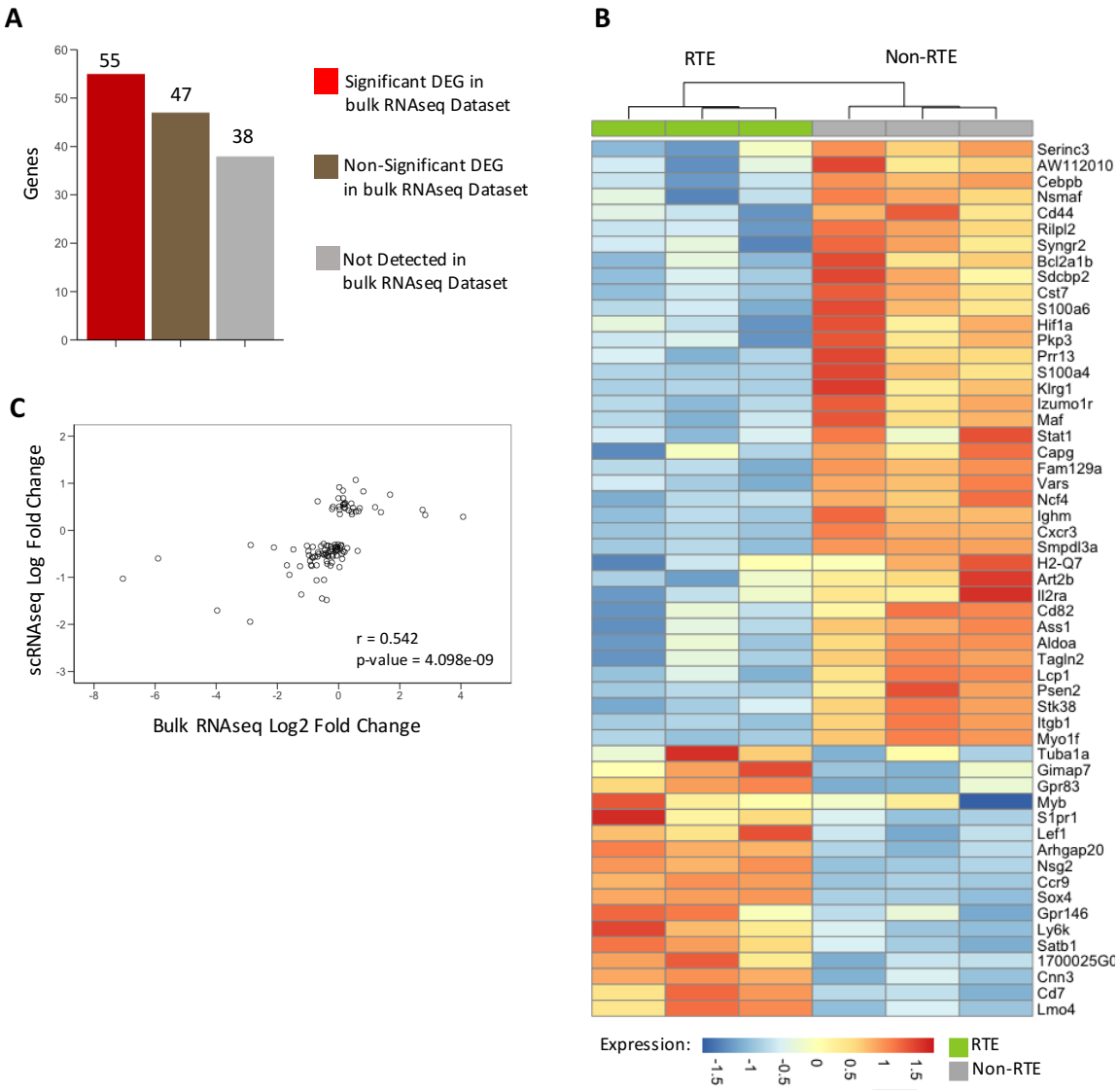
A
55
47
38
Genes
Significant DEG in bulk RNAseq Dataset
Non-Significant DEG in bulk RNAseq Dataset
Not Detected in bulk RNAseq Dataset
B
RTE
Non-RTE
Serinc3
AW112010
Cebpb
Nsmaf
Cd44
Rilpl2
Syngr2
Bcl2a1b
Sdcbp2
Cst7
S100a6
Hif1a
Pkp3
Prr13
S100a4
Klrg1
Izumo1r
Maf
Stat1
Capg
Fam129a
Vars
Ncf4
Ighm
Cxcr3
Smpdl3a
H2-Q7
Art2b
Il2ra
Cd82
Ass1
Aldoa
Tagln2
Lcp1
Psen2
Stk38
Itgb1
Myo1f
Tuba1a
Gimap7
Gpr83
Myb
S1pr1
Lef1
Arhgap20
Nsg2
Ccr9
Sox4
Gpr146
Ly6k
Satb1
1700025G0
Cnn3
Cd7
Lmo4
Expression:
-1.5
-1
-0.5
0
0.5
1
1.5
RTE
Non-RTE
C
scRNAseq Log Fold Change
r = 0.542
p-value = 4.098e-09
Bulk RNAseq Log2 Fold Change

Figure 5. 12 Changes in Gene Expression Identified in Treg scRNAseq Analysis are Less Consistent with Bulk RNAseq Analysis

Comparison of RTE and non-RTE DEGs detected from subsetted Treg scRNAseq analysis with DEGs detected by naïve SP4 Tconv Bulk RNAseq Analysis. **(A)** Barplot of the DEGs detected in the Treg scRNAseq dataset categorised by their relationship with the bulk RNAseq dataset. Genes are quantified in three categories: the gene is also a significant DEG in the bulk RNAseq dataset (red), the gene is a non-significant DEG in the bulk RNAseq dataset (brown), the gene was not detected in the bulk RNAseq dataset (grey). Numbers above bars indicate the total number of genes in each condition. **(B)** Heatmap showing the expression of the DEGs which are significant in both the Treg scRNAseq dataset and bulk RNAseq dataset (rows) by bulk RNAseq samples (columns). Columns are grouped by unsupervised clustering and are coloured by their sorted RTE (green) or non-RTE (grey) identity. Colour scale indicates gene expression level. **(C)** Plot comparing the fold changes (FCs) of all DEGs that were detected in both the bulk RNAseq dataset and the Treg scRNAseq dataset. Plot shows the FC of DEGs within the bulk RNAseq dataset against the same DEGs FC within the Treg scRNAseq dataset. Strength of the correlation given by Pearson's correlation coefficient (r) with associated p-value.

Of the two scRNAseq datasets, we anticipated that the greatest correlation would be observed between the Tconv dataset and the SP4-bulk dataset, given that Tconvs represent the majority of the SP4 T-cell population. Indeed, excluding those not detected in the SP4-bulk dataset, the vast majority of Tconv dataset DEGs also proved to be significant DEGs within the SP4-bulk dataset (Figure 5.11.A-B). Notable among these shared DEGs were the downregulated RTE DEGs *Ly6c1*, *Dapl1* and *Cd55* and the upregulated RTE DEGs *Sox4* and *Cd7* (Figure 5.11.B) all of which had previously proven distinguished differentiators of RTE and non-RTE identity, by fold change magnitude or PC1 contribution, within either or both the scRNAseq and bulk RNAseq datasets (respectively). In addition to a large proportion of shared significant DEGs, the fold changes of the detected DEGs showed a strong correlation between the two RNAseq datasets (Figure 5.11.C), further emphasising the consistency of changing expression patterns that characterise RTE identity across the two RNAseq datasets.

We also compared the SP4-bulk dataset with the Treg dataset, with the expectation that more discrepancies in the DEGs detected may be observed since Treg represent only a small proportion of the total SP4 T-cell population. Accordingly, excluding those not detected in the SP4-bulk dataset, around half of the Treg dataset DEGs also proved to be significant DEGs within the SP4-bulk dataset (Figure 5.12.A). Likely reflective of the expected disparity between the T-cell populations the two datasets represent. Interestingly again, among the shared significant DEGs were several previously highlighted for their PC1 contribution (SP4-bulk dataset) or fold change magnitude (Treg dataset), including *Sox4*, *Cd7* and *Ccr9* (Figure 5.12.B). Similarly, while fewer DEGs are shared between the Treg scRNAseq and SP4-bulk datasets, there is reasonable correlation

between the fold changes of the detected DEGs (Figure 5.12.C). However, the correlation between these two datasets is more modest than the strong correlation observed between Tconv and SP4-bulk dataset (Figure 5.11.C). This is in keeping with not only the expected discrepancy between Treg and total SP4 T-cell population but also the differences in DEGs detected between Treg and Tconv datasets (Figure 5.10). Further emphasising that analysis of SP4 T-cells as a gross population while possibly suffice to capture changes within a highly prevalent subset, may not be fully representative of changes occurring in more minor subsets.

Overall this comparative analysis between our three different RNAseq datasets highlighted some interesting consistent variation in gene expression between RTEs and non-RTEs. However, one limitation of all RNAseq analysis is that variation in gene expression does not guarantee variation in protein expression. Therefore, for robustness we intended to follow-up a selection of identified DEGs using Flow Cytometry analysis in Rag-GFP mice to look at DEG protein expression between defined RTE/non-RTEs. From this analysis, we hoped to reaffirm the findings in the RNAseq analysis and thereby gain further insight into RTE biology and potentially identify markers which could be used to discriminate RTEs by flow cytometry. We decided to focus on DEGs which appeared to be common to Tregs and Tconvs, as universal RTE markers would be most practical for future RTE discrimination. Similarly, we also sought to select those DEGs which presented as strong candidates to differentiate RTEs and non-RTEs. We therefore considered both the characteristics of the DEG's expression across the three RNAseq datasets alongside any documented relationship to T-cell development/function in the wider literature. Finally, we also considered the practicality of assessing these markers in the wet-lab, opting only for those

which may be possible to follow up by flow cytometry. Ultimately we selected five DEGs (Table 5.2), many of which have already been discussed in this section and therefore are only described briefly below.

Notably, *Cd7*, *Satb1* and *Sox4* all stood out as positive markers of RTEs whose upregulation was statistically significant across all three RNAseq datasets. Indeed, these markers have all been highlighted previously here for their prominence within the individual RNAseq datasets (being among either the top 100 DEGs contributing to PC1 in the SP4-bulk dataset analysis or DEGs within the top 10 fold change magnitudes in the Tconv/Treg dataset analysis) and for their documented association with thymic T-cell development. However, these three may pose a challenge for flow cytometry analysis as commercial available anti-mouse antibodies are un-conjugated and of variable clonality. Furthermore, Sox4 and Satb1 are intracellular which also presents some challenges considering the Rag-GFP system.

More straightforward protein targets are presented by the remaining DEGs, *Ccr9* and *Ly6a*, as both are surface expressed with commercially available conjugated monoclonal anti-mouse antibodies. Though on the other hand, these DEGs differential expression were not universally significant across the RNAseq datasets. However, *Ly6a* is likely only not universally significant because it was not detected in the SP4-bulk RNAseq dataset as its downregulation was significant and among the top 10 fold changes for both Tconvs and Tregs (Table 5.2). Furthermore, while Ly6A is expressed by some naïve SP4 T-cells[355], its expression varies across SP4 thymocyte development, and notably downregulation of Ly6A at certain thymocyte stages is important for developmental progression[356].

Similarly, CCR9, an aforementioned marker of SP8 RTEs (Table 5.1), was significantly upregulated in both the Treg dataset and the SP4-bulk dataset (where it also was a top 100 PC1 contributor) but not in the Tconv dataset. However, the Tconv and SP4-bulk datasets represent largely overlapping populations suggesting the uniformity of this DEG. Possibly the lack of significance within Tconvs is due to dropout issues with *Ccr9* in the scRNAseq as detection of *Ccr9* was low across cells.

Ultimately, due to time constraints, it was not feasible to complete this validation analysis within the PhD timeframe, however this selection of genes remains of outstanding interest to RTE biology and discrimination.

Table 5. 2 Details of Suspected Common DEGs between RTE and Non-RTEs Selected for Follow-Up Protein Validation Analysis

Marker	Type of RTE Marker	Expression in RNAseq Datasets						Relevance in Literature	Commercial Antibody Availability
		SP4 bulk RNAseq		Tconv scRNAseq		Treg scRNAseq			
		Adj P <0.05	Top PC1	Adj P <0.05	Top FC	Adj P <0.05	Top FC		
Sox4	Positive	✓	✓	✓	✓	✓	**X**	Regulator of thymocyte development [347,348]	Unconjugated Polyclonal
CD7	Positive	✓	✓	✓	✓	✓	✓	Marker of thymocyte development [350] Regulator of thymocyte function[351]	Unconjugated Monoclonal
Satb1	Positive	✓	**X**	✓	✓	✓	✓	Regulator of thymocyte development [352,357]	Unconjugated Monoclonal
Ly6a	Negative	**X** (Not detected)		✓	✓	✓	✓	Marker of Naïve SP4 T-cells, variable marker of SP4 thymocytes [355,356] Down-regulation linked to progression of thymocyte development stages[356]	Conjugated Monoclonal
CCR9	Positive	✓	✓	**X** (possible dropout)		✓	**X**	Mediator of SP8 RTE homing[313]	Conjugated Monoclonal

5.3 Discussion

5.3.1 Gene Expression Changes Characterising RTE Maturation

Overall our bioinformatics analysis, including dimensional reduction analysis and associated DEGs, did identify differences in the genetic profiles of SP4 RTEs and their mature counterparts including within Tconv and Treg subsets (Figure 5.6 – Figure 5.9). Furthermore, whilst the majority of RTE/non-RTE DEGs were not shared between Tconv and Treg subsets, there were some DEGs common to both (Figure 5.10). This mixture of shared and differential DEGs is suggestive of conserved and lineage specific features of RTE development (respectively) between Tregs and Tconvs. In addition to these global inferences, certain common and lineage specific DEGs also stand out for what they may suggest about Treg and Tconv RTE biology and in particular how this may link with or diverge from previously described gross SP4/SP8 RTE maturation.

5.3.1.1 Possible Common Features of Treg and Tconv RTEs

For instance, perhaps the most fundamental characteristic of gross SP4/SP8 RTEs is that upon thymic egress they require a period of post-thymic maturation prior to entering the naïve T-cell pool[157,199,342]. Similarly, our analysis suggested that Treg and Tconv RTEs may undergo a post-thymic maturation period as several prominent DEGs expressed by both subsets were linked with T-cell development and differentiation (Figure 5.7 – Figure 5.9). Furthermore, there may also be a common component to the post-thymic maturation of these two lineages. As notably both Treg and Tconv RTEs expressed higher levels of the TFs Satb1 and Sox4, both of which orchestrate T-cell development through mechanisms which may also be relevant to RTE maturation, as outlined below.

Firstly with regard to Sox4, initial reports suggested a role in early thymocyte development, as Sox4 deficiency results in impaired DP and SP thymocyte populations[347]. However subsequent work suggests that, within the αβ lineage, only iNKT-cells were reliant on Sox4, which regulated thymic iNKT-cell development by inducing MicroRNA-181 (Mir181) to enhance TCR mediated $Ca2^{+}$ flux[348]. Enhanced TCR signalling has previously been linked with gross SP4/SP8 RTEs as murine SP8 RTEs proved more responsive to both high-affinity and low-affinity antigens *in vitro*[346]. Furthermore observations of human cord blood (CB) SP4 T-cells (believed to primarily composed of RTEs) and SP4 RTEs showed enhanced TCR mediated $Ca2^{+}$ flux which they also associated with higher levels of Mir181[358]. In combination, this might suggest that, akin to its regulation of thymic iNKT-cell development, Sox4, via Mir181, regulates Treg and Tconv RTE maturation through altered TCR signalling.

Similarly, Satb1 has been heavily connected to thymocyte development not only as a regulator of early thymocyte development[357] but also as an orchestrator of later lineage decisions, including establishing SP4 and Treg lineages[352]. Furthermore, Satb1's regulation of T-cells extends beyond the thymus as it has also been linked to peripheral Th2 differentiation[359]. Interestingly one proposed regulator of Satb1 in the context of Th2 differentiation is the NF-κB signalling pathway[359], which has previously proved necessary in driving some features of RTE maturation[199]. Moreover Runx1, another suspected regulator of RTE maturation[200], is predicted as one of the top TFs bound by Satb1[360]. Therefore, Satb1 appears to represent both a downstream target and an upstream regulator of two known gross SP4/SP8 RTE maturation signalling pathways and thus in this manner may be able orchestrate Treg and Tconv RTE maturation.

Another described feature of gross SP4/SP8 RTEs, which our analysis may suggest as common to both Treg and Tconv RTEs, is their ability to home to non-lymphoid tissue. Studies suggest that bulk SP4 and SP8 RTEs homing to the liver or gut, respectively[313–315], with CCR9 a key mediator of SP8 RTE gut homing[313]. Notably, in our analysis, CCR9 was upregulated by both Treg and Tconv RTEs, thereby raising the possibility that these SP4 subsets also home to the gut via CCR9. However it should be noted that while previous analysis linking SP8 RTEs to the gut did not directly examine SP4 RTEs[313], they did transfer both SP4 and SP8 thymocytes and reported the ratio which homed to the peripheral lymph node versus the small intestine. The ratios of SP4 and SP8 thymocyte homing appeared quite similar suggesting some homing by SP4 thymocytes to the gut. However, this study also reported that *Ccr9*$^{-/-}$ and *Ccr9*$^{+/+}$ SP4 thymocytes exhibited equivalent homing abilities. Collectively suggesting, that SP4 RTEs can home to the gut and while CCR9 may be involved, it is non-essential. Therefore, CCR9 upregulation may not be indicative of enhanced gut homing ability of Treg or Tconv RTEs.

5.3.1.2 Possible Lineage Specific Features of Treg and Tconv RTEs

Thus far we have discussed possible common traits, suggested by common DEGs, between Treg and Tconv RTEs, however not all changes in gene expression were conserved between these lineages (Figure 5.10). These distinct DEGs between Treg and Tconv RTEs/non-RTEs may be indicative of lineage specific features of these RTE subsets. Furthermore, some of these lineage specific DEGs suggest that certain aspects of characterised gross SP4 RTE biology may only be prevalent within the Tconv lineage.

For instance, we noted higher expression of IL7Ra by non-RTEs relative to RTEs within the Tconv but not Treg population (Figure 5.8 and Figure 5.9). Upregulation of IL7Ra during post-thymic maturation of gross SP4 T-cells has previously been described and seems necessary for the homeostatic survival and proliferation of mature cells[157,199]. Notably IL-7 signalling has also been described as important in the homeostasis of mature Tregs[361]. Therefore, our observation that Treg RTEs and non-RTEs express comparable levels of IL7Ra, suggests their equivalent competency in responding to homeostatic signals. Implying that at least in some aspects of their phenotype Treg RTEs may be at a more mature stage of development compared to their Tconv RTE counterparts.

Similarly, our analysis may hint of differing susceptibilities of Treg and Tconv RTEs to complement. As we observed lower expression of the complement regulator CD55 by Tconv RTEs (relative to non-RTEs) but not Treg RTEs (Figure 5.8 and Figure 5.9). Previous studies of total gross SP4 RTEs also identified they expressed lower levels of CD55 relative to their mature counterparts[214], and importantly this reduced expression was linked with increased susceptibility of these RTEs to removal by complement[214]. Therefore, given that we observed no significant difference in CD55 expression between Treg RTEs and non-RTEs, this may suggest that Treg RTEs are more protected from complement as a population than Tconv RTEs. However, one caveat to this conclusion is that in our analysis we only detected expression of CD55 in relatively few individual Tregs. This may be an issue of dropout, but alternatively it might suggest that as a population Tregs largely lack CD55, in keeping with previous reports of low expression of CD55 by Tregs[362]. Furthermore this study also reported that within Tregs, protection from complement is mediated by Crry and CD59, not CD55[362]. As we did not detect Crry or CD59 in our Treg analysis, we cannot

address whether these markers are also expressed at comparable levels between Treg RTEs and non-RTEs. Therefore, the differing regulation of CD55 by Tconv and Treg RTEs in their transition to maturity may not be indicative of differing susceptibilities of the two RTE populations to complement.

Crucially though, the fact that both CD55 and IL7Ra are not significant DEGs associated with Treg RTE maturation highlights that previously described markers of gross SP4 RTEs may be subjective to the type of SP4 RTE. On this note, intriguingly many of the changes in gene expression which appeared unique to Treg RTEs/non-RTEs were more associated with differentiation of heterogeneous Treg subsets than known RTE markers (Figure 5.9). Notably Treg RTEs downregulated markers associated with eTreg differentiation (e.g. Klrg[85], S100a11, S100a4 and S100a6[101,104,353]) while upregulating cTreg markers (e.g. Bcl2[85], Klf2, Sell[354]). This predominance of a cTreg phenotype versus an eTreg phenotype in Treg RTEs and non-RTEs (respectively) may reflect the dominance of cTreg as a population on thymic egress. Indeed cTregs have previously been proposed as sole thymic leavers[85] and while our work disagrees with this homogenous view of thymic Treg development and export, our previous analysis of Treg RTEs does suggest a predominantly CD62L^{hi}/ cTreg-like phenotype (Figure 3.8). Therefore, this collection of DEGs linked to Treg heterogeneity, may reflect differences in the prevalence of Treg subsets on thymic export compared to within the mature population. Alternatively, these DEGs may be a consequence of our loose definition of Treg non-RTEs. As, while Tconv non-RTEs were defined as naïve T-cells, to exclude Rag-GFP^{-} effector cells which differentiate from mature peripheral naïve T-cells, Treg non-RTEs were simply defined as Rag-GFP^{-} due to the unclear timing of differentiation of Treg subsets. Therefore, it is possible that some of the variation

we identified may be independent of RTE maturation and instead associated with subsequent effector differentiation.

5.3.2 Similarity of SP4 RTE and Non-RTE Genetic Profiles

Importantly, though our analysis identifies statistically significant changes in gene expression between SP4 RTEs and their mature counterparts, these changes generally represented only modest fold changes in expression (Figure 5.7). This was also the case when SP4 cells were split into Tconv and Treg subsets (Figure 5.8 and Figure 5.9). These modest changes in gene expression suggest a large degree of similarity between the genetic profiles of RTEs and non-RTEs within these SP4 populations. As such our findings are reminiscent of previous RNAseq analysis comparing mature SP4 thymocytes (defined as $CD24^-$) with naïve SP4 T-cells[363]. Whilst this data is not a direct assessment of RTE maturation, as RTEs and non-RTEs are not separately identified within their defined naïve SP4 T-cell population, it does offer some insight into the changes occurring post-thymic egress. Encouragingly, in alignment with our own findings, among the genes upregulated by naïve SP4 T-cells, relative to mature SP4 thymocytes, were Dapl1, CD55 and Ly6C, which we identified as upregulated by mature naïve SP4 Tconvs with respect to RTEs. However, these DEGs were among only a handful of significant genes upregulated with a fold change of greater than 2. Thus, suggesting that the late stages of thymocyte development and the final mature naïve peripheral state are highly comparable. This combined with our own findings of relatively modest changes in gene expression between SP4/Treg/Tconv RTE and non-RTE populations might be suggestive that thymocyte development is largely completed intrathymically and that post-thymic maturation of RTEs is a subtler stage of T-cell development.

Furthermore, it is possible that in part the modest gene expression changes between SP4/Treg/Tconv RTEs and non-RTEs are a consequence of an ongoing progressive maturation within the RTE population. Indeed the proposed duration of the post-thymic maturation period undertaken by gross SP4/SP8 RTEs is between 2-3 weeks[342], a rather extended period of development especially considering that post-selection maturation is estimated as taking only 4-5 days[26]. Moreover previous investigations have demonstrated that gross SP4 RTEs grouped by Rag-GFP intensity as GFP^{high} or GFP^{low}, display differing expression of phenotypic markers with expression levels of the GFP^{lo} RTEs most similar to mature T-cells[157]. Suggesting that changes in phenotypic markers can be protracted over this prolonged period. There are also suggestions that this prolonged period of development may in fact encompass several independent development processes, as it was noted that upregulation of IL7Ra took only 6-9 days[199], and that different signalling pathways might contribute to different facets of RTE maturation[199,215]. Therefore, it is likely that SP4/Treg/Tconv RTEs do not represent a homogeneous distinct population but rather a complex heterogeneous mixture of cells at different stages of post-thymic maturation.

Interestingly, our scRNAseq clustering analysis of Tconvs (although not Tregs) identified distinct clusters within the RTE population (Figure 5.4). While these clusters are not fully explored here, it is tempting to speculate that these clusters may represent Tconv RTEs at different stages of maturation and consequently exhibiting subtle changes in gene expression. Furthermore, distinct clusters were also identified within the mature naïve Tconv population, again perhaps suggesting unappreciated subtle genetic changes within this population, possibly related to cell age or some unappreciated heterogeneity. To

further investigate how these clusters might fit with a progressive maturation within the Tconv RTE population, trajectory analysis tools could be utilised. In particular, RNA velocity analysis could be applied to our data to give more detailed insight into the possible progressive maturation of RTEs, as this tool uses information on unspliced and spliced mRNAs to predict cell progression in an unbiased manner[364].

5.3.3 Concluding Remarks

As summarised in Figure 5.13, overall in this chapter we identified differences in gene expression between SP4, Tconv and Treg RTEs and their mature counterparts. Some of these changes appear to be conserved between the two lineages while others are lineage specific, which may translate to shared and distinct traits of Treg and Tconv RTE maturation. However, while our analysis supports some form of post-thymic maturation of SP4 RTEs, it appears to be associated with only modest gene expression changes, implying an underlying similarity between SP4 RTEs and their mature counterparts. This similarity may help to explain the ongoing challenge in distinguishing RTEs from their mature counterparts and suggests they will remain a difficult population to confidently identify outside the Rag-GFP system.

A

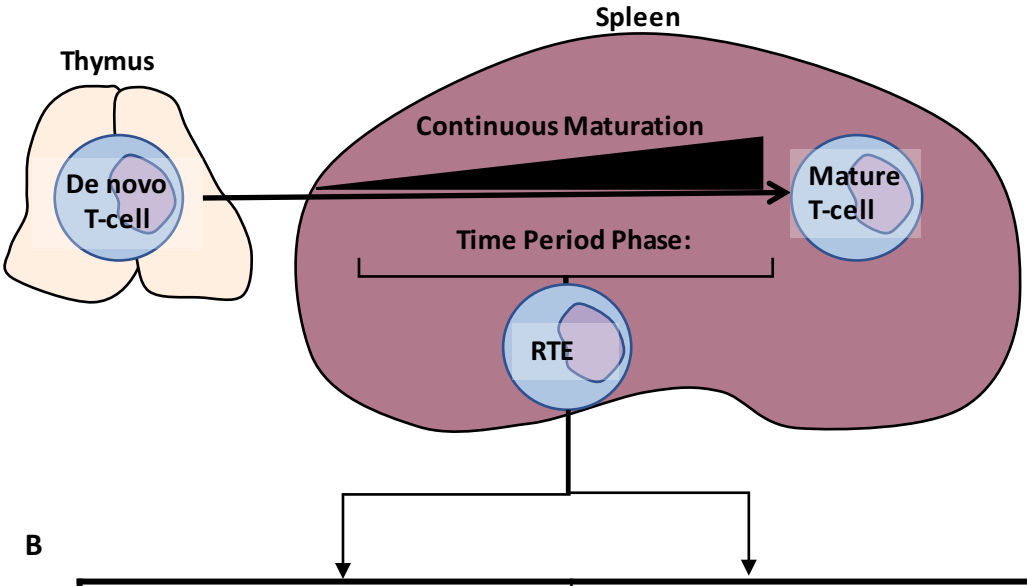

B

Tconv RTE ($CD25^-$ $Foxp3^-$)	Treg RTE ($CD25^+$ $Foxp3^+$)
Possible Common Features of RTEs*	
↓Maturity/ Evidence of ongoing T-cell development? ↑ Sox4 and Satb1: TFs linked to T-cell differentiation ↑ Overlap with thymocyte phenotype (e.g. ↑CD7, ↓Ly6a)	
↑ Responsivity to TCR signals? ↑Sox4 (possibly enhanced TCR signalling via Mir181)	
↑ Gut Homing Ability? ↑CCR9	
Possible Lineage Specific Features of RTEs*	
↑ Susceptibility to complement ↓CD55	= Susceptibility to complement? = CD55
↓Responsivity to Homeostatic Signals ↓IL7Rα	= Responsivity to Homeostatic Signals =IL7Rα
N/A	↑ Prevalence of cTreg phenotype ↑cTreg genes ↓ eTreg genes

*relative to mature counterparts

Figure 5. 13 Summary Diagram of SP4 RTE Development Stage

Proposed overview of **(A)** how broadly SP4 RTEs may fit within SP4 T-cell development and **(B)** specific features of the Treg and Tconv RTE subsets within the SP4 RTE population.

(A) Overall our analysis suggests that SP4 RTEs do not represent a molecularly distinct subpopulation between thymocyte and mature T-cell but rather SP4 RTEs seem to represent a stage in a progressive maturation.

(B) Comparison of distinguishing features of Treg and Tconv RTEs, relative to their mature counterparts. Distinguishing features are divided into possible common or lineage specific traits, based on whether there is evidence that the change is common or not to both types of RTEs, respectively. The suspected behaviour/characteristics of the RTE is detailed first, with the associated gene expression changes implying this trait detailed below.

CHAPTER SIX:
GENERAL DISCUSSION

Thymic Tregs are essential enforcers of peripheral tolerance and while the re-direction of auto-reactive thymocytes into the Treg lineage has become increasingly well characterised, there is still uncertainty surrounding the generation of thymic Tregs. Therefore, within our study we re-examined *de novo* thymic Treg development, to investigate the intrathymic and post-thymic processes which might contribute to a tolerance enforcing Treg population.

6.1 Considerations for Models Used to Investigate De Novo Treg Development

Our characterisation of intrathymic and post-thymic Treg development across this study was heavily dependent upon the Rag-GFPxFoxp3-RFP model. This model has proved a valuable tool in our analysis primarily for its ability to distinguish new and mature cells. Indeed our analysis, in agreement with recent studies[234,235], highlights the critical need to identify and exclude mature recirculating/retained cells in the thymus from investigations of *de novo* thymic Treg and Treg precursor populations. However, whilst here we utilised Rag-GFP to distinguish new and mature thymocytes, discriminatory cell markers for these populations are emerging[189,234]. For instance, CD73 reportedly distinguishes *de novo* and mature SP4 thymocytes as $CD73^-$ and $CD73^+$ respectively[189]. Similarly, *de novo* thymic Tregs and Treg precursors have also been described as largely $CCR6^-CCR7^+$ compared to $CCR6^+CCR7^-$ mature thymic counterparts[234]. Our analysis would support this latter definition in particular, as broadly we observed that all *de novo* Tregs were $CCR7^+$ and we detected only a few Tregs with slightly higher CCR6 levels (Figure 3.3). However, regarding the former, we identified a more prevalent proportion of Rag-GFP^+ Tregs with a higher expression of CD73 (Figure 3.3). This may reflect reports that while virtually all $CD73^-$ thymocytes are Rag-GFP^+, so too are approximately 15% of $CD73^+$ thymocytes[189]. Thereby

emphasising a need for caution when using such markers to discriminate new and mature thymic Tregs. As the *de novo* populations isolated, though potentially consisting entirely of newly produced cells, may not encapsulate the full diversity of the whole *de novo* population. Therefore, our analysis advocates that Rag-GFP remains the gold-standard for ensuring that all *de novo* Tregs are considered, as summarised in Figure 6.1.

Our analysis also highlights the benefit of combining Rag-GFP with Foxp3-RFP to identify thymic Tregs. One unique opportunity offered by this model was the possibility to obtain purified live Rag-GFP^{+} Tregs by cell sorting. This was essential for our analysis of CD62L^{hi} *de novo* Treg fate using RTOCs (Figure 3.6), and would be necessary for further experiments seeking to characterise the developmental potential of *de novo* thymic Treg or Treg precursor populations. Furthermore, investigations into the function of *de novo* thymic Tregs could also utilise this model to sort Treg populations for transfer into *in vivo* autoimmune models or *in vitro* suppression assays. This dual model was also beneficial in our characterisation analysis, as it enabled co-detection of Rag-GFP and Foxp3 without intracellular staining. Enabling us to identify *de novo* Tregs with minimal manipulation, and thereby gain a more representative view of thymic Treg development.

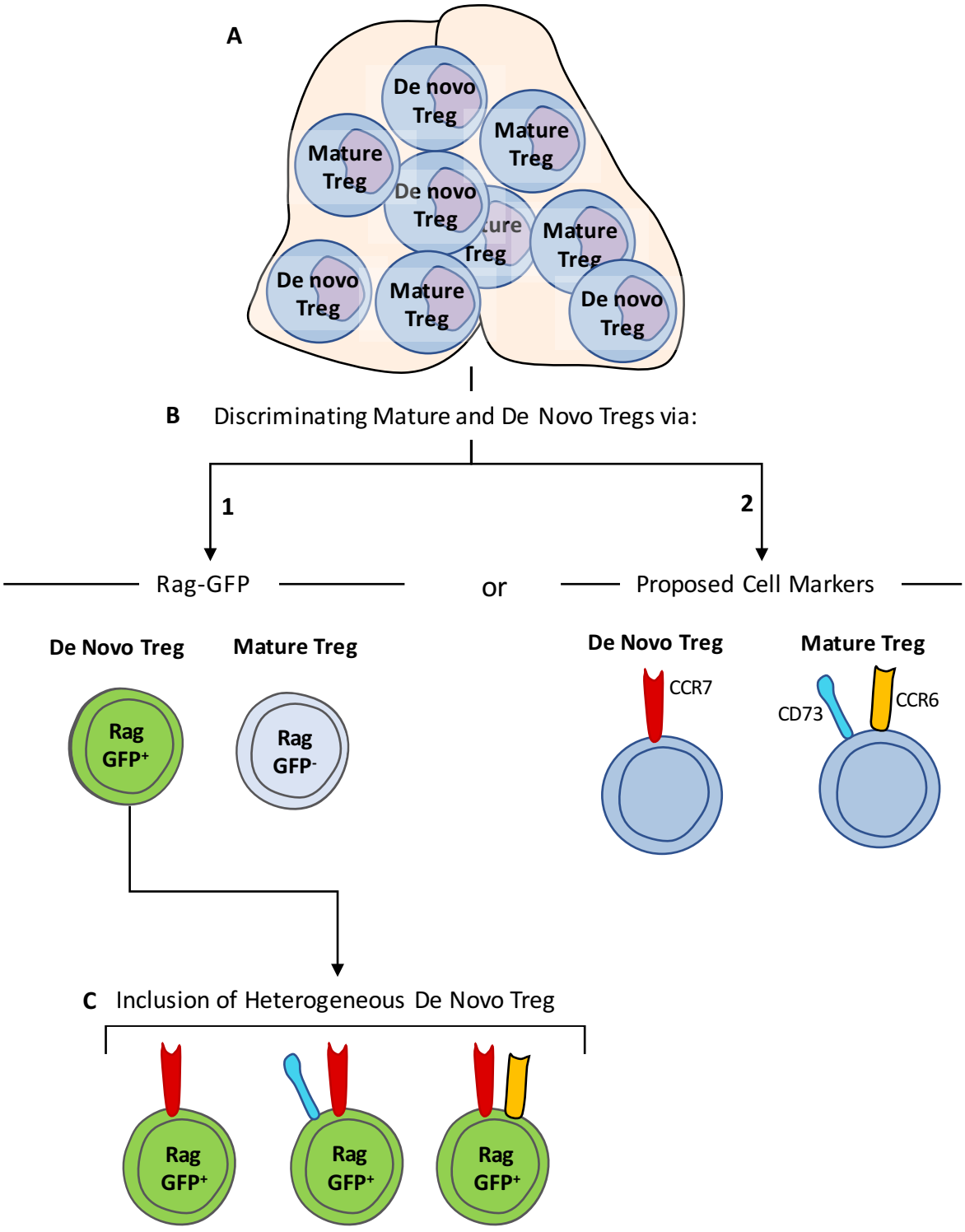
A
De novo Treg
Mature Treg
Mature Treg
De novo Treg
Mature Treg
De novo Treg
Mature Treg
De novo Treg
Mature Treg
De novo Treg
B Discriminating Mature and De Novo Tregs via:
1
2
Rag-GFP
or
Proposed Cell Markers
De Novo Treg
Mature Treg
Rag GFP+
Rag GFP-
De Novo Treg
Mature Treg
CCR7
CD73
CCR6
C Inclusion of Heterogeneous De Novo Treg
Rag GFP+
Rag GFP+
Rag GFP+

Figure 6. 1 Discriminating *De Novo* and Mature Thymic Tregs

An overview of different methods proposed to discriminate de novo and mature thymic Tregs, and the implications of our findings regarding these approaches.

(A) The thymic Treg population is a mixture of newly developing de novo Tregs and recirculating/retained mature Tregs. **(B)** To discriminate these two populations of Treg different approaches have been suggested. **(1)** Using Rag-GFP fluorescent models to discriminate de novo and mature Treg as Rag-GFP^{+} or Rag-GFP^{-}. **(2)** Alternatively cell markers CCR7, CCR6 and CD73 have been proposed to distinguish de novo and mature Treg as CCR7^{+}CCR6^{-}CD73^{-} or CCR7^{-}CCR6^{+}CD73^{+}.

(C) Importantly our analysis suggests that discriminating de novo Tregs as Rag-GFP^{+} ensures the inclusion of heterogeneous de novo Tregs Tregs which express CCR6 and CD73 (markers associated with a mature phenotype)

However, it was not always feasible to utilise the Rag-GFPxFoxp3-RFP reporter in our characterisation analysis, for instance in genetic KO models which lacked the Foxp3-RFP reporter component. Therefore, we adapted an alternative method to retain Rag-GFP while undertaking intracellular Foxp3 staining[317], acknowledging there were some limitations. Most notable was a slight reduction in the intensity of Rag-GFP, likely due to some leaching associated with the fixation process (Figure 3.17). As a consequence of this reduced intensity, it was more challenging to distinguish cells with lower levels of Rag-GFP, particularly RTEs, and so we may have failed to detect those RTEs with the lowest Rag-GFP levels. Therefore, it would be beneficial to generate genetic KOs on the Rag-GFPxFoxp3-RFP background. Another issue with this fixation approach was the poor detection of certain intracellular markers e.g. Ki67, therefore for some avenues of investigation it may still be necessary to sort populations on Rag-GFP before performing normal intracellular staining.

Our analysis also highlights a more fundamental issue with the Rag-GFP model as a reporter of cell age, which is that cellular proliferation can be a confounding factor. Our findings suggest that under conditions of intense proliferation, Rag-GFP can be diluted with each division and ultimately lost from the cell (Figure 4.2), meaning that under these circumstances loss of Rag-GFP is more an indicator of extensive proliferation rather than dramatically increased age. This issue may not be of such concern in the adult thymus, as our findings along with previous reports[339] suggest that adult SP4 thymocytes, including Tregs, undergo limited proliferation (Figure 4.18 and Figure 4.19). However, in circumstances where proliferation may be more prevalent such as in younger mice or under lymphopenic conditions, caution should be exercised in interpreting the age of Rag-

GFP$^-$ populations. Furthermore, it may also be prudent to establish whether differential proliferation of populations could be a contributing factor, when using Rag-GFP levels to compare the ages of Rag-GFP$^+$ cells.

In addition, while the long half-life of Rag-GFP was beneficial in terms of tracking the newly produced population through thymic development and early peripheral stages, it made differentiating the dynamics of similarly aged cells challenging. For instance, the large degree of overlap between Rag-GFP levels of *de novo* thymic Tregs and CD25$^-$Foxp3$^+$ Treg precursors meant Rag-GFP could not be used to infer their developmental order (Figure 3.13). A further complication to the comparison of average Rag-GFP levels between these populations, is that our analysis indicates that some CD25$^-$Foxp3$^+$ may be mature cells (Figure 3.14), possibly as a result of downregulation of CD25 by Tregs. As such, there may also be a need to distinguish precursors and mature thymocytes within the Rag-GFP$^+$CD25$^-$ Foxp3$^+$ population.

Finally, whilst Rag-GFP can distinguish new and old populations within the thymus it does not inform on their origin. Therefore it remains unclear whether the large Rag-GFP$^-$CD25$^-$ Foxp3$^+$ population we, and others[234], observed in the adult thymus is due to thymic retention or recirculation of these cells. This could be addressed, similar to the origin of Rag-GFP$^-$ Tregs[234,306], by grafting thymic lobes into congenically different hosts, and determining if mature graft cells are present within the graft and/or host thymus, indicating retention and/or recirculation, respectively.

Overall while there are some limitations associated with the Rag-GFPxFoxp3-RFP mouse, it does offer several unique advantages in studying *de novo* Treg development and as such it enabled us to identify underappreciated subtleties within Treg development.

6.2 Complexities and Distinctions of Thymic Treg Development

A primary interest of our study was the identification of intrathymic processes which may contribute to Treg development and hence ultimately the peripheral Treg population. We identified two intrathymic processes, heterogeneous differentiation and proliferation (limited to the neonate), which appear to contribute in a qualitative and quantitative manner to Treg development, respectively. The timing of both these intrathymic processes appeared to fit within a post-selection maturation period, that followed initial selection and divergence of autoreactive thymocytes into the Treg lineage. With regards to heterogeneous Treg differentiation, we identified that this process actively occurred within Treg thymocytes and resulted in the generation of two subsets (Figure 3.6). Our analysis, in keeping with previous suggestions[189], also hints of a role for thymic Treg precursors in this heterogeneous Treg differentiation pathway (Figure 3.15 and Figure 3.16). Similarly regarding intrathymic proliferation, we observed extensive active proliferation within both the Treg and $CD25^{+}Foxp3^{-}$ Treg precursor populations (Figure 4.5 and Figure 4.7).

This intrathymic timing is reminiscent of previously described post-selection maturation of Tconv thymocytes which notably features proliferation[191] and differentiation[191,192]. However, our observations of these post-selection processes in Tregs identify distinctions between the two lineages. Firstly, Tconvs differentiate to a singular endpoint, as evidenced by the described export of Tconvs with a uniform mature phenotype[192]. Meaning this

differentiation does not contribute to peripheral heterogeneity in the same way we suspect Treg differentiation does. While regarding proliferation, our direct comparison of Tregs and Tconvs suggested proliferation was more extensive in the Treg lineage, at least in the neonate. Therefore, our analysis suggests that intrathymic development of Tregs is subject to lineage specific post-selection processes.

Having identified differentiation and proliferation as contributors to thymic Treg development we were then interested in how these processes might be regulated. Our findings proved largely inconclusive, though some of our evidence suggested a role for the medulla. Firstly, mTEC^{hi} may be involved in mediating Treg differentiation (Figure 3.6). Furthermore γ_c cytokines IL-2 and IL-15 may drive Treg proliferation (Figure 4.13 and Figure 4.14), which earlier studies would indicate originates from thymic DCs[299]/autoreactive thymocytes[304] or mTEC[271], respectively. As such, unlike Tconv post-selection maturation[158], there may be a speculative role for the medulla in supporting post-selection processes of Treg development. Although, given the age restricted nature of proliferation but not differentiation, the medulla presumably mediates these by independent pathways.

It would therefore be interesting to assess these post-selection processes further in models with an altered thymic medulla. Including those where normal *de novo* thymic Treg development has been described, for instance, *Tnfrsf11b*$^{-/-}$ which show increased mTEC but normal bulk *de novo* thymic Tregs[308]. Our findings, would suggest there are greater subtleties to consider when characterising thymic Treg development alongside the main differentiation of Tregs from autoreactive precursors. As demonstrated by our

investigations of adult *Ltbr*$^{-/-}$, which identified that while reports of normal bulk *de novo* thymic Treg development were accurate[300], there was unappreciated altered differentiation within the Treg population (Figure 3.22). In addition, our analysis also identifies the importance of assessing any such models at neonatal as well as adult stages. As we found that extensive intrathymic proliferation within the Treg lineage was largely restricted to the neonate (Figure 4.18 and Figure 4.19). Indicating age should be considered a factor in post-selection maturation, and in keeping with other reports[232,233] that unique mechanisms of Treg development may be involved in the neonate.

Furthermore, considering the impact of age on post-selection mechanisms in thymic Treg development it is notable that we examined neonatal and early adult stages but not aged adults. Our observations, like others[235], indicate aging is associated with a quantitative reduction of *de novo* thymic Tregs and RTEs. However, whether aging also results in a qualitative change in thymic Tregs, linked with altered intrathymic differentiation, is less clear. Our analysis identified that, unlike proliferation, Treg differentiation was largely consistent across early neonatal life into young adulthood (Figure 3.4), however we did not examine older adult mice. Interestingly scRNAseq analysis suggests that peripheral Tregs from older adult mice, compared to younger adult mice, have a greater predominance of cells with an extreme regulatory phenotype[365]. It would therefore be interesting to assess whether altered intrathymic differentiation of thymic Tregs may contribute to this, and furthermore whether this altered balance may be linked to the changes in TEC distribution associated with thymic involution[227].

Another aspect of Treg development which our findings may suggest requires further consideration is the nature of Treg thymic egress. Historically opinion has been divided over whether thymic egress is an ordered linear process (conveyor belt model) or a stochastic process (lucky dip model)[153]. Recent evidence supports a conveyor belt model for Tconv thymocytes[26,192], however Treg emigration was not specifically addressed in this analysis therefore whether Tregs also follow this model is less clear. In fact, our findings on post-selection differentiation may suggest Tregs emigrate in a more stochastic manner. As we identified that while some CD62L^{hi} Tregs differentiated into CD62L^{lo} Tregs, there was evidence of thymic egress of both subsets (Figure 3.7 – Figure 3.9), indicating that pre- and post-differentiation there exists an option for Tregs to undergo thymic egress. In addition, our data hints that increasing thymic dwell time results in greater differentiation of CD62L^{hi} Tregs into CD62L^{lo} (Figure 3.6), suggesting that CD62L^{hi} Tregs with the potential to differentiate undergo thymic egress. In combination, this prompts speculation that unlike Tconvs, Tregs undergo a more stochastic thymic egress, with CD62L^{hi} Tregs able to leave or remain, differentiate to CD62L^{lo} Tregs and then leave. Alternatively, it might still be that within the two CD62L Treg subsets there exists an order to thymic egress with only the most mature CD62L^{hi} or CD62L^{lo} Tregs able to egress. Perhaps this could be assessed by labelling cells in the thymic PVS[192] of Rag-GFPxFoxp3-RFP mice, to identify CD62L^{hi} and CD62L^{lo} Tregs about to egress. The phenotype of these subsets could then be examined for expression of maturation markers or Rag-GFP levels, if there was uniformity within the subsets this would suggest only the most mature CD62L$^{hi/lo}$ Tregs leave, thus implying the two subsets follow a conveyor belt model.

Our characterisation of Tconv and Treg RTEs also has implications for post-thymic development of Tregs. We identified differences in the genetic profiles of Treg RTEs and their mature counterparts, suggestive of some further development of Treg RTEs in the periphery (Figure 5.9). Notably a small selection of gene expression changes observed between Treg RTEs and mature Tregs were also seen between Tconv RTEs and mature Tconvs (Figure 5.10). This is important as bulk SP4 RTEs, which predominantly consist of Tconv RTEs, are described to undergo an extended post-thymic maturation period on initial egress[26,157]. Therefore, these common changes might suggest elements of a shared post-thymic maturation programme for both Tregs and Tconvs.

However, there were also many differences between the genetic profiles of Treg and Tconv RTEs (Figure 5.7 – Figure 5.10). Raising the question of how comparable any post-thymic maturation of Tregs might be to previously described SP4 RTE post-thymic maturation. For instance, we identified mature levels of IL7Rα by Treg but not Tconv RTEs, implying that Treg RTEs might be more mature on thymic egress and hence require less peripheral development. Reminiscent of previous reports that expression of Treg signature genes is largely comparable between thymic and peripheral Tregs[366]. Furthermore, unlike Tconv RTEs, Treg RTEs may also be more functionally capable on thymic egress. As early transfer experiments identified bulk thymocytes contained cells capable of preventing autoimmune disease[367,368], a finding subsequently attributed to the presence of thymic $CD25^+$ Tregs which proved regulatory *in vitro*[369]. Collectively this suggests the thymus generates *de novo* Tregs similar in phenotype and function to their mature peripheral counterparts. However, a caveat of these earlier studies[366–369] is that mature thymic Tregs were not

excluded and therefore these mature cells may have masked the comparative immaturity of their younger counterparts.

Interestingly, our Treg RTE analysis may hint at some functional impairment, as we observed higher expression of Satb1 in Treg RTEs relative to mature Tregs (Figure 5.9). While Satb1 does drive SP4 and Treg development[352], it has also emerged that peripheral Tregs repress Satb1 to maintain their phenotype and function, with overexpression of Satb1 resulting in impaired regulatory function[370]. Whilst speculative, this may indicate that Treg RTEs with higher levels of Satb1 consequently have reduced functionality, paralleling reports of functional maturation of SP4 RTEs[157]. Therefore, it would be interesting to compare the regulatory capacities of *de novo* thymic Tregs, Treg RTEs, and mature peripheral Tregs using either *in vivo* autoimmune models or *in vitro* suppression assays, to assess whether there is a functional component to any post-thymic maturation. Furthermore, potential post-thymic maturation of Tregs also raises the question of how this process may be regulated. As discussed in Section 5.3 our analysis may suggest some intrinsic regulators, Satb1 and Sox4, which possibly connect to previously described pathways driving SP4 RTE maturation[199]. However how these intrinsic pathways are regulated by extrinsic factors is unclear. Indeed, generally the extrinsic drivers of SP4 RTE development have thus far remained elusive with the only clear requirement being access to SLOs[309] and an intact DC compartment[311]. While our characterisation of Treg RTEs identified some homing to non-lymphoid tissue, there appeared a greater preference for SLOs, which might suggest a similar dependence of Treg RTEs on these sites for maturation. It would therefore be interesting to determine if, without access to SLOs, Treg RTEs appeared altered and immature.

6.3 Concluding Remarks

In summary, our findings presented in this thesis offer greater insight into both the intrathymic and post-thymic development of Tregs. We identify that *de novo* thymic Tregs undergo two differential processes of post-selection maturation, differentiation and proliferation. Regarding differentiation, we identified that this process generated two egress competent subsets of Tregs across the lifespan. Supporting the notion that the thymus does contribute qualitatively to the diversity of the peripheral pool, although the exact relationship between the thymic Treg subsets we identified and previously described peripheral Treg subsets remains unclear. In contrast to this consistent intrathymic differentiation, intrathymic proliferation was largely restricted to neonatal Tregs and we suspect this proliferation may be involved in the rapid establishment of the Treg population at this stage. Hence this proliferation represents another age-dependent aspect of thymic Treg development exclusive to the neonate, further highlighting the importance of considering Treg development specifically at this stage. Finally, our comparison of the genetic profiles of Treg RTEs with their mature counterparts identified differences, suggesting Tregs undergo further post-thymic maturation on egress, as has been reported in the wider SP4 T-cell lineage. However, it is unclear exactly how similar such post-thymic maturation of Tregs might be to reported SP4 RTE maturation, as we found some evidence that Treg RTEs may be more mature. Overall our work highlights complexities of Treg development which warrant further investigation, not least regarding the mechanisms which control these processes, with our work suggesting roles for traditional regulators of thymic Treg development, such as mTEC and γ_c cytokines.

REFERENCES

1. Parkin J, Cohen B. An overview of the immune system. Lancet 2001;357(9270):1777–89.
2. Nikolich-Žugich J, Slifka MK, Messaoudi I. The many important facets of T-cell repertoire diversity. Nat Rev Immunol 2004;4(2):123–32.
3. Davis MM, Bjorkman PJ. T-cell antigen receptor genes and T-cell recognition. Nature 1988;334(6181):395–402.
4. Vantourout P, Hayday A. Six-of-the-best: unique contributions of γδ T cells to immunology. Nat Rev Immunol 2013;13(2):88–100.
5. Krovi SH, Gapin L. Invariant natural killer T cell subsets-more than just developmental intermediates. Front Immunol 2018;9:1393.
6. Itano AA, Jenkins MK. Antigen presentation to naive CD4 T cells in the lymph node. Nat Immunol 2003;4(8):733–9.
7. Vyas JM, Van Der Veen AG, Ploegh HL. The known unknowns of antigen processing and presentation. Nat Rev Immunol 2008;8(8):607–18.
8. Janeway CA. The T Cell Receptor as a Multicomponent Signalling Machine: CD4/CD8 Coreceptors and CD45 in T Cell Activation. Annu Rev Immunol 1992;10(1):645–74.
9. Von Boehmer H. CD4/CD8 lineage commitment: Back to instruction? J Exp Med 1996;183(3):713–5.
10. Andersen MH, Schrama D, thor Straten P, Becker JC. Cytotoxic T Cells. J Invest Dermatol 2006;126(1):32–41.
11. Luckheeram RV, Zhou R, Verma AD, Xia B. $CD4^+$T cells: differentiation and functions. Clin Dev Immunol 2012;2012:925135.
12. Kapsenberg ML. Dendritic-cell control of pathogen-driven T-cell polarization. Nat Rev Immunol 2003;3(12):984–93.
13. Acuto O, Michel F. CD28-mediated co-stimulation: A quantitative support for TCR signalling. Nat Rev Immunol 2003;3(12):939–51.
14. Lighvani AA, Frucht DM, Jankovic D, Yamane H, Aliberti J, Hissong BD, et al. T-bet is rapidly induced by interferon-γ in lymphoid and myeloid cells. Proc Natl Acad Sci USA 2001;98(26):15137–42.
15. Szabo SJ, Kim ST, Costa GL, Zhang X, Fathman CG, Glimcher LH. A novel transcription factor, T-bet, directs Th1 lineage commitment. Cell 2000;100(6):655–69.
16. Ivanov II, McKenzie BS, Zhou L, Tadokoro CE, Lepelley A, Lafaille JJ, et al. The Orphan Nuclear Receptor RORγt Directs the Differentiation Program of Proinflammatory IL-17+ T Helper Cells. Cell 2006;126(6):1121–33.
17. Zhou L, Ivanov II, Spolski R, Min R, Shenderov K, Egawa T, et al. IL-6 programs TH-17 cell differentiation by promoting sequential engagement of the IL-21 and IL-23 pathways. Nat Immunol 2007;8(9):967–74.
18. Gause WC, Wynn TA, Allen JE. Type 2 immunity and wound healing: evolutionary refinement of adaptive immunity by helminths. Nat Rev Immunol 2013;13(8):607–14.
19. Ouyang W, Ranganath SH, Weindel K, Bhattacharya D, Murphy TL, Sha WC, et al. Inhibition of Th1 development mediated by GATA-3 through an IL-4- independent mechanism. Immunity 1998;9(5):745–55.
20. Crotty S. T Follicular Helper Cell Differentiation, Function, and Roles in Disease. Immunity 2014;41(4):529–42.
21. Mellman I, Steinman RM. Dendritic cells: specialized and regulated antigen processing machines. Cell 2001;106(3):255–8.
22. Hubert F-X, Kinkel SA, Crewther PE, Cannon PZF, Webster KE, Link M, et al. Aire-deficient C57BL/6 mice mimicking the common human 13-base pair deletion mutation present with only a mild autoimmune phenotype. J Immunol 2009;182(6):3902–18.
23. Nagamine K, Peterson P, Scott HS, Kudoh J, Minoshima S, Heino M, et al. Positional cloning of the APECED gene. Nat Genet 1997;17(4):393–8.
24. Danke NA, Koelle DM, Yee C, Beheray S, Kwok WW. Autoreactive T Cells in Healthy

Individuals. J Immunol 2004;172(10):5967–72.
25. Cebula A, Kuczma M, Szurek E, Pietrzak M, Savage N, Elhefnawy WR, et al. Dormant pathogenic CD4+ T cells are prevalent in the peripheral repertoire of healthy mice. Nat Commun 2019;10(1):4882.
26. McCaughtry TM, Wilken MS, Hogquist KA. Thymic emigration revisited. J Exp Med 2007;204(11):2513–20.
27. Klein L, Kyewski B, Allen PM, Hogquist KA. Positive and negative selection of the T cell repertoire: What thymocytes see (and don't see). Nat Rev Immunol 2014;14(6):377–91.
28. Xing Y, Hogquist KA. T-Cell tolerance: Central and peripheral. Cold Spring Harb Perspect Biol 2012;4(6):1–15.
29. Sakaguchi S, Yamaguchi T, Nomura T, Ono M. Regulatory T Cells and Immune Tolerance. Cell 2008;133(5):775–87.
30. ElTanbouly MA, Noelle RJ. Rethinking peripheral T cell tolerance: checkpoints across a T cell's journey. Nat. Rev. Immunol.2021;21(4):257–67.
31. Schietinger A, Greenberg PD. Tolerance and exhaustion: Defining mechanisms of T cell dysfunction. Trends Immunol.2014;35(2):51–60.
32. Gershon RK, Kondo K. Cell interactions in the induction of tolerance: the role of thymic lymphocytes. Immunology 1970;18(5):723–37.
33. Gershon RK, Kondo K. Infectious immunological tolerance. Immunology 1971;21(6):903–14.
34. Gershon RK, Cohen P, Hencin R, Liebhaber SA. Suppressor T cells. J Immunol 1972;108(3):586–90.
35. Sakaguchi S, Sakaguchi N, Asano M, Itoh M, Toda M. Immunologic self-tolerance maintained by activated T cells expressing IL-2 receptor alpha-chains (CD25). Breakdown of a single mechanism of self-tolerance causes various autoimmune diseases. J Immunol 1995;155(3):1151–64.
36. Asano M, Toda M, Sakaguchi N, Sakaguchi S. Autoimmune disease as a consequence of developmental abnormality of a T cell subpopulation. J Exp Med 1996;184(2):387–96.
37. Hori S, Nomura T, Sakaguchi S. Control of regulatory T cell development by the transcription factor Foxp3. Science 2003;(299):1057–61.
38. Fontenot JD, Gavin MA, Rudensky AY. Foxp3 programs the development and function of CD4+CD25+ regulatory T cells. Nat Immunol 2003;4(4):330–6.
39. Khattri R, Cox T, Yasayko S-A, Ramsdell F. An essential role for Scurfin in CD4+CD25+ T regulatory cells. Nat Immunol 2003;4(4):337–42.
40. Brunkow ME, Jeffery EW, Hjerrild KA, Paeper B, Clark LB, Yasayko S-A, et al. Disruption of a new forkhead/winged-helix protein, scurfin, results in the fatal lymphoproliferative disorder of the scurfy mouse. Nat Genet 2001;27(1):68–73.
41. Blair PJ, Bultman SJ, Haas JC, Rouse BT, Wilkinson JE, Godfrey VL. CD4+CD8- T cells are the effector cells in disease pathogenesis in the scurfy (sf) mouse. J Immunol 1994;153(8):3764–74.
42. Lahl K, Loddenkemper C, Drouin C, Freyer J, Arnason J, Eberl G, et al. Selective depletion of Foxp3+ regulatory T cells induces a scurfy-like disease. J Exp Med 2007;204(1):57–63.
43. Kim JM, Rasmussen JP, Rudensky AY. Regulatory T cells prevent catastrophic autoimmunity throughout the lifespan of mice. Nat Immunol 2007;8(2):191–7.
44. Kim J, Lahl K, Hori S, Loddenkemper C, Chaudhry A, DeRoos P, et al. Cutting Edge: Depletion of Foxp3 + Cells Leads to Induction of Autoimmunity by Specific Ablation of Regulatory T Cells in Genetically Targeted Mice. J Immunol 2009;183(12):7631–4.
45. Bennett CL, Christie J, Ramsdell F, Brunkow ME, Ferguson PJ, Whitesell L, et al. The immune dysregulation, polyendocrinopathy, enteropathy, X-linked syndrome (IPEX) is caused by mutations of FOXP3. Nat Genet 2001;27(1):20–1.
46. Allan SE, Crome SQ, Crellin NK, Passerini L, Steiner TS, Bacchetta R, et al. Activation-

induced FOXP3 in human T effector cells does not suppress proliferation or cytokine production. Int Immunol 2007;19(4):345–54.
47. Liu W, Putnam AL, Xu-yu Z, Szot GL, Lee MR, Zhu S, et al. CD127 expression inversely correlates with FoxP3 and suppressive function of human CD4+ T reg cells. J Exp Med 2006;203(7):1701–11.
48. Chen X, Oppenheim JJ. Resolving the identity myth: Key markers of functional CD4 +FoxP3 + regulatory T cells. Int Immunopharmacol 2011;11(10):1489–96.
49. Rodríguez-Perea AL, Arcia ED, Rueda CM, Velilla PA. Phenotypical characterization of regulatory T cells in humans and rodents. Clin Exp Immunol 2016;185(3):281–91.
50. Klein L, Khazaie K, Von Boehmer H. In vivo dynamics of antigen-specific regulatory T cells not predicted from behavior in vitro. Proc Natl Acad Sci USA 2003;100(15):8886–91.
51. Takahashi T, Kuniyasu Y, Toda M, Sakaguchi N, Itoh M, Iwata M, et al. Immunologic self-tolerance maintained by CD25+CD4+ naturally anergic and suppressive T cells: induction of autoimmune disease by breaking their anergic/suppressive state. Int Immunol 1998;10(12):1969–80.
52. Onishi Y, Fehervari Z, Yamaguchi T, Sakaguchi S. Foxp3+ natural regulatory T cells preferentially form aggregates on dendritic cells in vitro and actively inhibit their maturation. Proc Natl Acad Sci USA 2008;105(29):10113–8.
53. Qureshi OS, Zheng Y, Nakamura K, Attridge K, Manzotti C, Schmidt EM, et al. Trans-endocytosis of CD80 and CD86: A molecular basis for the cell-extrinsic function of CTLA-4. Science 2011;332(6029):600–3.
54. Akkaya B, Oya Y, Akkaya M, Al Souz J, Holstein AH, Kamenyeva O, et al. Regulatory T cells mediate specific suppression by depleting peptide–MHC class II from dendritic cells. Nat Immunol 2019;20(2):218–31.
55. Pandiyan P, Zheng L, Ishihara S, Reed J, Lenardo MJ. CD4+CD25+Foxp3+ regulatory T cells induce cytokine deprivation–mediated apoptosis of effector CD4+ T cells. Nat Immunol 2007;8(12):1353–62.
56. Asseman C, Mauze S, Leach MW, Coffman RL, Powrie F. An essential role for interleukin 10 in the function of regulatory T cells that inhibit intestinal inflammation. J Exp Med 1999;190(7):995–1004.
57. Powrie F, Carlino J, Leach MW, Mauze S, Coffman RL. A critical role for transforming growth factor-beta but not interleukin 4 in the suppression of T helper type 1-mediated colitis by CD45RB(low) CD4+ T cells. J Exp Med 1996;183(6):2669–74.
58. Collison LW, Workman CJ, Kuo TT, Boyd K, Wang Y, Vignali KM, et al. The inhibitory cytokine IL-35 contributes to regulatory T-cell function. Nature 2007;450(7169):566–9.
59. Maj T, Wang W, Crespo J, Zhang H, Wang W, Wei S, et al. Oxidative stress controls regulatory T cell apoptosis and suppressor activity and PD-L1-blockade resistance in tumor. Nat Immunol 2017;18(12):1332–41.
60. Gondek DC, Lu L-F, Quezada SA, Sakaguchi S, Noelle RJ. Cutting edge: contact-mediated suppression by CD4+CD25+ regulatory cells involves a granzyme B-dependent, perforin-independent mechanism. J Immunol 2005;174(4):1783–6.
61. Liang B, Workman C, Lee J, Chew C, Dale BM, Colonna L, et al. Regulatory T Cells Inhibit Dendritic Cells by Lymphocyte Activation Gene-3 Engagement of MHC Class II. J Immunol 2008;180(9):5916–26.
62. Fallarino F, Grohmann U, Hwang KW, Orabona C, Vacca C, Bianchi R, et al. Modulation of tryptophan catabolism by regulatory T cells. Nat Immunol 2003;4(12):1206–12.
63. Yu X, Harden K, Gonzalez LC, Francesco M, Chiang E, Irving B, et al. The surface protein TIGIT suppresses T cell activation by promoting the generation of mature immunoregulatory dendritic cells. Nat Immunol 2009;10(1):48–57.
64. Coombes JL, Siddiqui KRR, Arancibia-Cárcamo C V., Hall J, Sun C-M, Belkaid Y, et al. A functionally specialized population of mucosal CD103+ DCs induces Foxp3+ regulatory T

cells via a TGF-β– and retinoic acid–dependent mechanism. J Exp Med 2007;204(8):1757.
65. Rubtsov YP, Rasmussen JP, Chi EY, Fontenot J, Castelli L, Ye X, et al. Regulatory T cell-derived interleukin-10 limits inflammation at environmental interfaces. Immunity 2008;28(4):546–58.
66. Groux H, O'Garra A, Bigler M, Rouleau M, Antonenko S, de Vries JE, et al. A CD4+T-cell subset inhibits antigen-specific T-cell responses and prevents colitis. Nature 1997;389(6652):737–42.
67. Chen Y, Kuchroo VK, Inobe J, Hafler DA, Weiner HL. Regulatory T cell clones induced by oral tolerance: suppression of autoimmune encephalomyelitis. Science 1994;265(5176):1237–40.
68. Kitagawa Y, Ohkura N, Kidani Y, Vandenbon A, Hirota K, Kawakami R, et al. Guidance of regulatory T cell development by Satb1-dependent super-enhancer establishment. Nat Immunol 2017;18(2):173–83.
69. Zheng Y, Josefowicz S, Chaudhry A, Peng XP, Forbush K, Rudensky AY. Role of conserved non-coding DNA elements in the Foxp3 gene in regulatory T-cell fate. Nature 2010;463(7282):808–12.
70. Floess S, Freyer J, Siewert C, Baron U, Olek S, Polansky J, et al. Epigenetic control of the foxp3 locus in regulatory T cells. PLoS Biol 2007;5(2):0169–78.
71. Zhou X, Bailey-Bucktrout SL, Jeker LT, Penaranda C, Martínez-Llordella M, Ashby M, et al. Instability of the transcription factor Foxp3 leads to the generation of pathogenic memory T cells in vivo. Nat Immunol 2009;10(9):1000–7.
72. Yang XO, Nurieva R, Martinez GJ, Kang HS, Chung Y, Pappu BP, et al. Molecular Antagonism and Plasticity of Regulatory and Inflammatory T Cell Programs. Immunity 2008;29(1):44–56.
73. Rubtsov YP, Niec RE, Josefowicz S, Li L, Darce J, Mathis D, et al. Stability of the regulatory T cell lineage in vivo. Science 2010;329(5999):1667–71.
74. Miyao T, Floess S, Setoguchi R, Luche H, Fehling HJ, Waldmann H, et al. Plasticity of Foxp3 + T Cells Reflects Promiscuous Foxp3 Expression in Conventional T Cells but Not Reprogramming of Regulatory T Cells. Immunity 2012;36(2):262–75.
75. Ohkura N, Hamaguchi M, Morikawa H, Sugimura K, Tanaka A, Ito Y, et al. T Cell Receptor Stimulation-Induced Epigenetic Changes and Foxp3 Expression Are Independent and Complementary Events Required for Treg Cell Development. Immunity 2012;37(5):785–99.
76. Schmitt EG, Haribhai D, Williams JB, Aggarwal P, Jia S, Charbonnier L-M, et al. IL-10 produced by induced regulatory T cells (iTregs) controls colitis and pathogenic ex-iTregs during immunotherapy. J Immunol 2012;189(12):5638–48.
77. Feuerer M, Hill JA, Kretschmer K, Von Boehmer H, Mathis D, Benoist C. Genomic definition of multiple ex vivo regulatory T cell subphenotypes. Proc Natl Acad Sci USA 2010;107(13):5919–24.
78. Haribhai D, Williams JB, Jia S, Nickerson D, Schmitt EG, Edwards B, et al. A requisite role for induced regulatory T cells in tolerance based on expanding antigen receptor diversity. Immunity 2011;35(1):109–22.
79. Thornton AM, Korty PE, Tran DQ, Wohlfert EA, Murray PE, Belkaid Y, et al. Expression of Helios, an Ikaros Transcription Factor Family Member, Differentiates Thymic-Derived from Peripherally Induced Foxp3 + T Regulatory Cells. J Immunol 2010;184(7):3433–41.
80. Yadav M, Louvet C, Davini D, Gardner JM, Martinez-Llordella M, Bailey-Bucktrout S, et al. Neuropilin-1 distinguishes natural and inducible regulatory T cells among regulatory T cell subsets in vivo. J Exp Med 2012;209(10):1713–22.
81. Szurek E, Cebula A, Wojciech L, Pietrzak M, Rempala G, Kisielow P, et al. Differences in expression level of Helios and neuropilin-1 do not distinguish thymus-derived from extrathymically-induced CD4+Foxp3+ regulatory T cells. PLoS One 2015;10(10):e0141161.
82. Josefowicz SZ, Niec RE, Kim HY, Treuting P, Chinen T, Zheng Y, et al. Extrathymically

generated regulatory T cells control mucosal TH2 inflammation. Nature 2012;482(7385):395–9.
83. Haribhai D, Lin W, Edwards B, Ziegelbauer J, Salzman NH, Carlson MR, et al. A central role for induced regulatory T cells in tolerance induction in experimental colitis. J Immunol 2009;182(6):3461–8.
84. Miyara M, Yoshioka Y, Kitoh A, Shima T, Wing K, Niwa A, et al. Functional delineation and differentiation dynamics of human CD4+ T cells expressing the FoxP3 transcription factor. Immunity 2009;30(6):899–911.
85. Smigiel KS, Richards E, Srivastava S, Thomas KR, Dudda JC, Klonowski KD, et al. CCR7 provides localized access to IL-2 and defines homeostatically distinct regulatory T cell subsets. J Exp Med 2014;211(1):121–36.
86. Lee JH, Kang SG, Kim CH. FoxP3 + T Cells Undergo Conventional First Switch to Lymphoid Tissue Homing Receptors in Thymus but Accelerated Second Switch to Nonlymphoid Tissue Homing Receptors in Secondary Lymphoid Tissues. J Immunol 2007;178(1):301–11.
87. Huehn J, Siegmund K, Lehmann JCU, Siewert C, Haubold U, Feuerer M, et al. Developmental stage, phenotype, and migration distinguish naive- and effector/memory-like CD4+ regulatory T cells. J Exp Med 2004;199(3):303–13.
88. Cretney E, Xin A, Shi W, Minnich M, Masson F, Miasari M, et al. The transcription factors Blimp-1 and IRF4 jointly control the differentiation and function of effector regulatory T cells. Nat Immunol 2011;12(4):304–11.
89. Koch MA, Tucker-Heard G, Perdue NR, Killebrew JR, Urdahl KB, Campbell DJ. The transcription factor T-bet controls regulatory T cell homeostasis and function during type 1 inflammation. Nat Immunol 2009;10(6):595–602.
90. Zheng Y, Chaudhry A, Kas A, DeRoos P, Kim JM, Chu TT, et al. Regulatory T-cell suppressor program co-opts transcription factor IRF4 to control TH2 responses. Nature 2009;458(7236):351–6.
91. Chaudhry A, Rudra D, Treuting P, Samstein RM, Liang Y, Kas A, et al. CD4+ regulatory T cells control TH17 responses in a stat3-dependent manner. Science 2009;326(5955):986–91.
92. Chung Y, Tanaka S, Chu F, Nurieva RI, Martinez GJ, Rawal S, et al. Follicular regulatory T cells expressing Foxp3 and Bcl-6 suppress germinal center reactions. Nat Med 2011;17(8):983–8.
93. Feuerer M, Herrero L, Cipolletta D, Naaz A, Wong J, Nayer A, et al. Lean, but not obese, fat is enriched for a unique population of regulatory T cells that affect metabolic parameters. Nat Med 2009;15(8):930–9.
94. Cipolletta D, Feuerer M, Li A, Kamei N, Lee J, Shoelson SE, et al. PPAR-γ is a major driver of the accumulation and phenotype of adipose tissue T reg cells. Nature 2012;486(7404):549–53.
95. Sefik E, Geva-Zatorsky N, Oh S, Konnikova L, Zemmour D, McGuire AM, et al. Individual intestinal symbionts induce a distinct population of RORγ+ regulatory T cells. Science 2015;349(6251):993–7.
96. Schiering C, Krausgruber T, Chomka A, Fröhlich A, Adelmann K, Wohlfert EA, et al. The alarmin IL-33 promotes regulatory T-cell function in the intestine. Nature 2014;513(7519):564–8.
97. Rodriguez RS, Pauli ML, Neuhaus IM, Yu SS, Arron ST, Harris HW, et al. Memory regulatory T cells reside in human skin. J Clin Invest 2014;124(3):1027–36.
98. Scharschmidt TC, Vasquez KS, Truong H-A, Gearty SV, Pauli ML, Nosbaum A, et al. A Wave of Regulatory T Cells into Neonatal Skin Mediates Tolerance to Commensal Microbes. Immunity 2015;43(5):1011–21.
99. Nosbaum A, Prevel N, Truong H-A, Mehta P, Ettinger M, Scharschmidt TC, et al. Cutting Edge: Regulatory T Cells Facilitate Cutaneous Wound Healing. J Immunol

2016;196(5):2010–4.
100. Li C, DiSpirito JR, Zemmour D, Spallanzani RG, Kuswanto W, Benoist C, et al. TCR Transgenic Mice Reveal Stepwise, Multi-site Acquisition of the Distinctive Fat-Treg Phenotype. Cell 2018;174(2):285-299.e12.
101. Miragaia RJ, Gomes T, Chomka A, Jardine L, Riedel A, Hegazy AN, et al. Single-Cell Transcriptomics of Regulatory T Cells Reveals Trajectories of Tissue Adaptation. Immunity 2019;50(2):493-504.e7.
102. Vasanthakumar A, Liao Y, Teh P, Pascutti MF, Oja AE, Garnham AL, et al. The TNF Receptor Superfamily-NF-κB Axis Is Critical to Maintain Effector Regulatory T Cells in Lymphoid and Non-lymphoid Tissues. Cell Rep 2017;20(12):2906–20.
103. Levine AG, Arvey A, Jin W, Rudensky AY. Continuous requirement for the TCR in regulatory T cell function. Nat Immunol 2014;15(11):1070–8.
104. Zemmour D, Zilionis R, Kiner E, Klein AM, Mathis D, Benoist C. Single-cell gene expression reveals a landscape of regulatory T cell phenotypes shaped by the TCR. Nat Immunol 2018;19(3):291–301.
105. Wei X, Zhang J, Gu Q, Huang M, Zhang W, Guo J, et al. Reciprocal Expression of IL-35 and IL-10 Defines Two Distinct Effector Treg Subsets that Are Required for Maintenance of Immune Tolerance. Cell Rep 2017;21(7):1853–69.
106. Vasanthakumar A, Moro K, Xin A, Liao Y, Gloury R, Kawamoto S, et al. The transcriptional regulators IRF4, BATF and IL-33 orchestrate development and maintenance of adipose tissue–resident regulatory T cells. Nat Immunol 2015;16(3):276–85.
107. Wyss L, Stadinski BD, King CG, Schallenberg S, McCarthy NI, Lee JY, et al. Affinity for self antigen selects Treg cells with distinct functional properties. Nat Immunol 2016;17(9):1093–101.
108. Miller JFAP. Immunological Function of the Thymus. Lancet 1961;278(7205):748–9.
109. Donskoy E, Goldschneider I. Thymocytopoiesis is maintained by blood-borne precursors throughout postnatal life. A study in parabiotic mice. J Immunol 1992;148(6):1604–12.
110. Yui MA, Rothenberg E V. Developmental gene networks: A triathlon on the course to T cell identity. Nat Rev Immunol 2014;14(8):529–45.
111. Lind EF, Prockop SE, Porritt HE, Petrie HT. Mapping precursor movement through the postnatal thymus reveals specific microenvironments supporting defined stages of early lymphoid development. J Exp Med 2001;194(2):127–34.
112. Foss DL, Donskoy E, Goldschneider I. The importation of hematogenous precursors by the thymus is a gated phenomenon in normal adult mice. J Exp Med 2001;193(3):365–74.
113. Chen ELY, Thompson PK, Zúñiga-Pflücker JC. RBPJ-dependent Notch signaling initiates the T cell program in a subset of thymus-seeding progenitors. Nat Immunol 2019;20(11):1456–68.
114. Rothenberg E V., Moore JE, Yui MA. Launching the T-Lineage Developmental Programme. Nat Rev Immunol 2008;8(1):9.
115. Porritt HE, Rumfelt LL, Tabrizifard S, Schmitt TM, Zúñiga-Pflücker JC, Petrie HT. Heterogeneity among DN1 Prothymocytes Reveals Multiple Progenitors with Different Capacities to Generate T Cell and Non-T Cell Lineages. Immunity 2004;20(6):735–45.
116. Masuda K, Kakugawa K, Nakayama T, Minato N, Katsura Y, Kawamoto H. T Cell Lineage Determination Precedes the Initiation of TCRβ Gene Rearrangement. J Immunol 2007;179(6):3699–706.
117. Plotkin J, Prockop SE, Lepique A, Petrie HT. Critical Role for CXCR4 Signaling in Progenitor Localization and T Cell Differentiation in the Postnatal Thymus. J Immunol 2003;171(9):4521–7.
118. Koch U, Fiorini E, Benedito R, Besseyrias V, Schuster-Gossler K, Pierres M, et al. Delta-like 4 is the essential, nonredundant ligand for Notch1 during thymic T cell lineage commitment. J Exp Med 2008;205(11):2515.

119. Capone M, Hockett RD, Zlotnik A. Kinetics of T cell receptor β, γ, and δ rearrangements during adult thymic development: T cell receptor rearrangements are present in CD44+CD25+ Pro-T thymocytes. Proc Natl Acad Sci USA 1998;95(21):12522–7.
120. Roth DB. V(D)J Recombination: Mechanism, Errors, and Fidelity. Microbiol Spectr 2014;2(6).
121. Dudley EC, Girardi M, Owen MJ, Hayday AC. α β and γ δ T cells can share a late common precursor. Curr Biol 1995;5(6):659–69.
122. Taghon T, Yui MA, Pant R, Diamond RA, Rothenberg E V. Developmental and molecular characterization of emerging β- and γδ-selected pre-T cells in the adult mouse thymus. Immunity 2006;24(1):53–64.
123. Falk I, Nerz G, Haidl I, Krotkova A, Eichmann K. Immature thymocytes that fail to express TCRβ and/or TCRγδ proteins die by apoptotic cell death in the CD44-CD25- (DN4) subset. Eur J Immunol 2001;31(11):3308–17.
124. Maillard I, Tu L, Sambandam A, Yashiro-Ohtani Y, Millholland J, Keeshan K, et al. The requirement for Notch signaling at the β-selection checkpoint in vivo is absolute and independent of the pre–T cell receptor. J Exp Med 2006;203(10):2239.
125. Trampont PC, Tosello-Trampont A-C, Shen Y, Duley AK, Sutherland AE, Bender TP, et al. CXCR4 acts as a costimulator during thymic β-selection. Nat Immunol 2010;11(2):162–70.
126. MacDonald HR, Budd RC, Howe RC. A CD3− subset of CD4−8+ thymocytes: a rapidly cycling intermediate in the generation of CD4+8+ cells. Eur J Immunol 1988;18(4):519–24.
127. Jones ME, Zhuang Y. Acquisition of a functional T cell receptor during T lymphocyte development is enforced by HEB and E2A transcription factors. Immunity 2007;27(6):860–70.
128. Carpenter AC, Bosselut R. Decision checkpoints in the thymus. Nat Immunol 2010;11(8):666–73.
129. Witt CM, Raychaudhuri S, Schaefer B, Chakraborty AK, Robey EA. Directed Migration of Positively Selected Thymocytes Visualized in Real Time. PLoS Biol 2005;3(6).
130. Huang C-Y, Kanagawa O. Ordered and Coordinated Rearrangement of the TCR α Locus: Role of Secondary Rearrangement in Thymic Selection. J Immunol 2001;166(4):2597–601.
131. Sun Z, Unutmaz D, Zou YR, Sunshine MJ, Pierani A, Brenner-Morton S, et al. Requirement for RORγ in thymocyte survival and lymphoid organ development. Science 2000;288(5475):2369–73.
132. Ioannidis V, Beermann F, Clevers H, Held W. The β-catenin-TCF-I pathway ensures CD4+CD8+ thymocyte survival. Nat Immunol 2001;2(8):691–7.
133. McCaughtry TM, Baldwin TA, Wilken MS, Hogquist KA. Clonal deletion of thymocytes can occur in the cortex with no involvement of the medulla. J Exp Med 2008;205(11):2575.
134. Melichar HJ, Ross JO, Herzmark P, Hogquist KA, Robey EA. Distinct Temporal Patterns of T Cell Receptor Signaling During Positive Versus Negative Selection in Situ. Sci Signal 2013;6(297):ra92.
135. Stritesky GL, Xing Y, Erickson JR, Kalekar LA, Wang X, Mueller DL, et al. Murine thymic selection quantified using a unique method to capture deleted T cells. Proc Natl Acad Sci USA 2013;110(12):4679–84.
136. Davey GM, Schober SL, Endrizzi BT, Dutcher AK, Jameson SC, Hogquist KA. Preselection thymocytes are more sensitive to T cell receptor stimulation than mature T cells. J Exp Med 1998;188(10):1867–74.
137. Azzam HS, DeJarnette JB, Huang K, Emmons R, Park C-S, Sommers CL, et al. Fine Tuning of TCR Signaling by CD5. J Immunol 2001;166(9):5464–72.
138. Li QJ, Chau J, Ebert PJR, Sylvester G, Min H, Liu G, et al. miR-181a Is an Intrinsic Modulator of T Cell Sensitivity and Selection. Cell 2007;129(1):147–61.
139. Bain G, Cravatt CB, Loomans C, Alberola-Ila J, Hedrick SM, Murre C. Regulation of the helix-loop-helix proteins, E2A and Id3, by the Ras-ERK MAPK cascade. Nat Immunol

2001;2(2):165–71.
140. Rivera RR, Johns CP, Quan J, Johnson RS, Murre C. Thymocyte selection is regulated by the helix-loop-helix inhibitor protein, Id3. Immunity 2000;12(1):17–26.
141. Palmer E. Negative selection - Clearing out the bad apples from the T-cell repertoire. Nat Rev Immunol 2003;3(5):383–91.
142. Zijlstra M, Bix M, Simister NE, Loring JM, Raulet DH, Jaenisch R. β2-Microglobulin deficient mice lack CD4-8+ cytolytic T cells. Nature 1990;344(6268):742–6.
143. Cosgrove D, Gray D, Dierich A, Kaufman J, Lemeur M, Benoist C, et al. Mice lacking MHC class II molecules. Cell 1991;66(5):1051–66.
144. Singer A, Adoro S, Park J-H. Lineage fate and intense debate: myths, models and mechanisms of CD4/CD8 lineage choice. Nat Rev Immunol 2008;8(10):788.
145. Itano A, Robey E. Highly Efficient Selection of CD4 and CD8 Lineage Thymocytes Supports an Instructive Model of Lineage Commitment. Immunity 2000;12(4):383–9.
146. Bosselut R, Feigenbaum L, Sharrow SO, Singer A. Strength of signaling by CD4 and CD8 coreceptor tails determines the number but not the lineage direction of positively selected thymocytes. Immunity 2001;14(4):483–94.
147. Brugnera E, Bhandoola A, Cibotti R, Yu Q, Guinter TI, Yamashita Y, et al. Coreceptor Reversal in the Thymus: Signaled CD4+8+ Thymocytes Initially Terminate CD8 Transcription Even When Differentiating into CD8+ T Cells. Immunity 2000;13(1):59–71.
148. Sinclair C, Seddon B. Overlapping and Asymmetric Functions of TCR Signaling during Thymic Selection of CD4 and CD8 Lineages. J Immunol 2014;192(11):5151–9.
149. Taniuchi I, Osato M, Egawa T, Sunshine MJ, Bae SC, Komori T, et al. Differential requirements for Runx proteins in CD4 repression and epigenetic silencing during T lymphocyte development. Cell 2002;111(5):621–33.
150. Muroi S, Naoe Y, Miyamoto C, Akiyama K, Ikawa T, Masuda K, et al. Cascading suppression of transcriptional silencers by ThPOK seals helper T cell fate. Nat Immunol 2008;9(10):1113–21.
151. He X, He X, Dave VP, Zhang Y, Hua X, Nicolas E, et al. The zinc finger transcription factor Th-POK regulates CD4 versus CD8 T-cell lineage commitment. Nature 2005;433(7028):826–33.
152. Ueno T, Saito F, Gray DHD, Kuse S, Hieshima K, Nakano H, et al. CCR7 signals are essential for cortex-medulla migration of developing thymocytes. J Exp Med 2004;200(4):493–505.
153. Scollay R, Godfrey DI. Thymic emigration: conveyor belts or lucky dips? Immunol Today 1995;16(6):268–73.
154. Romagnoli P, Dooley J, Enault G, Vicente R, Malissen B, Liston A, et al. The Thymic Niche Does Not Limit Development of the Naturally Diverse Population of Mouse Regulatory T Lymphocytes. J Immunol 2012;189(8):3831–7.
155. Yu W, Nagaoka H, Jankovic M, Misulovin Z, Suh H, Rolink A, et al. Continued RAG expression in late stages of B cell development and no apparent re-induction after immunization. Nature 1999;400(6745):682–7.
156. Kuwata N, Igarashi H, Ohmura T, Aizawa S, Sakaguchi N. Cutting Edge: Absence of Expression of RAG1 in Peritoneal B-1 Cells Detected by Knocking into RAG1 Locus with Green Fluorescent Protein Gene. J Immunol 1999;163(12):6355–9.
157. Boursalian TE, Golob J, Soper DM, Cooper CJ, Fink PJ. Continued maturation of thymic emigrants in the periphery. Nat Immunol 2004;5(4):418–25.
158. Cowan JE, Parnell SM, Nakamura K, Caamano JH, Lane PJL, Jenkinson EJ, et al. The thymic medulla is required for Foxp3+ regulatory but not conventional CD4+ thymocyte development. J Exp Med 2013;210(4):675–81.
159. Kurobe H, Liu C, Ueno T, Saito F, Ohigashi I, Seach N, et al. CCR7-dependent cortex-to-medulla migration of positively selected thymocytes is essential for establishing central tolerance. Immunity 2006;24(2):165–77.

160. Klein L, Robey EA, Hsieh C-S. Central CD4+ T cell tolerance: deletion versus regulatory T cell differentiation. Nat Rev Immunol 2019;19(1):7–18.
161. Lee H-M, Bautista JL, Scott-Browne J, Mohan JF, Hsieh C-S. A broad range of self-reactivity drives thymic regulatory T cell selection to limit responses to self. Immunity 2012;37(3):475.
162. Daniels MA, Teixeiro E, Gill J, Hausmann B, Roubaty D, Holmberg K, et al. Thymic selection threshold defined by compartmentalization of Ras/MAPK signalling. Nature 2006;444(7120):724–9.
163. Relland LM, Mishra MK, Haribhai D, Edwards B, Ziegelbauer J, Williams CB. Affinity-based selection of regulatory T cells occurs independent of agonist-mediated induction of Foxp3 expression. J Immunol 2009;182(3):1341–50.
164. Hinterberger M, Aichinger M, Prazeres da Costa O, Voehringer D, Hoffmann R, Klein L. Autonomous role of medullary thymic epithelial cells in central CD4+ T cell tolerance. Nat Immunol 2010;11(6):512–9.
165. Legoux FP, Lim J-B, Cauley AW, Dikiy S, Ertelt J, Mariani TJ, et al. CD4+ T Cell Tolerance to Tissue-Restricted Self Antigens Is Mediated by Antigen-Specific Regulatory T Cells Rather Than Deletion. Immunity 2015;43(5):896–908.
166. Malhotra D, Linehan JL, Dileepan T, Lee YJ, Purtha WE, Lu J V, et al. Tolerance is established in polyclonal CD4(+) T cells by distinct mechanisms, according to self-peptide expression patterns. Nat Immunol 2016;17(2):187–95.
167. Le Borgne M, Ladi E, Dzhagalov I, Herzmark P, Liao YF, Chakraborty AK, et al. The impact of negative selection on thymocyte migration in the medulla. Nat Immunol 2009;10(8):823–30.
168. Dzhagalov IL, Chen KG, Herzmark P, Robey EA. Elimination of self-reactive T cells in the thymus: a timeline for negative selection. PLoS Biol 2013;11(5):e1001566.
169. Sauer S, Bruno L, Hertweck A, Finlay D, Leleu M, Spivakov M, et al. T cell receptor signaling controls Foxp3 expression via PI3K, Akt, and mTOR. Proc Natl Acad Sci USA 2008;105(22):7797–802.
170. Khailaie S, Robert PA, Toker A, Huehn J, Meyer-Hermann M. A Signal Integration Model of Thymic Selection and Natural Regulatory T Cell Commitment. J Immunol 2014;193(12):5983–96.
171. Fontenot JD, Dooley JL, Farr AG, Rudensky AY. Developmental regulation of Foxp3 expression during ontogeny. J Exp Med 2005;202(7):901–6.
172. Wirnsberger G, Mair F, Klein L. Regulatory T cell differentiation of thymocytes does not require a dedicated antigen-presenting cell but is under T cell-intrinsic developmental control. Proc Natl Acad Sci USA 2009;106(25):10278–83.
173. Kishimoto H, Sprent J. Negative selection in the thymus includes semimature T cells. J Exp Med 1997;185(2):263–71.
174. McNeil LK, Starr TK, Hogquist KA. A requirement for sustained ERK signaling during thymocyte positive selection in vivo. Proc Natl Acad Sci USA 2005;102(38):13574–9.
175. Gray DHD, Kupresanin F, Berzins SP, Herold MJ, O'Reilly LA, Bouillet P, et al. The BH3-only proteins Bim and Puma cooperate to impose deletional tolerance of organ-specific antigens. Immunity 2012;37(3):451–62.
176. Apert C, Romagnoli P, van Meerwijk JPM. IL-2 and IL-15 dependent thymic development of Foxp3-expressing regulatory T lymphocytes. Protein Cell 2018;9(4):322–32.
177. Salomon B, Lenschow DJ, Rhee L, Ashourian N, Singh B, Sharpe A, et al. B7/CD28 Costimulation Is Essential for the Homeostasis of the CD4+CD25+ Immunoregulatory T Cells that Control Autoimmune Diabetes. Immunity 2000;12(4):431–40.
178. Hinterberger M, Wirnsberger G, Klein L. B7/CD28 in central tolerance: Costimulation promotes maturation of regulatory T cell precursors and prevents their clonal deletion. Front Immunol 2011;2:30.

179. Murray ME, Gavile CM, Nair JR, Koorella C, Carlson LM, Buac D, et al. CD28-mediated pro-survival signaling induces chemotherapeutic resistance in multiple myeloma. Blood 2014;123(24):3770–9.
180. Farrar MA, Owen DL. STAT5 and CD4+ T Cell Immunity. F1000Research 2017;6.
181. Burchill MA, Yang J, Vang KB, Moon JJ, Chu HH, Lio CWJ, et al. Linked T Cell Receptor and Cytokine Signaling Govern the Development of the Regulatory T Cell Repertoire. Immunity 2008;28(1):112–21.
182. Tai X, Erman B, Alag A, Mu J, Kimura M, Katz G, et al. Foxp3 transcription factor is pro-apoptotic and lethal to developing regulatory T cells unless counterbalanced by cytokine survival signals. Immunity 2013;38(6):1116.
183. Burchill MA, Yang J, Vogtenhuber C, Blazar BR, Farrar MA. IL-2 receptor beta-dependent STAT5 activation is required for the development of Foxp3+ regulatory T cells. J Immunol 2007;178(1):280–90.
184. Vang KB, Yang J, Mahmud SA, Burchill MA, Vegoe AL, Farrar MA. IL-2, -7, and -15, but Not Thymic Stromal Lymphopoeitin, Redundantly Govern CD4 + Foxp3 + Regulatory T Cell Development. J Immunol 2008;181(5):3285–90.
185. Tani-ichi S, Shimba A, Wagatsuma K, Miyachi H, Kitano S, Imai K, et al. Interleukin-7 receptor controls development and maturation of late stages of thymocyte subpopulations. Proc Natl Acad Sci USA 2013;110(2):612–7.
186. Soper DM, Kasprowicz DJ, Ziegler SF. IL-2Rβ links IL-2R signaling with Foxp3 expression. Eur J Immunol 2007;37(7):1817–26.
187. Marshall D, Sinclair C, Tung S, Seddon B. Differential requirement for IL-2 and IL-15 during bifurcated development of thymic regulatory T cells. J Immunol 2014;193(11):5525–33.
188. Lio C-WJ, Hsieh C-S. A two-step process for thymic regulatory T cell development. Immunity 2008;28(1):100–11.
189. Owen DL, Mahmud SA, Sjaastad LE, Williams JB, Spanier JA, Simeonov DR, et al. Thymic regulatory T cells arise via two distinct developmental programs. Nat Immunol 2019;20(2):195–205.
190. Bending D, Martín PP, Paduraru A, Ducker C, Marzaganov E, Laviron M, et al. A timer for analyzing temporally dynamic changes in transcription during differentiation in vivo. J Cell Biol 2018;217(8):2931–50.
191. Xing Y, Wang X, Jameson SC, Hogquist KA. Late stages of T cell maturation in the thymus involve NF-κB and tonic type i interferon signaling. Nat Immunol 2016;17(5):565–73.
192. James KD, Cosway EJ, Lucas B, White AJ, Parnell SM, Carvalho-Gaspar M, et al. Endothelial cells act as gatekeepers for LTβRdependent thymocyte emigration. J Exp Med 2018;215(12):2984–93.
193. Webb L V., Ley SC, Seddon B. TNF activation of NF-κB is essential for development of single-positive thymocytes. J Exp Med 2016;213(8):1399.
194. Webb L V, Barbarulo A, Huysentruyt J, Vanden Berghe T, Takahashi N, Ley S, et al. Survival of Single Positive Thymocytes Depends upon Developmental Control of RIPK1 Kinase Signaling by the IKK Complex Independent of NF-κB. Immunity 2019;50(2):348–61.
195. Sinclair C, Saini M, Van Der Loeff IS, Sakaguchi S, Seddon B. The long-term survival potential of mature T lymphocytes is programmed during development in the thymus. Sci Signal 2011;4(199):ra77.
196. Hare KJ, Jenkinson EJ, Anderson G. An Essential Role for the IL-7 Receptor During Intrathymic Expansion of the Positively Selected Neonatal T Cell Repertoire. J Immunol 2000;165(5):2410–4.
197. Tan JT, Dudl E, LeRoy E, Murray R, Sprent J, Weinberg KI, et al. IL-7 is critical for homeostatic proliferation and survival of naïve T cells. Proc Natl Acad Sci USA 2001;98(15):8732–7.
198. Seddon B, Zamoyska R. TCR and IL-7 Receptor Signals Can Operate Independently or

Synergize to Promote Lymphopenia-Induced Expansion of Naive T Cells. J Immunol 2002;169(7):3752–9.
199. Silv A, Cornish G, Ley SC, Seddon B. NF-κB signaling mediates homeostatic maturation of new T cells. Proc Natl Acad Sci USA 2014;111(9):E846-55.
200. Hsu FC, Shapiro MJ, Dash B, Chen CC, Constans MM, Chung JY, et al. An Essential Role for the Transcription Factor Runx1 in T Cell Maturation. Sci Rep 2016;6(1):23533.
201. Matloubian M, Lo CG, Cinamon G, Lesneski MJ, Xu Y, Brinkmann V, et al. Lymphocyte egress from thymus and peripheral lymphoid organs is dependent on S1P receptor 1. Nature 2004;427(6972):355–60.
202. Carlson CM, Endrizzi BT, Wu J, Ding X, Weinreich MA, Walsh ER, et al. Kruppel-like factor 2 regulates thymocyte and T-cell migration. Nature 2006;442(7100):299–302.
203. Fabre S, Carrette F, Chen J, Lang V, Semichon M, Denoyelle C, et al. FOXO1 Regulates L-Selectin and a Network of Human T Cell Homing Molecules Downstream of Phosphatidylinositol 3-Kinase. J Immunol 2008;181(5):2980–9.
204. Alfonso C, McHeyzer-Williams MG, Rosen H. CD69 down-modulation and inhibition of thymic egress by short- and long-term selective chemical agonism of sphingosine 1-phosphate receptors. Eur J Immunol 2006;36(1):149–59.
205. Bankovich AJ, Shiow LR, Cyster JG. CD69 suppresses sphingosine 1-phosophate receptor-1 (S1P1) function through interaction with membrane helix 4. J Biol Chem 2010;285(29):22328–37.
206. Yagi H, Kamba R, Chiba K, Soga H, Yaguchi K, Nakamura M, et al. Immunosuppressant FTY720 inhibits thymocyte emigration. Eur J Immunol 2000;30(5):1435–44.
207. Rosen H, Alfonso C, Surh CD, McHeyzer-Williams MG. Rapid induction of medullary thymocyte phenotypic maturation and egress inhibition by nanomolar sphingosine 1-phosphate receptor agonist. Proc Natl Acad Sci USA 2003;100(19):10907–12.
208. Zachariah MA, Cyster JG. Neural crest-derived pericytes promote egress of mature thymocytes at the corticomedullary junction. Science 2010;328(5982):1129–35.
209. Bréart B, Ramos-Perez WD, Mendoza A, Salous AK, Gobert M, Huang Y, et al. Lipid phosphate phosphatase 3 enables efficient thymic egress. J Exp Med 2011;208(6):1267–78.
210. Zamora-Pineda J, Kumar A, Suh JH, Zhang M, Saba JD. Dendritic cell sphingosine-1-phosphate lyase regulates thymic egress. J Exp Med 2016;213(12):2773.
211. Rieck M, Kremser C, Jobin K, Mettke E, Kurts C, Gräler M, et al. Ceramide synthase 2 facilitates S1P-dependent egress of thymocytes into the circulation in mice. Eur J Immunol 2017;47(4):677–84.
212. Jin R, Wang W, Yao J-Y, Zhou Y-B, Qian X-P, Zhang J, et al. Characterization of the In Vivo Dynamics of Medullary CD4 + CD8 − Thymocyte Development. J Immunol 2008;180(4):2256–63.
213. Berzins SP, Boyd RL, Miller JFAP. The role of the thymus and recent thymic migrants in the maintenance of the adult peripheral lymphocyte pool. J Exp Med 1998;187(11):1839–48.
214. Hsu F-C, Shapiro MJ, Chen MW, McWilliams DC, Seaburg LM, Tangen SN, et al. Immature Recent Thymic Emigrants Are Eliminated by Complement. J Immunol 2014;193(12):6005–15.
215. Hsu FC, Pajerowski AG, Nelson-Holte M, Sundsbak R, Shapiro VS. NKAP is required for T cell maturation and acquisition of functional competency. J Exp Med 2011;208(6):1291–304.
216. Zhang S, Zhang X, Wang K, Xu X, Li M, Zhang J, et al. Newly Generated CD4 + T Cells Acquire Metabolic Quiescence after Thymic Egress . J Immunol 2018;200(3):1064–77.
217. Hendricks DW, Fink PJ. Recent thymic emigrants are biased against the T-helper type 1 and toward the T-helper type 2 effector lineage. Blood 2011;117(4):1239.
218. Friesen TJ, Ji Q, Fink PJ. Recent thymic emigrants are tolerized in the absence of

inflammation. J Exp Med 2016;213(6):913–20.
219. Moore JWJ, Beattie L, Osman M, Owens BMJ, Brown N, Dalton JE, et al. CD4+ recent thymic emigrants are recruited into granulomas during leishmania donovani infection but have limited capacity for cytokine production. PLoS One 2016;11(9):e0163604.
220. Paiva RS, Lino AC, Bergman ML, Caramalho Í, Sousa AE, Zelenay S, et al. Recent thymic emigrants are the preferential precursors of regulatory T cells differentiated in the periphery. Proc Natl Acad Sci USA 2013;110(16):6494–9.
221. Bhaumik S, Giffon T, Bolinger D, Kirkman R, Lewis DB, Weaver CT, et al. Retinoic Acid hypersensitivity promotes peripheral tolerance in recent thymic emigrants. J Immunol 2013;190(6):2603–13.
222. Thangavelu G, Parkman JC, Ewen CL, Uwiera RRE, Baldwin TA, Anderson CC. Programmed death-1 is required for systemic self-tolerance in newly generated T cells during the establishment of immune homeostasis. J Autoimmun 2011;36(3–4):301–12.
223. Ellestad KK, Thangavelu G, Haile Y, Lin J, Boon L, Anderson CC. Prior to peripheral tolerance, newly generated CD4 T cells maintain dangerous autoimmune potential: Fas- and Perforin-independent autoimmunity controlled by programmed death-1. Front Immunol 2018;9:12.
224. Berkley AM, Hendricks DW, Simmons KB, Fink PJ. Recent Thymic Emigrants and Mature Naive T Cells Exhibit Differential DNA Methylation at Key Cytokine Loci. J Immunol 2013;190(12):6180–6.
225. Cunningham CA, Bergsbaken T, Fink PJ. Cutting Edge: Defective Aerobic Glycolysis Defines the Distinct Effector Function in Antigen-Activated CD8 + Recent Thymic Emigrants . J Immunol 2017;198(12):4575–80.
226. Cunningham CA, Hoppins S, Fink PJ. Cutting Edge: Glycolytic Metabolism and Mitochondrial Metabolism Are Uncoupled in Antigen-Activated CD8 + Recent Thymic Emigrants . J Immunol 2018;201(6):1627–32.
227. Chinn IK, Blackburn CC, Manley NR, Sempowski GD. Changes in primary lymphoid organs with aging. Semin Immunol 2012;24(5):309–20.
228. Hale JS, Boursalian TE, Turk GL, Fink PJ. Thymic output in aged mice. Proc Natl Acad Sci USA 2006;103(22):8447–52.
229. Jenkinson EJ, Jenkinson WE, Rossi SW, Anderson G. The thymus and T-cell commitment: the right niche for Notch? Nat Rev Immunol 2006;6(7):551–5.
230. Ueno T, Hara K, Willis MS, Malin MA, Höpken UE, Gray DHD, et al. Role for CCR7 Ligands in the Emigration of Newly Generated T Lymphocytes from the Neonatal Thymus. Immunity 2002;16(2):205–18.
231. Jiang Q, Su H, Knudsen G, Helms W, Su L. Delayed functional maturation of natural regulatory T cells in the medulla of postnatal thymus: Role of TSLP. BMC Immunol 2006;7(1):6.
232. Guerau-de-Arellano M, Martinic M, Benoist C, Mathis D. Neonatal tolerance revisited: A perinatal window for Aire control of autoimmunity. J Exp Med 2009;206(6):1245–52.
233. Yang S, Fujikado N, Kolodin D, Benoist C, Mathis D. Regulatory T cells generated early in life play a distinct role in maintaining self-tolerance. Science 2015;348(6234):589–94.
234. Cowan JE, McCarthy NI, Anderson G. CCR7 Controls Thymus Recirculation, but Not Production and Emigration, of Foxp3+T Cells. Cell Rep 2016;14(5):1041–8.
235. Thiault N, Darrigues J, Adoue V, Gros M, Binet B, Perals C, et al. Peripheral regulatory T lymphocytes recirculating to the thymus suppress the development of their precursors. Nat Immunol 2015;16(6):628–34.
236. Clise-Dwyer K, Huston GE, Buck AL, Duso DK, Swain SL. Environmental and Intrinsic Factors Lead to Antigen Unresponsiveness in CD4+ Recent Thymic Emigrants from Aged Mice. J Immunol 2007;178(3):1321–31.
237. Houston EG, Higdon LE, Fink PJ. Recent thymic emigrants are preferentially incorporated

only into the depleted T-cell pool. Proc Natl Acad Sci USA 2011;108(13):5366–71.
238. Min B, McHugh R, Sempowski GD, Mackall C, Foucras G, Paul WE. Neonates Support Lymphopenia-Induced Proliferation. Immunity 2003;18(1):131–40.
239. Opiela SJ, Koru-Sengul T, Adkins B. Murine neonatal recent thymic emigrants are phenotypically and functionally distinct from adult recent thymic emigrants. Blood 2009;113(22):5635–43.
240. Vaidya HJ, Briones Leon A, Blackburn CC. FOXN1 in thymus organogenesis and development. Eur J Immunol 2016;46(8):1826–37.
241. Gordon J, Wilson VA, Blair NF, Sheridan J, Farley A, Wilson L, et al. Functional evidence for a single endodermal origin for the thymic epithelium. Nat Immunol 2004;5(5):546–53.
242. Rossi SW, Jenkinson WE, Anderson G, Jenkinson EJ. Clonal analysis reveals a common progenitor for thymic cortical and medullary epithelium. Nature 2006;441(7096):988–91.
243. Luis TC, Luc S, Mizukami T, Boukarabila H, Thongjuea S, Woll PS, et al. Initial seeding of embryonic thymus by immune-restricted lympho-myeloid progenitors. Nat Immunol 2016;17(12):1424.
244. Klug DB, Carter C, Gimenez-Conti IB, Richie ER. Cutting Edge: Thymocyte-Independent and Thymocyte-Dependent Phases of Epithelial Patterning in the Fetal Thymus. J Immunol 2002;169(6):2842–5.
245. Nehls M, Pfeifer D, Schorpp M, Hedrich H, Boehm T. New member of the winged-helix protein family disrupted in mouse and rat nude mutations. Nature 1994;372(6501):103–7.
246. Blackburn CC, Augustine CL, Li R, Harvey RP, Malin MA, Boyd RL, et al. The nu gene acts cell-autonomously and is required for differentiation of thymic epithelial progenitors. Proc Natl Acad Sci USA 1996;93(12):5742–6.
247. Nowell CS, Bredenkamp N, Tetélin S, Jin X, Tischner C, Vaidya H, et al. Foxn1 regulates lineage progression in cortical and medullary thymic epithelial cells but is dispensable for medullary sublineage divergence. PLoS Genet 2011;7(11):e1002348.
248. Itoi M, Kawamoto H, Katsura Y, Amagai T. Two distinct steps of immigration of hematopoietic progenitors into the early thymus anlage. Int Immunol 2001;13(9):1203–11.
249. Kadouri N, Nevo S, Goldfarb Y, Abramson J. Thymic epithelial cell heterogeneity: TEC by TEC. Nat Rev Immunol 2020;20(4):239–53.
250. Murata S, Sasaki K, Kishimoto T, Niwa SI, Hayashi H, Takahama Y, et al. Regulation of CD8+ T cell development by thymus-specific proteasomes. Science 2007;316(5829):1349–53.
251. Florea BI, Verdoes M, Li N, Van Der Linden WA, Geurink PP, Van Den Elst H, et al. Activity-based profiling reveals reactivity of the murine thymoproteasome-specific subunit β5t. Chem Biol 2010;17(8):795–801.
252. Sasaki K, Takada K, Ohte Y, Kondo H, Sorimachi H, Tanaka K, et al. Thymoproteasomes produce unique peptide motifs for positive selection of CD8+ T cells. Nat Commun 2015;6(1):1–10.
253. Xing Y, Jameson SC, Hogquist KA. Thymoproteasome subunit-β5T generates peptide-MHC complexes specialized for positive selection. Proc Natl Acad Sci USA 2013;110(17):6979–84.
254. Nakagawa T, Roth W, Wong P, Nelson A, Farr A, Deussing J, et al. Cathepsin L: Critical role in Ii degradation and CD4 T cell selection in the thymus. Science 1998;280(5362):450–3.
255. Honey K, Nakagawa T, Peters C, Rudensky A. Cathepsin L regulates CD4+ T cell selection independently of its effect on invariant chain: A role in the generation of positively selecting peptide ligands. J Exp Med 2002;195(10):1349–58.
256. Gommeaux J, Grégoire C, Nguessan P, Richelme M, Malissen M, Guerder S, et al. Thymus-specific serine protease regulates positive selection of a subset of CD4+ thymocytes. Eur J Immunol 2009;39(4):956–64.
257. Nedjic J, Aichinger M, Emmerich J, Mizushima N, Klein L. Autophagy in thymic epithelium shapes the T-cell repertoire and is essential for tolerance. Nature 2008;455(7211):396–

400.
258. Wekerle H, Ketelsen UP, Ernst M. Thymic nurse cells. Lymphoepithelial cell complexes in murine thymuses: Morphological and serological characterization. J Exp Med 1980;151(4):925–44.
259. Nakagawa Y, Ohigashi I, Nitta T, Sakata M, Tanaka K, Murata S, et al. Thymic nurse cells provide microenvironment for secondary T cell receptor α rearrangement in cortical thymocytes. Proc Natl Acad Sci USA 2012;109(50):20572–7.
260. Gray DHD, Seach N, Ueno T, Milton MK, Liston A, Lew AM, et al. Developmental kinetics, turnover, and stimulatory capacity of thymic epithelial cells. Blood 2006;108(12):3777–85.
261. Gray D, Abramson J, Benoist C, Mathis D. Proliferative arrest and rapid turnover of thymic epithelial cells expressing Aire. J Exp Med 2007;204(11):2521–8.
262. Bornstein C, Nevo S, Giladi A, Kadouri N, Pouzolles M, Gerbe F, et al. Single-cell mapping of the thymic stroma identifies IL-25-producing tuft epithelial cells. Nature 2018;559(7715):622–6.
263. Anderson MS, Venanzi ES, Klein L, Chen Z, Berzins SP, Turley SJ, et al. Projection of an immunological self shadow within the thymus by the aire protein. Science 2002;298(5597):1395–401.
264. Sansom SN, Shikama-Dorn N, Zhanybekova S, Nusspaumer G, Macaulay IC, Deadman ME, et al. Population and single-cell genomics reveal the Aire dependency, relief from Polycomb silencing, and distribution of self-antigen expression in thymic epithelia. Genome Res 2014;24(12):1918–31.
265. Meredith M, Zemmour D, Mathis D, Benoist C. Aire controls gene expression in the thymic epithelium with ordered stochasticity. Nat Immunol 2015;16(9):942–9.
266. Brennecke P, Reyes A, Pinto S, Rattay K, Nguyen M, Kuchler R, et al. Single-cell transcriptome analysis reveals coordinated ectopic gene-expression patterns in medullary thymic epithelial cells. Nat Immunol 2015;16(9):933–41.
267. Takaba H, Morishita Y, Tomofuji Y, Danks L, Nitta T, Komatsu N, et al. Fezf2 Orchestrates a Thymic Program of Self-Antigen Expression for Immune Tolerance. Cell 2015;163(4):975–87.
268. Danan-Gotthold M, Guyon C, Giraud M, Levanon EY, Abramson J. Extensive RNA editing and splicing increase immune self-representation diversity in medullary thymic epithelial cells. Genome Biol 2016;17(1):1–13.
269. Derbinski J, Gäbler J, Brors B, Tierling S, Jonnakuty S, Hergenhahn M, et al. Promiscuous gene expression in thymic epithelial cells is regulated at multiple levels. J Exp Med 2005;202(1):33–45.
270. Aichinger M, Wu C, Nedjic J, Klein L. Macroautophagy substrates are loaded onto MHC class II of medullary thymic epithelial cells for central tolerance. J Exp Med 2013;210(2):287–300.
271. Cui G, Hara T, Simmons S, Wagatsuma K, Abe A, Miyachi H, et al. Characterization of the IL-15 niche in primary and secondary lymphoid organs in vivo. Proc Natl Acad Sci USA 2014;111(5):1915–20.
272. White AJ, Jenkinson WE, Cowan JE, Parnell SM, Bacon A, Jones ND, et al. An Essential Role for Medullary Thymic Epithelial Cells during the Intrathymic Development of Invariant NKT Cells. J Immunol 2014;192(6):2659–66.
273. Mahmud SA, Manlove LS, Schmitz HM, Xing Y, Wang Y, Owen DL, et al. Costimulation via the tumor-necrosis factor receptor superfamily couples TCR signal strength to the thymic differentiation of regulatory T cells. Nat Immunol 2014;15(5):473–81.
274. Herbin O, Bonito AJ, Jeong S, Weinstein EG, Rahman AH, Xiong H, et al. Medullary thymic epithelial cells and CD8α+dendritic cells coordinately regulate central tolerance but CD8α+cells are dispensable for thymic regulatory T cell production. J Autoimmun 2016;75:141–9.

275. Perry JSA, Lio CWJ, Kau AL, Nutsch K, Yang Z, Gordon JI, et al. Distinct contributions of Aire and antigen-presenting-cell subsets to the generation of self-tolerance in the thymus. Immunity 2014;41(3):414–26.
276. Akiyama T, Shimo Y, Yanai H, Qin J, Ohshima D, Maruyama Y, et al. The Tumor Necrosis Factor Family Receptors RANK and CD40 Cooperatively Establish the Thymic Medullary Microenvironment and Self-Tolerance. Immunity 2008;29(3):423–37.
277. Rossi SW, Kim MY, Leibbrandt A, Parnell SM, Jenkinson WE, Glanville SH, et al. RANK signals from CD4+3- inducer cells regulate development of Aire-expressing epithelial cells in the thymic medulla. J Exp Med 2007;204(6):1267–72.
278. Onder L, Nindl V, Scandella E, Chai Q, Cheng HW, Caviezel-Firner S, et al. Alternative NF-κB signaling regulates mTEC differentiation from podoplanin-expressing presursors in the cortico-medullary junction. Eur J Immunol 2015;45(8):2218–31.
279. Miragaia RJ, Zhang X, Gomes T, Svensson V, Ilicic T, Henriksson J, et al. Single-cell RNA-sequencing resolves self-antigen expression during mTEC development. Sci Rep 2018;8(1):1–13.
280. Lkhagvasuren E, Sakata M, Ohigashi I, Takahama Y. Lymphotoxin β Receptor Regulates the Development of CCL21-Expressing Subset of Postnatal Medullary Thymic Epithelial Cells. J Immunol 2013;190(10):5110–7.
281. Kozai M, Kubo Y, Katakai T, Kondo H, Kiyonari H, Schaeuble K, et al. Essential role of CCL21 in establishment of central self-tolerance in T cells. J Exp Med 2017;214(7):1925–35.
282. Lucas B, White AJ, Cosway EJ, Parnell SM, James KD, Jones ND, et al. Diversity in medullary thymic epithelial cells controls the activity and availability of iNKT cells. Nat Commun 2020;11(1):2198.
283. Miller CN, Proekt I, von Moltke J, Wells KL, Rajpurkar AR, Wang H, et al. Thymic tuft cells promote an IL-4-enriched medulla and shape thymocyte development. Nature 2018;559(7715):627–31.
284. Yano M, Kuroda N, Han H, Meguro-Horike M, Nishikawa Y, Kiyonari H, et al. Aire controls the differentiation program of thymic epithelial cells in the medulla for the establishment of self-tolerance. J Exp Med 2008;205(12):2827–38.
285. White AJ, Nakamura K, Jenkinson WE, Saini M, Sinclair C, Seddon B, et al. Lymphotoxin Signals from Positively Selected Thymocytes Regulate the Terminal Differentiation of Medullary Thymic Epithelial Cells. J Immunol 2010;185(8):4769–76.
286. Watanabe N, Wang YH, Lee HK, Ito T, Wang YH, Cao W, et al. Hassall's corpuscles instruct dendritic cells to induce CD4 +CD25+ regulatory T cells in human thymus. Nature 2005;436(7054):1181–5.
287. Wu L, Shortman K. Heterogeneity of thymic dendritic cells. Semin Immunol 2005;17(4):304–12.
288. Hadeiba H, Lahl K, Edalati A, Oderup C, Habtezion A, Pachynski R, et al. Plasmacytoid Dendritic Cells Transport Peripheral Antigens to the Thymus to Promote Central Tolerance. Immunity 2012;36(3):438–50.
289. Vobořil M, Brabec T, Dobeš J, Šplíchalová I, Březina J, Čepková A, et al. Toll-like receptor signaling in thymic epithelium controls monocyte-derived dendritic cell recruitment and Treg generation. Nat Commun 2020;11(1):2361.
290. Bonasio R, Scimone ML, Schaerli P, Grabie N, Lichtman AH, von Andrian UH. Clonal deletion of thymocytes by circulating dendritic cells homing to the thymus. Nat Immunol 2006;7(10):1092–100.
291. Baba T, Nakamoto Y, Mukaida N. Crucial Contribution of Thymic Sirp + Conventional Dendritic Cells to Central Tolerance against Blood-Borne Antigens in a CCR2-Dependent Manner. J Immunol 2009;183(5):3053–63.
292. Cosway EJ, Ohigashi I, Schauble K, Parnell SM, Jenkinson WE, Luther S, et al. Formation of the Intrathymic Dendritic Cell Pool Requires CCL21-Mediated Recruitment of CCR7 +

Progenitors to the Thymus. J Immunol 2018;201(2):516–23.
293. Lei Y, Ripen AM, Ishimaru N, Ohigashi I, Nagasawa T, Jeker LT, et al. Aire-dependent production of XCL1 mediates medullary accumulation of thymic dendritic cells and contributes to regulatory T cell development. J Exp Med 2011;208(2):383–94.
294. Atibalentja DF, Murphy KM, Unanue ER. Functional Redundancy between Thymic CD8α + and Sirpα + Conventional Dendritic Cells in Presentation of Blood-Derived Lysozyme by MHC Class II Proteins . J Immunol 2011;186(3):1421–31.
295. Koble C, Kyewski B. The thymic medulla: A unique microenvironment for intercellular self-antigen transfer. J Exp Med 2009;206(7):1505–13.
296. Hubert F-X, Kinkel SA, Davey GM, Phipson B, Mueller SN, Liston A, et al. Aire regulates the transfer of antigen from mTECs to dendritic cells for induction of thymic tolerance. Blood 2011;118(9):2462–72.
297. Proietto AI, Dommelen S van, Zhou P, Rizzitelli A, D'Amico A, Steptoe RJ, et al. Dendritic cells in the thymus contribute to T-regulatory cell induction. Proc Natl Acad Sci 2008;105(50):19869–74.
298. Coquet JM, Ribot JC, Bąbala N, Middendorp S, van der Horst G, Xiao Y, et al. Epithelial and dendritic cells in the thymic medulla promote CD4+Foxp3+ regulatory t cell development via the CD27-CD70 pathway. J Exp Med 2013;210(4):715–28.
299. Weist BM, Kurd N, Boussier J, Chan SW, Robey EA. Thymic regulatory T cell niche size is dictated by limiting IL-2 from antigen-bearing dendritic cells and feedback competition. Nat Immunol 2015;16(6):635–41.
300. Cosway EJ, Lucas B, James KD, Parnell SM, Carvalho-Gaspar M, White AJ, et al. Redefining thymus medulla specialization for central tolerance. J Exp Med 2017;214(11):3183–95.
301. Boehm T, Scheu S, Pfeffer K, Bleul CC. Thymic medullary epithelial cell differentiation, thymocyte emigration, and the control of autoimmunity require lympho-epithelial cross talk via LTβR. J Exp Med 2003;198(5):757–69.
302. Lancaster JN, Thyagarajan HM, Srinivasan J, Li Y, Hu Z, Ehrlich LIR. Live-cell imaging reveals the relative contributions of antigen-presenting cell subsets to thymic central tolerance. Nat Commun 2019;10(1):2220.
303. Leventhal DS, Gilmore DC, Berger JM, Nishi S, Lee V, Malchow S, et al. Dendritic Cells Coordinate the Development and Homeostasis of Organ-Specific Regulatory T Cells. Immunity 2016;44(4):847–59.
304. Owen DL, Mahmud SA, Vang KB, Kelly RM, Blazar BR, Smith KA, et al. Identification of Cellular Sources of IL-2 Needed for Regulatory T Cell Development and Homeostasis. J Immunol 2018;200(12):3926–33.
305. Hemmers S, Schizas M, Azizi E, Dikiy S, Zhong Y, Feng Y, et al. IL-2 production by self-reactive CD4 thymocytes scales regulatory T cell generation in the thymus. J Exp Med 2019;216(11):2466–78.
306. Yang E, Zou T, Leichner TM, Zhang SL, Kambayashi T. Both retention and recirculation contribute to long-lived regulatory T-cell accumulation in the thymus. Eur J Immunol 2014;44(9):2712–20.
307. Cowan JE, Baik S, McCarthy NI, Parnell SM, White AJ, Jenkinson WE, et al. Aire controls the recirculation of murine Foxp3+ regulatory T-cells back to the thymus. Eur J Immunol 2018;48(5):844–54.
308. McCarthy NI, Cowan JE, Nakamura K, Bacon A, Baik S, White AJ, et al. Osteoprotegerin-Mediated Homeostasis of Rank + Thymic Epithelial Cells Does Not Limit Foxp3 + Regulatory T Cell Development. J Immunol 2015;195(6):2675–82.
309. Houston EG, Nechanitzky R, Fink PJ. Cutting Edge: Contact with Secondary Lymphoid Organs Drives Postthymic T Cell Maturation. J Immunol 2008;181(8):5213–7.
310. Houston EG, Fink PJ. MHC Drives TCR Repertoire Shaping, but not Maturation, in Recent Thymic Emigrants. J Immunol 2009;183(11):7244–9.

311. Houston EG, Boursalian TE, Fink PJ. Homeostatic signals do not drive post-thymic T cell maturation. Cell Immunol 2012;274(1–2):39–45.
312. Dong J, Chen Y, Xu X, Jin R, Teng F, Yan F, et al. Homeostatic Properties and Phenotypic Maturation of Murine CD4+ Pre-Thymic Emigrants in the Thymus. PLoS One 2013;8(2):e56378.
313. Staton TL, Habtezion A, Winslow MM, Sato T, Love PE, Butcher EC. CD8+ recent thymic emigrants home to and efficiently repopulate the small intestine epithelium. Nat Immunol 2006;7(5):482–8.
314. Xu X, Zhang S, Jin R, Wang K, Li P, Lin L, et al. Retention and tolerance of autoreactive CD4+ recent thymic emigrants in the liver. J Autoimmun 2015;56:87–97.
315. Xu X, Jin R, Li M, Wang K, Zhang S, Hao J, et al. Liver sinusoidal endothelial cells induce tolerance of autoreactive CD4+ recent thymic emigrants. Sci Rep 2016;6(1):19861.
316. Horst AK, Neumann K, Diehl L, Tiegs G. Modulation of liver tolerance by conventional and nonconventional antigen-presenting cells and regulatory immune cells. Cell Mol Immunol 2016;13(3):277–92.
317. Heinen AP, Wanke F, Moos S, Attig S, Luche H, Pal PP, et al. Improved method to retain cytosolic reporter protein fluorescence while staining for nuclear proteins. Cytom Part A 2014;85(7):621–7.
318. Zabransky DJ, Nirschl CJ, Durham NM, Park B V., Ceccato CM, Bruno TC, et al. Phenotypic and functional properties of Helios + regulatory T cells. PLoS One 2012;7(3):e34547.
319. Mottet C, Uhlig HH, Powrie F. Cutting edge: cure of colitis by CD4+CD25+ regulatory T cells. J Immunol 2003;170(8):3939–43.
320. Denning TL, Kim G, Kronenberg M. Cutting edge: CD4+CD25+ regulatory T cells impaired for intestinal homing can prevent colitis. J Immunol 2005;174(12):7487–91.
321. Stuart T, Butler A, Hoffman P, Hafemeister C, Papalexi E, Mauck WM, et al. Comprehensive Integration of Single-Cell Data. Cell 2019;177(7):1888-1902.e21.
322. Love MI, Huber W, Anders S. Moderated estimation of fold change and dispersion for RNA-seq data with DESeq2. Genome Biol 2014;15(12):550.
323. Campbell DJ, Koch MA. Phenotypical and functional specialization of FOXP3+ regulatory T cells. Nat Rev Immunol 2011;11(2):119–30.
324. Mouri Y, Nishijima H, Kawano H, Hirota F, Sakaguchi N, Morimoto J, et al. NF-κB–Inducing Kinase in Thymic Stroma Establishes Central Tolerance by Orchestrating Cross-Talk with Not Only Thymocytes but Also Dendritic Cells. J Immunol 2014;193(9):4356–67.
325. Toomer KH, Yuan X, Yang J, Dee MJ, Yu A, Malek TR. Developmental Progression and Interrelationship of Central and Effector Regulatory T Cell Subsets. J Immunol 2016;196(9):3665–76.
326. Anderson G, Jenkinson EJ. Investigating Central Tolerance With Reaggregate Thymus Organ Cultures. Methods Mol Biol 2007;380:185–96.
327. Jenkinson EJ, Franchi LL, Kingston R, Owen JJT. Effect of deoxyguanosine on lymphopoiesis in the developing thymus rudiment in vitro: Application in the production of chimeric thymus rudiments. Eur J Immunol 1982;12(7):583–7.
328. Vahl JC, Drees C, Heger K, Heink S, Fischer JC, Nedjic J, et al. Continuous T cell receptor signals maintain a functional regulatory T cell pool. Immunity 2014;41(5):722–36.
329. Lucas B, James KD, Cosway EJ, Parnell SM, Tumanov A V, Ware CF, et al. Lymphotoxin β Receptor Controls T Cell Progenitor Entry to the Thymus. J Immunol 2016;197(7):2665–72.
330. Dujardin HC, Burlen-Defranoux O, Boucontet L, Vieira P, Cumano A, Bandeira A. Regulatory potential and control of Foxp3 expression in newborn CD4 + T cells. Proc Natl Acad Sci USA 2004;101(40):14473–8.
331. Samy ET, Wheeler KM, Roper RJ, Teuscher C, Tung KSK. Cutting Edge: Autoimmune Disease in Day 3 Thymectomized Mice Is Actively Controlled by Endogenous Disease-Specific Regulatory T Cells. J Immunol 2008;180(7):4366–70.

332. Jiang W, Anderson MS, Bronson R, Mathis D, Benoist C. Modifier loci condition autoimmunity provoked by Aire deficiency. J Exp Med 2005;202(6):805–15.
333. van Dierendonck JH, Keijzer -Rob, van de Velde CJH, Cornelisse CJ. Nuclear Distribution of the Ki-67 Antigen during the Cell Cycle: Comparison with Growth Fraction in Human Breast Cancer Cells. Cancer Res 1989;49(11):2999–3006.
334. Van Oijen MGCT, Medema RH, Slootweg PJ, Rijksen G. Positivity of the proliferation marker Ki-67 in noncycling cells. Am J Clin Pathol 1998;110(1):24–31.
335. Ceredig R, Waltzinger C. Neonatal mouse CD4+ mature thymocytes show responsiveness to interleuking 2 and interleukin 7: Growth in vitro of negatively selected Vβ 6- and Vβ 11-expressing CD4+ cells from (C57BL/6xDBA/2)F1 mice. Int Immunol 1990;2(9):869–77.
336. Kumar P, Marinelarena A, Raghunathan D, Ragothaman VK, Saini S, Bhattacharya P, et al. Critical role of OX40 signaling in the TCR-independent phase of human and murine thymic Treg generation. Cell Mol Immunol 2019;16(2):138–53.
337. Hare KJ, Wilkinson RW, Jenkinson EJ, Anderson G. Identification of a developmentally regulated phase of postselection expansion driven by thymic epithelium. J Immunol 1998;160(8):3666–72.
338. Ceredig R. Intrathymic proliferation of perinatal mouse αβ and §γ T cell receptor-expressing mature T cells. Int Immunol 1990;2(9):859–67.
339. Föhse L, Reinhardt A, Oberdörfer L, Schmitz S, Förster R, Malissen B, et al. Differential Postselection Proliferation Dynamics of αβ T Cells, Foxp3 + Regulatory T Cells, and Invariant NKT Cells Monitored by Genetic Pulse Labeling. J Immunol 2013;191(5):2384–92.
340. Henriques CM, Rino J, Nibbs RJ, Graham GJ, Barata JT. IL-7 induces rapid clathrin-mediated internalization and JAK3-dependent degradation of IL-7Rα in T cells. Blood 2010;115(16):3269–77.
341. Dakic A, Shao Q, D'Amico A, O'Keeffe M, Chen W, Shortman K, et al. Development of the Dendritic Cell System during Mouse Ontogeny. J Immunol 2004;172(2):1018–27.
342. Fink PJ. The biology of recent thymic emigrants. Annu Rev Immunol 2013;31(1):31–50.
343. McHeyzer-Williams LJ, McHeyzer-Williams MG. Developmentally Distinct Th Cells Control Plasma Cell Production In Vivo. Immunity 2004;20(2):231–42.
344. Cunningham CA, Helm EY, Fink PJ. Reinterpreting recent thymic emigrant function: defective or adaptive? Curr Opin Immunol 2018;51:1–6.
345. Lee CK, Kim K, Welniak LA, Murphy WJ, Muegge K, Durum SK. Thymic emigrants isolated by a new method possess unique phenotypic and functional properties. Blood 2001;97(5):1360–9.
346. Berkley AM, Fink PJ. Cutting edge: CD8+ recent thymic emigrants exhibit increased responses to low-affinity ligands and improved access to peripheral sites of inflammation. J Immunol 2014;193(7):3262–6.
347. Schilham MW, Moerer P, Cumano A, Clevers HC. Sox-4 facilitates thymocyte differentiation. Eur J Immunol 1997;27(5):1292–5.
348. Malhotra N, Qi Y, Spidale NA, Frascoli M, Miu B, Cho O, et al. SOX4 controls invariant NKT cell differentiation by tuning TCR signaling. J Exp Med 2018;215(11):2887–900.
349. McFarland RD, Douek DC, Koup RA, Picker LJ. Identification of a human recent thymic emigrant phenotype. Proc Natl Acad Sci USA 2000;97(8):4215–20.
350. Hao QL, George AA, Zhu J, Barsky L, Zielinska E, Wang X, et al. Human intrathymic lineage commitment is marked by differential CD7 expression: Identification of CD7- lympho-myeloid thymic progenitors. Blood 2008;111(3):1318–26.
351. Heinly CS, Sempowski GD, Lee DM, Patel DD, McDermott PM, Scearce RM, et al. Comparison of thymocyte development and cytokine production in CD7-deficient, CD28-deficient and CD7/CD28 double-deficient mice. Int Immunol 2001;13(2):157–66.
352. Kakugawa K, Kojo S, Tanaka H, Seo W, Endo TA, Kitagawa Y, et al. Essential Roles of SATB1 in Specifying T Lymphocyte Subsets. Cell Rep 2017;19(6):1176–88.

353. Delacher M, Imbusch CD, Hotz-Wagenblatt A, Mallm JP, Bauer K, Simon M, et al. Precursors for Nonlymphoid-Tissue Treg Cells Reside in Secondary Lymphoid Organs and Are Programmed by the Transcription Factor BATF. Immunity 2020;52(2):295-312.e11.
354. Luo CT, Liao W, Dadi S, Toure A, Li MO. Graded Foxo1 activity in Treg cells differentiates tumour immunity from spontaneous autoimmunity. Nature 2016;529(7587):532–6.
355. DeLong JH, Hall AO, Konradt C, Coppock GM, Park J, Harms Pritchard G, et al. Cytokine- and TCR-Mediated Regulation of T Cell Expression of Ly6C and Sca-1. J Immunol 2018;200(5):1761–70.
356. Bamezai A, Palliser D, Berezovskaya A, McGrew J, Higgins K, Lacy E, et al. Regulated expression of Ly-6A.2 is important for T cell development. J Immunol 1995;154(9):4233–9.
357. Alvarez JD, Yasui DH, Niida H, Joh T, Loh DY, Kohwi-Shigematsu T. The MAR-binding protein SATB1 orchestrates temporal and spatial expression of multiple genes during T-cell development. Genes Dev 2000;14(5):521–35.
358. Palin AC, Ramachandran V, Acharya S, Lewis DB. Human Neonatal Naive CD4 + T Cells Have Enhanced Activation-Dependent Signaling Regulated by the MicroRNA miR-181a . J Immunol 2013;190(6):2682–91.
359. Khare SP, Shetty A, Biradar R, Patta I, Chen ZJ, Sathe A V., et al. NF-κB signaling and IL-4 signaling regulate SATB1 expression via alternative promoter usage during Th2 differentiation. Front Immunol 2019;10:667.
360. Chorro L, Suzuki M, Chin SS, Williams TM, Snapp EL, Odagiu L, et al. Interleukin 2 modulates thymic-derived regulatory T cell epigenetic landscape. Nat Commun 2018;9(1):5368.
361. Simonetta F, Gestermann N, Martinet KZ, Boniotto M, Tissières P, Seddon B, et al. Interleukin-7 influences FOXP3+CD4+ regulatory T cells peripheral homeostasis. PLoS One 2012;7(5):e36596.
362. Li Q, Nacion K, Bu H, Lin F. Mouse CD4+CD25+ T regulatory cells are protected from autologous complement mediated injury by Crry and CD59. Biochem Biophys Res Commun 2009;382(1):223–6.
363. Mingueneau M, Kreslavsky T, Gray D, Heng T, Cruse R, Ericson J, et al. The transcriptional landscape of αβ T cell differentiation. Nat Immunol 2013;14(6):619–32.
364. La Manno G, Soldatov R, Zeisel A, Braun E, Hochgerner H, Petukhov V, et al. RNA velocity of single cells. Nature 2018;560(7719):494–8.
365. Elyahu Y, Hekselman I, Eizenberg-Magar I, Berner O, Strominger I, Schiller M, et al. Aging promotes reorganization of the CD4 T cell landscape toward extreme regulatory and effector phenotypes. Sci Adv 2019;5(8):eaaw8330.
366. Hill JA, Feuerer M, Tash K, Haxhinasto S, Perez J, Melamed R, et al. Foxp3 Transcription-Factor-Dependent and -Independent Regulation of the Regulatory T Cell Transcriptional Signature. Immunity 2007;27(5):786–800.
367. Saoudi A, Seddon B, Fowell D, Mason D. The thymus contains a high frequency of cells that prevent autoimmune diabetes on transfer into prediabetic recipients. J Exp Med 1996;184(6):2393–8.
368. Sakaguchi S, Takahashi T, Nishizuka Y. Study on cellular events in post-thymectomy autoimmune oophoritis in mice: II. Requirement of lyt-1 cells in normal female mice for the prevention of oophoritis. J Exp Med 1982;156(6):1577–86.
369. Itoh M, Takahashi T, Sakaguchi N, Kuniyasu Y, Shimizu J, Otsuka F, et al. Thymus and autoimmunity: production of CD25+CD4+ naturally anergic and suppressive T cells as a key function of the thymus in maintaining immunologic self-tolerance. J Immunol 1999;162(9):5317–26.
370. Beyer M, Thabet Y, Müller RU, Sadlon T, Classen S, Lahl K, et al. Repression of the genome organizer SATB1 in regulatory T cells is required for suppressive function and inhibition of effector differentiation. Nat Immunol 2011;12(9):898–907.

APPENDIX: SUPPLEMENTARY DATA ACCOMPANYING CHAPTER FIVE

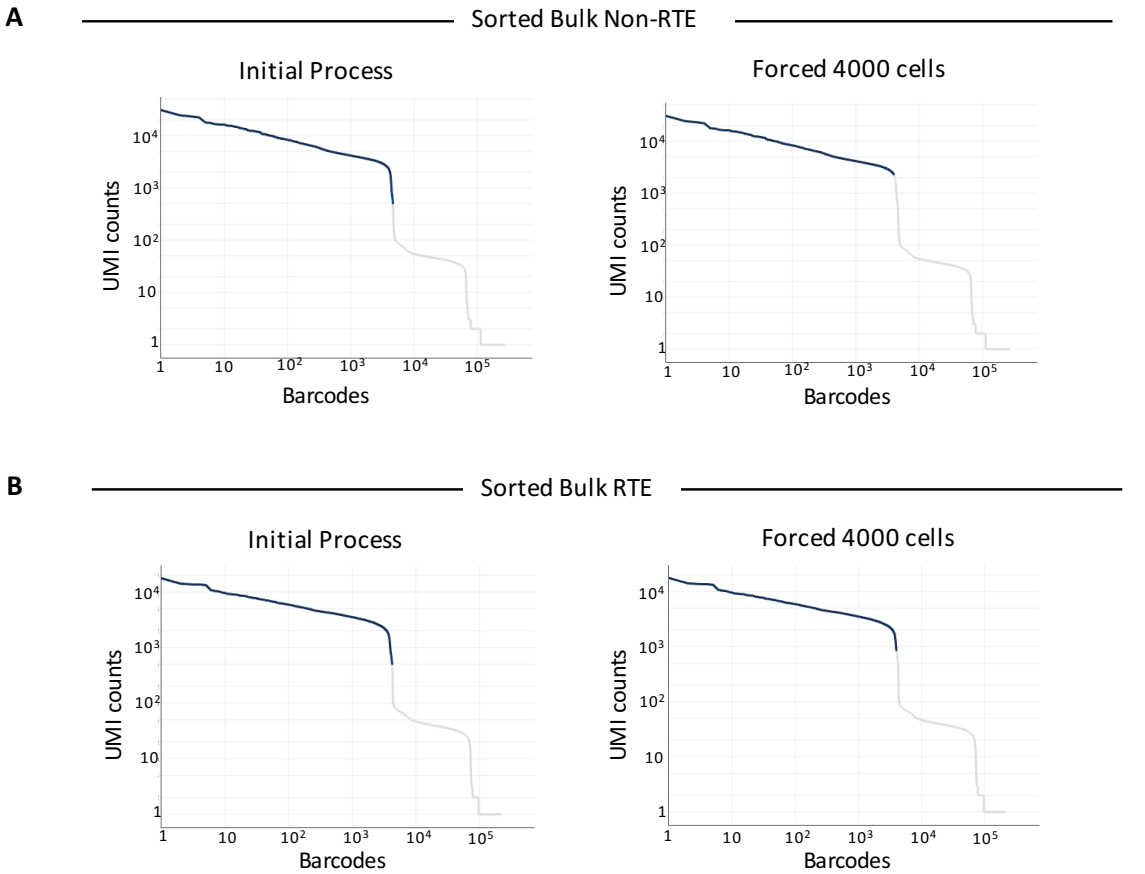
A
Sorted Bulk Non-RTE
Initial Process
Forced 4000 cells
UMI counts
Barcodes
B
Sorted Bulk RTE
Initial Process
Forced 4000 cells
UMI counts
Barcodes

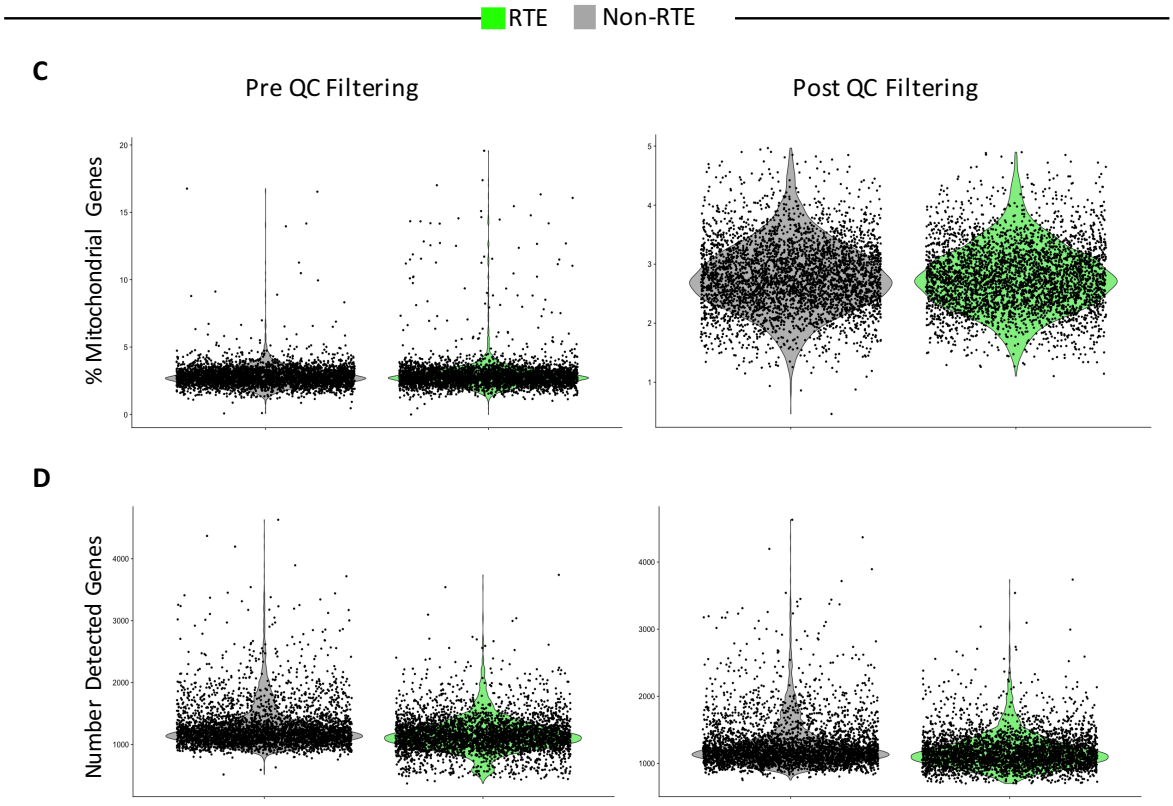
RTE
Non-RTE
C
Pre QC Filtering
Post QC Filtering
% Mitochondrial Genes
D
Number Detected Genes

Figure S. 1 Detail of QC Steps Taken in Processing scRNAseq Dataset from Figure 5.2

(A-B) Removal of suspected empty droplets from processed scRNAseq dataset. Barcode Rank plots from the output summary of Cell Ranger Pipeline processing of scRNAseq **(A)** Non-RTE or **(B)** RTE samples. Plots on the left are from processing using default settings while plots on the left are from processing where the algorithm was forced to return 4000 cells. The blue line indicates detected cells while the grey indicates background empty droplets.

(C-D) Removal of low quality cells from processed scRNAseq dataset. Violin plots of **(C)** the **%** mitochondrial genes and **(D)** the number of unique genes detected in cells from pooled Non-RTE (grey) and RTE (green) scRNAseq dataset. Plots are generated from the dataset either prior (left) or post (right) to the enforcement of quality control steps to remove cells with >5 mitochondrial genes and <700 unique genes.

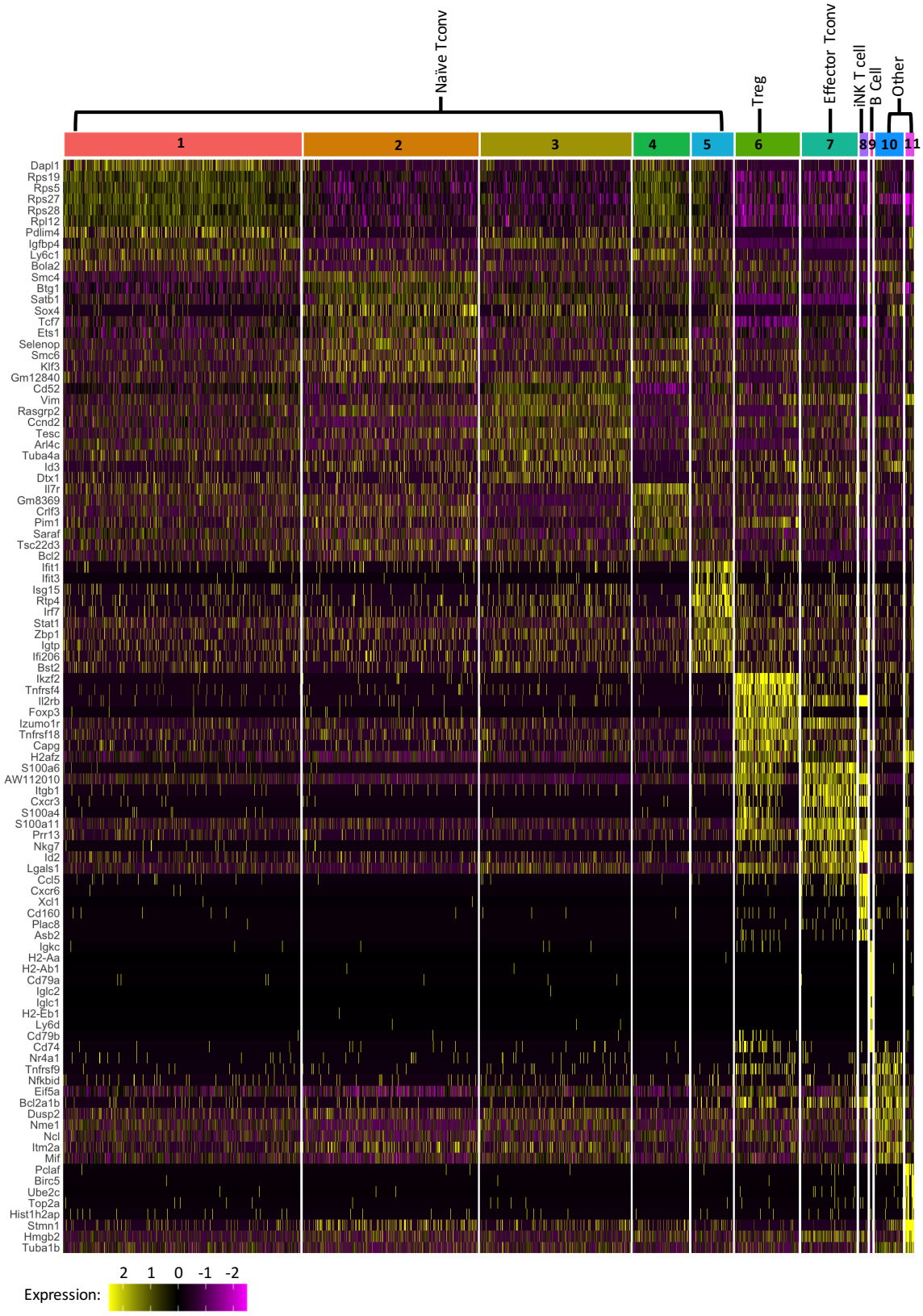
Naïve Tconv
Treg
Effector Tconv
iNK T cell
B Cell
Other
1
2
3
4
5
6
7
8
9
10
11
Dapl1
Rps19
Rps5
Rps27
Rps28
Rpl12
Pdlim4
Igfbp4
Ly6c1
Bola2
Smc4
Btg1
Satb1
Sox4
Tcf7
Ets1
Selenop
Smc6
Klf3
Gm12840
Cd52
Vim
Rasgrp2
Ccnd2
Tesc
Arl4c
Tuba4a
Id3
Dtx1
Il7r
Gm8369
Crlf3
Pim1
Saraf
Tsc22d3
Bcl2
Ifit1
Ifit3
Isg15
Rtp4
Irf7
Stat1
Zbp1
Igtp
Ifi206
Bst2
Ikzf2
Tnfrsf4
Il2rb
Foxp3
Izumo1r
Tnfrsf18
Capg
H2afz
S100a6
AW112010
Itgb1
Cxcr3
S100a4
S100a11
Prr13
Nkg7
Id2
Lgals1
Ccl5
Cxcr6
Xcl1
Cd160
Plac8
Asb2
Igkc
H2-Aa
H2-Ab1
Cd79a
Iglc2
Iglc1
H2-Eb1
Ly6d
Cd79b
Cd74
Nr4a1
Tnfrsf9
Nfkbid
Eif5a
Bcl2a1b
Dusp2
Nme1
Ncl
Itm2a
Mif
Pclaf
Birc5
Ube2c
Top2a
Hist1h2ap
Stmn1
Hmgb2
Tuba1b
2 1 0 -1 -2
Expression:

Figure S. 2 Enlarged Heatmap of Total RTE and Non-RTE Clusters DEGs Originally Presented in Figure 5.3.B

Heatmap shows the expression of the 10 most positively DEGs for each cluster, with the colour scale indicating gene expression level. Cluster identities, including assigned cell subset identity, are given above.

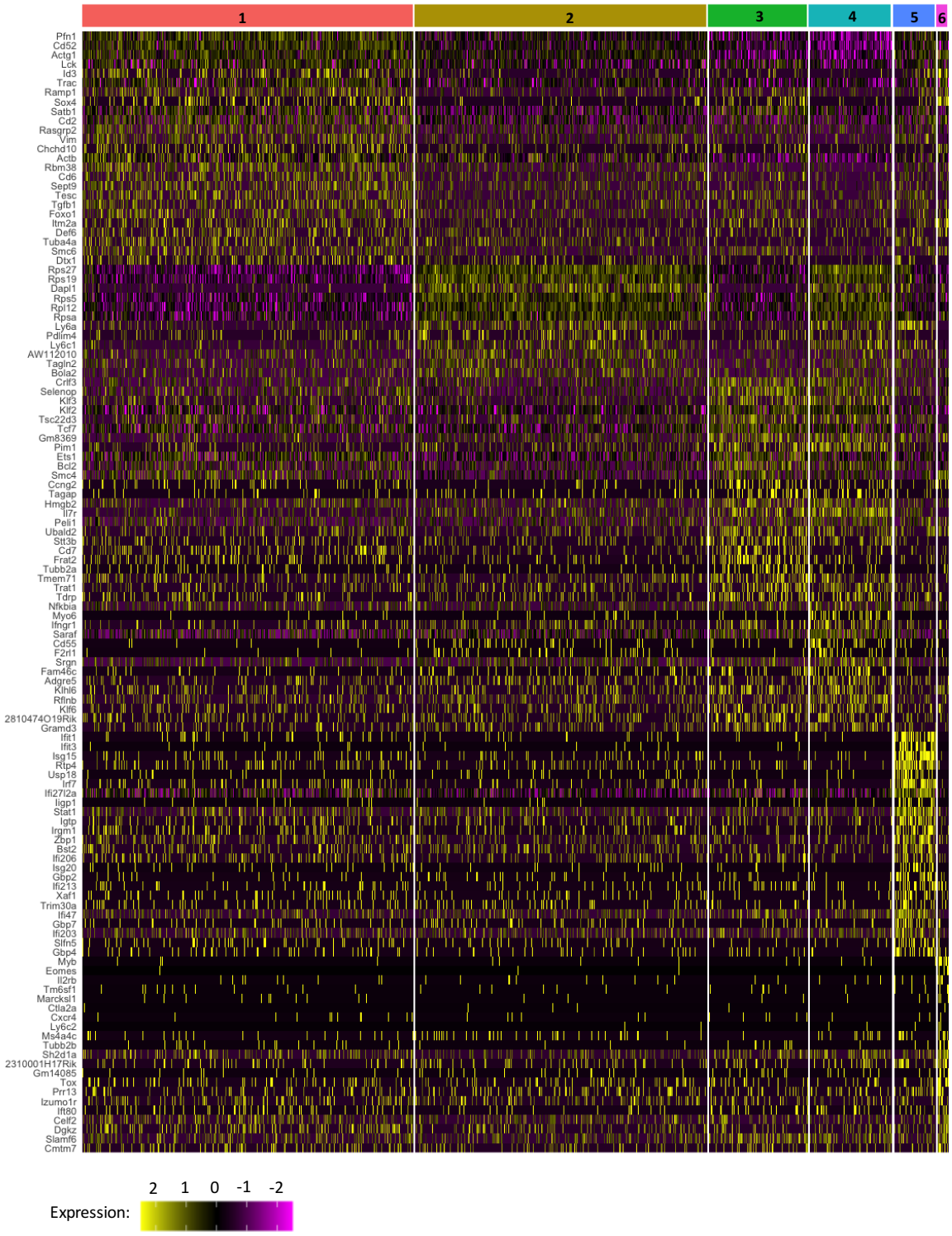
1
2
3
4
5
6
Pfn1
Cd52
Actg1
Lck
Id3
Trac
Ramp1
Sox4
Satb1
Cd2
Rasgrp2
Vim
Chchd10
Actb
Rbm38
Cd6
Sept9
Tesc
Tgfb1
Foxo1
Itm2a
Def6
Tuba4a
Smc6
Dtx1
Rps27
Rps19
Dapl1
Rps5
Rpl12
Rpsa
Ly6a
Pdlim4
Ly6c1
AW112010
Tagln2
Bola2
Crlf3
Selenop
Klf3
Klf2
Tsc22d3
Tcf7
Gm8369
Pim1
Ets1
Bcl2
Smc4
Ccng2
Tagap
Hmgb2
Il7r
Peli1
Ubald2
Stt3b
Cd7
Frat2
Tubb2a
Tmem71
Trat1
Tdrp
Nfkbia
Myo6
Ifngr1
Saraf
Cd55
F2rl1
Srgn
Fam46c
Adgre5
Klhl6
Rflnb
Klf6
2810474O19Rik
Gramd3
Ifit1
Ifit3
Isg15
Rtp4
Usp18
Irf7
Ifi27l2a
Iigp1
Stat1
Igtp
Irgm1
Zbp1
Bst2
Ifi206
Isg20
Gbp2
Ifi213
Xaf1
Trim30a
Ifi47
Gbp7
Ifi203
Slfn5
Gbp4
Myb
Eomes
Il2rb
Tm6sf1
Marcksl1
Ctla2a
Cxcr4
Ly6c2
Ms4a4c
Tubb2b
Sh2d1a
2310001H17Rik
Gm14085
Tox
Prr13
Izumo1r
Ift80
Celf2
Dgkz
Slamf6
Cmtm7
2
1
0
-1
-2
Expression:

Figure S. 3 Enlarged Heatmap of Naïve Tconv Clusters DEGs Originally Presented in Figure 5.4.B

Heatmap shows the expression of the 25 most positively DEGs for each cluster, with the colour scale indicating gene expression level. Cluster identities are given above.

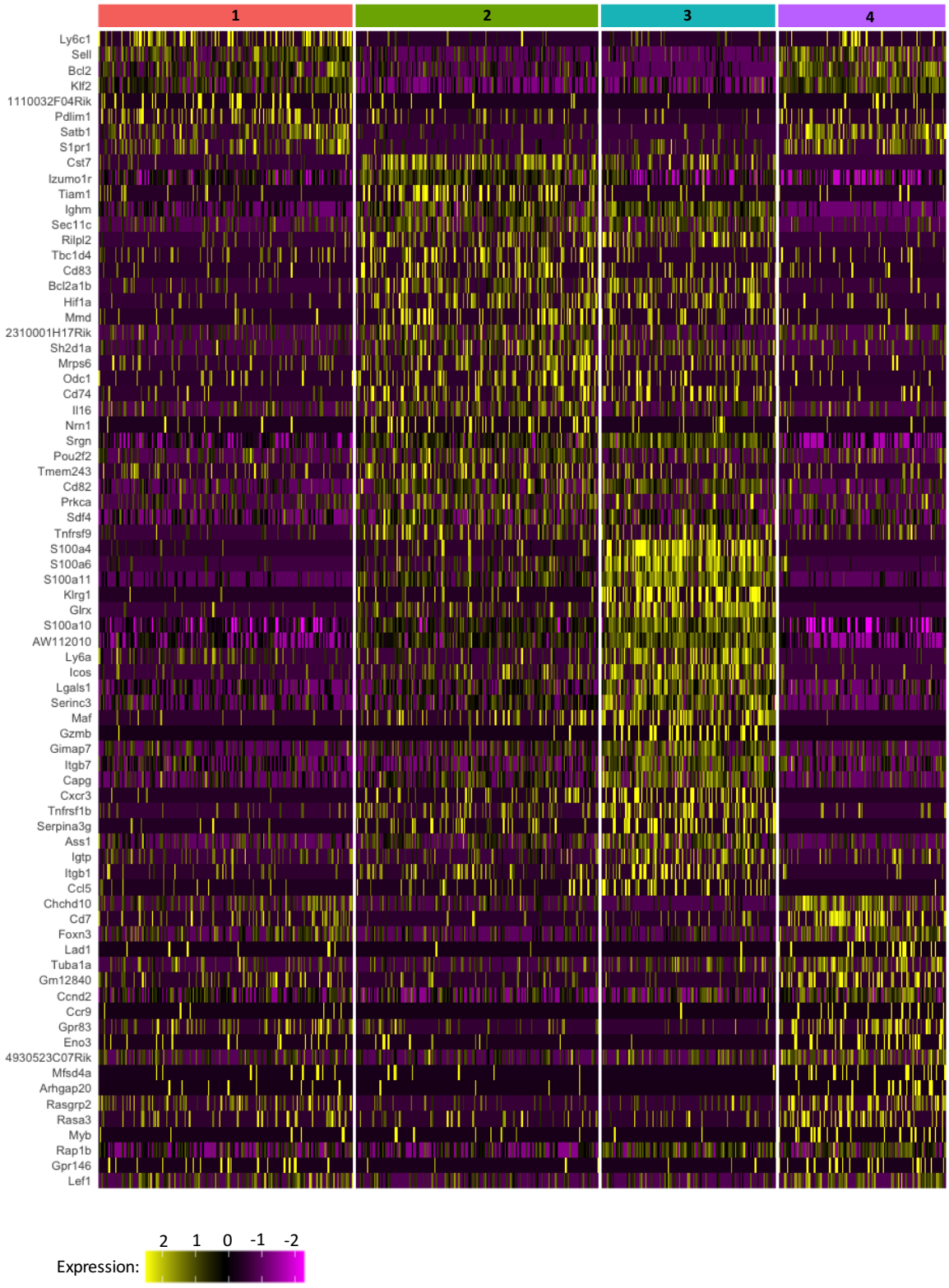
1
2
3
4
Ly6c1
Sell
Bcl2
Klf2
1110032F04Rik
Pdlim1
Satb1
S1pr1
Cst7
Izumo1r
Tiam1
Ighm
Sec11c
Rilpl2
Tbc1d4
Cd83
Bcl2a1b
Hif1a
Mmd
2310001H17Rik
Sh2d1a
Mrps6
Odc1
Cd74
Il16
Nrn1
Srgn
Pou2f2
Tmem243
Cd82
Prkca
Sdf4
Tnfrsf9
S100a4
S100a6
S100a11
Klrg1
Glrx
S100a10
AW112010
Ly6a
Icos
Lgals1
Serinc3
Maf
Gzmb
Gimap7
Itgb7
Capg
Cxcr3
Tnfrsf1b
Serpina3g
Ass1
Igtp
Itgb1
Ccl5
Chchd10
Cd7
Foxn3
Lad1
Tuba1a
Gm12840
Ccnd2
Ccr9
Gpr83
Eno3
4930523C07Rik
Mfsd4a
Arhgap20
Rasgrp2
Rasa3
Myb
Rap1b
Gpr146
Lef1
Expression:
2 1 0 -1 -2

Figure S. 4 Enlarged Heatmap of Treg Clusters DEGs Originally Presented in Figure 5.4.C

Heatmap shows the expression of the 25 most positively DEGs for each cluster, with the colour scale indicating gene expression level. Cluster identities are given above.

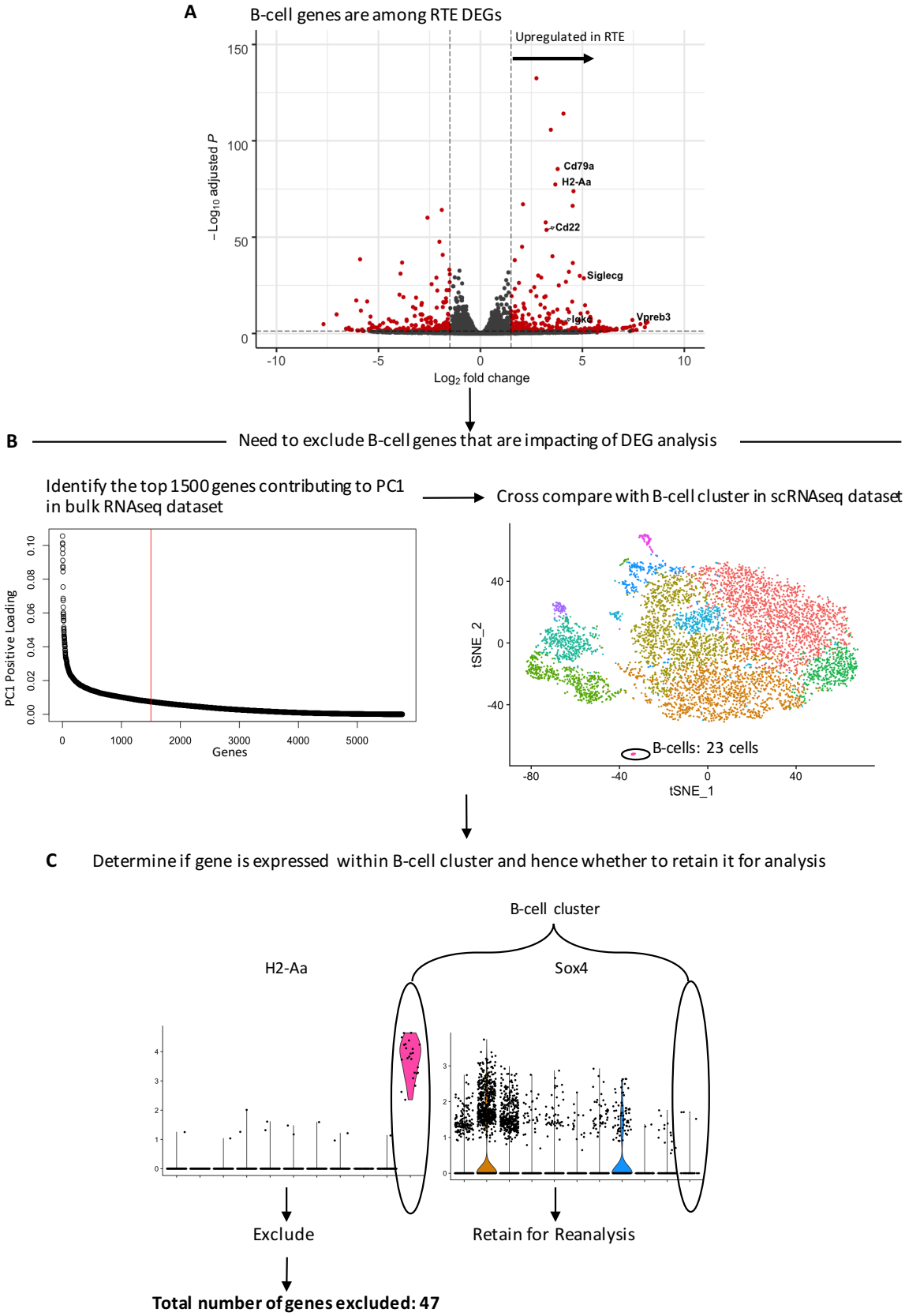
A
B-cell genes are among RTE DEGs
Upregulated in RTE
Cd79a
H2-Aa
Cd22
Siglecg
Vpreb3
Igkc
−Log10 adjusted P
Log2 fold change
B
Need to exclude B-cell genes that are impacting of DEG analysis
Identify the top 1500 genes contributing to PC1 in bulk RNAseq dataset
Cross compare with B-cell cluster in scRNAseq dataset
PC1 Positive Loading
Genes
tSNE_2
tSNE_1
B-cells: 23 cells
C
Determine if gene is expressed within B-cell cluster and hence whether to retain it for analysis
B-cell cluster
H2-Aa
Sox4
Exclude
Retain for Reanalysis
Total number of genes excluded: 47

Figure S. 5 Specifics of Removal of B-cell Genes from Bulk RNAseq datasets from Figure 5.5

Schematic giving an overview of the process of identifying and removing contaminating B-cell genes from bulk RNAseq datasets. In brief, **(A)** initial differential gene expression analysis flagged genes known to characterise B-cells as positively upregulated within the RTE samples. Therefore **(B)** the 1500 genes making the largest positive contribution to PC1 were identified and their expression assessed across the different cellular populations within the scRNAseq dataset which had been identified to contain a B-cell cluster. **(C)** If the genes were found to be highly expressed by the B-cell cluster they were excluded from the analysis, otherwise the gene was retained. This process resulted in the exclusion of 47 genes.

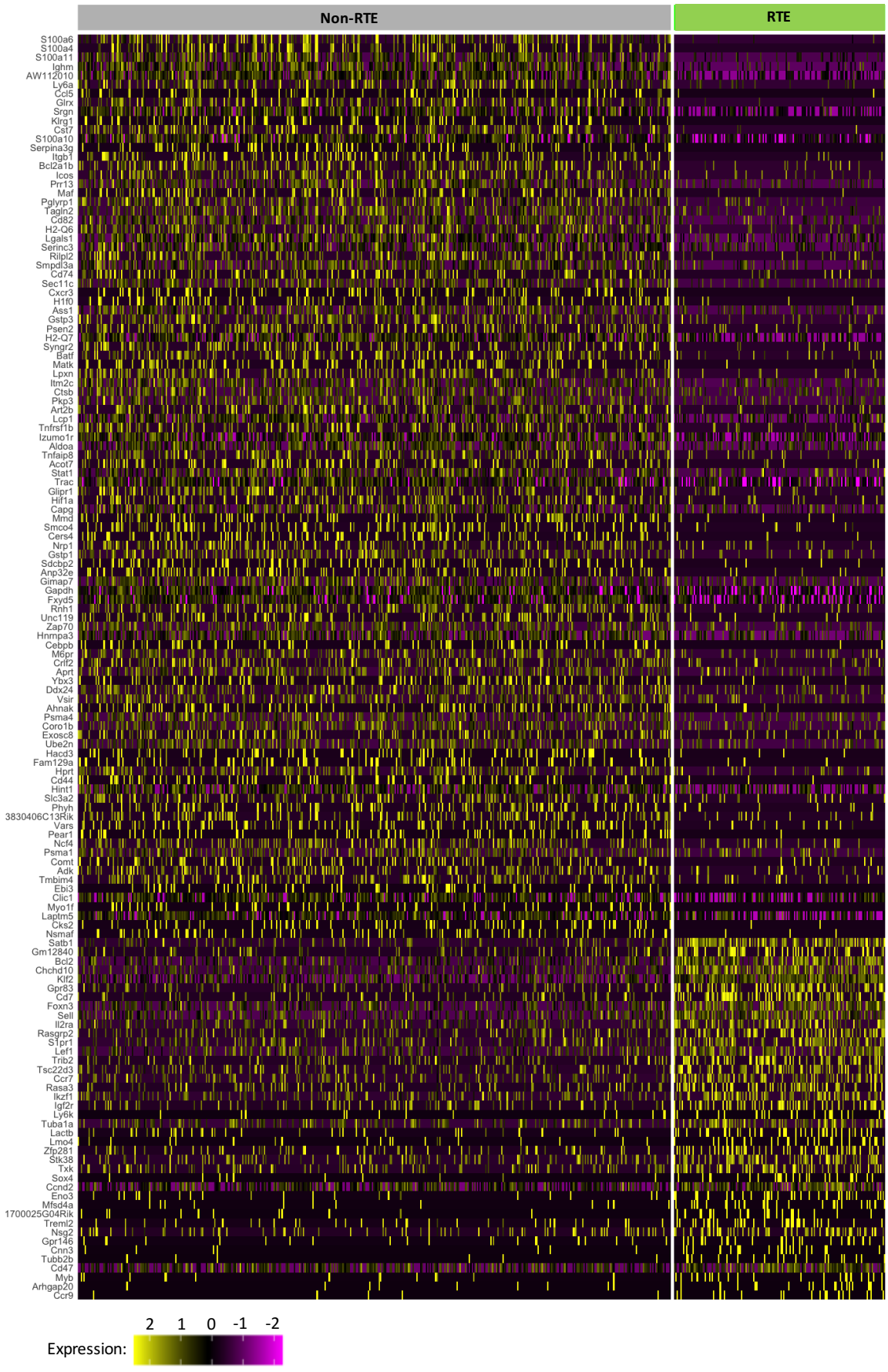
Non-RTE
RTE
S100a6
S100a4
S100a11
Ighm
AW112010
Ly6a
Ccl5
Glrx
Srgn
Klrg1
Cst7
S100a10
Serpina3g
Itgb1
Bcl2a1b
Icos
Prr13
Maf
Pglyrp1
Tagln2
Cd82
H2-Q6
Lgals1
Serinc3
Rilpl2
Smpdl3a
Cd74
Sec11c
Cxcr3
H1f0
Ass1
Gstp3
Psen2
H2-Q7
Syngr2
Batf
Matk
Lpxn
Itm2c
Ctsb
Pkp3
Art2b
Lcp1
Tnfrsf1b
Izumo1r
Aldoa
Tnfaip8
Acot7
Stat1
Trac
Glipr1
Hif1a
Capg
Mmd
Smco4
Cers4
Nrp1
Gstp1
Sdcbp2
Anp32e
Gimap7
Gapdh
Fxyd5
Rnh1
Unc119
Zap70
Hnrnpa3
Cebpb
M6pr
Crlf2
Aprt
Ybx3
Ddx24
Vsir
Ahnak
Psma4
Coro1b
Exosc8
Ube2n
Hacd3
Fam129a
Hprt
Cd44
Hint1
Slc3a2
Phyh
3830406C13Rik
Vars
Pear1
Ncf4
Psma1
Comt
Adk
Tmbim4
Ebi3
Clic1
Myo1f
Laptm5
Cks2
Nsmaf
Satb1
Gm12840
Bcl2
Chchd10
Klf2
Gpr83
Cd7
Foxn3
Sell
Il2ra
Rasgrp2
S1pr1
Lef1
Trib2
Tsc22d3
Ccr7
Rasa3
Ikzf1
Igf2r
Ly6k
Tuba1a
Lactb
Lmo4
Zfp281
Stk38
Txk
Sox4
Ccnd2
Eno3
Mfsd4a
1700025G04Rik
Treml2
Nsg2
Gpr146
Cnn3
Tubb2b
Cd47
Myb
Arhgap20
Ccr9
2 1 0 -1 -2
Expression:

Figure S. 6 Enlarged Heatmap of DEGs between Treg RTE and Non-RTE Originally Presented in Figure 5.9.E

Heatmap of all significant ($p<0.05$) DEGs (rows), with cells grouped as RTE or Non-RTE (columns) as indicated. Colour scale indicates gene expression level. Cells identity as RTE vs Non-RTE given above.

Table S. 1 Contaminating B-cell Genes Identified and Removed from SP4-Bulk Dataset

B-cell Gene	Identification Reference
H2-Aa	Genes found specifically in B-cell scRNAseq cluster and supported as B-cell markers by literature
Igkc	
H2-Ab1	
Pax5	
Cd79a	
Ms4a1	
H2-Eb1	
Siglecg	
H2-DMb2	
Ebf1	
Cd180	
Napsa	
Fcrla	
Fgd2	
Ctsh	
Lmo2	
Blnk	
Mef2c	
Srpk3	
Kmo	
Cd22	
Lyn	
Bank1	
Bcar3	
H2-DMb1	
Lrrk2	
Hhex	
Vpreb3	
Bcl11a	
Il4i1	
H2-Eb2	
Fcgr2b	
Prr5	Genes found in B-cell scRNAseq cluster with little documentation in literature
Hck	
Trim7	
Cbfa2t3	
Tifa	
Fam43a	Genes found in B-cell scRNAseq cluster but literature supports as also being found on T-cells
Pkig	
Sdc4	
Pxdc1	
Syk	Genes found in B-cell scRNAseq cluster but with low expression or also found in other clusters
Ly6d	
Faim3	Genes not found in scRNAseq search but have a link to B-cells in literature
Iglv1	
Igj	
Ppapdc1b	

Table S. 2 Specifics of DEGs (between RTEs and Non-RTEs) of Literature Genes Detected within the SP4-Bulk Dataset

Gene	Log2 Fold Change	Adjusted p-value
Cd3e	1.84E-01	1.43E-01
Cd3g	4.48E-01	1.71E-04
Dgkz	1.29E-01	2.51E-01
Pdcd1	-8.53E-01	2.08E-02
Ctla4	-5.18E-01	3.43E-03
Itga4	-6.67E-01	1.87E-09
Itgb7	-1.93E-01	5.59E-02
Ccr9	4.07E+00	7.75E-115
Itgb1	-1.26E+00	1.11E-29
Dnmt3a	6.58E-01	8.06E-07
Ly6c1	-1.08E+00	7.19E-22
Cd28	-1.04E-01	4.59E-01
Slc2a1	-2.93E-01	8.47E-02
Hk2	-1.16E+00	1.02E-01
Slc7a5	-3.35E-01	4.73E-02
Tfrc	1.09E-02	9.61E-01
Mtor	-1.77E-01	2.67E-01
Rptor	-4.69E-01	4.61E-03
Cd55	-2.01E+00	5.43E-48

Table S. 3 Specifics of DEGs identified between RTEs and Non-RTEs, which are Top 100 Contributors to PC1, within the SP4-Bulk Dataset

Gene	Log2 Fold Change	Adjusted p-value
Sox4	2.745746475	3.34E-133
Ccr9	4.072214866	7.75E-115
Nt5e	-2.595951871	1.65E-60
Dapl1	-2.421160451	8.67E-09
Tmie	2.08724549	1.91E-67
Cd55	-2.010331535	5.43E-48
Ttc39b	-1.89461762	1.72E-64
Ndrg1	2.041868872	1.95E-45
Fam46a	-1.848527644	2.94E-41
Arhgap20	2.833458264	1.26E-30
Cd7	1.684222806	9.47E-24
Stmn1	1.683789154	1.67E-38
Ptpn13	-3.918485114	1.37E-31
Dnaja4	-2.158186743	1.59E-29
Kcnh2	1.88896824	7.92E-27
Vangl2	2.640961038	1.24E-24
Jup	2.981231012	1.36E-29
Fam129a	-2.114458106	6.96E-23
Itga6	-1.394417088	4.19E-05
Klf4	-1.523954843	1.27E-33
Klrd1	-2.393668981	3.53E-26
Cxcr3	-5.901509606	5.99E-39
Gpr68	-3.84188846	2.74E-37
Myo6	-1.50090622	3.02E-31
Ptms	1.369950883	3.05E-32
Klhl5	-1.505596443	3.61E-27
Itm2a	1.26523701	2.88E-28
Car2	2.742422232	5.72E-20
H2-Q5	-1.677201728	3.19E-17
Ppm1j	-1.538351137	4.70E-23
Gsn	1.352887551	3.19E-26
Il18r1	-1.659408155	4.81E-23
Itgb1	-1.260101913	1.11E-29
Ptprf	3.132131406	1.95E-19
Glipr2	-1.346518155	4.62E-25
Ikzf2	-1.322451574	4.62E-25
Maf	-1.689103449	6.81E-19
Nedd4	2.469530751	1.29E-22
Cnn3	1.385521219	7.08E-22
Ager	1.52972178	5.62E-20
Smo	4.531230209	4.40E-37
Tiam1	-1.824868848	5.91E-17
Marcks	3.197272546	6.68E-20
Kif1b	-1.149415001	4.25E-17
Trp53inp2	2.111079837	3.73E-16

Nhsl1	1.845003168	2.01E-12
Ramp1	1.177651931	4.11E-24
Eif4e3	1.263350558	2.50E-20
Pdlim4	-1.191585131	6.20E-18
Adam19	-1.135368861	2.21E-17
Sidt1	-1.075686385	3.34E-29
Kcnmb4	1.704355307	7.82E-15
Jun	-1.026830906	4.11E-33
Acsbg1	-1.718651511	6.69E-17
Sntb1	-1.377485481	1.37E-09
Gm14085	-1.08032843	1.44E-14
Acvrl1	1.143048945	1.42E-13
AW112010	-1.220374132	2.29E-13
Pde8a	-1.787490649	9.80E-17
Cebpb	-1.476945362	8.23E-14
Ampd1	1.243208586	2.18E-11
Itih5	1.284775894	1.10E-15
Abcb1a	-3.154945677	3.16E-19
Myo1f	-2.874929063	1.89E-16
S100a4	-3.969924478	9.40E-21
D8Ertd82e	-1.19332044	5.09E-19
Id3	1.131023791	1.44E-18
Ly6c1	-1.07727284	7.19E-22
Tmem108	2.138228768	3.58E-14
Wscd2	-1.843333642	2.31E-14
Tagap	-0.983687461	1.37E-19
Zbtb10	-1.229786312	9.05E-10
S100a6	-2.891527676	1.79E-15
Plxnd1	1.44337822	3.93E-14
P2rx7	-1.090602743	1.29E-12
Dlg4	1.022614009	1.41E-18
Coro2a	-1.251253127	7.32E-14
Acpp	-1.224578571	3.80E-13
Inpp4b	-0.906538073	9.03E-10
Ephb6	0.983853345	1.69E-19
Top2a	1.032145673	1.26E-15
Adgre5	-0.897566107	1.48E-26
Fos	-0.896683346	3.15E-19
Tlr7	1.504389374	2.44E-12
Ncf4	-1.034533934	4.02E-14
Tagln2	-0.901642171	8.85E-18
Ms4a4c	-1.169590507	1.20E-11
Chdh	2.177848102	1.80E-13
Atm	-0.882093864	0.025692434
Smpdl3a	-0.932739313	8.07E-18
Prkar2a	-1.191397671	4.70E-11
Gvin1	-2.936863255	1.41E-10
Ntrk3	-2.143080194	4.65E-14
Nacc2	-1.127503662	5.28E-11

Ddr1	-1.20430888	2.62E-11
Gngt2	1.175821099	6.21E-12
Cuedc1	1.443555074	1.24E-11
Rapgef6	-0.805482651	1.37E-14
Brdt	1.45459727	1.22E-11
Map3k12	1.136564154	2.84E-11

Table S. 4 Specifics of all DEGs Identified Between RTEs and Non-RTEs within the Tconv scRNAseq Dataset

Gene	Average Log Fold Change	Adjusted p-value
Dapl1	-1.279007268	<2.225E-3080
Satb1	0.545301464	2.13E-131
Ly6a	-0.614607694	1.26E-127
Sox4	0.717511535	3.32E-105
Ly6c1	-0.538565866	3.65E-104
AW112010	-0.451030114	1.70E-82
Ramp1	0.515763857	7.84E-79
Id3	0.649696589	6.41E-77
Ly6e	-0.272084124	2.23E-70
Cd7	0.498578165	2.86E-64
Pdlim4	-0.406530635	3.00E-63
Tagln2	-0.341495953	2.73E-57
Itm2a	0.501518095	8.50E-53
Rasgrp1	0.433136961	1.89E-51
Gstp1	-0.303618965	3.14E-50
Bola2	-0.321625986	5.93E-49
Smc4	0.445780325	6.96E-48
Cd55	-0.251406029	1.18E-44
Tesc	0.417213504	1.86E-43
Snrnp70	0.368920756	2.07E-43
Rasgrp2	0.382817652	5.60E-43
Smc6	0.409952725	2.72E-42
Foxn3	0.430636441	2.49E-40
Stmn1	0.408407696	8.47E-39
Il7r	-0.304962054	1.71E-32
Ccnd3	0.329362287	5.71E-31
H2afv	0.294096154	1.65E-29
Cd6	0.36728677	3.06E-28
Spint2	0.318122759	3.81E-28
Chchd10	0.396848995	1.01E-27
Chd3	0.312223664	7.20E-27
Phpt1	0.314374103	7.97E-27
Frat2	0.317580824	2.75E-26
Abhd8	0.310788321	4.17E-24

Table S. 5 Specifics of all DEGs Identified Between RTEs and Non-RTEs within the Treg scRNAseq Dataset

Gene	Average Log Fold Change	Adjusted p-value
Ighm	-1.449085504	4.35E-29
AW112010	-1.364966824	7.81E-28
Satb1	1.070032389	9.25E-26
Klf2	0.844537343	1.09E-22
S100a11	-1.482709272	1.44E-22
Srgn	-1.042461916	1.20E-20
S100a6	-1.944963554	1.96E-18
Bcl2	0.916523716	3.47E-16
Chchd10	0.87593728	8.92E-16
Glrx	-1.054340057	4.71E-15
Cst7	-0.947453008	1.58E-13
S100a10	-0.782952374	2.83E-13
Cd7	0.758086977	1.66E-12
Sell	0.681323669	2.39E-12
Foxn3	0.684074407	7.25E-12
Prr13	-0.743785716	1.17E-11
Ly6a	-1.351832432	5.05E-11
S100a4	-1.705930894	8.78E-11
Smpdl3a	-0.65049719	1.35E-10
Pglyrp1	-0.736934694	2.03E-10
Tagln2	-0.736217314	3.18E-10
Cd82	-0.712791439	4.74E-10
H2-Q7	-0.559847086	3.11E-09
H2-Q6	-0.70272313	4.35E-09
Bcl2a1b	-0.76003102	8.20E-09
Gpr83	0.827212411	2.13E-08
Icos	-0.753172659	2.24E-08
Lpxn	-0.547164762	3.79E-08
Sec11c	-0.60764206	4.81E-08
Maf	-0.74358759	5.57E-08
Gapdh	-0.432811135	1.46E-07
Stat1	-0.486669049	1.76E-07
Syngr2	-0.557995544	3.73E-07
Lcp1	-0.52398237	4.00E-07
Itgb1	-0.76472058	7.46E-07
Rilpl2	-0.654937783	8.36E-07
Serinc3	-0.687032518	9.89E-07
Fxyd5	-0.43013716	9.99E-07
Gstp3	-0.571526933	1.32E-06
Trac	-0.481212272	2.94E-06
Lgals1	-0.701583574	3.91E-06
Psen2	-0.569357444	7.62E-06
Matk	-0.554288796	1.01E-05
Sox4	0.435855483	1.40E-05
Cnn3	0.383844089	1.42E-05
Tubb2b	0.355657934	1.60E-05

Lef1	0.569583822	1.73E-05
Gstp1	-0.448602934	2.05E-05
Ctsb	-0.532461371	2.14E-05
Mfsd4a	0.417910277	2.26E-05
Acot7	-0.497028795	2.41E-05
Trib2	0.5684872	2.86E-05
Cxcr3	-0.599507689	3.40E-05
Aldoa	-0.506187389	4.42E-05
Cers4	-0.458029995	4.80E-05
Tnfaip8	-0.498996529	5.67E-05
Unc119	-0.420736302	8.94E-05
Izumo1r	-0.51797624	9.67E-05
Ccr9	0.286665118	1.00E-04
Ass1	-0.585172949	0.000110635
S1pr1	0.578878517	0.000112444
Klrg1	-1.029203528	0.000113691
Itm2c	-0.537983723	0.000135323
Serpina3g	-0.767872992	0.000144419
Batf	-0.554795226	0.000169682
Pkp3	-0.53004612	0.0001771
Rnh1	-0.421033669	0.000199636
Art2b	-0.52913507	0.000254571
Anp32e	-0.44681072	0.000267681
Hint1	-0.350440815	0.000301795
1700025G04Rik	0.406660205	0.000362226
Hnrnpa3	-0.409288899	0.000384598
H1f0	-0.598278018	0.000422372
Mmd	-0.462023202	0.000625754
Smco4	-0.459024579	0.000648008
Eno3	0.424519849	0.000704155
Cd74	-0.642895708	0.000734003
Tnfrsf1b	-0.518298252	0.000809152
Hif1a	-0.469536163	0.000994274
Sdcbp2	-0.447134201	0.001162845
Gm12840	1.005451764	0.001439623
Aprt	-0.402189242	0.001871967
Il2ra	0.615741314	0.002011238
Rasgrp2	0.602588365	0.002045995
Ccnd2	0.426263791	0.002124627
Arhgap20	0.325549159	0.002595696
Fam129a	-0.364586476	0.002980913
Cebpb	-0.406384913	0.003254477
Ikzf1	0.498797711	0.003390407
Gimap7	-0.43826417	0.003765174
Igf2r	0.492040502	0.003836071
Hprt	-0.355068394	0.004321827
Cd44	-0.351602246	0.004850983
Zap70	-0.409735058	0.004858628
Lactb	0.470251883	0.004955166

Ube2n	-0.367152537	0.005174138
Zfp281	0.468119223	0.005180504
Stk38	0.453197957	0.006385507
Capg	-0.469045518	0.006628262
Ahnak	-0.383406952	0.007033615
Glipr1	-0.470732944	0.007329523
Clic1	-0.313999323	0.007553963
Nrp1	-0.453162218	0.007755608
Ccl5	-1.063406999	0.008173953
Ly6k	0.490998998	0.009601488
Nsg2	0.398124459	0.010915797
Phyh	-0.346720692	0.01223747
Tmbim4	-0.325402812	0.012326
Txk	0.441139175	0.012407351
Pear1	-0.335712349	0.012505807
Coro1b	-0.377777625	0.012560021
M6pr	-0.406073613	0.014019035
Comt	-0.327110262	0.014829636
Laptm5	-0.305108323	0.014985034
Ybx3	-0.400431308	0.015300532
Rasa3	0.500487033	0.015422248
Hacd3	-0.36662698	0.017692551
Myb	0.338687273	0.01770434
Lmo4	0.469868226	0.017987171
Psma4	-0.378739121	0.018124653
Crlf2	-0.405827165	0.018857621
Ncf4	-0.330261773	0.020590438
Nsmaf	-0.287055219	0.028445205
Psma1	-0.328039596	0.028586099
Myo1f	-0.313004798	0.029421945
Ebi3	-0.317660221	0.029421945
Tuba1a	0.475428505	0.031009451
Gpr146	0.396087732	0.031806883
Cd47	0.342228338	0.032630508
Ccr7	0.542096084	0.035841843
Cks2	-0.301762144	0.03874788
Vars	-0.338308222	0.040205894
Vsir	-0.392012853	0.040557484
Treml2	0.406629066	0.041406553
Adk	-0.325618881	0.041513366
3830406C13Rik	-0.338536316	0.045735909
Tsc22d3	0.548177541	0.046339644
Exosc8	-0.375966844	0.046554588
Slc3a2	-0.347436535	0.049340043
Ddx24	-0.396144306	0.049817347